Development of Surface-Modified Liposomes for Drug Delivery Applications

A Dissertation Presented for the

Doctor of Philosophy

Degree

The University of Tennessee, Knoxville

Megan L. Qualls

May 2023

Acknowledgements

My graduate school career would not have been possible without the mentors, colleagues, friends, and family who supported me along the way. First, I would like to thank my advisor Dr. Michael Best who has provided guidance and support throughout my graduate school years. He is an excellent mentor because of his wide range of knowledge, passion for the field of chemistry, and genuine and professional demeanor towards students. He has always been patient and open to answering any questions and has provided unwavering support even through difficult times. His influence has shaped me into the researcher I am today, for which I am very grateful. I am very lucky to have him as a research advisor and to have the opportunity to work and learn in the Best lab.

Special thanks to Dr. Constance Bailey, Dr. Brian Long, and Dr. Todd Reynolds for serving on my dissertation committee. I appreciate all of the insightful questions and advice during defenses which both deepened my understanding and improved my research projects. Their academic excellence and strong work ethics are attributes I hope to emulate in my career. I would also like to thank the collaborators who I have had the pleasure of working with on most of my projects. Dr. Joshua Baccile and Dillon McBee have been unparalleled research associates and I am very thankful to have had the opportunity to learn new cell study skills through our collaborations. I am also thankful for Dr. Deidra Mountain, Dr. Sam Mattern-Schain, Dr. Todd Reynolds, and Yue Aeric Zhou for assistance with cell studies on various projects; Dr. John Brantley for polymer collaborations; Jaydeep Kolape for guidance at the Advanced Microscopy and Imaging Center; and Dr. Carlos Steren for assistance and maintenance of the NMR facilities. Thanks to the faculty, staff, and graduate students in the Chemistry Department for providing a positive environment. Special thanks to Dr. Lauren Anderson for providing a model of considerate leadership and passion for teaching which I continuously strive to replicate.

I would like to thank all Best Group Members who I have had the privilege of working with and learning from over the years. I am particularly thankful for previous graduate student and current post-doctoral scholar Dr. Jinchao Lou who has provided endless advice and opportunities which

have greatly impacted my graduate school journey. I am exceptionally grateful for my lab mates Ruhani Sagar and Christelle Ancajas with whom I simultaneously began graduate school and joined the Best lab. We have undergone every step of the process together and they have provided unequaled support and companionship. In addition to being a true friend and confidante both in the lab and in life, Ruhani Sagar has a determination for discovery, knowledge, truth, and justice and an astonishing work ethic which I hope to mirror in my life and career. Additionally, I'd like to thank my undergraduate research assistant Hannah Hagewood who I had the privilege of mentoring for providing a refreshing eagerness to learn. I am also thankful for Dr. Xiaoyu Zhang, Alexa Watson, Sara Barker, Matt Johnson, Justin Kirby, Brooke Smith, Mayesha Mustafa, Kazi Shahriar, Michael Kadiri, and many other colleagues.

I'd like to thank the many people who provided me opportunities prior to graduate school, without which I would never have had the opportunity of a Ph.D. career in chemistry. I would like to thank my undergraduate research advisor Dr. Dallas Donohoe for providing my first research experience in the Cellular and Molecular Nutrition Department and UTK which inspired me to pursue a career in research. Working in the lab allowed me to learn research skills and concepts which I still use to this day. Additionally, I'd like to thank Dr. Curtis Anderson who encouraged me to pursue chemistry research, and thanks to Dr. Brian Long who provided the opportunity to participate in research. The organic synthesis techniques, passion and drive for research I learned during that time provided a platform for my future research and inspired me to pursue graduate school in chemistry.

I would like to thank the people who served as my strong support system throughout my life, my family and friends. The Pence family has provided so much love and support over my life, and I strive to make them proud. I am thankful that they have always believed in me and continuously model what it means to live a kind and meaningful life. I am thankful for my grandmother Dorel Davis Elliot for providing a safe and loving environment in the midst of chaos, and I wish you could be here today to see me accomplish something you always believed I could. I am blessed to have a supportive and loving father, Brian Pence, who has always encouraged me to follow my

passions in life. His ability to overcome impossible challenges in life inspires me every day. I am grateful for my brother Brian Christopher Pence, sister-in-law Lindsey Pence, niece Naomi Pence, and nephew Theodore Pence for their love and support. I am especially grateful for my amazing sister Gabrielle Pence whose endurance, love, and ability to see the beautiful things in life continuously inspires me. For many years my life was challenging, and the future was never certain, but I am forever grateful to my family for never doubting that I could find a path and accomplish my goals. I love them very much and hope to make them proud. I am also thankful to my friends Sophia Cook, Adrian Cross, Mason Thornton, Chris Justice, Katie Green, and Derek Dougal for being supportive friends, keeping me grounded, and providing laughs and precious memories. I am additionally thankful for my father and mother in-law, Donald and Linda Qualls, for their continuous love and support.

The person who deserves the most thanks in my life is my husband and best friend, Christopher Qualls, without whom my journey through graduate school would have never been possible. He is the most kind, loving, smart, trustworthy, consistent, and genuine person I have ever met, and is the only person who truly sees me. I am incredibly blessed that he has loved and supported me through the toughest times, the late nights, and the tears and self-doubt, and has never once stopped believing in me. He was the first person to encourage me to apply for graduate school and has been my daily advocate and encourager over the last five years. His unending love, patience, and support has allowed me to achieve this milestone in life, and as I look into our future together, I am excited to go on more adventures, experience more life, start a family, and spend our years growing together. I love you very much and hope I've made you proud.

Abstract

Liposomes are spherical vesicles composed of a lipid bilayer membrane that assembles around an internal aqueous core. This duality gives liposomes the ability to encapsulate both hydrophobic cargo within the lipid bilayer and hydrophilic cargo in the aqueous core, making them versatile molecular carriers for drug delivery. Liposome platforms have many advantages and are promising drug delivery carriers, and research is ongoing to improve their designs for continued clinical applications. Many liposome types have been developed, but further work is needed to improve surface modification, site-specific targeting, and triggered cargo release in order to further the therapeutic applications of these platforms. In this dissertation, we mainly present the development of surface-modified and stimuli-responsive liposomal platforms via rationally designed synthetic lipids.

In Chapter 2, we present a liposome platform incorporating a headgroup modified cyclic disulfide lipid (CDL) for the dual purpose of enhancing cell entry and functionalizing the liposome membrane through thiol-disulfide exchange. In Chapter 3, we develop a headgroup modified liposome platform incorporating bis-boronic acid lipids (BBALs) to increase valency in order to achieve selective saccharide sensing and enhance cell surface recognition based on carbohydrate binding interactions. In Chapter 4, we utilize a slightly different strategy in which we chemically modified the headgroups of the non-bilayer lipid DOPE to achieve responsive lipids that show alteration in self-assembly properties upon thiol and cysteine addition. In Chapter 5, we present advances towards an ROS-responsive synthetic system for use in artificial ROS signal transduction. Following the synthesis of the synthetic lipids in all these projects, we evaluated their respective activities using the appropriate techniques including fluorescence-based assays to measure surface binding, conjugation, or cargo release. Changes to liposome nanoparticle morphology were additionally probed using dynamic light scattering (DLS) and electron microscopy (EM) techniques. Finally, enhancements in cell delivery were analyzed through fluorescence-based microscopy experiments.

Table of Contents

Chapter 1. Introduction to Lipids, Liposomes, Nanotechnology, Drug Delivery 1

1.1. Lipids in biological systems 1

1.2. Lipid structure and properties 1

1.3. Lipid self-assembly and liposomes 3

1.3.1. Lipid packing parameter and self-assembly of lipids 3

1.3.2. Background of liposomes 8

1.3.3. Liposome membrane phase transition 8

1.3.4. Methods of liposome preparation 9

1.3.5. Characterization of liposomes 14

1.4. Liposomes and drug delivery nanocarriers 15

1.4.1. Introduction of drug delivery nanocarriers 15

1.4.2. Liposomes as drug delivery nanocarriers 19

1.4.3. Liposome surface decoration to improve drug delivery 21

1.4.4. Liposomes and triggered release 24

1.5. Summary and outlook 25

Chapter 2. Development of Cyclic Disulfide Liposomes for Membrane Functionalization and Cellular Delivery 28

2.1. Abstract 29

2.2. Introduction 30

2.2.1. Introduction to disulfide bonds and thiols and biological relevance 30

2.2.2. Reactions of disulfide bonds and thiols 30

2.2.3. Factors influencing the reactivity of disulfide bonds and thiols 31

2.2.4. Disulfide bond use in materials chemistry and nanomedicine 33

2.2.5. Introduction to cyclic disulfide liposomes 34

2.3. Design of cyclic disulfide liposomes 37

2.4. Microplate-based liposome assay to detect membrane functionalization 39

2.4.1. Assay overview 39

2.4.2. Microplate immobilization and membrane functionalization results 39

2.4.3. IAM terminated microplate assay 41

2.5. Dynamic light scattering studies 41

2.6. Transmission electron microscopy studies 45

2.7. NMR experiment before and after liposome preparation 45

2.8. Cellular delivery studies 49
2.8.1. Cellular imaging 49
2.8.2. Quantification of cellular delivery 51
2.9. MTS cellular viability assay 51
2.10. Development of alternative lipid structure for cyclic disulfide liposomes 56
2.10.1. Design of alternative disulfide lipid 56
2.10.2. Microplate-based liposome Biotin-PEG-SH assay with alternative lipid 56
2.10.3. Microplate-based liposome Rhodamine-PEG-SH assay with alternative lipid .. 59
2.10.4. DLS of liposomes containing alternative lipid 2.3 62
2.10.5. TEM of alternative lipid 62
2.10.6. Cellular delivery study with alternative lipid 62
2.11. Alternative microplate assay designs for CDLs 2.1 and 2.2 65
2.12. Conclusions 67
2.13. Synthesis and experimental procedure 69
Chapter 3. Bis-Boronic Acid Liposomes for Carbohydrate Recognition and Cellular Delivery 76
3.1. Abstract 77
3.2. Introduction 78
3.2.1. Introduction to boronic acids 78
3.2.2. Boronate anion equilibrium 79
3.2.3. Boronic acid-diol equilibrium 82
3.2.4. Introduction to boronic acids in nanomaterials for drug delivery 87
3.2.5. Introduction to boronic acid liposomes 89
3.3. Design and synthesis of bis-boronic acid liposomes 95
3.4. Microplate assay for detection of mucin-liposome binding 96
3.4.1. Assay overview 96
3.4.2. Microplate liposome immobilization results 100
3.4.3. BBAL liposomes Rd-dextran binding assay results 100
3.4.4. BBAL liposome mucin binding competition assay results 102
3.4.5. Microplate catechol binding competition assay results 105
3.5. Dynamic light scattering studies 105
3.6. Transmission electron microscopy studies 108
3.7. Cellular delivery studies with vascular smooth muscle cells 108

3.7.1. Quantification of cellular delivery 108
3.7.2. Cellular delivery imaging 111
3.7.3. Delivery of liposomes encapsulating polar dye sulforhodamine B 111
3.7.4. Dynamic light scattering of liposomes used in cellular experiments..... 114
3.8. Other attempted mammalian BBAL cell delivery studies..... 114
3.8.1. Overview of attempted mammalian BBAL cell delivery studies 114
3.8.2. Attempted BBAL U87 cell delivery study results 116
3.8.3. Attempted BBAL MDA-MB-231 cell delivery study results 116
3.8.4. Attempted BBAL A375 cell delivery study results..... 120
3.9. Cellular delivery studies with *Candida albicans*..... 120
3.9.1. Overview of Candida albicans BBAL liposome cellular delivery..... 120
3.9.2. Cellular delivery of bis-boronic acid delivery to *C. albicans*..... 125
3.10. Alternative bis-boronic acid assays attempted 128
3.10.1. Attempted Nile red release assays 128
3.10.2. Attempted Alizarin Red S. competition assay 129
3.10.3. Attempted alternative microplate assay designs for BBALs 3.1a-d..... 132
3.11. Initial design and synthesis of bis-boronic acid lipid 139
3.11.1. Initial design of bis-boronic acid lipid 139
3.12. Alternative boronic acid polymer liposomes 141
3.12.1. Design of boronic acid polymer lipid..... 141
3.12.2. Synthesis of BOPLIPs 142
3.12.3. Nile red (NR) release assay with BOPLIP liposomes 144
3.12.4. Dynamic light scattering BOPLIP studies..... 148
3.12.5. Transmission electron microscopy studies of BOPLIP liposomes 151
3.12.6. Sulforhodamine B release assay with BOPLIP liposomes..... 151
3.12.7. Attempted cellular delivery studies..... 153
3.13. Conclusions..... 156
3.14. Synthesis and experimental procedure 156
Chapter 4. General Thiol and Cysteine Responsive Liposomes 173
4.1. Abstract..... 174
4.2. Introduction 175
4.3. Design and synthesis of general thiol-responsive liposomes 178
4.4. Nile red release assays with 4.1a 180

4.5. Dynamic light scattering 4.1a studies 182
4.6. TLC analysis of thiol-mediated cleavage of free lipid 4.1a 182
4.7. Mass spectrometry evidence of DOPE formation 187
4.8. Synthesis of alternative general thiol-responsive lipid 4.1b 190
4.9. Attempted cargo dye release assays with alternative lipid 4.1b 190
4.10. TLC analysis of thiol-mediated cleavage of free lipid 4.1b 193
4.11. Mass spectrometry evidence of DOPE formation 195
4.12. Design and study of cysteine-responsive liposomes 195
4.13. Nile red release assays with 4.2a-c 199
4.13.1. Screen of cysteine-responsive liposome formulations for Nile Red release assay 199
4.13.2. Nile Red release assay with cysteine-responsive liposomes 202
4.14. Dynamic light scattering studies with 4.2a 209
4.15. 6-Carboxyfluorescein release assay with 4.2a 209
4.16. TLC analysis of cysteine-mediated cleavage of free lipid 211
4.17. Time-dependent NMR experiment 215
4.18. Mass spectrometry evidence of DOPE formation 216
4.19. Conclusion 222
4.20. Synthesis and experimental procedure 223
Chapter 5. Advances Toward ROS Triggered Artificial Transmembrane Signaling with Synthetic Integral Membrane Proteins 241
5.1. Abstract 242
5.2. Introduction 243
5.3. Design and synthesis of ROS triggered synthetic integral membrane proteins 245
5.4. Conclusions 252
5.5. Synthesis and experimental procedure 252
Appendix 292
Vita 293

List of Tables

Table 1.1 Phase transition temperatures of common glycerophospholipids. 11
Table 2.1 Summary of microplate assay designs and treatments explored for CDL 2.1 and 2.2 membrane decoration with thiol-tagged fluorophore. 68
Table 3.1 Ionization constants (pK_as) for common boronic acids. Data is from a book by Dr. Dennis Hall.[251] 81
Table 3.2 Association constants (K_{eq}) of phenylboronic acid with diols. Data courtesy of paper reported by Wang et. al.[274] 85
Table 3.3 Association constants (K_{eq}) of 3-AcPBA and DAPBA with diols at various pH. Data courtesy of paper reported by Sumerlin et. al.[273] 86
Table 3.4 Chemical structures of compounds that compose *C. albicans* cell wall. 124
Table 3.5 Summary of formulations and treatments explored Nile Red release using BBAL liposomes with various percentages of 3.1a, 3.1b, 3.1d, or PC. 130
Table 3.6 Summary of formulations and treatments explored with ARS competition assay using 3.1a or 3.1b. 133
Table 3.7 Summary of microplate assay designs and treatments explored to assess 3.1a-d carbohydrate binding. 136
Table 3.8 Summary of formulations explored for hydrophilic SRB release assay using BOPLIP 3.1.16 and different percentages of Egg-PC, DPPC, DOPE, PA, and DOTAP. 154
Table 4.1 Summary of formulations explored for NR release assay using 4.1a and different percentages of Egg-PC, DOPE, and PA. 185
Table 4.2 Summary of formulations explored for CF release assay using 4.1a, 4.1b and different percentages of DPPC, Egg-PC, DOPE, and PA. 194
Table 4.3 Summary of formulations explored for NR release assay using lipid 4.2a and different percentages of Egg-PC, DOPE, PA, and DOTAP. 203
Table 4.4 Summary of formulations explored for NR release assay using lipid 4.2b and different percentages of Egg-PC, DPPC, DOPE, and PA. 205
Table 4.5 Summary of formulations explored for CF release assay using lipid 4.2a and different percentages of DPPC, Egg-PC, DOPE, and PA. 212

List of Figures

Figure 1.1 General structure of glycerophospholipids and common headgroups. 4
Figure 1.2 Common fatty acids and their chemical structures. 5
Figure 1.3 Typical lipid assemblies as determined by CPP and curvature. 7
Figure 1.4 Liposome classification based on size and lamellarity. 10
Figure 1.5 Representative graph describing membrane phase transition temperature (T_m). .. 10
Figure 1.6 Liposome preparation via lipid thin-film hydration method. 13
Figure 1.7 Summary of current nanoparticle carriers. 18
Figure 1.8 Advancements in surface modified liposomes. 23
Figure 1.9 Methods of altering lipid bilayer packing to cause cargo release. 26
Figure 2.1 Previously reported disulfide and thiol lipids utilized in liposome NPs. 35
Figure 2.2 Microplate assay for detection of disulfide mediated membrane functionalization. 40
Figure 2.3 Analysis of surface thiol conjugation. 42
Figure 2.4 Microplate assay for detection of IAM terminated disulfide mediated membrane functionalization. 44
Figure 2.5 DLS results for liposomes containing different percentages of 2.1 and 2.2. 46
Figure 2.6 DLS results of liposomes containing different percentages of 2.1 and 2.2 after Biotin-PEG-SH treatment. 47
Figure 2.7 TEM results of 2.1 liposomes. 48
Figure 2.8 H-NMR analysis for liposomes composed of 100% 2.1 before and after liposome formation. 50
Figure 2.9 Enhanced liposomal delivery to MDA-MB-231 cells driven by 2.1 and 2.2. 52
Figure 2.10 PC control liposomal delivery to MDA-MB-231 cells. 52
Figure 2.11 2.1 Liposomal enhanced delivery to MDA-MB-231 cells. 53
Figure 2.12 2.2 Liposomal enhanced delivery to MDA-MB-231 cells. 54
Figure 2.13 Quantification of liposomal enhanced delivery to MDA-MB-231 cells. 55
Figure 2.14 MTS assay to assess cell viability of MDA-MB-231 cells after liposome treatment. 57
Figure 2.15 Analysis of surface thiol conjugation of 2.3 liposomes. 60
Figure 2.16 Analysis of surface thiol-fluorophore conjugation of 2.3 liposomes. 63
Figure 2.17 DLS results of 2.3 liposomes. 64
Figure 2.18 TEM results of 2.3 liposomes. 64
Figure 2.19 Attempted 2.3 liposomal delivery to MDA-MB-231 cells. 66
Figure 3.1 Chemical structures of organoboron compounds. 80
Figure 3.2 Boronic acid structure and equilibrium dissociation in water. 80
Figure 3.3 Mono-boronic acid lipid by Best and coworkers for cellular delivery driven by carbohydrate binding. 94

Figure 3.4 Cartoon depicting microplate assay for detection of mucin-liposome binding..... 99
Figure 3.5 Analysis of microplate immobilization of BBAL liposomes..... 101
Figure 3.6 Analysis of BBAL liposome Rd-dextran binding microplate assay. 103
Figure 3.7 Raw fluorescence values from microplate analysis of Rd-dextran binding to immobilized BBAL liposomes. 104
Figure 3.8 Analysis of BBAL liposome mucin binding microplate competition assay. 106
Figure 3.9 Raw fluorescence values from mucin binding competition assay. 107
Figure 3.10 Catechol bis-boronic acid binding competition assay. 109
Figure 3.11 Dynamic light scattering studies of BBALs. 110
Figure 3.12 TEM images of Bis-boronic acid liposomes 110
Figure 3.13 VSMC cell binding experiment. 112
Figure 3.14 Liposomal SRB delivery to VSMCs. 113
Figure 3.15 Dynamic Light Scattering of BBAL liposomes used in cellular experiments. 115
Figure 3.16 Bis-boronic acid U87 cell delivery study results. 117
Figure 3.17 Bis-boronic acid MDA-MB-231 63X cell delivery study results 118
Figure 3.18 Bis-boronic acid MDA-MB-231 40X cell delivery study results. 119
Figure 3.19 Bis-boronic acid A375 4X cell delivery study results. 121
Figure 3.20 Bis-boronic acid A375 4X cell delivery study results. 121
Figure 3.21 *C. albicans* cell wall composition. 123
Figure 3.22 *C. albicans* cell delivery images and flow cytometry analysis..... 127
Figure 3.23 Hydrophobic Nile Red dye release assay for BOPLIP liposomes. 146
Figure 3.24 Monosaccharide hydrophobic Nile Red dye release assay for BOPLIP liposomes. 147
Figure 3.25 DLS results for BOPLIP liposomes treated with Neu5Ac..... 149
Figure 3.26 DLS results for BOPLIP liposomes treated with monosaccharides..... 150
Figure 3.27 Transmission electron microscopy images of BOPLIP liposomes..... 152
Figure 3.28 BOPLIP liposome MDA-MB-231 cell delivery study results. 155
Figure 4.1 Hydrophobic NR dye release after Cys treatment for liposomes containing various percentages of 4.1a. 183
Figure 4.2 Hydrophobic NR dye release after GSH treatment for liposomes containing various percentages of 4.1a. 184
Figure 4.3 DLS results for 4.1a liposomes treated with Cys and GSH. 186
Figure 4.4 TLC analysis of thiol-mediated cleavage 4.1a. 188
Figure 4.5 Mass spectrum including a peak matching DOPE after treating free lipid 4.1a with Cys. 189
Figure 4.6 TLC analysis of thiol-mediated cleavage 4.1b. 196
Figure 4.7 Lipid 4.1b samples from TLC study. 196

Figure 4.8 Mass spectrum including a peak matching DOPE after treating free lipid 4.1b with Cys. 197
Figure 4.9 Nile Red release from 4.2a-c liposomes 208
Figure 4.10 DLS results for 4.2a liposomes treated with Cys. 210
Figure 4.11 TLC analysis of thiol-mediated cleavage 4.2a. 214
Figure 4.12 Time-dependent NMR analysis for lipid 4.2a in $CDCl_3$:CD_3OD:D_2O = 65:25:4 (v/v) upon treatment with Cys. 217
Figure 4.13 Time-dependent NMR analysis for lipid 4.2b in $CDCl_3$:CD_3OD:D_2O = 65:25:4 (v/v) upon treatment with Cys. 218
Figure 4.14 Time-dependent NMR analysis for lipid 4.2c in $CDCl_3$:CD_3OD:D_2O = 65:25:4 (v/v) upon treatment with Cys. 219
Figure 4.15 Mass spectrum including a peak matching lipid 4.3a and DOPE after treating free lipid 4.2a with Cys. 220
Figure 4.16 Mass spectrum including a peak matching DOPE after treating free lipid 4.2b with Cys. 220
Figure 4.17 Mass spectrum including a peak matching DOPE after treating free lipid 4.2c with Cys. 221
Figure 5.1 Design of lipid bilayer spanning compounds 5.1a-b. 249

List of Schemes

Scheme 2.1 Thiol pK_a and thiol-disulfide exchange reaction. 32
Scheme 2.2 Design strategy for cyclic disulfide liposomes. 38
Scheme 2.3 Reaction of 2.1 with iodoacetamide. 43
Scheme 2.4 Design of alternative disulfide lipid 2.3. 58
Scheme 3.1 Structures of *o*-aminomethylphenylboronic acids as a function of pH. 84
Scheme 3.2 Structures of bis-boronic acid sensor for differentiation between enantiomers of glucose by Shinkai and coworkers. 92
Scheme 3.3 Chemical Structures of bis-boronic Acids 3.1.2a-z reported by Wang and coworkers. 93
Scheme 3.4 Design strategy for bis-boronic acid liposomes. 97
Scheme 3.5 Synthetic route for BBALs 1a-d. 98
Scheme 3.6 Synthetic route for initial bis-boronic acid lipid 3.1.10 140
Scheme 3.7 Synthesis of boronic acid polymer lipid 3.1.16. 143
Scheme 4.1 Thiol responsive lipid 4.1a design. 179
Scheme 4.2 The synthetic route for accessing 4.1a. 181
Scheme 4.3 The synthetic strategy for accessing 4.1b. 191
Scheme 4.4 Design for cysteine-responsive lipids. 200
Scheme 4.5 The synthetic scheme to access lipids 4.2a-c. 201
Scheme 5.1 Design of ROS-responsive artificial signal transduction system. 248
Scheme 5.2 Design of the full signaling cascade of compounds 5.1a-b. 249
Scheme 5.3 Synthetic scheme for accessing transmembrane signaling molecules 5.8 and 5.10. 250
Scheme 5.4 Synthetic design of signaling molecules 5.1a and 5.1b. 251

List of Abbreviations

AA	Asparagusic acid
AcOH	Acetic Acid
3-AcPBA	3-Acetamidophenylboronic acid
ACVA	4,4'-Azobis-(4-cyanovaleric acid)
ADP	Adenosine diphosphate
AFM	Atomic force microscopy
AIBN	Azobisisobutyronitrile
AMP	Adenosine monophosphate
AmpB	Amphotericin B
Ar	Argon
ARS	Alizarin Red S.
ATP	Adenosine triphosphate
ATRP	Atom transfer radical polymerization
AuNP	Gold nanoparticle
BBAL	Bis-boronic acid lipid
BIBB	α-Bromoisobutyryl bromide
Biotin-cap-PE	1,2-Dioleoyl-*sn*-glycero-3-phosphoethanolamine -*N*-(cap biotinyl) (sodium salt)
Biotin-PEG-SH	Biotin-PEG-thiol
BOPLIP	Boronic acid polymer lipids
BSA	Bovine serum albumin
C. albicans	*Candida albicans*
CAM	Carbamidomethyl
CD_3OD	Deuterated methanol
$CDCl_3$	Deuterated chloroform
CDL	Cyclic disulfide lipid
CF	6-Carboxyfluorescein
$CHCl_3$	Chloroform
ClR	Chloro-rhodamine
CO_2	Carbon dioxide
COVID-19	Coronavirus Disease 2019
CPK	Corey–Pauling–Koltun
CPP	Critical packing parameter
Cryo-TEM	Cryogenic transmission electron microscopy
CSSC	Carbon-sulfur-sulfur-carbon
Cys	Cysteine
DAPBA	2-Dimethylaminomethylphenylboronic acid
DAPI	4',6-Diamidino-2-phenylindole

DART	Direct analysis in real time
DCE	1,2-Dichloroethane
DCM	Dichloromethane
DET	Diethylenetriamine
DIEA	Diisopropylethylamine
DLPC	Dilauroyl phosphatidylcholine
DLS	Dynamic light scattering
DMAP	4-(Dimethylamino)pyridine
DMCP	1,2-Dimyristoleoyl-*sn*-glycero-3-phosphocholine
DMEM	Dulbecco's Modified Eagle Medium
DMF	*N*,*N*-Dimethylformamide
DMPC	Dimyristoyl phosphatidylcholine
DMPE	Dimyristoyl phosphatidylethanolamine
DMPS	Dimyristoyl phosphatidylserine
DOPA	Dioleoyl phosphatidic acid
DOPC	Dioleoyl phosphatidylcholine
DOPE	Dioleoyl phosphatidylethanolamine
DOPG	Dioleoyl phosphatidylglycerol
DOPS	Dioleoyl phosphatidylserine
DOTAP	1,2-Dioleoyl-3-trimethylammonium propane
Dox-HCl	Doxorubicin hydrochloride
DPPA	Dipalmitoyl phosphatidic acid
DPPC	Dipalmitoyl phosphatidylcholine
DPPE	Dipalmitoyl phosphatidylethanolamine
DPPG	Dipalmitoyl phosphatidylglycerol
DPPS	Dipalmitoyl phosphatidylserine
DSIL	Disulfide-based self-immolative linker
DSILL	Disulfide-based self-immolative linker lipid
DSPC	Distearoyl phosphatidylcholine
DSPG	Dioleoyl phosphatidylglycerol
DTT	Dithiothreitol
EDC	*N*-(3-Dimethylaminopropyl)-*N*'-ethylcarbodiimide
EDCI	1-Ethyl-3-(3-dimethylaminopropyl)carbodiimide hydrochloride
EDG	Electron donating group
EDTA	Ethylenediaminetetraacetic acid
EE	Encapsulation efficiency
Egg-PC	L-α-Phosphatidylcholine from chicken egg
ELISA	Enzyme-linked immunosorbent assay
EM	Electron microscopy
EPR	Enhanced permeation and retention

ER	Endoplasmic reticulum
ESI	Electrospray ionization
EtOAc	Ethyl acetate
EtOH	Ethanol
EWG	Electron-withdrawing groups
FA	Fatty acyl
FADH	Flavin adenine dinucleotide
FBP	D-Fructose-1,6-biphosphate
FBS	Fetal bovine serum
FDA	Food and Drug Administration
FP	D-Fructose-6-phosphate
FR	Folate receptor
FRET	Fluorescence resonance energy transfer
FSC	Forward scatter
GlcNAc	*N*-Acetylglucosamine
GPC	Gel permeation chromatography
GPCR	G-protein coupled receptors
GPI	Glycosylphosphatidylinositol
GPI-AP	Glycosylphosphatidylinositol anchored protein
GSH	Glutathione
GUV	Giant unilamellar vesicles
H_2O_2	Hydrogen peroxide
HB	Heparin-biotin
HCl	Hydrochloric acid
HEPES	4-(2-Hydroxyethyl)-1-piperazineethanesulfonic acid
Hex	Hexane
HOBt	Hydroxybenzotriazole
HPLC	High performance liquid chromatography
HRMS	High-resolution mass spectrometry
HRP	Horseradish peroxidase
IAM	Iodoacetamide
ICU	Intensive care unit
IP_3	*myo*-Inositol 1,4,5-trisphosphate
K_2CO_3	Potassium carbonate
KI	Potassium iodide
$KMnO_4$	Potassium permanganate
LA	Lipoic acid
LC-MS	Liquid chromatography–mass spectrometry
LNP	Lipid nanoparticles
LPC	*lyso*-Phosphatidylcholine

LUV	Large unilamellar vesicles
MDA-MB-231	M.D. Anderson - Metastatic Breast 231
MeOH	Methanol
MFI	Mean fluorescence intensity
MHz	Megahertz
MIP	Molecularly imprinted polymer
MLV	Multilamellar vesicle
MQ	Milli-Q water
mRNA	Messenger ribonucleic acid
MS	Mass spectrometry
MsOH	Methanesulfonic acid
MTP-PE	Muramide-tripeptide-phosphatidylethanolamine
MTS	3-(4,5-Dimethylthiazol-2-yl)-5-(3-carboxymethoxyphenyl) -2-(4-sulfophenyl)-2H-tetrazolium, inner salt
MUC2	Mucin-2
MW	Molecular weight
Na_2SO_4	Sodium sulfate
$NaBH_4$	Sodium borohydride
NaCl	Sodium chloride
NAD^+	Nicotinamide adenine dinucleotide
NADH	Nicotinamide adenine dinucleotide + hydrogen
$NaHCO_3$	Sodium bicarbonate
NaOH	Sodium hydroxide
NBD	1,2-dioleoyl-*sn*-glycero-3-phosphoethanolamine -*N*-(7-nitro-2-1,3-benzoxadiazol-4-yl) (ammonium salt)
Neu5Ac	*N*-Acetylneuraminic acid
Neu5Gc	*N*-Glycolylneuraminic acid
NMR	Nuclear magnetic resonance
NO_2	Nitro
NP	Nanoparticle
NR	Nile red
NS	Negative-staining
NT	No treatment
OD	Optical density
OH	Hydroxyl
OMe	Methoxy
p-TsOH	*p*-Toluenesulfonic acid
PA	Phosphatidic acid
PBA	Phenyl boronic acid
PBS	Phosphate-buffered saline

PC	L-α-Phosphatidylcholine
PDI	Polydispersity index
PDsI	Protein disulfide isomerase
PE	Phosphatidylethanolamine
PEG	Polyethylene glycol
PEG-PE	1,2 Distearolyl-*sn*-glycero-3-phosphoethanolamine -*N*-[amino(polyethylene glycol)-2000] (ammonium salt)
PET	Photoinduced-electron-transfer
PG	Phosphatidylglycerol
PI	Phosphatidylinositol
PIP_ns	Phosphoinositides
PS	Phosphatidylserine
PTA	Phosphotungstic acid
PTFE	Polytetrafluoroethylene
PVD	Peripheral vascular disease
QM	1,4-Quinone-methide
RBF	Round bottom flask
Rd-PE	1,2-Dioleoyl-*sn*-glycero-3-phosphoethanolamine -*N*-(lissamine rhodamine B sulfonyl)(ammonium salt)
RES	Reticuloendothelial system
R_f	Retention factor
RFP	Red fluorescent protein
RFU	Relative fluorescence units
RNA	Ribonucleic acid
ROS	Reactive oxygen species
RPM	Revolutions per minute
rt	Room temperature
SANS	Small-angle neutron scattering
SAXS	Small-angle X-ray scattering
SEC	Size exclusive chromatography
SH	Thiol
SH-PEG-Fc	SH-PEG-Fluorescein
SH-PEG-Rd	SH-PEG-Rhodamine
Sias	Sialic acids
SIL	Self-immolative linker
SLeX	Sialyl lewis x
SO_2Cl_2	Sulfuryl chloride
SRB	Sulforhodamine B
SSC	Side scatter
STEM	Scanning transmission electron microscopy

SUV	Small unilamellar vesicles
T2DM	Type 2 diabetes mellitus
TACA	Tumor associated carbohydrate antigens
TBDMS-Cl	*tert*-Butyldimethylsilyl chloride
TCEP	Tris(2-carboxyethyl)phosphine hydrochloride
TEA/Et3N	Triethylamine
TEG	Tetraethylene glycol
TEM	Transmission electron microscopy
TGC	Tight glycemic control
THF	Tetrahydrofuran
TLC	Thin layer chromatography
T_m	Phase transition temperature
TOF	Time-of-Flight
U-87 MG	Uppsala 87 Malignant Glioma
UPLC	Ultra-performance liquid chromatography
UV	Ultraviolet
VSMC	Vascular smooth muscle cell
YPD	Yeast extract peptone dextrose
ZS	Zetasizer

Chapter 1. Introduction to Lipids, Liposomes, Nanotechnology, Drug Delivery

1.1. Lipids in biological systems

Lipids are a major type of biomolecule present in the body, with other categories including nucleic acids, carbohydrates, and proteins. Lipids are unique from these other structures because they are individual molecules which behave as assemblies to accomplish various functions. Lipids have diverse roles in important biological functions including serving as energy storage sources, participating in membrane signaling pathways, and maintaining rigid cell structures. Storage lipids serve as energy reservoirs and are encased in lipid droplets filled with neutral lipids, most commonly triacylglycerol and sterol esters, surrounded by a phospholipid monolayer.[1] Lipids are organic molecules which are characterized by their solubility in non-polar organic solvent and are either insoluble or poorly soluble in water. They are generally amphiphilic molecules composed of esters or amides of fatty acids that contain both a hydrophilic and a hydrophobic region. Lipids self-assemble in water according to the hydrophobic effect driven by entropy, with the hydrophilic portions of the lipids being exposed to water and hydrophobic portions aggregating inward to avoid interaction with water.[2] These self-assemblies can yield rigid cellular membranes. In biological systems, self-assembled lipid bilayer membranes allow cells to form compartments, or spatially separate different regions of the cell, to allow for physical decoupling of physiological processes on either side of the membrane. These compartmentalization systems are important for maintaining cell homeostasis, such as ion balance, and are selectively permeable in order to allow communication across the two sides of a bilayer. Additionally, some lipids play important roles as cellular messengers and signaling molecules that influence inflammation,[3] immunity,[4] cell division,[5] membrane trafficking,[6] metabolism and development.[7]

1.2. Lipid structure and properties

The three categories of membrane lipids are the glycerophospholipids, sterols, and sphingolipids. Lipids are divided into groups depending on their chemical structure. Sterols such as cholesterol are naturally occurring and serve important roles in maintaining the integrity and fluidity of cell membranes and acting as precursors for the synthesis of steroid hormones, bile acids, and

vitamins.[8] Sphingolipids are vital structural and signaling molecules which are composed of a long-chain sphingoid base backbone linked to a fatty acyl (FA) chain and a polar headgroup.[9] While both sterols and sphingolipids are important components of biological membranes, glycerophospholipids will be discussed in more depth due to their relevance to the dissertation work herein, including an overview of their structure and properties.

The general structure of common glycerophospholipids is shown in Figure 1.1 and is composed of three main sections including the two acyl chains, a glycerol backbone, and a headgroup.[10] A wide range of diversity exists within natural glycerophospholipids resulting from variation of the headgroup and fatty acid tails, the latter of which vary in degrees of saturation and length. Fatty acid tails are typically 12-20 carbons long and are attached to glycerol via ester or ether bonds at the *sn*-1 and *sn*-2 positions of glycerol.[11] Common free fatty acids are shown in Figure 1.2, which contain a free carboxylic acid group and acyl tail with varying degrees of saturation and length. The delta nomenclature describes the chain length, degree and location of unsaturation. It is known that glycerophospholipids typically have low degrees of unsaturation on the *sn*-1 chain, but conversely the *sn*-2 chain usually has more unsaturation with up to four double bonds.[12]

The naturally occurring glycerophospholipid headgroups are also diverse in structure and are attached to the *sn*-3 position of the glycerol backbone through a phosphodiester group. For example, commonly occurring glycerophospholipids contain headgroups of choline, ethanolamine, serine, glycerol, or variously phosphorylated inositol. Phosphatidic acid (PA), for which the headgroup is simply a phosphate, is an anionic lipid which serves as a key building block of phospholipid synthesis and a major lipid second messenger for cell signaling.[13] Phosphatidylcholine (PC) possesses a choline headgroup composed of a phosphorylcholine esterified glycerol at the *sn*-3 position. PCs are the most abundant phospholipids in eukaryotic cells and the composition of the FA tail plays a key role in regulating the physical properties of membranes, since more unsaturation increases membrane fluidity.[14] Also, at physiological conditions PC is a zwitterionic lipid containing a positively charged quaternary ammonium group and a negatively charged phosphodiester. Phosphatidylethanolamine (PE), a glycerophospholipid

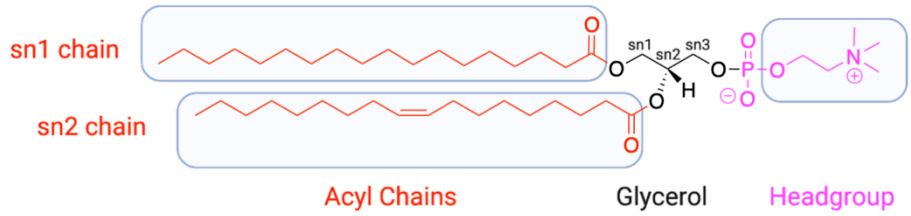
with an ethanolamine headgroup, is also zwitterionic under physiological conditions and is the second most abundant phospholipid in mammalian cells. Lipids such as PE are involved in promoting membrane fusion and fission events due to the intrinsic biophysical properties of possessing a small headgroup.[15] Phosphatidylserine (PS) has a serine headgroup and is the major anionic phospholipid.[16] PS is found extensively enriched in the inner leaflet of the plasma membrane, and loss of PS asymmetry is an early indicator of apoptosis and signals initiation of blood clotting.[17, 18] Phosphatidylglycerol (PG), also anionic, possesses a glycerol headgroup and functions as a precursor of cardiolipin and a required signaling molecule for various cellular functions.[19] Both PS and PG have one negative charge at physiological pH. Phosphoinositides contain a *myo*-inositol headgroup, which can present as the parent phosphatidylinositol (PI) and the variably phosphorylated phosphoinositides (PIP_ns), in which various combinations of hydroxyl groups on the inositol can be phosphorylated. Although they comprise a class of low abundance anionic lipids, PI and PIP_ns play key roles in non-vesicular lipid transport, membrane homeostasis and trafficking, and cell signaling pathways.[20]

1.3. Lipid self-assembly and liposomes

1.3.1. Lipid packing parameter and self-assembly of lipids

The structural characteristics of lipids greatly influences their behavior in aqueous solution. Due to their amphiphilic nature of having a hydrophilic headgroup and hydrophobic tail, lipids can self-assemble in aqueous solution into structures including spherical micelles, cylindrical micelles, spherical bilayers, and planar bilayers.[21] The assembly type that lipids display is driven by factors including entropic properties, thermodynamics, variations in the aqueous environment, and the spatial molecular geometry of the lipid.

The critical packing parameter (CPP) of lipids was first reported by Israelachvili et. al.[22] and is used to describe the structural shape of different hydrocarbon amphiphiles and understand the formation of micelle or bilayer assemblies. The CPP is calculated by first determining the cross-sectional area of the headgroup and the length and volume occupied by the hydrophobic tail(s).



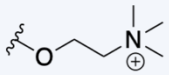
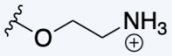
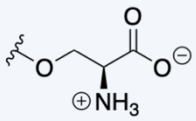
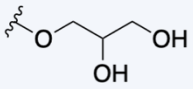
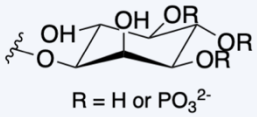
Common Glycerophospholipids	Headgroup	Headgroup Structure
Phosphatidic acid (PA)	None	
Phosphatidylcholine (PC)	Choline	
Phosphatidylethanolamine (PE)	Ethanolamine	
Phosphatidylserine (PS)	Serine	
Phosphatidylglycerol (PG)	Glycerol	
Phosphatidylinositol (PI) or Phosphoinositides (PIP_n)	Inositol	

Figure 1.1 General structure of glycerophospholipids and common headgroups. The structural features of glycerophospholipids include the two acyl chains, glycerol backbone, and phosphodiester headgroup. The lipid classification depends on the different headgroup structures. Common lipids have diverse headgroups structures, including phosphate only (PA) (anionic lipid), choline (PC) and ethanolamine (PE) (zwitterionic lipids), serine (PS) and glycerol (PG) (anionic lipids), and inositol (PI) and phosphorylated inositol (PIP_n).

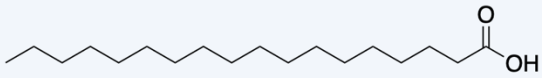
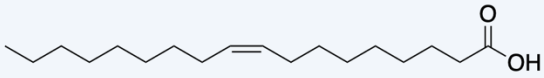
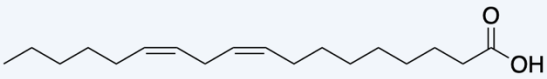
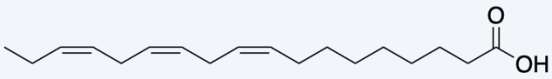
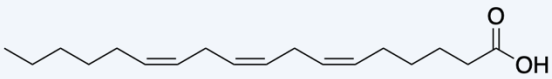
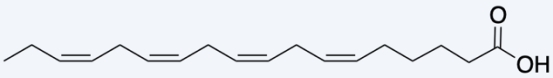
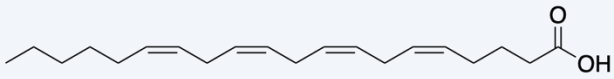
Common Fatty Acids	Delta Nomenclature	Fatty Acid Structure
Stearic acid	(18:0)	
Oleic acid	(18:1)Δ^{9}	
Linoleic acid	(18:2)$\Delta^{6,9}$	
α-Linoleic acid	(18:3)$\Delta^{3,6,9}$	
γ-Linolenic acid	(18:3)$\Delta^{6,9,12}$	
Stearidonic acid	(18:4)$\Delta^{3,6,9,12}$	
Arachidonic acid	(20:4)$\Delta^{6,9,12,15}$	

Figure 1.2 Common fatty acids and their chemical structures. Commonly occurring fatty acids contain a free carboxylic acid group and acyl tail with varying degrees of saturation and length. The delta nomenclature describes the chain length, degree and location of unsaturation.

The equation to calculate the CPP is $\mathrm{CPP} = \frac{v}{a_0 l_C}$ were v is the tail volume, a_0 is the cross-sectional area of the headgroup, and l_0 is the length of the tail(s). There are three types of typical assemblies which can be determined by the CPP, associated curvature and lipid shape including spherical micelles, inverted micelles, and bilayers (Figure 1.3). First, spherical micelles are mono-layer lipid aggregates which have the hydrophilic heads facing outward and hydrophobic regions aggregated inward to form a hydrophobic core. These assemblies form when the CPP is less than 1/3, indicating the lipids have a positive curvature and are shaped like an inverted cone-shape. These lipids are characterized by having a larger head area and smaller tail area, such as *lyso*-phosphatidylcholine (LPC), which only has one tail in the *sn*-1 position and forms micelles in aqueous solutions.

Second, inverted micelles (hexagonal phase) are also mono-layers and display their hydrophobic regions facing outward while the hydrophilic heads face inward surrounding a small aqueous core. These assemblies are driven by a CPP value greater than 1, meaning that the lipids have a cone shape in which the tail area is larger in comparison to the head area, resulting in negative curvatures. A representative lipid of this type is lipid PE, which has a small unmethylated amine headgroup. This effect can be exacerbated by the introduction of unsaturation in the acyl chains via *cis* double bonds, adding kinks in the tails which increase both the hydrophobic region and cone shape of the lipids. An example of this type is dioleoylphosphatidylethanolamine (DOPE), which bears a *cis* double bond on each tail at the ninth carbon (18:1 (Δ^9-Cis). Third, spherical bilayers are composed of a two-layered sheet with hydrophilic heads pointing both outside and inside, resulting in a hydrophobic bilayer and an internal aqueous core. These lipids possess a CPP near 1 with similarly sized headgroups and acyl chains, and thus display cylindrical geometry and prefer to form bilayer assemblies. A representative lipid class of this type includes the PC lipids, and it follows that these are the most abundant glycerophospholipids in mammalian cell bilayer membranes due to their natural preference to form bilayers. It is important to note that if lipid types are mixed in a sample, the self-assembly type depends on the composition of the lipid mixture. For example, if a small portion of non-bilayer forming lipids are mixed among a larger percentage of bilayer forming lipids, the resulting assembly may remain a bilayer vesicle.

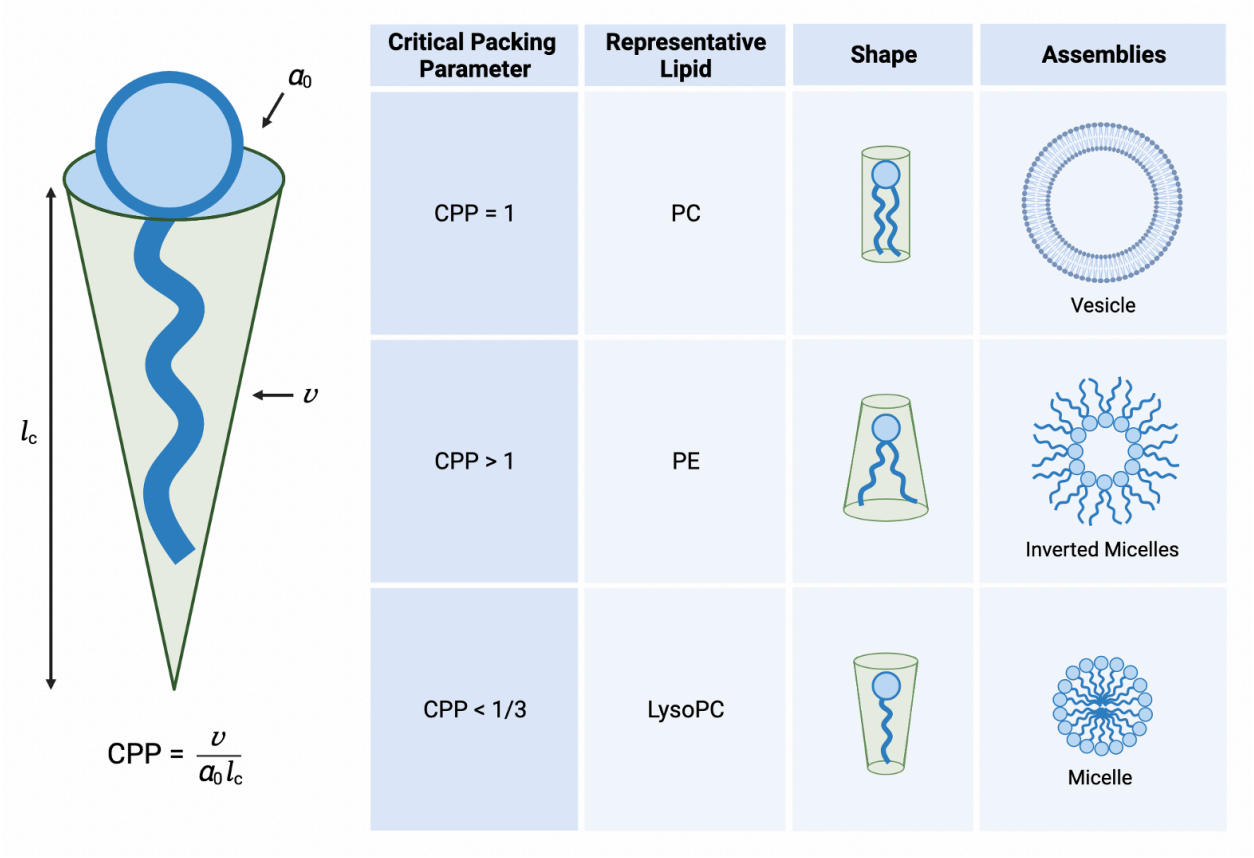


Figure 1.3 Typical lipid assemblies as determined by CPP and curvature. The three types of typical assemblies which can be determined by the CPP and associated curvature a lipid shape including bilayer vesicles, inverted micelles, and spherical micelles. CPP is calculated by the equation $\mathrm{CPP} = \frac{v}{a_0 l_C}$ were v is the tail volume, a_0 is the cross-sectional area of the headgroup, and l_0 is the length of the tail(s). CPP = 1 indicates that lipids display cylindric geometry and prefer to form bilayer assemblies, as represented by PC lipids. CPP > 1 indicates that the lipids have a conical shape in which the tail area is larger in comparison to the head area, resulting in negative curvature and formation of inverted micelles, as demonstrated by PE lipids. CPP < 1/3 indicates the lipids have positive curvature and are shaped like an inverted cone-shape, assembling into spherical micelles as represented by lyso-PC.

However, if the abundance of non-bilayer forming lipids exceeds a certain threshold, the assembly will no longer form stable vesicles. Vesicle stability can therefore be tuned by varying the composition of the lipid mixture containing both bilayer and non-bilayer forming lipids.

1.3.2. Background of liposomes

The most common lipid assembly is the liposome which is comprised of a spherical vesicle with a hydrophobic bilayer and aqueous inner core. Liposomes were first discovered in 1965 by Dr. Alec Douglas Bangham when a negative stain was added to dry phospholipids while testing a new electron microscope.[23, 24] The images showed bilayer vesicles, and due to their similarity to images of plasma membranes, the images served as the first evidence for the cell membrane being a bilayer lipid structure. Liposomes can be classified into different categories depending on their size and lamellarity. The sizes of liposomes are categorized based on the diameter of the vesicle and lamellarity refers to the number of bilayers in the vesicle. A unilamellar vesicle has only one bilayer while a multilamellar vesicle (MLV) is composed of multiple layers of bilayers. As seen in Figure 1.4, small unilamellar vesicles (SUVs) have a vesicle diameter smaller than 100 nm and consist of one bilayer membrane. Large unilamellar vesicles (LUVs) exhibit diameters between 100 and 1000 nm with one bilayer, and giant unilamellar vesicles (GUVs) have diameters greater than 1 μm. MLVs have layers of bilayers and can be various sizes, and multivesicular vesicles have smaller vesicles in the aqueous core of a larger vesicle.

1.3.3. Liposome membrane phase transition

In addition to the critical packing parameter, there are additional lipid properties that are important features to consider in order to achieve the desired assembly. For instance, it is important to understand membrane phase behavior which can give insight to membrane fluidity. At different temperatures, lipids can exist in either ordered or disordered phase. The temperature needed to pass from the ordered gel phase to the disordered fluid crystalline phase is referred to as the phase transition temperature (T_m) of the lipid or formulation.[25] As described in the representative graph in Figure 1.5, below the T_m the hydrocarbon chains are fully extended and closely packed, and above the T_m the hydrocarbon chains become fluid and randomly

oriented. Phase transition is responsible for liposome permeability, a key function in order for compounds such as therapeutic drugs to cross the liposome membrane. It follows that permeability is dependent on the T_m of the lipid mixture, and liposomes are most permeable as they transition from ordered gel to disordered fluid phase.[26, 27] A table showing the T_m values of commonly used glycerophospholipids is included in Table 1.1. A few factors can influence T_m including chain length, unsaturation, and headgroup type and charge.[28] For example, longer chain length increases the T_m due to enhanced van der Waals interactions between adjacent lipid molecules.[29] Since there is more energy needed to overcome these interactions and enter the disordered fluid crystalline phase, the T_m is higher. In contrast, T_m is lowered by increases in unsaturation of the hydrocarbon chains, particularly the presence of *cis* double bonds. The kinks introduced by the *cis* double bonds disrupt the orderly packing of the lipid tails and less energy is then required to further disrupt membrane packing and achieve phase transition.

1.3.4. Methods of liposome preparation

Various methods can be used to prepare liposomes to achieve variations in the size, lamellarity, and encapsulation efficiency of the liposomes. The most conventional preparation method was reported by Bangham and et. al. in 1976 and was originally named the Bangham method, although it is widely known today as the lipid thin-film hydration method.[31, 32] This method, as shown in Figure 1.6, involves first creating solutions of compositional lipids in organic solvent (chloroform or methanol), and transferring precise aliquots to a small vial. Then, the solvent is completely removed, and aqueous buffer is used to rehydrate the lipids at a temperature above the lipids' T_m, resulting in a liposome suspension. The steps performed during and after hydration will then determine the size and lamellarity of liposomes formed. For example, MLVs with heterogeneous size distribution can be formed with intense agitation during hydration, while gentle hydration will result in GUVs. To form smaller vesicles of more uniform sizes, additional size-reducing steps are needed. Probe or bath sonication during hydration can be used to form SUVs with homogeneous sizes; however, this technique can cause liposome damage, lipid de-esterification from local warming, and metal contamination from the sonication probe.[33-35] Also, bath sonication can result in low encapsulation efficacy, phospholipid and encapsulated

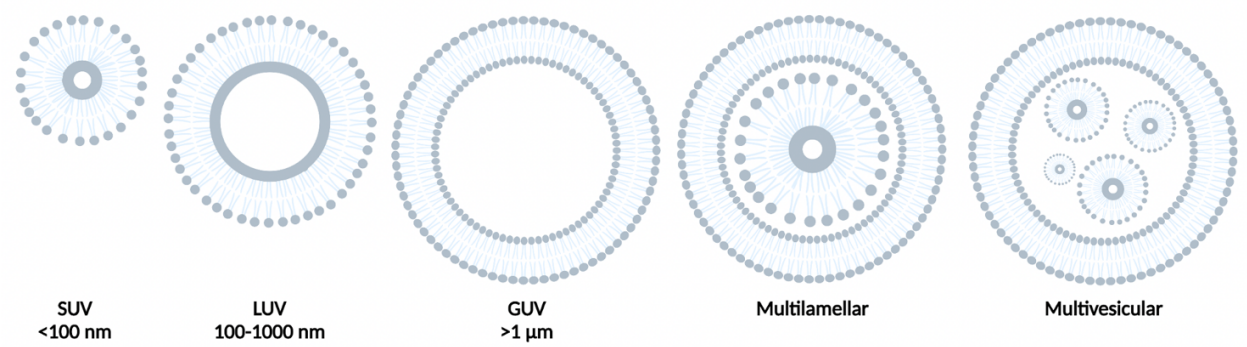


Figure 1.4 Liposome classification based on size and lamellarity. Liposome classification includes SUVs which have a vesicle diameter smaller than 100 nm and have one bilayer membrane. LUVs have diameters between 100 and 1000 nm with one bilayer, and GUVs have diameters greater than 1 µm. MLVs have layers of bilayers and can be various sizes, while multivesicular vesicles have smaller vesicles in the aqueous core of a larger vesicle. The figure is based on the work reported by deMello et al.[30]

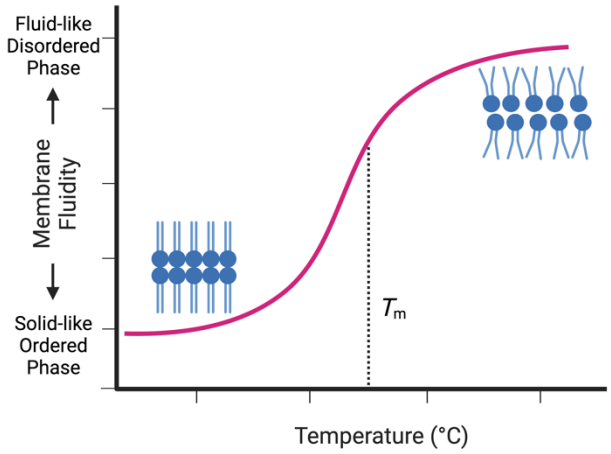


Figure 1.5 Representative graph describing membrane phase transition temperature (T_m). The temperature needed to pass from the ordered gel phase to the disordered fluid crystalline phase is referred to as the phase transition temperature (T_m) of the lipid. Below T_m the lipids are in the ordered gel phase with the hydrocarbon chains fully extended and closely packed. Above the T_m the hydrocarbon chains become fluid randomly oriented.

Table 1.1 Phase transition temperatures of common glycerophospholipids.

Glycerophospholipid Name	T_m (°C)
12:0 Dilauroyl phosphatidylcholine (DLPC)	-2
14:0 Dimyristoyl phosphatidylcholine (DMPC)	24
16:0 Dipalmitoyl phosphatidylcholine (DPPC)	41
18:0 Distearoyl phosphatidylcholine (DSPC)	55
18:1 Dioleoyl phosphatidylcholine (DOPC)	-17
14:0 Dimyristoyl phosphatidylserine (DMPS)	35
16:0 Dipalmitoyl phosphatidylserine (DPPS)	54
18:1 Dioleoyl phosphatidylserine (DOPS)	-11
16:0 Dipalmitoyl phosphatidic acid (DPPA)	65
18:1 Dioleoyl phosphatidic acid (DOPA)	-4
14:0 Dimyristoyl phosphatidylethanolamine (DMPE)	50
16:0 Dipalmitoyl phosphatidylethanolamine (DPPE)	63
18:1 Dioleoyl phosphatidylethanolamine (DOPE)	-16
16:0 Dipalmitoyl phosphatidylglycerol (DPPG)	41
18:0 Dioleoyl phosphatidylglycerol (DSPG)	55
18:1 Dioleoyl phosphatidylglycerol (DOPG)	-18
18:1 1,2-Dioleoyl-3-trimethylammonium propane (DOTAP)	0

compound degradation, and high size polydispersity.

Most liposomes in this dissertation were prepared using extrusion, an effective method to reduce particle size by extruding the liposome solutions through a polycarbonate membrane made up of defined pore sizes (1 mm - 25 nm).[36-38] Several passes through the polycarbonate membrane filter results in the formation of LUVs with narrow-size distributions and dimensions close to the membrane pore sizes. Homogeneity also depends on the number of passes through the membrane. For very rigid lipid mixtures (high T_m), a heating block can be arranged around the extruder to allow for extrusion above the T_m of the phospholipids.

A select few liposome types in this dissertation were prepared using the ethanol injection method, in which an ethanolic solution of lipids is first heated to increase solubility, and then injected dropwise into an aqueous solution, which disperses the lipids in the aqueous phase and results in the formation of bilayer planar fragments. After the ethanol is removed by either dialysis or rotary evaporation, the lipid fragments fuse and form unilamellar vesicles.[39, 40] In this method, heated hydration is not required. The ethanol injection method has certain advantages over the thin-film method including avoiding lipid or cargo degradation from heat,[41] better solubility of some lipids in ethanol compared to chloroform or methanol, and greater vesicle stability[42] compared to thin-film methods. However, a major drawback of this method is that minute differences in preparation parameters such as injection velocity, injection hole diameter, vortex rate, composition of the aqueous phase, lipid concentration, ratio of ethanol and its residual amount, and dimensions of reaction vessel can greatly influence the size and dispersity of liposomes formed.[43, 44] Other liposome preparation methods include detergent depletion method, ether injection method, reverse-phase evaporation method, freeze-drying (lyophilization) method, supercritical fluid-assisted methods, microfluidic (channel) methods, and membrane contactor method.[39]

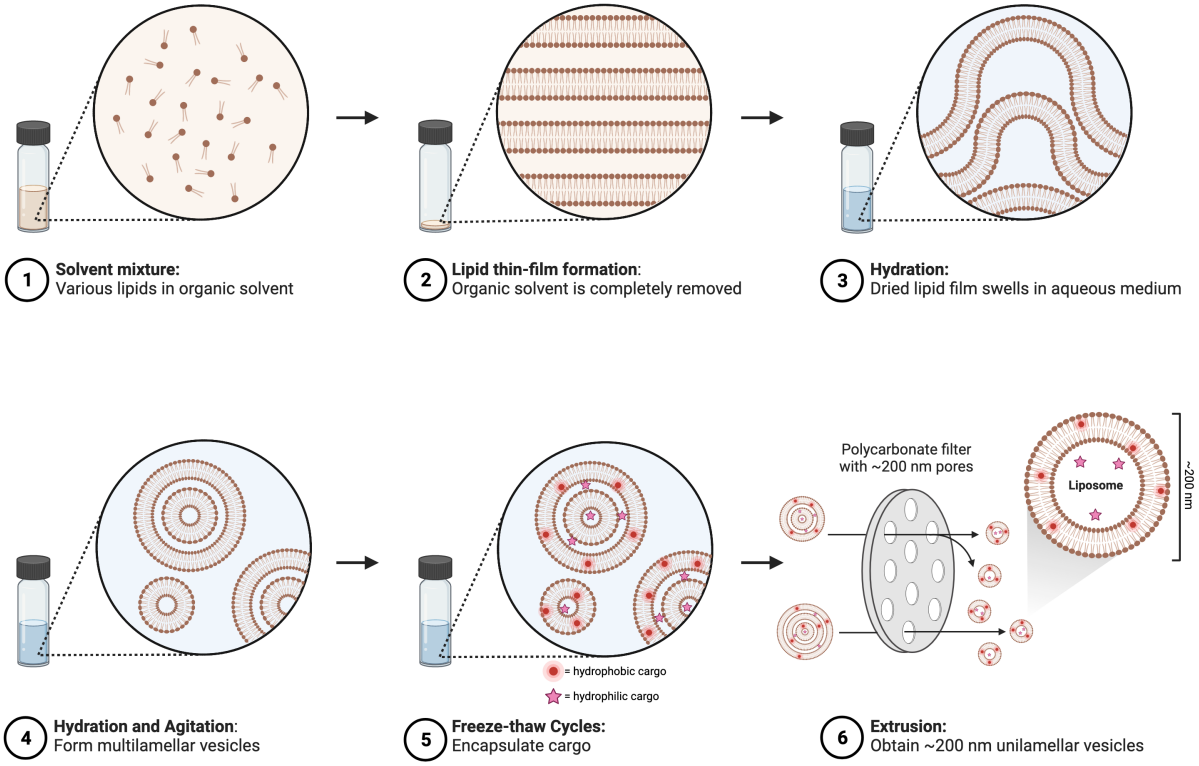


Figure 1.6 Liposome preparation via lipid thin-film hydration method. First, compositional lipids in organic solvent are combined in a small vial. Then, the solvent is completely removed, and aqueous buffer is used to rehydrate the lipids, swelling the lipid film. Next, intense agitation during heated hydration above the T_m of the lipids results in the formation of multilamellar vesicles (MLVs) with heterogeneous size distribution. Freeze-thaw cycles are performed to aid in cargo encapsulation, followed by extrusion through a polycarbonate membrane made up of defined pore sizes (typically ~200 nm) to form homogenous LUVs of defined size (~200 nm).

1.3.5. Characterization of liposomes

It is important to characterize liposomes to confirm proper formation, batch to batch reproducibility, and stability of the liposome dispersions. There are various techniques used to characterize liposomes, which will be discussed in the following section. The two major characteristics of liposome solutions include their vesicle size and polydispersity index (PDI) since liposome size is key for physiological applications. Methods of size measurement include dynamic light scattering (DLS), size exclusive chromatography (SEC), nuclear magnetic resonance spectroscopy (NMR), and microscopy techniques such as transmission electron microscopy (TEM), cryogenic-TEM (Cryo-TEM), atomic force microscopy (AFM), or fluorescence microscopy.[45, 46] The most widely used method is DLS due to its easy and efficient technique, and DLS can also be used to characterize the size of polymers, proteins, colloidal dispersions, and other nanoparticles types. In DLS, small particles are suspended in aqueous solution and a laser is applied to the sample, resulting in scattering at different intensities depending on the Brownian motion of the particles or molecules. A detector is used to measure the resulting scattering of the incident light and analyze their Brownian motion to give an average particle size and size distribution according to the Stokes-Einstein equation. DLS typically has a measurement range of 20 - 1000 nm, and was the primary technique used in this dissertation to verify proper liposomal size and homogeneity.

Another important property of liposomes is their encapsulation efficiency (EE%), particularly for drug delivery purposes. To measure EE%, unencapsulated cargo must first be removed by an appropriate method such as ultracentrifugation, dialysis, or size exclusion chromatography (SEC). Then, release of encapsulated cargo is accomplished by addition of solvent (ethanol, acetonitrile, or methanol) or a surfactant such as Triton X-100 to accomplish destruction of the liposome structure. Various techniques can be used to analyze the content and calculate EE% including fluorescence or UV-Vis spectroscopy, high performance liquid chromatography (HPLC), ultra-performance liquid chromatography (UPLC), or liquid chromatography–mass spectrometry (LC-MS).[46, 47] Another key characteristic of liposomes is zeta potential. Zeta potential measures the surface charge of liposomes in solution, which is determined by lipid composition. Liposomes can

have positive or negative charge or no charge depending on lipid composition. Zeta potential can be measured by DLS using fluctuations in the scattered light. A final parameter of liposomes which should be investigated is lamellarity, the number of bilayer membranes, to assess applications. Common techniques used to characterize lamellarity are cryo-TEM analysis,[48, 49] small-angle X-ray scattering (SAXS), and small-angle neutron scattering (SANS).[49-52]

1.4. Liposomes and drug delivery nanocarriers

1.4.1. Introduction of drug delivery nanocarriers

Traditional therapeutics are administered as free drugs through physiological routes including sublingual, oral, inhalation, rectal, intravenous, intramuscular, and subcutaneous.[53] These conventional delivery methods suffer from drug instability, limited solubility, poor biodistribution, uncontrolled release, off-site effects, slow absorption, enzymatic deterioration, and poor localization in clinical applications.[54] Incorporating a drug into a nanocarrier is an efficient method to improve drug solubility and achieve sustained and targeted delivery of drug. Extensive work is underway to develop various types of nanocarriers to achieve enhanced circulation, improve biodistribution and targeted delivery to ultimately improve drug pharmacokinetic parameters and reduce harmful side effects.

Current nanoparticle (NP) carriers are divided into three categories, as described in Figure 1.7, including polymeric, inorganic, and lipid-based nanoparticles.[55] The first category is polymeric and includes polymersomes,[56] dendrimers,[57] polymer micelles,[58] and nanospheres.[59] Polymeric NPs are made from monomers or polymers of natural or synthetic materials, which allows for a wide range of structures and characteristics. Delivery of both hydrophilic and hydrophobic compounds is possible since therapeutics can be trapped in the polymer matrix, encapsulated in the NP core, or conjugated to the polymer or NP surface. Polymeric NPs are fair drug delivery carriers because they are water soluble, biocompatible, biodegradable, biomimetic, stable during storage, and can easily be modified with surface targeting groups.[60] However, due to the significant drawbacks of high risk of particle aggregation and toxicity, there are only a small

number of polymeric NP therapeutics currently approved by the Food and Drug Administration (FDA) and used in the clinic.[61]

The second category is inorganic NPs and includes nanostructures synthesized with silica, gold, iron, or graphene materials. Examples include gold NPs (AuNPs),[62] iron oxide NPs,[63] quantum dots,[64] calcium phosphate and mesoporous silica NPs,[65] and carbon nanotubes.[66] Because of their radioactive, magnetic, or plasmonic properties, inorganic NPs are particularly stable and are useful for imaging, photothermal therapies, and diagnostics, and many have been found capable of gene and drug delivery.[67-69] Of these, AuNPs are the most widely studied due to their unique photothermal properties caused by free surface electrons, which continually oscillate at frequencies depending the AuNPs physical parameters.[70] AuNPs can also be easily functionalized with imaging and targeted delivery groups.[71] Although there are over a dozen AuNPs in various stages of clinical trials, these technologies are not progressing at the same rate as organic liposome-based nanoparticle drugs.[72] The major limitation in the clinical application of most inorganic NPs, including AuNPs and other formulations using heavy metals, is their low solubility and toxicity concerns.[73, 74]

Conversely, lipid-based NPs are the third category and they have been shown to overcome the drawbacks of other NP types, making them one of the most promising drug delivery candidates. This category includes liposomes, lipid nanoparticles (LNPs), and emulsions. All lipid-based NPs offer remarkable benefits including self-assembly in aqueous environment, high bioavailability and biocompatibility, formulation simplicity, large payload capability, and a tunable range of physicochemical properties which can be modulated to vary their biological characteristics.[75-77] Due to these advantages, lipid-based NPs are the largest category of FDA-approved nanomedicines.[61, 78]

The first subset of lipid-based NPs to be discussed includes the LNPs. LNPs are similar to liposomes, but differ because they contain micelles within the core of a larger vesicle, and are commonly used to deliver nucleic acids.[79] LNPs are usually made up of bulk phospholipids,

stabilizing cholesterol, biocompatibility enhancing PEGylated lipids, and most importantly, cationic or ionizable lipids that complex with negatively charged genetic material and facilitate endosomal escape.[80, 81] It is necessary to mention that the latest, and most remarkable, use of LNPs is as the delivery vehicle in the Coronavirus Disease 2019 (COVID-19) messenger RNA (mRNA) vaccines developed by Pfizer/BioNTech and Moderna in response to the COVID-19 pandemic.[82, 83] Both LNP compositions were similar and followed the typical formula of containing an ionizable lipid, PEGylated lipid, bulk phospholipid (distearoylphosphatidylcholine (DSPC)), and cholesterol.[84, 85] Their molar ratios were cationic lipid:PEG-lipid:cholesterol:DSPC of 46.3:1.6:42.7:9.4 for the Pfizer formulation, and 50:1.5:38.5:10 for the Moderna formulation, and vesicle were 80 - 100 nm in size, allowing for ~100 molecules of mRNA per LNP.[86-90] The cationic lipids from Pfizer (ALC-0315) and Moderna (SM-102) both contain tertiary amines (ALC-0315 pK_a = 6.09, SM-102 pK_a = 6.75) which are protonated (and thus positively charged) at low pH, allowing for complexing with mRNA during preparation at pH 4, but are neutral at physiological pH in order to reduce toxic side-effects.[91, 92] It is considered a requirement for LNPs to shed their external PEG layer before internalization into the cell, after which it is thought that the low-pH environment of the endosome (pH = 6.8–5.9 in early endosomes, pH = 5.5–5.0 in late endosomes)[93] leads to re-ionization of the cationic lipids, causing particle disassembly.[94, 95] Electrostatic and hydrophobic interactions between the LNPs and the anionic lipids naturally found in the endosomal membrane are believed to disrupt the membrane and allow mRNA escape into the cytosol.[95] These recent advancements in LNP carriers have caused an explosion of interest in lipid-based nanotechnologies and their applications in a diverse range of fields including drug delivery, medical imaging, nutrition, cosmetics, agriculture, and nanoreactors.[96]

The second subset of lipid-based NPs to be discussed is the liposome, which has been considered a promising drug delivery vesicle type for over two decades. Liposomes are an evergreen nanocarrier with long-standing interest because they are low-cost, biocompatible, have tunable delivery, are easy to modify, and offer fast administration. Due to their importance in this dissertation, a more detailed discussion of liposomes as drug delivery nanocarriers including an overview of their drug delivery background, necessary liposomal sizes and physical parameters,

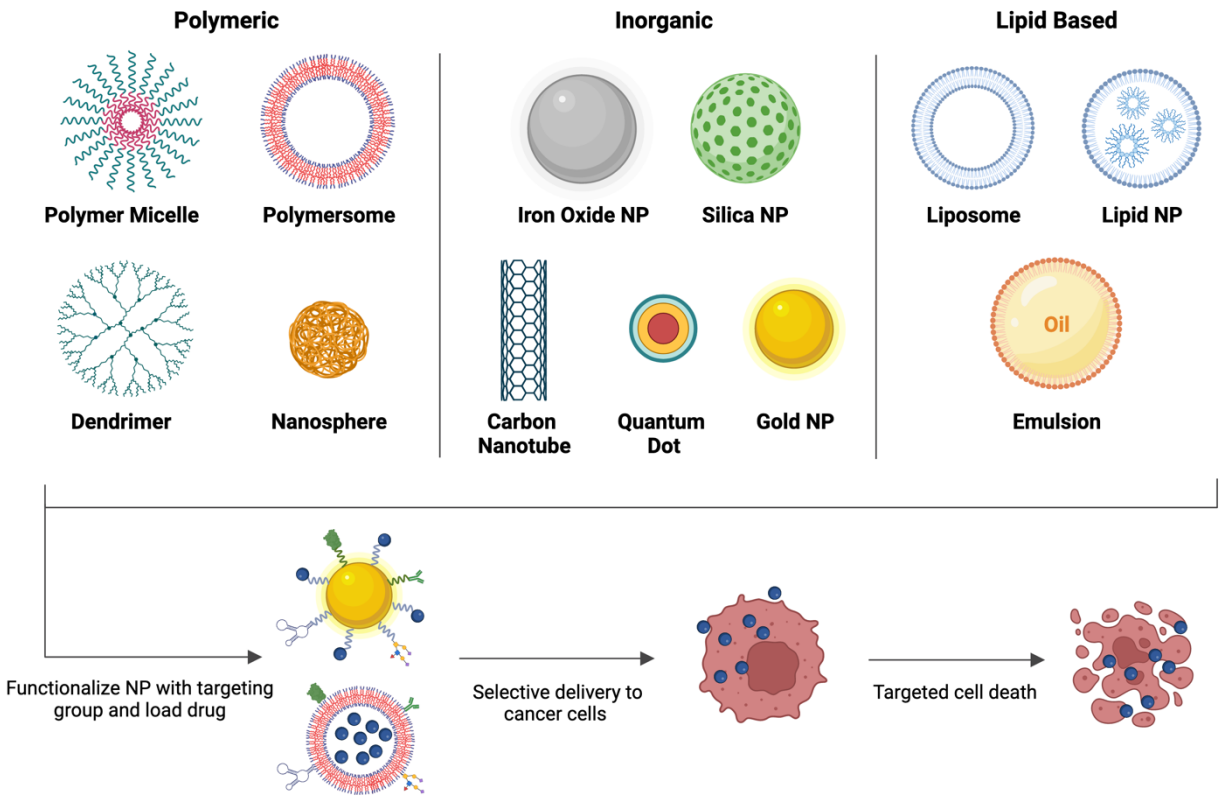


Figure 1.7 Summary of current nanoparticle carriers. Current NP carriers are divided into three categories including polymeric, inorganic, and lipid-based nanoparticles. Each class has numerous advantages and disadvantages regarding delivery, cargo, and biological response, and the proper NP can be selected to suit specific applications. This figure is inspired by a figure by Langer et al.[55]

surface charge, EE%, surface modification, site-specific targeting, and triggered release can be found in the following sections.

1.4.2. Liposomes as drug delivery nanocarriers

Liposomes were the first nanoparticles developed, and their promising application as drug delivery carriers was identified shortly after their discovery. The original idea of employing liposomes as drug delivery carriers was proposed by Gregoriadis et. al. in the early 1970s.[97, 98] Since then, liposomes have been widely investigated as delivery vehicles for small molecular drugs, imaging agents, nucleic acids, and proteins.[99-103] Research has continued for decades and many liposome-based drug and gene delivery systems have been developed, entered FDA clinical trials, and been approved for therapeutic use. Because of this, liposomes are known as the first nanomedicine type to be FDA approved for clinical use.[104] As discussed before, liposomes are composed of a hydrophobic bilayer membrane surrounding an aqueous hydrophilic core, so they are able to encapsulate either hydrophilic and/or hydrophobic contents, making then versatile for therapeutic use. The first FDA approved liposome nanomedicine was Doxil/Caelyx (Johnson & Johnson) and was introduced to the market in 1995 for the delivery of the anti-cancer drug doxorubicin hydrochloride (Dox-HCl) to treat ovarian cancer, Kaposi's sarcoma, and myeloid melanoma. Today, there are fourteen FDA-approved liposomal drugs available for use in the clinic, six of which have been approved since 2010. Additional representative examples of FDA-approved liposomal drugs include AmBisome (Gilead Sciences) to deliver amphotericin B (AmpB) against systemic fungal infections, Mepact (Takeda) to deliver muramide-tripeptide-phosphatidylethanolamine (MTP-PE) to treat osteosarcoma, and Vyxeos (Jazz Pharmaceuticals) which delivers daunorubicin and cytarabine to treat leukemia.[105] In comparison to free drugs, liposome platforms are uniquely biocompatible[106] and are capable of improving drug solubility, protecting against degradation, reducing toxicity[107] and negative side effects,[108] and overall improving the pharmacokinetic properties[109] and therapeutic index[110] of drugs. It is important to note that improving the solubility of therapeutics with liposomal carriers is a substantial accomplishment, given that more than 40% of cancer treatment drugs that are developed have poor hydrophilicity, which greatly limits their uses when freely administered. [111]

A few conditions need to be considered while developing liposomes for drug delivery applications, including particle size, surface charge, and EE%. Liposomes employed for drug delivery applications typically need particle sizes ~100 - 200 nm in order to take advantage of the enhanced permeation and retention (EPR) effect. This phenomenon describes the massive and irregular neovascularization in cancerous tissue that is developed in order to meet the tumor's elevated demands for nutrient and oxygen supplies.[112] Tumors are also known to lack efficient drainage of the lymphatic systems, which results in the passive retention of anticancer macromolecular drugs like liposomes.[113] This leaky and distended vasculature within the tumor sites allows liposomal entry, and poor drainage results in liposome accumulation, which improves drug delivery. Liposomes that are ~100 - 200 nm in size have also been shown to enhance fusion with cell membranes to their advanced curvature.[114, 115] Additionally, liposomes of this size display longer circulation times compared to larger liposomes (> 400 nm), which tend to be cleared by the reticuloendothelial system (RES).

Another liposomal parameter to consider is surface charge which can change the liposomal properties.[116] Depending on the compositional lipids, liposomes can have either neutral, negative, or positive charges. Charge interactions can occur between liposomes and counterions or multiple adjacent liposomes, influencing vesicle stability. For example, liposomes with the same charge experience electrostatic repulsion and are less likely to aggregate. In comparison, neutral liposomes tend to aggregate over time. To improve stability, charged lipid such as *N*-[1(2,3-dioleoyloxy)propyl]-*N,N,N*- trimethylammonium chloride (DOTAP) can be formulated in the liposome, which has been shown to improve cell recognition, interaction, and entry by electrostatic attraction to the cell membrane.[117, 118] Additionally, charged lipids can be useful for encapsulating charged compounds, as was discussed in the COVID-19 LNP examples.

The final parameter is EE% which describes the efficiency of the liposomes for encapsulating cargo for delivery purposes. Liposomes can load hydrophobic cargo in the bilayer membrane and hydrophilic cargo in the aqueous core. The thin-film hydration liposome preparation technique is known to result in low EE% since the cargo is non-specifically entrapped during the preparation.

Certain strategies can be taken to enhance EE%, such as loading cargo along a transmembrane gradient (pH gradient[119] or ammonium sulfate gradient[120]) or employing freeze-thaw cycles, which are particularly useful for enhancing EE% of hydrophilic cargo.[121] It is known that repeated cycles of freezing and thawing help to disrupt the bilayer via the formation of ice crystals during the freezing step. The insertion of ice crystals in the bilayer results in an increase in the internal aqueous volume of the liposome.[122] Additionally, it has been reported that the internal volume can increase 10 - 50x the original volume after freeze-thaw cycling due to the fusion of small vesicles to form larger liposomes.[123] The vesicles also tend to reassemble into unilamellar vesicles, which again increases the internal aqueous volume.[124] These factors all contribute to enhancement of the EE% after freeze-thaw cycles due to increasing the internal volume.

1.4.3. Liposome surface decoration to improve drug delivery

Liposome nanocarriers have many advantages, although a few aspects have hindered the application of liposomal drug delivery. When liposomes were first developed, they were composed of charged lipids, neutral lipids, and cholesterol (Figure 1.8A). These liposomes did improve the pharmacokinetics of drugs, but they had many issues. Specifically, short circulation lifetime of liposomes in the body was a major issue, as they were quickly cleared from the bloodstream. Also, these simple liposome systems lacked any targeting or selective delivery capabilities. Although the EPR effect allows for some accumulation of these liposomes in tumor tissue, there were no other factors to allow for more specific delivery to diseased cells over healthy cells. Recent improvements in liposome membrane functionalization have been developed to allow for increased circulation time and selective targeted delivery.

To increase liposome circulation times and improve stability, “stealth” stabilized liposomes were introduced, which have a hydrophilic polyethylene glycol (PEG) polymer chains conjugated on the liposomes surface (Figure 1.8B).[125] The PEG coating protects the liposomes from degradation by providing a steric barrier shield between the liposome and processes like opsonization. Opsonization marks foreign particles like liposomes with proteins, making them more visible to phagocytic cells (monocytes, macrophages, neutrophils and dendritic cells).[126] After

opsonization, phagocytosis occurs, which is the engulfing and destruction or removal of the liposome from the bloodstream. Without PEGylation, nanoparticles can undergo opsonization within minutes of entering the bloodstream. Because PEGylated liposomes are shielded from this process, their circulation time is enhanced, thereby enhancing the EPR effect by increasing the likelihood of liposome accumulation in the tumor vasculature. Also, the length and density of PEG has been shown to influence liposomal circulation time and *in vivo* biodistribution.[127]

The second drawback to traditional liposomes, non-specific delivery, is a major field of liposomal development. Ligand-targeted liposomal systems have been developed to achieve site-specific delivery of drugs to certain pathological cells, organs or tissues. These systems can selectively recognize groups that are commonly overexpressed in diseased cells. Various types of ligands have been used to achieve targeted delivery to specific cell types including small molecule, antibody, carbohydrate, aptamer, peptide, and protein (Figure 1.8C). It is important to ensure proper position of ligands on the liposome surface in order to optimize surface-substrate interaction. Therefore, these targeting moieties are typically either attached to the end of a surface PEG chain or incorporated into the liposome membrane as a headgroup functionalized lipid. Antibodies have great specificity for the associated antigen and are therefore a widely studied targeting ligand. The antibody is typically attached to the terminal end of a PEG chain.[128] These antibody decorated liposomes are known as immunoliposomes and are being developed using a variety of antibodies or antibody fragments for the treatment of not only cancer, but also inflammatory and cardiovascular diseases, autoimmune and degenerative diseases, and infectious pathologies.[129] Another common target is the folate receptor (FR), which is unregulated in cancer cells.[130] This receptor binds with the small molecule folic acid, which can be added to the liposome surface. It has been shown that liposomes functionalized with folic acid can achieve specific drug delivery to cancer cells.[131] Newer generations of liposomes can combine targeting groups with imaging agents, resulting in theranostic liposomes (Figure 1.8D) .[132]

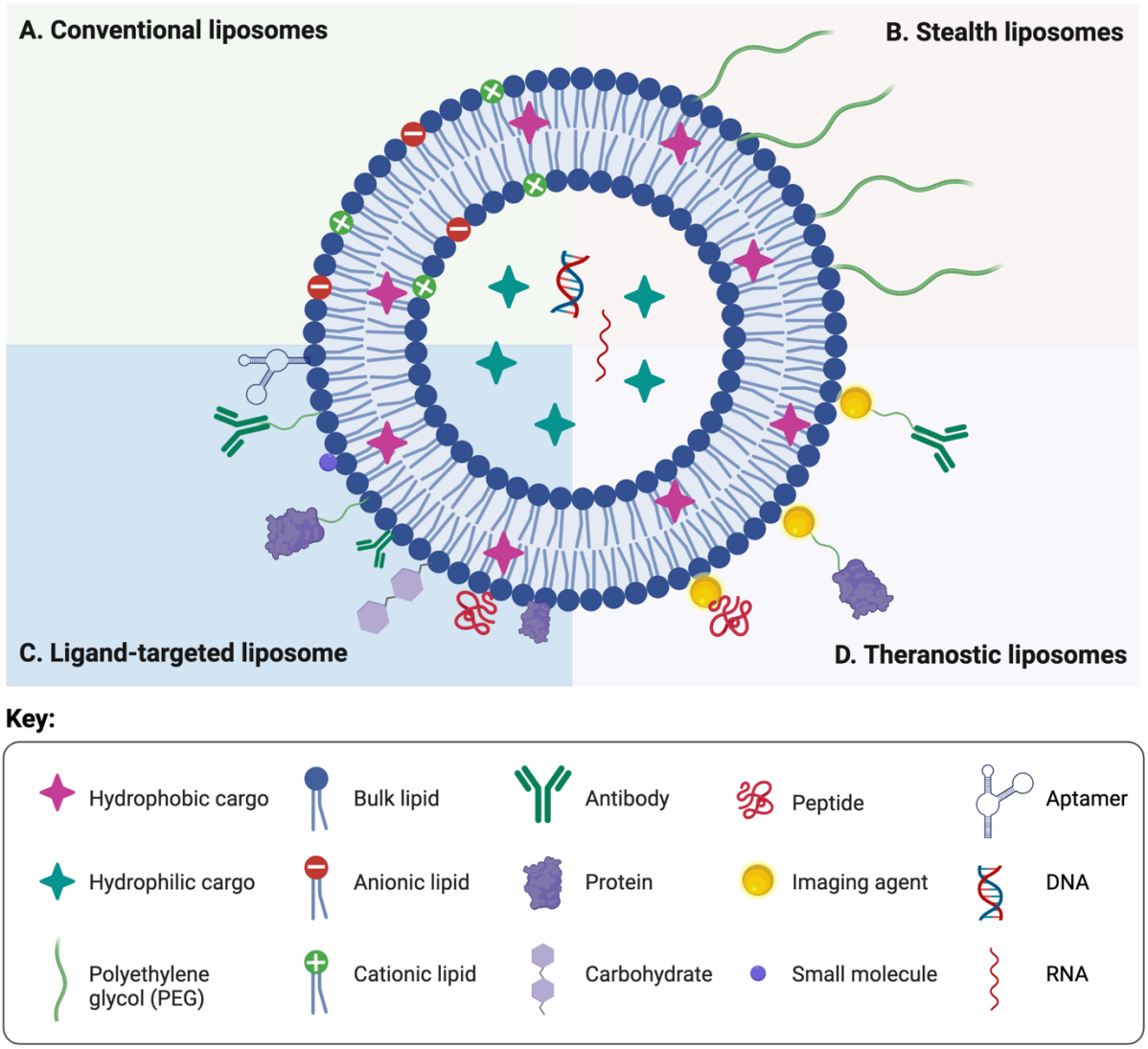


Figure 1.8 Advancements in surface modified liposomes. (A) Traditional liposomes composed of charged lipids, neutral lipids, and cholesterol. (B) Stealth stabilized liposomes with hydrophilic PEG polymer chains conjugated on the liposomes surface. (C) Targeting ligands including small molecule, antibody, carbohydrate, peptide, aptamer, and protein selectively recognize groups that are commonly overexpressed in diseased cells. (D) Theranostic liposomes can combine targeting groups with imaging agents. This image is inspired by the work of Hua et. al.[133]

1.4.4. Liposomes and triggered release

While active targeting ligands such as antibodies allow for site-controlled delivery of the vesicles, strategies are also needed to allow for quick and efficient drug release from the liposome to increase drug efficacy and reduce adverse effects. Therefore, another key area of development is the necessary breakdown of the liposome bilayer in order to release therapeutic cargo. While the breakdown of the membrane is not efficient in typical liposome systems, progress is being made toward the development of stimuli-responsive liposomes platforms that can release cargo upon specific trigger exposure.[134, 135] Cargo release mechanisms can also be developed which leverage disease-associated stimuli to selectively delivery liposome contents to diseased cells compared to healthy cells. This selective delivery can be exploited to reduce harmful side effects and improve liposome efficacy by encouraging maximum content release from liposomes and enabling selective delivery to diseased cells for therapeutic applications. Therefore, the development of triggered release platforms that employ stimuli-responsive liposomes which release cargo upon exposure to a specific trigger has emerged as a vibrant research area.

An important aspect in developing stimuli-responsive liposome systems is to form liposomes that are stable during circulation but undergo sufficient alterations in packing properties after encountering the desired stimulus to destabilize the bilayer and induce cargo release. A few known strategies for altering lipid bilayer packing properties are represented in Figure 1.9, including modification of the lipid headgroup,[136-140] loss of acyl chain,[141-143] conformational change,[144-148] and binding interactions.

There are two categories of triggered release based on the microenvironment which most systems fall into, namely passive release and active release. Passive release exploits pathophysiological differences in the microenvironment of healthy cells compared to diseased cells including pH,[149] redox environment,[150] enzyme expression,[151] and metabolite concentrations.[152-155] Active release employs changes in external stimuli such as light,[156-158] heat,[159, 160] or ultrasound.[161, 162] Controlled cargo release based on the cellular microenvironment embodies the technological forefront of the field; however, the number of targeted release

strategies remains meager and these platforms have not yet entered clinical applications because of unresolved challenges. Recently, our group has supplied notable contributions by developing liposomes that respond to light,[163] calcium,[164, 165] zinc,[166] enzymes,[167] reactive oxygen species (ROS),[168] and phosphorylated metabolites (adenosine triphosphate (ATP)[169] and inositol (1,4,5)-trisphosphate (IP_3)[170]). As indicated, a particular area of interest is the creation of liposomes that respond to small organic biomolecules that are overexpressed in and around diseased cells.[171] The origin of this interest is due to other stimuli being unsuitable for clinical use. For example, passive release methods often suffer from minimal differences between healthy and diseased cells. Analogously, active release suffers from difficulty in delivering physical stimuli that leaves healthy cells undamaged. Targeting small organic biomolecules can address these challenges, and organic metabolites and functional groups offer exciting stimuli for triggering cargo release because they are known to be highly overexpressed in diseased cells compared to their healthy counterparts.

1.5. Summary and outlook

It has been demonstrated that liposomes are effective drug delivery carriers, and research is ongoing to improve their designs for continued clinical applications. While many liposome types have been developed, further work is needed to improve surface modification, site-specific targeting, and triggered release in order to further the therapeutic applications of these platforms.

Through the work described in this dissertation, we sought to advance this field by developing various surface modified and stimuli-responsive liposomal platforms via synthetic lipids. In Chapter 2, we present a liposome platform incorporating a headgroup modified cyclic disulfide lipid (CDL) for the dual purpose of enhancing cell entry and functionalizing the liposome membrane through thiol-disulfide exchange. In Chapter 3, we describe the development of a headgroup modified liposome platform incorporating bis-boronic acid lipids (BBALs) to increase valency in order to achieve selective saccharide sensing and enhance cell surface recognition based on carbohydrate binding interactions. In Chapter 4, we utilize a slightly different strategy

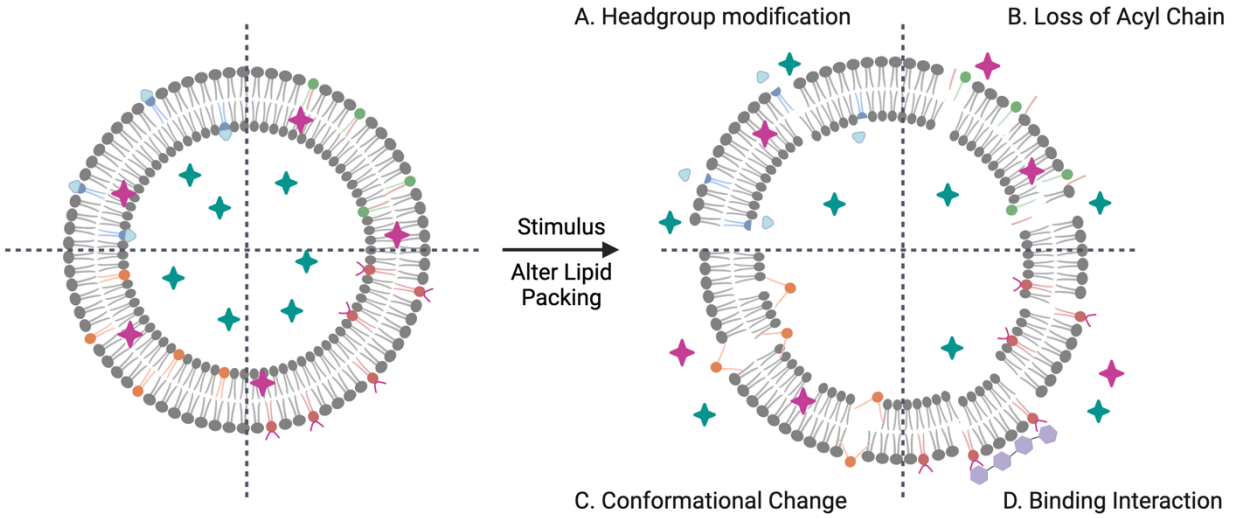


Figure 1.9 Methods of altering lipid bilayer packing to cause cargo release. Established strategies for altering lipid bilayer packing properties to yield cargo release include (A) modification of the lipid headgroup, (B) loss of acyl chain, (C) conformational change, and (D) binding interactions. This image is inspired by the work by Best et. al.[172]

in which we chemically modified the headgroups of the non-bilayer lipid DOPE to achieve responsive lipids that show alteration in self-assembly properties upon thiol and cysteine addition. In Chapter 5, we present advances towards an ROS-responsive synthetic system for use in artificial ROS signal transduction. As discussed in the chapters below, our approaches show promising enhancements in a range of functions including enhancing membrane decoration, cellular delivery, saccharide sensing, and controlled release associated with the disease environments to ultimately advance clinical liposome applications.

Chapter 2. Development of Cyclic Disulfide Liposomes for Membrane Functionalization and Cellular Delivery

A version of this chapter was originally published by Megan L. Qualls, et al.:

Qualls, Megan L.; Lou, Jinchao; McBee, Dillon P.; Baccile, Joshua A.; Best, Michael D., Cyclic Disulfide Liposomes for Membrane Functionalization and Cellular Delivery, *Chemistry a European Journal* 2022, *28* (45), e202201164.

In Chapter 2, MLQ designed and performed all microplate-based assays. JL synthesized and characterized the lipids. MLQ performed all liposome preparation and all DLS, TEM and NMR analysis of all liposomes. DPM prepared cells for liposome analysis. MLQ performed cellular delivery experiments, cellular imaging, and cytotoxicity analysis. MLQ, JL, JAB, and MDB contributed to the writing of the manuscript. MDB directed the project.

2.1. Abstract

Liposomes are effective therapeutic delivery nanocarriers due to their ability to encapsulate and enhance the pharmacokinetic properties of wide-ranging therapeutics. Two primary areas in which improvement is needed for liposomal drug delivery is to enhance the ability to infiltrate cells and to easily functionalize the liposome surface. Herein, we report a liposome platform incorporating a cyclic disulfide lipid (CDL) for the dual purpose of enhancing cell entry and functionalizing the liposome membrane through thiol-disulfide exchange. In order to accomplish this, **2.1** and **2.2**, composed of lipoic acid (LA) or asparagusic acid (AA) appended to a lipid scaffold, were designed and synthesized. A fluorescence-based microplate immobilization assay was implemented to show that these compounds enable convenient membrane decoration through reaction with thiol-functionalized small molecules. Additionally, fluorescence microscopy experiments indicated dramatic enhancements in cellular delivery when CDLs were incorporated within liposomes. These results demonstrate that multifunctional CDLs serve as an exciting liposome system for surface decoration and enhanced cellular delivery.

2.2. Introduction

2.2.1. Introduction to disulfide bonds and thiols and biological relevance

Disulfide bonds are fundamental building blocks for molecular structures and are formed via intermolecular and intra-domain covalent bonds between two thiol-containing cysteine (Cys) residues in peptides and proteins.[173] In addition to protein stabilizing structural purposes, disulfide formation is also responsible for the diverse and dynamic functional properties of many enzymes and for protection against oxidative damage.[174] Protein activity and location are controlled by redox-active disulfide bonds, which respond to the redox potential of the cell. These bonds can be categorized as intramolecular protein disulfides and mixed disulfides that involve small molecules like glutathione (GSH). Unlike fixed structural disulfides, redox-active disulfides are highly dynamic and are regulated by changes in the oxidation or reduction state in the cellular environment.[175] Eukaryotic systems exhibit tight regulation on the formation of disulfide bonds in secreted proteins, which is carried out by oxidoreductases (typically of the protein disulfide isomerase (PDsI) family)[176] located in the endoplasmic reticulum (ER).[173] In addition to their biological relevance, disulfide bonds have been utilized in nanomaterials for drug delivery purposes to produce stimulus-responsive and/or self-healing materials for therapeutic applications.[177] Due to the relevance of disulfide-thiol chemistry in the following chapter, these interactions will be further discussed including the reactions of disulfide bond and thiols, factors that influence disulfide-thiol reactions, and current applications of disulfide-thiol interactions in materials chemistry and nanomedicine**.**

2.2.2. Reactions of disulfide bonds and thiols

In proteins, disulfide bonds form between two spatially proximal thiol moieties of Cys residues through reactions comprised of a two-electron oxidation process beginning with the reduced sulfhydryl groups of Cys (S-H) and resulting in an oxidized cystine (S-S) residue. Two Cys thiols may react spontaneously *in vitro* to form a disulfide bond, coupled with gain of electrons by an acceptor such as molecular oxygen.[173] In biological systems, disulfide bonds are usually formed via thiol-disulfide exchange reactions in which a thiolate anion nucleophile (Scheme 2.1A) attacks an existing disulfide bond (RS-SR) to yield a new mixed disulfide and free thiol species (Scheme

2.1B).[178] Although these *in vivo* reaction are slow, they can be accelerated through enzymatic catalysis.[179, 180] The fact that the S-S bond can be easily broken and reformed is a crucial aspect of many biochemical processes and makes this an important field of chemistry to study. Platforms have been developed which utilize the disulfide bond for therapeutic drug delivery in which the sulfhydryl-disulfide bond exchange reaction is leveraged.[181] In these cases, the nanomaterial possesses a disulfide bond which can undergo sulfhydryl-disulfide bond exchange reaction with biological thiols such as GSH or Cys.

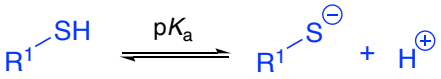
GSH is a thiol-containing tripeptide of glutamic acid, Cys, and glycine, and Cys is a thiol containing amino acid. The intracellular concentration of GSH (0.5–10 mM) is ~1000 fold higher compared to the extracellular environment (2–20 μM),[182] which has been harnessed in redox-responsive drug delivery systems to trigger release of drugs in cancer cells.[182] It has also been shown that GSH levels are elevated in tumor cells including bone marrow, breast, colon, larynx, and lung cancers in order to protect the cells from excessive ROS and to confer resistance to several chemotherapeutic drugs.[183-185] Additionally, Cys is an analyte that is significantly upregulated during cancer onset and is responsible for producing GSH to combat oxidative conditions and maintaining cellular homeostasis and cancer cell survival.[186]

2.2.3. Factors influencing the reactivity of disulfide bonds and thiols

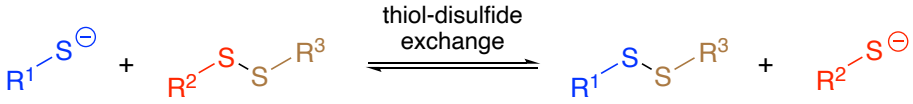
The stability of a disulfide bond is described by the bond's redox potential, which specifies the tendency to be reduced in a given redox environment.[187] The redox potentials of cellular disulfides are typically measured as compared to a GSH standard, and negative redox potentials are considered more stable and therefore less likely to participate in thiol-disulfide exchange. Protein disulfide redox potentials have been reported to range from −95 to −470 mV.[175] Factors that influence the reactivity and redox potential of disulfide bonds and include pK_a, entropy, and bond-strain energy.[187-189]

The thiol-disulfide exchange kinetics are influenced by the pK_a of the nucleophilic thiol as well as the pK_a of the thiol leaving group. The pK_a values of common thiols range from 5.24 to 11.22.[189]

A.



B.



Scheme 2.1 Thiol pK_a and thiol-disulfide exchange reaction. (A) The pK_a of the thiol describes the conversion from thiol to thiolate anion. (B) The thiol-disulfide exchange reaction occurs in which a thiolate anion nucleophile attacks an existing disulfide bond to yield a new mixed disulfide and free thiolate species

For example, the pK_a of Cys is 8.3, resulting in protonation at physiological pH and suppressed reactivity.[190] Conversely, it has also been shown that thiol pK_a values significantly below the pH of the solution tend to signify decreased nucleophilicity of the thiolate, also resulting in lessened reactivity. Hence, the rate constant is highest when the thiol pK_a is equal to or near the pH of the solution.[191] In contrast, decreased pK_a of the leaving group thiol increases the rate of thiol-disulfide exchange, regardless of the pH of the solution, and thiol addition to an asymmetrical disulfide will result in the thiol with the lowest pK_a acting as the leaving group.[192] Entropy also influences the stability of disulfide bonds, and entropic barriers including rotation and translation affect the rate of formation. For example, while intermolecular disulfide bonds are entropically disfavored, intramolecular disulfide bonds in proteins become more favored as the two Cys become closer in the primary sequence. This is due to a decrease in the conformational freedom and increase in the orientations that would permit disulfide bond formation, which overall reduce the entropic barrier of disulfide-bond formation.[193] Also, disulfide bonds are less stable if the newly formed disulfide bond presents an increase in strain. The preferred dihedral angle for disulfides is ±90°, and studies suggests that deviation from this preferred angle could lead to an elevation in redox potential ranging from 10 to 100 millivolts.[194]

2.2.4. Disulfide bond use in materials chemistry and nanomedicine

The flexibility of disulfide chemistry has generated significant interest in the biomedical arena, where it is being used to create nanoparticles with disulfide components for more advanced forms of disease therapy. The disulfide bond has been developed into nanoparticles largely because of the increased concentration of GSH and Cys in intramolecular and intra-tumor environments, which can act as endogenous disulfide cleaving agents to the nanoparticles. The disulfide bond is stable both during blood circulation and extracellularly, but after entering tumor cells, it will undergo a sulfhydryl-disulfide bond exchange reaction with GSH and Cys in the cytoplasm. The cleavage of disulfide bonds can be designed to induce NP responses such as drug release. Because the disulfide bond is a well-studied dynamic covalent bond which exchanges quickly and reversibly with a thiol or thiolate, it has been utilized in a broad range of applications including controlling protein conformations,[195] mediating cellular redox homeostasis,[196, 197]

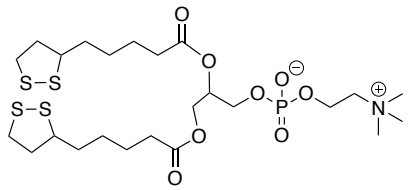
cellular drug delivery using dendrimer[198] and polymerizome NPs,[199] prodrug therapeutics,[200] dynamic self-assembly,[201-203] self-healing materials,[204, 205] and inorganic/organic hybrid polymers.[206, 207]

For example, Ling et. al. recently reported disulfide cross-linked liposomes which were assembled from a dimeric lipoic acid-derived glycerophosphorylcholine conjugate that possessed cyclic disulfide groups in the lipid tail (Figure 2.1A).[208] The drug Dox-HCl was encapsulated in the liposome core and the disulfide tails were cross-linked with dithiothreitol (DTT). Their lipid NP system showed remarkable thiol-sensitive release of payload upon cellular uptake by cancer cells. In another example, Koyanagi et. al. described a cholesterol-integrated tetraether lipid with a cleavable disulfide bond in the lipid headgroup which was designed to respond to the reducing environment of the cell (Figure 2.1B).[138] Intracellular headgroup cleavage upon cellular uptake by cancer cells resulted in release of encapsulated Dox-HCl and cell death. Additionally, a headgroup thiol-modified phospholipid, 1,2-dipalmitoyl-*sn*-glycero-3-phosphothioethanol, which is commercially available, was shown to form liposomes up to 100 mol% in the lipid formulation and allowed these liposomes to adsorb onto AuNPs (Figure 2.1C).[209]

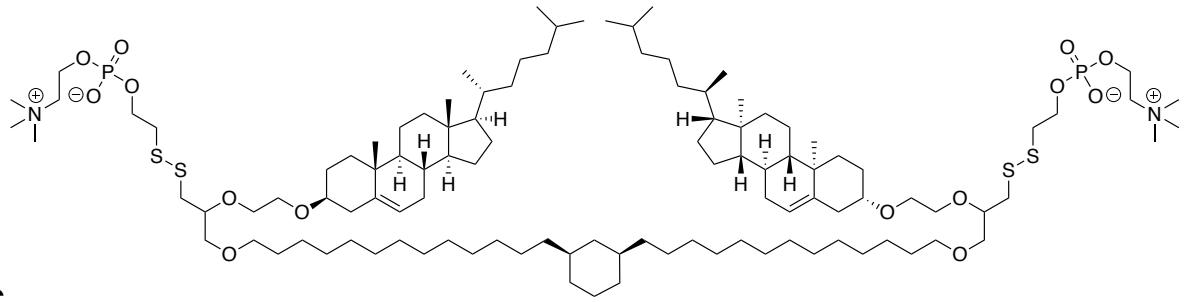
2.2.5. Introduction to cyclic disulfide liposomes

Liposomes are spherical vesicles composed of a lipid bilayer membrane that assembles around an internal aqueous core. This duality gives liposomes the ability to encapsulate both hydrophobic cargo within the lipid bilayer and hydrophilic contents in the aqueous core, making them versatile molecular carriers for drug delivery. In certain situations, liposomes exhibit improved delivery to diseased tissue, such as through the EPR effect that exploits the leaky vasculatures proximal to tumors. Liposomes can also be designed with passive triggered release mechanisms that take advantage of conditions associated with diseased cells, such as acidity,[210-213] enzymatic expression,[214, 215] metabolites,[146, 147, 216] and redox conditions.[217, 218] However, there are drawbacks to these stimuli since they must exhibit significant differences between diseased sites and healthy sites in order to drive selectivity.[219, 220] Intensive efforts are underway to achieve broader enhancements in cellular delivery by attaching moieties to liposomal surfaces that can

A.



B.



C.

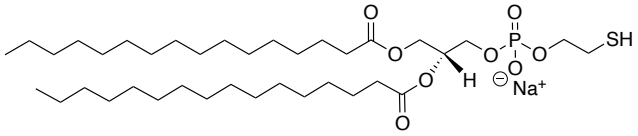


Figure 2.1 Previously reported disulfide and thiol lipids utilized in liposome NPs. (A) Dimeric lipoic acid-derived glycerophosphorylcholine conjugate with cyclic disulfide groups in the lipid tail reported by Ling et. al. for Dox-HCl encapsulation and thiol-sensitive cargo release.[208] (B) Cholesterol-integrated tetraether lipid with a cleavable disulfide bond in the lipid headgroup by Koyanagi et. al. for Dox encapsulation and intracellular release.[208] (C) Headgroup thiol-modified phospholipid allows liposomes to adsorb onto AuNPs.

enhance cell delivery.[166, 172, 221-225] While groups including antibodies, peptides, carbohydrates, proteins, and other small molecules are effective,[226, 227] the attachment of complex and expensive biomolecules onto liposome surfaces is challenging and impractical for clinical applications. The engineering of cell penetrating moieties directly into the membrane bilayer using designer lipid analogs likely provides a more efficient approach for enhancing cellular delivery characteristics.

It has been shown that certain nanoparticles can exploit cell-surface thiols such as Cys to enhance cellular uptake.[228] For example, disulfides can drive the entry of liposomes,[229] peptides,[230] proteins,[231] viruses,[232, 233] and fluorophores [234] into cells through dynamic covalent disulfide exchange with thiols on the cell surface that initiate cell uptake. To react with free thiols, nanoparticles can be designed with disulfide groups that are able to exchange with exofacial thiols. Further, studies have shown that increased ring tension of disulfides dramatically improves cellular uptake, with the two highest tensions for common cyclic disulfides being AA and LA, which have carbon-sulfur-sulfur-carbon (CSSC) dihedral angles of 27° and 35°, respectively.[235]

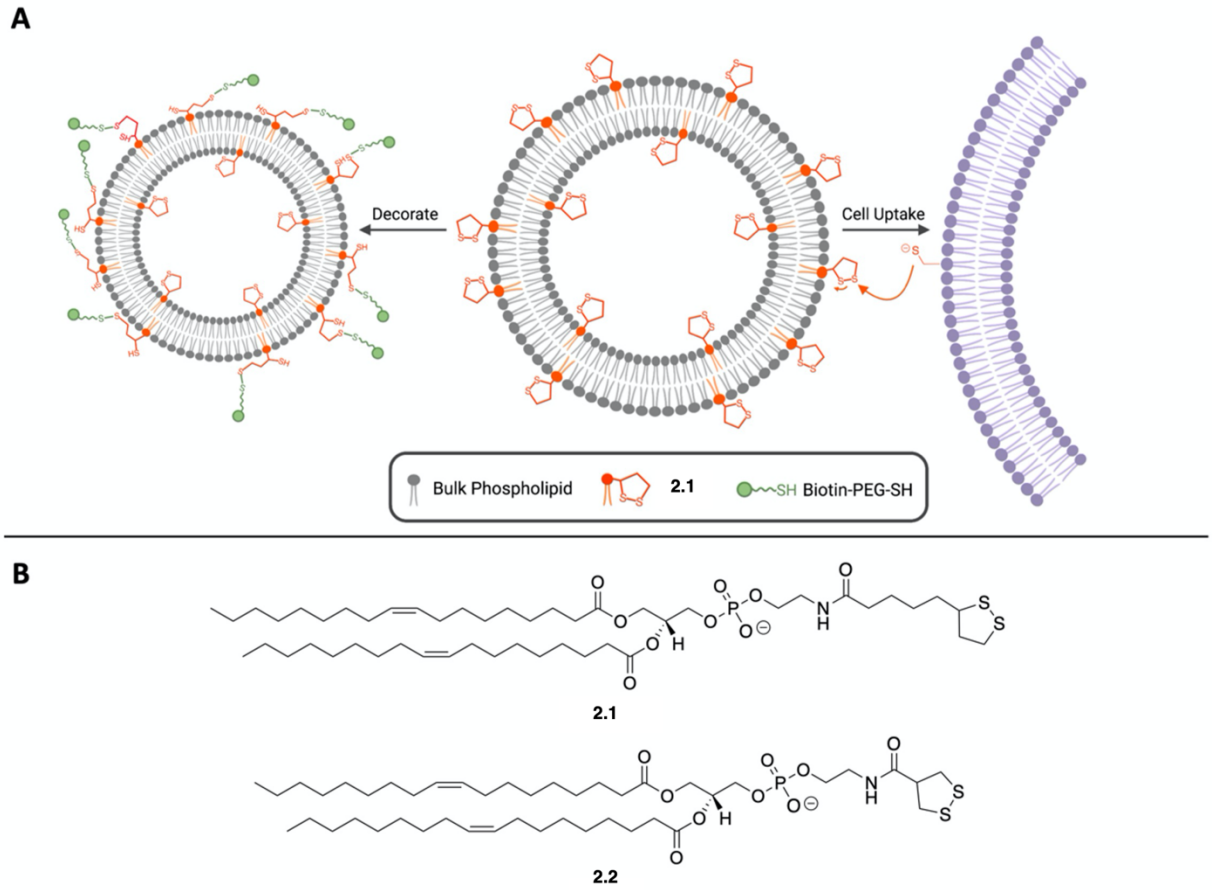
The ability to functionalize liposome surfaces in a convenient manner is additionally an important area of study to increase the therapeutic applications of liposomes by adding accessories such as fluorescent reporter tags, targeting moieties including proteins or peptides, drugs, and/or other small molecules. One approach for liposome membrane functionalization relies on the synthesis of functionalized lipid conjugates followed by formulation or post-insertion. Alternatively, liposomes can be functionalized *in situ* using lipid anchors containing reactive moieties for conjugation reactions such as amide[236] and thiol-maleimide coupling,[237] imine[238] and hydrazone linkage,[239] click chemistry,[240] and the Staudinger ligation.[241] The thiol disulfide exchange remains a relatively underexplored reaction for liposome surface functionalization.

In this Chapter, we present a promising new means by which we may enhance the ability of liposomes to infiltrate cells and to easily functionalize the liposome surface. The thiol disulfide

exchange reaction was chosen as the foundation of the lipid. To achieve this goal, lipids were synthesized which can react with free thiols and were incorporated into liposomes. The synthetic lipids bear a cyclic disulfide located at the lipid headgroup to react with free thiols either from synthetic compounds or as side chains presented on cell-surfaces and thereby facilitate membrane functionalization and enhancement of cellular delivery. In this chapter, a comprehensive evaluation of this delivery platform is presented including the design and synthesis of the multifunctional lipid, analysis of membrane decoration with a fluorescence-based microplate immobilization assay, characterization of liposome morphology containing the lipids, and assessment of enhancements in cellular delivery with fluorescence microscopy.

2.3. Design of cyclic disulfide liposomes

Herein, we describe a liposomal platform that enables both facile membrane functionalization and enhancement of cellular delivery. We hypothesized that compounds bearing a cyclic disulfide located at the lipid headgroup would be invaluable for both purposes. This is because cyclic disulfides presented at liposome aqueous interfaces are expected to react with free thiols either from synthetic compounds or as side chains presented on cell-surfaces, generating a covalent bond that could be exploited for functionalization or to promote cell delivery. To achieve these goals, we developed two synthetic lipids composed of 1,2-dioleoyl-*sn*-glycero-3-phosphoethanolamine (DOPE) functionalized with either LA or AA (**2.1** and **2.2**, respectively, Scheme 2.2). Compounds **2.1** and **2.2** were designed with the cyclic disulfide moiety linked to the phospholipid headgroup so this reactive tag could be presented at the aqueous interface of the membrane. In accordance, it is expected to be accessible for both reacting with thiols on cell surfaces to drive cell entry as well as with synthetic compounds containing free thiols for the purpose of decorating liposome membranes. Synthesis of **2.1** and **2.2** was performed in collaboration with Dr. Jinchao Lou in our group. These compounds were synthesized via amide coupling reactions of DOPE with either LA to form **2.1** or AA to form **2.2**.



Scheme 2.2 Design strategy for cyclic disulfide liposomes. (A) Cartoon illustration of cyclic disulfide liposomes containing **2.1** facilitating liposome membrane functionalization with Biotin-PEG-SH as well as enhancing cellular delivery due to exchange with thiols on the cell-surface. (B) Chemical structures of **2.1** and **2.2** which were synthesized via amide coupling reactions of DOPE with either LA to form **2.1** or AA to form **2.2**.

2.4. Microplate-based liposome assay to detect membrane functionalization

2.4.1. Assay overview

Following CDL synthesis, we moved on to study the ability of **2.1** and **2.2** to facilitate liposome membrane functionalization via disulfide exchange with free thiols. To accomplish this, a two-step assay was developed in which reaction with a functionalized thiol was evaluated using a microplate immobilization strategy (Figure 2.2). The benefits of conducting a microplate assay include rapid screening and the ability to separate unreacted liposomes through microplate wash steps. This assay exploited protocols our group previously developed for immobilizing intact liposomes that include biotinylated lipids onto streptavidin-coated microplates.[242] In the first step, liposomes formulated with varying percentages of **2.1** or **2.2** and fluorescently labeled with 1% rhodamine L-α-phosphatidylethanolamine (Rd-PE) were incubated with biotin-PEG-thiol reagent (Biotin-PEG-SH, molecular weight (MW) 1K) to allow for disulfide conjugation and liposome surface functionalization (Figure 2.2A). In the second step, the resulting liposomes were incubated with streptavidin-coated microplates, and rigorous washes were performed to remove unbound liposomes, after which fluorescence measurements were acquired to detect liposomes that were successfully functionalized and immobilized onto microplate surfaces (Figure 2.2B).

2.4.2. Microplate immobilization and membrane functionalization results

To perform this assay, liposomes were initially prepared composed of either 0%, 5%, 10%, 30%, 50%, 75%, or 99% **2.1** or **2.2,** 1% Rd-PE, and the remainder Egg-PC (99%, 94%, 89%, 69%, 49%, 24% or 0%, respectively). Liposomes were prepared through traditional thin-film preparation techniques including thin-film formation, hydration, freeze-thaw cycling, and extrusion through 200 nm membranes to form uniform liposomes of desired size. Then, 0.5 mM liposome solutions were incubated with 5 mM Biotin-PEG-SH to allow for disulfide conjugation and surface functionalization and then incubated with streptavidin-coated microplates to allow for biotin immobilization of the functionalized liposomes. After washing away any unbound liposomes from the plate, immobilization was assessed via increases in Rd-PE fluorescence. As seen in Figure 2.3, surface conjugation was shown to be dependent on the percentage of **2.1** (Relative Fluorescence Units (RFU) = 5% **2.1**, ~ 20,300; 10% **2.1**, ~ 48,000; 30% **2.1**, ~ 99,700; 50% **2.1**, ~ 113,000; 75%

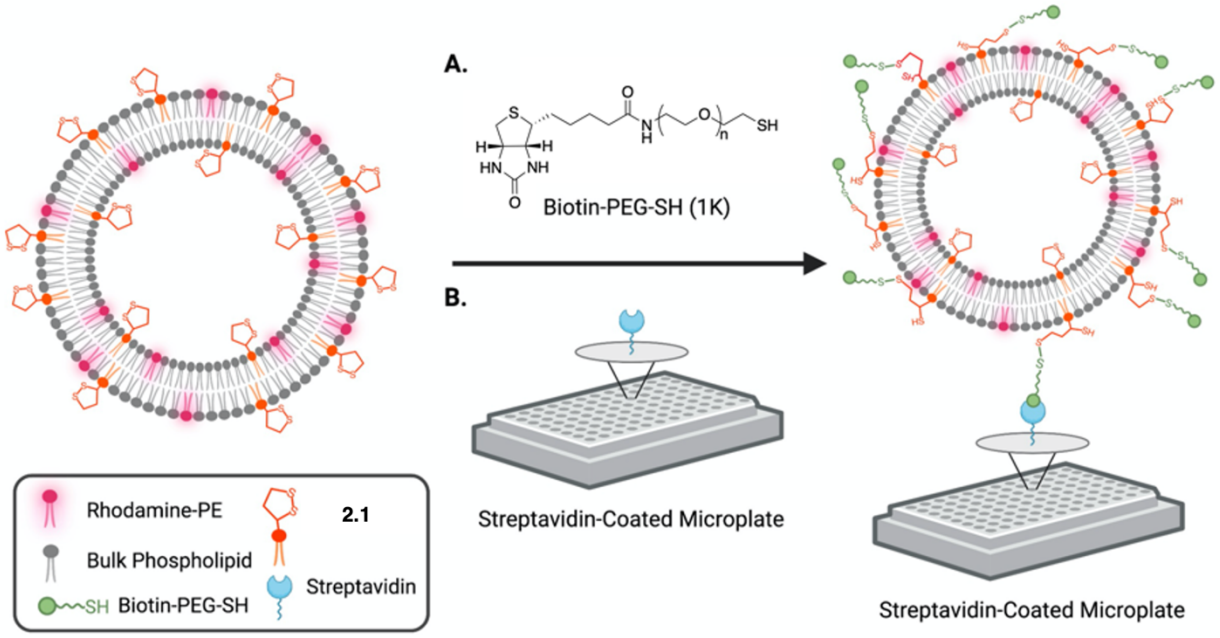


Figure 2.2 Microplate assay for detection of disulfide mediated membrane functionalization. (A) Rd-PE labeled liposomes containing **2.1** or **2.2** are incubated with Biotin-PEG-SH reagent (MW 1K) to functionalize the liposome surface via disulfide conjugation. (B) Biotin functionalized liposomes are then immobilized onto streptavidin-coated microplates.

2.1, ~ 109,700; 99% **2.1**, ~ 115,000;) and **2.2** (RFU = 5% **2.2**, ~ 21,500; 10% **2.2**, ~ 51,700; 30% **2.2**, ~ 63,900; 50% **2.2**, ~ 103,100; 75% **2.2**, ~ 102,600; 99% **2.2**, ~ 194,300) incorporated within the liposomes. Liposomes containing 99% **2.2** showed the greatest extent of liposome immobilization driven by disulfide conjugation.

2.4.3. IAM terminated microplate assay

To continue improving liposome membrane functionalization, a modified microplate assay protocol was designed with the addition of the terminating thiol-reactive agent iodoacetamide (IAM), which reacts with free thiols. IAM is a sulfhydryl-reactive alkylating reagent which is commonly used to block reduced Cys residues for protein characterization.[243] It is possible that after the cyclic disulfide conjugates to the Biotin-PEG-SH, the free thiol in the headgroup could re-close the cyclic disulfide and release the Biotin-PEG-SH. This release would therefore decrease membrane functionalization efficiency and liposome immobilization on the streptavidin-coated microplate. To probe this, a step was added after Biotin-PEG-SH conjugation in which the samples were incubated with IAM to prevent restoration of the cyclic disulfide (Scheme 2.3). Adding a terminator reagent after conjugation with the Biotin-PEG-SH could help by reacting with the free thiol and preventing reclosure, which would improve Biotin-PEG-SH labeling. Improvement in Biotin-PEG-SH labeling was assessed as indicated by increase in fluorescence intensity from Rd-PE labeled liposome immobilized by Biotin-PEG-SH on the streptavidin-coated microplate. The results of this assay indicated that IAM addition did improve microplate immobilization results. Liposomes with 50% **2.1** had similar results to liposomes without IAM, but 99% **2.1** liposome immobilization was improved ~3 fold with IAM treatment (Figure 2.4A). For liposomes containing 50% **2.2** and 99% **2.2**, immobilization was improved by more than ~5 fold (Figure 2.4B) with IAM treatment. This study demonstrated that post-functionalization of liposome membranes containing **2.1** and **2.2** can be improved with the addition of the terminating thiol-reactive agent.

2.5. Dynamic light scattering studies

Once synthetic lipids are incorporated into liposomes, they can potentially change liposome size and morphology due to alterations to lipid self-assembly. Also, addition of compounds used for

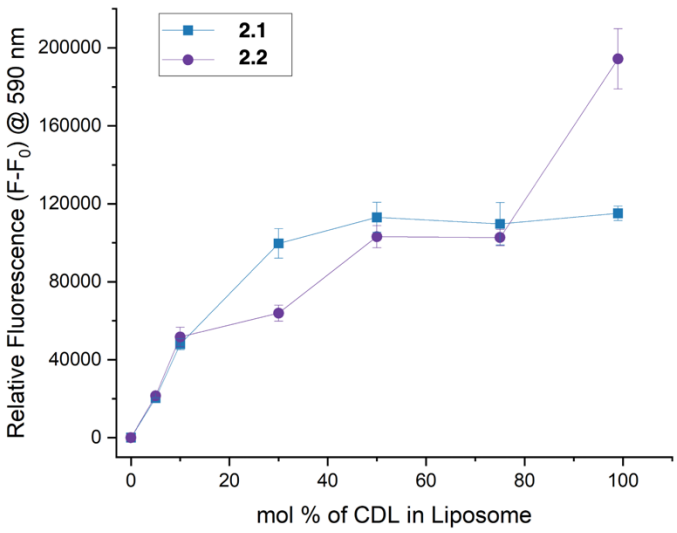
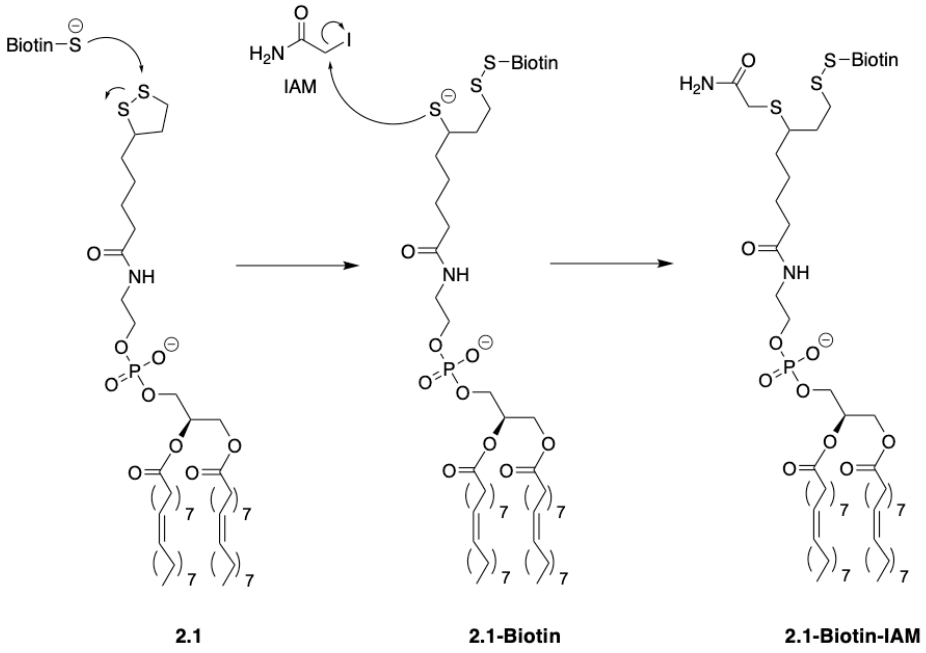


Figure 2.3 Analysis of surface thiol conjugation. Microplate immobilization results for fluorescent Rd-PE labeled CDL liposomes containing 0%, 5%, 10%, 30%, 50%, 75% or 99% lipid **2.1** or **2.2**, 1% Rd-PE, and the remainder Egg-PC (99%, 94%, 89%, 69%, 49%, 24%, or 0%, respectively). Liposome labeling and subsequent immobilization was assessed based on increases in Rd-PE fluorescence, and surface conjugation was shown to be dependent on the percentage of **2.1** and **2.2** in the liposomes with 99% **2.2** exhibiting the greatest conjugation. Error bars represent standard errors of at least three replicates.



Scheme 2.3 Reaction of 2.1 with iodoacetamide. Alkylation of **2.1** with IAM after **2.1** thiol-disulfide conjugation with Biotin-PEG-SH results in the covalent addition of a carbamidomethyl (CAM) group and prevents the formation of disulfide bonds.

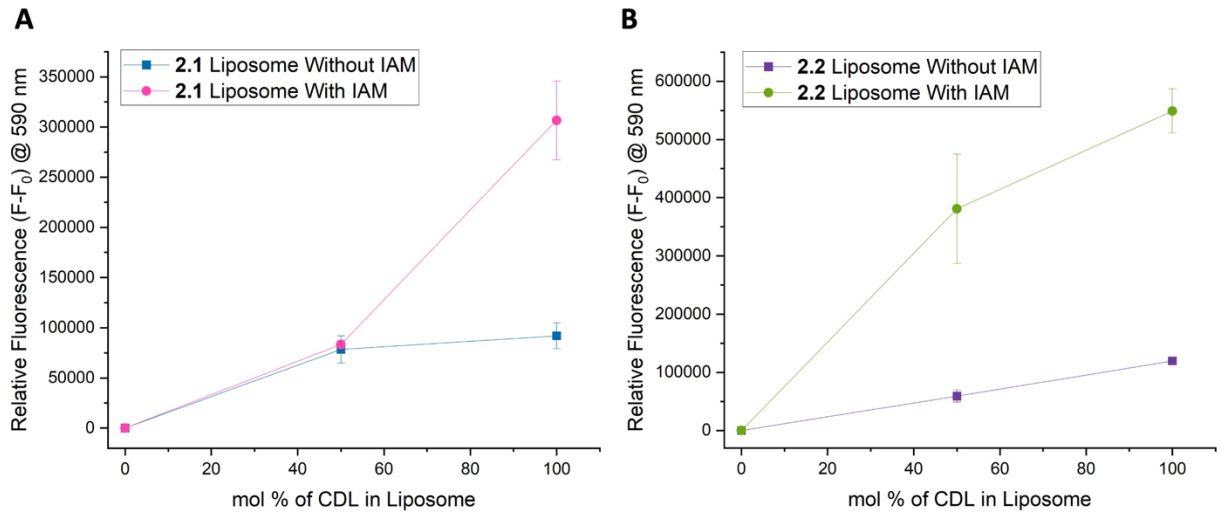


Figure 2.4 Microplate assay for detection of IAM terminated disulfide mediated membrane functionalization. Microplate immobilization results for fluorescent Rd-PE labeled CDL liposomes containing 0%, 50%, or 99% lipid **2.1** or **2.2**, 1% Rd-PE, and the remainder Egg-PC (99%, 49%, 0%, respectively). Liposome labeling, IAM treatment, and subsequent immobilization was assessed based on increases in Rd-PE fluorescence, and surface conjugation was shown to be improved with IAM treatment. Error bars represent standard errors of at least three replicates.

membrane functionalization could potentially cause issues such as disruption of the membrane bilayer during thiol-disulfide conjugation with synthetic CDLs. Therefore, it is important to probe for changes in particle sizes, both before and after membrane functionalization. To accomplish this, we next analyzed the structural characteristics of liposomes containing **2.1** or **2.2** to evaluate morphology. First, we employed DLS analysis to probe particle sizes. These showed that liposomes containing 0%, 10%, 30%, 50%, 75%, or 99% of either **2.1** (Figure 2.5A) or **2.2** (Figure 2.5B) and 1% Rd-PE formed stable vesicles of sizes within the expected diameter range following extrusion. Raw distribution curves are included in Figure 2.5C-D. Increasing the mol% of CDL incorporated within liposomes caused small decreases in vesicle diameters, however, all samples maintained average diameters below 200 nm, which is within the range that is beneficial due to the EPR effect. We also assessed the size of liposomes containing 0%, 10%, 30%, 50%, 75%, or 99% of either **2.1** or **2.2** after treatment with 5 mM Biotin-PEG-SH to probe the morphology of liposomes after treatment. There was no major change in liposome size or uniformity after Biotin-PEG-SH incubation (Figure 2.6A-B). Raw distribution curves are included in Figure 2.6C-D. These data indicate that the synthetic CDLs form remarkably stable liposomes, even up to 99% liposome incorporation, and that membrane conjugation did not induce significant morphology changes in these cases.

2.6. Transmission electron microscopy studies

Lipid nanoparticle stability was further examined by electron microscopy (EM) experiments. Liposomes containing 100% **2.1** lipid were negatively stained with phosphotungstic acid (PTA), which is one of the most commonly used anionic negative-staining (NS) stains for examining liposome structure.[244] The **2.1** liposomes presented with circular cross-sections exhibiting traditional morphology (Figure 2.7), which further verified the formation of stable liposomes even at 100% **2.1** incorporation.

2.7. NMR experiment before and after liposome preparation

To continue analyzing the **2.1** liposomes, and particularly any changes in lipid stability, we next investigated the lipid structure before and after liposome formation by NMR analysis. Strained

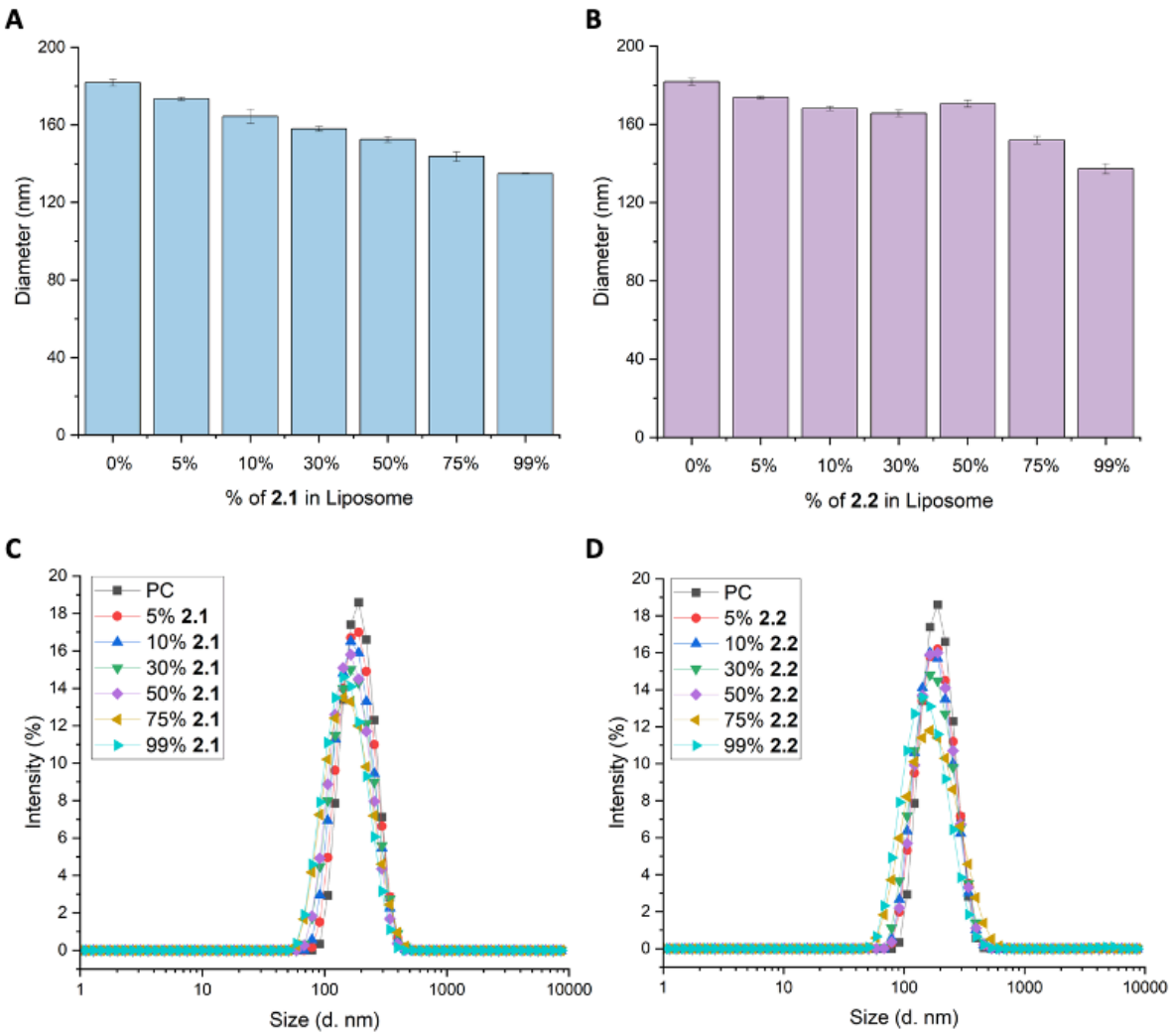


Figure 2.5 DLS results for liposomes containing different percentages of 2.1 and 2.2. DLS results for liposomes containing 0%, 5%, 10%, 30%, 50%, 75%, or 99% lipid (A) **2.1** or (B) **2.2**, 1% Rd-PE, and the remainder Egg-PC (99%, 94%, 89%, 69%, 49%, 24%, or 0%, respectively). Full DLS spectra results of liposomes containing 5%, 10%, 30%, 50%, 75%, or 99% lipid (C) **2.1** or (D) **2.2** with 1% Rd-PE and the remainder Egg-PC PC (99%, 94%, 89%, 69%, 49%, 24% or 0%, respectively). DLS size distribution plots show small decreases in particle size as mol% of CDL was increased. Error bars represent standard errors of at least three replicates.

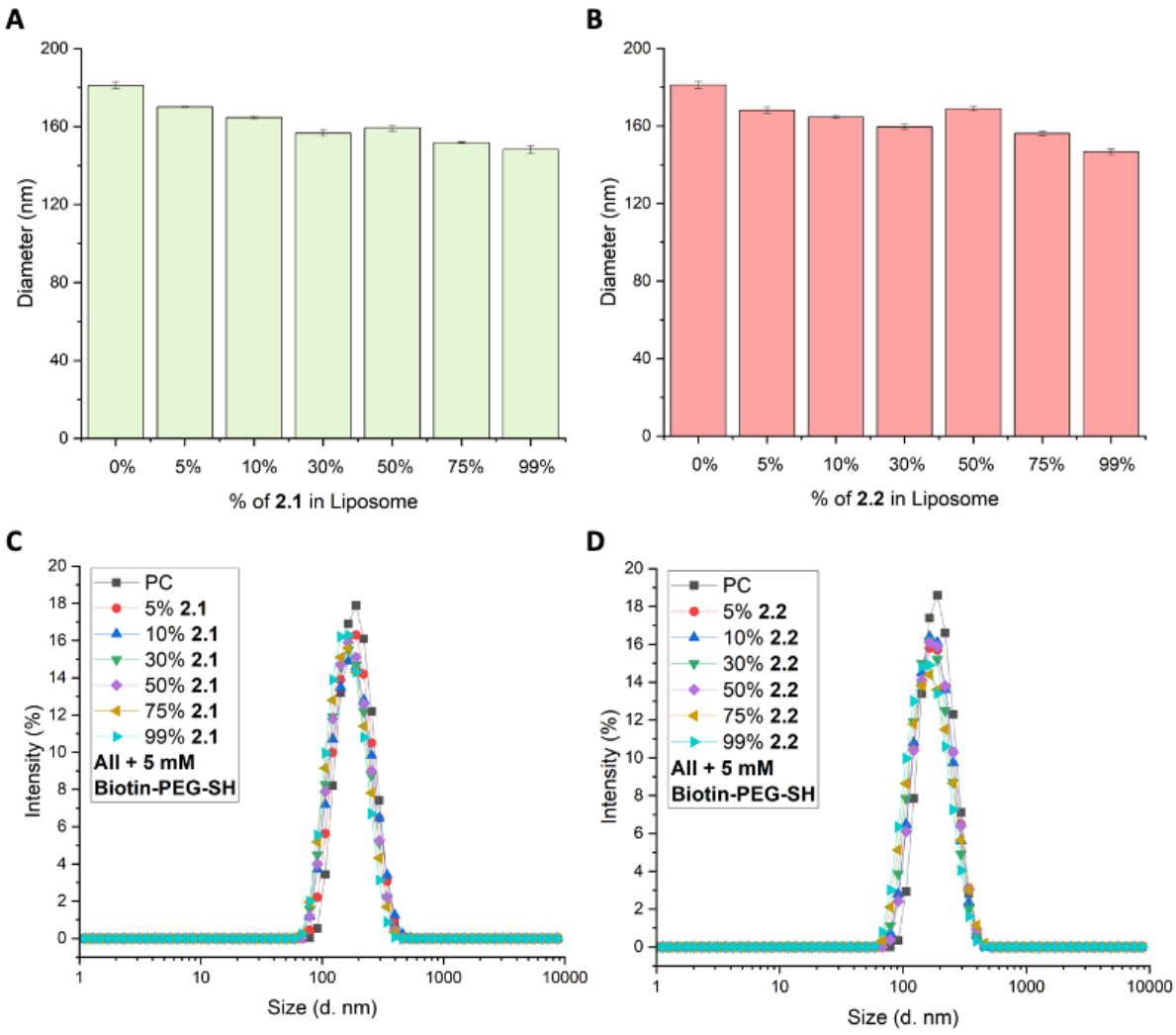


Figure 2.6 DLS results of liposomes containing different percentages of 2.1 and 2.2 after Biotin-PEG-SH treatment. DLS results of liposomes containing 0%, 5%, 10%, 30%, 50%, 75%, or 99% lipid (A) **2.1** or (B) **2.2** with 1% Rd-PE and the remainder Egg-PC PC (99%, 94%, 89%, 69%, 49%, 24% or 0%, respectively) after treatment with 5 mM Biotin-PEG-SH. Full DLS spectra results of liposomes containing 0%, 5%, 10%, 30%, 50%, 75%, or 99% lipid (C) **2.1** or (D) **2.2** with 1% Rd-PE and the remainder Egg-PC PC (99%, 94%, 89%, 69%, 49%, 24% or 0%, respectively) after treatment with 5 mM Biotin-PEG-SH. Error bars represent standard errors of at least three replicates.

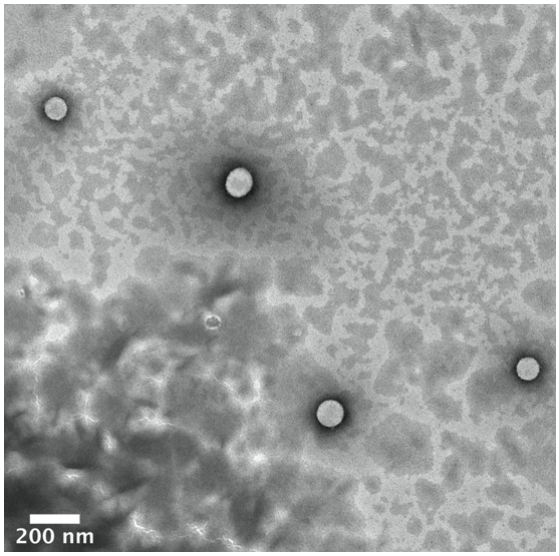


Figure 2.7 TEM results of 2.1 liposomes. Representative TEM image of liposomes containing 100% **2.1**. Samples presented with circular cross-section showing traditional liposome morphology. Liposomes were stained with 1.0% (w/v) solution of neutral PTA and scale bar represents 200 nm.

cyclic disulfides can undergo polymerization, and it was important to ensure that the liposome preparation procedure was not causing polymerization. To perform this experiment, liposomes composed of 100% **2.1** were prepared in buffer following the usual methods, and then the water was fully evaporated. The resulting lipid film was dissolved in deuterated methanol/deuterated chloroform ($CD_3OD/CDCl_3$) 20/80 (v/v), filtered through a polytetrafluoroethylene (PTFE) filter, and transferred into an NMR tube for analysis. At this point, lipid **2.1** was freely dissolved and was not self-assembled. Spectra were taken and compared to spectra of free lipid **2.1** that had not undergone the liposome preparation steps.

As shown in Figure 2.8, the spectra of both **2.1** (no liposome preparation) (Figure 2.8, trace A) and **2.1**, which did undergo liposome formation and then deconstruction (Figure 2.8, trace B), showed that lipids were intact and had not undergone polymerization. These data demonstrate that CDLs remain intact after liposome preparation.

2.8. Cellular delivery studies

2.8.1. Cellular imaging

We next assessed the ability of **2.1** and **2.2** to accomplish our other goal, which is to enhance the entry of liposomes into cells. These experiments were performed in collaboration with Dr. Joshua Baccile's lab in UTK Chemistry. Graduate student Dillon McBee from the Baccile group contributed to these studies in terms of maintaining cell cultures and plating cells for experiments. Liposomes containing **2.1** or **2.2** were expected to enhance delivery of liposomes by chemically reacting with thiol moieties presented on cell surfaces, such as the Cys side chains of membrane-associated proteins. Such bioconjugation events can trigger cell entry pathways such as membrane fusion or pinocytosis. These experiments were conducted using human epithelial breast cancer cells (MDA-MB-231), which were incubated with liposomes containing either 99.92%, 90%, 75%, 60%, or 25% **2.1** or **2.2**, otherwise composed of Egg-PC, along with 0.08% Rd-PE as a fluorescent marker of liposome localization. Liposomes lacking **2.1** or **2.2** (replaced by PC) were employed as negative controls. Following 1 hr incubation, cells were washed with buffer, fixed with 4% paraformaldehyde, and stained with 4',6-diamidino-2-

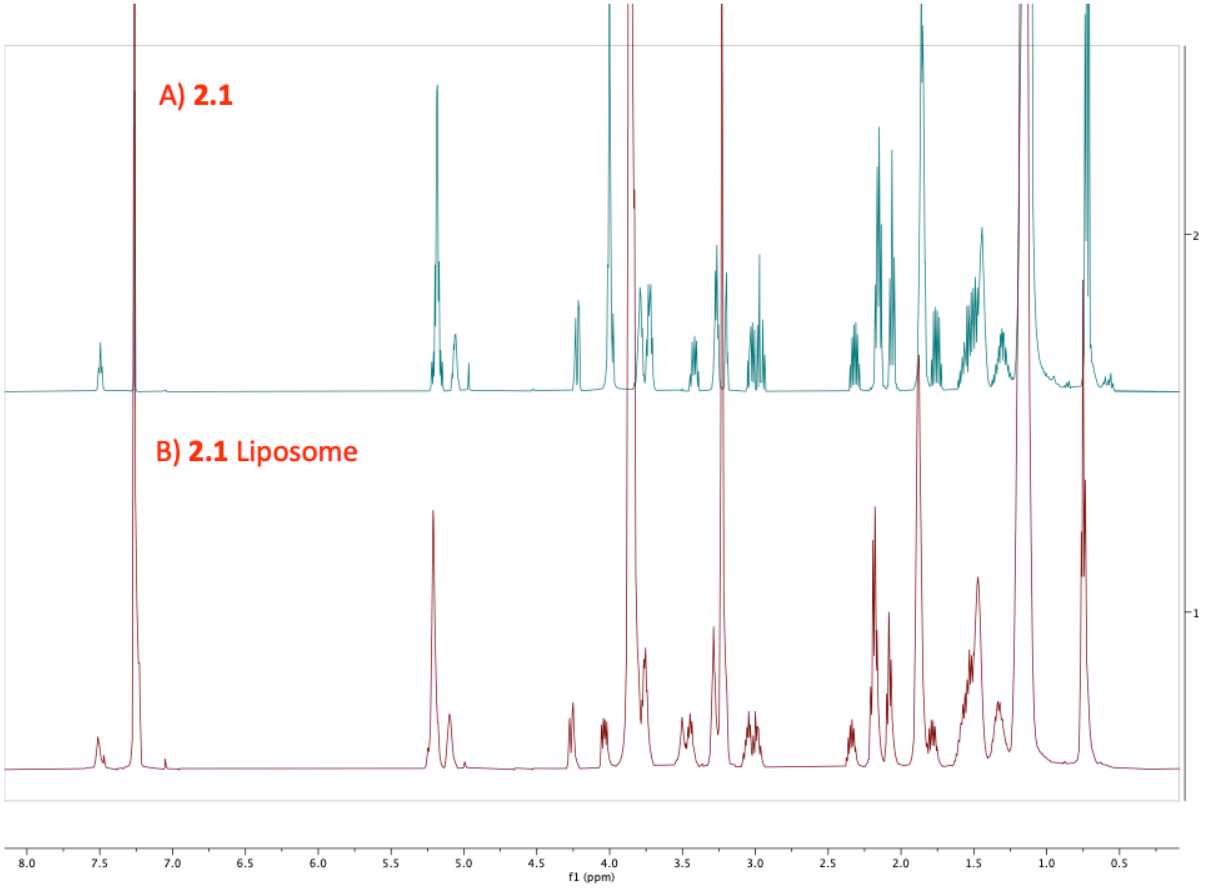


Figure 2.8 H-NMR analysis for liposomes composed of 100% 2.1 before and after liposome formation. Liposomes were prepared at 2 mM and water was removed before re-dissolving the mixture in $CD_3OD/CDCl_3$ 20/80 v/v for NMR analysis. NMR spectra showed that **2.1** remained intact after liposome formation. Trace A: **2.1** standard; Trace B: **2.1** solubilized after forming 100% **2.1** liposomes.

phenylindole (DAPI). Fluorescence microscopy was used to image cells and evaluate the presence of Rd-PE resulting from liposome uptake. Cell-associated Rd-PE fluorescence was quantified using Gen5 software. Representative images show that cells treated with liposomes containing 99.92% **2.1** or **2.2** (Figure 2.9A, Figure 2.9F) exhibited dramatically enhanced fluorescence (Rd-PE, red), followed by a decrease in delivery corresponding to the percentage of **2.1** or **2.2** in the liposome formulation: 90% **2.1** or **2.2** (Figure 2.9B, Figure 2.9G), 75% **2.1** or **2.2** (Figure 2.9C, Figure 2.9H), 60% **2.1** or **2.2** (Figure 2.9D, Figure 2.9I), 25% **2.1** or **2.2** (Figure 2.9E, Figure 2.9J). Cells treated with PC control liposomes lacking **2.1** showed only DAPI stain (Figure 2.10).

2.8.2. Quantification of cellular delivery

The Rd-PE quantification calculated from 4X images (Figure 2.11, Figure 2.12) shown in Figure 2.13 further demonstrates dose-dependent **2.1** and **2.2** delivery enhancement, with RFU readings for **2.1** and **2.2** liposomes, respectively, at ~15,700 and ~16,000 for 99.92% CDL liposomes, ~8,400 and ~8,400 for 90% CDL liposomes, ~5,000 and ~6,800 for 75% CDL liposomes, ~4,200 and ~6,000 for 60% CDL liposomes, ~3,300 and ~4,600 for 25% CDL liposomes, ~3,200 for PC control liposomes, and ~2,300 for cells that did not receive any liposome treatment (NT). When background fluorescence is accounted for, there was more than a fourteen-fold increase in fluorescence between the cells treated with 99.92% **2.1** or 99.92% **2.2** liposomes, compared to PC control liposomes. There was significant increase in delivery of **2.2** liposomes compared to equimolar amounts of **2.1** at molar percentages of 25%, 60%, and 75%, which could be due to the increased reactivity of the AA disulfide compared to the LA disulfide. Differences in cellular delivery between **2.1** and **2.2** liposomes at higher percentages (≥ 90%) were not found to be statistically different ($p > 0.5$) which can be attributed to the enhanced activities at these percentages. Due to the similarity of 25% **2.1** liposomes to PC control readings, delivery enhancement appears to be negligible at that percentage.

2.9. MTS cellular viability assay

Cell viability in the presence of liposomes containing **2.1** and **2.2** was also measured via a 3-(4,5-dimethylthiazol-2-yl)-5-(3-carboxymethoxyphenyl)-2-(4-sulfophenyl)-2H-tetrazolium, inner salt

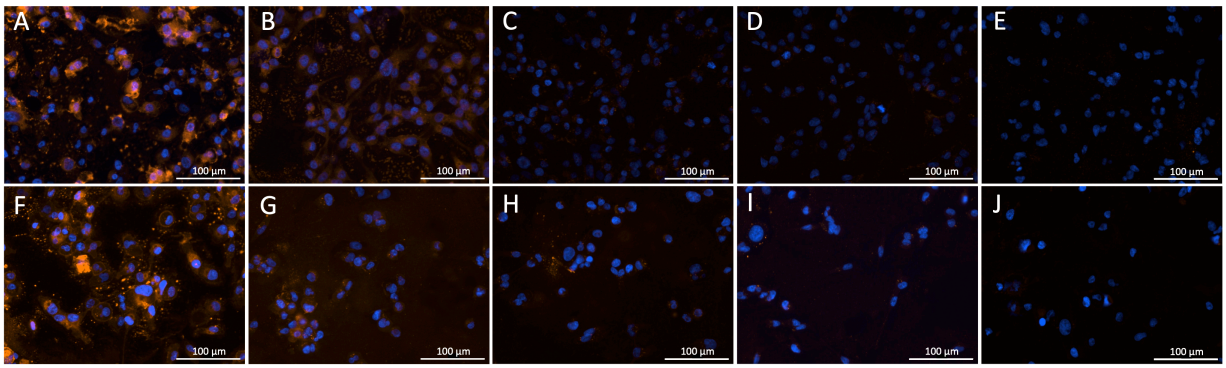


Figure 2.9 Enhanced liposomal delivery to MDA-MB-231 cells driven by 2.1 and 2.2. Representative 20X images show MDA-MB-231 cells treated with liposomes containing 0.08% Rd-PE and (A) 99.92% **2.1**, (B) 90% **2.1**, (C) 75% **2.1**, (D) 60% **2.1**, (E) 25% **2.1**, (F) 99.92% **2.2**, (G) 90% **2.2**, (H) 75% **2.2**, (I) 60% **2.2**, (J) 25% **2.2**, with the remainder of the liposome composed of Egg-PC. Images demonstrate that **2.1** and **2.2** enhanced delivery to cells in a manner that is dependent on the percentage of CDL in the liposome formulation, as indicated by Rd-PE fluorescence. The scale bars depict 100 µm. DAPI is shown in blue. Rd-PE is shown in red.

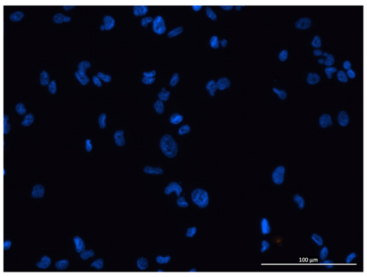


Figure 2.10 PC control liposomal delivery to MDA-MB-231 cells. Representative 20X image shows MDA-MB-231 cells treated with liposomes containing 0.08% Rd-PE and 99.92% Egg-PC. The scale bar depicts 100 µm. DAPI is shown in blue. Rd-PE is shown in red.

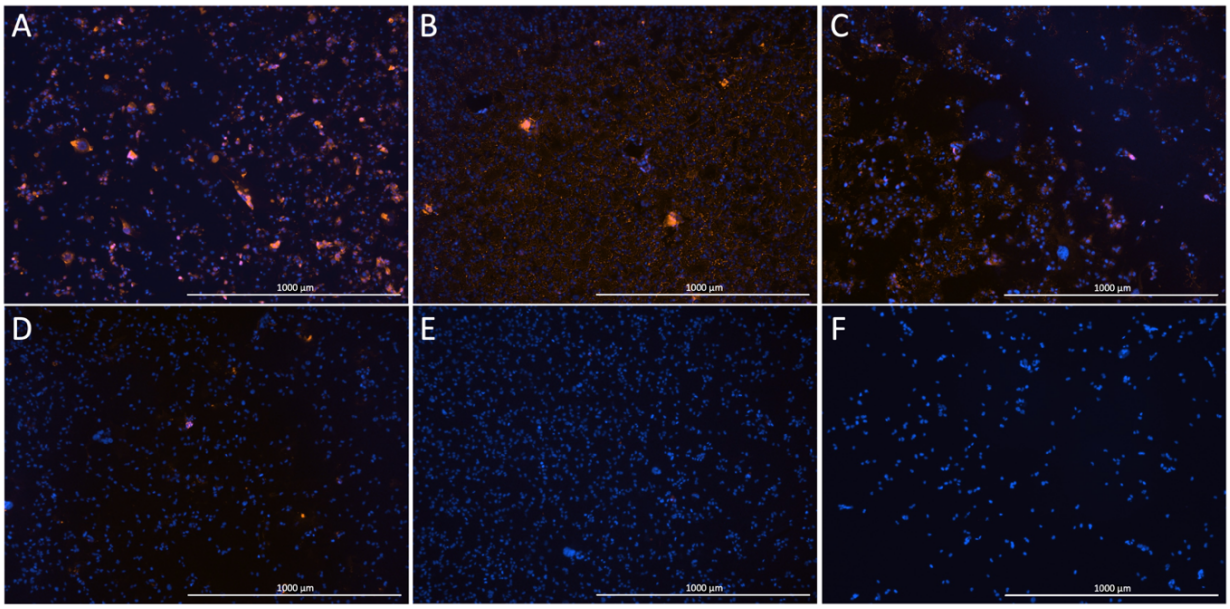


Figure 2.11 2.1 Liposomal enhanced delivery to MDA-MB-231 cells. Representative 4X images show MDA-MB-231 cells treated with liposomes containing and (A) 99.92% **2.1**, (B) 90% **2.1**, (C) 75% **2.1**, (D) 60% **2.1**, (E) 25% **2.1**, or (F) 0% **2.1** with 0.08% Rd-PE and the remainder of the liposome composed of Egg-PC. Images demonstrate that **2.1** enhanced delivery to cells in a manner dependent on the percentage of **2.1** in the liposome formulation, as indicated by Rd-PE fluorescence. The scale bars depict 1000 µm. DAPI is shown in blue. Rd-PE is shown in red.

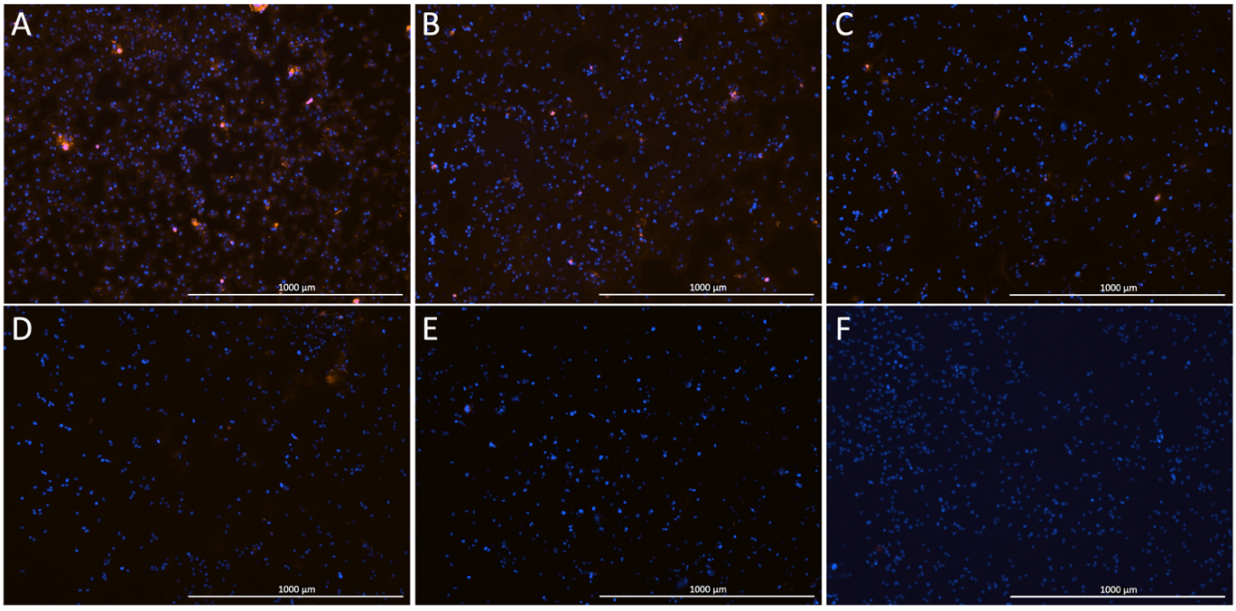


Figure 2.12 2.2 Liposomal enhanced delivery to MDA-MB-231 cells. Representative 4X images show MDA-MB-231 cells treated with liposomes containing and (A) 99.92% **2.2**, (B) 90% **2.2**, (C) 75% **2.2**, (D) 60% **2.2**, (E) 25% **2.2**, or (F) 0% **2.2** with 0.08% Rd-PE and the remainder of the liposome composed of Egg-PC. Images demonstrate that **2.2** enhanced delivery to cells in a manner dependent on the percentage of **2.2** in the liposome formulation, as indicated by Rd-PE fluorescence. The scale bars depict 1000 µm. DAPI is shown in blue. Rd-PE is shown in red.

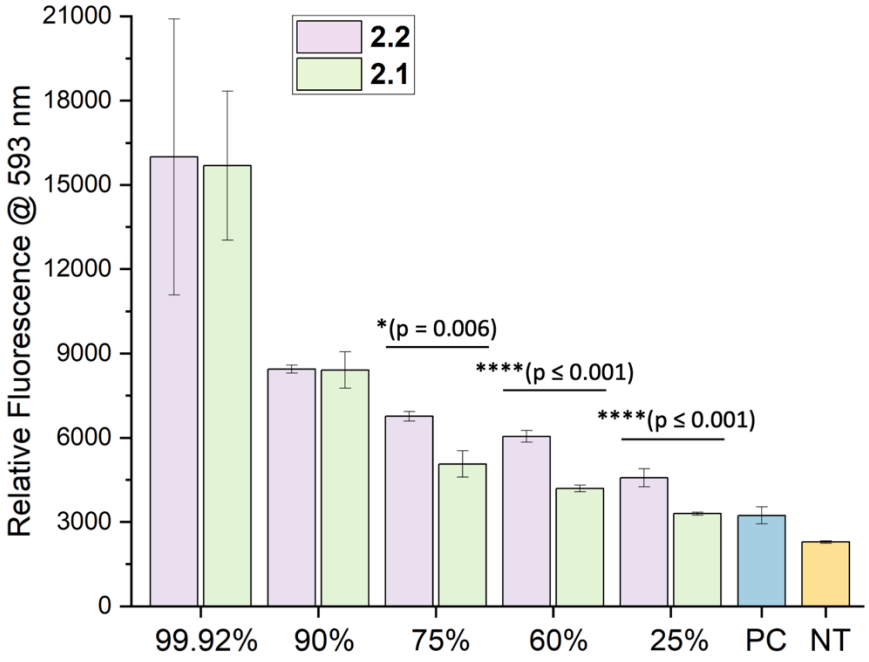


Figure 2.13 Quantification of liposomal enhanced delivery to MDA-MB-231 cells. Quantification shows Rd-PE fluorescence from cells treated with Rd-PE labeled liposomes containing 99.92% **2.1** (green) or **2.2** (purple), 90% **2.1** or **2.2**, 75% **2.1** or **2.2**, 60% **2.1** or **2.2**, 25% **2.1** or **2.2**, PC control liposome, or no treatment (NT). As shown, **2.1** and **2.2** enhanced delivery to cells in a manner that is dependent on the percentage of CDL in the liposome. Statistical analysis (*t* test) indicates that there is a significant increase in uptake of **2.2** liposomes compared to **2.1** liposomes at percentages of 25% ($p = 1.3 \times 10^{-6}$), 60% ($p = 3.3 \times 10^{-4}$), and 75% ($p = 0.006$). N = 6-8. Error bars represent standard errors of at least three replicates.

(MTS) assay using 0%, 25%, 60%, 75%, 90%, and 100% **2.1** or **2.2** liposomes at concentrations of 0.0016, 0.008, 0.04, 0.2, and 1 mM. Our results showed minimal changes in cell growth in all samples, which indicates that CDL liposomes do not cause cytotoxicity (Figure 2.14A-B).

2.10. Development of alternative lipid structure for cyclic disulfide liposomes

2.10.1. Design of alternative disulfide lipid

In a slightly different design, lipid **2.3** was synthesized by introducing a tetraethylene glycol (TEG) linker in between the disulfide headgroup and the triazole lipid backbone. Synthesis of **2.3** was performed in collaboration with Dr. Jinchao Lou in our group. Two hydrophobic alkyl tails were included so that the compound will be incorporated into the lipid bilayer. The presence of the hydrophilic TEG linker is designed to encourage the disulfide ring to be accessible on the liposome membrane surface in order to improve surface conjugation. This linker also provides distance between the liposome surface and the disulfide binding unit to enhance thiol conjugation ability. Following lipid formation, we moved on to the evaluation of thiol conjugation properties of the liposomes containing **2.3**.

2.10.2. Microplate-based liposome Biotin-PEG-SH assay with alternative lipid

Following **2.3** creation, we moved on to study the ability of the lipid to facilitate liposome membrane functionalization via disulfide exchange with free thiols. To accomplish this, a two-step assay was developed in which reaction with a functionalized thiol was evaluated using a microplate immobilization strategy. This assay was similar to the immobilization assay used for **2.1** and **2.2**, but with slightly adjusted protocol. Similar to the previous assay, this assay exploited protocols our group previously developed for immobilizing intact liposomes that include biotinylated lipids onto streptavidin-coated microplates.[242] The assays differ because in this version, Biotin-PEG-SH is first immobilized onto streptavidin-coated microplates, yielding a thiol-coated surface, instead of being first intubated with disulfide liposome solution. This surface coating method proved more successful with **2.3** liposomes compared to the pre-incubation method. In the first assay step, Biotin-PEG-SH (1K, 10 mM) was incubated on a streptavidin-coated microplate to allow for Biotin-PEG-SH immobilization on the plate (Figure 2.15A). In the

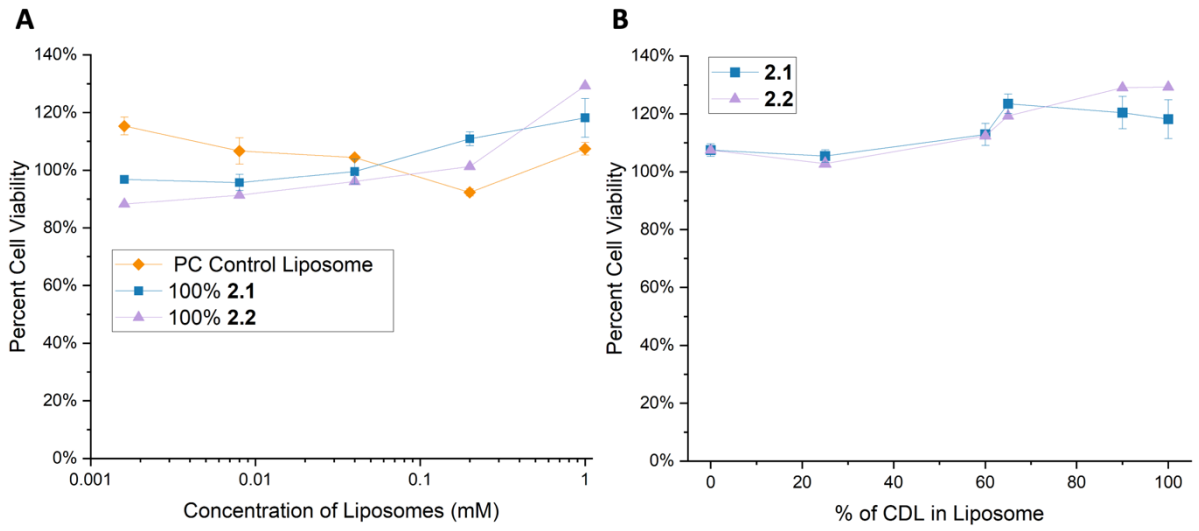
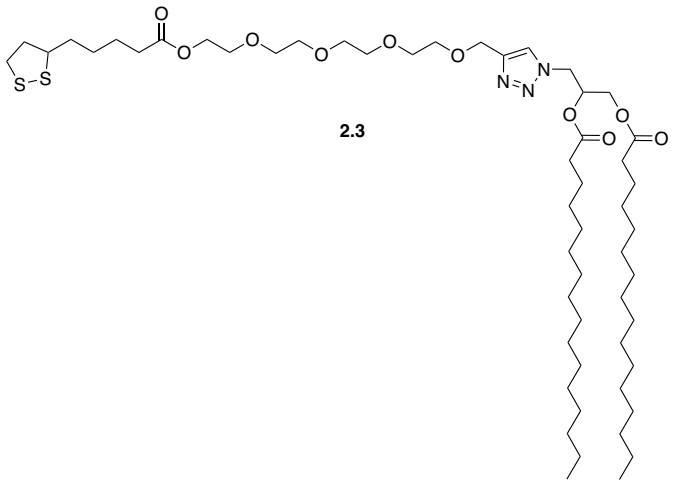


Figure 2.14 MTS assay to assess cell viability of MDA-MB-231 cells after liposome treatment. MTS assay indicates CDL liposomes do not affect cell viability. (A) MDA-MB-231 cells treated with 0.0016, 0.008, 0.04, 0.2, and 1 mM of liposomes composed of 100% PC (PC Control), 100% **2.1**, or 100% **2.2**. (B) MDA-MB-231 cells were treated with 1 mM of liposomes composed of either 0%, 25%, 60%, 75%, 90%, or 100% **2.1** or **2.2**. Cells were incubated with liposomes for 1 hr, washed and incubated for 24 hr, after which MTS reagent was used to assess cell viability. Viability of 100% corresponds with cells treated with buffer only. Error bars represent standard errors of at least three replicates.



Scheme 2.4 Design of alternative disulfide lipid 2.3. Lipid **2.3** includes two hydrophobic alkyl tails to allow the compound to be incorporated into the lipid bilayer, and a hydrophilic TEG linker was designed to improve surface conjugation via (1) encouraging the disulfide ring to be accessible on the liposome membrane surface, and (2) providing distance between the liposome surface and the reactive disulfide unit.

second step, various concentrations of liposomes (0 - 800 µM) formulated with varying percentages (0 - 30%) of **2.3** and fluorescently labeled with 1% Rd-PE were incubated on the microplate to allow for disulfide conjugation and liposome surface functionalization (Figure 2.15B). Rigorous washes were performed after each step to remove unbound Biotin-PEG-SH and/or liposomes, after which fluorescence measurements were acquired to detect liposomes that were successfully functionalized and immobilized onto the microplate surface.

To perform this assay, liposomes were initially prepared composed of either 0%, 5%, 10%, 20%, or 30% **2.3**, 1% Rd-PE, and the remainder Egg-PC (99%, 94%, 89%, 79%, or 69%, respectively). Liposomes were prepared through traditional thin-film preparation techniques including thin-film formation, hydration, freeze-thaw cycling, and extrusion through 200 nm membranes to form uniform liposomes of desired size. Then, 10 mM Biotin-PEG-SH was allowed to incubate on the streptavidin-coated microplates to allow for biotin immobilization to create a thiol-coated surface. After washing away any unbound Biotin-PEG-SH, 0 - 800 µM liposome solutions were incubated on the microplate to allow for disulfide conjugation and immobilization on the microplate. After washing away any unbound liposomes from the plate, immobilization was assessed via increases in Rd-PE fluorescence. As seen in Figure 2.15C, surface conjugation was shown to be dependent on the percentage of **2.3** incorporated within the liposomes (RFU at 800 µM = 0% **2.3**, ~ 13,800; 5% **2.3**, ~ 24,300; 10% **2.3**, ~ 30,200; 20% **2.3**, ~ 47,400; 30% **2.3**, ~ 56,000). Liposomes containing 30% **2.3** showed the greatest extent of liposome immobilization driven by disulfide conjugation.

2.10.3. Microplate-based liposome Rhodamine-PEG-SH assay with alternative lipid

After analyzing liposome membrane conjugation with Biotin-PEG-SH, we next designed an assay to assess membrane functionalization with a thiol tagged fluorophore. To accomplish this, a two-step assay was developed in which reaction with a rhodamine functionalized thiol was evaluated using a microplate immobilization strategy. Similarly to previous assays, this assay exploited protocols our group previously developed for immobilizing intact liposomes that include biotinylated lipids onto streptavidin-coated microplates.[242] In the first step, liposomes

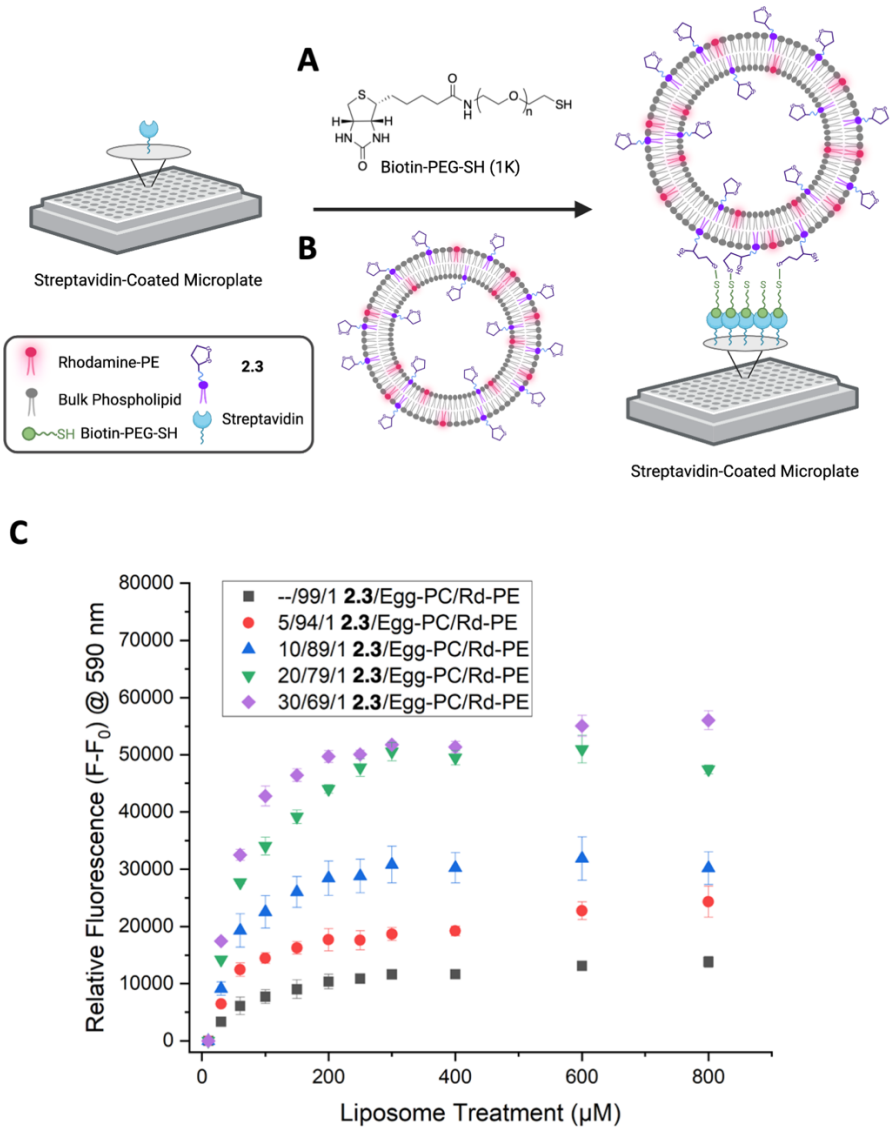


Figure 2.15 Analysis of surface thiol conjugation of 2.3 liposomes. (A) Biotin-PEG-SH was first incubated on a streptavidin-coated microplate to allow for immobilization. (B) Then, **2.3** liposomes were incubated on the microplate to allow for disulfide conjugation. (C) Liposome formulations containing different percentages of **2.3** lipid (0 - 30%), 1% rhodamine-PE, and the remainder Egg-PC were incubated on a thiol-coated microplate. Immobilization is assessed toward increase in Rd-PE fluorescence, and surface conjugation was shown to be dependent on the percentage of **2.3** lipid in the liposomes with 30% **2.3** having the highest conjugation and 0% **2.3** the lowest. Error bars represent standard errors of at least three replicates.

formulated with varying percentages of **2.3** and 1% biotin labeled phosphatidylethanolamine (18:1 Biotinyl Cap PE (1,2-dioleoyl-*sn*-glycero-3-phosphoethanolamine-*N*-(cap biotinyl) (sodium salt)) (Biotin-cap-PE) were incubated with Rhodamine-PEG-thiol reagent (Rd-PEG-SH, MW 1K) to allow for disulfide conjugation and liposome surface fluorescence tag functionalization (Figure 2.16A). In the second step, the resulting liposomes were incubated with streptavidin-coated microplates, and rigorous washes were performed to remove unbound liposomes and/or Rd-PEG-SH, after which fluorescence measurements were acquired to detect liposomes that were successfully fluorescently tagged and immobilized onto microplate surfaces (Figure 2.16B).

To perform this assay, liposomes were initially prepared composed of either 0% or 30% **2.3**, 1% Biotin-cap-PE, and the remainder Egg-PC (99%, or 69%, respectively). Liposomes were prepared through traditional thin-film preparation techniques including thin-film formation, hydration, freeze-thaw cycling, and extrusion through 200 nm membranes to form uniform liposomes of desired size. Then, 0.5 mM liposome solutions were incubated with various concentrations of Rd-PEG-SH (0 µM, 0.1 mM, 0.5 mM, 1 mM, 3 mM, 5 mM) to allow for disulfide conjugation and surface functionalization. The samples were incubated on streptavidin-coated microplates to allow for biotin immobilization of the functionalized liposomes. After washing away any unbound liposomes from the plate, fluorescence tagging was assessed via increases in Rd-PE fluorescence. As seen in Figure 2.16C, surface conjugation was shown to increase with the presence of **2.3** incorporated within the liposomes (RFU at 5 mM Rd-PEG-SH = 0% **2.3**, ~ 45,800; 30% **2.3**, ~ 115,700). Liposomes containing 30% **2.3** did show the greatest extent of fluorescence tagging driven by disulfide conjugation; however, at the highest fluorescence (5 mM Rd-PEG-SH treatment) there was only an approximate ~2.5-fold increase in fluorescence functionalization in the liposomes containing 30% **2.3** compared to liposomes lacking **2.3**.

A possible drawback to this assay could be that once the Rd-PEG-SH compounds are conjugated onto liposomes, the bulky PEG surrounding the liposome surface may make it harder for the biotin tag to be accessed and bind to the streptavidin-coated microplate. Because of that, we

may not be able to immobilize **2.3** containing liposomes that are conjugating more extensively to the Rd-PEG-SH since the fluorophore is blocking biotin binding. This could be causing a false depression in the fluorescence reading, when in reality the **2.3** containing liposome surface fluorescent tagging could be much higher.

2.10.4. DLS of liposomes containing alternative lipid 2.3

The successful preparation of uniform liposomes with formulations including synthetic lipid **2.3** was then probed. First, we employed DLS analysis to assess particle sizes of liposome formulations used in the microplate-based liposome Biotin-PEG-SH assay. These results showed that liposomes containing 0%, 5%, 10%, 20%, or 30%, or **2.3,** 1% Rd-PE, with the remainder Egg-PC (99%, 94%, 89%, 79%, or 69%, respectively) formed stable vesicles of sizes within the expected diameter range (100 - 200 nm) following extrusion (Figure 2.17A). Raw distribution curves are included in Figure 2.17B. Incorporation of 5 mol% **2.3** increased the average vesicle diameters by ~50 nm, but increasing the mol% from 10% - 30% caused small decreases in vesicle diameters. At all formulations, samples maintained average diameters below 200 nm, which is within the range that is beneficial due to the EPR effect. These data indicate that this synthetic CDL with TEG linker forms uniform liposomes at up to at least 30 mol% liposome incorporation.

2.10.5. TEM of alternative lipid

Next, lipid nanoparticle stability was again examined by electron microscopy (EM) experiments. Liposomes containing 30% **2.3** and 70% Egg-PC were negatively stained with PTA and imaged with TEM. The **2.3** liposomes presented with circular cross-sections exhibiting traditional morphology (Figure 2.18), which showed that vesicles with **2.3** lipid incorporation form stable liposomes.

2.10.6. Cellular delivery study with alternative lipid

We next assessed the ability of **2.3** to enhance the entry of liposomes into cells, similar to the studies performed with lipids **2.1** and **2.2**. These experiments were performed in collaboration with Dr. Joshua Baccile's lab in UTK Chemistry. Graduate student Dillon McBee from the Baccile

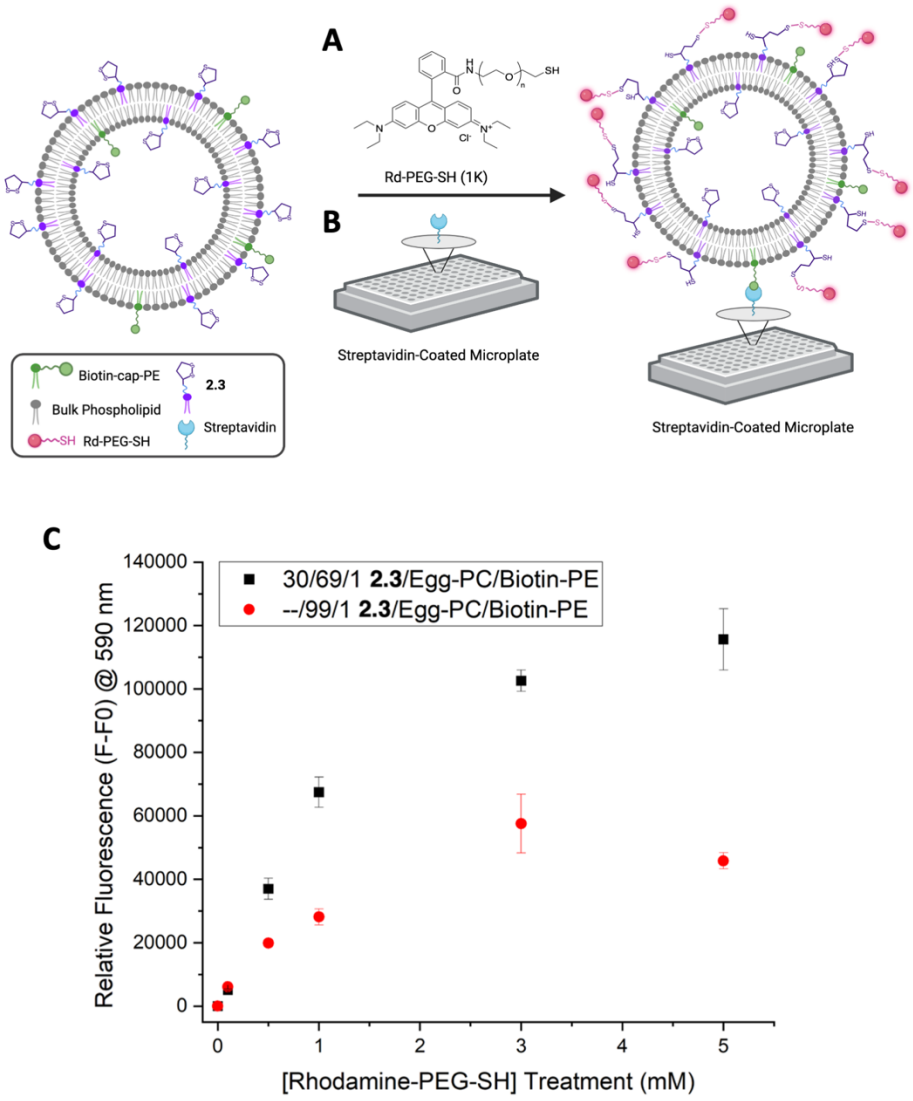


Figure 2.16 Analysis of surface thiol-fluorophore conjugation of 2.3 liposomes. (A) First, **2.3** liposomes were incubated with Rhodamine-PEG-thiol reagent to allow for disulfide conjugation. (B) Then, the liposomes were added to streptavidin-coated microplates, incubated, and washed. (C) Liposome formulations containing either 0% or 30% **2.3** lipid, 1% rhodamine-PE, 1% Biotin-cap-PE, and the remainder Egg-PC were studied. Surface functionalization with the fluorophore is assessed toward increase in Rd-PE fluorescence, and surface functionalization was shown to be increased with the presence of **2.3** lipid in the liposomes with 30% **2.3** having higher decoration than 0% **2.3**. Error bars represent standard errors of at least three replicates.

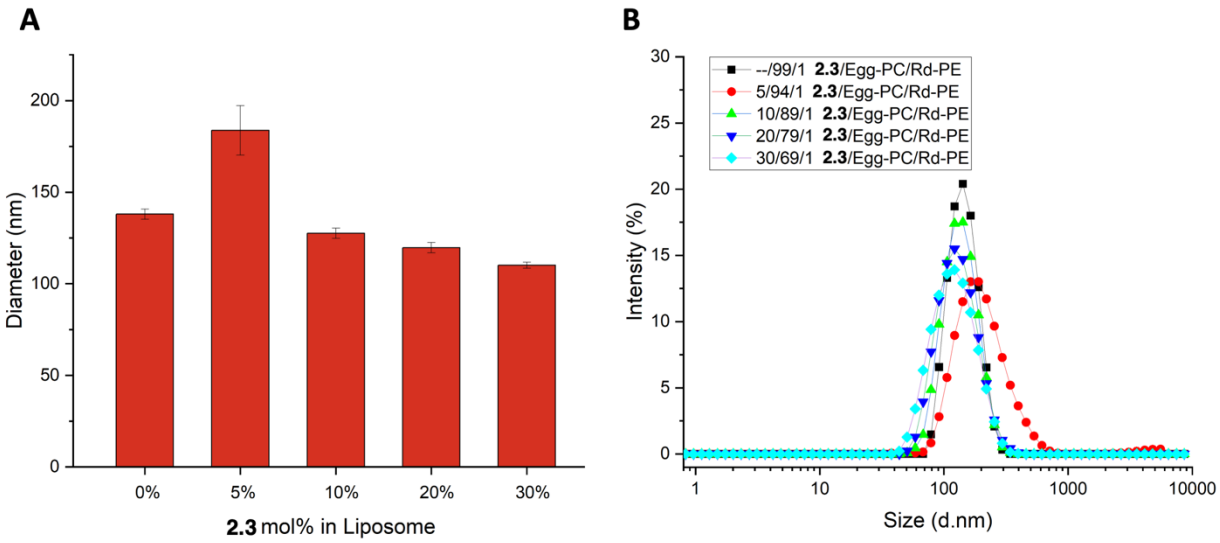


Figure 2.17 DLS results of 2.3 liposomes. (A) Liposomes containing either 0, 5%, 10%, 20%, or 30% **2.3,** 1% Rd-PE, and the remainder Egg-PC (99%, 94%, 89%, 79%, or 69%, respectively) were formed in uniform size in the expected size range of 100 - 200 nm. (B) DLS size distribution plots of the same liposome formulations. Error bars represent standard errors of at least three replicates.

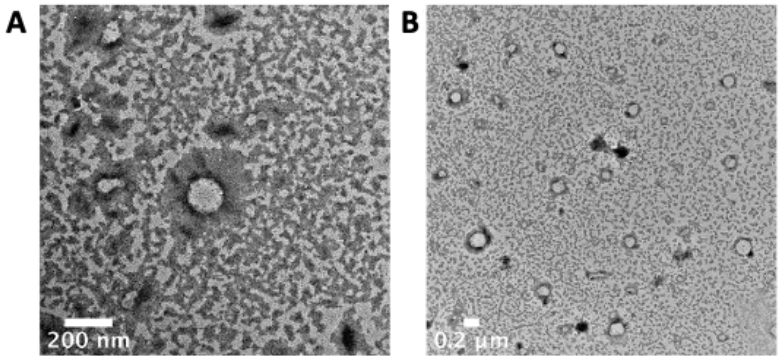


Figure 2.18 TEM results of 2.3 liposomes. TEM images of liposomes containing 30% **2.3** and 70% Egg-PC show a circular cross-section showing traditional liposome morphology. Liposomes were stained with 1.0% (w/v) solution of neutral PTA, and scale bars represent 200 nm.

group contributed to these studies in terms of maintaining cell cultures and plating cells for experiments. These experiments were conducted using human epithelial breast cancer cells (MDA-MB-231). Liposomes containing **2.3** were expected to enhance delivery of liposomes by chemically reacting with thiol moieties presented on cell surfaces, such as the Cys side chains of membrane-associated proteins, which can trigger cell entry pathways. Also, due to the results seen in the thiol-fluorophore conjugation assay (Figure 2.16), a similar experiment was attempted in which a cell targeting group, folic acid (FA), was appended to the liposome surface of **2.3** liposomes prior to their addition to cells. FA has been widely used as a cancer targeting group for the treatment and imaging of cancers due to the overexpression and random distribution of glycoprotein folate receptors (FRs) on a multitude of cancers of epithelial origin, including breast,[245] lung, kidney and ovarian cancers,[246] with up to 100–300 times higher expression (1–10 million receptor copies per cell)[247, 248] in carcinomas compared to healthy cells.[249] To perform this experiment, a compound in which folic acid was appended to a free thiol via a PEG linker (FA-PEG-SH, 2K) was purchased and pre-incubated at concentrations of 0 mM - 10 mM FA-PEG-SH with 1 mM of 20% or 30% **2.3** liposome. Liposomes were otherwise composed of Egg-PC, along with 0.08% Rd-PE as a fluorescent marker of liposome localization. After pre-incubation with FA-PEG-SH, liposomes were added to cells and incubated for 1 hr, followed by washing cells with buffer, fixing with 4% paraformaldehyde, and staining with DAPI. Fluorescence microscopy was used to image cells and evaluate the presence of Rd-PE resulting from liposome uptake. Images represent cells treated with 30% **2.3** liposome with no pre-treatment (Figure 2.19A), 0.05 mM or 0.25 FA-PEH-SH pre-treatment (Figure 2.19B-C) for 2 hr at rt, and 20% **2.3** liposome with 2 mM, 5 mM, or 10 mM FA-PEH-SH pre-treatment for 4 hr at 37C (Figure 2.19D-F). These representative images of MDA-MB-231 cells demonstrate that **2.3** did not enhance delivery to cells either alone or after conjugation with targeting group FA-PEG-SH, as indicated by lack of Rd-PE fluorescence.

2.11. Alternative microplate assay designs for CDLs 2.1 and 2.2

Prior to the success of the SH-PEG-Biotin conjugation assay, additional assay designs were developed in attempts to demonstrate thiol-mediated liposome membrane functionalization

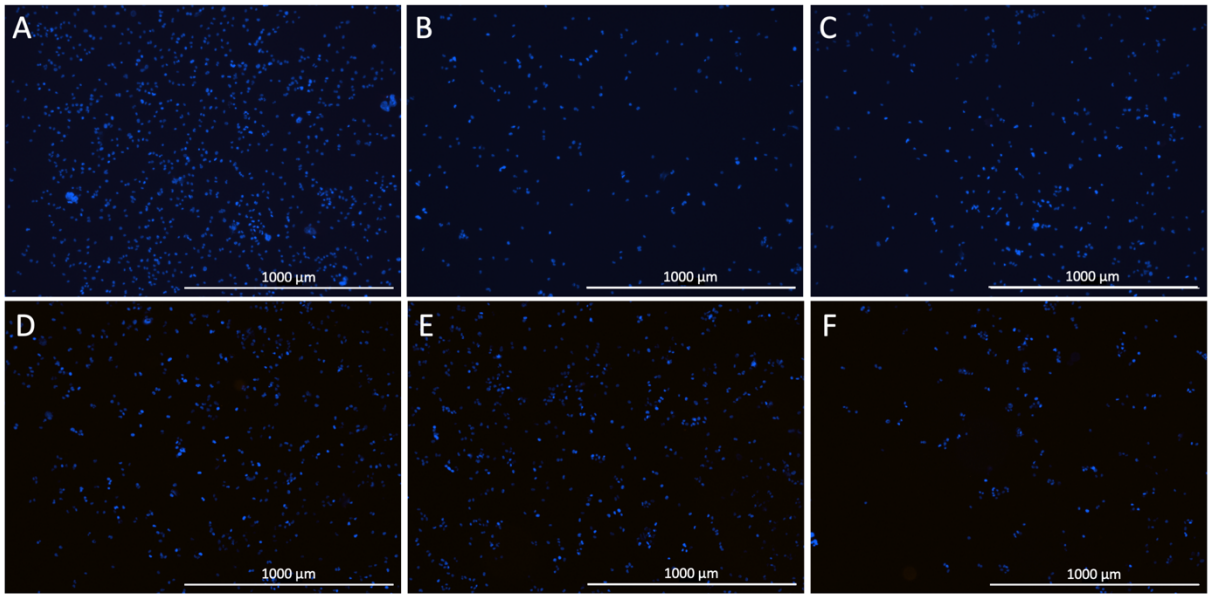


Figure 2.19 Attempted 2.3 liposomal delivery to MDA-MB-231 cells. Representative 4X images show MDA-MB-231 cells treated with 1 mM liposomes containing 30% **2.3** (0.3 mM) receiving either (A) no pre-treatment, or pre-incubation for 2 hr at room temperature (rt) with (B) 0.05 mM FA-PEG-SH or (C) 0.25 mM FA-PEG-SH. Liposomes were also prepared at 1 mM with 20% **2.3** (0.2 mM) and pre-incubated with (D) 2 mM FA-PEG-SH, (E) 5 mM FA-PEG-SH, or 10 mM FA-PEG-SH before addition to cells. The liposomes all contained 0.08% Rd-PE and the remainder of the liposome was composed of Egg-PC. All images demonstrate that **2.3** did not enhance delivery to cells either alone or after conjugation with targeting group FA-PEG-SH, as indicated by lack of Rd-PE fluorescence. The scale bars depict 1000 µm. DAPI is shown in blue. Rd-PE is shown in red.

with CDLs **2.1** and **2.2**. First, an immobilization assay was designed in which **2.1** liposomes were successfully immobilized onto a streptavidin microplate due to incorporation of 1% Biotin-cap-PE in the liposomes, although increasing the mol% of **2.1** in the liposome above 10% did result in lower immobilization efficiency. This assay was used as a precursor to other assay designs. Secondly, a thiol-fluorophore assay was developed as an attempt to demonstrate CDL-facilitated membrane decoration with a fluorescent tag. In this design, CDL liposomes composed of various percentages (0 - 99%) of **2.1** or **2.2** were first immobilized on a microplate via the previously mentioned Biotin-cap-PE immobilization technique. Then, various concentrations (0 - 5mM) of either SH-PEG-Fluorescein (SH-PEG-Fc, MW 1K) or SH-PEG-Rhodamine (SH-PEG-Rd, MW 1K) were introduced to the microplate wells and allowed to incubate and undergo thiol-disulfide conjugation between the CDL and free thiol of the fluorophore. In an alternative design, **2.1** or **2.2** liposomes (1% Biotin-cap-PE) were first incubated with SH-PEG-Rd or SH-PEG-Fc in vials at various pH (7.4, 8, 11), temperature (rt, 37°C, 50°C), and buffer types (phosphate-buffered saline (PBS) and 4-(2-hydroxyethyl)-1-piperazineethanesulfonic acid (HEPES) before addition to the microplate in order to allow for better mixing between the liposomes with the thiol-fluorophore and enhanced conjugation reaction conditions (pH and heat). However, these assays were not able to sufficiently demonstrate liposome membrane decoration with thiol-tagged fluorophores.

2.12. Conclusions

In conclusion, we have developed a multifunctional liposome platform based on LA and AA functionalized DOPE lipids, which achieves our two synergistic goals of enhancing liposomal cell delivery as well as thiol-mediated liposome membrane functionalization. CDLs were capable of forming stable liposomes at up to 100% molar percentage of the liposome formulation and were effective for thiol derivatization resulting in surface modification. Liposome cell infiltration was also studied, and the results show that CDL liposomes dramatically enhanced cell delivery to mammary adenocarcinoma cells. This multifunctional liposome system could provide notable nanocarriers for facile decoration and efficient therapeutic cargo delivery to cancer tissues based on cell surface thiols. While additional studies are needed to explore the therapeutic applications of these liposome systems, these results demonstrate that cyclic disulfide liposomes could serve

Table 2.1 Summary of microplate assay designs and treatments explored for CDL 2.1 and 2.2 membrane decoration with thiol-tagged fluorophore.

Entry	Lipid	Mol%	Assay Protocol	Fluorophore Type, []	Incubation Time, Temp	Buffer Type, pH
1	**2.1**	0-10%	1. Liposome immobilization onto plate (500 μM) 2. Incubate 2 hr, wash 3. Add SH-PEG-Fluorophore to wells 4. Incubate 1 hr, wash, analyze	SH-PEG-Fc 0-5 mM	1 hr, rt	PBS pH 8
2	**2.2**	0-99%		SH-PEG-Rd 0-0.5 mM	2 hr, rt	PBS pH 8
3	**2.1**	0-50%	1. Liposome incubation with SH-PEG-Fluorophore (various times) 2. Immobilization onto plate (500 μM) 3. Incubate 1 hr, wash, analyze	SH-PEG-Fc 0-1 mM	1 hr, rt	PBS pH 8
4	**2.1**	0-10%		SH-PEG-Fc 0-0.5 mM	1 hr, rt or 50°C	PBS pH 8 or 10
5	**2.1**	0-99%		SH-PEG-Rd 5 mM	12 hr, rt	PBS pH 8
6	**2.2**	0-99%		SH-PEG-Rd 5 mM	12 hr, rt	PBS pH 8
7	**2.1**	0-99%		SH-PEG-Rd 2 mM	12 hr, rt	HEPES (1mM) pH 7.4
8	**2.2**	0-99%		SH-PEG-Rd 2 mM	12 hr, rt	HEPES (1mM) pH 7.4

as a promising nanotechnology platform for cellular delivery. Future work will be aimed at continuing to enhance the activity and sensitivity of the disulfide headgroup to further amplify the liposomal membrane functionalization and cellular delivery.

2.13. Synthesis and experimental procedure

General experimental

Reagents and solvents were generally purchased from Sigma-Aldrich or Fisher Scientific and used as received. SH-PEG-Biotin (MW = 1K) and Rhodamine B-PEG-Thiol (Rd-PEG-SH) (MW = 1K) were purchased from Biopharma PEG Scientific Inc. (Watertown, MA). Pierce™ streptavidin-coated high-capacity plates (Black, 96-Well) were purchased from Thermo-Fisher Scientific. Egg-PC (L-α-phosphatidylcholine, mixed isomers from chicken eggs), Rd-PE (L-α-phosphatidylethanolamine-*N*-(lissamine rhodamine B sulfonyl) (ammonium salt)), and 18:1 Biotinyl Cap PE (Biotin-cap-PE) (1,2-dioleoyl-*sn*-glycero-3-phosphoethanolamine-*N*-(cap biotinyl) (sodium salt)) were purchased from Avanti Polar Lipids, Inc. (Alabaster, AL). Dry solvents were obtained from a Pure Solv MD-7 solvent delivery system purchased from Innovative Technologies, Inc. Column chromatography was performed using 230 – 400 mesh silica gel purchased from Sorbent Technologies (Norcross, GA). NMR spectra were obtained using a Varian 500 MHz spectrometer. Mass spectra were obtained with JEOL DART-AccuTOF and Waters Synapt G2-Si mass spectrometers (Milford, MA). Liposome extruder and polycarbonate membranes were obtained from Avestin (Ottawa, Canada). Water for liposome preparation and assays was purified via a Millipore water system (≥18 MW·cm triple water purification system). Small quantities (<5 mg) were weighed on a Mettler Toledo XS105 dual range analytical balance. DLS measurements were performed using a Malvern Zetasizer Nano ZS instrument equipped with a He-Ne 633 nm laser and a temperature controller at a scattering angle of 173°. Plots were generated using Origin Pro 2022. Fluorometric analysis was performed using Gen5 software and Cytation 1 Cell Imaging Multimode Microplate Reader (BioTek Instruments, Winooski, VT) with an RFP filter (Ex 531 / Em 593 nm) and DAPI filter (Ex 377 / Em 447 nm). All error bars in plots show the standard errors of at least three experimental replicates.

Preparation of liposomes for biotinylation microplate assay

Stock solutions of 5 mM **2.1, 2.2**, and **2.3**, 0.5 mM Rd-PE, and 32.46 mM Egg-PC were prepared in chloroform and were stored at −20 °C after preparation. To prepare liposomes, a thin film was created by pipetting the appropriate volumes of the stock solution of each lipid component into a clean vial according to calculations to obtain a mixture of 2 mM of total lipid content with the desired molar percentage of each component. As an example, for 200 µL of 2 mM liposomes composed of 50% **2.1**, 49% PC, and 1% Rd-PE, 40 µL **2.1** stock (200 nmol), 6 µL Egg-PE stock (196 nmol), and 8 µL Rd-PE stock (4 nmol) were combined. A nitrogen stream was then used to evaporate the solvent and the resulting lipid film was subsequently dried for at least 1 hr under vacuum. Then, the lipids were hydrated with 1 mM HEPES (pH = 7.4) at 60 °C in a water bath for 3 sets of 20 min with vortexing after each set. Liposomes then underwent 10 freeze-thaw cycles between a -80 °C dry ice-acetone bath and a 60 °C water bath, and vortexing was performed at a low speed between each cycle. Last, the liposome solutions were extruded through a 200 nm membrane filter for 15 passes using a LiposoFast extruder (Avestin, Inc.) and were stored at 4 °C for use within 1 day.

Disulfide liposome 2.1 and 2.2 biotinylation microplate assay

Microplate liposome immobilization experiments were performed using black streptavidin-coated 96-well microplates. The wash buffer that was used was 1 mM HEPES, pH 7.4. Liposomes were prepared according to the procedure above composed of 0%, 5%, 10%, 30%, 50%, 75%, and 99% **2.1** or **2.2**, 1% Rd-PE, and the remainder Egg-PC (99%, 94%, 89%, 69%, 49%, 24% or 0%, respectively) at a concentration of 1 mM. For the first step of the assay, a stock solution of 50 mM Biotin-PEG-SH (MW 1K) was prepared consisting of 45 mg Biotin-PEG-SH dissolved in 900 µL buffer. A stock solution of 0.5 M IAM was created by dissolving 9.248 mg IAM in 100 µL buffer. To begin the assay, liposomes and Biotin-PEG-SH were diluted in a vial to achieve 150 µL of solution containing 500 µM of liposome and 5 mM Biotin-PEG-SH. To accomplish this, 75 µL of 1 mM liposome, 15 µL of 50 mM Biotin-PEG-SH, and 60 µL of buffer were combined. These solutions were then incubated at 37 °C in a water bath for 2 hr. In experiments in which IAM was used, 2.1 µL of a 0.5 M IAM solution was then added to liposome solutions in place of buffer for

a final concentration of 7 mM and volume of 150 µL and incubated at rt for 30 min. Next, the microplate wells that were to be used for analysis were washed with 250 µL of wash buffer for 30 min. This was removed, followed by introduction of 100 µL of the appropriate liposome solution and then incubated for 1 hr. Next, these solutions were removed, and the wells were washed with 2 × 250 µL wash buffer for 3 minutes each with low shaking. Finally, 100 µL of MilliQ water was added to each well. The microplate was then analyzed for fluorescence using a microplate reader with excitation at 530 +/- 20 nm and emission wavelength of 590 +/- 20 nm. The RFU was determined according to the equation below where F_0 is the fluorescence measurement of 500 µM liposome containing 0% CDL treatment on the microplate, and F is the fluorescence measurement at 590 nm of the corresponding liposome treatment (5%, 10%, 30%, 50%, 75%, and 99% **2.1** or **2.2**). RFU @ 590 nm = ($F - F_0$). Replicates were performed using at least 3 batches of liposomes.

Disulfide liposome 2.3 biotinylation microplate assay

Microplate liposome immobilization experiments were performed using black streptavidin-coated 96-well microplates. The wash buffer that was used was 1 mM HEPES, pH 7.4. Liposomes were prepared according to the procedure above composed of 0%, 5%, 10%, 20%, or 30% **2.3**, 1% Rd-PE, and the remainder Egg-PC (99%, 94%, 89%, 79%, 69%, respectively) at a concentration of 800 µM. For the first step of the assay, a solution of 10 mM Biotin-PEG-SH (MW 1K) was prepared consisting of 22 mg Biotin-PEG-SH dissolved in 2.2 mL buffer. Next, the microplate wells that were to be used for analysis were washed with 250 µL of wash buffer for 30 min. To begin the assay, 100 µL of the 10 mM Biotin-PEG-SH solution was added to each microplate well and incubated at rt for 1 hr. Next, these solutions were removed, and the wells were washed with 3 × 250 µL wash buffer for 3 minutes each with low shaking. Liposomes were diluted with buffer in the appropriate microplate wells to achieve 100 µL of solution containing either 0 µM, 10 µM, 30 µM, 60 µM, 100 µM, 150 µM, 200 µM, 250 µM, 300 µM, 400 µM, 600 µM, or 800 µM of liposome. These solutions were then added incubated in the microplate at rt for 12 hr. Next, these solutions were removed, and the wells were washed with 2 × 250 µL wash buffer for 3 minutes each with low shaking. Finally, 100 µL of MilliQ water was added to each well. The microplate was then

analyzed for fluorescence using a microplate reader with excitation at 530 +/- 20 nm and emission wavelength of 590 +/- 20 nm. The RFU was determined according to the equation below where F_0 is the fluorescence measurement at 590 nm 0 μM liposome treatment (buffer only) on the microplate, and F is the fluorescence measurement at 590 nm of the corresponding liposome treatment at the associated concentration treatment (either 10 μM, 30 μM, 60 μM, 100 μM, 150 μM, 200 μM, 250 μM, 300 μM, 400 μM, 600 μM, or 800 μM). RFU @ 590 nm = ($F – F_0$). Replicates were performed using at least 3 batches of liposomes.

Disulfide liposome 2.3 fluorophore conjugation microplate assay

Microplate liposome immobilization experiments were performed using black streptavidin-coated 96-well microplates. The wash buffer that was used was 1x PBS pH 8. Liposomes were prepared according to the procedure above composed of 0%, or 30% **2.3**, 1% Biotin-PE, and the remainder Egg-PC (99% or 69%, respectively) at a concentration of 2 mM. For the first step of the assay, a stock solution of 50 mM Rd-PEG-SH (MW 1K) was prepared consisting of 10 mg Biotin-PEG-SH dissolved in 200 μL buffer. To begin the assay, liposomes and Biotin-PEG-SH were diluted in a vial to achieve 150 μL of solution containing 500 μM of liposome and various concentrations of Rd-PEG-SH (0 mM, 0.1 mM, 0.5 mM, 1 mM, 3 mM, 5 mM). These solutions were then incubated at rt for 2 hr. Next, the microplate wells that were to be used for analysis were washed with 250 μL of wash buffer for 30 min. This was removed, followed by introduction of 100 μL of the appropriate liposome solution and then incubated for 1 hr. Next, these solutions were removed, and the wells were washed with 2 × 250 μL wash buffer for 3 minutes each with low shaking. Finally, 100 μL of MilliQ water was added to each well. The microplate was then analyzed for fluorescence using a microplate reader with excitation at 530 +/- 20 nm and emission wavelength of 590 +/- 20 nm. The RFU was determined according to the equation below where F_0 is the fluorescence measurement of 500 μM liposome treated with 0 μM Rd-PEG-SH, and F is the fluorescence measurement at 590 nm of the corresponding liposome treatment (0%, or 30% **2.3**) treated with either 0.1 mM, 0.5 mM, 1 mM, 3 mM, or 5 mM Rd-PEG-SH. RFU @ 590 nm = ($F – F_0$). Replicates were performed using at least 3 batches of liposomes.

Dynamic light scattering (DLS) analysis of liposome size

DLS measurements were carried out with a Malvern Zetasizer Nano ZS instrument equipped with a 4.0 mW laser operating at l = 633 nm. Samples were prepared by diluting the liposome solutions before and after treatment 10 times with 1 mM HEPES pH 7.4. All samples were determined at a scattering angle of 173° at 20 °C. The data reported were the average of three tests with error bars indicating standard error.

Transition electron microscope (TEM) analysis

Liposomes (2 mM) were prepared according to the standard liposome preparation procedure mentioned above. For TEM studies, a drop (5−10 µL) of liposome solution was immobilized onto a thin carbon film supported by a 200-mesh copper grid (for 1 min) and then stained (for 1 min) with a 1.0% (w/v) solution of neutral PTA. After drying, the samples were stored in a desiccator overnight prior to examination. Images were collected using a JEOL 1400 Flash microscope operating with a beam energy of 80 keV and associated Gatan One View camera and processed with ImageJ software. Scale bar on image denotes 200 nm.

NMR analysis of 2.1 before and after liposome formation.

For analysis of free lipid, **2.1** was dissolved in a mixture of $CD_3OD/CDCl_3$ 20/80 (v/v) and 0.5 mL solution was transferred into an NMR tube for analysis. For NMR analysis of **2.1** after liposome formation, 0.5 mL of 2 mM liposomes composed of 100% **2.1** were prepared in PBS pH 7.4. The water was removed under reduced pressure and the vial was placed under vacuum for 1 hr. To prepare NMR samples, the residue was dissolved in 0.5 mL $CD_3OD/CDCl_3$ 20/80 (v/v), filtered through a PTFE filter, and transferred into an NMR tube for analysis. NMR spectra were analyzed by MestReNova.

MDA-MB-231 cell culture

Human epithelial breast cancer cells (MDA-MB-231) were obtained from ATCC (Manassas, VA). Cells were grown in 100 mm plates and then plated at 1×10^4 cells per well in a 96-well plate with clear flat bottom for cell delivery experiments. Cells were grown for 48 hr to reach 80%

confluency in Dulbecco's modified eagle medium (DMEM, Gibco) supplemented with 10% (v:v) fetal bovine serum (FBS, Gibco), 50 U/mL penicillin/streptomycin (Gibco). Incubation was performed at 37 °C under 5% CO_2 with 95% humidity.

MDA-MB-231 liposomal cell delivery experiments.

Lipid-dependent cell delivery was measured as previously described.[216] Briefly, liposomes containing 0.08% Rd-PE and 25%, 60%, 75%, 90%, or 99.92% **2.1** or **2.2**, with the rest of the liposome consisting of Egg-PC were prepared at 2 mM lipid concentration and diluted to 1 mM using PBS pH 7.4 containing 0.5 mM $MgCl_2$ and 0.9 mM $CaCl_2$ (PBS^{++}). At 80% confluence, cells were treated with 200 µL per well of the corresponding 1 mM liposome solutions and incubated for 1 hr at 37°C. Cells were washed two times with 200 µL PBS^{++} pH 7.4, then fixed for 30 min at 37 °C by addition of 100 µL per well of 4% paraformaldehyde. Then, cells were washed two times with 200 µL PBS^{++} pH 7.4 and stained with NucBlue™ Fixed Cell ReadyProbes™ Reagent (DAPI, Fisher Scientific). Fluorometric analysis was performed using Gen5 software and Cytation 1 Cell Imaging Multimode Microplate Reader (BioTek Instruments, Winooski, VT) with a red fluorescence protein (RFP) filter (Ex 531 / Em 593 nm) and DAPI filter (Ex 377 / Em 447 nm). Fluorescence microscopy images were acquired on the Cytation 1 Reader using 20X and 4X magnification which provided representative cell delivery images. Average RFP fluorescence units for each sample were determined from images taken at 4X magnification. Replicates were performed using at least 3 batches of liposomes.

Cell viability assay

Cell viability after liposome treatment was measured as previously described.[148] Liposomes (2 mM) containing 0% (PC control) or 25%, 60%, 75%, 90%, or 100% **2.1** or **2.2** without any content encapsulation were prepared using the standard liposome preparation procedure described above and diluted to 1 mM, 200 µM, 40 µM, 8 µM, 1.6 µM, or 0 µM liposomes using PBS^{++}. Cells were then treated with 100 µL per well of either the corresponding 1 mM solutions of liposomes (0%, 25%, 60%, 75%, 90%, or 100% **2.1** or **2.2**) or with the corresponding 200 µM, 40 µM, 8 µM, 1.6 µM, or 0 µM solutions of liposomes (0% or 100% **2.1** or **2.2**) and incubated for 1 hr at 37°C.

Cells were washed two times with 200 µL PBS^{++} pH 7.4 and incubated in 100 µL phenol free DMEM containing 10% FBS for 24 hr. Finally, 10 µL MTS reagent (Promega G3582) was added to each well, incubated for 1.5 hr, and 490 nm absorbance was measured using the Cytation 1 Cell Imaging Multimode Microplate Reader with Gen5 software. Replicates were performed using at least 3 batches of liposomes.

Chapter 3. Bis-Boronic Acid Liposomes for Carbohydrate Recognition and Cellular Delivery

A version of this chapter was originally published by Megan L. Qualls, et al.:

Qualls, Megan L.; Hagewood, Hannah; Lou, Jinchao; Mattern-Schain, Samuel I.; Zhang, Xiaoyu; Mountain, Deidra J.; Best, Michael D., Bis-Boronic Acid Liposomes for Carbohydrate Recognition and Cellular Delivery. *ChemBioChem* 2022, *23* (21), e202200402.

In Chapter 3, MLQ synthesized and characterized all bis-boronic acid lipids. MLQ performed all liposome preparation, designed and performed all microplate-based assays, and completed all DLS and TEM analysis. HH assisted with dextran binding assay and mucin competition binding assay analysis. SIM prepared VSMC cells for liposome analysis and performed cellular delivery, quantification, and SRB delivery. XZ contributed to the design of the bis-boronic acid lipids. MLQ, JL, SIM, DJM, and MDB contributed to the writing of the manuscript. MDB directed the project.

Additional experiments in Chapter 3 include contributions from collaborators Dillon P. McBee, Dr. Joshua A. Baccile, Dr. Todd B. Reynolds, Yue Zhou, Dr. Alan D. Fried, Dr. Brian P. Jacobs, Dr. Breanna J. Wilson, and Dr. Johnathan N. Brantley. DPM prepared U87, MDA-MB-231, and A375 cells for analysis under the direction of JAB. YZ prepared *C. albicans* cells for analysis under the direction of TBR. For these cell types, MLQ performed all cellular delivery experiments, confocal microscopy cellular imaging, flow cytometry, and associated quantification. ADF, BPJ, and BJW synthesized the boronic acid monomer and performed the polymerization to form the boronic acid polymer lipid under the direction of JNB.

3.1. Abstract

Liposomes are effective therapeutic nanocarriers due to their ability to encapsulate and enhance the pharmacokinetic properties of a wide range of drugs and diagnostic agents. A primary area in which improvement is needed for liposomal drug delivery is to maximize the delivery of these nanocarriers to cells. Cell membrane glycans provide exciting targets for liposomal delivery since they are often densely clustered on cell membranes and glycan overabundance and aberrant glycosylation patterns are a common feature of diseased cells. Herein, we report a liposome

platform incorporating bis-boronic acid lipids (BBALs) to increase valency in order to achieve selective saccharide sensing and enhance cell surface recognition based on carbohydrate binding interactions. In order to vary properties, multiple BBALs (**3a-d**) with variable linkers in between the binding units were designed and synthesized. Fluorescence-based microplate screening of carbohydrate binding showed that these compounds exhibit varying binding properties depending on their structures. Additionally, fluorescence microscopy experiments indicated enhancements in cellular association when BBALs were incorporated within liposomes. These results demonstrate that multivalent BBALs serve as an exciting glycan binding liposome system for targeted delivery.

3.2. Introduction

3.2.1. Introduction to boronic acids

Boron containing compounds are found in high concentrations in nature. Boron-based acids include borinic acid, boronic acid, and boric acid, which can each form either neutral or anionic esters upon reaction with diols or divalent ligands and loss of water (Figure 3.1). While there are many types of organoboron compounds, the boronic acid is the most studied boron-containing functional group in organic and medicinal chemistry. Due to their unique structural properties, binding ability, and their promising anticancer, antibacterial, and antiviral activity, the use of boronic acids in nanoparticle and drug design has flourished in the last decade.[250] Boronic acids are trivalent organic compound composed of a boron in planar geometry with one carbon-based substituent and two hydroxyl groups.[251] They are synthetically derived from boric acids which feature three hydroxyl groups. Boronic acids do not fulfill the octet rule since the boron atom is deficient of two electrons and thus is sp^2-hybridized with only six valence electrons. The resulting sp^2-hybridized boron atom has a vacant p orbital, which confers Lewis acidity (Figure 3.2A). Although boronic acids may exist as mixtures of free boronic acid with anhydride forms such as the 6-membered boroxine while in dehydrated solid form, most arylboronic acids are chemically stable, have extended shelf-stability, and can be handled in air without special precautions.

3.2.2. Boronate anion equilibrium

Boronic acids can act as hydrogen bond donors, but in aqueous solutions it is rare for them to behave as Brønsted acids, as would be evidenced by loss of a proton from a B–OH moiety (Figure 3.2B). In most cases, boronic acids behave as Lewis acids through a dissociation equilibrium involving two water molecules, and typically have a pK_a in the range of 5 - 9. The pK_a of a boronic acid is defined as the pH at which 50% of the boronic acid exists as the hydroxyboronate anion species. This Lewis acid characteristic of the boronic acid group has interested chemists for over a century, and Lorand and Edwards were the first to report the complexing equilibria of boronic acid and polyols, which elucidated that the boronate ion is the conjugate base of boronic acid.[252] Boronic acid acidity is indicated by its ability to ionize water to produce hydronium ions, and thus boronic acids with lower pK_a have more electrophilic boron atoms, which results in the formation of the anionic tetrahedral boronate anions. Many biomaterial platforms involving boronic acids rely on a shift in solubility or reactivity, which can be decided by the transition from the hydrophobic neutral boronic acid to the anionic hydroxyboronate or boronate ester. Because of this, boronic acid pK_a must be considered when designing these systems, and it follows that it would be detrimental to use a boronic acid with a pK_a much higher than physiological pH (7.35 – 7.42), since it may not perform well within physiological conditions.

The pK_a values of commonly used boronic acids are shown in Table 3.1, as reported by Dr. Dennis Hall.[251] There are modifications that can influence boronic acid acidity, and a general trend is that arylboronic acids tend to have lower pK_a values than alkylboronic acids. Bulky groups proximal to the boron atom cause steric hindrance on the formation of the tetrahedral boronate ion, resulting in higher pK_a values. For example, 3-methoxyphenylboronic acid (pK_a = 8.0) exhibits a lower pK_a than 2-methoxyphenylboronic acid (pK_a = 9.0) due to decreased steric hindrance. Also, electron-withdrawing groups (EWGs) on the phenyl ring of arylboronic acids decrease the pK_a since they result in the boron atom becoming even more electrophilic. Addition of ester and nitro EWGs on a phenylboronic acid decreases the pK_a from 8.9 to 6.9. Another method to lower the pK_a of boronic acids is by introducing an *ortho*-dialkylaminomethyl substituent on the phenyl ring, known as Wulff-type boronic acids. [253] Addition of this *o*-aminomethyl group enhances boronic

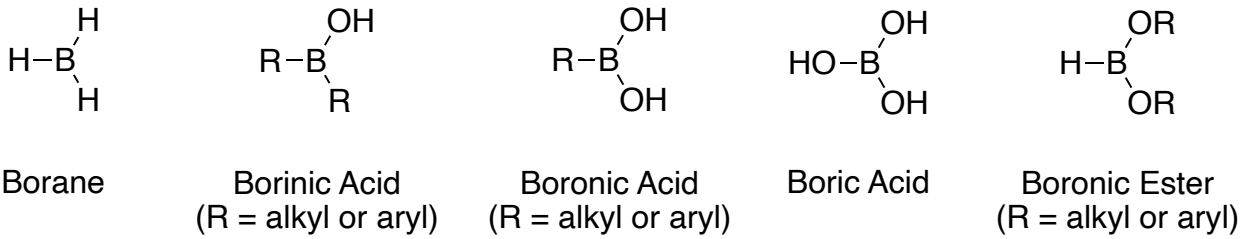


Figure 3.1 Chemical structures of organoboron compounds. Boron-based acids include borane, borinic acid, boronic acid, boric acid, and boronic ester. The nomenclature depends on the substituents bonded to boron atom.

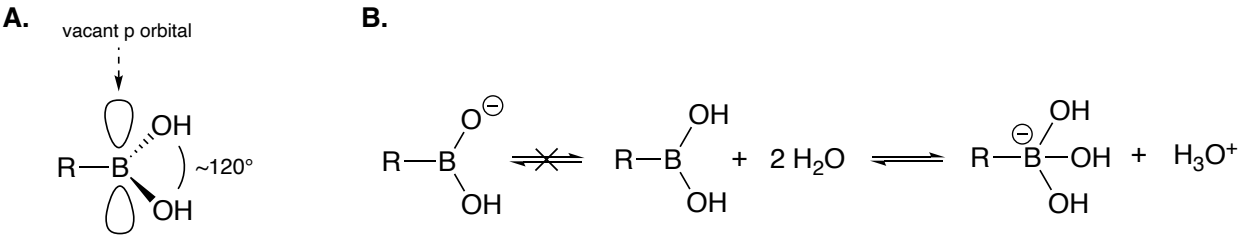


Figure 3.2 Boronic acid structure and equilibrium dissociation in water. (A) The boron atom of the boronic acid is deficient of two electrons and thus is sp^2-hybridized with only six valence electrons, resulting in an empty p orbital. (B) In aqueous solutions it is rare for boronic acids to behave as Brønsted acids. Typically, boronic acids behave as Lewis acids which show a dissociation equilibrium involving two water molecules, and typically have a pK_a in the range of 5 - 9.

Table 3.1 Ionization constants (pK_as) for common boronic acids. Data is from a book by Dr. Dennis Hall.[251]

Organoboron Compound	**pK_a**
Boric acid $B(OH)_3$	9.0
Methylboronic acid	10.4
Phenylboronic acid	8.9
3,5-Dichlorophenylboronic acid	7.4
3,5-Bis(trifluoromethyl)phenylboronic acid	7.2
2-Methoxyphenylboronic acid	9.0
3-Methoxyphenylboronic acid	8.7
4-Methoxyphenylboronic acid	9.3
4-Carboxyphenylboronic acid	8.4
2-Nitrophenylboronic acid	9.2
4-Nitrophenylboronic acid	7.1
4-Bromophenylboronic acid	8.6
4-Fluorophenylboronic acid	9.1
2-Methylphenylboronic acid	9.7
3-Methylphenylboronic acid	9.0
4-Methylphenylboronic acid	9.3
3,5-Dimethylphenylboronic acid	9.1
3-Methoxycarbonyl-5-nitrophenylboronic acid	6.9
2-Fluoro-5-nitrophenylboronic acid	6.0
3-Pyridylboronic acid	4.0, 8.2
3-Benzyl-3-pyridyliumboronic acid	4.2
Quinolinylboronic acid	4.0, 10

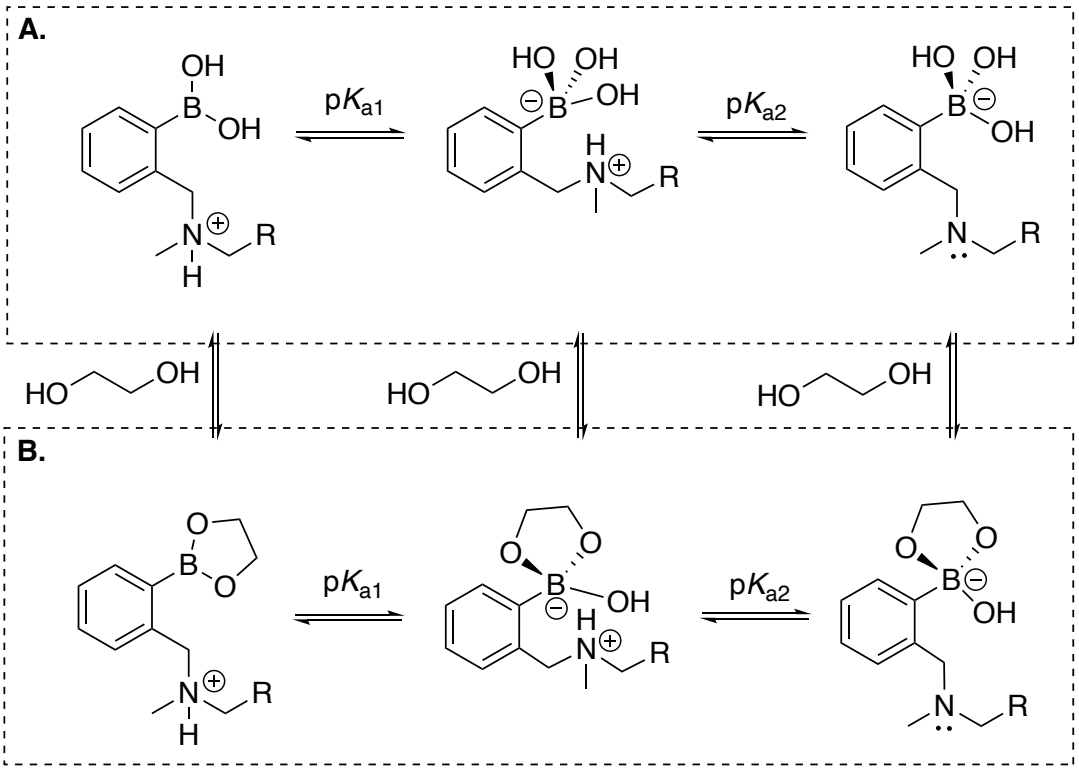
acid affinity towards diols at neutral pH; however, the reason underlying how the group accomplishes this feat was long debated.[254-263] A landmark treatise was published by Dr. Binghe Wang, Dr. Tony James, and Dr. Eric Anslyn which, combined a body of work from various groups in order to finally discern the role that the *o*-aminomethyl group plays in influencing the pK_a and molecular recognition properties of phenylboronic acids.[264, 265] They described two reasons why *o*-aminomethyl effect boronic acids. First, they argue that the electron-withdrawing nature of the *o*-aminomethyl and field effect from the ammonium ion were responsible for lowering the pK_a of the proximal boronic acid. Second, that there is an intramolecular hydrogen bond between the anionic hydroxyboronate and the ammonium cation which facilitates inserted solvent leaving group departure since the ammonium group can act as a general acid-catalyst, resulting in the liberation of the inserted solvent.

3.2.3. Boronic acid-diol equilibrium

Another important interaction is the boronic acid-diol equilibrium. The B–O covalent bonds of boronic acids can undergo a reversible exchange with the hydroxy group of alcohols and carboxylic acids. Boronic acids also have the unique ability to form cyclic esters with polyols and carbohydrates, which was first characterized in a landmark paper by Lorand and Edwards in 1959.[252] This interaction of boron and diol plays a key roles in plant growth,[266] bacterial quorum sensing,[267] nanomaterials for biomedical applications,[268] purification of glycoproteins, nucleotides and carbohydrate transporters,[269] and as protecting groups for carbohydrates[270, 271] Although the study of the boron-diol interaction began as early as 1832 in the pioneering work of Jean-Baptiste Biot, Edwards and coworkers were the first to report quantitative affinities of boric and phenylboronic acids with diols and monosaccharides. These affinities were measured by the pH depression method. The main conclusion at the time was that the binding equilibrium favors formation of boronate ions in higher pH aqueous solutions. Although previous work has shown that the binding affinity of a boronic acid is often related to the pK_a of the boronic acid, the most effective diol binding does not always occur near or above the pK_a of the boronic acid.[272] Due to their specific importance in this dissertation, Scheme 3.1 shows an overview of the structure and associated pK_a values of *o*-aminomethylphenylboronic acids both with and without a diol such as a sugar, hydroxycarboxylate or catechol as a function of pH. As reported by Anslyn

et. al., the first pK_a of *o*-aminomethylphenylboronic is typically between 5 - 7 and results in solvent insertion, resulting in the hydroxylation of the boronic acid/ester and yielding a direct solvent inserted structure. Then, the second pK_a value of *o*-aminomethylphenylboronic acids or boronate esters corresponds to the deprotonation of the ammonium ion and has been found to be between 11 - 12.

The dynamic exchange of B–OH groups is due to boron's vacant p orbital. Specifically, an associative mechanism facilitated by rapid proton transfers has been shown to drive the reaction between boronic acids and alcohols in neutral or slightly alkaline aqueous solutions. In *o*-aminomethylphenylboronic, a mechanism is influenced by the *o*-aminomethyl group which speeds up the sugar binding by an intramolecular general acid-catalysis of inserted solvent leaving group departure from the boronic acid.[265] Factors that influence the association constant (K_{eq}) between a boronic acid and a diol include boronic acid pK_a, diol pK_a, dihedral angle of the diol, stabilization of the boronate center, and steric hindrance.[273] Association constants of phenyl boronic acid (PBA) with diols are included in Table 3.2,[274] and association constants of 3-acetamidophenylboronic acid (3-AcPBA) and 2-dimethylaminomethylphenylboronic acid (DAPBA) with diol Alizarin Red S (ARS), sorbitol, fructose, and glucose at various pH are included in Table 3.3.[273] As summarized in Table 3.1, a 2002 report by Wang et. al. analyzed boronic acid - diol complexation including phenylboronic acid with many diol types at pH 7.4. They found that 1,2-dihydroxyphenyl-containing compounds, such as ARS and catechol, had the highest affinities for PBA with K_{eq} values of 1300 and 830 M^{-1}, respectively. Following that, high affinities (K_{eq} = 110–370 M^{-1}) for PBA were seen with sorbitol, fructose, tagatose, mannitol, sorbose, and 1,4-anhydroerythritol. Compounds with moderate affinities for PBA (K_{eq} = 13–30 M^{-1}) included erythronic-γ-lactone, arabinose, ribose, sialic acid, *cis*-1,2-cyclopentanediol, glucuronic acid, galactose, xylose, and mannose. Weak affinities (K_{eq} = 0.67–4.6 M^{-1}) for PBA were seen from D-Glucose, diethyl tartrate, maltose, lactose, and sucrose. Additionally, the K_{eq} values for 3-AcPBA (pK_a = 8.5) and Wulff type boronic acid DAPBA (pK_a = 5.3) with diol ARS, sorbitol, fructose, and glucose at various pH are included in Table 3.3. It was found that for both DAPBA and 3-AcPBA, the conditions with the highest K_{eq} values were either pH at 7.4 or 8.7, depending on the diol.



Scheme 3.1 Structures of *o*-aminomethylphenylboronic acids as a function of pH. The structures and *o*-aminomethylphenylboronic acids as influenced by pH (low pH on the left to high pH on the right), in the (A) absence or (B) presence of diol. pK_{a1} of *o*-aminomethylphenylboronic is typically between 5 - 7 and results in solvent insertion, hydroxylation of the boronic acid/ester and yields a direct solvent inserted structure. pK_{a2} value of *o*-aminomethylphenylboronic acids or boronate esters corresponds to the deprotonation of the ammonium ion and has been found to be between 11 - 12. This scheme is adapted from a scheme by Ansley et. al.[265]

Table 3.2 Association constants (K_{eq}) of phenylboronic acid with diols. Data courtesy of paper reported by Wang et. al.[274]

Diol	$K_{eq}(M^{-1})$	**Diol**	$K_{eq}(M^{-1})$
Alizarin Red S.	1300	Sialic acid	21
Catechol	830	cis-1,2-Cyclopentane diol	20
D-sorbitol	370	Glucuronic acid	16
Il-fructose	160	D-galactose	15
D-tagatose	130	D-xylose	14
D-mannitol	120	D-mannose	13
L-sorbose	120	D-glucose	4.6
1,4-Anhydroerythritol	110	Diethyl tartrate	3.7
D-erythronic-y-lactone	30	Maltose	2.5
L-arabinose	25	Lactose	1.6
D-ribose	24	Sucrose	0.67

Table 3.3 Association constants (K_{eq}) of 3-AcPBA and DAPBA with diols at various pH. Data courtesy of paper reported by Sumerlin et. al.[273]

Boronic acid - pK_a	**3-AcPBA (pK_a = 8.5)**	**DAPBA (pK_a = 5.3)**
Diol = ARS		
pH 5.2	1220 (110)	17400 (680)
pH 7.4	2200 (73)	600 (34)
pH 8.7	490 (38)	43 (1.2)
Diol = Sorbitol		
pH 5.2	6.5 (0.2)	130 (5.6)
pH 7.4	610 (13)	380 (20)
pH 8.7	3200 (190)	230 (1.4)
Diol = Fructose		
pH 5.2	n/d	4 (0.2)
pH 7.4	350 (11)	64 (2.0)
pH 8.7	1400 (50)	9.6 (0.3)
Diol = Glucose		
pH 5.2	n/d	n/d
pH 7.4	8.1 (0.7)	n/d
pH 8.7	30 (0.9)	n/d

Apart from solution pH, the geometry of the hydroxyl groups located in the diol binding moieties plays a key role in influencing boronic acid binding. The relative affinity of boronates for diols that exist in most carbohydrates follow the order of cis 1,2-diol > cis 1,3-diol >> trans 1,2-diol. Hence, some saccharides will have naturally higher affinity than others. For example, K_{eq} values between methylboronic acid and 1,3-propanediol, 1,2-ethanediol and 1,2,3-propanetriol, were found to be 2.5, 5.5 and 38, respectively as determined by pH titration and ^{11}B NMR spectroscopy. The preferred K_{eq} of 1,2,3-propanetriol was due to the cis-diol geometry.[275]

3.2.4. Introduction to boronic acids in nanomaterials for drug delivery

Due to their versatility, boronic acid compounds have been used extensively for developing platforms for biomedical applications. The reversible reaction between boronic acid and 1,2-*cis*-diols or 1,3-*cis*-diols to form boronic esters according to the pH of the solution allows these groups to be utilized as a diol-responsive and/or pH responsive material. Specifically, platforms have been developed utilizing boronic acids as responsive functional groups for stimuli responsive platforms induced by stimuli including pH, ROS, and diols, as well as using boronic acids as targeting ligands. The pH responsive design category includes boronic acid based pH triggers for disassembly of polymeric micelles and release of drug cargo,[276-279] pH-responsive cross-linkers to control hydrogel formation and dissociation,[280-283] pH-responsive conjugation linkers for controlled release of therapeutic agents, [284, 285] and pH-responsive mesoporous silica nanoparticles with boronic acid surface coating to enable controlled release of cargo.[286-288] In the ROS responsive category, designs include a hydrophilicity switch trigger group to disrupt polymer assemblies to release therapeutic cargo,[289, 290] a polymer degradation trigger group to control drug release,[291, 292] and as ROS-responsive protein prodrugs for controlled therapeutic delivery.[293-295]

The diol-responsive category includes boronic acid based glucose sensor compounds for diol-triggered protein and insulin release,[296] boronic acid–diol complexation triggered glucose-responsive polymeric micelles via for insulin delivery,[297] glucose responsive polymer micelles for triggered cargo release,[298] a glucose-responsive self-healing hydrogel,[299] and an ATP-responsive fluorophore for theranostic applications.[300] Two particularly noteworthy commercial

developments of diol-responsive boronic acid-based systems are the Eversense system by Senseonics and the Glysure Ltd system. Both of these sensors use fluorescent *ortho*-aminomethylphenylboronic acids to continuously monitor glucose for patients with diabetes. The Eversense system is based on the first glucose selective fluorescent sensor developed by James, Sandanayake and Shinkai in 1994,[301, 302] and Glysure is based on the fluorescent design by Arimori, Frimat and James in 2001.[303, 304] The Eversense system consists of a small implantable fluorescence-based sensor, a transmitter, and a mobile app for displaying glucose values and trends. Glysure is a fiber optic fluorescent sensor used by patients in Intensive Care Units (ICUs) to enable Tight Glycemic Control (TGC).

The final category of boronic acid-based systems for biomedical applications is using boronic acids as targeting ligands. As discussed, boron-containing molecules can interact with biological targets and undergo dynamic covalent interactions with diol containing compounds. These diols can exist either in the diol-containing biomolecules such as sugars, carbohydrates, or glycans, or as residues in disease-associated proteins. Boronic acid based platforms have been shown to interfere with signaling pathways, inhibit enzymes, and target glycoproteins for enhanced nanoparticle uptake.[305] For these applications, major issues to overcome are binding affinities for the selected target and ensuring a pK_a at or below the physiological range, but both of these issues have been addressed by employing Wulff-type boronic acids.[306]

The boronic acid functional group has been extensively used to target surface saccharides on gram-positive bacteria and sialic acids (Sias), a family of sugar structures on glycoproteins expressed on hyperactivated cells. The boronic acids in the bacterial detecting systems have been shown to bind to the saccharide-rich peptidoglycan cell wall and diol-containing lipopolysaccharides on the cell surface. These systems have contained fluorescent probes,[307] artificial receptors,[308] and antibacterial agents.[309] Platforms for targeting Sias on mammalian cell surfaces have also comprised an exciting area of development. Saccharides such as Sias at the terminal ends of cellular surface glycoconjugates play key roles in cell signaling; however, they are overexpressed in a hyperactive state such as cancer and immunity.[310] Detection of Sias can

be beneficial for monitoring, analyzing, or delivering cargo to the cells, but efficient and selective binding is difficult. To address this, Otsuka et al. employed Wulff-type boronic acids which were found to form intramolecular B-O bonds with the glycerol side chain of Sias, resulting in a ~7 times higher K_{eq} for Sias than for glucose.[311] Since then, this strategy of complexing PBA biointerface materials and Sias has been developed to achieve broad applications related to cancers such as biodetection and biosensing,[312] controllable drug delivery and release,[313] and bio-separation.[314] Boronic acid-based molecularly imprinted polymers (MIPs) have also been used to develop Sia targeting MIP nanoparticles for cancer imaging.[315-317] Although great progress has been made to develop boronic acid-based platforms for triggered response to microenvironmental conditions and targeted delivery based on cell surface saccharides, more work is needed to achieve selective and efficient substrate binding, enhanced delivery, and release of therapeutics.

3.2.5. Introduction to boronic acid liposomes

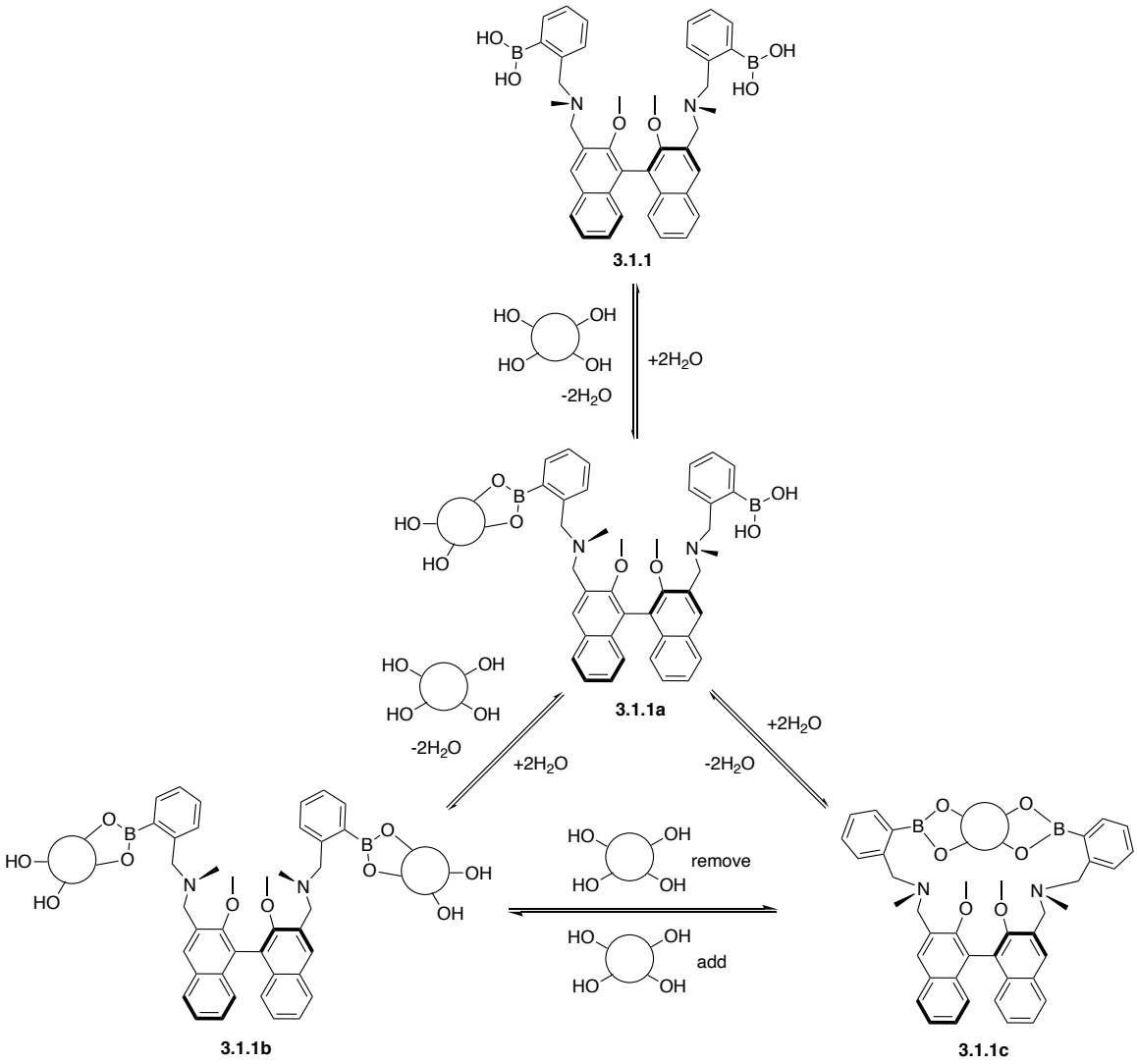
Liposomes are spherical vesicles composed of a lipid bilayer membrane that assembles around an internal aqueous core. This duality gives liposomes the ability to encapsulate both hydrophobic cargo within the lipid bilayer and hydrophilic cargo in the aqueous core, making them versatile molecular carriers for drug delivery. In certain situations, liposomes exhibit enhanced delivery to diseased tissue, such as through EPR effect that exploits the leaky vasculatures proximal to tumors. Intensive efforts are underway to achieve broader enhancements in cell delivery by attaching targeting ligands to liposomal surfaces that distinguish between specific cell types based on disease-associated receptors.[318] While molecular sensing groups including antibodies, peptides, carbohydrates, proteins, and other small molecules can be appended to liposome surfaces,[226, 227] the attachment of complex and expensive biomolecules is challenging and impractical for clinical applications. The engineering of molecular recognition properties directly into the membrane bilayer using designer lipid analogs likely provides a more efficient approach for enhancing cellular delivery characteristics.

Cell surface carbohydrates offer a compelling recognition target due to the extensive variations in structures and abundance on different cell types, including variation between different diseased and healthy cells. For example, Mucin 1, an important tumor-associated antigen, is both overexpressed and aberrantly glycosylated in adenocarcinomas.[319] A combination of alterations in the mucin core peptide, mucin subcellular localization or expression, and dysregulation of various glycosyltransferases leads to the formation of truncated *O*-linked glycans and aberrant mucin glycosylation patterns on human cancer cells.[320] This incorrect glycosylation commonly results in the formation of truncated glycans terminating in Sia, a functionalized version of *N*-acetylneuraminic acid.[321-323] For example, it is estimated that there are as many as 10^9 Sia residues on multiple sialylated antigens per tumor cell.[324] Indeed, Sia overabundance correlates with a range of cancers including gastric, colon, pancreatic, liver, lung, prostate, and breast cancers.[325] A liposomal delivery vesicle engineered to recognize particular carbohydrate motifs would be a significant advancement in cancer nanotherapies.

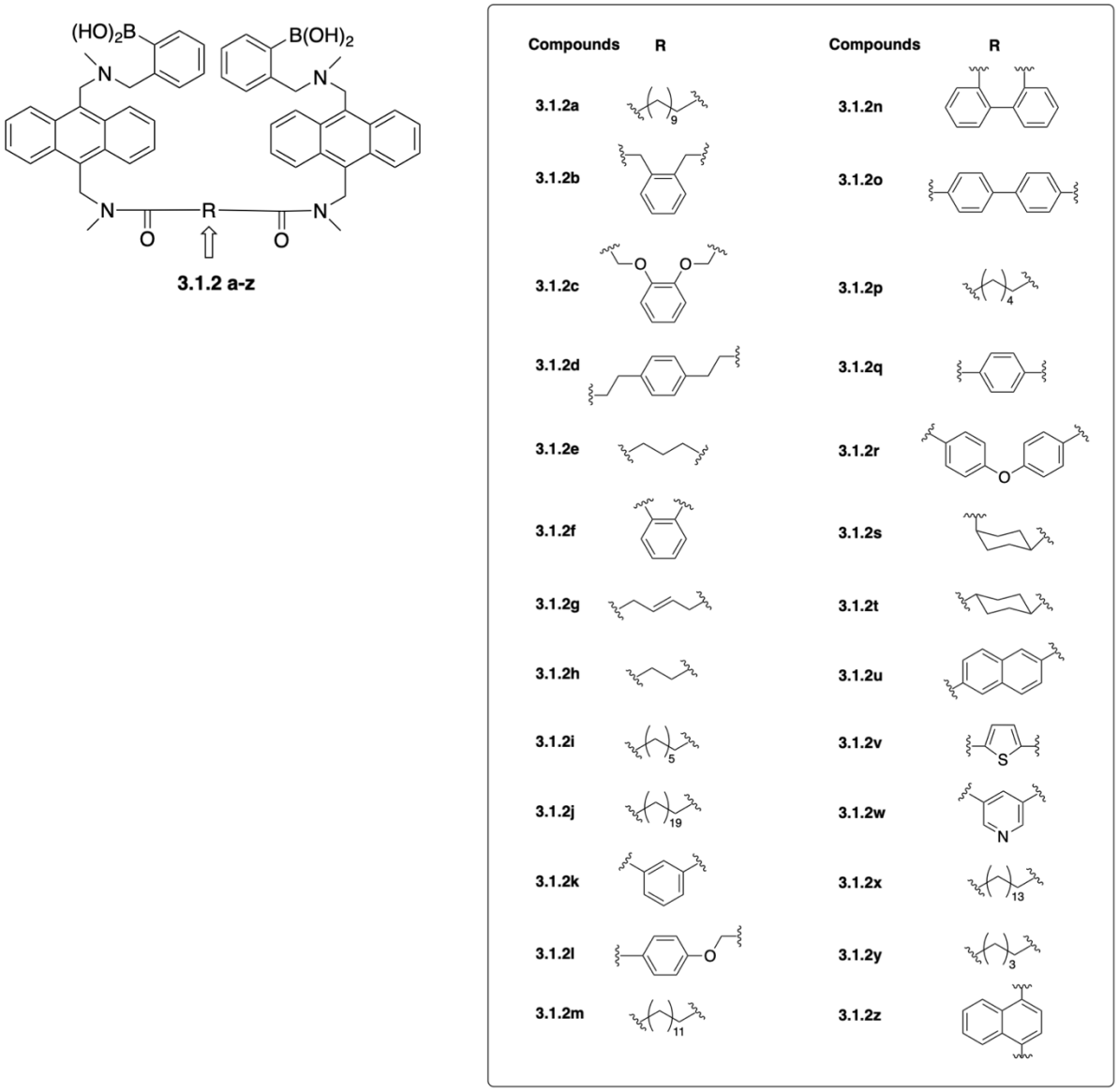
Our approach to exploiting cell surface glycosylation patterns for enhancing cellular delivery entails the decoration of liposomal surfaces with boronic acid recognition groups. Boronic acids have been extensively used as sensors for carbohydrates through the reversible formation of boronate esters via the binding of carbohydrates moieties including diols.[272, 274, 326-335] While these individual interactions are weak in aqueous solution with association constant (K_a) values of less than 1,000 for phenylboronic acids and naturally occurring sugars, affinities towards carbohydrates are known to be dramatically enhanced through multivalent binding interactions.[336-341] For example, PBA has an association constant toward glucose of 4.6 M^{-1} while a synthetic multivalent boronic acid compound by Drueckhammer and co-workers exhibited a glucose binding constant of 4.0×10^4 M^{-1}.[342] Similarly, Shinkai and co-workers reported a selective glucose sensor (**3.1.1**) that overcomes the low affinity of single boronic acid sensors for glucose at physiological pH by using a bis-boronic acid (Scheme 3.2).[343] This bis-boronic acid sensor has a chiral binaphthol core and twin aminoboronates, which use a photoinduced-electron-transfer (PET) system to differentiate between enantiomers of glucose and emit a fluorescence signal. Indeed, sensors containing more than one boronic acid can exhibit greater

carbohydrate binding selectivity based on the precise display of functional groups on guests.[302, 344, 345] For example, Wang and co-workers developed a family of anthracene-based fluorescent bis-boronic acid sensors (**3.1.2a-z**) that showed specific affinity for the target carbohydrate sialyl Lewis x (SLeX), which is frequently overexpressed on cancer cells (Scheme 3.3).[346] This affinity was tuned by synthesizing bis-boronic acid molecules with various linkers in search of the optimal arrangement. Twenty-six linkers were screened of different length, rigidity, and spatial orientation between two boronic acid binding units, which either increased or decreased the binding affinities toward the target carbohydrate (SLeX). Of these compounds, the bis-boronic acids linked with a *p*-xylene linker (**3.1.2q**) showed the highest binding selectivity for SLeX and was able to specifically label SLeX -expressing cells.

Previously, our group reported that liposomes containing lipids with single boronic acid moieties were effective for enhancing cell delivery driven by carbohydrate binding (Figure 3.3).[153] This synthetic lipid was composed of a boronic acid directly attached to an amino glycerolipid scaffold. An *ortho*-(alkylaminomethyl)phenylboronic acid binding unit was employed since the phenyl group has been shown to stabilize the boronic acids, and incorporation of nitrogenous bases in an *ortho*-methyl position to the PBA has been shown to increase the rate of boronate ester formation and diol exchange in neutral aqueous solution under physiological conditions.[257] These type of internally coordinated boronic acids are also referred to as Wulff-type boronic acids.[273] Through prior investigation by our lab, these mono-boronic acid lipids were shown to bind the glycosaminoglycan heparin through a microplate binding assay approach, and the lipids also enhanced cell entry driven by carbohydrate binding. In this case, the carbohydrate binding also caused membrane destabilization and cargo release from the liposome. Even though these compounds were monovalent, it was reasoned that the fluid multivalent environment of the membrane could enable enhanced avidity in binding interactions. Broadening this investigation to bis-boronic acid lipids (BBALs) poses a compelling opportunity for achieving multivalent binding interactions between cell surface carbohydrates and boronic acid lipids to ultimately enhance cell delivery for drug delivery applications. Additionally, by varying the spatial arrangement of the two boronic acids, we sought to probe for potential binding selectivity and



Scheme 3.2 Structures of bis-boronic acid sensor for differentiation between enantiomers of glucose by Shinkai and coworkers. Possible complexes of bis-boronic acid sensor **3.1.1** (*R* or *S*) by Shinkai et. al. with saccharides. Sensor **3.1.1** can differentiate between enantiomers of glucose. Four main species exist including non-fluorescent **3.1.1** and **3.1.1a**, fluorescent species **3.1.1b**, a non-cyclic 1:2 complex, and **3.1.1c**, a cyclic 1:1 complex. Adapted from Shinkai et. al.[343] with permission from Springer Nature.



Scheme 3.3 Chemical Structures of bis-boronic Acids 3.1.2a-z reported by Wang and coworkers. Structures of library of bis-boronic acid sensors **3.1.2a-z** by Wang et. al., which show specific affinity for the target carbohydrate SLeX. Compounds consist of dimeric anthracene-based fluorescent sensors with bis-boronic acid binding units whose affinity was tuned by synthesizing bis-boronic acid molecules with various length linkers (**3.1.2a-z**) between the two boronic acid binding units. The bis-boronic acid linked with a *p*-xylene linker (**3.1.2q**) showed the highest binding selectivity for SLeX and was able to specifically label SLeX -expressing cells.

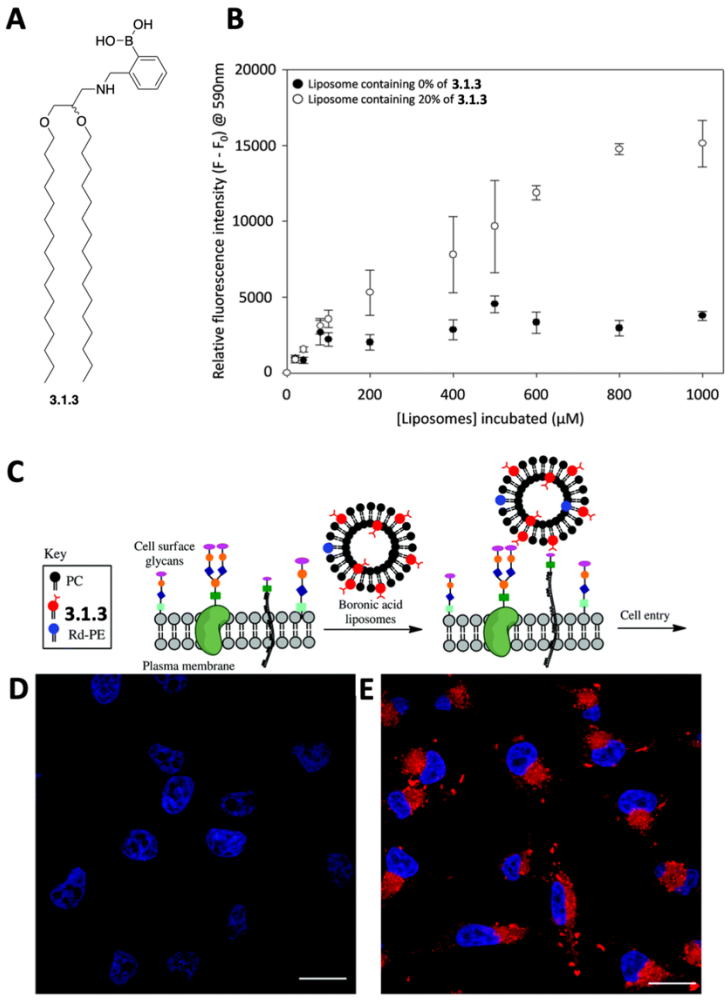


Figure 3.3 Mono-boronic acid lipid by Best and coworkers for cellular delivery driven by carbohydrate binding. (A) Structure of mono-boronic acid **3.1.3** with single boronic acid binding unit and amino glycerolipid scaffold. (B) Results from microplate binding assay indicating successful binding of fluorescently labeled boronic acid liposomes to immobilized heparin–biotin. (C) Cartoon depicting cell surface carbohydrates driving liposome cell entry. (D) Fluorescence image of A375 melanoma cells treated with control liposomes lacking **3.1.3**. (E) Fluorescence image A375 melanoma cells treated liposomes composed of 10% **3.1.3** yielded a dramatic enhancement in fluorescence. Reproduced from Best et. al.[153] with permission from The Royal Society of Chemistry.

elucidate BBAL(s) with optimized binding activity.

In this Chapter, we present a carbohydrate-targeting liposome cell delivery platform with the goals of enabling the binding of various carbohydrates and enhancing cell association in mammalian cells. This platform is accomplished by introducing bis-boronic acids, which have previously been shown to exhibit carbohydrate binding selectivity, into lipid structures. To achieve these goals, lipids were designed and synthesized that can bind selectively to carbohydrates and were incorporated into liposomes. The synthetic BBALs contain two internally coordinated boronic acids within the lipid headgroup, which can engage in multivalent binding interactions between cell surface carbohydrates and boronic acid lipids on the liposome membrane and thereby facilitate carbohydrate selectivity and ultimately enhance cell delivery. In this chapter, a comprehensive evaluation of this delivery platform is presented including the design and synthesis of the BBALs, characterization of liposome morphology containing the lipids, analysis of carbohydrate and glycoprotein binding ability with a fluorescence-based microplate competitive displacement assay, assessment of enhancements in cellular association using fluorescence microscopy, and examination of the ability of our liposome platform to deliver internal cargo to cells for drug delivery applications

3.3. Design and synthesis of bis-boronic acid liposomes

Our BBAL design (**3.1a-d**, Scheme 3.4B) incorporates two boronic acid units into the lipid headgroup so these binding moieties will be available at the liposome surface. Additionally, two hydrophobic alkyl tails were included so that the compound will be incorporated into the lipid bilayer. Finally, four BBALs were synthesized in which the boronic acids were attached via variable linkers to modulate their spacing to probe for variation in binding properties. Aromatic tethers were used to introduce rigidity into these structures. Since it is difficult to predict the exact spacing needed between boronic acid binding units that would fit disease associated carbohydrate targets, we designed lipid structures composed of linkers of different length and rigidity buttressing the two boronic acid groups. We synthesized lipids with *m*-xylene (**3.1a**) and *p*-xylene (**3.1b**) linkers, as well as slightly longer and more rigid naphthyl (**3.1c**) and biphenyl (**3.1d**) linkers. In this manner, each lipid is capable of forming two distinct binding interactions

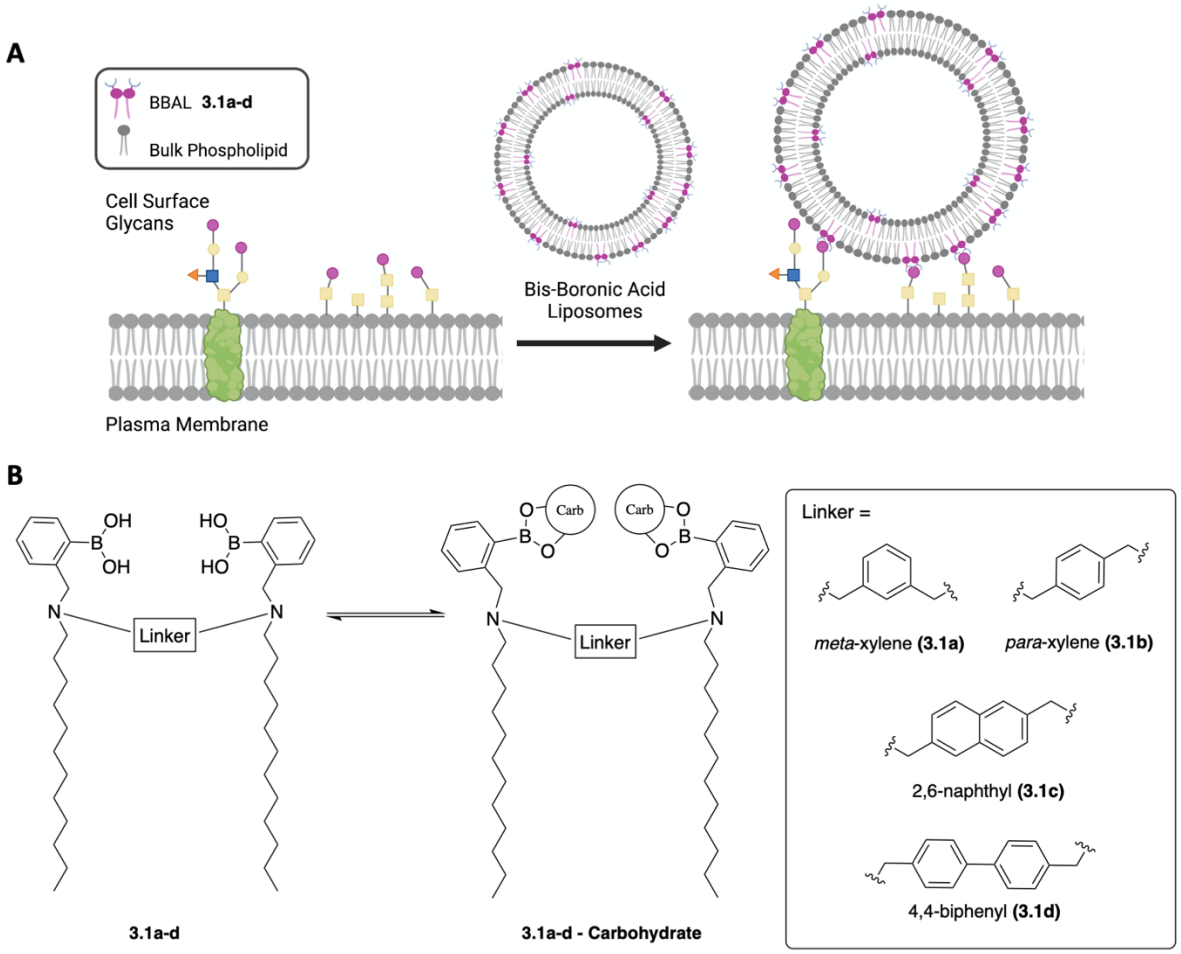
with cell surface glycans, whether that occurs through binding of two separate carbohydrate moieties (as depicted in Scheme 3.4A) or via divalent binding to one glycan sequence.

The synthetic strategy for accessing BBALs **3.1a-d** is shown in Scheme 3.5. We previously reported the synthesis and activity of monovalent boronic acid lipid **3.1.5**, obtained from reductive amination between commercially available 2-formylphenylboronic acid (**3.1.4**) and dodecylamine.[153] The secondary amino group of intermediate **3.1.5** was then treated with either *m*-xylene dibromide, *p*-xylene dibromide, 2,6-bis(bromomethyl)naphthalene, or 4,4'-bis(bromomethyl)-1,1'-biphenyl to produce dimeric products **3.1a**, **3.1b**, **3.1c**, or **3.1d**, respectively. Following BBAL synthesis, we moved on to the evaluation of the carbohydrate binding properties of liposomes containing **3.1a-d.**

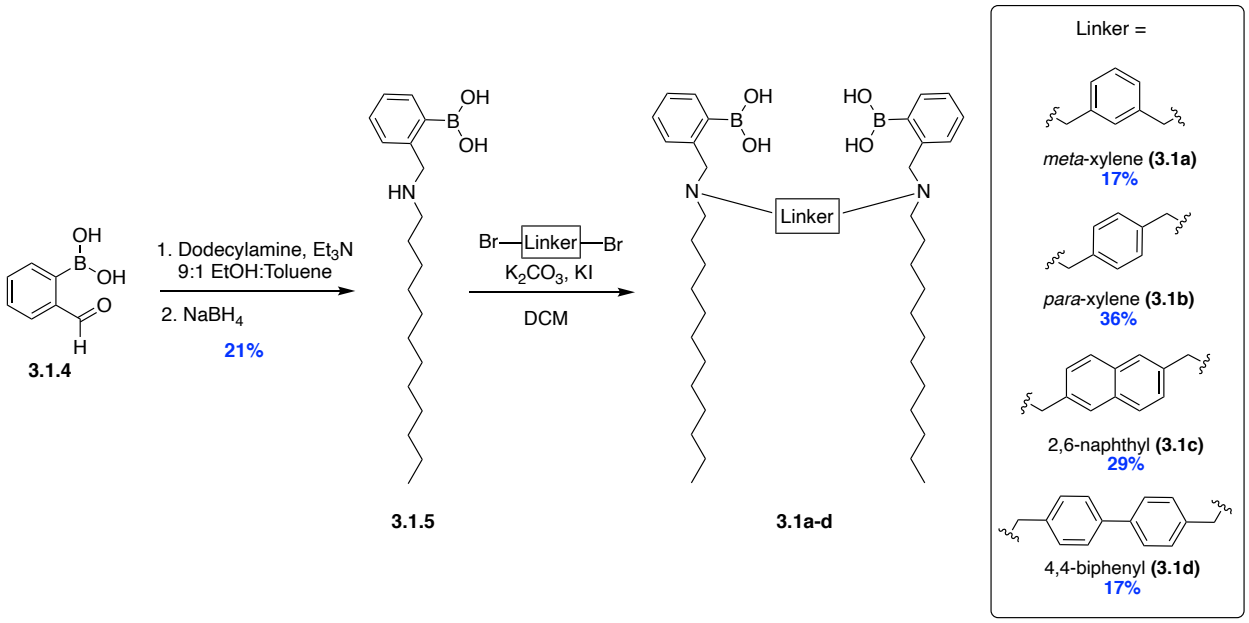
3.4. Microplate assay for detection of mucin-liposome binding

3.4.1. Assay overview

To study and compare the carbohydrate binding properties of liposomes incorporating different BBALs, a three-step competitive assay was developed in which binding to two different glycans could be evaluated using a microplate immobilization strategy (Figure 3.4). The benefits of conducting a microplate assay include the rapid screening of several experiments and the ability to separate unbound glycans through microplate wash steps. This assay exploited protocols for immobilizing intact liposomes including a small percentage of biotinylated lipids onto streptavidin-coated microplates.[347] In the first step, liposomes formulated with BBALs **3.1a**, **3.1b**, **3.1c,** or **3.1d** (20%), biotin labeled PE (biotin–cap–PE) (1%), and the remainder L-α-phosphatidylcholine (PC, mixed isomers from chicken egg) were immobilized onto streptavidin-coated microplates at varying concentrations (Figure 3.4A). In the second step, binding was assessed using a rhodamine-labeled derivative of dextran (Rd-dextran), which is a polysaccharide predominately comprised of α-(1,6)-linked glucose units (Figure 3.4B). This was selected since bacteria use dextran as an extracellular polysaccharide biofilm coating for protection and to evade host phagocytes,[348-350] and because a fluorescent conjugate is commercially available. In the final step, an unlabeled sample of the cancer-associated glycoprotein mucin was added to



Scheme 3.4 Design strategy for bis-boronic acid liposomes. (A) Cartoon illustration of liposome binding to cell surface glycans by forming multiple contacts using BBALs. (B) Structures of BBALs **3.1a-d** and anticipated binding mode toward carbohydrates. These compounds include variable linkers to modulate the spacing of boronic acid binding groups.



Scheme 3.5 Synthetic route for BBALs 1a-d. Compound **3.1.4** was reacted with dodecylamine to form **3.1.5**, which was reacted with alkyl halide linkers *m*-xylene dibromide, *p*-xylene dibromide, 2,6-bis(bromomethyl)naphthalene, or 4,4'-bis(bromomethyl)-1,1'-biphenyl to produce dimeric bis-boronic acid products **3.1a**, **3.1b**, **3.1c**, or **3.1d**, respectively.

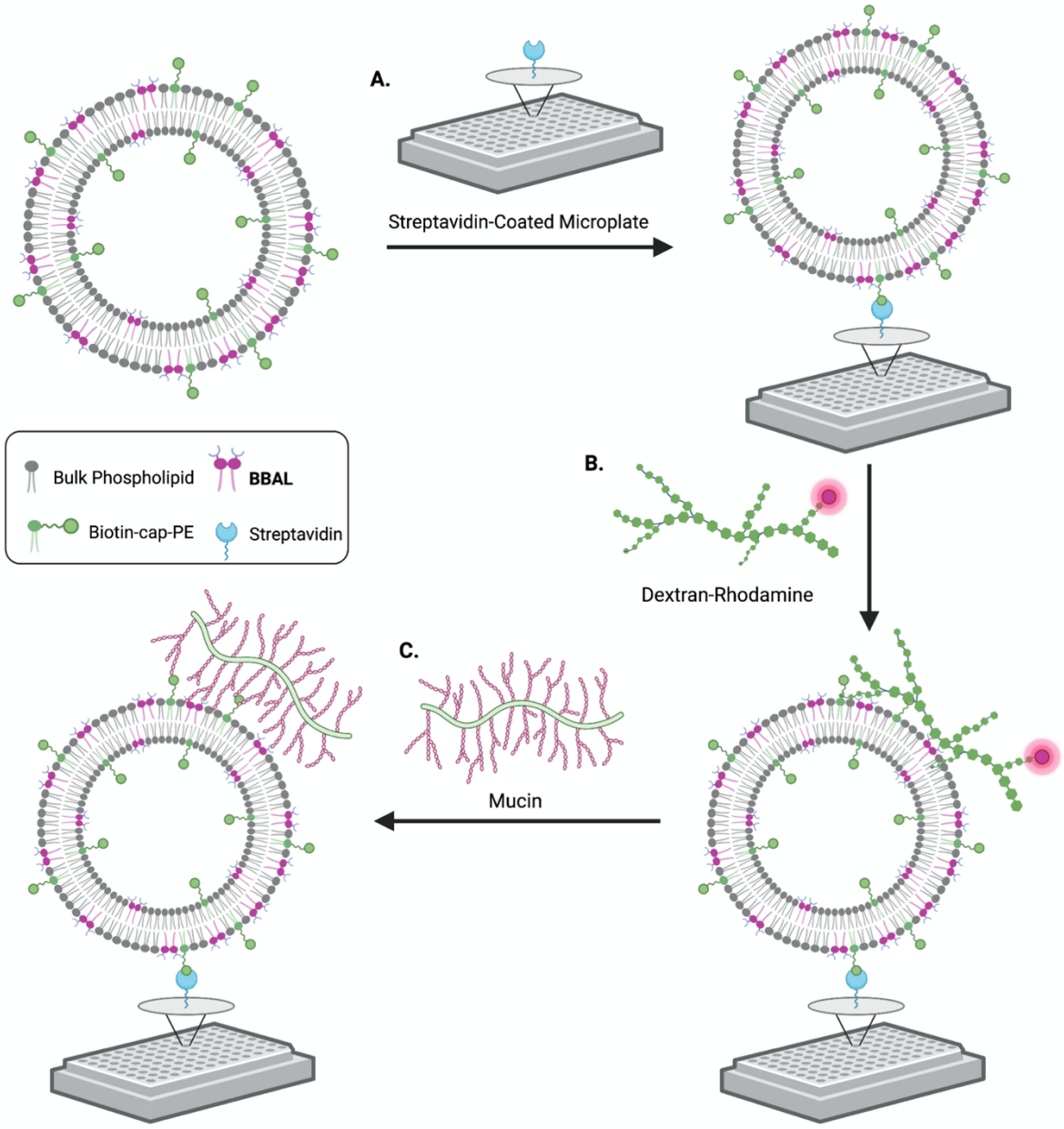


Figure 3.4 Cartoon depicting microplate assay for detection of mucin-liposome binding. (A) Bis-boronic acid liposomes containing small percentages of Biotin-cap-PE were immobilized onto streptavidin-coated microplates. (B) Binding was initially assessed toward Rd-dextran. (C) The microplate was next treated with unlabeled mucin glycoprotein to determine the ability to competitively displace Rd-dextran from liposome binding. Washes were performed after each step to remove unbound species.

competitively displace bound Rd-dextran from immobilized liposomes (Figure 3.4C). After each step of this assay, rigorous washes were performed to remove unbound liposomes and/or carbohydrates, after which fluorescence measurements were acquired. This assay allows for analysis of binding to two different carbohydrate motifs, and detection of the binding of unlabeled mucin glycoproteins is enabled through a competitive displacement approach.

3.4.2. Microplate liposome immobilization results

To ensure successful immobilization of liposome formulations containing different BBALs onto the microplate surfaces, fluorescently-tagged unilamellar liposomes were first studied containing 0% or 20% BBALs **3.1a**, **3.1b**, **3.1c,** or **3.1d** or monovalent boronic acid lipid **3.1.5**, 0% or 1% Biotin-cap-PE, 1% rhodamine L-α-phosphatidylethanolamine (Rd-PE), and the remainder of the liposome formulation consisting of PC (79%, 99%; or 78%, 98%, respectively) (Figure 3.5A). Standard liposome preparation procedures were performed to generate liposomes of uniform size including thin film liposome formation, hydration, freeze-thaw, and extrusion through a 200 nm membrane. Streptavidin-coated microplates were then treated with various dilutions of the fluorescent liposomes, allowed to incubate, and then washed to remove unbound liposomes. Inclusion of 20% **3.1a**, **3.1b**, **3.1c**, **3.1d**, or **3.1.5** only slightly decreased liposome immobilization compared to PC control liposomes, and liposomes containing 0% Biotin-cap-PE (replaced by PC) exhibited minimal background fluorescence (Figure 3.5B). These results demonstrate that all liposome formulations were effectively immobilized onto streptavidin-coated microplates via interaction with the Biotin-cap-PE lipid anchor, thus ensuring proper liposome immobilization before moving on to carbohydrate-binding experiments.

3.4.3. BBAL liposomes Rd-dextran binding assay results

For carbohydrate binding assays, liposomes did not include Rd-PE as a fluorescent tag but were otherwise immobilized in the same manner as described above (Figure 3.6A). We next assessed the ability of BBALs **3.1a-d** to enable binding of liposomes to Rd-dextran. To do so, Rd-dextran was added to a plate on which unlabeled bis-boronic acid liposomes had been immobilized at various concentrations. After incubation and washing, we observed that all BBALs yielded

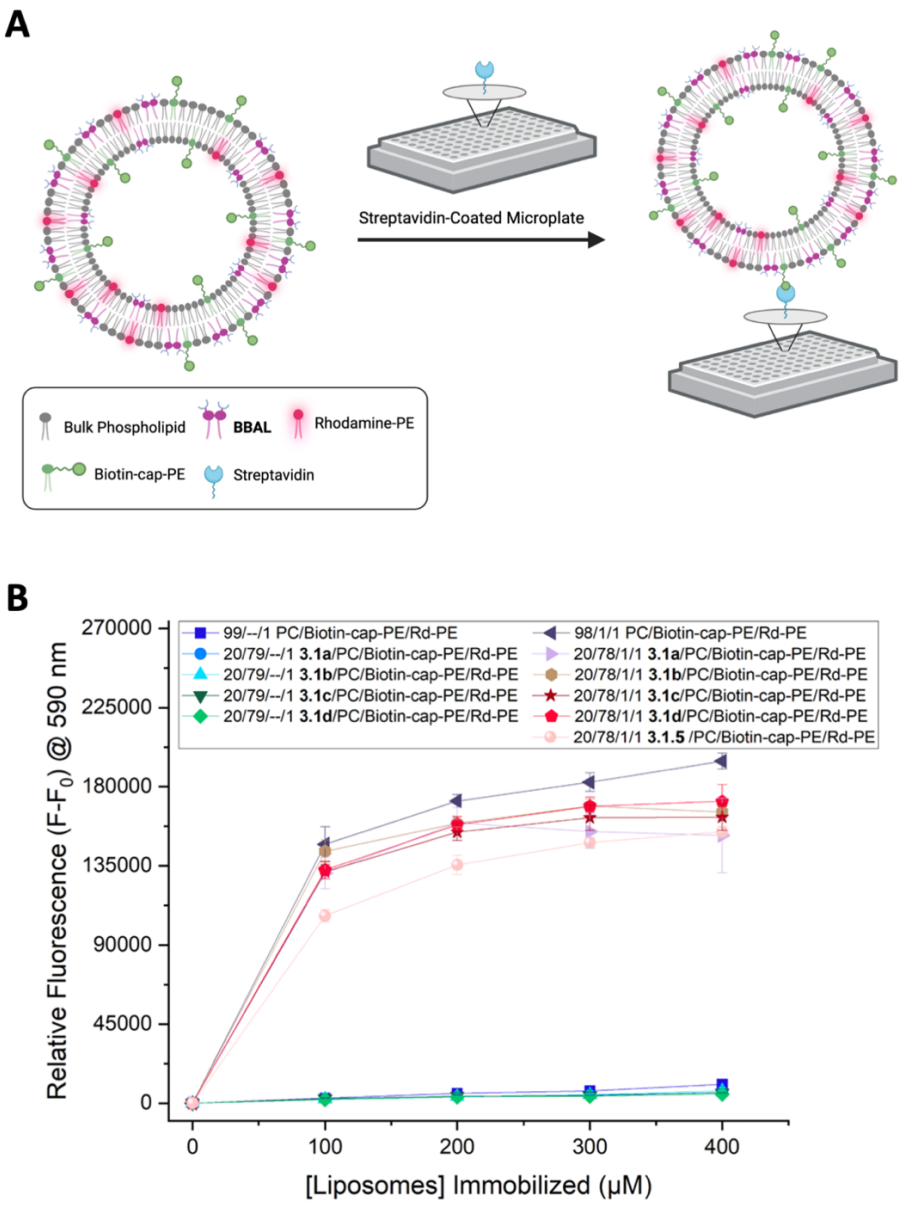


Figure 3.5 Analysis of microplate immobilization of BBAL liposomes. (A) Overview of microplate immobilization assay step. (B) Immobilization experiments utilized liposome formulations including 0% or 1% Biotin-cap-PE, 1% Rd-PE, 20% of **3.1a**, **3.1b**, **3.1c**, **3.1d**, or **3.1.5** and the remainder PC. Positive control PC liposomes showed slightly greater immobilization, indicated by increases in Rd-PE fluorescence, while negative control liposomes lacking Biotin-cap-PE anchor showed virtually no fluorescence. Error bars represent standard errors of at least three replicates.

increased fluorescence indicating Rd-dextran binding when included within immobilized liposomes at concentrations of 0 - 400 μM (Figure 3.6B). The BBALs with a naphthyl linker (**3.1c**) and *meta*-xylene linker (**3.1a**) showed the strongest binding of the BBALs with ~47% and ~85% fluorescence increases, respectively. On the contrary, liposomes with 20% lipid **3.1.5** showed essentially no signal increase and were comparable to PC liposomes lacking any boronic acid lipids. It should be noted that **3.2.5** has only a single lipid chain, compared to the BBALs that have two, which could influence membrane properties. For example, **3.2.5** could be more easily removed from liposomes. The raw fluorescence readings for liposome-dextran binding assays are also included in Figure 3.7. These results provided evidence that BBALs promote increased Rd-dextran binding compared to controls, and that the identity of the linker type and therefore spacing of boronic acid moieties in the lipid headgroup influenced the carbohydrate binding ability. This variable binding activity was intended, and we expect that this phenomenon results from the precise geometric display of the two boronic acid moieties and their fit with carbohydrate guests.

3.4.4. BBAL liposome mucin binding competition assay results

This assay was next used to assess mucin glycoprotein binding to BBAL liposomes using a competition assay (Figure 3.8A). Assays employing competitive displacement of labeled ligands have long been used to characterize binding interactions in molecular sensing.[334, 351, 352] To assess mucin glycoprotein preferential binding, mucin was added to microplates that had previously been treated with 500 μM liposomes containing 20% **3.1.a**, **3.1.b**, **3.1.c**, or **3.1.d** and then subjected to 5 μg/mL Rd-dextran and washed as described above. Solutions of mucin were then added to the microplate at various concentrations including 1 mg/mL, 5 mg/mL, 10 mg/mL, 20 mg/mL, and 30 mg/mL. After mucin incubation, the plate was vigorously washed again to remove unbound Rd-dextran and/or mucin. In cases where mucin outcompetes Rd-dextran for binding, this would cause unbound Rd-dextran to be washed away, which would be evidenced by a decrease in the percent of initial fluorescence intensity. We observed that all 20% BBAL liposomes showed more substantial mucin binding and Rd-dextran displacement (~27-46% fluorescence decrease at 40 mg/mL mucin) compared to PC and 20% **3.1.5** liposomes (~6% and

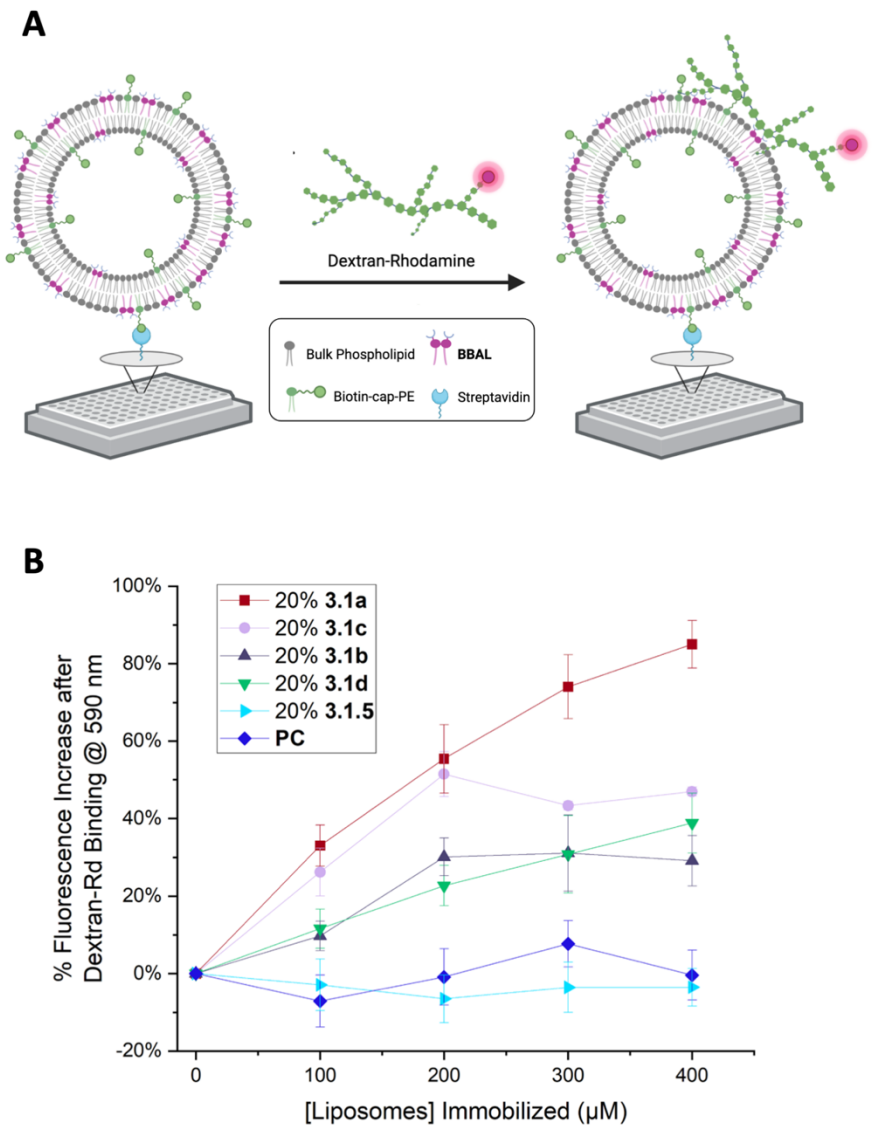


Figure 3.6 Analysis of BBAL liposome Rd-dextran binding microplate assay. (A) Overview of microplate assay step of Rd-dextran binding to immobilized bis-boronic acid liposomes. (B) Immobilization of increasing amounts of liposomes containing 20% of **3.1.a**, **3.1.b**, **3.1.c**, or **3.1.d** led to enhanced Rd-dextran binding compared to control PC liposomes, with **3.1.a** and **3.1.c** yielding the strongest results. Liposomes containing monovalent boronic acid lipid **3.1.5** yielded minimal fluorescence and was comparable to negative PC control liposomes lacking any boronic acid lipid.

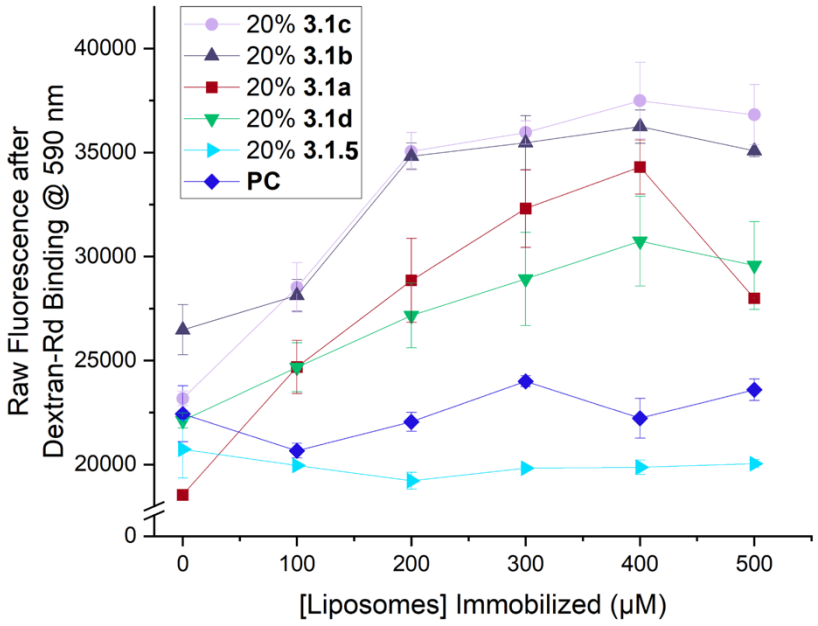


Figure 3.7 Raw fluorescence values from microplate analysis of Rd-dextran binding to immobilized BBAL liposomes. Immobilization of increasing amounts of liposomes containing 20% of **3.1a**, **3.1b**, **3.1c**, or **3.1d** led to enhanced Rd-dextran binding compared to control PC liposomes or liposomes containing 20% monovalent boronic acid lipid **3.1.5**, which yielded minimal signal. Error bars represent standard errors of at least three replicates.

~11% fluorescence decrease at 40 mg/mL mucin, respectively) (Figure 3.8B). In this case, **3.1a** demonstrated the greatest displacement of Rd-dextran by mucin compared to the other BBALs, as shown by a ~46% fluorescence decrease at 40 mg/mL mucin. The raw fluorescence readings for liposome-mucin binding assays are also included in Figure 3.9. These results provide further support that BBALs result in variable carbohydrate binding selectivity based on their linker groups changing the precise display of boronic acid functional groups, and that binding is also influenced by the structures of bound carbohydrates. This also demonstrates that all BBALs show stronger Rd-dextran and mucin binding than mono-boronic acid **3.1.5**, which can be attributed to multivalency.

3.4.5. Microplate catechol binding competition assay results

For additional validation that this carbohydrate binding and competition assay is effective for measuring competitive displacement, we also performed experiments in which 20% **3.1a** liposomes that had been treated with Rd-dextran were subjected to different concentrations of catechol, which is known to exhibit a higher binding affinity toward boronic acids than monosaccharides.[274] Accordingly, we observed the expected dose-dependent decrease in fluorescence correlating with catechol concentration, which further supports our competition assay design (Figure 3.10).

3.5. Dynamic light scattering studies

We also probed the successful preparation of stable liposomes with formulations including synthetic lipids **3.1.a**, **3.1.b**, **3.1.c**, and **3.1.d**. We first employed DLS analysis to assess particle sizes of liposome formulations containing BBALs in the mol% used in the microplate-based liposome assays. Liposomes containing 0%, 10%, or 20% **3.1.a**, **3.1.b**, **3.1.c**, or **3.1.d** and the remainder Egg-PC (100%, 90%, or 80%, respectively) were assessed, and the results showed that the liposomes formed stable vesicles of sizes within the expected diameter range (100 - 200 nm) following extrusion (Figure 3.11A). Raw distribution curves are included in Figure 3.11B. At all formulations, samples maintained average diameters below 200 nm, which is within the range that is beneficial due to the EPR effect. These data indicate that these synthetic BBALs form stable

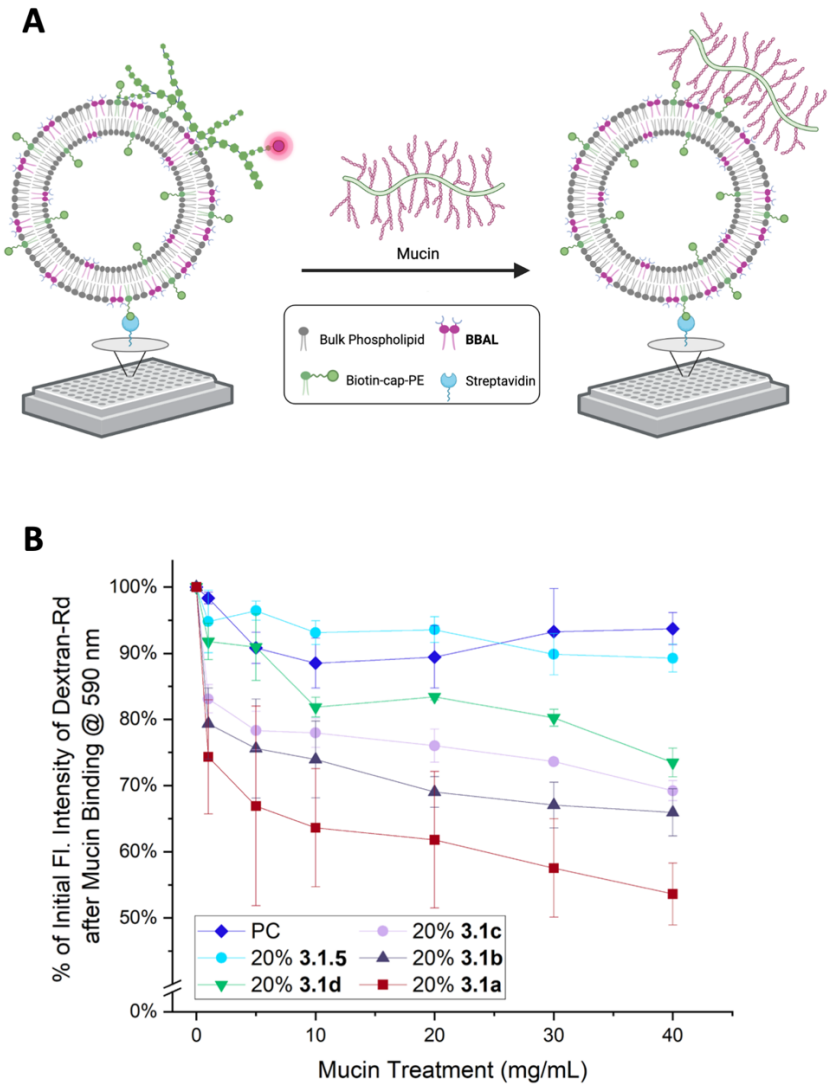


Figure 3.8 Analysis of BBAL liposome mucin binding microplate competition assay. (A) Overview of microplate assay step of Rd-dextran binding to immobilized bis-boronic acid liposomes. (B) Liposomes containing 20% of **3.1.a**, **3.1.b**, **3.1.c**, or **3.1.d** were immobilized onto a microplate at 500 µM, followed by treatment with 5 µg/mL of Rd-dextran. Next, liposomes were treated with various concentrations of mucin glycoprotein. Results show greater displacement of Rd-dextran by mucin using all BBALs tested compared to PC liposomes as well as liposomes containing **3.1.5**. BBAL **3.1a** yielded the greatest signal change. Error bars represent standard errors of at least three replicates.

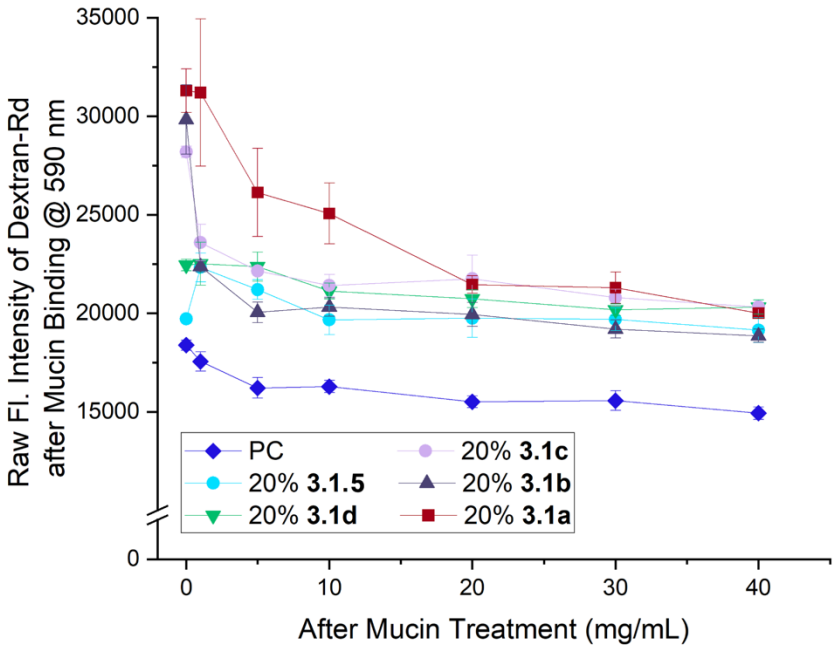


Figure 3.9 Raw fluorescence values from mucin binding competition assay. Raw fluorescence values after treatment with mucin and displacement of Rd-dextran from liposomes. Results show greater dose-dependent displacement of Rd-dextran by mucin using all BBALs tested compared to PC liposomes or liposomes containing **3.2.5**. BBAL **3.1a** yielded the greatest signal change. Error bars represent standard errors of at least three replicates.

liposomes at up to 20 mol% liposome incorporation.

3.6. Transmission electron microscopy studies

Next, lipid nanoparticle stability was further analyzed by TEM experiments. Liposomes containing 20% **3.1a** lipid (with the remainder composed of Egg-PC) were mounted on a copper grid and negatively stained with 5% uranyl acetate, a cationic stain commonly used for NS to examine liposome structure.[353] The **3.1a** liposomes appear to have circular cross-sections exhibiting traditional morphology (Figure 3.12), which further verified the formation of stable liposomes at up to 20% **3.1a** incorporation.

3.7. Cellular delivery studies with vascular smooth muscle cells

Having confirmed carbohydrate binding by liposomes containing BBALs, we next moved to assess the ability of these compounds to drive cellular association using fluorescence microscopy analysis. We began by studying mammalian cell delivery using vascular smooth muscle cells (VSMCs) due to the importance of this cell type as a target for peripheral vascular disease (PVD).[354] The following experiments involving VSMCs were performed in collaboration with Dr. Deidra Mountain's lab at the University of Tennessee Medical Center, Knoxville, Department of Surgery. The studies were led by postdoctoral researcher Dr. Sam Mattern-Schain from the Mountain lab. For these studies, liposomes containing 1% Rd-PE were used to analyze liposome localization following cell incubation. Following preliminary experiments, we proceeded with compound **3.1c**, which exhibited promising activity. Liposomes were prepared using the ethanol injection method with 0%, 10%, or 20% BBAL **3.1c**; 1% Rd-PE; 5% PEG-PE; and the remainder consisted of a 7:3 mixture of DOPC:Cholesterol (94%, 84%, or 74%, respectively). After VSMC cells were incubated with liposomes for 24 hr, cells were washed thoroughly before collection or imaging.

3.7.1. Quantification of cellular delivery

The extent of Rd-PE-labeled liposomal association to VSMCs was quantified by measuring Rd-PE fluorescence of cell lysate supernatant. Figure 3.13A shows that cells treated with liposomes containing 10% **3.1c** exhibited increased fluorescence compared to cells treated with liposomes

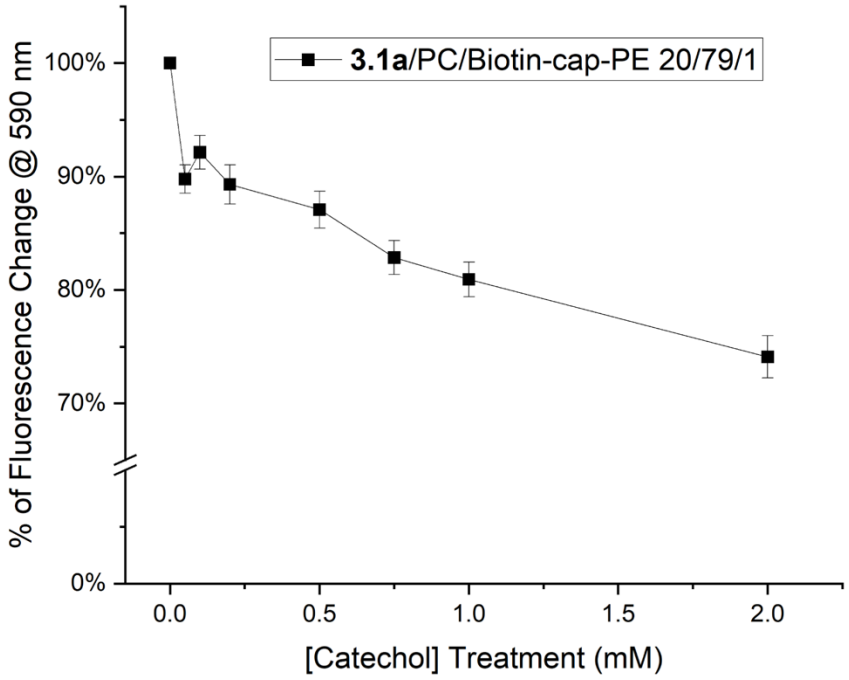


Figure 3.10 Catechol bis-boronic acid binding competition assay. Results show dose-dependent decreases in the percent of fluorescence caused by treatment with catechol and displacement of Rd-dextran from 20% **3.1a** liposomes. Error bars represent standard errors of at least three replicates.

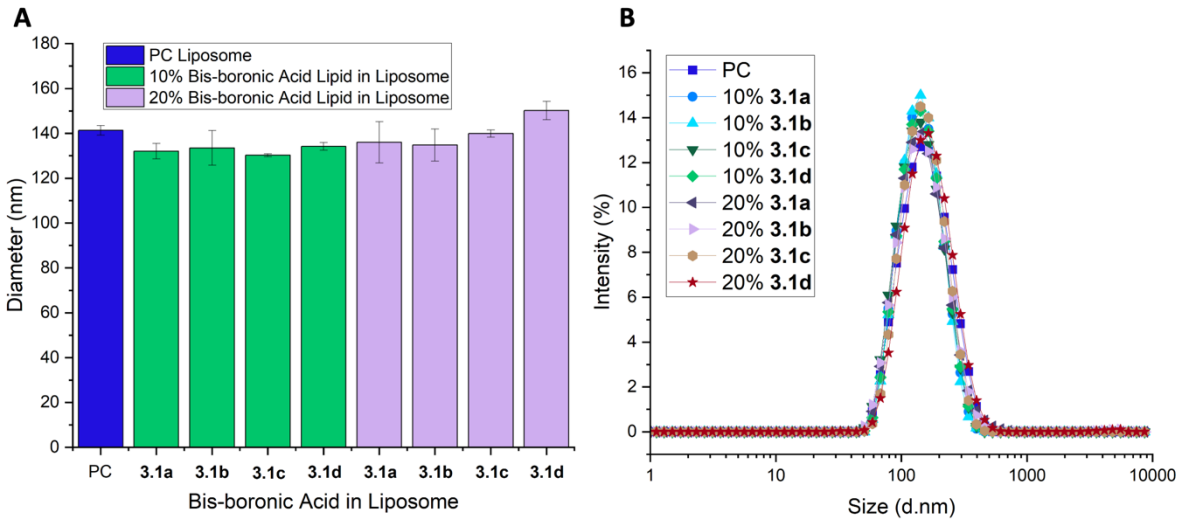


Figure 3.11 Dynamic light scattering studies of BBALs. DLS analysis of liposomes containing 0%, 10%, or 20% BBAL **3.1a-d** with the remainder PC (100%, 90%, or 80%, respectively). All formulations formed stable and uniform liposomes. Error bars represent standard errors of at least three replicates.

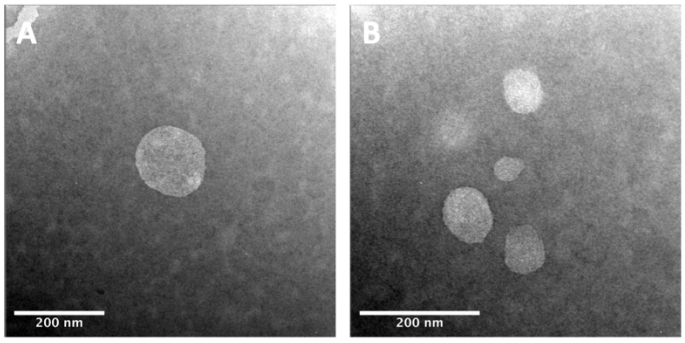


Figure 3.12 TEM images of Bis-boronic acid liposomes. Representative TEM images of liposomes containing 20% **3.1a** and 80% PC. Images indicate spherical liposomes in the desired size range (<200 nm). Scale bars represent 200 nm.

containing 0% **3.1c**, followed by an even more dramatic increase in fluorescence from cells treated with liposomes containing 20% **3.1c**.

3.7.2. Cellular delivery imaging

Fluorescence microscopy images were acquired as a representative visualization of cellular association of liposomes. These images confirm that cells treated with liposomes containing 10% or 20% **3.1c** demonstrate enhanced cell association (Figure 3.13D and Figure 3.13E, respectively) compared to cells treated with liposomes lacking BBAL (Figure 3.13C), while untreated cells showed only DAPI stain (Figure 3.13B). It is difficult to interpret the localization of liposome components since fluorescent lipid Rd-PE and other lipid components can dissociate from the liposomes during or after cell delivery. However, it is clear that the inclusion of BBAL **3.1c** enhances liposomal labeling of cells.

3.7.3. Delivery of liposomes encapsulating polar dye sulforhodamine B

A study was also conducted to assess the ability of our liposome platform to deliver internal cargo, which is the ultimate goal for drug delivery applications. Liposomes composed of either 10% or 20% **3.1c** were first prepared with polar dye sulforhodamine B (SRB) encapsulated within their aqueous interiors at a self-quenching concentration (50 mM) within the BBAL liposomes. Release and dilution of SRB into the cellular environment results in dequenching of the SRB fluorescence, resulting in an increase in SRB fluorescence emission. To perform the experiment, VSMC cells were treated with the SRB loaded BBAL liposomes, incubated to allow for cell entry and SRB delivery, after which residual liposome washed away and SRB delivery analyzed in two ways. First, cell lysate supernatant was prepared, and the delivery of SRB was quantified within the cell lysates by measuring residual SRB fluorescence. As shown in Figure 3.14A, cell lysate fluorescence readings indicate increases in SRB delivery with 10% and 20% BBAL **3.1c** incorporated within the membrane. Second, fluorescence microscopy images were also obtained which further confirm that VSMCs treated with liposomes containing 10% **3.1c** (Figure 3.14D) or 20% **3.1c** (Figure 3.14E) exhibited increased SRB delivery compared to cells treated with liposomes containing 0% **3.1c** (Figure 3.14C). Altogether, these results indicate that incorporation

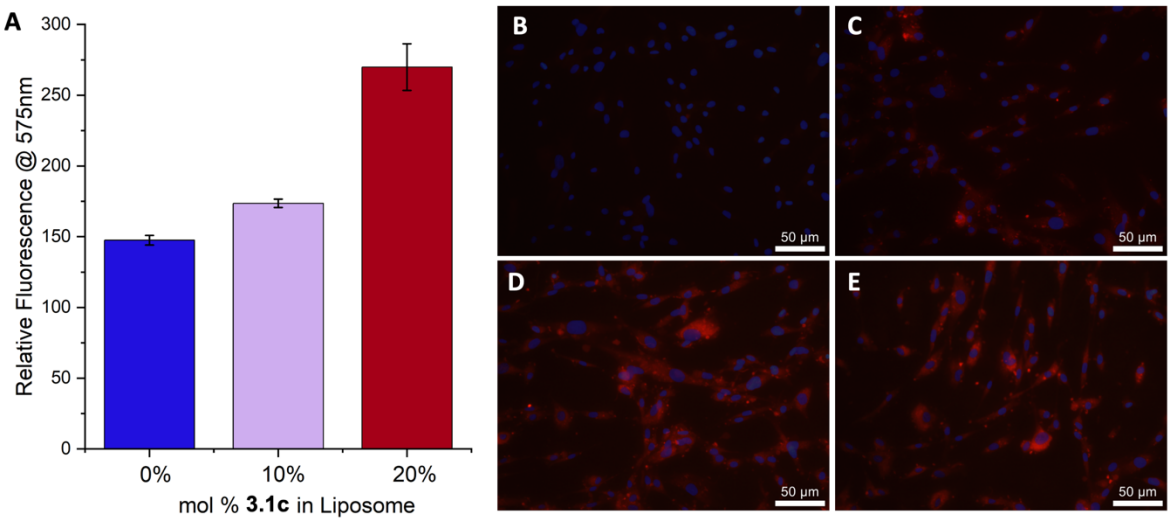


Figure 3.13 VSMC cell binding experiment. (A) Cell lysate quantification shows liposomes containing either 10% or 20% **3.1c** had greater cell association than liposomes lacking **3.1c**. (B) Untreated VSMCs show DAPI stain only. (C) Cells treated with 0% **3.1c** liposomes show minimal fluorescence while cells treated with (D) 10% **3.1c** and (E) 20% **3.1c** bis-boronic acid fluorescent liposomes showed increased membrane binding as indicated by Rd-PE fluorescence. The scale bars depict 50 µm. DAPI is shown in blue. Rd-PE is shown in red. Error bars represent standard error of at least three replicates.

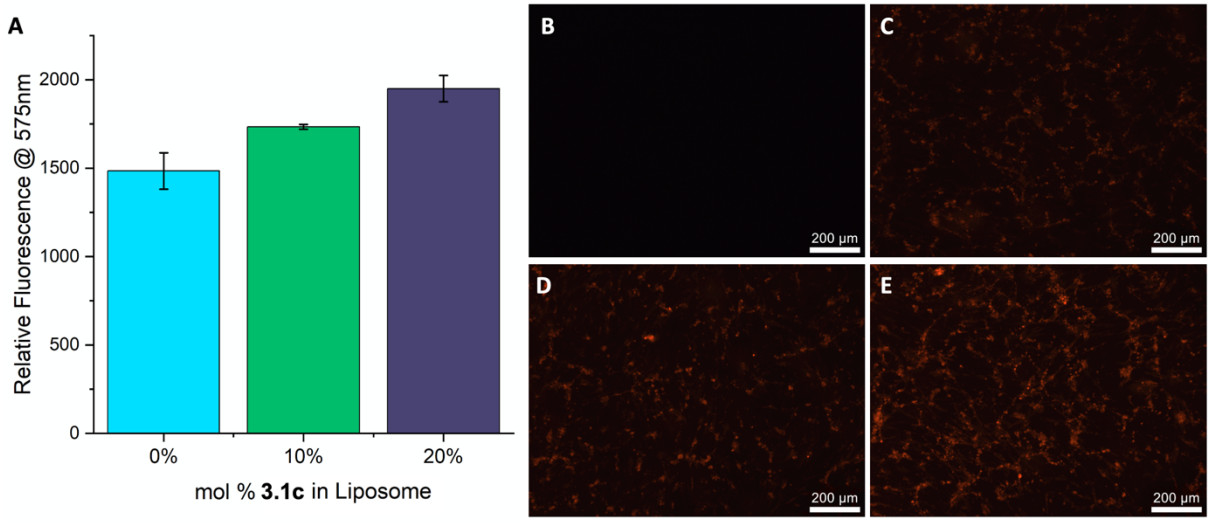


Figure 3.14 Liposomal SRB delivery to VSMCs. (A) Cell lysate quantification shows liposomes containing either 10% or 20% **3.1c** demonstrated greater SRB delivery than liposomes lacking **3.1c**. Cell images show that: (B) untreated VSMCs do not show signal, (C) Cells treated with 0% **3.1c** liposomes show minimal fluorescence while cells treated with (D) 10% **3.1c** and (E) 20% **3.1c** fluorescent liposomes showed increased SRB delivery, as indicated by SRB fluorescence. The scale bars depict 200 µm. Rd-PE is shown in red. Error bars represent standard error of at least three replicates.

of BBALs into liposomal delivery vesicles enhanced their association with VSMCs and achieved internal cargo delivery to the cells.

3.7.4. Dynamic light scattering of liposomes used in cellular experiments

Since cellular delivery experiments were completed with more complex liposome formulations and prepared with the ethanol injection technique, we again probed the stability of these formulations. The ethanol injection technique produces liposomes between 30 - 170 nm on average, which is smaller on average than liposomes prepared with the thin-film method.[355] Also, the size can be influenced by the concentration of lipids and the injection speed. When using this technique, liposomes are dissolved in ethanol, injected into the aqueous (buffer) phase during rapid vortexing, and then the ethanol is removed by either rotary evaporation, centrifugation, or dialysis. Liposomes were prepared with 0%, 10%, or 20% BBAL **3.1c**, 1% Rd-PE, 5% PEG-PE, and the remainder consisted of a 7:3 mixture of DOPC:Cholesterol (94%, 84%, or 74%). DLS analysis was then used to assess particle sizes of liposome formulations. The three liposome formulations were assessed, and the results showed that the liposomes formed stable vesicles of sizes between 50 - 70 nm, which is within the expected diameter range for ethanol injection technique following extrusion (Figure 3.15). These data indicate that the BBAL formulations for cell experiments were stable and uniform.

3.8. Other attempted mammalian BBAL cell delivery studies

3.8.1. Overview of attempted mammalian BBAL cell delivery studies

In addition to confirming enhancement of cellular delivery with VSMC cells, multiple studies were done with other cell types in attempts to demonstrate enhancements in cellular delivery driven by the presence of BBALs in liposomes. These experiments were performed in collaboration with Dr. Joshua Baccile's lab in UTK Chemistry. Graduate student Dillon McBee from the Baccile group contributed to these studies in terms of maintaining cell cultures and plating cells for experiments. These experiments were conducted using either U87 human glioblastoma cell line, MDA-MB-231 human epithelial breast cancer cell line, or A375 human malignant melanoma cell line. Liposomes containing **3.1a-d** were expected to enhance delivery of liposomes by binding carbohydrates which are overexpressed and aberrantly glycosylated on cancer cell surfaces. Such

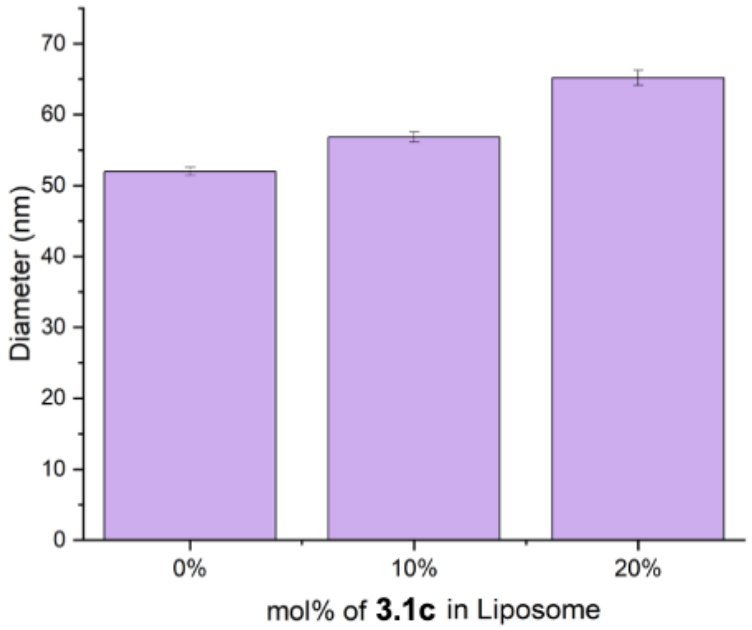


Figure 3.15 Dynamic Light Scattering of BBAL liposomes used in cellular experiments. DLS analysis of liposomes containing 0%, 10%, or 20% BBAL **3.1c**, 1% Rd-PE, 5% PEG-PE, with the remainder a 7:3 mixture of DOPC:Cholesterol (94%, 84%, or 74%). Liposomes were prepared with the ethanol injection technique. All formulations formed stable and uniform liposomes. Error bars represent standard errors of at least three replicates.

binding events can trigger cell entry pathways such as membrane fusion or pinocytosis. In these experiments, cancer cells (U87, MDA-MB-231, or A375) were incubated with liposomes containing various percentages (0%, 10%, 20%, or 50%) of either **3.1a** or **3.1c**, which had shown the most promising results in the microplate carbohydrate binding assays. The liposomes were otherwise composed of Egg-PC, along with 0.08% Rd-PE as a fluorescent marker of liposome localization. Liposomes lacking **3.1a** or **3.1c** (replaced by PC) were employed as negative controls. Cells were plated either on glass coverslips or in 96-well plates, and liposomes were added to the cells and allowed to incubate for 1 hr at 37 °C. Following 1 hr incubation, cells were washed with buffer, fixed with 4% paraformaldehyde, and either mounted with DAPI containing mountant (for coverslips) or stained with DAPI solution (for 96 well plates). Fluorescence microscopy was used to image cells and evaluate the presence of Rd-PE resulting from liposome association with cells. Cell-associated Rd-PE fluorescence was quantified using Gen5 software.

3.8.2. Attempted BBAL U87 cell delivery study results

Cell delivery studies with the U87 human glioblastoma cell line were performed first. Representative images in Figure 3.16 show that U87 cells treated with liposomes containing 20% **3.1a** (Figure 3.16E,H) or 20% **3.1c** (Figure 3.16I,L) displayed minimally enhanced fluorescence (Rd-PE, red) compared to cells treated with control liposomes containing 0% BBAL (Figure 3.16A,D).

3.8.3. Attempted BBAL MDA-MB-231 cell delivery study results

Next, cell delivery studies with MDA-MB-231 human epithelial breast cancer cell line were performed. Representative images of cells taken with a 63x oil immersion objective are shown in Figure 3.17. Similar to the cell study with U87 cells, these images show that cells treated with liposomes containing 20% **3.1a** (Figure 3.17E,H) or 20% **3.1a** (Figure 3.17I,L) did not exhibit enhanced fluorescence (Rd-PE, red) compared to cells treated with control liposomes containing 0% BBAL (Figure 3.17A,D). Representative images of MDA-MB-231 cells taken with a 40x objective likewise show that cells treated with liposomes containing 0% BBAL (Figure 3.18A,D) had visually identical fluorescence compared to liposomes containing 20% **3.1a** (Figure 3.18E,H), 20% **3.1a** (Figure 3.18I,L), or 20% of mono-boronic 20% **3.1.5** (Figure 3.18M,P).

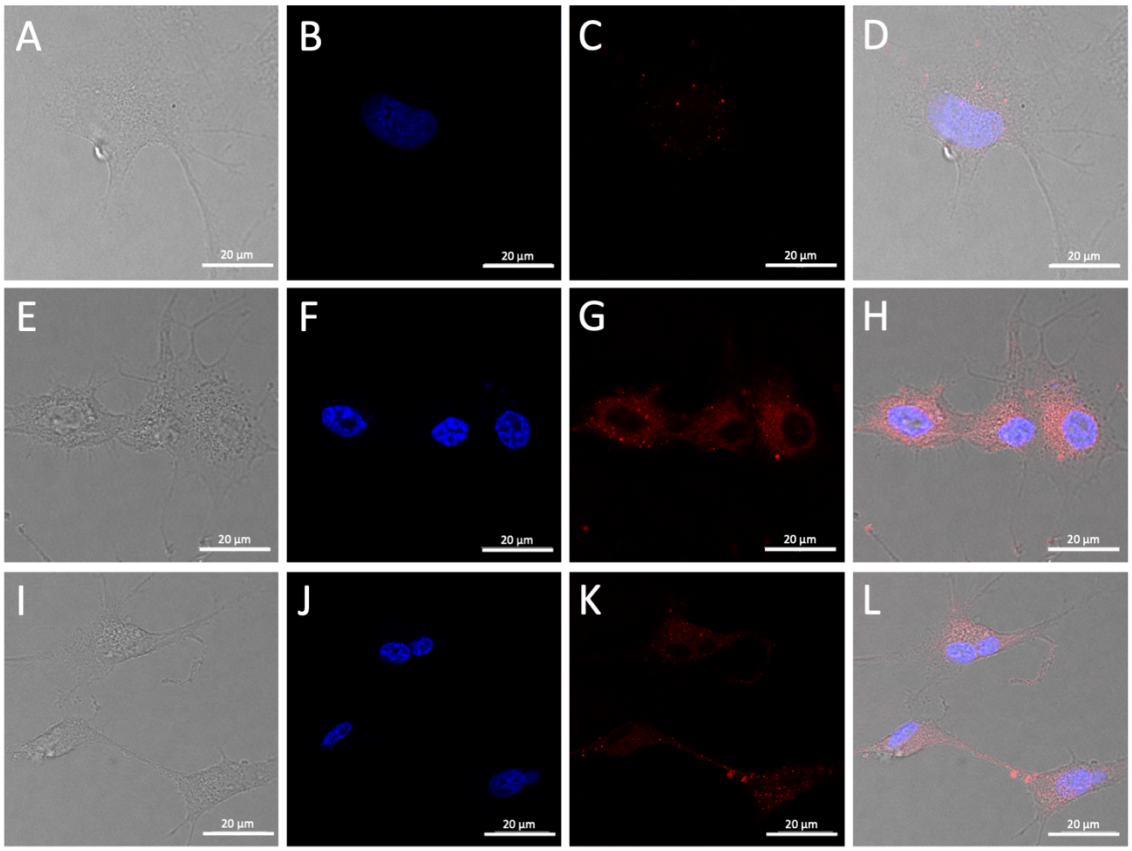


Figure 3.16 Bis-boronic acid U87 cell delivery study results. Representative 63X images show separate channels of U87 cells treated with liposomes containing 0.08% Rd-PE including (A) brightfield 0% BBAL, (B) DAPI only 0% BBAL, (C) Rd-PE only 0% BBAL, and (D) overlay 0% BBAL; (E) brightfield 20% **3.1a**, (F) DAPI only 20% **3.1a**, (G) Rd-PE only 20% **3.1a**, and (H) overlay 20% **3.1a**; (I) brightfield 20% **3.1c**, (J) DAPI only 20% **3.1c**, (K) Rd-PE only 20% **3.1c**, and (L) overlay 20% **3.1c**. Images demonstrate that **3.1a** and **3.1b** did not enhance delivery to U87 cells, as indicated by Rd-PE fluorescence. The scale bars depict 20 µm. DAPI is shown in blue. Rd-PE is shown in red.

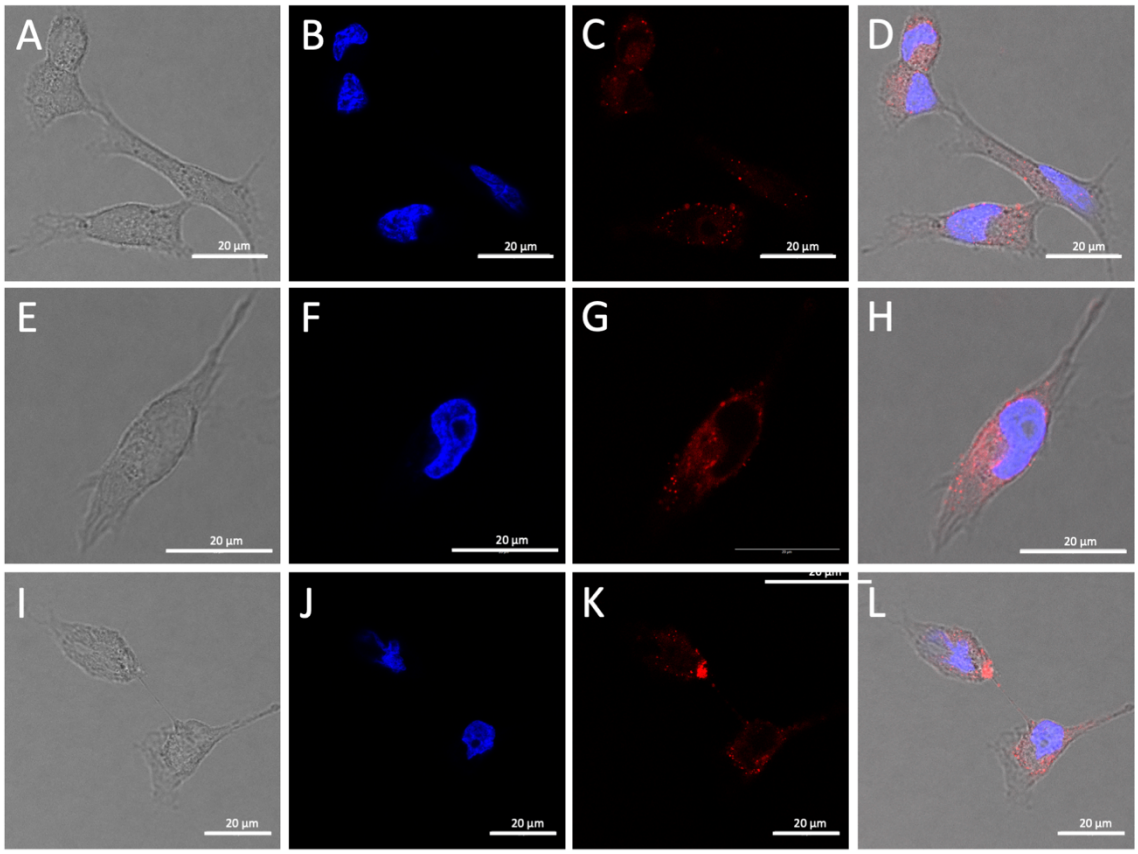


Figure 3.17 Bis-boronic acid MDA-MB-231 63X cell delivery study results. Representative 63X images show separate channels of MDA-MB-231 cells treated with liposomes containing 0.08% Rd-PE including (A) brightfield 0% BBAL, (B) DAPI only 0% BBAL, (C) Rd-PE only 0% BBAL, and (D) overlay 0% BBAL; (E) brightfield 20% **3.1a**, (F) DAPI only 20% **3.1a**, (G) Rd-PE only 20% **3.1a**, and (H) overlay 20% **3.1a**; (I) brightfield 20% **3.1c**, (J) DAPI only 20% **3.1c**, (K) Rd-PE only 20% **3.1c**, and (L) overlay 20% **3.1c**. Images demonstrate that **3.1a** and **3.1b** did not enhance delivery to MDA-MB-231 cells, as indicated by Rd-PE fluorescence. The scale bars depict 20 µm. DAPI is shown in blue. Rd-PE is shown in red.

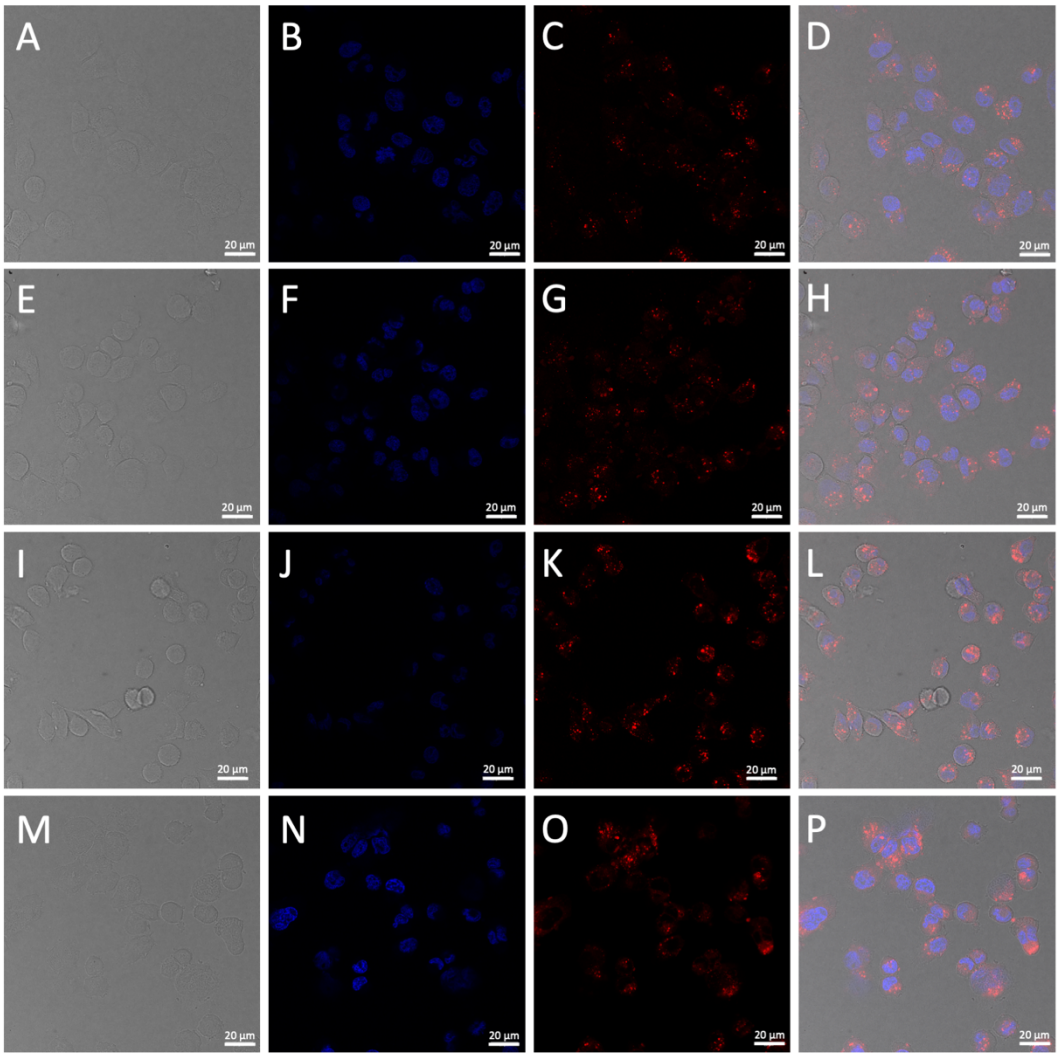


Figure 3.18 Bis-boronic acid MDA-MB-231 40X cell delivery study results. Representative 40X images show separate channels of MDA-MB-231 cells treated with liposomes containing 0.08% Rd-PE including (A) brightfield 0% BBAL, (B) DAPI only 0% BBAL, (C) Rd-PE only 0% BBAL, and (D) overlay 0% BBAL; (E) brightfield 20% **3.1a**, (F) DAPI only 20% **3.1a**, (G) Rd-PE only 20% **3.1a**, and (H) overlay 20% **3.1a**; (I) brightfield 20% **3.1c**, (J) DAPI only 20% **3.1c**, (K) Rd-PE only 20% **3.1c**, (L) overlay 20% **3.1c**; and (M) DAPI only 20% **3.2.5**, (N) Rd-PE only 20% **3.2.5**, and (O) overlay 20% **3.2.5**. Images demonstrate that **3.1a**, **3.1b**, or **3.2.5** did not enhance delivery to MDA-MB-231 cells, as indicated by Rd-PE fluorescence across all treatment types. The scale bars depict 20 µm. DAPI is shown in blue. Rd-PE is shown in red.

3.8.4. Attempted BBAL A375 cell delivery study results

Last, cell delivery studies with A375 human malignant melanoma cell lines were performed, which are the same cells that were used in the cellular delivery experiments with the mono-boronic acid lipid. In the mono-boronic acid liposome studies, the inclusion of the lipid in liposomes did indeed show enhancements in cellular delivery to A375 cells.[216] Representative images in Figure 3.19 show that A375 cells treated with 1 mM or 2 mM of liposomes containing of 20% **3.1a** (Figure 3.19B,G), 30% **3.1a** (Figure 3.19C,H), 40% **3.1a** (Figure 3.19D,I), or 50% **3.1a** (Figure 3.19E,J) did not exhibit enhanced liposome delivery fluorescence compared to cells treated with control liposomes containing 0% **3.1a** (Figure 3.19A,F). In the same way but in regard to lipid **3.1c**, representative images in Figure 3.20 show that A375 cells treated with 1 mM or 2 mM of liposomes containing of 20% **3.1c** (Figure 3.20B,G), 30% **3.1c** (Figure 3.20C,H), 40% **3.1c** (Figure 3.20D,I), or 50% **3.1c** (Figure 3.20E,J) also did not improve liposome delivery to cells compared to cells treated with control liposomes lacking **3.1c** (Figure 3.20A,F).

3.9. Cellular delivery studies with *Candida albicans*

3.9.1. Overview of Candida albicans BBAL liposome cellular delivery

In addition to confirming enhancement of cellular delivery with VSMC cells and attempting experiments with other mammalian cells, delivery to non-mammalian cells was probed as well. We began by assessing if BBALs **3.1a-d** could enhance cell delivery to *Candida albicans* (*C. albicans*) yeast cells. These experiments were performed in collaboration with Dr. Todd Reynolds' lab in UTK Microbiology. Graduate student Yue Zhou from the Reynolds group contributed to these studies in terms of maintaining cell cultures and preparing cells for experiments.

The following application we pursued involved boronic acid liposomes as therapeutic agents for fungal infections. Fungal infections can be difficult to treat and are associated with high rates of morbidity and mortality in immunocompromised patient populations who are at higher risk of developing infections.[356] Boric acid and other organoboron compounds have been used as topical therapeutics for candidiasis in cases when conventional treatment with azole antifungals fails.[357, 358] Failure of conventional treatment can lead to recurrent infections and the development of

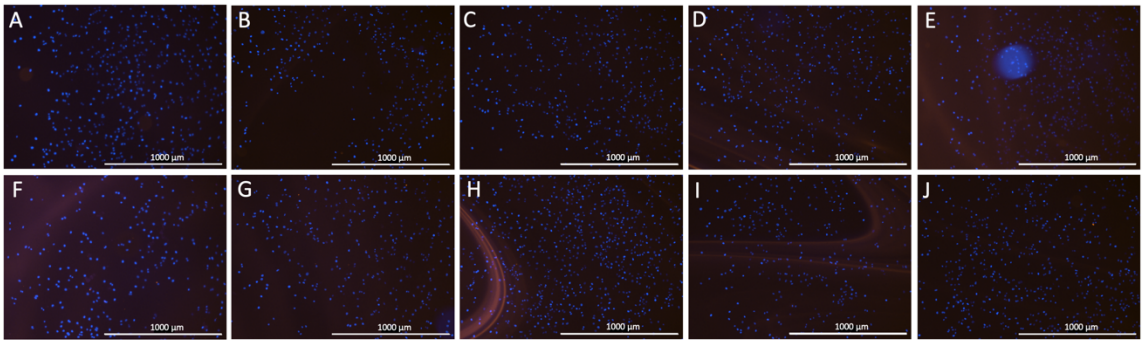


Figure 3.19 Bis-boronic acid A375 4X cell delivery study results. Representative 4X images show A375 cells treated with liposomes containing 0.08% Rd-PE and (A) 1 mM 0% **3.1a**, (B) 1 mM 20% **3.1a**, (C) 1 mM 30% **3.1a**, (D) 1 mM 40% **3.1a**, (E) 1 mM 50% **3.1a**; or (F) 2 mM 0% **3.1a**, (G) 2 mM 20% **3.1a**, (H) 2 mM 30% **3.1a**, (I) 2 mM 40% **3.1a**, or (F) 2 mM 50% **3.1a**. Images demonstrate that **3.1a** did not enhance delivery to A375 cells, as indicated by minimal Rd-PE fluorescence across all treatment types. The scale bars depict 1000 µm. DAPI is shown in blue. Rd-PE is shown in red.

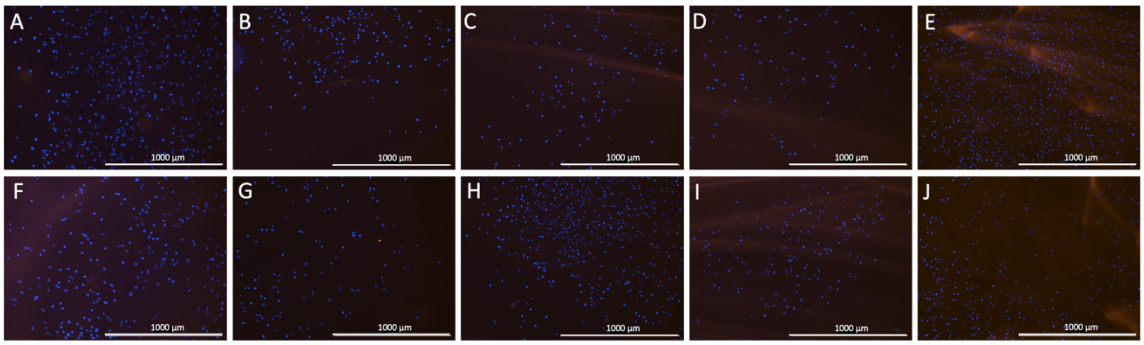


Figure 3.20 Bis-boronic acid A375 4X cell delivery study results. Representative 4X images show A375 cells treated with liposomes containing 0.08% Rd-PE and (A) 1 mM 0% **3.1c**, (B) 1 mM 20% **3.1c**, (C) 1 mM 30% **3.1c**, (D) 1 mM 40% **3.1c**, (E) 1 mM 50% **3.1c**; or (F) 2 mM 0% **3.1c**, (G) 2 mM 20% **3.1c**, (H) 2 mM 30% **3.1c**, (I) 2 mM 40% **3.1c**, or (F) 2 mM 50% **3.1c**. Images demonstrate that **3.1c** did not enhance delivery to A375 cells, as indicated by minimal Rd-PE fluorescence across all treatment types. The scale bars depict 1000 µm. DAPI is shown in blue. Rd-PE is shown in red.

drug-resistant microbes. Although they are widely used, not much is known about the mechanism of antifungal effects of boric acid and other organoboron compounds. It has been shown that boric acid slowly compromises *C. albicans* cellular integrity, but sudden, destructive membrane damage is not believed to be the primary antifungal effect of boric acid. However, boric acid treatment has been shown to reduce ergosterol concentration in the yeast membrane and suppress the formation of invasive hyphae.[359] These findings suggest that boric acid treatment may weaken the cellular membrane and make fungal cells more susceptible to azole therapy. Another study showed that organoboron concentration as low as 0.625% w/v (0.1 M) resulted in greater than ten-fold inhibition of *C. albicans* growth.[360] Consequently, pairing azole antifungal treatment with bis-boronic acid liposomes delivery could lead to a more efficient antifungal therapy.

Further, *C. albicans* has an exterior surface coating of mannoproteins which we expected the BBALs could bind to (Figure 3.21). The composition of yeast cell wall varies by species, but there are some common similarities such as chitin (β-1,4-*N*-acetylglucosamine) and β-1,3(β-1,6)-glucans, both being core elements that provide strength to the cell wall. The third similarity is that the outer cell wall is covered with mannan, a highly branched complex carbohydrate with an α-1,6 backbone as well as α-1,2 and α-1,3-linked mannose (Man) sidechains.[361] Some sidechains are further branched through phosphodiester bonds and *C. albicans* uniquely has some sidechains that terminate in β-1,2 mannose residues.[362] The mannose is attached to the cell wall via proteins linked to the remnant of a glycosylphosphatidylinositol (GPI) anchor. The GPI anchored proteins (GPI-APs) have a core structure of protein-CO-NH_2-CH_2-CH_2-PO_4-6-Manα1,2Manα1,6Manα1,4GlcNα1,6-*myo*-inositol phospholipid, but this structure is modified during biosynthesis and transfer to the cell wall.[363] The GPI-APs on the yeast cell wall are a remnant of GPI anchors which have lost the phospholipid segment after cleavage between Man-1 and GlcN and are instead attached to mostly β-1,6 or β-1,3 glucan in the cell wall via the reducing end of Man-1 residues.[364] The GPI remnant also has a fourth Man linked α-1,2 to the third Man and an ethanolamine phosphate on the third Man, which forms an amide bond with the α-carboxyl of the C-terminal amino acid of the protein.[364] This outer mannan layer was seen

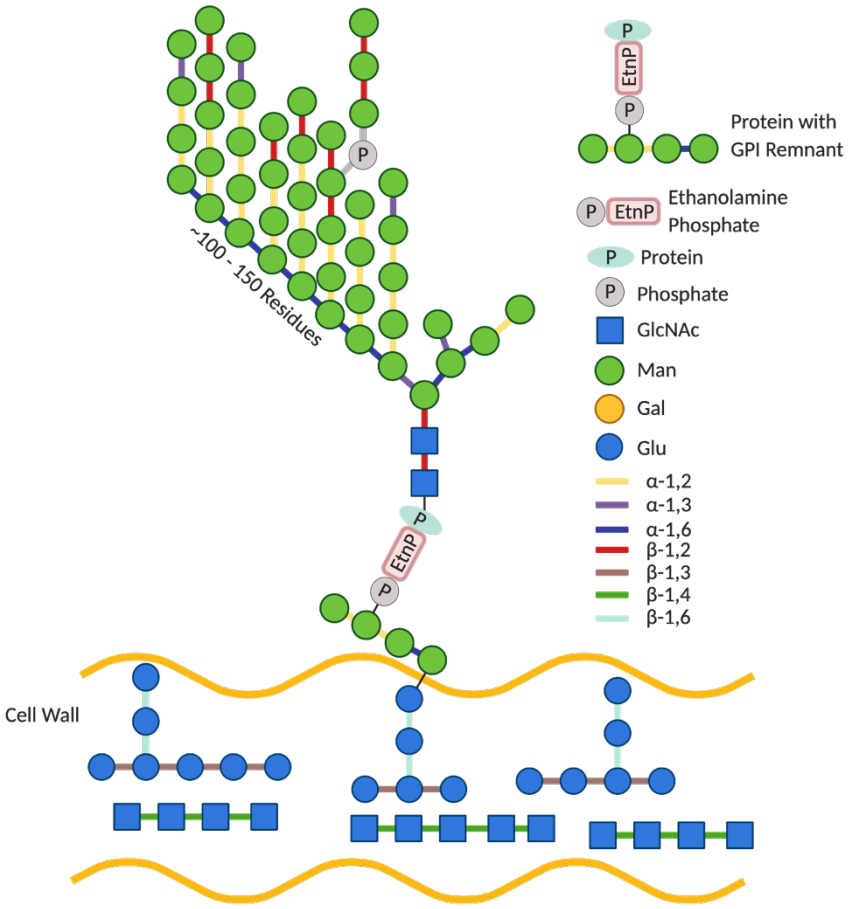


Figure 3.21 *C. albicans* cell wall composition. *C. albicans* cell wall consisting of chitin (β-1,4-*N*-acetylglucosamine) and β-1,3(β-1,6)-glucans in the core and highly branched α-1,2; α-1,3; and β-1,2 mannose sidechains, some of which terminate in β-1,2 mannosyl residues.[15]

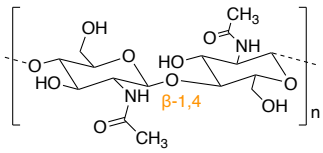
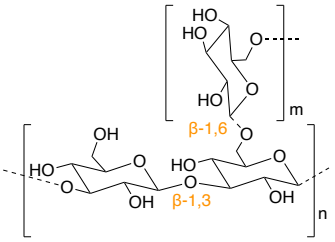
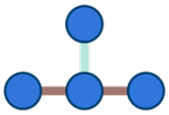
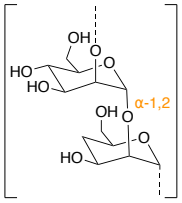
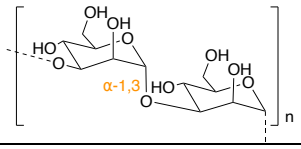
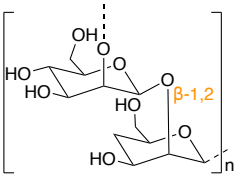
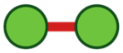
Sugar Name	Chemical Structure	Figure 8 Representation
β-1,4-*N*-acetylglucosamine (Chitin)		
β-1,3(β-1,6)-glucans		
α-1,2 Mannose		
α-1,3 Mannose		
β-1,2 Mannose		

Table 3.4 Chemical structures of compounds that compose *C. albicans* cell wall. Yeast cell wall chemical structures including chitin (β-1,4-*N*-acetylglucosamine); β-1,3(β-1,6)-glucans; and α-1,2; α-1,3; and β-1,2 linked mannose.

as a possible target for boronic acid liposomes. Table 3.4 shows the chemical structures of chitin (β-1,4-N-acetylglucosamine);[365] β-1,3(β-1,6)-glucans;[366] and α-1,2; α-1,3; and β-1,2 mannose.[367]

Therefore, experiments were performed to examine the effect of bis-boronic acid liposomes on *C. albicans*, with the hypothesis that binding interactions between BBALs and mannoproteins could drive improvements in infection-associated cellular glycan recognition and enhance liposomal membrane binding, cell entry, and delivery for therapeutic applications.

3.9.2. Cellular delivery of bis-boronic acid delivery to *C. albicans*

We next moved to assess delivery to *C. albicans* cells since this microorganism is the most prevalent cause of fungal infections that are very difficult to treat.[368-370] Additionally, *C. Albicans* cell surfaces are densely decorated with mannose-rich oligosaccharides that may be targeted by boronic acid liposomes.[368, 370, 371] First, confocal fluorescence laser scanning microscopy experiments were used to evaluate the delivery of 20% **3.1a** or **3.1c** liposomes containing 1% nitrobenzoxadiazole (NBD) labeled lipid (1,2-dioleoyl-*sn*-glycero-3-phosphoethanolamine-*N*-(7-nitro-2-1,3-benzoxadiazol-4-yl) (ammonium salt) (NBD-PE) as a fluorescent marker. In this study, strain SC5314 (wildtype) of *C. albicans* was used, which has been previously described.[372] To prepare the cells for studies, cells were cultured in 5 mL yeast extract peptone dextrose (YPD) media (1% Bacto yeast extract, 2% Bacto peptone, and 2% dextrose) and shaken at 30 °C and 250 rpm overnight. The next day, cells were diluted to OD_{600} = 0.1 in 50 mL fresh YPD media and were spun down when OD_{600} reaches 1.0. The cell pellets were washed three times with 30 mL PBS to remove residual nutrients and were left in 5 mL fresh PBS to be shaken at 30 °C and 250 rpm overnight. On day three, cells were diluted to final OD_{600} = 1.0 in PBS with each liposome treatment at a final concentration of 1 mM, with a total volume of 500 μL. Cells were incubated with these liposome formulations for 8 hr at 37 °C, and then washed to remove residual unbound liposomes. After fixing with 3.7% paraformaldehyde, washing, and mounting on glass slides, the cells were imaged. Samples were used immediately and were kept on ice (0 °C) during sample preparation for fluorescence microscopy and flow cytometry studies. Liposome association was

evaluated based on the fluorescent signal from NBD-PE, which was collected upon excitation at 458 nm with an Ar ion laser and emission collected 470 - 560 nm.

As seen in the representative images in Figure 3.22, cells treated with control PC liposomes lacking BBALs (Figure 3.22A) exhibited minimal fluorescence while those subjected to liposomes containing 20% of either **3.1a** or **3.1c** (Figure 3.22B, Figure 3.22C) showed slightly enhanced fluorescence resulting from labeled liposomes. Delivery is not particularly strong in this case, which can be attributed to challenges associated with the complex cell wall of *C. albicans.* Additionally, *C. albicans* cellular delivery was quantified with flow cytometry. Samples were prepared similarly as for fluorescence microscopy, but after fixing and washing, cell pellets were resuspended in PBS (OD_{600} = 1.0) and kept on ice for flow cytometry with FACSCalibur LSR II flow cytometer (Becton Dickinson). After exclusion of debris (forward scatter area (FSC-A) vs side scatter area (SSC-A) plot) and gating for single cells (forward scatter width (FSC-W) vs FSC-A), NBD-PE fluorescence intensity was recorded in the PE-A channel. Flow cytometry data were obtained for 8,000 - 10,000 gated events per sample. Replicates were analyzed on the same day and data analysis was performed using FlowJo software (v.10.11 FlowJo LLC, OR, USA). Untreated cells were also prepared as a negative control, which consisted of cells treated with buffer (no liposome) but were otherwise prepared the same. As seen in Figure 3.22D-E, flow cytometry results confirmed that when compared to cells that received no treatment, there was an increase in significance of delivery of 20% **3.1a** (p=4.3×10^{-4}) or **3.1c** (p=5.5×10^{-4}) liposomes as compared to 0% BBAL liposomes (p=2.0×10^{-3}). However, neither differences in cellular delivery directly between 20% **3.1a** or **3.1c** liposomes and 0% BBAL liposomes, nor differences between 20% **3.1a** and **3.1c,** were found to be statistically different (p>0.05). Nevertheless, these results support that bis-boronic liposomes mildly enhanced yeast cell delivery driven by carbohydrate binding. While additional studies are needed to explore the yeast glycan binding applications of this liposome system, these results suggest that BBALs **3.1a-d** could potentially serve as promising nanocarriers for yeast cellular delivery.

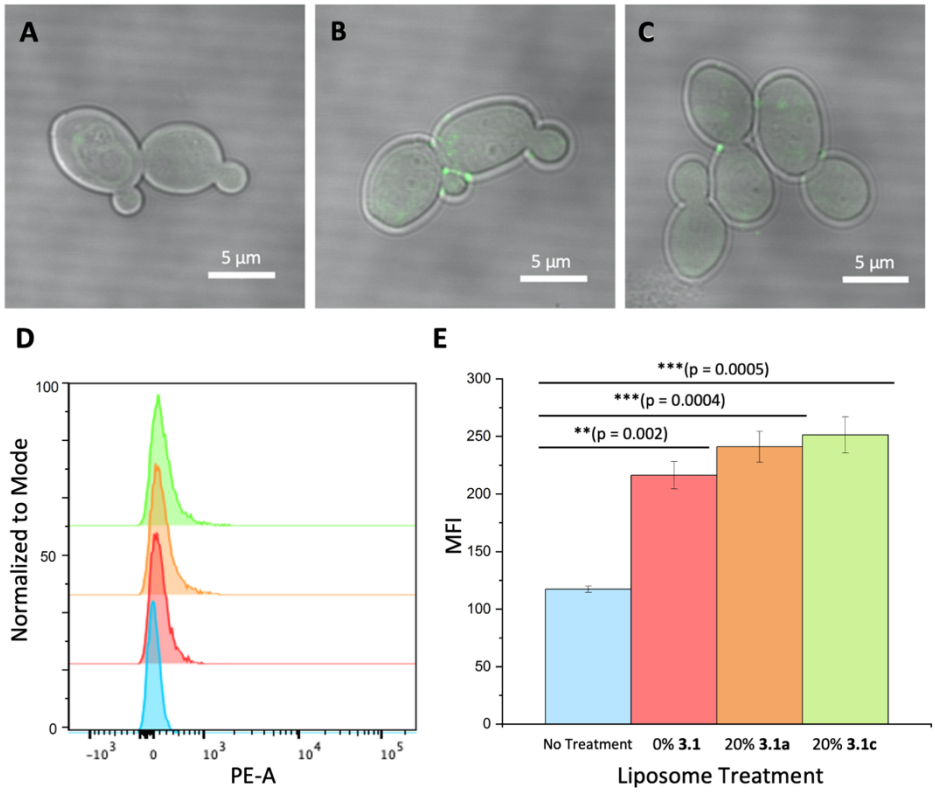


Figure 3.22 *C. albicans* cell delivery images and flow cytometry analysis. Merged images of bright field and NBD fluorescence (green) show that cells treated with liposomes containing 20% **3.1a** (B) or 20% (C) **3.1c** resulted in slightly enhanced fluorescence compared to (A) control liposomes lacking BBAL compound. All liposomes contained 1% NBD-PE and were otherwise composed of Egg-PC. Scale bars depict 5 µm and NBD-PE fluorescence is shown in green. (D) Representative flow cytometry histograms of *C. albicans* cells that have been incubated with (bottom row) no treatment, (second row) 0% BBAL liposome, (third row) 20% **3.1a** liposome, and (top row) 20% **3.1c** liposome. The x-axis represents NBD-PE fluorescence detected in the PE-A channel and the y-axis represents the relative number of cells for three biological replicates. (E) Statistical analysis (*t* test) of the mean fluorescence intensity (MFI) indicates that there is an increase in significance of uptake when **3.1a** (p=4.3×10^{-4}) or **3.1c** (p=5.5×10^{-4}) are incorporated in the liposomes vs. control liposomes lacking BBAL (p=2.0×10^{-3}) when compared to cells that received no treatment (*, 0.01 < p ≤ 0.05; **, 0.001 < p ≤ 0.01; ***, 0.0001 < p ≤ 0.001; ****, p ≤ 0.0001). N=3. Error bars represent standard errors of at least three replicates.

3.10. Alternative bis-boronic acid assays attempted

3.10.1. Attempted Nile red release assays

Prior to developing the carbohydrate binding assays, various other studies were done in attempts to assess the functionality of BBALs **3.1a-d**. First, a Nile red (NR) release assay was used to probe the release of non-polar cargo from liposomes containing **3.1a-d**, since NR is a common hydrophobic dye used for membrane examination.[373] NR is incorporated within the bilayer membrane of liposomes and only fluoresces when encapsulated there. Once liposomes are triggered and NR is released into aqueous media, it is no longer soluble and therefore no longer fluorescent.[374] Thus, the release of NR can be tracked by reductions in fluorescence. It was originally hypothesized that interaction between lipids **3.1a-d** and carbohydrate triggers could lead to release of non-polar cargo due to reorganization of the lipid bilayer. Similar results were seen in experiments performed with the mono-boronic acid lipid, in which liposomes containing 20% **3.1.3** were treated with 5 Units of heparin and the liposomes released 50% of the NR cargo. Heparin, an anticoagulant consisting of repeating disaccharide units of sulfated iduronic acid/glucuronic acid and glucosamine residues, was used as a model carbohydrate in those studies because it had previously been shown to bind to boronic acids in a multivalent manner.[375, 376] Hence, studies were done with lipids **3.1a-d** and various carbohydrates in order to assess if binding could lead to membrane disruption and cargo release.

Liposomes were prepared by incorporating varying percentages (0 - 50%) of **3.1a-d** along with common bulk lipids such as phosphatidylcholine (Egg-PC), and 5% NR was also included in all formulations. Standard thin film liposome preparation was used to prepare unilamellar liposomes, including creation of lipid mixtures in chloroform, drying to films, hydrating, freeze/thaw cycling, and extrusion through 200 nm filter for at least 15 passes. After taking an initial fluorescence scan, samples were treated with a screen of carbohydrate triggers at various concentrations, including heparin; glycoprotein mucin; polysaccharide guar; horseradish peroxidase (HRP); small sugars such as glucose, galactose, mannose, *N*-acetylneuraminic acid (Neu5Ac); and other non-carbohydrate small molecules including ATP, adenosine diphosphate (ADP), adenosine monophosphate (AMP), D-fructose-6-phosphate (FP), D-fructose-1,6-

biphosphate (FBP), GSH, nicotinamide adenine dinucleotide + hydrogen (NADH), nicotinamide adenine dinucleotide NAD^+, and flavin adenine dinucleotide (FADH). Since dilution effects can also cause fluorescence signal decreases, blank samples were also run, in which liposome was treated with buffer or Milli-Q water (MQ) only and release was monitored. No formulation or treatment was found that caused NR release from liposomes containing **3.1a-d** without having an effect on control liposomes lacking **3.1a-d**. This could be due to the fact that the lipids are not inherently designed to undergo triggered conformational change upon binding diols of carbohydrates, such as shifting from a cylindrical, membrane forming lipid to a cone shaped, non-bilayer forming lipid. Without this change in bilayer packing parameters, NR release may not be possible. Future studies could be aimed at designing a more rigid lipid scaffold which could encourage a larger change in cone angle and facilitate a shift to non-bilayer properties which results in NR release. A summary of liposome formulations, treatments, and results is shown in Table 3.5.

3.10.2. Attempted Alizarin Red S. competition assay

Following attempts of NR release assays, we set out to begin analyzing the binding properties of BBALs **3.1a-d**. First, ARS titration, which is a general optical reporter for studying the binding of boronic acids with carbohydrates, was attempted. ARS is widely used because it displays a change in color and fluorescence intensity upon binding boronic acid, and can be used both quantitatively and qualitatively to study carbohydrate–boronic acid interactions.[377-379] The general theory of the assay is that ARS shows a dramatic increase in fluorescence when complexed to boronic acids in aqueous solutions at physiological pH due to a shift in photophysical properties. Additionally, this assay can be performed in a 2-step manner in order to further measure the binding affinity of boronic acids.[380] After initial interaction between boronic acids and ARS, a second step can be performed in which a separate carbohydrate is added to the mixture which competes for binding. In this case, there are two competing equilibria in the fluorescence assay, the first is between the boronic acid and the ARS, which is measured by an increase in fluorescence due to boronate formation. After the separate carbohydrate is added, the second equilibrium occurs between the boronic acid binding with the carbohydrate,

Table 3.5 Summary of formulations and treatments explored Nile Red release using BBAL liposomes with various percentages of 3.1a, 3.1b, 3.1d, or PC.

Entry	% 3.1a-d	% Egg-PC	Stable?	Treatment	Outcome
1	0	100	Yes	Buffer	Minimal Release (<10%)
2	10 **3.1a**	90	Yes		
3	10 **3.1c**	90	Yes		
4	0	100	Yes	10 units Heparin	~10% release
5	10 **3.1a**	90	Yes		
6	10 **3.1c**	90	Yes		
7	0			20 units Heparin (buffer)	~15% background release
8	10 **3.1a**	90	Yes		~15% release
9	10 **3.1c**	90	Yes		~15% release
10	0	100	Yes	MQ	~5% release
				10 units Heparin (MQ)	~5% release
11	10 **3.1a**	90	Yes	MQ	~15% release
				10 units Heparin (MQ)	~15% release
12	20 **3.1a**	80	Yes	MQ	~10% release
				10 units Heparin (MQ)	~10% release
13	30 **3.1a**	70	Yes	MQ	~10% release
				10 units Heparin (MQ)	~10% release
14	40 **3.1a**	60	Yes	MQ	~15% release
				10 units Heparin (MQ)	~15% release
15	0	100	Yes	0-2mM Mucin	~30% background release
16	10 **3.1a**	90	Yes		~20% release
17	10 **3.1c**	90	Yes		~20% release

Table 3.5 Continued

Entry	% 3.1a-d	% Egg-PC	Stable?	Treatment	Outcome
18	0	100	Yes	0-0.2 mg/mL Guar	~15% background release
19	10 **3.1a**	90	Yes		~15% release
20	10 **3.1c**	90	Yes		~15% release
21	10 **3.1a**	90	Yes	Glucose, galactose, mannose (0-10mM)	~5% increase in fluorescence
22	10 **3.1a**	90	Yes	N-Acetylneuraminic acid (0-30 mM)	~7% increase in fluorescence
23	0	100	Yes	ATP, ADP, AMP, FP, FBP, GSH, NADH, NAD^+ (0-10 mM)	~0-15% background release
				FADH (0-10 mM)	~50% background release
24	10 **3.1a**	90	Yes	ATP, ADP, AMP, FP, FBP, GSH, NADH, NAD^+ (0-10 mM)	~0-15% release
				FADH (0-10 mM)	~60% background release
25	10 **3.1d**	90	Yes	ATP, ADP, AMP, FP, FBP, GSH, NADH, NAD^+ (0-10 mM)	~0-10% release
				FADH (0-10 mM)	~60% background release

and subsequently displacing the ARS that had previously been bound. This release of ARS results in a decrease in fluorescence intensity. Hence, the binding of boronic acid to the separate carbohydrate can be indirectly measured by a decrease in ARS fluorescence intensity.

To perform this assay, liposomes were prepared by incorporating varying percentages (0 - 10%) of **3.1a** or **3.1b** along with common bulk lipids such as phosphatidylcholine (Egg-PC). Standard thin film liposome preparation was used to prepare unilamellar liposomes, including creation of lipid mixtures in chloroform, drying to films, hydrating, freeze/thaw cycling, and extrusion through 200 nm filter for at least 15 passes. Samples were also tested that contained free lipid **3.1a** or **3.1d**. After taking an initial fluorescence scan, ARS was titrated into the sample and fluorescence scans acquired after each ARS addition. Once a plateau was reached, various separate carbohydrates were then titrated into the mixture including *N*-acetylneuraminic acid (Neu5Ac) and heparin. Fluorescence readings were taken after each carbohydrate addition as well. The results of this assay, as summarized in Table 3.6, indicated that although fluorescence increased upon ARS addition, fluorescence also increased when the separate carbohydrate was added. Altogether, these titrations show that compounds **3.1a** and **3.1b** did bind to ARS as expected for a boronic acid sensor, but either they did not show binding affinity towards the carbohydrates attempted, or the carbohydrates used had unwanted interactions with the ARS causing it to increase in fluorescence intensity.

3.10.3. Attempted alternative microplate assay designs for BBALs 3.1a-d

Prior to the success of the Rd-dextran binding and mucin competition binding assays, additional assay designs were pursued in attempts to demonstrate boronic acid-mediated liposome binding to carbohydrates using BBALs **3.1a-d**. First, an HRP binding assay adapted from a previous report[341] was performed in which liposomes containing **3.1a-d** and 1% Biotin-cap-PE were prepared and immobilized onto a streptavidin microplate, followed by treatment with glycoprotein HRP (~40 kDa), which has previously been shown to bind boronic acids.[216] HRP can bind boronic acids because is composed of diverse carbohydrates including *N*-acetylglucosamine (GlcNAc), mannose, fucose and xylose units composing the complex oligosaccharides.[381, 382] Then,

Table 3.6 Summary of formulations and treatments explored with ARS competition assay using 3.1a or 3.1b.

Entry	% **3.1a-b**	% Egg-PC	ARS treatment	Fluorescence Outcome	Carb Treatment	Fluorescence Outcome
1	0	100	0.2mM	↓~20%	13.5 mM Neu5Ac	↓~25%
2	10 **3.1a**	90	0.2mM	↑~90%	13.5 mM Neu5Ac	↑~120%
3	10 **3.1b**	90	0.3mM	↑~45%	12.4 mM Neu5Ac	↑~80%
4	0.2 mM free **3.1a**	--	0.2mM	↑~600%	15.5 mM Neu5Ac	↑~1400%
5	0.2 mM free **3.1b**	--	0.1mM	↑~800%	14.1 mM Neu5Ac	↑~900%

the presence of bound HRP was assessed using the Pierce SuperSignal ELISA Femto Maximum Sensitivity Substrate kit, in which HRP is used to catalyze the excitation of luminol, resulting in chemiluminescence that indicates the presence of HRP bound on the liposome surface. The trials of this assay, as summarized in Table 3.7 entries 1.1-1.11, demonstrated mild enhancement of HRP binding by the BBAL liposomes. The two issues that persisted were that the assay did not perform consistently and also there was high background luminescence from control liposomes.

A second assay type was attempted in which a streptavidin microplate was first treated with a heparin-biotin (HB, ~15kDa) conjugate to immobilize the heparin on the plate, after which thorough wash was used to remove unbound substrate. We have previously used this assay to study boronic acid and heparin binding interactions.[216] Heparin, a polysaccharide commonly used as a model carbohydrate, is an anticoagulant consisting of complex heterogeneous mixtures of repeating disaccharide units of uronic acid (D-glucuronic or L-iduronic acid), D-glucosamine, or *N*-acetyl-D-glucosamine, which all display various degrees of sulfation on each monosaccharide unit, ranging from zero to tri-sulfation.[383] Heparin has previously been shown to bind to boronic acids in a multivalent manner.[375, 376] Following heparin coating on the microplate, liposomes composed of various percentages of BBAL **3.1a-d** and tagged with fluorescence 1% Rd-PE were added to the wells to allow for binding to the immobilized heparin. After incubation and washing to remove unbound liposomes, Rd-PE fluorescence was analyzed in order to observe the extent of liposome binding to the plate. An additional step was attempted in which after washing away excess HB, a blocking 1% bovine serum albumin (BSA) solution was added to each well, followed by 1 hr incubation, washing, and then the assay continued the same with liposome treatment. BSA blocking is a common step in immunoassays, and in this case the goal was to use BSA to prevent non-specific liposome binding on the microplate by blocking the leftover space available on the solid surface once the HB has been immobilized.[384] The trials of this assay are summarized in Table 3.7 entries 2.1-2.6 and involve attempts at optimizing the various treatment concentrations and incubation times. However, this assay design was also hindered by high background fluorescence from control liposomes and inconsistent results.

Third, an enzyme-linked immunosorbent assay (ELISA) was adapted from a previously reported assay in an attempt to analyze binding between the boronic acids of BBAL liposomes and mucin glycoprotein.[341] To begin, solutions containing various concentrations and formulations of BBAL **3.1a-d** liposomes were immobilized on a streptavidin microplate via incorporation of 1% Biotin-PEG-PE lipid. After washing away unbound liposomes, solutions of mucin were introduced to the wells and allowed to bind with the liposomes, followed again by thorough washing. A blocking step was performed with 1% BSA, followed by addition of a primary mucin antibody (Ab_1, ELISA Polyclonal Antibody to Porcine Mucin 2 (MUC2)), incubation, and washing. Then, an HRP-conjugated secondary antibody (Ab_2, HRP-Goat Anti-Rabbit Secondary Antibody) was added, allowed to associate with the primary antibody, then washed away. Finally, Pierce SuperSignal ELISA Femto Maximum Sensitivity Substrate was added, and the resulting chemiluminescence was measured to indicate the presence of HRP, and by association, the presence of mucin bound to the liposomes. The trials of this assay are summarized in Table 3.7 entries 3.1-3.9 and involved attempts at optimizing the concentration of liposome, mucin, Ab_1 and Ab_2, as well as incubation times and washing techniques. Although initial assays indicated moderate enhancements in mucin binding based on the presence of lipids **3.1a-d** in liposomes, further experiments showed that the assay results were highly variable and not consistently reproducible.

In a fourth attempt to develop an assay to demonstrate binding between BBAL **3.1a-d** liposomes and carbohydrates, a mucin immobilization protocol was explored. The protocol for this assay was as follows: first, a biotin-tagged mucin primary antibody was immobilized onto a streptavidin microplate, followed by coating the plate with mucin and allowing the antibody to bind to the mucin and form a mucin coated surface. After thorough washing to remove unbound mucin, fluorescent tagged liposomes (1% Rd-PE) containing various percentages of lipids **3.1a-d** were added to the plate, incubated, washed and then Rd-PE fluorescence measurements were taken. Binding of **3.1a-d** liposome to the mucin-coating surface was to be indicated by increases in Rd-PE fluorescence compared to control liposomes lacking **3.1a-d**. Despite optimization of concentrations and incubations times of mucin antibody and liposome treatments (Table 3.7 entries 4.1-4.4), this assay was not capable of distinguish binding of mucin to BBAL liposome

Table 3.7 Summary of microplate assay designs and treatments explored to assess 3.1a-d carbohydrate binding.

Entry	Lipid	Mol%	[] Liposome	Other Notes	Assay Protocol
1.1	**3.1a**	0-10	0-200 μM	• Black plate • [HRP] = 100 ng/mL • PBS Buffer (pH=8)	**HRP Binding Chemiluminescence Assay** 1. Immobilize liposome onto microplate (various []), incubate 1 hr, wash x3 with buffer 2. Treat with HRP (various []), incubate 1 hr, wash x3 with buffer 3. Add HRP substrate and measure chemiluminescence
1.2	**3.1a**	0-10	0-200 μM	• Biotin-PEG-PE • [HRP] = 100 ng/mL • PBS Buffer (pH=8)	
1.3	**3.1a**	0-10	0-250	• White plate • [HRP] = 100 ng/mL • PBS Buffer (pH=8)	
1.4	**3.1a**	0-10	0-250 μM	• White plate • No shaking plate during incubation • [HRP] = 100 ng/mL • PBS Buffer (pH=8)	
1.5	**3.1a**	0-10	0-200 μM	• Black plate • No shaking plate during incubation • [HRP] = 100 ng/mL • PBS Buffer (pH=8)	
1.6	**3.1a-d**	0-10	0-200 μM	• White plate • No shaking plate during incubation • [HRP] = 100 ng/mL • PBS Buffer (pH=8)	
1.7	**3.1a**	0-10	500 μM	• [HRP] = 0.5 μg/mL – 0.1 mg/mL • PBS Buffer (pH=8)	
1.8	**3.1a**	0-10	0-300 μM	• HEPES (1mM) Buffer (pH=7.4) • [HRP] = 5 μg/mL	
1.9	**3.1a**	0-10	0-1 mM	• HEPES (1mM) Buffer (pH=7.4) • [HRP] = 5 μg/mL	
1.10	**3.1a**	0-10	0-125 μM	• HEPES (1mM) Buffer (pH=7.4) • [HRP] = 5 μg/mL	
1.11	**3.1a**	0-10	0-125 μM	• HEPES (1mM) Buffer (pH=7.4) • [HRP] = 5 μg/mL	

Table 3.7 Continued

Entry	Lipid	Mol%	[] Liposome	• Other Notes	Assay Protocol
2.1	**3.1a**	0-10	0-1 mM	• 1 µg/mL HB • Liposome incubation: 2 hr • PBS Buffer (pH=8)	**Heparin-Biotin Binding Assay** 1. Immobilize HB onto microplate (various []), incubate 1 hr, wash x3 2. Treat with Rd-PE tagged BBAL liposomes (various []), incubate (various times), wash x3 3. Add HRP substrate and measure chemiluminescence
2.2	**3.1a**	0-10	0-1 mM	• 10 µg/mL HB • Liposome incubation: 12 hr • PBS Buffer (pH=8)	
2.3	**3.1a**	0-10	0-1 mM	• Step added: BSA blocking step between HB immobilization and liposome treatment • 10 µg/mL HB • Liposome incubation: 2 hr • PBS Buffer (pH=8)	
2.4	**3.1a**	0-10	0-1 mM	• Tried 1%, 5%, and 10% Rd-PE label in the liposomes • 10 µg/mL HB • Liposome incubation: 2 hr • PBS Buffer (pH=8)	
2.5	**3.1a**	0-10	0-1 mM	• HEPES (1mM) Buffer (pH=7.4) • 10 µg/mL HB • Liposome incubation: 2 hr	
2.6	**3.1a** **3.1d**	0-10	0-1 mM	• 50 µg/mL HB • Liposome incubation: 2 hr • PBS Buffer (pH=8)	
3.1	**3.1a**	0-10	0.5 mM	• Mucin = 0-1 mg/mL • Ab_1 = 0-20 µg/mL • Ab_2 = 1:2000 • HEPES pH 7.4	**Mucin Binding ELISA** 1. Immobilize liposome onto microplate (various []), incubate 1 hr, wash x3 2. Treat with 1% BSA, incubate 2 hr, wash x3 3. Treat with mucin (various []), incubate (various times), wash x3 4. Treat with Ab_1, (various []), incubate 2 hr, wash x3 5. Treat with Ab_2, (various []), incubate 1 hr, wash x3 6. Add HRP substrate and measure chemiluminescence
3.2	**3.1a -d 3.1.5**	0-10	0-0.5 mM	• Mucin = 1 mg/mL • Ab_1 = 2 µg/mL • Ab_2 = 1:2,000 • HEPES pH 7.4	
3.3	**3.1d**	0-10	0-1.1 mM	• Mucin = 1 mg/mL • Ab_1 = 2 µg/mL • Ab_2 = 1:2,000 • HEPES pH 7.4	
3.4	**3.1d**	0-10	0-0.6 mM	• Mucin = 1 mg/mL • Ab_1 = 2 µg/mL • Ab_2 = 1:2,000 – 1:20,000 • HEPES pH 7.4	

Table 3.7 Continued

Entry	Lipid	Mol%	[] Liposome	• Other Notes	Assay Protocol
3.5	**3.1d**	0-10	0-0.5 mM	• Mucin = 1 mg/mL • Ab_1 = 2 µg/mL vs. 0 µg/mL • Ab_2 = 1:5,000 • HEPES pH 7.4	**Cont. Mucin Binding ELISA**
3.6	**3.1.5**	20	0-0.5 mM	• Mucin = 1 mg/mL • Ab_1 = 2 µg/mL • Ab_2 = 1:5,000 • HEPES pH 7.4	
3.6	**3.1a** **3.1d**	5	0-0.5 mM	• Mucin = 1 mg/mL • Ab_1 = 2 µg/mL • Ab_2 = 1:5,000 • HEPES pH 7.4	
3.7	**3.1a -d**	10	0-0.5 mM	• Mucin = 1 mg/mL • Ab_1 = 2 µg/mL • Ab_2 = 1:5,000 • HEPES pH 7.4	
3.8	**3.1d**	10	0-0.5 mM	• Mucin = 1 mg/mL • Ab_1 = 2 µg/mL • Ab_2 = 1:5,000 • PBS pH 8	
3.9	**3.1d**	10	0-0.5 mM	• Biotin-cap-PE vs. Biotin-PEG_4-PE • Mucin = 1 mg/mL • Ab_1 = 2 µg/mL • Ab_2 = 1:5,000 • HEPES pH 7.4	
4.1	**3.1d**	0-10	2 mM	• Biotin-mucin Ab_1 = 0-20 µg/mL • Ab_1 incubation = 1 hr • Black plate • PBS pH 8	**Mucin Capture Assay** 1. Immobilize biotin-mucin Ab_1 on microplate, incubate (various time), wash x3 2. Treat plate with mucin (1 mg/mL), incubate 1 hr, wash x3 3. Treat plate with Rd-PE tagged liposomes, incubate 1hr, wash x3, measure Rd-PE fluorescence
4.2	**3.1d**	0-10	0–2 mM	• Biotin-mucin Ab_1 = 5 µg/mL • Ab_1 incubation = 1 hr or 2 hr • Black plate • PBS pH 8	
4.3	**3.1d**	0-10	2 mM	• Biotin-mucin Ab_1 = 0-10 µg/mL • Ab_1 incubation = 2 hr • Black plate • HEPES pH 8.5	
4.4	**3.1d**	0-10	0-2 mM	• Biotin-mucin Ab_1 = 5 µg/mL • Ab_1 incubation = 2 hr • Black plate • HEPES pH 8.5	

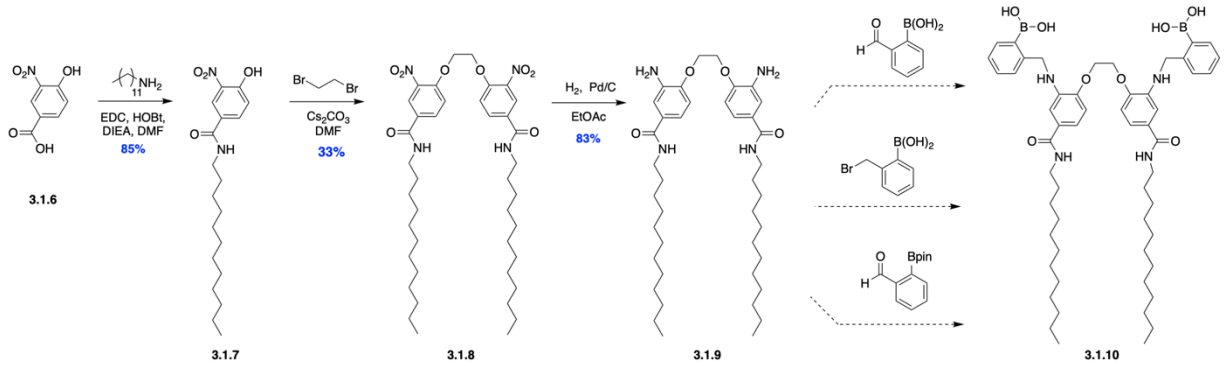
compared to control liposome due to high levels of non-specific background fluorescence from control liposomes.

3.11. Initial design and synthesis of bis-boronic acid lipid

3.11.1. Initial design of bis-boronic acid lipid

We initially designed BBAL **3.1.10** with the goal of enhancing liposomal cell delivery and content release in the presence of aberrant glycosylation. Similar to the successfully produced BBALs **3.1a-d**, compound **3.1.10** was designed to have two boronic acids incorporated into the headgroup of this lipid and two hydrophobic hydrocarbon tails so that the compound will be incorporated into the lipid bilayer. The compound was also designed to bind diols upon treatment with carbohydrates to form boronate esters, which can cause a disturbance in the membrane bilayer and trigger release of contents. Since this lipid has a more rigid scaffold, it was hypothesized that binding could cause constriction of the headgroup to alter tail presentation, altering the 3-dimensional shape of the lipid to resemble a cone-shaped lipid. Cone-shaped lipids are non-bilayer forming lipids and would destabilize the membrane by creating defects and pressure in the membrane.[385] These transformations would cause membrane destabilization and release of contents. Therefore, lipid **3.1.10** was designed to drive binding interactions with carbohydrates and glycoproteins to enhance disease-associated cellular glycan recognition and triggered release of cargo, thereby improving liposomal cell delivery and release.

The synthetic route we designed for BBAL **3.1.10** is shown in Scheme 1 and was inspired by a calcium-responsive lipid synthesized by Lou et. al.[386] We began with 4-hydroxy-3-nitrobenzoic acid (**3.1.6**), which underwent an amide coupling reaction with dodecylamine to establish the amide-linked hydrophobic lipid chain of **3.1.7**. Then, two equivalents of **3.1.7** were reacted with dibromoethane to produce the bridge of **3.1.8**. Subsequently, the nitro groups of **3.1.8** were reduced with Pd/C to unveil the amine groups of **3.1.9**, which paves the way for the final step to produce **3.1.10**. Attempts were made to complete the final step with reductive amination with 2-formylphenyl boronic acid or protected 2-Formylphenylboronic acid pinacol ester, or alkylation with 2-bromophenylboronic acid. Several attempts were made under varying conditions, but



Scheme 3.6 Synthetic route for initial bis-boronic acid lipid 3.1.10 4-Hydroxy-3-nitrobenzoic acid (**3.1.6**) underwent an amide coupling reaction with dodecylamine to form **3.1.7**. Then, two equivalents of **3.1.7** were reacted with dibromoethane to produce the bridge of **3.1.8**. Last, the nitro groups of **3.1.8** were reduced with Pd/C to form the amine groups of **3.1.9**. Attempts at producing **3.1.10** were not successful.

each resulted in a messy reaction. Realizing that coupling this lipid scaffold with boronic acids may cause issues, we pursued the synthesis plan as described previously in this Chapter.

3.12. Alternative boronic acid polymer liposomes

3.12.1. Design of boronic acid polymer lipid

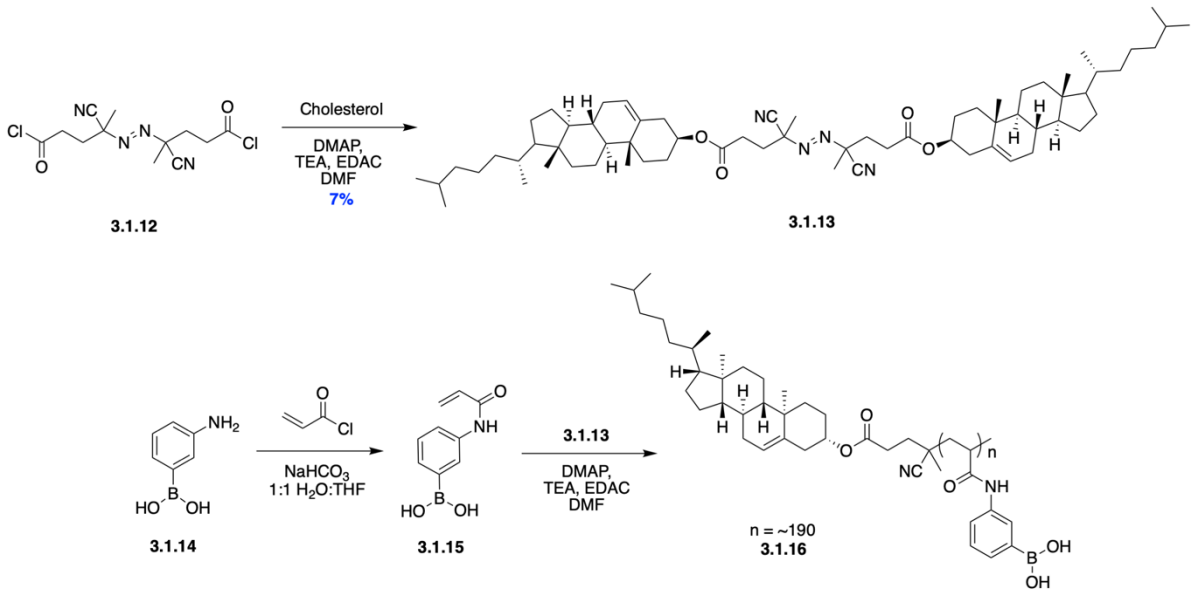
In addition to developing bisboronic acid lipids, we pursued boronic acid polymer lipids (BOPLIPs) for cell delivery and release by carbohydrate binding. As previously discussed, a limitation of boronic acid lipids is their low binding affinity in aqueous media. While presentation on a membrane surface increases valency, this could be further extended by introducing polymers incorporating numerous boronic acid groups. Our original boronic acid lipids could also be limited by the fact that the boronic acids sit close to the liposome membrane, limiting interaction capabilities. This is especially problematic in clinical liposomes, which are usually decorated with stealth polymers to increase their circulation time in the body, but could block smaller boronic acid lipids from cell surface binding.[387] These issues can be improved by extending the boronic acid binding unit further away from the lipid bilayer. Both of these solutions can be achieved by implementing BOPLIPs. Therefore, we designed a lipid-functionalized polymerization initiator and then polymerized boronic acid acrylamide monomers using that initiator. The resulting compound, a single lipid with long boronic acid chain branching off, was incorporated into liposomes to study the ability to form binding interactions with carbohydrates and glycoproteins to enhance disease-associated cellular glycan recognition and cargo release to improve liposomal cell delivery and release. These experiments were performed in collaboration with Dr. Johnathan Brantley's lab in UTK Chemistry. Collaborators Dr. Alan Fried, Dr. Brian Jacobs, and Dr. Breanna Wilson from the Brantley lab contributed to these studies in terms of synthesizing monomer **3.1.15** and polymer **3.1.16**.

In cancer cells, Mucin 1, a heavily glycosylated protein, is both overexpressed and aberrantly glycosylated resulting in truncated O-linked glycans which terminate in Sias.[319, 322, 323, 388, 389] In addition, dozens of tumor associated carbohydrate antigens (TACAs) have been documented, and a majority of these TACAs have Sias as terminal sugars.[390, 391] These naturally occurring Sias have been categorized into 50 types, and the two most predominantly appearing Sias in

mammals are *N*-Acetylneuraminic acid (Neu5Ac) and its hydroxylated derivative, *N*-glycolylneuraminic acid (Neu5Gc).[392-395] Further, there is a significant difference in sialylation patterns and concentration between normal cells and their malignant equivalents. Aberrant and overexpressed Sia encourages cancer metastasis by enhancing migration and tissue invasion, therefore it is relevant to develop platforms that are specific for Sia glycans.[396, 397] Also, Neu5Ac has two different structural features that can be targeted with a boronic acid, an extended glycerol sidechain and an α-hydroxyacid-type arrangement of the hemiketal at the anomeric position.[398] The Sias on the cancer cell membranes are the target of the polymer boronic acid liposomes. Studies were done with polymer lipid **3.1.16** and Neu5Ac in order to assess if binding could lead to membrane disruption and cargo release. Hence, Neu5Ac was used as a model glycan in these studies to test for Sias sensitivity.

3.12.2. Synthesis of BOPLIPs

The synthesis of boronic acid polymer lipid **3.1.16** is shown in Scheme 3.7. We first determined that the initiator design was crucial since it is used to install the lipid tail. The cholesterol-modified azobisisobutyronitrile (AIBN)-derived initiator **3.1.13** was prepared according to work originally by Bertozzi et. al.[399] First, 4,4'-azobis-(4-cyanovaleric acid) (ACVA) (**3.1.12**) underwent *N*-(3-Dimethylaminopropyl)-*N*'-ethylcarbodiimide (EDC)-mediated coupling with cholesterol to yield initiator **3.1.13**. A separate reaction to couple **3.1.12** and octadecylamine to form an alternative initiator proved unsuccessful. Then, **3.1.14** was combined with acryloyl chloride to make borylated acrylamide monomer **3.1.15**, which then underwent free-radical polymerization with initiator **3.1.13** to form polymer **3.1.16**. The polymer has a long chain of boronic acid binding units, and a lipid-functionalized initiator will provide a single lipid tail to allow the molecule to rest in the liposome bilayer. Characterization with ^{1}H-NMR and gel permeation chromatography (GPC) solubilized in *N*,*N*-dimethylformamide (DMF) indicated that the polymer has an average weight of ~15kDa, which equates to an average of 190 boronic acid repeat units per polymer. Attempts were also made to employ the more controllable atom transfer radical polymerization (ATRP) method using a borylated acrylamide monomer and either an octadecylamine or



Scheme 3.7 Synthesis of boronic acid polymer lipid 3.1.16. First, ACVA (**3.1.12**) underwent EDC-mediated coupling with cholesterol to yield initiator **3.1.13**. Then, **3.1.14** was combined with acryloyl chloride to make borylated acrylamide monomer **3.1.15**, which then underwent free-radical polymerization with initiator **3.1.13** to form polymer **3.1.16**.

cholesterol functionalized α-bromoisobutyryl bromide (BIBB), but neither polymerization proved successful.

3.12.3. Nile red (NR) release assay with BOPLIP liposomes

Once BOPLIP **3.1.16** was synthesized, studies began to analyze the polymer's triggered release properties using fluorescence cargo dye release assays. We hypothesized that upon the diols of Neu5Ac binding the multitude of boronic acid units available around the liposomal surface, that the cholesterol anchor could be dragged throughout or pulled from the membrane, causing collapse of membrane integrity and release of cargo. First, a NR release assay was used to probe the release of non-polar cargo form the liposomal membrane of liposomes containing **3.1.16**, since NR is a common hydrophobic dye used for membrane examination.[373] NR is incorporated within the bilayer membrane of liposomes and only fluoresces when encapsulated there. Once liposomes are triggered and NR is released into aqueous media, it is no longer soluble and therefore no longer fluorescent.[400] Thus, the release of NR will be tracked by reductions in fluorescence.

Liposomes were prepared by incorporating either 0% or 0.11% of **3.1.16** along with 100% or 99.89% bulk lipid Egg-PC, and 5% NR was also included in all formulations. Liposome preparation was performed using the ethanol injection technique previously described.[354] This technique was used because polymer lipid **3.1.16** proved to have limited solubility in water, making the thin film liposome preparation method unsuitable. Briefly, lipids were dissolved in chloroform, combined as indicated, and dried under nitrogen gas to create lipid films. Lipid films were resuspended in 100% molecular grade ethanol and mixed for 60 minutes at 40 °C. Ethanolic lipid solutions were then injected dropwise into filtered phosphate buffered saline (PBS). Liposomes were then purified from ethanol via rotary evaporation. After evaporation, the final volume for each sample was measured, and all samples were adjusted to the originally calculated aqueous volume for each sample with MQ. Liposomes were extruded through a 200 nm filter for at least 15 passes. DLS experiments were performed to verify the successful formation of the stable liposomes, which will be discussed later. After taking an initial fluorescence scan, samples were treated with a screen of carbohydrate triggers at various concentrations, including Neu5Ac and small sugars

such as glucose, galactose, and mannose. Since dilution effects or unstable liposome formulations can also cause fluorescence signal decreases, blank samples were also run, in which liposome was treated with buffer only and release was monitored.

As seen in Figure 3.23A, addition of Neu5Ac to liposomes containing 0.11% **3.1.16** resulted in dose-dependent decreases in NR fluorescence indicating release over 25 minutes. For example, 5 mM Neu5Ac treatment resulted in a decrease in NR fluorescence less than ~12%, and 40 mM Neu5Ac treated liposomes showed a ~33% NR fluorescence decrease. The dose-dependent NR release trend from **3.1.16** liposomes was observed for all Neu5Ac treatment concentrations (10mM, ~20% release; 15mM, ~22% release; 20mM, ~28% release; 30mM, ~33% release). A leakage study was conducted in which buffer was instead added to **3.1.16** liposomes and release was measured over time, which yielded minimal NR fluorescence decrease (<3% release). Control experiments were also run with liposomes lacking **3.1.16**, which indicated Neu5Ac did slightly influence the liposomes, but less intensely compared to liposomes containing **3.1.16** (Figure 3.23B). Treatment of Egg-PC only liposomes with 20mM Neu5Ac resulted in~7% release, 30mM Neu5Ac in 12% release, and 40 mM Neu5Ac in 14% release. Figure 3.23C shows that 0.11% **3.1.16** liposomes are pink and uniform, indicating encapsulated NR before Neu5Ac treatment, but after treatment the NR has been released into the aqueous environment and has precipitated from the solution. Conversely, 0% **3.1.16** liposomes retain the same color and encapsulated NR both before and after Neu5Ac treatment.

A study was also done in which 0.11% **3.1.16** liposomes (Figure 3.24A) and PC only control liposomes (Figure 3.24B) were treated with 40 mM of other monosaccharides including glucose, galactose, and mannose. The monosaccharide treatments resulted in minimal NR release (<10%) from both 0% and 0.11% **3.1.16** liposomes, demonstrating sensitivity for Neu5Ac in particular, which may be due to the compounds each having multiple sites for the boronic acid polymers to bind. Altogether, these experiments demonstrate that **3.1.16** liposomes appear to undergo triggered release of hydrophobic cargo in response to treatment with Neu5Ac.

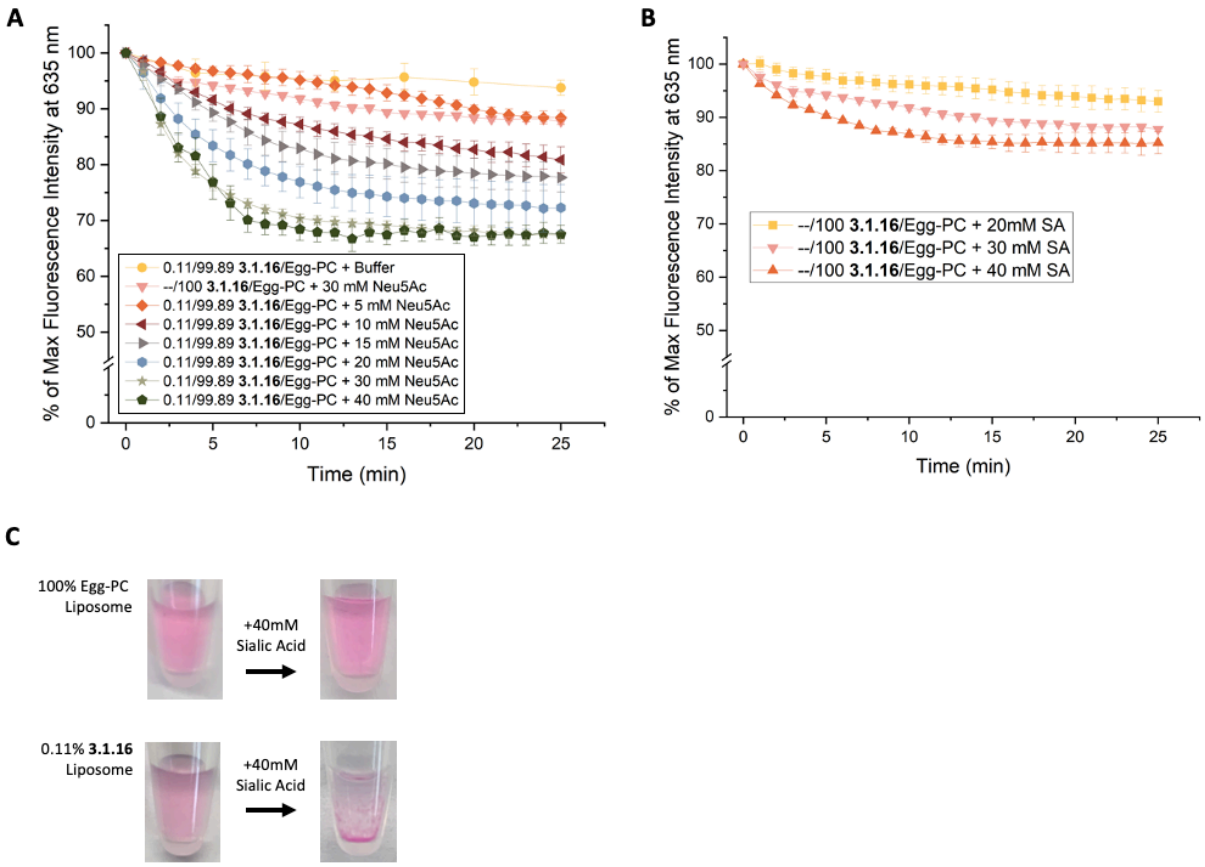


Figure 3.23 Hydrophobic Nile Red dye release assay for BOPLIP liposomes. (A) Liposomes composed of either 0% or 0.11% **3.1.16** with the remainder Egg-PC (100% or 99.89%), and 5% NR were treated with various concentrations (0 - 40 mM) of Neu5Ac. Results show a dose-dependent decrease in NR fluorescence after Neu5Ac treatment over 25 min, with 30 mM treatment showing over 33% release. (B) Control liposomes lacking **3.1.16** show slight NR release when treated with 20 - 40 mM Neu5Ac. (C) Pictures of liposome solutions before and after Neu5Ac treatment. Top left: initial 100% Egg-PC liposomes; top right: Egg-PC liposomes after Neu5Ac treatment. Bottom left: initial 0.11% **3.1.16** liposomes; bottom right: 0.11% **3.1.16** liposomes after Neu5Ac treatment. Pink precipitate was only observed at the bottom of the Eppendorf tube when **3.1.16** liposomes were treated with Neu5Ac. Error bars represent standard errors of at least three replicates.

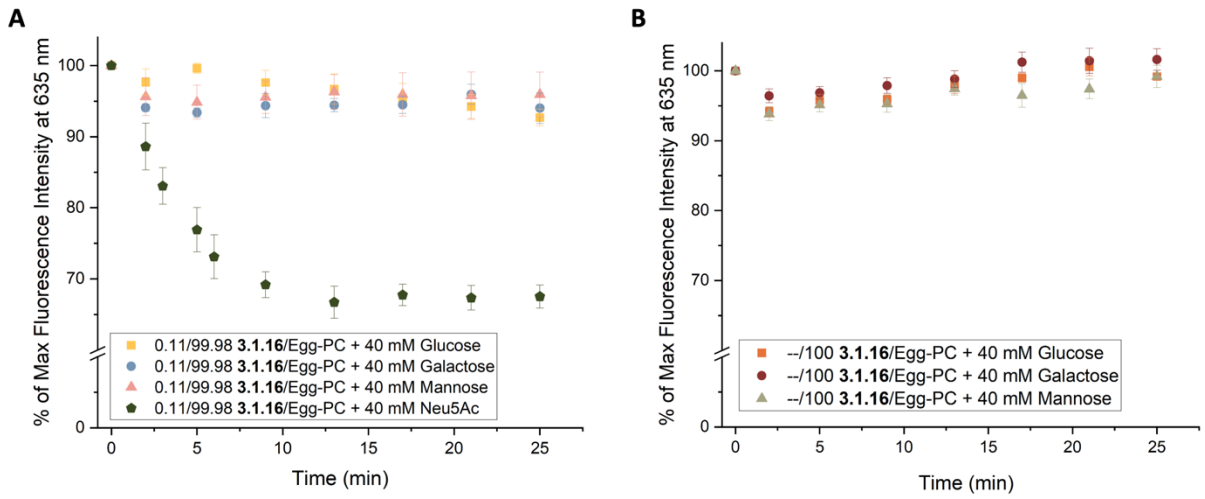


Figure 3.24 Monosaccharide hydrophobic Nile Red dye release assay for BOPLIP liposomes. (A) Liposomes composed of 0% or 0.11% **3.1.16** with the remainder Egg-PC (100% or 99.89%), and 5% NR were treated with 40 mM of monosaccharides glucose, galactose, mannose, or Neu5Ac. Results show minimal decrease in NR fluorescence (<10%) after sugar treatments, and 33% release after treatment with Neu5Ac. (B) Liposomes composed of 100% Egg-PC (100%) and 5% NR were treated with 40 mM of monosaccharides glucose, galactose, or mannose (40 mM) resulting in minimal decrease in NR fluorescence (<10%) after treatments. Error bars represent standard errors of at least three replicates.

3.12.4. Dynamic light scattering BOPLIP studies

Following the experiments demonstrating NR release from **3.1.16** liposomes, we moved on to test if the cargo release was accompanied by a change in liposome vesicle morphology. Since the addition of Neu5Ac resulted in NR cargo release from **3.1.16** liposomes, it is important to probe for changes in particle sizes both before and after Neu5Ac treatment. First, liposomes underwent DLS analysis to probe particle sizes before and after treatments. These showed that liposomes containing 0.11% **3.1.16** pre-Neu5Ac treatment had average diameters < 200 nm (Figure 3.25A) and polydispersity indices (PDI) ~0.2 (Figure 3.25B), which are both in the desirable size range (diameter ≤ 200, PDI ≤ 0.2), indicating stable liposomes were formed with up to at least 0.11% **3.1.16** incorporation. PDI is a measurement which describes the distribution of particle size of a sample. Pre-Neu5Ac treatment, the diameters of the 0.11% **3.1.16** liposomes were approximately twice the diameter of the PC-only liposomes, but this could be due to the 15 kDa polymer surrounding the liposome surface. When treated with Neu5Ac (5 – 40mM), PC-only liposomes showed no changes in size or PDI that would result from non-specific interactions. After treatment with just 5 mM Neu5Ac, liposomes with 0.11% **3.1.16** showed dramatic size increases, and the subsequent Neu5Ac treatment resulted in similar changes in size. Liposomes with 0.11% **3.1.16** also showed sizable increases in PDI to ~0.7-0.8 after all Neu5Ac treatments, indicating that membranes did undergo significant morphological changes driven by Neu5Ac when polymer lipid **3.1.16** was present in the membrane. Raw distribution curves are included in Figure 3.25C-D.

Additionally, DLS was examined after treatment with monosaccharides glucose, galactose, and mannose. Upon treatment with 40 mM monosaccharides, Egg-PC-only control liposomes did not show any meaningful size or PDI change, indicating there were no interactions occurring (Figure 3.26A). After 0.11% **3.1.16** liposomes were treated with the saccharides, there was no change in vesicle size although the PDI of the samples did increase slightly (~0.3) (Figure 3.26B). Raw distribution curves are included in Figure 3.26C-D. Altogether, these data indicate that the BOPLIPs form uniform liposomes, undergo morphological changes driven by Neu5Ac when polymer lipid **3.1.16** is present in the membrane, but are not affected by other small saccharides.

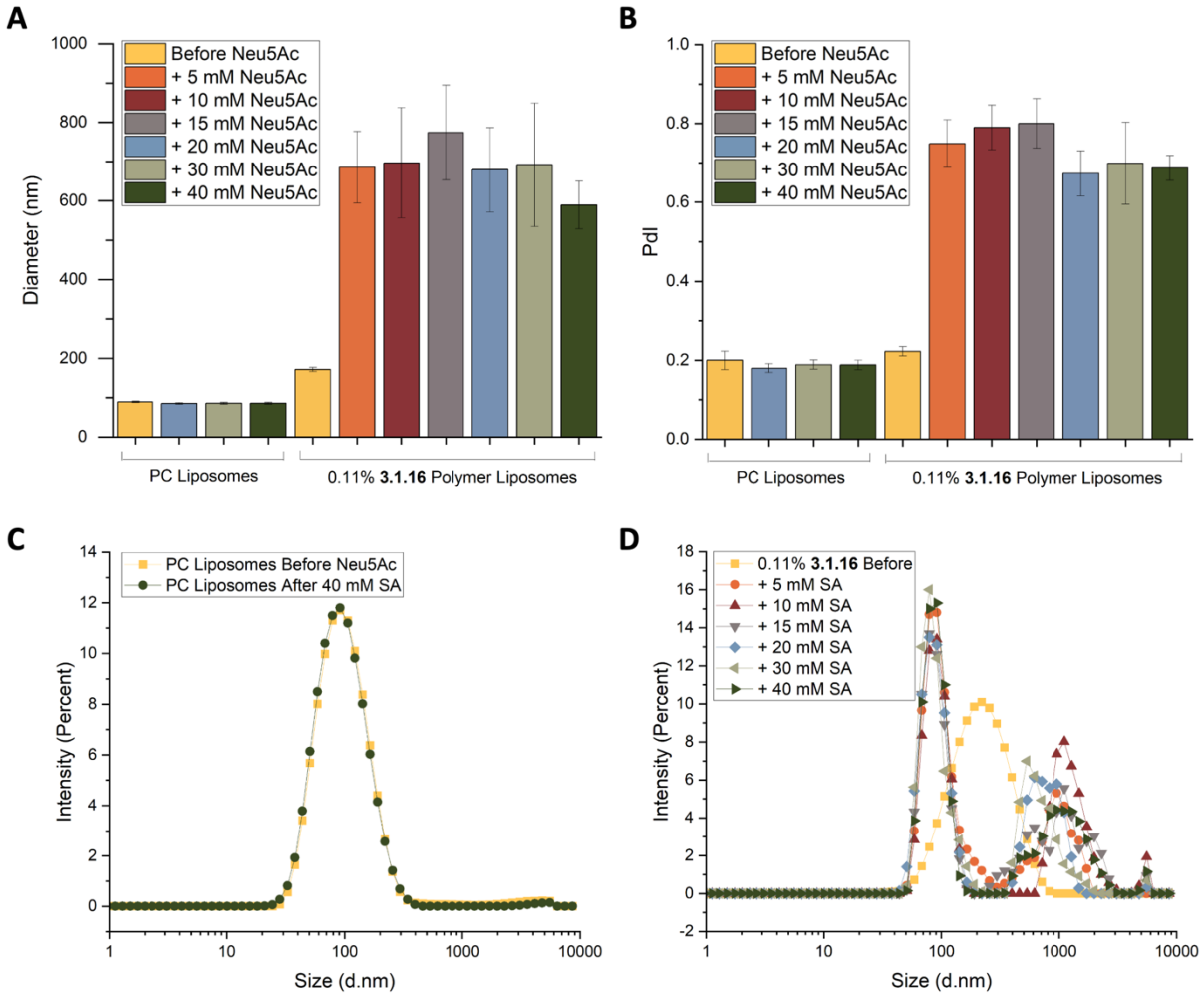


Figure 3.25 DLS results for BOPLIP liposomes treated with Neu5Ac. DLS results for liposomes containing 0% or 0.11% lipid **3.1.16**, 100% or 99.9% Egg-PC, and 5% NR treated with 0 - 40mM Neu5Ac. (A) After Neu5Ac treatment, PC-only liposomes average diameter (nm) did not change, while 0.11% **3.1.16** liposomes underwent dramatic size increase. (B) PDI of PC-only liposomes remained unchanged after treatment, but 0.11% **3.1.16** liposome PDI increased substantially. (C) Raw distribution curves of PC-only samples show no change in vesicle size distribution. (D) Raw distribution curves of 0.11% **3.1.16** liposome shows pronounced change in vesicle size distribution after 5-40mM Neu5Ac treatment, including the appearance of smaller (≤100 nm) and larger (+800 nm) formations. Error bars represent standard errors of at least three replicates.

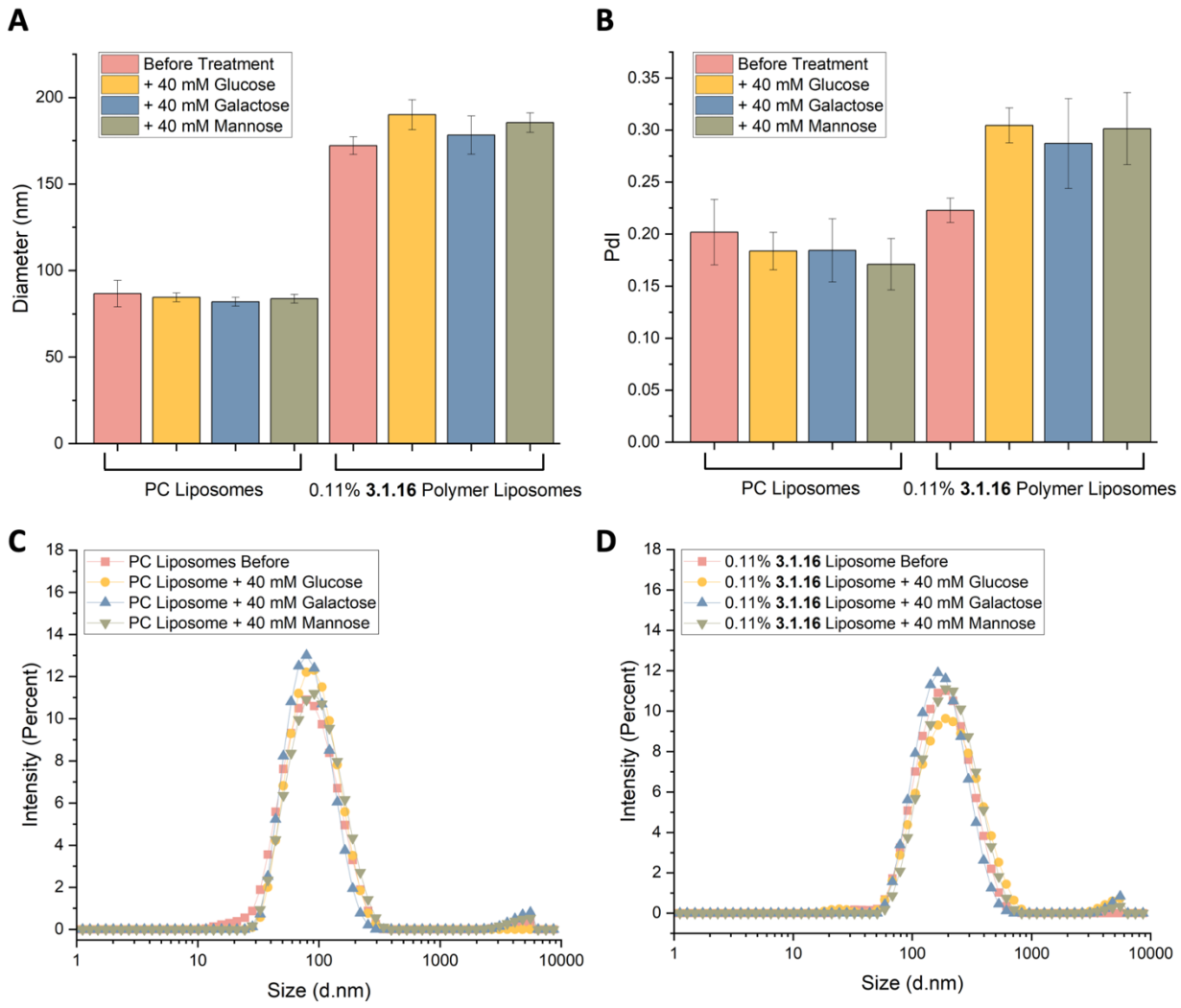


Figure 3.26 DLS results for BOPLIP liposomes treated with monosaccharides. DLS results for liposomes containing 0% or 0.11% lipid **3.1.16**, 100% or 99.9% Egg-PC, and 5% NR treated with 40 mM of monosaccharides glucose, galactose, or mannose. (A) After saccharide treatment, PC-only and 0.11% **3.1.16** liposomes average diameter (nm) did note change. (B) PDI of PC-only liposomes slightly decreased after treatment, and 0.11% **3.1.16** liposome PDI slightly increased. Raw distribution curves of (C) PC-only liposomes and (D) 0.11% **3.1.16** liposomes show no change in vesicle size distribution. Error bars represent standard errors of at least three replicates.

3.12.5. Transmission electron microscopy studies of BOPLIP liposomes

Scanning transmission electron microscopy (STEM) experiments were also performed to further understand changes in vesicle morphology and lipid self-assembly driven by Neu5Ac binding. Images were taken using liposomes containing 0% or 0.11% of **3.1.16** before and after treatment with 40 mM Neu5Ac. As seen in Figure 3.27, PC-only liposomes before (Figure 3.27A) and after (Figure 3.27B) adding Neu5Ac, as well as liposomes containing 0.11% of **3.1.16** pre-Neu5Ac treatment (Figure 3.27C), show similar depictions of unilamellar liposomes with defined membranes of the expected sizes. The images of liposomes containing 0.11% of **3.1.16** after treatment with Neu5Ac show that these vesicles have undergone significant changes in liposome morphology, including the formation of complicated aggregates (Figure 3.27D).

3.12.6. Sulforhodamine B release assay with BOPLIP liposomes

After seeing promising results from the NR hydrophobic release assay, we then moved on to examine the release of hydrophilic cargo. Contrary to hydrophobic cargo which resides in the membrane bilayer, hydrophilic contents are encapsulated in the interior aqueous core of the liposome. Membrane disruption is also required to release hydrophilic contents. To perform these studies, SRB was utilized as the hydrophilic fluorescent cargo dye because it is water soluble and commonly used in release assays of this type. The SRB is first encapsulated within the liposomes at high concentration to cause self-quenching of the fluorescence due to collisional effects within the liposome.[401] Once the dye is released from the liposome, it will be diluted into the surrounding buffer, resulting in an increase in fluorescence.

To prepare liposomes, a similar procedure was used compared to the NR release assay, but in this case the liposomes were hydrated with a 20 mM SRB buffer solution. After standard ethanol injection liposome preparation, a size exclusion column (SEC) was used after extrusion to remove unencapsulated dye. The release assay was conducted by adding Neu5Ac to the liposome solution and monitoring fluorescence over 18 hrs. At the end of the experiment, Triton X-100 detergent was added to the liposomes to destroy the bilayer and release 100% of the SRB content. This provides a fluorescence end-point of total release, and all other fluorescence

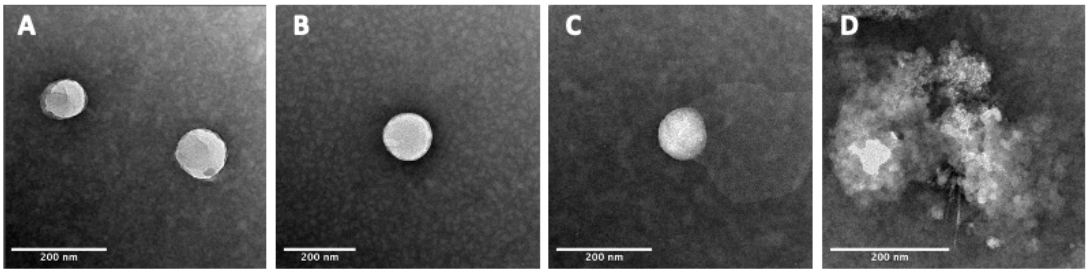


Figure 3.27 Transmission electron microscopy images of BOPLIP liposomes. (A) Representative TEM image of PC-only liposomes before Neu5Ac treatment show intact liposomes. (B) PC-only liposomes after Neu5Ac treatment show no change in liposome morphology. (C) Liposomes containing 0.11% of **3.1.16** pre-Neu5Ac treatment show similar depictions of unilamellar liposomes with defined membranes of the expected size. (D) Image of liposomes containing 0.11% of **3.1.16** after treatment with Neu5Ac indicates these vesicles have undergone significant changes in liposome morphology. Liposomes were stained with 1.0% (w/v) solution of neutral PTA and scale bar represents 200 nm.

readings were normalized by calculating percent release compared to total release. Various liposomes formulations containing **3.1.16** were explored with the goal of finding a combination that is stable and retains SRB cargo without Neu5Ac, but releases cargo after Neu5Ac treatment, similar to the NR release results. Also, it was necessary that liposomes with the same formulation but lacking **3.1.16** must retain SRB both before and after Neu5Ac. Lipids including Egg-PC, 1,2-dipalmitoyl-*sn*-glycero-3-phosphocholine (DPPC), 1,2-dioleoyl-*sn*-glycero-3-phosphoethanolamine (DOPE), PA (L-α-phosphatidic acid sodium salt from chicken eggs), DOTAP (1,2-dioleoyl-3-trimethylammonium-propane, chloride salt). As summarized in Table 3.4, most of the attempted formulations both with and without **3.1.16** showed significant background release without any Neu5Ac treatment, indicating the liposomes were non-specifically leaking SRB. Of the formulations that retained SRB without Neu5Ac, addition of Neu5Ac destabilized the liposomes with and without **3.1.16**. indicating that this release was not specific.

3.12.7. Attempted cellular delivery studies

After successful demonstration of NR release and morphological changes driven by **3.1.16** liposomes interacting with saccharide Neu5Ac, we moved to fluorescence microscopy studies to explore if **3.1.16** liposomes could enhance cellular association. We began by studying MDA-MB-231 human epithelial breast cancer cell line due to the importance of analyzing applications with cancer cells. For these studies, liposomes containing 0.01% Rd-PE were used to analyze liposome localization following cell incubation. Liposomes were prepared using the ethanol injection method with 0% or 0.11% **3.1.16**, 99.99% or 99.79% Egg-PC, and 0.01% Rd-PE. After A375 cells were incubated with liposomes for 1 hr, cells were washed thoroughly before imaging. Fluorescence microscopy images in Figure 3.28 were acquired as a representative visualization of cellular association of liposomes. These images indicate that liposomes containing 0.11% **3.1.16** (Figure 3.28E-H) did not improve liposome delivery to cells compared to control liposomes lacking **3.1.16** (Figure 3.28A-D).

Table 3.8 Summary of formulations explored for hydrophilic SRB release assay using BOPLIP 3.1.16 and different percentages of Egg-PC, DPPC, DOPE, PA, and DOTAP.

Entry	% 3.1.16	% Egg-PC	% DPPC	% DOPE	% PA	% DOTAP	Neu5Ac (mM)	Outcome
1	--	100	--	--	--	--	0	Background release, ~30%
							20, 40	~35% release
2	0.1	99.9	--	--	--	--	0	Background release, ~40%
							20, 40	~45% release
3	--	75	25	--	--	--	0	Background release, ~30%
							40	~50% release
4	0.1	74.5	25	--	--	--	0	Background release, ~25%
							40	~50% release
5	--	50	50	--	--	--	0	Background release, ~45%
							40	~50% release
6	0.1	49.9	50	--	--	--	0	Background release, ~15%
							40	~10% release
7	--	90	--	--	--	10	0	Background release, ~25%
							40	~30% release
8	0.1	89.9	--	--	--	10	0	Background release, ~40%
							20, 40	~50% release
9	--	85	--	--	--	15	0	Background release, ~20%
							20, 40	~25% release
10	0.1	84.9	--	--	--	15	0	Background release, ~25%
							20, 40	~35% release
11	--	80	--	--	--	20	0	Background release, ~20%
							20, 40	~25% release
12	0.1	79.9	--	--	--	20	0	Background release, ~25%
							20, 40	~30% release
13	--	40	--	50	10		0	<5% background release
							20, 40	~40% release
14	0.1	39.9	--	50	10		0	<5% background release
							20, 40	~40% release

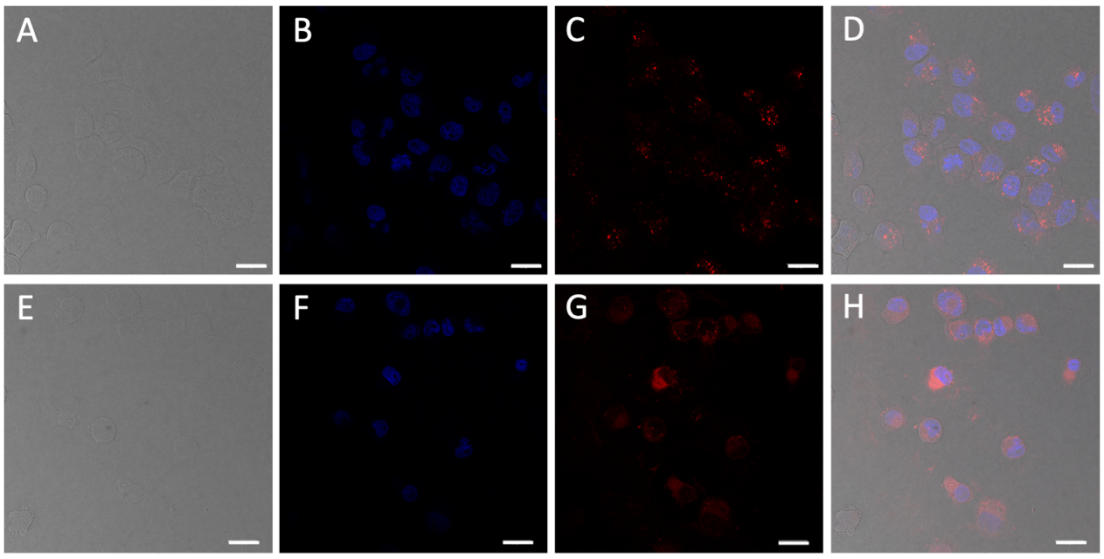


Figure 3.28 BOPLIP liposome MDA-MB-231 cell delivery study results. Representative 40X images show MDA-MB-231 cells treated with liposomes containing 0.08% Rd-PE and (A) brightfield PC-only, (B) DAPI PC-only, (C) Rd-PE PC-only, and (D) overlay PC-only; (E) brightfield 0.11% **3.1.16**, (F) DAPI 0.11% **3.1.16**, (G) Rd-PE 0.11% **3.1.16**, and (H) overlay 0.11% **3.1.16**. Images demonstrate that **3.1.16** did not enhance delivery to MDA-MB-231 cells, as indicated by similar Rd-PE fluorescence across all treatment types. The scale bars depict 20 µm. DAPI is shown in blue. Rd-PE is shown in red.

3.13. Conclusions

In conclusion, we have developed a carbohydrate-targeting liposome cell delivery platform using BBALs **3.1a-d** as multivalent lipids for binding to cell surface glycans. Carbohydrate binding assays using immobilized liposomes containing BBALs **3.1a-d** demonstrated that these compounds enable the binding of dextran and mucin, and that binding activity is variable depending upon the specific structural features of the BBAL. In addition, results from cellular microscopy imaging experiments and quantitative cell association assays show that bis-boronic acid liposomes exhibited enhanced cell association in mammalian cells. This glycan-targeted liposome system could provide worthy nanocarriers for enhanced cellular delivery based on the composition and abundance of cell surface carbohydrates. In addition, boronic acid polymer lipid **3.1.16** was developed, which releases hydrophobic cargo in response to disease associated stimuli. Future work will be aimed at further examination and modulation of boronic acid binding abilities to enhance cell type-specific liposomal delivery in addition to increasing the number of boronic acid moieties in the lipid headgroup to further leverage multivalent binding to cell surfaces.

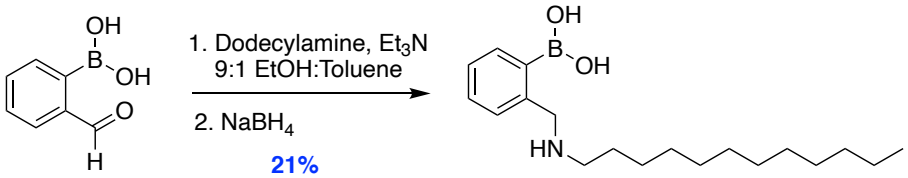
3.14. Synthesis and experimental procedure

General experimental

Reagents and solvents were generally purchased from Sigma-Aldrich or Fisher Scientific and used as received. Rhodamine B labeled dextran (Rd-dextran, 10,000 MW, neutral) was purchased from Thermo-Fisher Scientific and Mucin from porcine stomach (Type III, bound Sia 0.5-1.5 %, partially purified powder) was purchased from Sigma-Aldrich, Inc. PC (L-α-phosphatidylcholine, mixed isomers from chicken eggs), Rd-PE (L-α-phosphatidylethanolamine-*N*-(lissamine rhodamine B sulfonyl) (ammonium salt)), 18:1 Biotinyl Cap PE (Biotin-cap-PE) (1,2-dioleoyl-sn-glycero-3-phosphoethanolamine-N-(cap biotinyl) (sodium salt)), DOPE (1,2-dioleoyl-sn-glycero-3-phosphocholine), cholesterol, and 1,2 distearolyl-*sn*-glycero-3-phosphoethanolamine -*N*-[amino(polyethylene glycol)-2000] (ammonium salt) (PEG-PE) were purchased from Avanti Polar Lipids, Inc. (Alabaster, AL). Dry solvents were obtained from a Pure Solv MD-7 solvent delivery system purchased from Innovative Technology, Inc. Column chromatography was performed using 230 – 400 mesh silica gel purchased and 32-63 μm neutral alumina from Sorbent

Technologies. NMR spectra were obtained using Varian 300 or 500 MHz spectrometers. Mass spectra were obtained with JEOL DART-AccuTOF and Waters Synapt G2-Si mass spectrometers (Milford, MA). Liposome extruder and polycarbonate membranes were obtained from Avestin (Ottawa, Canada). Water for liposome preparation and assays was purified via a Millipore water system (≥18 MW·cm triple water purification system). Small quantities (<5 mg) were weighed on a Mettler Toledo XS105 dual range analytical balance. DLS measurements were performed using a Malvern Zetasizer Nano ZS instrument equipped with a He-Ne 633 nm laser and a temperature controller at a scattering angle of 173°. Plots were generated using Origin Pro 2021. All error bars in plots show the standard errors of at least three experimental replicates. Microplate fluorometric analysis was performed using Gen5 software and Synergy 2 Multi-Detection Microplate Reader (BioTek Instruments, Winooski, VT). Fluorometric analysis of VSMC cells was performed using a Glomax multi microplate reader with a 575 nm filter (Promega, Madison, WI), and fluorescence microscopy images were obtained using a BX51 Olympus microscope with an Olympus Q-color camera (Olympus Corporation, Shinjuku, Tokyo, Japan). All error bars in plots show the standard errors of at least three experimental replicates.

Synthesis



3.1.4 **3.1.5**

(2-((Dodecylamino)methyl)phenyl)boronic acid (3.1.5)[153]

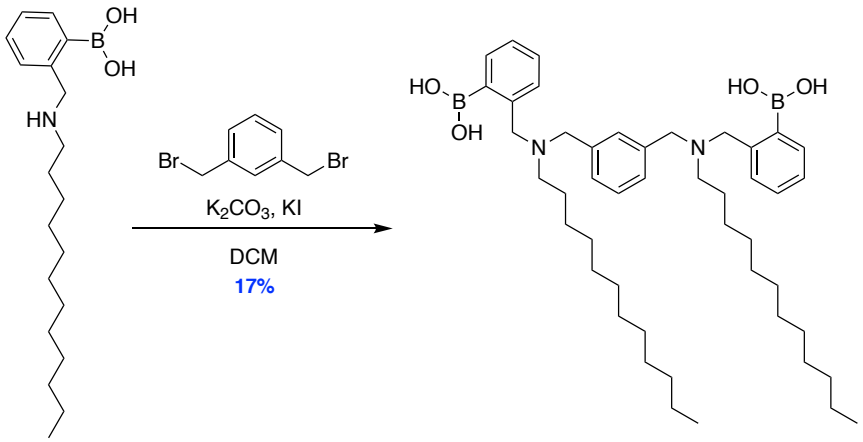
In a round-bottomed flask, 2-formylphenylboronic acid (0.89 g, 5.929 mmol) and TEA (1.09 g, 10.78 mmol) were dissolved in 30 mL of a mixture of ethanol/toluene (90:10). Then, dodecan-1-amine (1 g, 5.39 mmol) was added, and a Dean-Stark trap was attached to the round-bottom flask and filled with 10 mL of the same solvent mixture. After refluxing at 100 °C for 16 hr, the reaction mixture was cooled to 0 °C using an ice bath and sodium borohydride ($NaBH_4$, 0.82 g, 21.56 mmol) was added slowly, after which the reaction mixture was further stirred for 2 hr at

0°C. The reaction was quenched by adding 3 mL H_2O and then the solvent was removed under reduced pressure. The crude was then extracted with 30 mL chloroform ($CHCl_3$) and washed 3 x 50mL with water, dried over sodium sulfate (Na_2SO_4), and filtered and concentrated under reduced pressure. The crude product was purified with column chromatography packed with silica with an increasing gradient elution of 100% $CHCl_3$ to 10% methanol (MeOH)-$CHCl_3$ to afford compound **3.2.5** as a white solid (1.3622 g, 4.27 mmol, 80% yield).

^{1}H-NMR (500 MHz, 10% MeOD – $CDCl_3$): δ 7.34 – 7.29 (m, 1H), 7.09 – 7.01 (m, 2H), 6.97 – 6.92 (m, 1H), 4.09 (s, 1H), 3.82 (s, 2H), 2.70 – 2.64 (m, 2H), 1.52 (t, *J* = 7.8 Hz, 2H), 1.24 – 1.04 (m, 18H), 0.71 (t, *J* = 6.8 Hz, 3H). ^{13}C-NMR (126 MHz, 10% MeOD – $CDCl_3$): δ 144.5, 134.3, 131.2, 130.7, 126.6, 57.6, 51.7, 35.7, 33.5, 33.4, 33.3, 33.2, 31.0, 30.9, 26.5, 17.8. ^{11}B NMR (160 MHz, 10% MeOD – $CDCl_3$) δ 9.70.

Bis-boronic acid lipids with spacers (3.1a-e)

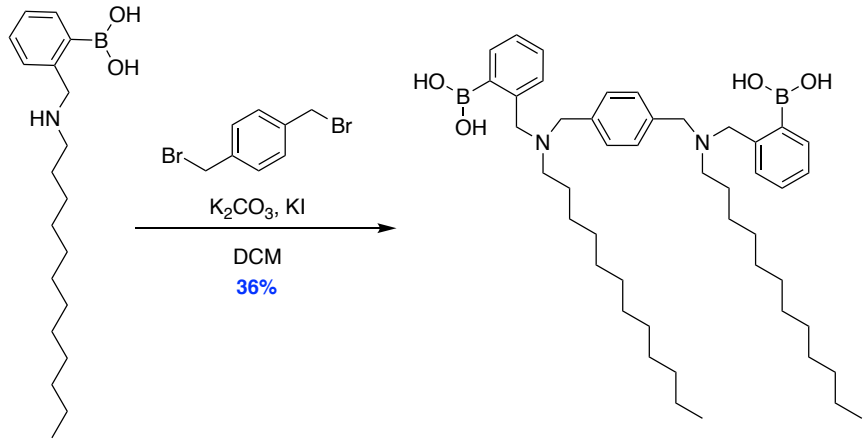
Compound **3.1.5** (100mg, 0.31 mmol) was dissolved in 10 mL of dry dichloromethane (DCM) along with the corresponding dibromide linker (*m*-xylene dibromide for **3.1a**, *p*-xylene dibromide for **3.1b**, 2,6-bis(bromomethyl)naphthalene for **3.1c**, or 4,4'-bis(bromomethyl)-1,1'-biphenyl for **3.1d**) (0.16 mM, 0.51 eq), potassium carbonate (69 mg, 0.50 mmol) and potassium iodide (KI, 1 mg). The reaction mixture was heated to reflux at 68 °C for 16 hr. The solvent was removed under reduced pressure and the crude product was purified with column chromatography packed with alumina with an increasing gradient elution of 100% DCM to 3% MeOH-DCM to afford the products.



3.1.5 **3.1a**

((((1,3-Phenylenebis(methylene))bis(dodecylazanediyl))bis(methylene))bis(2,1-phenylene))diboronic acid (3.1a)

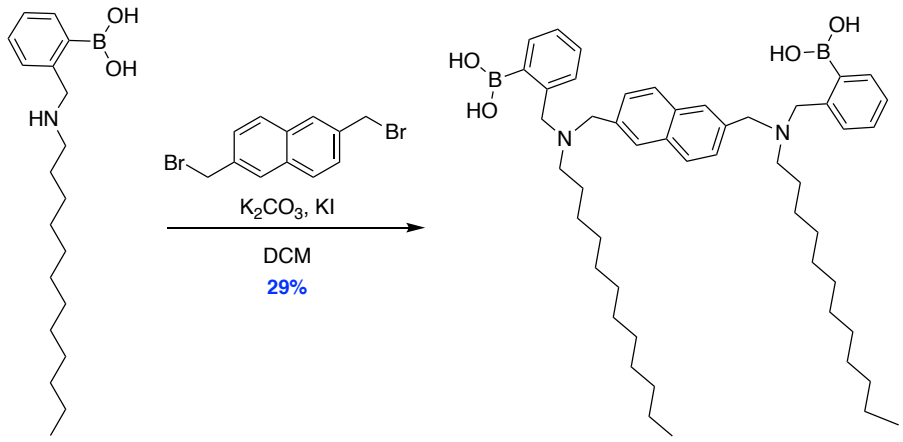
Product was a white solid (19.8 mg, 0.027mmol, 17% yield) R_f = 0.2 (2% MeOH-DCM). ^{1}H NMR (500 MHz, 10% MeOD – $CDCl_3$): δ 7.70 (d, *J* = 6.2 Hz, 2H), 7.21 – 7.13 (m, 5H), 7.10 – 7.01 (m, 5H), 3.63 (s, 4H), 3.23 (s, 4H), 2.32 – 2.25 (m, 4H), 1.43 – 1.34 (m, 4H), 1.14 – 0.95 (m, 38H), 0.75 (t, *J* = 6.9 Hz, 6H). ^{13}C-NMR (126 MHz, 10% MeOD – $CDCl_3$): δ 141.33, 135.81, 131.06, 130.61, 129.67, 128.87, 128.60, 127.21, 61.03, 56.72, 51.77, 31.81, 29.52, 29.44, 29.40, 29.23, 29.19, 27.25, 24.52, 22.56, 13.89. ^{11}B NMR (160 MHz, 10% MeOD – $CDCl_3$) δ = 29.84. MS-ESI [M^- -H_2O] calcd for $C_{46}H_{74}B_2N_2O_4$: 721.5651; Found: 721.5687.



3.1.5 **3.1b**

((((1,4-Phenylenebis(methylene))bis(dodecylazanediyl))bis(methylene))bis(2,1-phenylene))diboronic acid (3.1b)

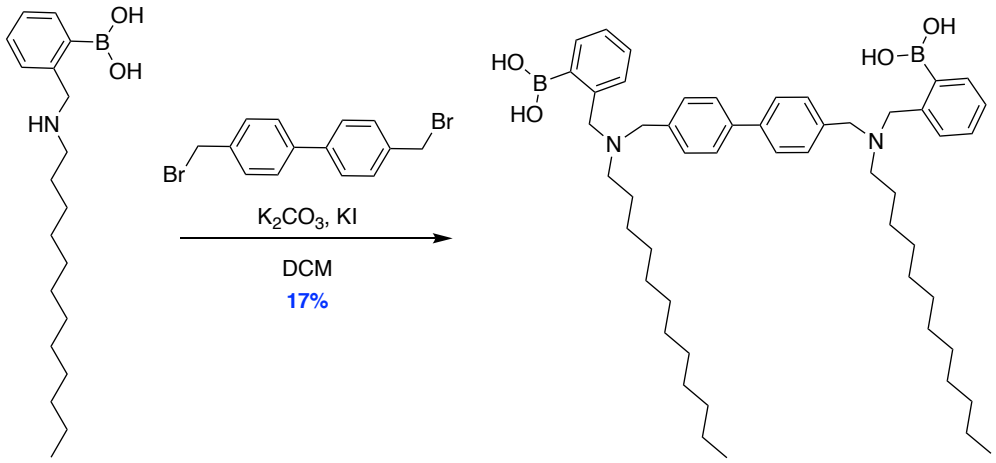
Product was a white solid (41.1 mg, 0.055 mmol, 36% yield) R_f = 0.2 (2% MeOH-DCM).^{1}H NMR (500 MHz, 10% MeOD – $CDCl_3$): δ 7.70 (d, *J* = 6.5 Hz, 2H), 7.21 – 7.14 (m, 4H), 7.11 (s, 4H), 7.06 – 7.02 (m, 2H), 3.64 (s, 4H), 3.49 (s, 4H), 2.33 – 2.25 (m, 4H), 1.43 – 1.34 (m, 4H), 1.20 – 0.94 (m, 45H), 0.75 (t, *J* = 7.0 Hz, 6H). ^{13}C-NMR (126 MHz, 10% MeOD – $CDCl_3$): δ 141.32, 135.74, 130.90, 129.39, 129.16, 127.46, 126.97, 126.73, 60.99, 56.18, 51.83, 32.74, 31.80, 29.50, 29.42, 29.37, 29.22, 29.18, 27.20, 24.40, 22.56, 13.87. ^{11}B NMR (160 MHz, 10% MeOD – $CDCl_3$) δ 28.52. MS-ESI [M^{+2}] calcd for $C_{46}H_{74}B_2N_2O_4$: 371.2997; Found: 371.3005.



3.1.5 3.1c

((((Naphthalene-2,6-diylbis(methylene))bis(dodecylazanediyl))bis(methylene))bis(2,1-phenylene))diboronic acid (3.1c)

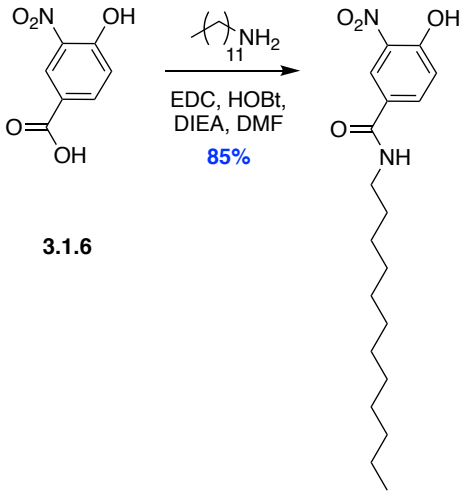
Product was a white solid (17.7 mg, 0.022 mmol, 29% yield) R_f = 0.2 (2% MeOH-DCM). ^{1}H NMR (500 MHz, 10% MeOD – CDCl3): δ 7.68 (d, *J* = 8.4 Hz, 4H), 7.59 (s, 2H), 7.31 (d, *J* = 8.4 Hz, 2H), 7.19 – 7.12 (m, 4H), 7.07 – 7.02 (m, 2H), 3.72 (m, 8H), 2.37 (s, 4H), 1.45 (s, 4H), 1.22 – 0.92 (m, 42H), 0.73 (t, *J* = 7.0 Hz, 7H). ^{13}C-NMR (126 MHz, 10% MeOD – $CDCl_3$): δ 135.65, 132.64, 130.39, 129.43, 128.60, 128.18, 127.92, 127.72, 127.46, 127.31, 60.79, 56.74, 52.29, 31.79, 29.56, 29.48, 29.46, 29.37, 29.30, 29.20, 29.11, 28.88, 27.08, 23.7, 22.54, 13.86. ^{11}B NMR (160 MHz, 10% MeOD – $CDCl_3$) δ 29.11. MS-ESI [M^{+2}] Calcd for $C_{50}H_{76}B_2N_2O_4$: 396.3074; Found: 396.3076.



3.1.5 3.1d

((((([1,1'-Biphenyl]-4,4'-diylbis(methylene))bis(dodecylazanediyl))bis(methylene))bis(2,1-phenylene))diboronic acid (3.1d)

Product was a white solid (6.5 mg, 0.008 mmol, 17% yield). R_f = 0.2 (2% MeOH-DCM). ^{1}H NMR (500 MHz, 10% MeOD – $CDCl_3$) δ 7.58 (s, 2H), 7.39 (d, *J* = 7.9 Hz, 4H), 7.17 (d, *J* = 7.8 Hz, 4H), 7.13 – 7.06 (m, 4H), 7.00 – 6.94 (m, 2H), 3.67 (s, 4H), 3.56 (s, 4H), 2.31 (t, *J* = 9.2 Hz, 4H), 1.38 (t, *J* = 7.6 Hz, 4H), 1.06 – 0.97 (m, 42H), 0.71 – 0.60 (m, 6H).^{13}C-NMR (126 MHz, 10% MeOD – $CDCl_3$): δ 140.23, 135.62, 134.11, 130.63, 130.00, 127.98, 127.75, 127.15, 127.12, 127.11, 61.31, 57.18, 52.29, 31.78, 30.44, 29.48, 29.39, 29.32, 29.19, 29.12, 28.55, 27.09, 24.92, 22.53, 13.85. ^{11}B NMR (160 MHz, 10% MeOD – $CDCl_3$) δ 29.53**.** MS-ESI [M^- -H_2O] Calcd for $C_{52}H_{78}B_2N_2O_4$ 797.5964; Found 797.5937. MS-ESI [M+H]$^+$: Calcd for $C_{52}H_{78}B_2N_2O_4$ 817.6226; Found 817.6174.



3.1.6

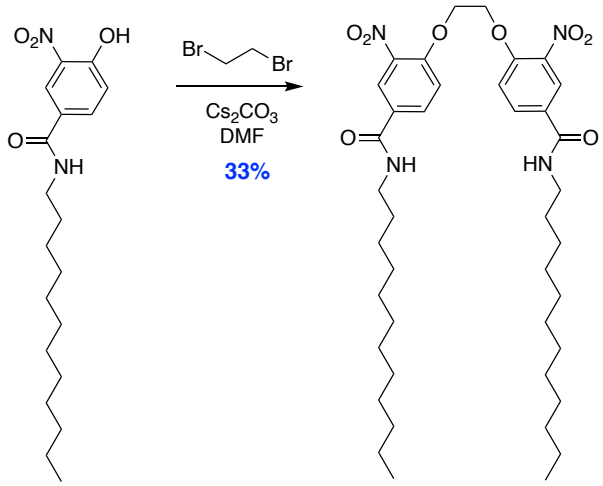
3.1.7

***N*-dodecyl-4-hydroxy-3-nitrobenzamide (3.1.7)**

4-Hydroxy-3-nitrobenzoic acid (**3.1.6**, 1.9997 g, 10.92 mmol, 1 eq), dodecan-1-amine (3.0561 g, 16.488 mmol, 1.51 eq) and hydroxybenzotriazole (HOBt, 2.2161 g, 16.4 mmol, 1.5 eq) were dissolved in 30 mL DMF under Ar. The solution was cooled to 0 °C and stirred for 5 min. Then, 1-ethyl-3-(3-dimethylaminopropyl)carbodiimide hydrochloride (EDCl) (3.1439 g, 16.4 mmol, 1.5 eq) and *N,N*-Diisopropylethylamine (DIEA, 4.755 mL, 24.324 mmol, 2.22 eq) were added to the reaction. The opaque orange mixture was warmed to rt and stirred for 5 hrs. To quench the reaction, 3 mL of water was added, and the mixture was poured into 50 mL of 1M HCl. EtOAc

(100 mL) was then added to the mixture and the organic layer was washed with water (5 x 50 mL) and brine (2 x 50 mL). The organic layer was next reduced under pressure and recrystallized with 95% ethanol to obtain **3.1.7** as a light-yellow solid. (3.253 g, 9.282 mmol, 85% yield).

^{1}H NMR (300 MHz, cdcl$_3$) δ 10.76 (s, 1H), 8.50 (d, *J* = 2.3 Hz, 1H), 8.06 (dd, *J* = 8.8, 2.3 Hz, 1H), 7.23 (d, *J* = 8.8 Hz, 1H), 6.08 (s, 1H), 3.48 – 3.42 (m, 2H), 1.63 (t, *J* = 7.1 Hz, 2H), 1.26 (s, 21H), 0.91 – 0.85 (m, 3H).



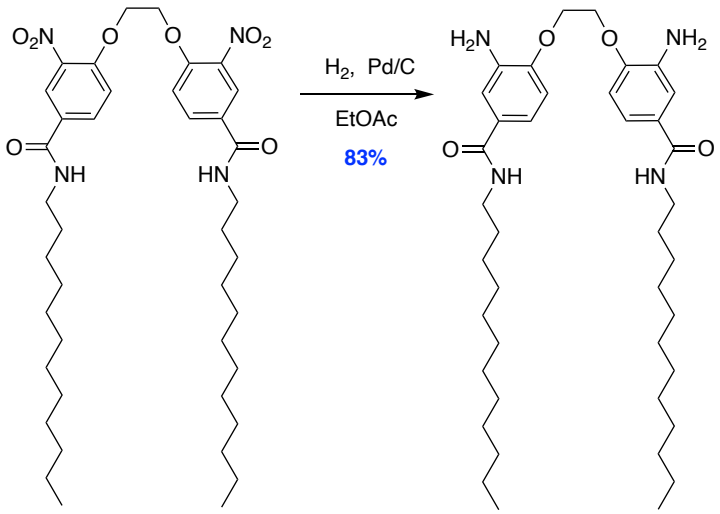
3.1.7 **3.1.8**

4,4'-(Ethane-1,2-diylbis(oxy))bis(*N*-dodecyl-3-nitrobenzamide (3.1.8)

Compound **3.1.7** (0.5687 g, 1.6227 mmol, 1 eq) was combined with oven-dried Cs_2CO_3 (1.5861 g, 4.868 mmol, 3 eq) under nitrogen and dissolved in DMF (15 mL). Then, 1,2-dibromoethane (0.070 mL, 0.8086 mmol, 0.5 eq) was added and the mixture was refluxed for 24 hrs. The mixture was cooled to rt and 100 mL water was added to form a yellow suspension, followed by extraction with $CHCl_3$ (2x 50mL). The organic phases were then collected and washed with water (3 x 50 mL) and brine (1x 50 mL). After being dried over Na_2SO_4, filtered, and concentrated under reduced pressure, the crude was subjected to a silica gel column chromatography using gradient elution from 50% EtOAc in hexanes to 10% MeOH in $CHCl_3$ to obtain **3.1.8** as a pale-yellow solid (194.6 mg, 0.2677 mmol, 33% yield). R_f = 0.5 (5% MeOH/EtOAc).

^{1}H NMR (300 MHz, cdcl$_3$) δ 8.20 (d, *J* = 2.2 Hz, 2H), 8.01 (d, *J* = 8.5 Hz, 2H), 7.27 (s, 1H), 7.25 (s, 1H), 6.14 (s, 2H), 4.61 (s, 4H), 3.45 (q, *J* = 6.7 Hz, 4H), 1.63 (t, *J* = 6.9 Hz, 4H), 1.26 (d, *J* = 1.8 Hz,

44H), 0.87 (d, *J* = 7.0 Hz, 7H). HRMS-DART: $[M+H]^+$ calcd for $C_{40}H_{63}N_4O_8$, 727.4646, found 727.3738.

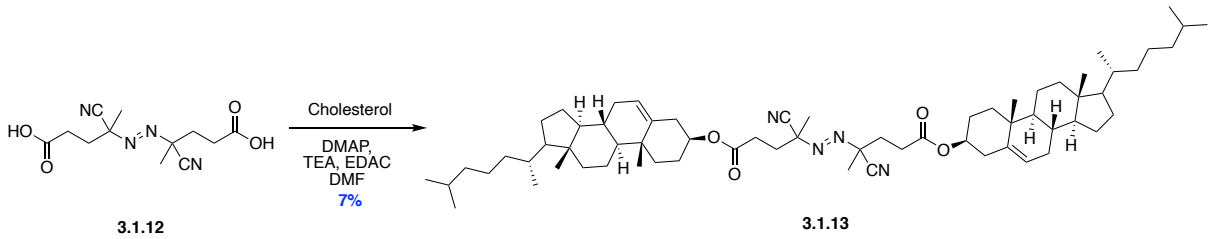


3.1.8 **3.1.9**

4,4'-(Ethane-1,2-diylbis(oxy))bis(3-amino-*N*-dodecylbenzamide) (3.1.9)

Compound **3.1.8** (0.0625 g, 0.0859 mmol) and 10% Pd/C (0.0188 g, 30% weight of compound **3.1.8**) were dissolved in 10 mL EtOAc under Ar. Then, the Ar was replaced by a hydrogen atmosphere using two balloons and the reaction mixture was further stirred under H_2 for 48 hr at rt. The Pd/C was removed by filtration over celite. After the removal of solvent under reduced pressure, the crude product was purified with column chromatography packed with alumina using eluant of 100% $CHCl_3$ to 1% MeOH-$CHCl_3$ to afford compound **2.3** (47.6 mg, 0.0713 mmol, 83%) as light-yellow solid. Rf = 0.4 (7.5% MeOH-$CHCl_3$). After the solution was and concentrated under reduced pressure, the crude was subjected to column chromatography packed with alumina using gradient elution from 100% $CHCl_3$ to 1% MeOH in $CHCl_3$ to afford **3.1.9** (47.6 mg, 0.0713 mmol, 83%) as a light-yellow solid. Rf = 0.4 (7.5% MeOH-$CHCl_3$).

^{1}H NMR (300 MHz, CD_3OD) δ 7.11 – 7.07 (m, 4H), 6.73 – 6.69 (m, 2H), 4.24 (s, 4H), 1.35 (d, *J* = 7.1 Hz, 4H), 1.02 (s, 49H), 0.66 – 0.61 (m, 8H). HRMS-DART: $[M+H]^+$ calcd for $C_{40}H_{66}N_4O_4$, 667.5162, found 667.4663.



3.1.12 3.1.13

Cholesterol-tailed initiator (3.1.13) Bis((3*S*,8*S*,9*S*,10*R*,13*R*,14*S*)-10,13-dimethyl-17-((*R*)-6-methylheptan-2-yl)-2,3,4,7,8,9,10,11,12,13,14,15,16,17-tetradecahydro-1*H*-cyclopenta[*a*]phenanthren-3-yl) 4,4'-((*E*)-diazene-1,2-diyl)bis(4-cyanopentanoate)

To a solution of 4,4'-azobis(4-cyanovaleric acid) (0.0500 g, 0.1784 mmol, 1 eq) in CH_2Cl_2 (50 mL) was added 4-(dimethylamino)pyridine (DMAP, 0.0218 g, 0.1784 mmol, 1eq), TEA (0.102 mL, 0.7318 mmol, 4.1 eq) and cholesterol (0.2758 g, 0.7133 mmol, 4 eq). The solution was stirred for 15 min and EDC (0.1368 g, 0.7136 mmol, 4 eq) was added. The solution was stirred in the dark for 18 hr under N_2, then diluted in DCM (30 mL), washed with water (5 x 100 mL), brine (200 mL). After being dried over Na_2SO_4, filtered, and concentrated under reduced pressure, the crude was subjected to a silica gel column chromatography using gradient elution from hexanes to 10% EtOAc in hexanes to obtain **3.1.13** as a white solid (12.72 mg, 0.0125 mmol, 7% yield).

^{1}H NMR (600 MHz, $CDCl_3$) δ 5.38 (d, *J* = 5.0 Hz, 2H), 4.63 (tq, *J* = 11.3, 4.2 Hz, 2H), 2.52 – 2.45 (m, 4H), 2.43 – 2.37 (m, 2H), 2.33 – 2.27 (m, 6H), 2.03 – 1.94 (m, 4H), 1.88 – 1.79 (m, 6H), 1.73 (s, 6H), 1.62 – 1.41 (m, 18H), 1.39 – 1.31 (m, 6H), 1.30 – 1.21 (m, 4H), 1.19 – 1.06 (m, 14H), 1.03 – 0.96 (m, 12H), 0.91 (d, *J* = 6.5 Hz, 6H), 0.86 (dd, *J* = 6.6, 2.7 Hz, 12H), 0.68 (s, 6H). ^{13}C NMR (151 MHz, $CDCl_3$δ 170.68, 139.41, 122.85, 74.79, 71.92, 56.67, 56.12, 50.00, 42.30, 39.71, 39.50, 38.04, 36.91, 36.56, 36.17, 35.77, 33.18, 31.89, 31.83, 29.40, 28.21, 28.00, 27.70, 24.26, 23.98, 23.81, 22.80, 22.55, 21.01, 19.28, 18.70, 11.84.

Preparation of BBAL liposomes for microplate assays

Stock solutions of 5 mM **3.1a**, **3.1b**, **3.1c**, **3.1d**, and **3.2.5**; 5 mM Biotin-cap-PE; and 5 mM rhodamine-PE were prepared in a 50:50 v/v mixture of methanol and chloroform and were stored at −20 °C after preparation. To prepare liposomes, a thin film was created by pipetting the appropriate volumes of the stock solution of each lipid component into a clean vial according to

calculations to obtain a mixture of 0.5 mM of total lipid content with the desired molar percentage of each component. As an example, for 500 µL of 0.5 mM liposomes composed of 20% **3.1a**, 1% Biotin-cap-PE, and 79% PC, 10 µL **3.1a** stock (50 nmols), 0.5 µL of Biotin-cap-PE stock (2.5 nmols), and 6.1 µL of PC (197.5 nmols) were combined. A nitrogen stream was then used to evaporate the solvent and the resulting lipid film was subsequently dried for at least 1 hr under vacuum. Then, the lipids were hydrated with 1 × PBS (pH = 8) at 60 °C in a water bath for 3 sets of 20 min with vortexing after each set. Liposomes then underwent 10 freeze-thaw cycles between a -80 °C dry ice-acetone bath and a 60 °C water bath, and vortexing was performed at a low speed between each cycle. Lastly, the liposome solutions were extruded through a 200 nm membrane filter for 15 passes using a LiposoFast extruder (Avestin, Inc.) and were stored at 4 °C for use within 1 day.

BBAL liposome microplate immobilization assay

Microplate liposome immobilization experiments were performed using black streptavidin-coated 96-well microplates. The wash buffer that was used was 1x PBS, pH 8. First, the wells that were to be used for analysis were washed with 250 µL of wash buffer for 30 min. This was removed, followed by introduction of different concentrations of liposomes with and without 1% Biotin-cap-PE (100 µL of solutions 0, 100, 200, 300, 400, 500 µM in wash buffer) and then incubated for 1 hr. The liposomes were composed of 0 or 20% of either **3.1a**, **3.1b**, **3.1c**, **3.1d**, and **3.2.5**; 0% or 1% Biotin-cap-PE; 1% Rhodamine-PE and the remainder PC (98%/99% or 78%/79%). Next, these solutions were removed, and the wells were washed 3 × 250 µL with wash buffer for 3 minutes each. Finally, 100 µL of MilliQ water was added to each well. The microplate was then analyzed for fluorescence using a microplate reader with excitation at 530 +/- 20 nm and emission wavelength of 590 +/- 20 nm. The RFU was determined according to the equation below where F_0 is the fluorescence measurement of 0 µM liposome treatment on the microplate, and F is the fluorescence measurement at 590 nm of the corresponding liposome treatment (100, 200, 300 or 400 µM). RFU @ 590 nm = $(F - F_0)$.

BBAL liposome binding dextran-rhodamine assay

Microplate liposome-dextran binding experiments were performed using black streptavidin-coated 96-well microplates. The wash buffer that was used was 1x PBS pH 8. First, the wells that were to be used for analysis were washed with 250 µL of wash buffer for 30 min. This was removed, followed by introduction of different concentrations of 1% Biotin-cap-PE functionalized liposomes (100 µL of solutions 0, 100, 200, 300, 400, 500 µM in wash buffer) and then incubated for 1 hr. The liposomes were composed of 0 or 20% of either **3.1a**, **3.1b**, **3.1c**, **3.1d**, and **3.2.5**; 1% Biotin-cap-PE; and the remainder PC (99% or 79%). Next, these solutions were removed, and the wells were washed 3 × 250 µL with wash buffer for 3 minutes each. Following this, 100 µL of 5 µg/mL Rd-dextran was added to each well, followed by a 1h incubation. The solution was removed and then the wells were washed 3 × 250 µL with wash buffer for 3 minutes each. Finally, 100 µL of MilliQ water was added to each well. The microplate was then analyzed for fluorescence using a microplate reader with excitation at 530 +/- 20 nm and emission wavelength of 590 +/- 20 nm. The percent fluorescence increase was determined according to the equation below where F_0 is the fluorescence measurement of 0 µM liposome treatment on the microplate, and F is the fluorescence measurement at 590 nm of the corresponding liposome treatment (100, 200, 300 or 400 µM). Fluorescence Increase after Rd-dextran Binding @ 590 nm = $(((F/F_0)*100)-100)$.

BBAL mucin binding competition assay

The protocol from the Rd-dextran microplate assay was first performed similar to as described above. Experiments were performed using black streptavidin-coated 96-well microplates. The wash buffer that was used was 1x PBS pH 8. First, the wells that were to be used for analysis were washed with 250 µL of wash buffer for 30 min. This was removed, followed by introduction of 1% Biotin-cap-PE functionalized liposomes (100 µL of 500 µM solution in wash buffer) and then incubated for 1 hr. The liposomes were composed of 0 or 20% of either **3.1a**, **3.1b**, **3.1c**, **3.1d**, and **3.2.5**; 1% Biotin-cap-PE; and the remainder PC (99% or 79%). Next, these solutions were removed, and the wells were washed 3 × 250 µL with wash buffer for 3 minutes each. Following this, 100 µL of 5 µg/mL Rd-dextran was added to each well, followed by a 1h incubation. The

solution was removed and then the wells were washed with 3 × 250 µL wash buffer for 3 minutes each. Then, 100 µL of MilliQ water was added to each well and an initial fluorescence reading was taken using a microplate reader with excitation 530 +/- 20 nm and emission wavelength of 590 +/- 20 nm. Next, a solution of 40 mg/mL mucin from porcine stomach (Type III, bound Sia 0.5-1.5) was created by dissolving 60 mg in 1.5 mL wash buffer, and various concentrations were added to the wells of the microplate (1, 5, 10, 20, and 30 mg/mL) in wash buffer and incubated for 13 hr at 4 °C. The solution was removed and then the wells were washed 3 × 250 µL with wash buffer for 3 minutes each. Finally, 100 µL of MilliQ water was added to each well. The microplate was then analyzed for fluorescence using a microplate reader with excitation 530 +/- 20 nm and emission wavelength of 590 +/- 20 nm. The percent of initial fluorescence intensity of Rd-dextran after mucin binding was determined according to the equation below where F_0 is the fluorescence measurement at 590 nm after the Rd-dextran binding step, and F is the fluorescence measurement at 590 nm after the competition assay final washing step. To account for background Rd-dextran fluctuations, the fluorescence decrease from initial (F_0-F) after 0 µM mucin treatment ($F_{0\mu M\ Muc}$) was added to the subsequent readings. Percent of Initial Fluorescence Intensity of Rd-dextran after Mucin Binding @ 590 nm = $((F+F_{0\mu M\ Muc})/F_0)*100$.

BBAL liposome catechol binding assay

The protocol for the Rd-dextran microplate binding assay was first performed similar to as described above. Experiments were performed using black streptavidin-coated 96-well microplates. The wash buffer that was used was 1x PBS pH 8. First, the wells that were to be used for analysis were washed with 250 µL of wash buffer for 30 min. This was removed, followed by introduction of 1% Biotin-cap-PE functionalized liposomes (100 µL of 500 µM solution in wash buffer) that were incubated for 1 hr. The liposomes were composed of 20% **3.1a**, 1% Biotin-cap-PE, and the remainder PC (79%). Next, these solutions were removed, and the wells were washed 3 × 250 µL with wash buffer for 3 minutes each. Following this, 100 µL of 5 µg/mL Rd-dextran was added to each well, followed by a 1 hr incubation. The solution was removed and then the wells were washed with 3 × 250 µL wash buffer for 3 minutes each. Next, a solution of 100 mM catechol was created by dissolving 11 mg of catechol in 1 mL wash buffer, which was then diluted to 2 mM

catechol stock and various concentrations in wash buffer were added to the wells of the microplate (0, 0.05, 0.1, 0.2, 0.5, 0.75, 1, or 2 mM) and incubated for 1 hr. These solutions were then removed and then the wells were washed with 3 × 250 µL wash buffer for 3 minutes each. Finally, 100 µL of MilliQ water was added to each well. The microplate was then analyzed for fluorescence using a microplate reader with excitation 530 +/- 20 nm and emission wavelength of 590 +/- 20 nm. The percent fluorescence change was determined according to the equation below where F_0 is the fluorescence measurement of 0 mM catechol treatment on the microplate, and F is the fluorescence measurement at 590 nm of the corresponding catechol treatment (0.05, 0.1, 0.2, 0.5, 0.75, or 1, 2 mM). Fluorescence change after catechol binding @ 590 nm = $((F/F_0)*100)$.

Dynamic light scattering (DLS) analysis of liposome size

DLS measurements were carried out with a Malvern Zetasizer Nano ZS instrument equipped with a 4.0 mW laser operating at l = 633 nm. Samples were prepared by diluting the liposome solutions before and after treatment 10 times with 1 x PBS pH 8. All samples were determined at a scattering angle of 173° at 20 °C. The data reported are the averages of three tests with error bars indicating standard error.

Transition electron microscope (TEM) BBAL analysis

Liposomes containing 20% of **3.1a** and otherwise composed of PC (2 mM) without any dye encapsulation were prepared according to the standard liposome preparation procedure mentioned above. For TEM studies, a drop (5−10 µL) from each solution was immobilized onto a thin carbon film supported by a 200-mesh copper grid (for 1 min) and then stained (for 1 min) with 5% uranyl acetate. After drying for 1 hr the samples were washed three times with distilled water for 10 min. Images were collected using a JEOL 1400 Flash microscope operating with a beam energy of 80 keV and a Gatan One View camera and then processed with ImageJ software. Scale bars on images denote 200 nm.

Preparation of BBAL liposomes for cell association experiments

Lipids and cholesterol were purchased from Avanti Polar Lipids (Alabaster, AL, USA). All liposomes were assembled via a modified ethanol injection technique previously described.[354] Briefly, lipids were dissolved in chloroform, combined as indicated, and dried under nitrogen gas to create lipid films. Lipid films were resuspended in 100% molecular grade ethanol and mixed for 60 minutes at 40 °C. Ethanolic lipid solutions were then injected dropwise into filtered phosphate buffered saline (PBS). For cell association experiments using internal aqueous dye SRB, the ethanolic lipids were injected into filtered PBS with 50 mM SRB. Liposomes were then purified from ethanol via overnight dialysis against PBS at 4 °C using 300 kD Float-A-Lyzer™ G2 dialysis devices (Spectrum labs, Rancho Dominguez, CA). One buffer exchange after 12 hr of dialysis followed by at least 2 more hr of dialysis ensured efficient purification for experiments that utilize the lipophilic Rd-PE dye. If SRB was present during injection, a minimum of 24 hr of dialysis was employed with at least 4 buffer exchanges to sufficiently remove unencapsulated dye. After dialysis, the final volume for each sample was measured, all samples were normalized to the highest volume and said volume was used to determine treatment amounts for experimental assays such that all samples received equimolar lipid content. Liposomes were extruded to 100 nm using polycarbonate membrane Nanosizers™ (T&T scientific, Knoxville, TN), stored at 4 °C, and used within 24 hr.

Vascular smooth muscle cell (VSMC) culture

Human aortic smooth muscle cells (LifeLine Cell Technology, Walkersville, MD) were maintained as cryopreserved primary cultures of single-donor cells. Cells were grown in T75 flasks and then plated at 1.5×10^5 cells per well (6-well plate) for cell association experiments. Cells were grown to 60 - 80% confluency in VascuLife growth medium composed of VascuLife Basal Medium and VascuLife smooth muscle cell growth supplement kit with gentamicin and amphotericin (LifeLine Cell Technology). Incubation was performed at 37 °C under 5% CO_2 with 95% humidity. Before liposomal treatment, cells were made quiescent by treating overnight with DMEM (Thermofisher Scientific) with gentamicin and amphotericin.

Vascular smooth muscle cell (VSMC) liposomal cell association experiments

Lipid-dependent cell association was measured as previously described.[354] Briefly, at ~80% confluence cells were treated in DMEM for 24 hr with 50 µM of liposomes containing 0%, 10%, or 20% **3.1c**, 1% Rd-PE, 5% PEG-PE, and the remainder of each liposome composed of DOPC and Cholesterol at a 7:3 ratio (94%, 84%, or 74%). Cells were washed three times in PBS, lysed with 1 mL of 1% Triton X-100, and centrifuged at 12,000 RPM for 5 min at 4 °C to remove debris. Cell lysate (200 µL) supernatants were plated in duplicate in 96-well plates and association of rhodamine-labeled liposomes was quantified within the cell lysates by measuring residual Rd-PE. Fluorometric analysis, performed using a Glomax multi microplate reader with a 575 nm filter (Promega, Madison, WI), determined average fluorescence units for each sample, minus baseline fluorescence of nontreated controls receiving no rhodamine source within each experimental replicate. Replicate studies always used fresh batches of liposomes. Fluorescence microscopy using 400X magnification (40X lens, 10X eyepiece/camera) with 200 ms (Rhodamine detection) or 50 ms (DAPI, bright field) exposures across all groups provided qualitative representative cell association images using a BX51 Olympus microscope with an Olympus Q-color camera (Olympus Corporation, Shinjuku, Tokyo, Japan).

***C. Albicans* cell delivery study**

For these experiments the SC5314 (wildtype) strain of *C. albicans* was used, which has been described previously.[402] Liposome treatments were prepared as described above, with 0% or 20% **3.1a** or **3.1c**, 79 or 99% PC, and were labeled with 1% NBD-PE for fluorescence detection. Cells were cultured in 5 mL YPD media (1% Bacto yeast extract, 2% Bacto peptone, and 2% dextrose (Thermo Fisher Scientific)), and shaken at 30 °C and 250 rpm overnight. The next day, cells were diluted to OD_{600} = 0.1 in 50 mL fresh YPD media and were spun down when OD_{600} reached 1.0. The cell pellets were washed three times with 30 mL 1 x PBS to remove residual nutrients and were left in 5 mL fresh 1 x PBS to be shaken at 30 °C and 250 rpm overnight. On day three, cells were diluted to final OD_{600} = 1.0 in 1 x PBS with each liposome treatment at a final concentration of 1mM, in the total volume of 500 µL. Cells were incubated with liposomes for 8h, then washed

three times with 500 µL 1 x PBS to remove residual liposomes. Cells were then fixed by addition of 500 µL of 3.7 % paraformaldehyde (dissolved in 1 x PBS buffer, pH 7.4), incubated for 15 min, then washed with 500 µL of 1 x PBS. Cells were finally resuspended in 500 µL 1 x PBS and then imaged with an inverted confocal laser scanning microscope (SP8, Leica). The fluorescent signal from the NBD-PE was collected upon excitation at 458 nm with an Ar ion laser and emission was collected 470 - 560 nm. Images were processed with ImageJ software. Scale bars on images denote 5 µm.

Preparation of BOPLIPs for hydrophobic nile red release assays

Stock solutions of 1 mM **3.1.16**, 5 mM Nile Red, and 32.46 mM Egg PC were prepared in chloroform and were stored at −20 °C after preparation. Proper volumes of each stock solution were pipetted into a clean vial to obtain the desired percentage of each component. As an example, to make 800 µL of a 2 mM liposome solution containing 94.9% PC, 0.11% BOPLIP, and 5% NR, 51.51 µL of PC, 1.76 µL of BOPLIP, and 17.6 µL of NR was added to a vial. The solvents were then removed, and the resulting solid was further dried under vacuum for at least two hr to yield a lipid film. After that, the lipid film was dissolved with 586.3 µL ethanol at 40 °C for 40 minutes to increase solubility. Then, 533 µL (90 %) of the ethanol mixture (not to exceed 40% of the total ethanol/aqueous solution) was added dropwise with constant vortexing to 800 µL 1x PBS pH 8 to achieve an ethanol/aqueous ratio of 40/60. The ethanol was then carefully removed via rotary evaporation and the samples were adjusted to their proper volume of 800 µL with MQ water to achieve a final solution of 2 mM liposome in 1 x PBS pH 8. Then, the liposome solutions were extruded through a 200 nm polycarbonate membrane for 15 passes with a LiposoFast extruder (Avestin, Inc.).

Analysis of nile red release assay with BOPLIPs

For fluorescence-based release studies, 50 µL samples of liposome vesicles were added into a sub-micro cuvette cell (Starna Cells, Inc). First, an initial fluorescence scan was obtained (excitation wavelength of 552 nm, emission wavelength scanned from 580 nm to 700 nm, excitation slit = 5 nm, emission slit = 10 nm). For NR release studies with different concentrations

of Neu5Ac, 2 mM of 0.11% **3.1.16** liposome samples encapsulating 5% NR were used. Stock solutions of 200 mM Neu5Ac, glucose, galactose, and mannose were made in 1 x PBS pH 8 buffer. For example, a 200 mM Neu5Ac stock solution was prepared by dissolving 12.37 mg Neu5Ac in 200 µL of 1 x PBS pH 8 buffer. To prepare the liposome treatment solutions containing 5 – 40 mM saccharide treatment, aliquots ranging from 1.5 µL - 10 µL of the 200 mM stock solution were then added into 50 µL liposome solution in a cuvette and fluorescence scans were taken every minute for 25 minutes. Data presented in plots indicate emission intensity values at 635 nm, which were converted into a percentage of initial fluorescence intensity based on the initial scan before adding stimuli. To demonstrate that the dilution effect is not responsible for NR release, control samples were run by treating liposomes with 10 µL of 1x PBS pH 8 and measuring fluorescence. Experiments were run at least 3 times with different batches of liposomes. Averaged data were reported with error bars denoting standard error.

Transition electron microscope (TEM) BOPLIP analysis.

Liposomes containing 0% or 0.11% **3.1.16** and otherwise composed of PC (2 mM) without any dye encapsulation were prepared according to the ethanol injection liposome preparation procedure mentioned above. Liposomes were treated with Neu5Ac and allowed to incubate for 25 min. For TEM studies, a drop (5−10 µL) of liposome solution was immobilized onto a thin carbon film supported by a 200-mesh copper grid (for 1 min) and then stained (for 1 min) with a 1.0% (w/v) solution of neutral PTA. After drying, the samples were stored in a desiccator overnight prior to examination. Images were collected using a JEOL 1400 Flash microscope operating with a beam energy of 80 keV. Images were collected using a Gatan One View camera and processed with ImageJ software. Scale bars on images denote 200 nm.

Chapter 4. General Thiol and Cysteine Responsive Liposomes

Experiments in Chapter 4 include contributions from Megan L. Qualls, Dr. Jinchao Lou, and Dr. Michael D. Best. MLQ designed all synthetic routes and synthesized and characterized all compounds. MLQ performed all liposome preparation, liposomal dye release assays, and DLS analysis. MLQ performed characterization of all lipid decomposition with TLC, NMR, and MS. MLQ and MDB contributed to the design of the general thiol-responsive lipids. MLQ, JL, and MDB contributed to the design of the cysteine-responsive lipids. MLQ and MDB contributed to the writing of Chapter 4. MDB directed the project.

4.1. Abstract

Liposomes are effective therapeutic delivery nanocarriers due to their ability to encapsulate and enhance the pharmacokinetic properties of wide-ranging therapeutics. The development of stimuli-responsive liposomes in which cargo release is controlled based on the microenvironment has emerged as an exciting area of research. Thiol-containing molecules provide a family of promising targets for triggered release with multiple opportunities for enhancing delivery and advancing the development of molecular-responsive liposomal platforms for drug delivery. As seen in Chapter 2, thiol functionalities present on cell surface proteins can be exploited for chemical reactions to drive liposome uptake; however, these reactions could also be harnessed to facilitate cargo release. Despite the opportunity of using thiols to drive cargo release, few thiol-responsive triggered liposomal platforms have been reported. Additionally, the thiol-containing amino acid Cys is an analyte that is significantly upregulated during cancer onset and is responsible for GSH production, which combats oxidative conditions, maintaining cellular homeostasis and cancer cell survival.[186] Because of this, we pursued the design and synthesis of two classes of stimuli-responsive liposomes, those that generally respond to thiols, and also lipid switches that are activated specifically by Cys. In order to accomplish this, lipid switches with thiol or Cys reactive headgroups appended to self-immolating lipid scaffolds were created. Fluorescence-based triggered release assays were implemented to show that these compounds enable the *in-situ* creation of non-membrane forming lipids upon reaction with thiols or Cys, resulting in membrane destabilization and release of internalized cargo. These results demonstrate that lipids which respond both generally to thiol-containing biomolecules as well as

selectively to Cys serve as exciting liposome systems for harnessing disease-associated thiols to trigger liposomal release.

4.2. Introduction

Liposomal nanoparticles are effective therapeutic carriers for encapsulating a wide range of therapeutic agents and enhancing their pharmacokinetic properties.[403] Previous advancements in liposome design, including polymer coatings (PEG) which enhance circulation time,[404] functionalities such as cationic lipids to promote cell entry,[405, 406] and targeting motifs like antibodies to enable selective delivery to diseased cells, have resulted in clinically approved liposome formulations.[407] Even so, improvements are needed to enhance liposome delivery properties and continue to improve their therapeutic achievements.

While liposomes decorated with active targeting ligands such as antibodies allow for site-controlled delivery of the vesicles, strategies are needed to allow for quick and efficient drug release from the liposome to increase drug efficacy and reduce adverse effects. Therefore, a key area of development is the necessary breakdown of the liposome bilayer in order to release therapeutic cargo. While the breakdown of the membrane is not efficient in typical liposome systems, progress is being made toward the development of stimuli-responsive liposomes platforms that can release cargo upon specific trigger exposure.[134, 135] Cargo release mechanisms can also be developed which leverage disease-associated stimuli to selectively delivery liposome contents to diseased cells compared to healthy cells. This selective delivery can be exploited to reduce harmful side effects and improve liposome efficacy by encouraging maximum content release from liposomes and enabling selective delivery to diseased cells for therapeutic applications. Therefore, the development of triggered release platforms that employ stimuli-responsive liposomes which release cargo upon exposure to a specific trigger has emerged as a vibrant research area.

There are two categories of triggered release based on the microenvironment which most systems fall into, namely passive release and active release. Passive release exploits

pathophysiological differences in the microenvironment of healthy cells compared to diseased cells including pH,[149] redox environment,[150] enzyme expression,[151] and metabolite concentrations.[152-155] Active release employs changes in external stimuli such as light,[156-158] heat,[159, 160] or ultrasound.[161, 162] Controlled cargo release based on cellular microenvironment embodies the technological forefront of the field; however, the number of targeted release strategies remains meager and these platforms have not yet entered clinical applications because of unresolved challenges. Recently, our group has supplied notable contributions by developing liposomes that respond to light,[163] calcium,[164, 165] zinc,[166] carbohydrates,[408, 409] enzymes,[167] reactive oxygen species (ROS),[168] and phosphorylated metabolites ATP[169] and inositol (1,4,5)-trisphosphate (IP_3)[170]). In addition, a liposome platform was designed to interact with free thiols to facilitated membrane decoration and enhance cellular uptake.[410] A particular area of interest is the creation of liposomes that respond to small organic biomolecules that are overexpressed in and around diseased cells.[171] The origin of this interest is due to other stimuli being unsuitable for clinical use. For example, passive release methods often suffer from minimal differences between healthy and diseased cells. Additionally, active release suffers from difficulty in delivering physical stimuli that leaves healthy cells undamaged.

Targeting small organic biomolecules can address these challenges, and organic metabolites and functional groups offer exciting stimuli for triggering cargo release because they can be highly overexpressed in diseased cells compared to their healthy counterparts. Thiol-containing molecules provide a family of promising targets for triggered release with multiple opportunities for enhancing delivery and advancing the development of molecular-responsive liposomal platforms for drug delivery. As seen in Chapter 2, thiol functionalities present on cell surface proteins can be exploited for chemical reactions to drive liposome uptake. Additionally, it is known that the thiol-containing amino acid Cys and tripeptide GSH are significantly upregulated during cancer onset.[186] Although it is an exciting opportunity to harness the reactions of disease-associated thiols to facilitate nanoparticle cargo release, few thiol-responsive triggered liposomal platforms have been reported. Previously, thiol-responsive NPs have been reported including dendrimers[198] and polymerizome NPs,[199] prodrug therapeutics,[200] and dynamic self-

assemblies.[201-203] Also, the previously discussed thiol-responsive liposome systems include lipids with thiol responsive tails[208] or headgroups[138, 411] which showed thiol-sensitive release of payload upon thiol treatment or cellular uptake by cancer cells. Since few systems have been developed, this is an exciting area of triggered liposome release.

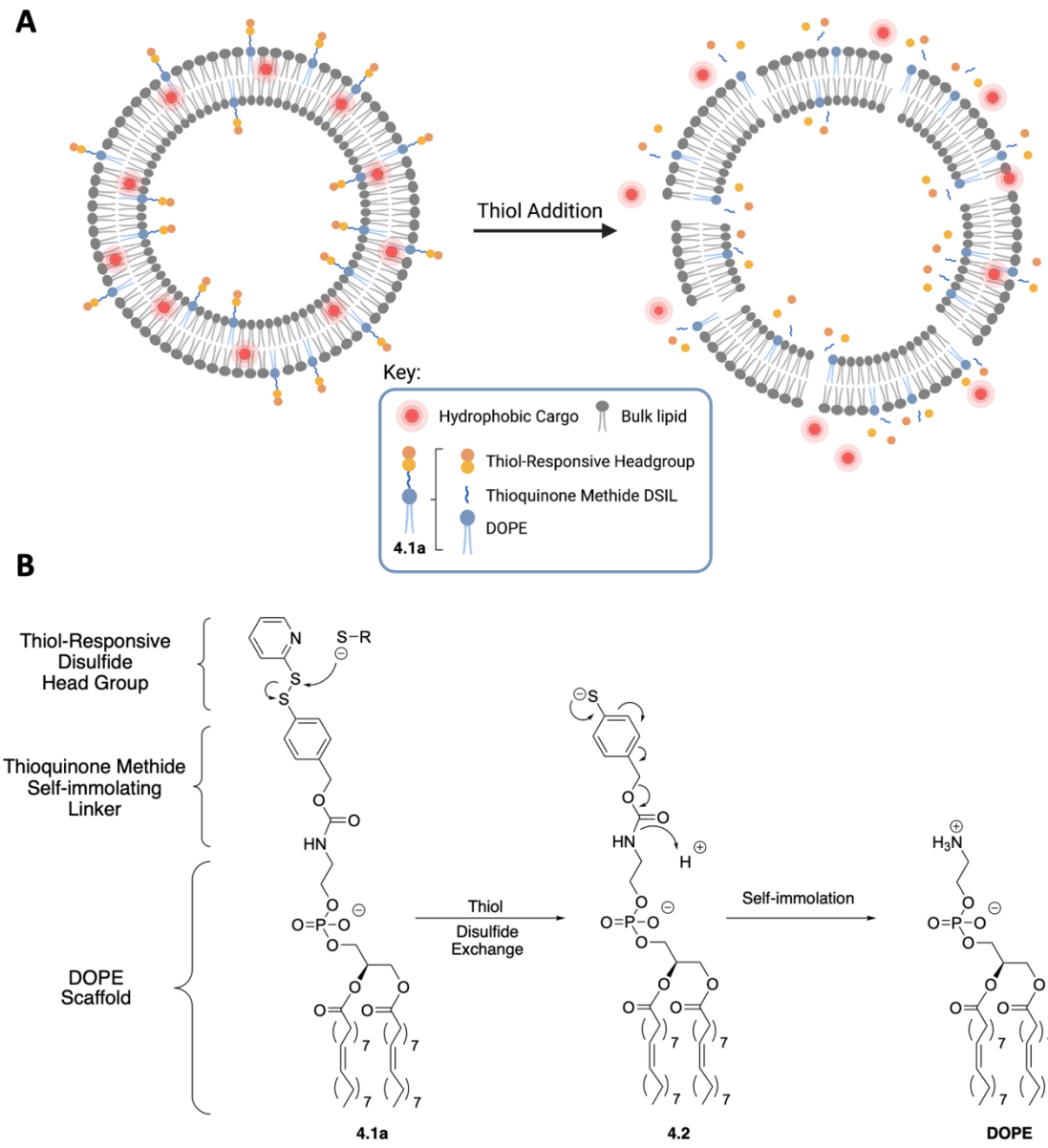
Hence, to further these goals we developed a family of synthetic lipid switches designed to undergo programmed structural alterations in the presence of thiols in general, or specifically Cys, that perturb liposomal membranes and drive the release of contents. In order to accomplish this, lipid switches with thiol or Cys reactive headgroups appended to a self-immolating lipid scaffold were created. Upon reaction with general thiol-containing biomolecules or Cys, the *in-situ* creation of non-membrane forming lipids is designed to facilitate membrane disruption and cargo release. These general thiol and Cys responsive liposome systems can enable further advancements in achieving maximum cargo release in response to the disease cell environment.

In this Chapter, we present a promising advancement in the emerging area of metabolite-responsive liposomes by harnessing important biomolecular targets that are upregulated in disease states as stimuli. We developed two classes of stimuli-responsive liposomes including panels of lipid switches that drive release through either reaction with general thiol-containing biomolecules, and also lipid switches that are designed to be activated specifically by Cys. In this chapter, a comprehensive evaluation of this delivery platform is presented including the design and synthesis of the thiol and Cys triggered lipids, assessment of triggered self-immolation and release of non-bilayer forming lipid, analysis of fluorescence-based triggered release assays to assess if these switches result in membrane destabilization and release of internalized cargo, and characterization of liposome morphology containing the lipids. The results of the experiments will demonstrate if these lipids serve as exciting liposome systems for harnessing disease-associated thiols to trigger liposomal release.

4.3. Design and synthesis of general thiol-responsive liposomes

Our initial lipid switch **4.1a** was designed to respond to general thiol-containing biomolecules and induce liposomal cargo release (Scheme 4.1A). The switch is designed with a disulfide functionality in the lipid headgroup that can undergo exchange with an intracellular thiol such as Cys or GSH (Scheme 4.1B). Once the exchange reaction has taken place, a self-immolating group will be uncaged (**4.2**), which undergoes the thioquinone methide cascade rearrangement mechanism, resulting in triggered fragmentation (1,6-elimination) and release of free DOPE. Similar disulfide-based self-immolative linkers (DSILs) have previously been used to successfully release therapeutic drugs,[412, 413] proteins,[414, 415] imaging probes,[416, 417] and even cleave vesicle PEG coating resulting in release of therapeutic cargo.[418] Once free DOPE has been released, membrane disruption is likely to occur since DOPE is a non-bilayer lipid that perturbs membrane packing. Hence, we will herein report DSIL lipids (DSILLs) that undergo triggered release of encapsulated liposomal contents in response to biologically relevant thiols.

Comparable strategies have been previously reported in which triggered lipid self-immolation and release of DOPE is harnessed to cause membrane disruption and liposomal content release in response to stimuli including reduction conditions,[218, 419] light,[420] and enzymes.[421] Formation of the non-bilayer lipid DOPE is hypothesized to disrupt the liposome membrane and cause release of hydrophobic or hydrophilic liposomal cargo because of the change in membrane packing. As previously discussed, lipid self-assembly is determined by the head-to-tail size ratio of the lipids composing the mixture.[422] For example, lipids with comparable head and tail volumes such as PC prefer to form bilayer liposome structures. Conversely, lipids such as DOPE which have small headgroups compared to tails prefer non-bilayer packing including the hexagonal phase H_{II}.[423] It follows that self-assembly properties can be modified by increasing or decreasing the headgroup volume. For example, *N*-acylation of the amine group of DOPE has been shown to allow the lipids to form stable bilayer membranes.[424] This strategy will be used to provide a switch in lipid packing properties upon cleavage of the large headgroup and DOPE formation, enabling membrane disruption and the release of encapsulated cargo.



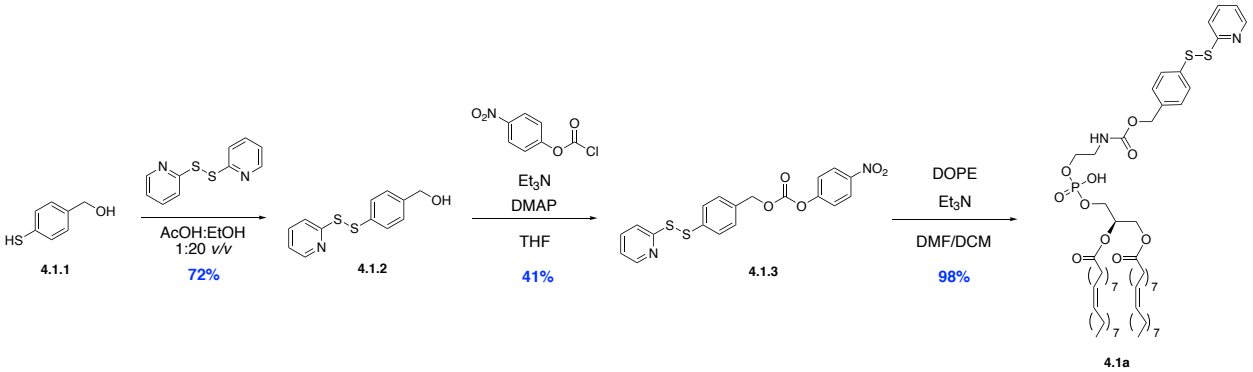
Scheme 4.1 Thiol responsive lipid 4.1a design. (A) Cartoon illustration of liposomal release driven by thiol addition. (B) Structure of thiol-responsive lipid **4.1a** and its decomposition mechanism upon stimulus addition. The disulfide headgroup of **4.1a** is expected to undergo exchange with an intracellular thiol such as Cys or GSH, leading to DSILL breakdown as shown in **4.2**. This breakdown releases the non-bilayer-forming lipid DOPE by 1,6-elimination, which can disrupt membrane packing and trigger release of liposomal contents.

The synthesis strategy for accessing **4.1a** is shown in Scheme 4.2. To begin, 4-mercaptobenzyl alcohol (**4.1.1**) underwent a thiol exchange reaction with 2,2′-dipyridyl disulfide to form **4.1.2**. Then, the hydroxyl of **4.1.2** was activated using 4-nitrophenyl chloroformate to form **4.1.3**. Last, **4.1.3** was coupled with DOPE to form **4.1a**. Following lipid synthesis, we moved on to the evaluation of thiol conjugation and liposome content release properties of the liposomes containing **4.1a**.

4.4. Nile red release assays with 4.1a

Following the synthesis of prospective thiol-responsive lipid **4.1a**, we began to evaluate release of the hydrophobic dye NR. After screening various liposome formulations, we determined that liposomes composed of 20 - 40% **4.1a**, 50% DOPE, 10% PA, and the remaining Egg-PC (20%, or 0%, respectively) in addition to 5% NR was the most promising formulation in terms of maximizing triggered release while minimizing background leakage. Liposomes were prepared through traditional thin-film liposome preparation techniques including thin-film formation, hydration, freeze-thaw cycling, and extrusion through 200 nm membranes to form uniform liposomes of desired size. Negative control liposomes lacking **4.1a** (replaced by Egg-PC) were also prepared. The samples were treated with 10 mM Cys, GSH, or buffer only and fluorescence readings were taken over time at room temperature. A summary of liposome formulations explored is included in Table 4.1.

As shown in Figure 4.1, addition of Cys resulted in dose-dependent decreases in NR fluorescence depending on the mol% of **4.1a** in the liposome over 12 hr, indicating NR release. For example, 20% **4.1a** liposome treated with Cys resulted in a decrease in NR fluorescence of ~27%, and 40% **4.1a** liposomes treated with Cys showed a sizable ~46% NR fluorescence decrease. Control liposomes lacking **4.1a** indicated minimal ~10% release from unspecific interactions. Control studies were conducted in which 1 x PBS pH 7.4, was instead added to the liposomes and release was measured over time, which yielded small NR fluorescence decrease over 12 hr (0% **4.1a**, ~2 % release; 20% **4.1a**, ~3% release; 40% **4.1a**, ~13% release). For comparison, liposome samples were also treated with 10 mM GSH and monitored over 12 hr. The 20% **4.1a** liposomes treated



Scheme 4.2 The synthetic route for accessing 4.1a. To begin, 4-Mercaptobenzyl alcohol (**4.1.1**) underwent a thiol exchange reaction with 2,2'-dipyridyl disulfide to form **4.1.2**. Then, the hydroxyl group of **4.1.2** was activated using 4-nitrophenyl chloroformate to form **4.1.2**. Last, **4.1.2** was coupled with DOPE to form **4.1a**.

with GSH resulted in a maximum ~16% decrease in NR fluorescence, which is lower compared to the ~27% release caused by Cys (Figure 4.2A). Similarly, 40% **4.1a** liposome treated with GSH showed a maximum of ~22% release, less than the ~46% release from Cys treatment (Figure 4.2B). It is notable that 0% **4.1a** liposomes also showed comparatively high maximum release of 13% after GSH treatment (Figure 4.2C). Altogether, these experiments demonstrate that **4.1a** liposomes undergo notable triggered release of hydrophobic cargo in response to Cys and minimally in response to GSH.

4.5. Dynamic light scattering 4.1a studies

Following the experiments demonstrating NR release from **4.1a** liposomes, we moved on to test if the cargo release was accompanied by a change in liposome vesicle morphology. Since the addition of Cys and GSH resulted in NR cargo release from **4.1a** liposomes, it is important to probe for changes in particle sizes both before and after Cys treatment. First, liposomes underwent DLS analysis to probe particle sizes before and after treatments. Liposomes were used which were comprised of 0%, 20%, or 40% **4.1a**, 50% DOPE, 10% PA, and otherwise Egg-PC (40%, 20%, or 0%, respectively) as well as 5% NR, and were treated with either buffer, 10 mM GSH, or 10 mM Cys and incubated for 12 hr. These results showed that liposomes containing 0%, 20%, or 40% **4.1a** had average diameters < 200 nm (Figure 4.3A) and polydispersity indices (PDI) ≤ 0.2 (Figure 4.3B) before and after treatment, which are both in the desirable size range (diameter ≤ 200, PDI ≤ 0.2). These results indicate that stable liposomes were formed with up 40% **4.1a** incorporation, and addition of thiols did not cause major changes in vesicle morphology. Raw distribution curves are included in Figure 4.3C-D.

4.6. TLC analysis of thiol-mediated cleavage of free lipid 4.1a

After synthesizing DSILL **4.1a** and assessing liposome release characteristics, we moved on to begin studying the compound's reactivity with the thiol-containing metabolites Cys and GSH. A thin layer chromatography (TLC) analysis was first performed in order to gain a simple understanding of the lipid's reactivity. The analysis was performed by treating 2 mM solutions of free **4.1a** lipid with no treatment (Figure 4.4, lane 1), 1.5 mM GSH (Figure 4.4, lane 2), or 1.5 mM

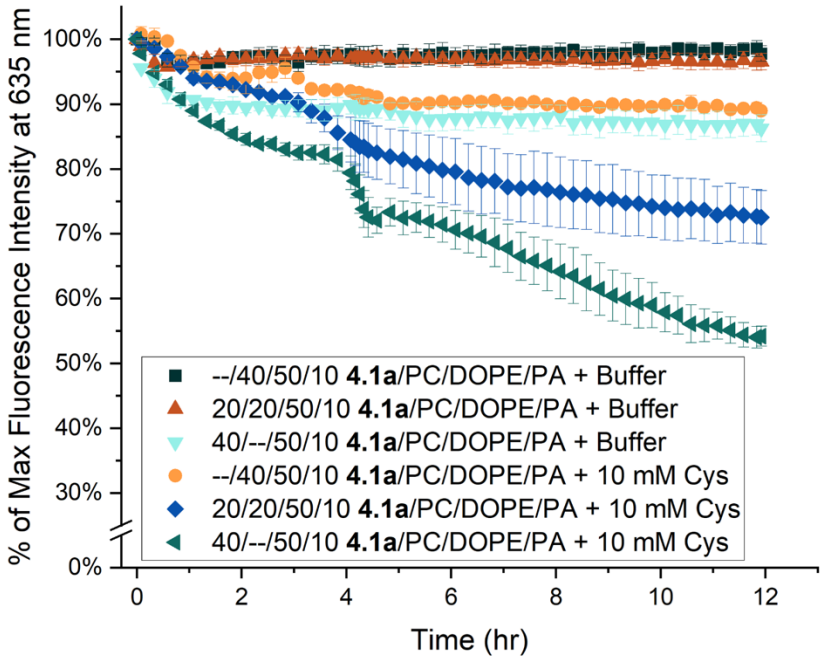


Figure 4.1 Hydrophobic NR dye release after Cys treatment for liposomes containing various percentages of 4.1a. Liposomes containing either 0%, 20%, or 40% **4.1a**, 50% DOPE, 10% PA, and otherwise Egg-PC (40%, 20%, or 0%, respectively) as well as 5% NR were treated with 10 mM of Cys. Results indicate that NR release was dependent on the percentage of **4.1a** in liposomes, with 20% **4.1a** liposomes releasing ~27% and 40% **4.1a** liposomes releasing ~46% over 12 hr. Error bars represent standard errors of at least three replicates.

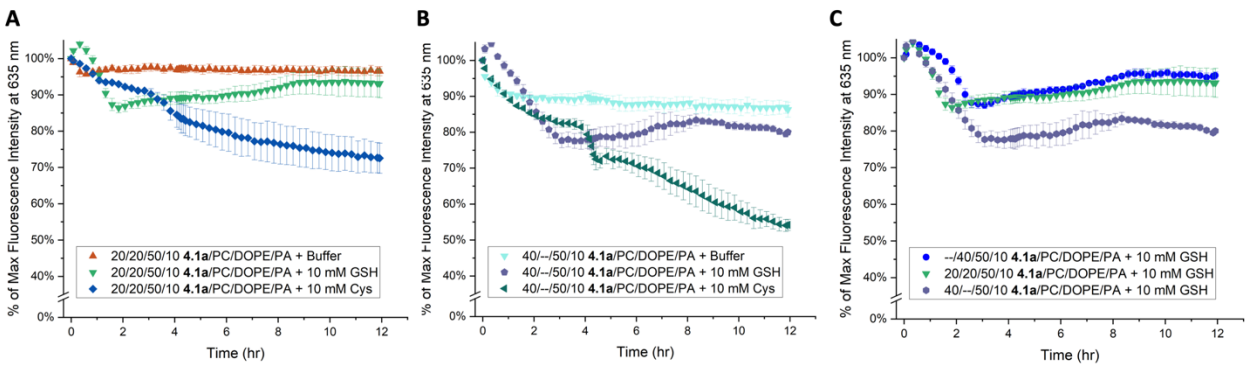


Figure 4.2 Hydrophobic NR dye release after GSH treatment for liposomes containing various percentages of 4.1a. Liposomes containing either 0%, 20%, or 40% **4.1a**, 50% DOPE, 10% PA, and otherwise Egg-PC (40%, 20%, or 0%, respectively) as well as 5% NR were treated with 10 mM of GSH. Results indicate that NR release was dependent on the percentage of **4.1a** in liposomes, with (A) 20% **4.1a** liposomes releasing ~15% and (B) 40% **4.1a** liposomes releasing ~20% over 12 hr; however, release was lower compared to Cys treatment in both cases. (C) Also, 0% **4.1a** liposomes showed a sizable ~15% release when treated with GSH. Error bars represent standard errors of at least three replicates.

Table 4.1 Summary of formulations explored for NR release assay using 4.1a and different percentages of Egg-PC, DOPE, and PA.

Entry	% 4.1a	% Egg-PC	% DOPE	% PA	% NR	Stable?	Cys (mM)	Outcome
1	--	95	--	--	5	Yes	10	~14% release
2	5	90	--	--	5	Yes	10	~0% release
3	25	70	--	--	5	Yes	1	~12% release
4	50	45	--	--	5	Yes	1	~16% release
5	75	20	--	--	5	No	10	--
6	95	--	--	--	5	No	10	--
7	--	45	45	10	5	Yes	10	~15% release
8	--	40	50	10	5	Yes	10	~10% release
9	20	25	45	10	5	Yes	10	~30% release
10	20	20	50	10	5	Yes	10	~25% release
11	30	15	45	10	5	Yes	10	~45% release
12	30	10	50	10	5	Yes	10	~35% release
13	40	5	45	10	5	Yes	10	~60% release
14	40	--	50	10	5	Yes	10	~45% release

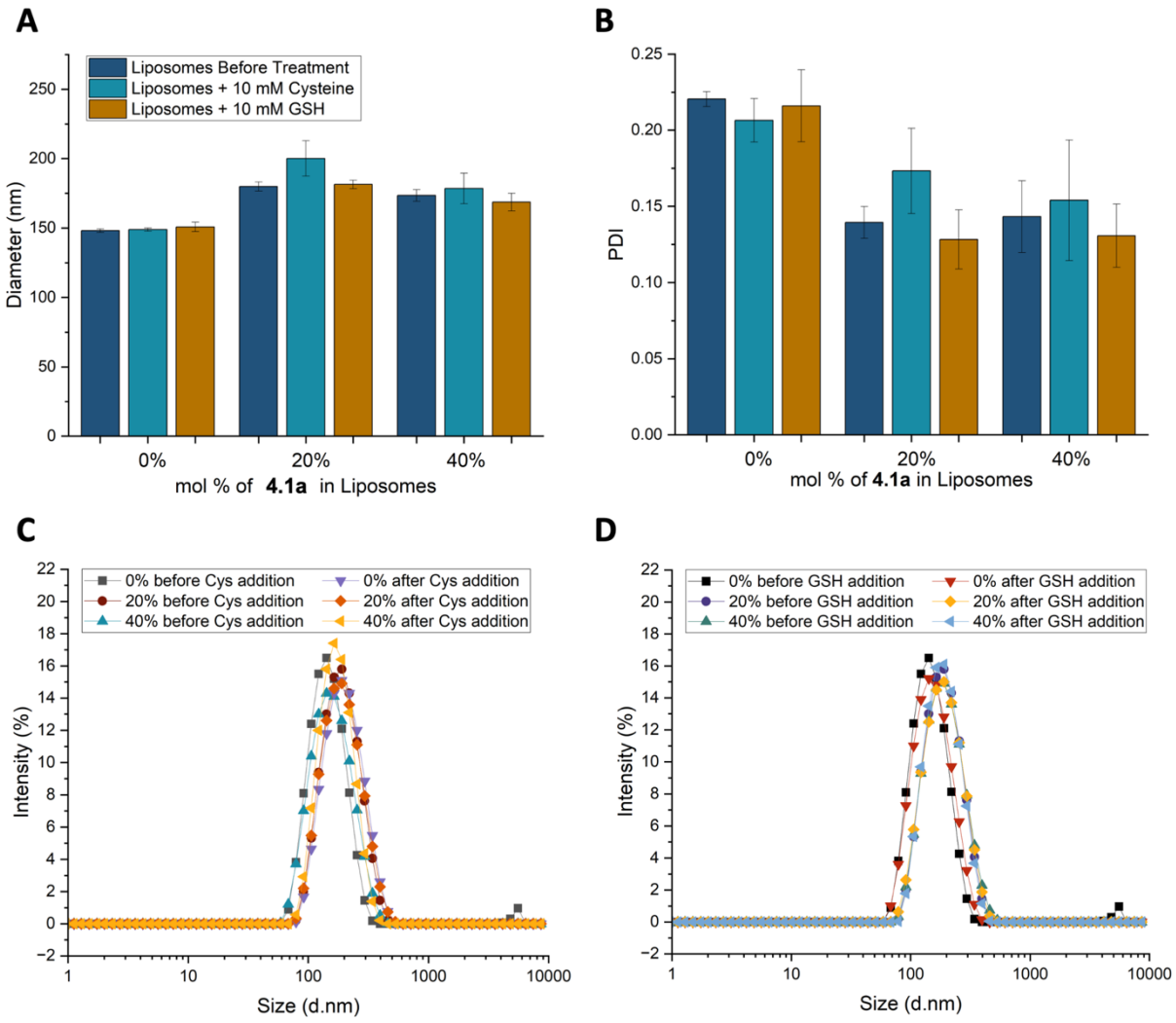


Figure 4.3 DLS results for 4.1a liposomes treated with Cys and GSH. DLS results for liposomes containing 0%, 20%, or 40% **4.1a**, 50% DOPE, 10% PA, and otherwise Egg-PC (40%, 20%, or 0%, respectively) as well as 5% NR which were treated with either buffer, 10 mM GSH, or 10 mM Cys. (A) Average diameters of samples before and after treatment were < 200 nm and (B) PDI for all samples ~0.2 or below. (C) Raw distribution curves of 10 mM Cys treated samples show no change in vesicle size distribution. (D) Raw distribution curves of 10 mM GSH treated samples show no change in vesicle size distribution. Error bars represent standard errors of at least three replicates.

Cys (Figure 4.4, lane 3). After treatment, the solution suspending the samples had a final ratio of 65:25:4 chloroform:methanol:water ($CHCl_3$:MeOH:H_2O) to maintain solubility of both lipid **4.1a** and thiols. Samples were incubated over 3 hr, but small aliquots were used to prepare TLC plates at 0 min, 5 min, 10 min, 15 min, 20 min, 25 min, and 3 hr. The samples were compared to a 2 mM DOPE standard shown on the far left. These TLC plates were first photographed under a UV lamp (Figure 4.4A-G) and again after staining with potassium permanganate ($KMnO_4$) and heating mildly (Figure 4.4H-N).

The results show that lipid **4.1a** reacted with GSH slowly, showing the **4.1a** spot fading and the appearance of 3 new spots after 3 hr. Conversely, lipid **4.1a** appeared to react with Cys at a faster rate, showing the **4.1a** spot fading and 3 new spots appearing after 5 minutes. By 3 hr most of the **4.1a** spot was gone and there was a new spot similar to the DOPE spot (DOPE R_f = 0.2); however, this spot was very faint. This shows that lipid **4.1a** is decomposing faster when treated with Cys compared to treatment with GSH, but it is difficult to elucidate the precise products being formed using this method. Also, the behavior of the lipid may be different in respect to reaction speed and substrate specificity when dissolved in 65:25:4 $CHCl_3$:MeOH:H_2O compared to when it is incorporated in a liposome in aqueous buffer.

4.7. Mass spectrometry evidence of DOPE formation

Mass spectrometry analysis was also performed to study DOPE release from lipid **4.1a**. To perform this experiment, lipid **4.1a** was prepared in $CHCl_3$/CH_3OH=65/25 (v/v), after which an aliquot of Cys solution in H_2O was added to achieve a final solution of 500 μM of **4.1a** and 1 mM Cys in a solution of $CHCl_3$/CH_3OH/H_2O=65/25/4 (v/v) in a vial. The samples were incubated for 12 hr and MS spectra were taken. As shown in the spectra of lipid **4.1a** (Figure 4.5) treated with Cys, the DOPE peak could be clearly observed, indicating that these lipids underwent all steps to fully decompose and release free DOPE.

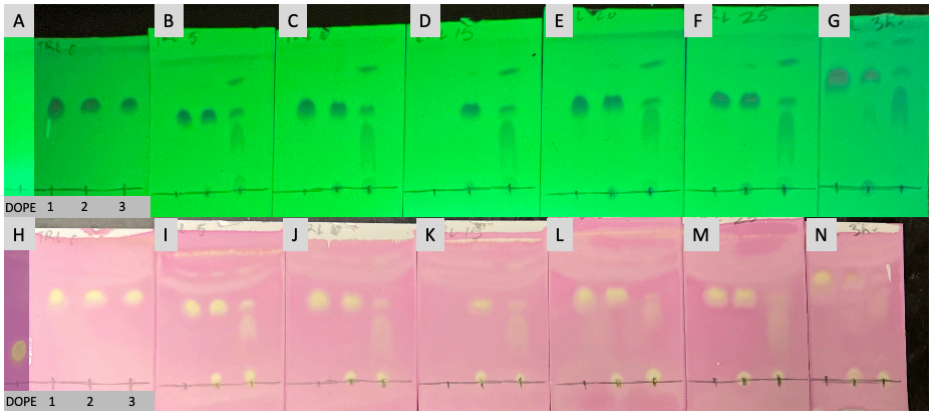


Figure 4.4 TLC analysis of thiol-mediated cleavage 4.1a. TLC analysis of 2 mM free lipid **4.1a** suspended in 65:25:4 $CHCl_3$:MeOH:H_2O with no treatment (lane 1) or treated with 1.5 mM GSH (lane 2) or 1.5 mM Cys (lane 3). A DOPE 2 mM standard is shown on the far left. Samples were incubated over 3 hr, TLC plates spotted, eluted in 20:80 MeOH:$CHCl_3$, and imaged under UV light at (A) 0 min, (B) 5 min, (C) 10 min, (D) 15 min, (E) 20 min, (F) 25 min, and (G) 3 hr. Plates were also stained with $KMnO_4$ at (H) 0 min, (I) 5 min, (J) 10 min, (K) 15 min, (L) 20 min, (M) 25 min, and (N) 3 hr. Lipid **4.1a** reacted with GSH slowly resulting in **4.1a** fading slightly after 3 hr. Lipid **4.1a** reacted with Cys quickly, showing Lipid **4.1a** spot fading and 3 new spots appearing after 5 minutes, and by 3 hr most of the **4.1a** spot was gone and there was a faint new spot in the area DOPE appears (DOPE R_f = 0.2).

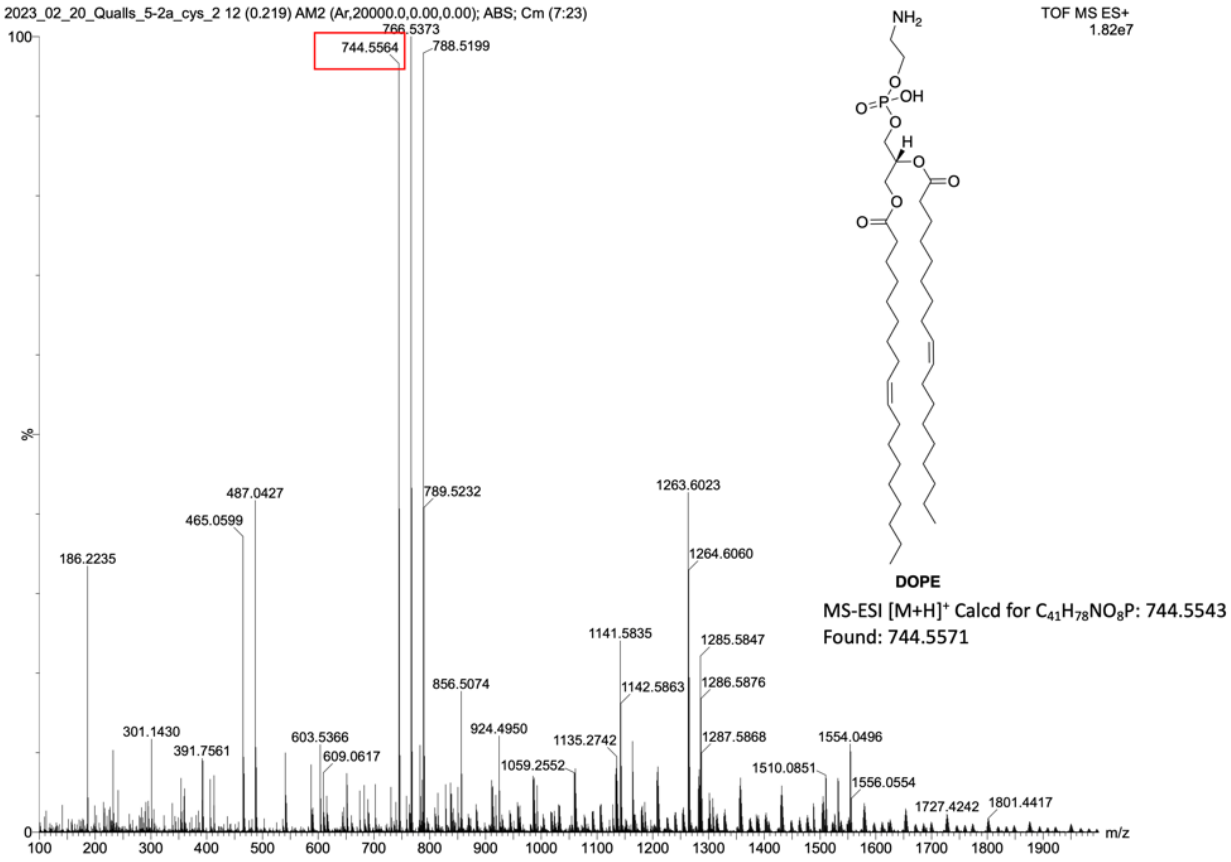


Figure 4.5 Mass spectrum including a peak matching DOPE after treating free lipid 4.1a with Cys.

4.8. Synthesis of alternative general thiol-responsive lipid 4.1b

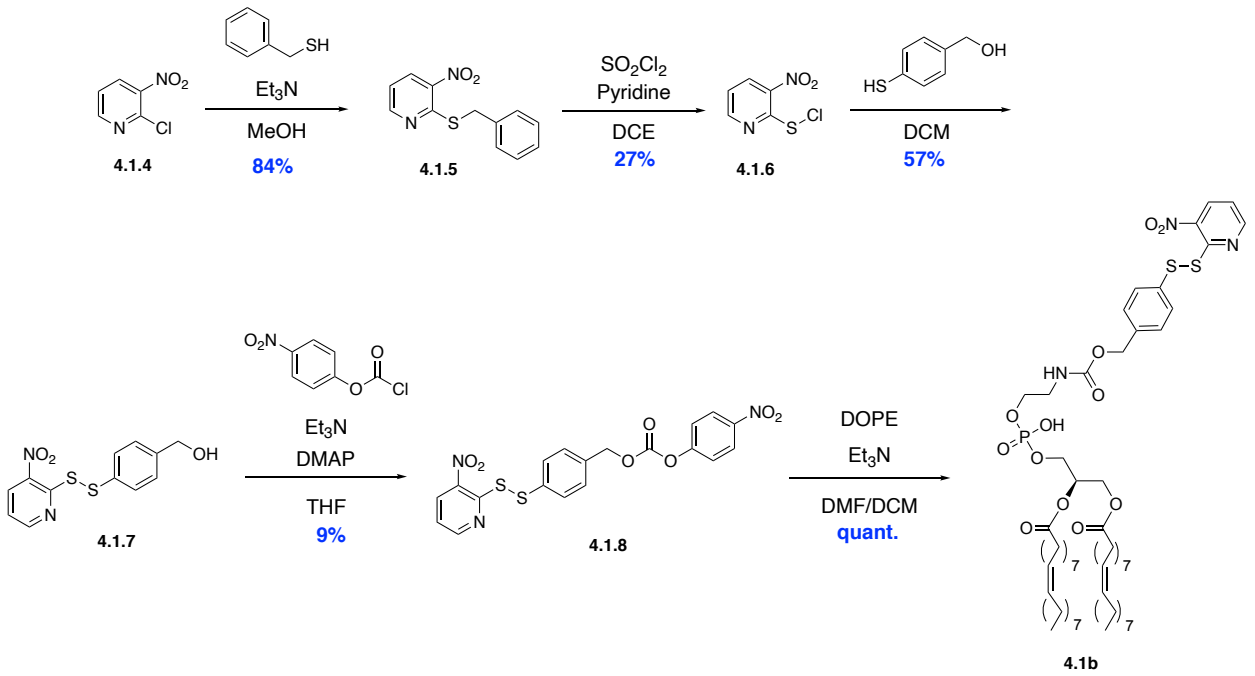
In an effort to maximize the DSILL activity, an alternate lipid was designed and synthesized. The core structure of **4.1a** was modified, as an electron withdrawing (EW) nitro group was added to the pyridyl group to produce **4.1b**. It has previously been shown that this nitro pyridyl group can enhance the disulfide exchange reaction, and it was hypothesized that if the reaction could proceed more quickly, then cargo release could see improvements in speed and/or extent.

The synthetic strategy for accessing **4.1b** is shown in Scheme 4.3. First, 2-chloro-3-nitropyridine (**4.1.4**) was reacted with benzyl mercaptan to give **4.1.5**. Then sulfuryl chloride (SO_2Cl_2) was used to convert the sulfide of **4.1.5** to a sulfenyl chloride (**4.1.6**) which was then reacted with 4-mercaptobenzyl alcohol to give **4.1.7**. Next, 4-nitrophenol chloroformate was used to produce the activated *p*-Nitrophenol carbonate **4.1.8**, which was then treated with DOPE to form **4.1b** in quantitative yield. Following lipid synthesis, we moved on to evaluation of thiol reactivity and the triggered NR release properties of the liposomes containing **4.1b**.

4.9. Attempted cargo dye release assays with alternative lipid 4.1b

Following the synthesis of lipid **4.1b**, we attempted trials of hydrophobic NR dye release assays. The first formulation of 30% **4.1b**, 10% Egg-PC, 50% DOPE, and 10% PA was chosen because of preliminary studies with lipid **4.1a**. These samples showed high stability before treatment and considerable NR release after treatment with Cys. Liposomes were prepared through traditional thin-film liposome preparation techniques including thin-film formation, hydration, freeze-thaw cycling, and extrusion through 200 nm membranes to form uniform liposomes of desired size. The samples were treated with 10 mM Cys, and fluorescence readings were taken over time at room temperature.

After treating 30% **4.1b** liposomes with 10 mM Cys, there was a 40 - 50% increase in fluorescence at 635 nm within 30 min. Trials were run with 5 mM Cys, 10 mM Cys, and 1 mM TCEP treatment, which gave the same result. Increases in NR fluorescence indicate that there could be either emission interference of a different fluorophore, or a non-polar additive is causing NR to become



Scheme 4.3 The synthetic strategy for accessing 4.1b. First, 2-chloro-3-nitropyridine (**4.1.4**) was reacted with benzyl mercaptan to give **4.1.5**. Then SO_2Cl_2 was used to convert the sulfide of **4.1.5** to a sulfenyl chloride (**4.1.6**) which was then reacted with 4-mercaptobenzyl alcohol to give **4.1.7**. Next, 4-nitrophenol chloroformate was used to produce the activated *p*-nitrophenol carbonate **4.1.8**, which was then treated with DOPE to form **4.1b** in quantitative yield.

more solubilized. It was thought that the yellow color formed after treating **4.1b** with Cys could be fluorescent itself and affect NR fluorescence, but that was found to likely not be the case. After treating **4.1b** liposome (containing 5% NR) with Cys, the emission of NR from 580 nm – 700 nm did not undergo any x-axis shifts in fluorescence, and no additional emission curves appeared. To analyze the fluorescence outside of the liposome, a separate study was performed in which 2 mM free lipid **4.1b** and 0.1 mM NR was dissolved in 65/25/4 $CHCl_3$/MeOH/H_2O, and after addition of 10 mM TCEP there was no change in the emission spectra. This indicated that the self-immolation products from **4.1b** are likely not fluorescent or changing NR fluorescence. Hereby, there could be non-specific interactions occurring between **4.1b** immolation products and NR which are causing increases in fluorescence. In either case, these interactions result in the NR assay not being compatible with lipid **4.1b**.

Following NR assay attempts, a hydrophilic release assay was also attempted with 6-carboxyfluorescein (CF), which is encapsulated in the aqueous core commonly and is used in release assays of this type.[425-427] The dye CF is first encapsulated at high concentration to cause fluorescence self-quenching and release from the liposome results in increase in fluorescence. To prepare liposomes, a similar procedure was used compared to the NR release assay, but in this case the liposomes were hydrated with a 50 mM CF buffer solution. After standard this film liposome preparation, a size exclusion column (SEC) was used after extrusion to remove unencapsulated dye. The release assay was conducted by adding 1 mM Cys, 10 mM Cys, or 1 mM TCEP to the liposome solution and monitoring fluorescence over 24 hrs. At the end of the experiment, Triton X-100 detergent was added to the liposomes to destroy the bilayer and release 100% of the SRB content. This provides a fluorescence end-point of total release, and all other fluorescence readings were normalized by calculating percent release compared to total release.

Various liposomes formulations containing **4.1a** and **4.1b** were explored with the goal of finding a combination that is stable and retains CF cargo without Cys or TCEP, but releases cargo after treatment. Also, it was necessary that liposomes with the same formulation but lacking **4.1a** or

4.1b must retain CF both before and after treatment. Liposome formulations were attempted with lipids including Egg-PC, DPPC, DOPE, and PA. Altogether, these release assays were attempted with lipid **4.1b** but none gave promising results. As summarized in Table 4.2, most of the attempted formulations showed significant background release with only buffer treatment, both with and without **4.1a**/**4.1b**, indicating non-specific leakage. For example, although liposomes with 30% **4.1a**, 40% Egg-PC, 20% DOPE, and 10% PA indicated ~96% CF release after 10 mM Cys treatment, the same liposomes showed ~46% CF release when treated with buffer only, indicating the liposomes are unstable and leaking CF.

4.10. TLC analysis of thiol-mediated cleavage of free lipid 4.1b

After synthesizing DSIL lipid **4.1b** and probing liposome release characteristics, we again moved to assess its reactivity with the biologically relevant thiols Cys and GSH. A TLC analysis was performed to gain a simple understanding of the lipid's reactivity. The analysis was performed by treating 2 mM solutions of free **4.1b** lipid with either no treatment (Figure 4.6, lane 2), 1.5 mM tris(2-carboxyethyl)phosphine hydrochloride (TCEP) (Figure 4.6, lane 3), 1.5 mM GSH (Figure 4.6, lane 4), or 1.5 mM Cys (Figure 4.6, lane 5). After treatment, the solution suspending the samples had a final ratio of 65:25:4 $CHCl_3$:MeOH:H_2O to maintain solubility of both lipid **4.1b** and thiols. The samples were compared to a DOPE standard shown in lane 1. Samples were incubated over 30 min, but small aliquots were used to prepare TLC plates at 0 min, 1 min, 5 min, 10 min, 15 min, 20 min, 25 min, and 30 min. These TLC plates were first photographed under a UV lamp (Figure 4.6A-G) and again after staining with $KMnO_4$ and heating mildly (Figure 4.6H-N).

The results indicate lipid **4.1b** reacted with TCEP quickly (lane 3), forming at least 3 new spots including a spot at R_f = ~0.2, which could be DOPE, and the full disappearance of the **4.1b** spot by 10 min. Lane 4 indicates **4.1b** did not react quickly with GSH and most **4.1b** remained at 3 hr incubation. Lane 5 indicates that **4.1b** reacted very quickly with Cys treatment with the full disappearance of **4.1b** after 1 min and the formation of 3 new spots, but lacking a DOPE spot. The spot at R_f = 0.8 formed lanes 3, 4, and 5 was yellow before staining, which is characteristic of the nitro pyridyl leaving group. The **4.1b** samples also underwent a color change from clear

Table 4.2 Summary of formulations explored for CF release assay using 4.1a, 4.1b and different percentages of DPPC, Egg-PC, DOPE, and PA.

Entry	% 4.1a	% 4.1b	% DPPC	% Egg-PC	% DOPE	% PA	Treatment	Outcome
1	30	--	--	10	50	10	Buffer	~41% release
							1 mM Cys	~23% release
							10 mM Cys	~57% release
							1 mM TCEP	~20% release
2	--	30	--	10	50	10	Buffer	~34% release
							1 mM Cys	18% release
							10 mM Cys	~24% release
							1 mM TCEP	~17% release
2	--	--	30	10	50	10	Buffer	~10% release
							1 mM Cys	~8% release
							10 mM Cys	~9% release
							1 mM TCEP	~9% release
4	30	--	--	40	20	10	Buffer	~46% release
							1 mM Cys	~35% release
							10 mM Cys	~96% release
							1 mM TCEP	~19% release
5	--	30	--	40	20	10	Buffer	~16% release
							1 mM Cys	~18% release
							10 mM Cys	~48% release
6	--	--	30	40	20	10	Buffer	~7% release
							1 mM Cys	~13% release
							10 mM Cys	~10% release

(Figure 4.7A) before treatment to yellow when treated with TCEP (Figure 4.7B) or Cys (Figure 4.7D). Only a faint yellow color appeared when treated with GSH (Figure 4.7C).

Overall, these results show that lipid **4.1b** is decomposing faster when treated with Cys compared to treatment with GSH, but it is not forming the expected DOPE spot. Interestingly, lipid treated with TCEP could be forming DOPE. However, it is difficult to elucidate the products being formed using this method. As previously stated, the lipid's behavior with respect to reaction speed and trigger sensitivity may differ once we move on to liposome studies when it is incorporated in liposomes and dissolved in aqueous buffer.

4.11. Mass spectrometry evidence of DOPE formation

Mass spectrometry analysis was also performed to study DOPE release from lipid **4.1b**. To perform this experiment, lipid **4.1b** was dissolved in $CHCl_3/CH_3OH$=65/25 (v/v), after which an aliquot of Cys solution in H_2O was added to achieve a final solution of 500 μM of **4.1b** and 1 mM Cys in a solution of $CHCl_3/CH_3OH/H_2O$=65/25/4 (v/v) in a vial. The samples were incubated for 12 hr and MS spectra were taken. As shown in the spectra of **4.1b** (Figure 4.8) upon treatment with Cys, the DOPE peak could be clearly observed, indicating that these lipids underwent all steps to fully decompose and release free DOPE.

4.12. Design and study of cysteine-responsive liposomes

While we expect the prior compounds (**4.1a-b**) can generally respond to thiols including Cys, it would be beneficial to develop lipid switches that selectively respond to Cys due to the upregulation of this compound in cancer environments. To achieve this goal, we adapted a Cys-responsive element and appended it to a variation of the self-immolating DOPE lipid (Scheme 4.4A). This Cys-responsive acryloyl moiety has been recently developed for selective recognition and response to Cys. Most commonly, the group is used in conjunction with latent fluorophores to achieve Cys sensing fluorescent probes, and in recent years, a multitude of probe designs which share this acryloyl appendage have been reported.[428-451] The group is an acrylate moiety which works by a thiol-Michael addition with the nucleophilic thiol group of Cys, and then

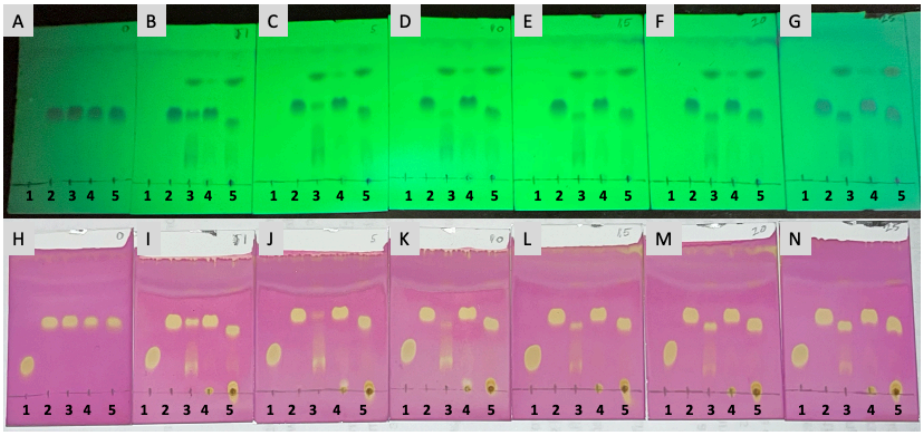


Figure 4.6 TLC analysis of thiol-mediated cleavage 4.1b. TLC analysis of 2 mM free lipid **4.1b** with various thiol treatments suspended in 65:25:4 $CHCl_3$:MeOH:H_2O. DOPE 2 mM standard (lane 1), 2mM **4.1b** with no treatment (lane 2), 2 mM **4.1b** + 1.5 mM TCEP (lane 3), 2 mM **4.1b** + 1.5 mM GSH (lane 4), or 2 mM **4.1b** + 1.5 mM Cys (lane 5). Plates imaged under UV light at (A) 0 min, (B) 1 min, (C) 5 min, (D) 10 min, (E) 15 min, (F) 20 min, and (G) 30 min and stained with $KMnO_4$ at (H) 0 min, (I) 1 min, (J) 5 min, (K) 10 min, (L) 15 min, (M) 20 min, and (N) 30 min. Lane 3 indicates lipid **4.1b** reacted quickly with TCEP resulting in the disappearance of the **4.1b** spot by 10 min. Lane 4 indicates **4.1b** did not react quickly with GSH and most **4.1b** remained. Lane 5 indicates that **4.1b** reacted quickly with Cys treatment resulting in disappearance of **4.1b** spot after 1 min, but lacking a new DOPE spot.

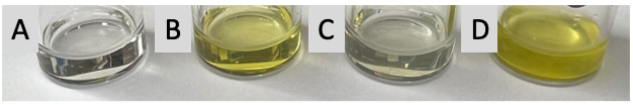


Figure 4.7 Lipid 4.1b samples from TLC study. Image showing the yellow color of (A) lipid **4.1b** no treatment, (B) 2 mM **4.1b** + 1.5 mM TCEP, (C) 2 mM **4.1b** + 1.5 mM GSH), and (D) 2 mM **4.1b** + 1.5 mM Cys.

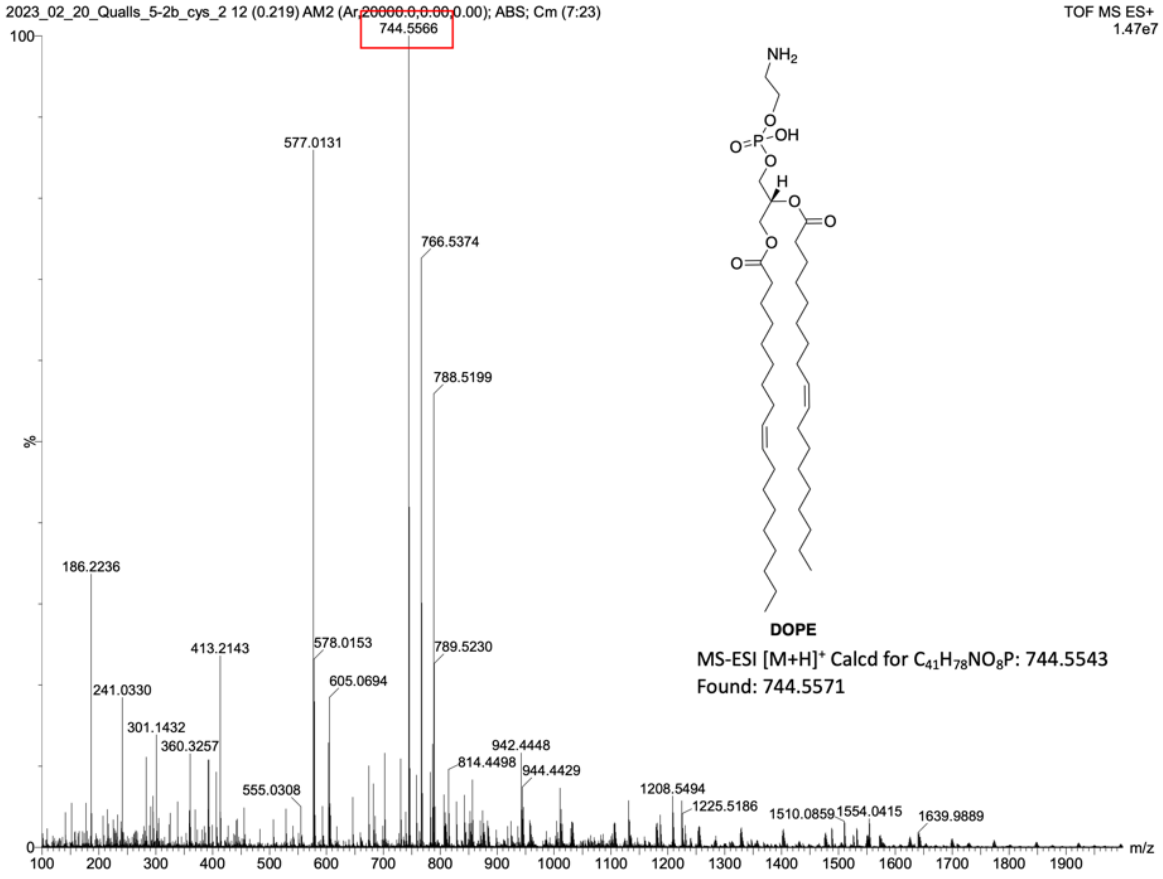


Figure 4.8 Mass spectrum including a peak matching DOPE after treating free lipid 4.1b with Cys.

intramolecular cyclization occurs, which yields a stable seven-member heterocyclic compound. This cyclization allows for Cys selectivity since it requires a proximal amino group.

Interestingly, one previously published design used the acrylate group together with a carbamate-based self-eliminating linker (SIL) in order to release a free fluorophore.[439] Taking inspiration from this probe, our design includes this Cys specific acrylate group appended via a self-immolating linker to a DOPE lipid scaffold (**4.2a-c**) (Scheme 4.4B). In this design, the Cys sulfhydryl group undergoes thiol-Michael addition to the α,β-unsaturated double bond in the reactive acryl moiety to form a thioether (**4.3a-c**). In the second step, the amine group of Cys initiates a nucleophilic attack on the carbonyl carbon of the SIL, thereby forming a cyclized thiolactam product (**4.4a-c**). The lactam formation produces a phenoxide anion similar to the previous examples, which initiates the self-immolation cascade reaction including quinone methide formation and finally release of the linker, carbon dioxide (CO_2), and DOPE lipid.

In addition to the basic Cys responsive lipid design (**4.2a**), we also produced modified lipids in an attempt to enhance the kinetics of self-immolation, which could help release DOPE faster and cause more efficient cargo release. Similar strategies have been applied before, in which electron withdrawing groups (EWGs) have been employed to increase self-immolation kinetics compared to electron donating groups (EDGs), which can either slow or have little effect on self-immolation kinetics.[452] It is known that an increase in the electron density on the aromatic ring increases the speed of the self-immolation reaction by facilitating de-aromatization and also stabilizing the transient positive charge formed at the benzylic position during the elimination leading to the quinone methide intermediate.[453] Indeed, self-immolation rate has been shown to be greatly accelerated by appending electron-donating groups such as OMe and NHMe onto the aromatic ring.[454-458] In the opposite way, a decrease in the electron density on the aromatic ring tends to diminish the speed of the self-immolation reaction by destabilizing the positively charged transition state, which slows down the reaction. SILs containing aromatic rings substituted with EWGs, such as NO_2, CO_2Me, or F exhibit a half-life of self-immolation larger than their unsubstituted analogues.[452, 454, 456, 458] However, it is also important to consider the possible

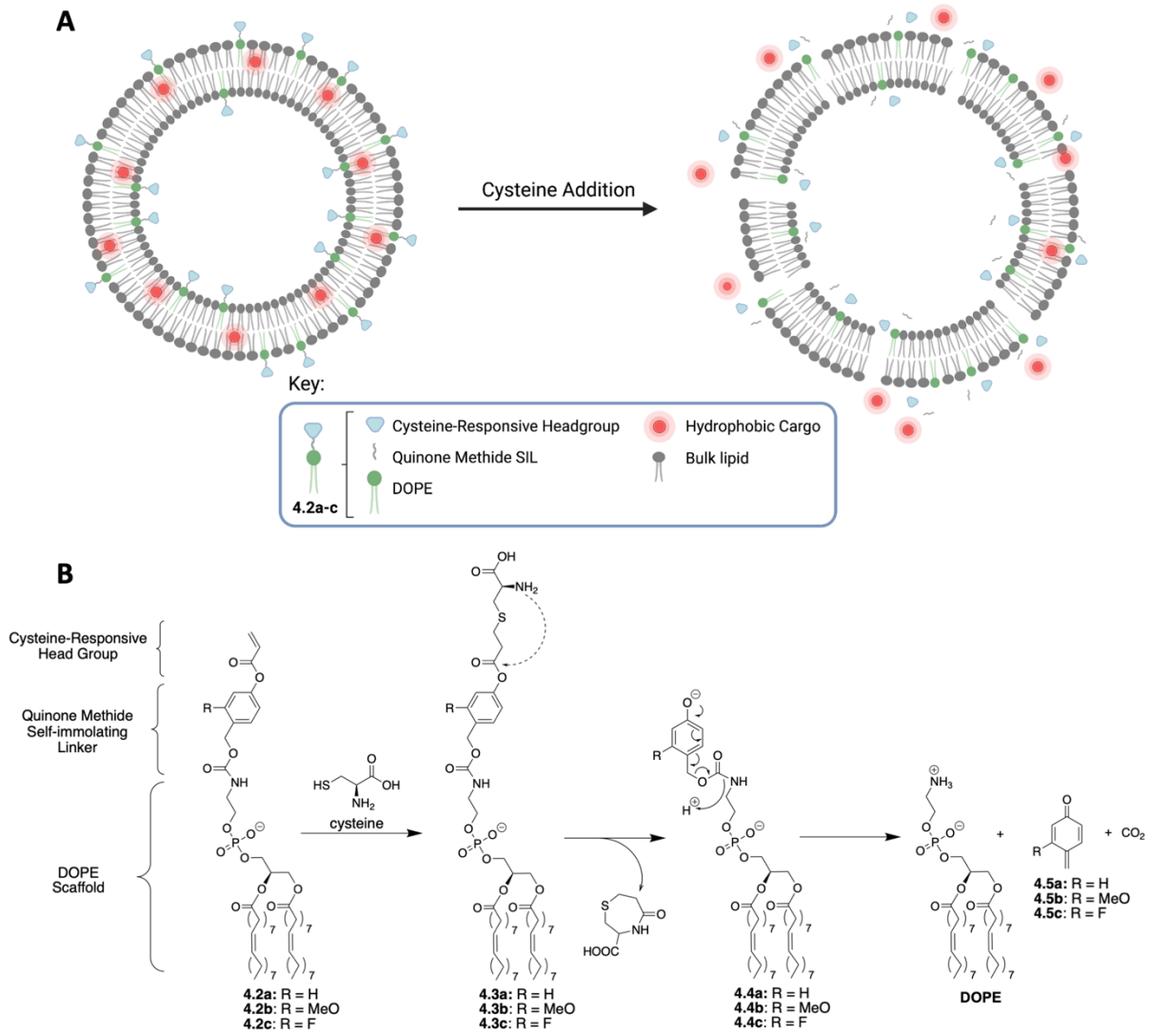
effects of EDGs or EWGs on the Cys responsive acrylate moiety. For instance, while EDG groups are known to speed up SIL decomposition, they could potentially make the acryl moiety less electrophilic, which could slow down the nucleophilic attack by Cys during the Michael addition between the Cys sulfhydryl group and the unsaturated double bond, which could result in slower liposomal release. On the other hand, while EWGs on the SIL are known to slow down self-immolation, they could produce the opposite effect by making the acryl moiety more electrophilic, potentially speeding up the Michael addition between the Cys and double bond, resulting in faster reactions and improved release profile. To assess the relationship between these phenomena and reaction speed and to determine which groups could result in more efficient liposomal cargo release, we designed and synthesized two additional lipids.

To accomplish this goal, we designed a lipid bearing an electron donating methoxy group (**4.2b**) to speed up the immolation as well as an electron withdrawing fluorine (**4.2c**) to render these compounds more electrophilic (Scheme 4.4). The synthetic scheme to access lipids **4.2a-c** is outlined in Scheme 4.5. First, either 4-hydroxybenzyl alcohol (**4.1.9a**), 4-(hydroxymethyl)-3-methoxyphenol (**4.1.9b**), or 3-fluoro-4-(hydroxymethyl)phenol (**4.1.9c**) were caged with acryloyl chloride to form **4.1.10a**, **4.1.10b**, or **4.1.10c**, respectively. These compounds were reacted with 4-nitrophenol chloroformate to form activated carbonates **4.1.11a**, **4.1.11b**, or **4.1.11c**, respectively. These were then treated with DOPE to make **4.2a**, **4.2b**, and **4.2c**.

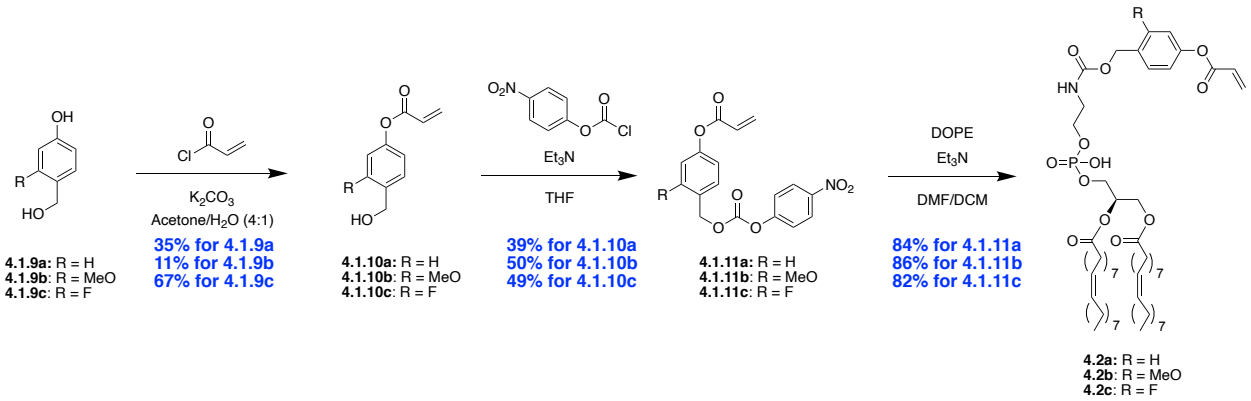
4.13. Nile red release assays with 4.2a-c

4.13.1. Screen of cysteine-responsive liposome formulations for Nile Red release assay

Following the synthesis of Cys responsive lipids **4.2a-c**, we began to evaluate release of the hydrophobic dye NR. We first screened a host of liposome formulations including lipids Egg-PC, DOPE, PA, DOTAP, and various percentages of **4.2a** (Table 4.3) and **4.2b** (Table 4.4). Liposomes were treated with various triggers including 1 mM – 10 mM Cys. For comparison, buffer treatment and 10 mM GSH were also analyzed. Liposomes were allowed to incubate for 5-12 hr and fluorescence scans taken routinely. Throughout all liposome screens, there was no sizable (>20%) NR release from any formulation or treatment type. We determined that the most



Scheme 4.4 Design for cysteine-responsive lipids. (A) Cartoon illustration of liposomal release driven by Cys addition. (B) Design includes a Cys specific acrylate group appended via a SIL to a DOPE lipid scaffold (**4.2a-c**). SILs with an EDG (**4.2b**), or EWG (**4.2c**), or neither (**4.2a**). The Cys sulfhydryl group undergoes Michael addition to the α,β-unsaturated double bond in the reactive acryl moiety to form a thioether (**4.3a-c**). Then, the amine group of Cys initiates a nucleophilic attack on the carbonyl carbon of the SIL linker, forming a cyclized thiolactam product. The lactam formation produces a phenoxide anion (**4.4a-c**) which initiates the self-immolation cascade reaction resulting in quinone methide formation (**4.5a-c**) and release of linker, CO_2, and DOPE lipid.



Scheme 4.5 The synthetic scheme to access lipids 4.2a-c. First, either 4-hydroxybenzyl alcohol (**4.1.9a**), 4-(hydroxymethyl)-3-methoxyphenol (**4.1.9b**), or 3-fluoro-4-(hydroxymethyl)phenol (**4.1.9c**) were caged with acryloyl chloride to form **4.1.10a**, **4.1.10b**, or **4.1.10c**, respectively. These compounds were reacted with 4-nitrophenyl chloroformate to form activated carbonates **4.1.11a**, **4.1.11b**, or **4.1.11c**, respectively. These were then treated with DOPE to make **4.2a**, **4.2b**, and **4.2c**.

promising liposome formulations in terms of maximizing triggered release were 30% **4.2a-c**, 10% Egg-PC, 50% DOPE, 10% PA; or 60% **4.2a**/**4.2b**, 30% DOPE, 10% PA, both in addition to 5% NR. Negative control liposomes lacking **4.2a-c** (replaced by Egg-PC) were also prepared.

Liposomes were prepared through traditional thin-film liposome preparation techniques including thin-film formation, hydration, freeze-thaw cycling, and extrusion through 200 nm membranes to form uniform liposomes of desired size. The samples were treated with 1 - 10 mM Cys, 10 mM GSH, or buffer only and fluorescence readings were taken over time at room temperature. A summary of liposome formulations explored is included in Table 4.3 (**4.2a** formulations) and Table 4.4 (**4.2b** formulations).

4.13.2. Nile Red release assay with cysteine-responsive liposomes

As shown in Figure 4.9, addition of Cys resulted in small decreases in NR fluorescence depending on the presence of **4.2a** or **4.2b** lipid in the liposome over 5 hr, indicating NR release. For example, at 30% lipid incorporation in the liposome, **4.2a** liposomes treated with Cys resulted in a decrease in NR fluorescence of ~11%, compared to **4.2b** which decreased ~16%, and **4.2c** decreased ~7%, which could be due to fluctuations in immolation speed (Figure 4.9A). At 60% incorporation, similar NR decrease was shown with **4.2a** liposomes **(**~9% release) and **4.2b** liposomes **(**~15% release), and 60% **4.2c** did not form stable liposomes (Figure 4.9B). When comparing the lipid types to each other, it can be seen that at 30% or 60% lipid incorporation, lipid **4.2b** did show an increased amplitude of release compared to **4.2a** liposomes over time in both cases, while 30% **4.2c** liposomes exhibited lessened release. Control liposomes lacking **4.2a-c** indicated minimal ~3% release after Cys treatment from unspecific interactions. While the extent of release was minor in this case and resulted from a high concentration of Cys (10 mM), these lipids are the first of their kind, and variations on the design of the Cys responsive headgroup or lipid tail could be prepared in order to yield greater contributions to liposomal release properties. Altogether, these experiments demonstrate that **4.2a-c** liposomes undergo slight triggered release of hydrophobic cargo in response to Cys.

Table 4.3 Summary of formulations explored for NR release assay using lipid 4.2a and different percentages of Egg-PC, DOPE, PA, and DOTAP.

Entry	% 4.2a	% Egg-PC	% DOPE	% PA	% DOTAP	% NR	Stable?	°C	Treatment	Outcome
1	--	45	45	10	--	5	Yes	rt	10 mM Cys	<1% release
2	--	40	50	10	--	5	Yes	rt	10 mM Cys	<1% release
3	20	25	45	10	--	5	Yes	rt	10 mM Cys	~7% release
4	20	20	50	10	--	5	Yes	rt	10 mM Cys	~7% release
5	30	15	45	10	--	5	Yes	rt	10 mM Cys	<1% release
6	30	10	50	10	--	5	Yes	rt	10 mM Cys	~10% release
7	40	5	45	10	--	5	Yes	rt	10 mM Cys	~4% release
8	40	--	50	10	--	5	Yes	rt	10 mM Cys	~8% release
9	50	--	40	10	--	5	Yes	rt	10 mM Cys	~10% release
10	60	--	30	10	--	5	Yes	rt	10 mM Cys	~11% release
11	--	40	50	--	10	5	Yes	rt	10 mM Cys	~3% release
12	20	20	50	--	10	5	Yes	rt	10 mM Cys	~5% release
13	30	10	50	--	10	5	Yes	rt	10 mM Cys	~3% release
14	40	--	50	--	10	5	Yes	rt	10 mM Cys	~3% release
15	--	45	50	--	5	5	Yes	rt	10 mM Cys	~5% release
16	20	25	50	--	5	5	Yes	rt	10 mM Cys	~5% release
17	30	15	50	--	5	5	Yes	rt	10 mM Cys	~5% release
18	40	--	50	--	5	5	Yes	rt	10 mM Cys	~5% release
19	--	40	50	10	--	5	Yes	30	1 mM Cys	~4% release

Table 4.3 Continued

Entry	% 4.2a	% Egg-PC	% DOPE	% PA	% DOTAP	% NR	Stable?	°C	Treatment	Outcome
20	60	--	30	10	--	5	Yes	30	1 mM Cys	~3% release
21	--	40	50	10	--	5	Yes	30	10 mM Cys	~12% release
22	60	--	30	10	--	5	Yes	30	10 mM Cys	~12% release
23	--	40	50	10	--	5	Yes	37	10 mM Cys	~40% release
24	20	20	50	10	--	5	Yes	37	10 mM Cys	~10% release
25	--	95	--	--	--	5	Yes	rt	10 mM Cys	~14% release
26	5	90	--	--	--	5	Yes	rt	1 mM Cys	~5% release
27	50	45	--	--	--	5	Yes	rt	5 mM Cys	~10% release
28	75	20	--	--	--	5	No	rt	--	--
29	95	--	--	--	--	5	No	rt	--	--
30	--	40	50	10	--	5	Yes	rt	Buffer pH = 10	~0% release
31	60	--	30	10	--	5	Yes	rt	Buffer pH = 10	~15% release
32	--	40	50	10	--	5	Yes	rt	10 mM Cys pH = 10	~0% release
33	60	--	30	10	--	5	Yes	rt	10 mM Cys pH = 10	~12% release

Table 4.4 Summary of formulations explored for NR release assay using lipid 4.2b and different percentages of Egg-PC, DPPC, DOPE, and PA.

Entry	% 4.2b	% DPPC	% Egg-PC	% DOPE	% PA	% NR	Stable?	°C	Treatment	Outcome
1	30	--	--	60	10	5	Yes	rt	Buffer	~5% release
									10 mM Cys	~9% increase
									10 mM GSH	~4% release
2	30	--	10	50	10	5	Yes	rt	Buffer	~6% release
									10 mM Cys	~15% release
									10 mM GSH	~5% release
2	30	--	20	40	10	5	Yes	rt	Buffer	~3% release
									10 mM Cys	~2% increase
									10 mM GSH	~0% release
4	30	--	30	30	10	5	Yes	rt	Buffer	~5% release
									10 mM Cys	~0% increase
									10 mM GSH	~0% release
5	30	--	40	20	10	5	Yes	rt	Buffer	~3% release
									10 mM Cys	~2% increase
									10 mM GSH	~2% increase
6	30	--	50	10	10	5	Yes	rt	Buffer	~5% release
									10 mM Cys	~9% increase
									10 mM GSH	~4% release
7	30	--	60	--	10	5	Yes	rt	Buffer	~4% release
									10 mM Cys	~4% increase
									10 mM GSH	~4% release
8	--	30	--	60	10	5	Yes	rt	Buffer	~2% release
									10 mM Cys	~1% increase
									10 mM GSH	~5% release
9	--	30	10	50	10	5	Yes	rt	Buffer	~12% release
									10 mM Cys	~4% release
									10 mM GSH	~5% release
10	--	30	20	40	10	5	Yes	rt	Buffer	~10% release
									10 mM Cys	~6% release
									10 mM GSH	~7% release
11	--	30	30	30	10	5	Yes	rt	Buffer	~12% release
									10 mM Cys	~1% release
									10 mM GSH	~4% release
12	--	30	40	20	10	5	Yes	rt	Buffer	~9% release
									10 mM Cys	~4% increase
									10 mM GSH	~3% release

Table 4.4 Continued

Entry	% 4.2b	% DPPC	% Egg-PC	% DOPE	% PA	% NR	Stable?	°C	Treatment	Outcome
13	--	30	50	10	10	5	Yes	rt	Buffer	~6% release
									10 mM Cys	~6% release
									10 mM GSH	~0% release
14	--	30	60	--	10	5	Yes	rt	Buffer	~6% release
									10 mM Cys	~6% increase
									10 mM GSH	~3% release
15	40	--	--	50	10	5	Yes	rt	Buffer	~5% increase
									10 mM Cys	~4% increase
									10 mM GSH	~0% release
16	40	--	10	40	10	5	Yes	rt	Buffer	~10% release
									10 mM Cys	~9% release
									10 mM GSH	~7% release
17	40	--	20	30	10	5	Yes	rt	Buffer	~8% release
									10 mM Cys	~6% release
									10 mM GSH	~2% release
18	40	--	30	20	10	5	Yes	rt	Buffer	~5% release
									10 mM Cys	~1% release
									10 mM GSH	~6% release
19	40	--	40	10	10	5	Yes	30	Buffer	~1% release
									10 mM Cys	~5% increase
									10 mM GSH	~5% increase
20	40	--	50	--	10	5	Yes	30	Buffer	~4% release
									10 mM Cys	~7% increase
									10 mM GSH	~7% increase
21	--	40	--	50	10	5	Yes	30	Buffer	~11% release
									10 mM Cys	~2% release
									10 mM GSH	~3% increase
22	--	40	10	40	10	5	Yes	30	Buffer	~9% release
									10 mM Cys	~6% release
									10 mM GSH	~8% release
23	--	40	20	30	10	5	Yes	37	Buffer	~10% release
									10 mM Cys	~8% release
									10 mM GSH	~8% release
24	--	40	30	20	10	5	Yes	37	Buffer	~14% release
									10 mM Cys	~14% release
									10 mM GSH	12% release
25	--	40	40	10	10	5	Yes	rt	Buffer	~14% release
									10 mM Cys	~12% release
									10 mM GSH	~14% release

Table 4.4 Continued

Entry	% 4.2b	% DPPC	% Egg-PC	% DOPE	% PA	% NR	Stable?	°C	Treatment	Outcome
26	--	40	50	--	10	5	Yes	rt	Buffer	~10% release
									10 mM Cys	~11% release
									10 mM GSH	~11% release
27	50	--	--	40	10	5	Yes	rt	Buffer	~13% release
									10 mM Cys	~2% increase
									10 mM GSH	~0% release
28	50	--	10	30	10	5	Yes	rt	Buffer	~9% release
									10 mM Cys	~1% release
									10 mM GSH	~3% release
29	50	--	20	20	10	5	Yes	rt	Buffer	~10% release
									10 mM Cys	~5% release
									10 mM GSH	~2% release
30	50	--	30	10	10	5	Yes	rt	Buffer	~11% release
									10 mM Cys	~2% release
									10 mM GSH	~3% increase
31	50	--	40	--	10	5	Yes	rt	Buffer	~10% release
									10 mM Cys	~2% increase
									10 mM GSH	~4% increase
32	--	50	--	40	10	5	Yes	rt	Buffer	~6% release
									10 mM Cys	~1% increase
									10 mM GSH	~1% release
33	--	50	10	30	10	5	Yes	rt	Buffer	~4% release
									10 mM Cys	~1% release
									10 mM GSH	~0% release
34	--	50	20	20	10	5	Yes	rt	Buffer	~5% release
									10 mM Cys	~0% release
									10 mM GSH	~3% release
35	--	50	30	10	10	5	Yes	rt	Buffer	~7% release
									10 mM Cys	~4% release
									10 mM GSH	~6% release
36	--	50	40	--	10	5	Yes	rt	Buffer	~8% release
									10 mM Cys	~6% release
									10 mM GSH	~0% release

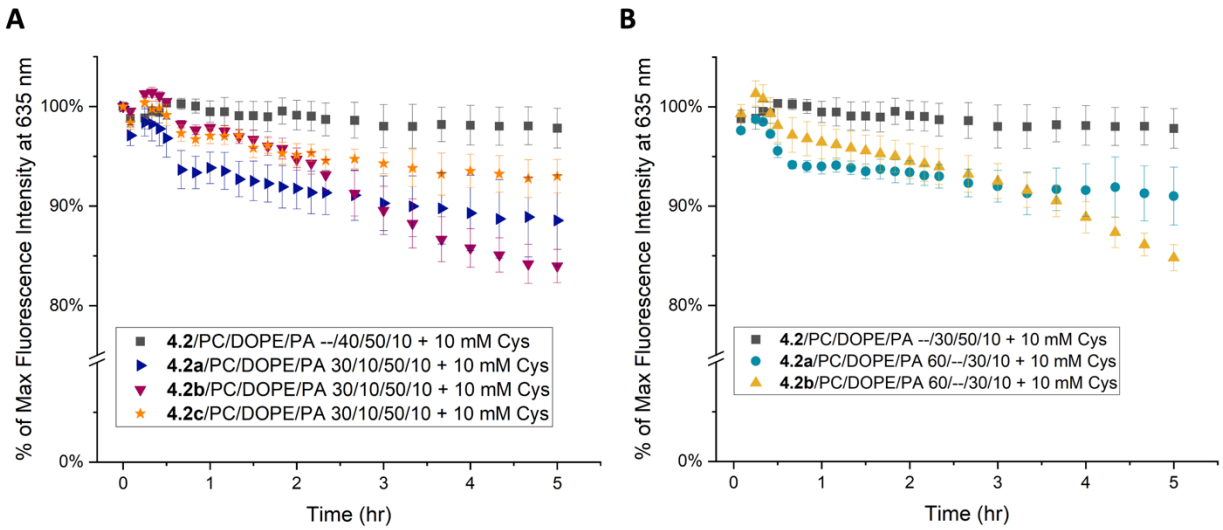


Figure 4.9 Nile Red release from 4.2a-c liposomes. (A) Liposomes were composed of 0% **4.2a**, 40% Egg-PC, 50% DOPE, and 10% PA; 30% **4.2a**, 10% Egg-PC, 50% DOPE, 10% PA; 30% **4.2b**, 10% Egg-PC, 50% DOPE, 10% PA; or 30% **4.2c**, 10% Egg-PC, 50% DOPE, 10% PA, in addition to 5% NR treated with 10 mM Cys. Release resulted from incorporation of 30% **4.2a (**~10% NR release), 30% **4.2b (**~16% NR release), and 30% **4.2c (**~7% NR release). (B) Liposomes were composed 0% **4.2b**, 40% Egg-PC, 50% DOPE, and 10% PA; 60% **4.2a**, 30% DOPE, 10% PA; and 60% **4.2b**, 30% DOPE, 10% PA, each in addition to 5% NR treated with 10 mM Cys. Release resulted from incorporation of 60% **4.2a (**~11%), 60% **4.2b (**~16%). These results show that compound **4.2b** containing an EWG exhibits minimally enhanced release activity over time in both cases. Error bars represent standard errors of at least three replicates.

4.14. Dynamic light scattering studies with 4.2a

Following the experiments establishing slight NR release from **4.2a** and **4.2b** liposomes, we moved on to test if the cargo release was accompanied by a change in liposome vesicle morphology. DLS was used to probe liposome particle sizes both before and after Cys treatment. Liposomes were used which were comprised of 0% **4.2a**, 40% Egg-PC, 50% DOPE, 10% PA; 30% **4.2a**, 10% Egg-PC, 50% DOPE, 10% PA; or 60% **4.2a**, 30% DOPE, 10% PA, both in addition to 5% NR. All liposomes were treated with either buffer, or 10 mM Cys, and incubated for 5 hr. These results showed that liposomes containing 0%, 30%, or 60% **4.2a** had average diameters < 200 nm (Figure 4.10A) and polydispersity indices (PDI) < 0.2 (Figure 4.10B) before and after treatment, which are both in the desirable size range (diameter ≤ 200, PDI ≤ 0.2). These results indicate that stable liposomes were formed with up to 60% **4.2a** incorporation, and addition of Cys did not cause major changes in vesicle morphology. Raw distribution curves are included in Figure 4.10C. We have previously observed cases in which cargo release does not cause significant changes to liposome size, which suggests that fusion is not occurring in these systems. [163, 168] This could also imply that membrane perturbation is not dramatic and may signify that further optimization of the lipid design is needed.

4.15. 6-Carboxyfluorescein release assay with 4.2a

Following NR assay attempts, a hydrophilic release assay was also attempted with CF, which is encapsulated in the aqueous core commonly and is used in release assays of this type.[425-427] The dye CF is first encapsulated at high concentration to cause fluorescence self-quenching, and release from the liposome results in increase in fluorescence. To prepare liposomes, a similar procedure was used compared to the NR release assay, but in this case the liposomes were hydrated with a 50 mM CF buffer solution. After standard this film liposome preparation, a size exclusion column (SEC) was used after extrusion to remove unencapsulated dye. The release assay was conducted by adding 10 mM Cys, 10 mM GSH, or buffer to the liposome solution and monitoring fluorescence over 24 hrs. At the end of the experiment, Triton X-100 detergent was added to the liposomes to destroy the bilayer and release 100% of the SRB content. This provides

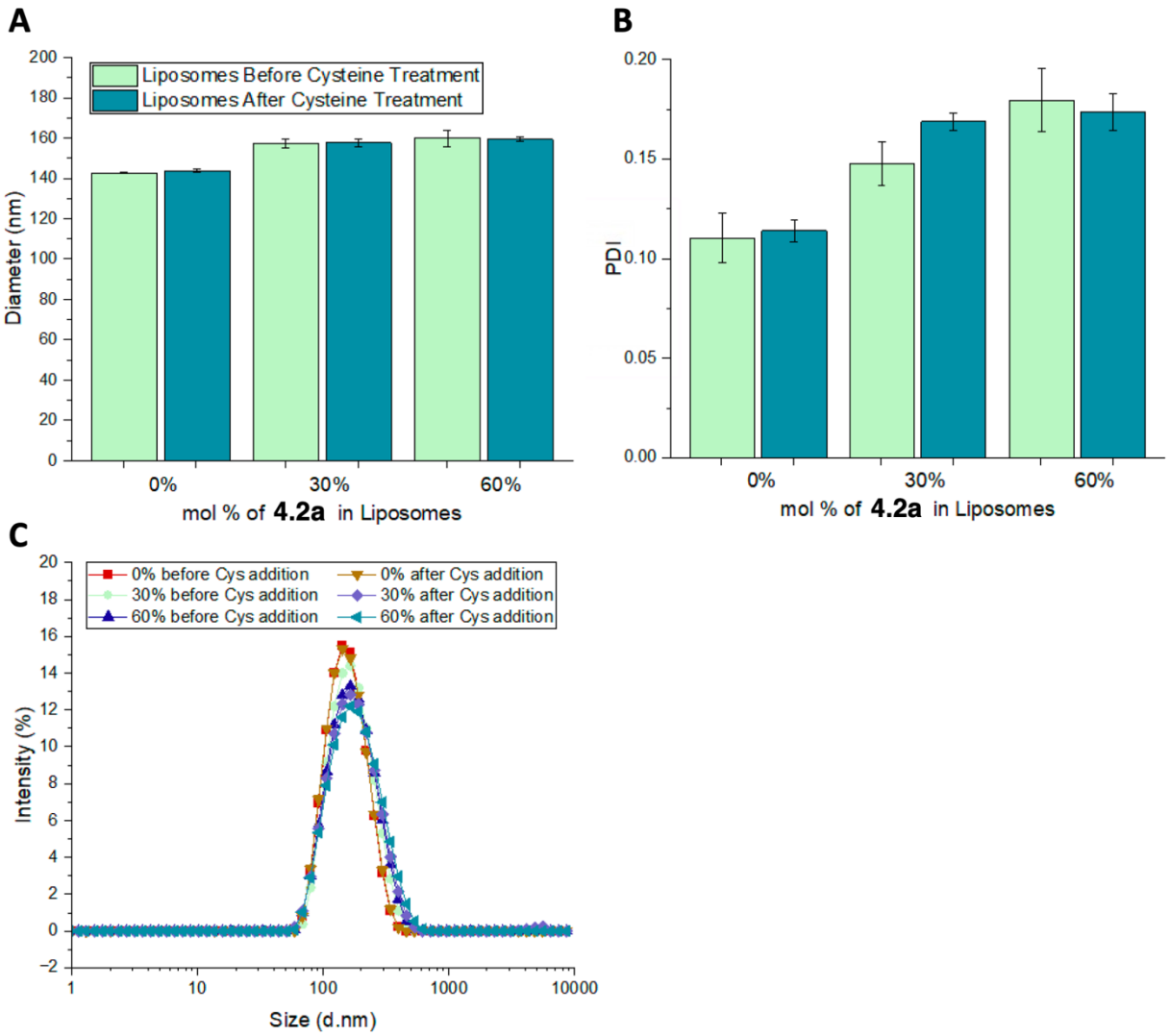


Figure 4.10 DLS results for 4.2a liposomes treated with Cys. DLS results for liposomes containing 0% **4.2a**, 40% Egg-PC, 50% DOPE, 10% PA; 30% **4.2a**, 10% Egg-PC, 50% DOPE, 10% PA; or 60% **4.2a**, 30% DOPE, 10% PA, as well as 5% NR. All liposomes were treated with either buffer or 10 mM Cys. (A) Average diameters of samples before and after treatment were < 200 nm and (B) PDI for all samples were < 0.2. (C) Raw distribution curves of samples before and after 10 mM Cys treatment showed no change in vesicle size distribution. Error bars represent standard errors of at least three replicates.

a fluorescence end-point of total release, and all other fluorescence readings were normalized by calculating percent release compared to total release.

Various liposomes formulations containing **4.2a** were explored with the goal of finding a combination that is stable and retains CF cargo without Cys treatment, but releases cargo after treatment. Also, it was necessary that liposomes with the same formulation but lacking **4.2a** must retain SRB both before and after treatment. Liposome formulations were attempted with lipids including Egg-PC, DPPC, DOPE, and PA. As summarized in Table 4.5, most of the attempted formulations showed minimal background release with buffer treatment, but also showed minimal release when treated with Cys, indicating that they are too stable. Conversely, a few formulations such as 40% **4.2a**, 50% DOPE, and 10% PA showed considerable release when treated with 10 mM Cys (~30%), but also showed high background release of ~30%, indicating the liposomes are unstable and leaking CF. Altogether, these release assays were attempted with lipid **4.2a** but none gave promising results.

4.16. TLC analysis of cysteine-mediated cleavage of free lipid

After synthesizing Cys responsive SIL lipid **4.2a** and exploring liposome release characteristics, we began analyzing the lipid's reactivity and selectivity towards the biologically relevant thiol Cys as compared to GSH. Again, a TLC analysis was performed to gain a simple understanding of the lipid's reactivity. The analysis was performed by treating 2 mM solutions of free **4.2a** lipid with either no treatment (Figure 4.11, lane 1), 1.5 mM GSH (Figure 4.11, lane 2), or 1.5 mM Cys (Figure 4.11, lane 3). After treatment, the solution suspending the samples had a final ratio of 65:25:4 $CHCl_3$:MeOH:H_2O to maintain solubility of both lipid **4.2a** and thiols. The samples were compared to a 2 mM DOPE standard shown on the far left. Samples were incubated over 30 min, but small aliquots were used to prepare TLC plates at 0 min, 5 min, 10 min, 15 min, 20 min, 25 min, and 3 hr. These TLC plates were first photographed under a UV lamp (Figure 4.11A-G) and again after staining with $KMnO_4$ and heating mildly (Figure 4.11H-N).

The results indicate lipid **4.2a** did not react with GSH and maintained the initial spot. Conversely,

Table 4.5 Summary of formulations explored for CF release assay using lipid 4.2a and different percentages of DPPC, Egg-PC, DOPE, and PA.

Entry	% 4.2a	% DPPC	% Egg-PC	% DOPE	% PA	Stable?	Treatment	Outcome
1	30	--	15	45	10	Yes	Buffer	~7% release
							10 mM Cys	~6% release
							10 mM GSH	~6% release
2	30	--	20	40	10	Yes	Buffer	~6% release
							10 mM Cys	~4% release
							10 mM GSH	~4% release
3	30	--	30	30	10	Yes	Buffer	~6% release
							10 mM Cys	~5% release
							10 mM GSH	~4% release
4	30	--	40	20	10	Yes	Buffer	~6% release
							10 mM Cys	~5% release
							10 mM GSH	~5% release
5	30	--	50	10	10	Yes	Buffer	~10% release
							10 mM Cys	~9% release
							10 mM GSH	~10% release
6	--	30	15	45	10	Yes	Buffer	~3% release
							10 mM Cys	~1% release
							10 mM GSH	~2% release
7	--	30	20	40	10	Yes	Buffer	~2% release
							10 mM Cys	~1% release
							10 mM GSH	~1% release
8	--	30	30	30	10	Yes	Buffer	~1% release
							10 mM Cys	~0% release
							10 mM GSH	~1% release
9	--	30	40	20	10	Yes	Buffer	~2% release
							10 mM Cys	~2% release
							10 mM GSH	~2% release
10	--	30	50	10	10	Yes	Buffer	~3% release
							10 mM Cys	~2% release
							10 mM GSH	~2% release
11	40	--	10	40	10	Yes	Buffer	~9% release
							10 mM Cys	~8% release
							10 mM GSH	~8% release
12	40	--	20	30	10	Yes	Buffer	~12% release
							10 mM Cys	~8% release
							10 mM GSH	~7% release

Table 4.5 Continued

Entry	% 4.2a	% DPPC	% Egg-PC	% DOPE	% PA	Stable?	Treatment	Outcome
13	40	--	30	20	10	Yes	Buffer	~17% release
							10 mM Cys	~13% release
							10 mM GSH	~13% release
14	40	--	40	10	10	Yes	Buffer	~16% release
							10 mM Cys	~16% release
							10 mM GSH	~15% release
15	40	--	50	--	10	Yes	Buffer	~30% release
							10 mM Cys	~34% release
							10 mM GSH	~47% release
16	--	40	10	40	10	Yes	Buffer	~3% release
							10 mM Cys	~3% release
							10 mM GSH	~2% release
17	--	40	20	30	10	Yes	Buffer	~2% release
							10 mM Cys	~2% release
							10 mM GSH	~2% release
18	--	40	30	20	10	Yes	Buffer	~3% release
							10 mM Cys	~2% release
							10 mM GSH	~2% release
19	--	40	40	10	10	Yes	Buffer	~3% release
							10 mM Cys	~3% release
							10 mM GSH	~3% release
20	--	40	50	--	10	Yes	Buffer	~6% release
							10 mM Cys	~7% release
							10 mM GSH	~7% release

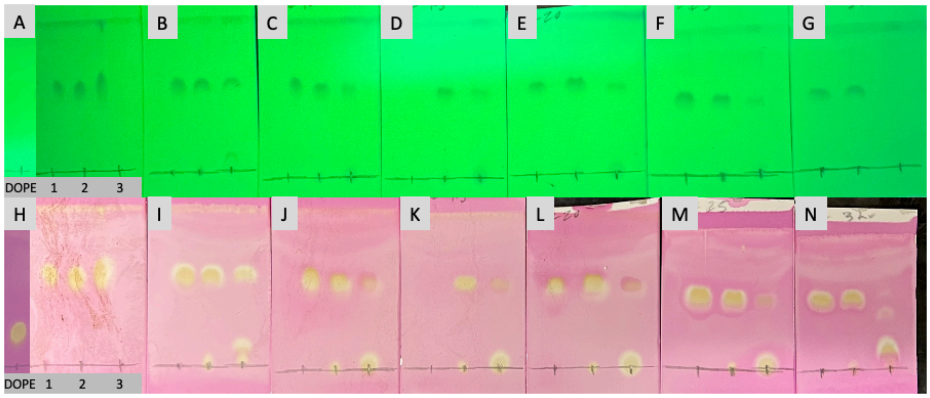


Figure 4.11 TLC analysis of thiol-mediated cleavage 4.2a. TLC analysis of 2 mM free lipid **4.2a** suspended in 65:25:4 $CHCl_3$:MeOH:H_2O with no treatment (lane 1), 1.5 mM GSH (lane 2) or 1.5 mM Cys (lane 3). A DOPE 2 mM standard is shown on the far left. Samples were incubated over 3 hr, TLC plates spotted, eluted in 20:80 MeOH:$CHCl_3$, and imaged under UV light at (A) 0 min, (B) 5 min, (C) 10 min, (D) 15 min, (E) 20 min, (F) 25 min, and (G) 3 hr. Plates were also stained with $KMnO_4$ at (H) 0 min, (I) 5 min, (J) 10 min, (K) 15 min, (L) 20 min, (M) 25 min, and (N) 3 hr. Lipid **4.2a** did not react with GSH and maintained the initial spot. Lipid **4.2a** reacted with Cys quickly, showing lipid **4.2a** spot fading at 10 min and gone at 30 min. Two new spots appear, including a faint new spot similar to the pure DOPE spot (DOPE R_f = 0.2).

lipid **4.2a** reacted with Cys quickly, showing the lipid **4.2a** spot fading at 10 min and almost fully decomposing at 25 min. Two new spots appear, including a faint new spot similar to the pure DOPE spot at 3 hr (DOPE R_f = 0.2). These results indicate that **4.2a** is decomposing faster when treated with Cys compared to treatment with GSH and it appears to be forming the expected DOPE spot after 3 hr incubation with Cys. As previously stated, this preliminary study only gives a preview of the lipid's performance. Behavior in respect to reaction speed and trigger sensitivity may differ once we move on to liposome studies when it is incorporated in liposomes and dissolved in aqueous buffer.

4.17. Time-dependent NMR experiment

To continue analyzing the different properties of lipids **4.2a-c** in terms of reaction speed and DOPE release, and particularly any discrepancy due to differences in electron density around the aromatic ring of the SIL, we investigated the release mechanism further. We began by studying the products resulting from reaction of free lipids **4.2a-c** with Cys by time-dependent NMR analysis. To perform this experiment, lipids **4.2a-c** were dissolved in $CDCl_3/CD_3OD/D_2O$=65/25/4 (v/v) in an NMR tube, and an initial scan was taken. Then, a separate sample of **4.2a-c** was prepared in $CDCl_3/CD_3OD$=65/25 (v/v), after which an aliquot of Cys solution in D_2O was added to achieve a final solution of 2 mM of either **4.2a**, **4.2b**, or **4.2c**, and 2 mM Cys in a solution of $CDCl_3/CD_3OD/D_2O$=65/25/4 (v/v) in an NMR tube. Spectra were then taken over time.

As shown in Figure 4.12, addition of Cys to the headgroup of **4.2a** took place gradually over the 22 hr time frame, as indicated by significant drop in the alkene protons of the acryl headgroup at ~6.06, ~6.33, and ~6.61 ppm. The aromatic protons also shifted from ~7.40 and ~7.12 ppm to ~7.39 and ~7.09 ppm (Figure 4.12, trace A-F). It is difficult to deduce if a new peak at ~2.95 ppm appeared, which would correspond to the methylene peak next to the amino moiety of the headgroup of DOPE, because overlapping Cys peaks in that region. The benzylic methylene peak also shifted slightly from ~5.09 to ~5.08 ppm after 10 min, and a new signal began appearing at ~4.98 ppm. No change was observed for the DOPE tail alkene protons at ~5.35 ppm or other DOPE peaks below ~2.8 ppm, indicating that Cys did not react with the DOPE tail under these conditions.

Similar results were seen in the **4.2b** sample treated with Cys. In this case, the lipid reacted faster with Cys compared to lipid **4.2a**, as indicated by the disappearance of alkene protons of the acryl headgroup (~6.06, ~6.33, and ~6.61 ppm) after 60 min incubation (Figure 4.13, trace A-C). After 10 min, the aromatic protons also shifted from ~7.35, 6.72, and ~6.69 ppm to ~7.34 ~6.71, and 6.66 ppm, respectively, and additional peaks in the aromatic region appeared at ~7.09, ~6.39, and ~6.44 ppm (Figure 4.13, trace A-B). The benzylic methylene peak also shifted slightly from ~5.11 to ~5.12 ppm, however, no new methylene signal appeared. It was again difficult to observe if a new methylene DOPE peak appeared at ~2.95 ppm due to overlapping Cys peaks. No change was observed for the DOPE tail alkene protons at ~5.35 ppm or other DOPE signals below ~2.8 ppm, indicating that Cys did not react with the DOPE tail under these conditions.

Lipid **4.2c** displayed similar results as well, with the quick disappearance of alkene protons of the acryl headgroup (~6.08, ~6.32, and ~6.62 ppm) after 10 min incubation (Figure 4.14, trace A-B). Additionally, the aromatic protons at ~6.94 ppm disappeared and new peaks in the aromatic region appeared at ~7.20, ~6.95, ~6.90, ~6.66, ~6.60, and ~6.55 ppm (Figure 4.14, trace A-F). The benzylic methylene peak again shifted slightly from ~5.14 to ~5.13 ppm, and an additional singlet at ~5.03 ppm appeared gradually over the 22 hrs. No change was observed for the DOPE tail alkene protons at ~5.35 ppm or other DOPE signals below ~2.8 ppm.

4.18. Mass spectrometry evidence of DOPE formation

Mass spectrometry analysis was also performed to study DOPE release from lipids **4.2a-c**. To perform this experiment, lipids **4.2a-c** were dissolved in $CHCl_3/CH_3OH$=65/25 (v/v), after which an aliquot of Cys solution in H_2O was added to achieve a final solution of 500 μM of either **4.2a**, **4.2b**, or **4.2c**, and 1 mM Cys in a solution of $CHCl_3/CH_3OH/H_2O$=65/25/4 (v/v) in a vial. The samples were incubated for 12 hr and MS spectra were taken. As shown in Figure 4.15, addition of Cys to lipid **4.2a** resulted in the formation of compound **4.3a** as well as a very small peak for DOPE, indicating that this lipid did not efficiently complete the intramolecular attack, cyclized thiolactam release, and/or self-immolation. Conversely, in the spectra of lipid **4.2b** (Figure 4.16)

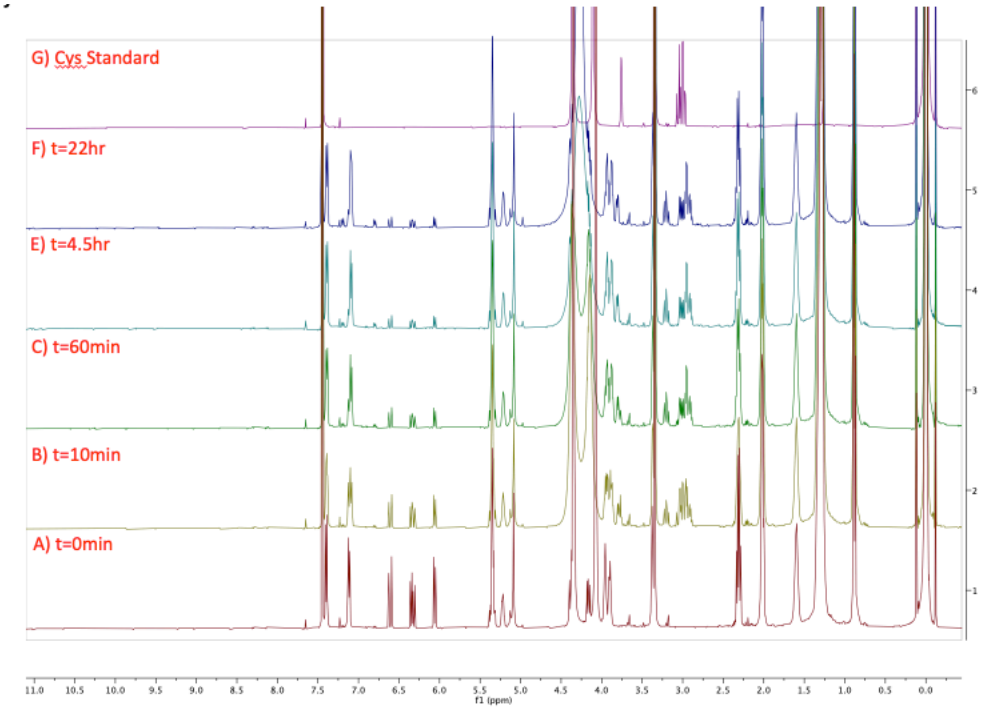


Figure 4.12 Time-dependent NMR analysis for lipid 4.2a in $CDCl_3$:CD_3OD:D_2O = 65:25:4 (v/v) upon treatment with Cys. Trace A: lipid **4.2a** before Cys addition. Trace B to F: spectra for lipid **4.2a** after Cys treatment taken over time. Trace G: Cys standard.

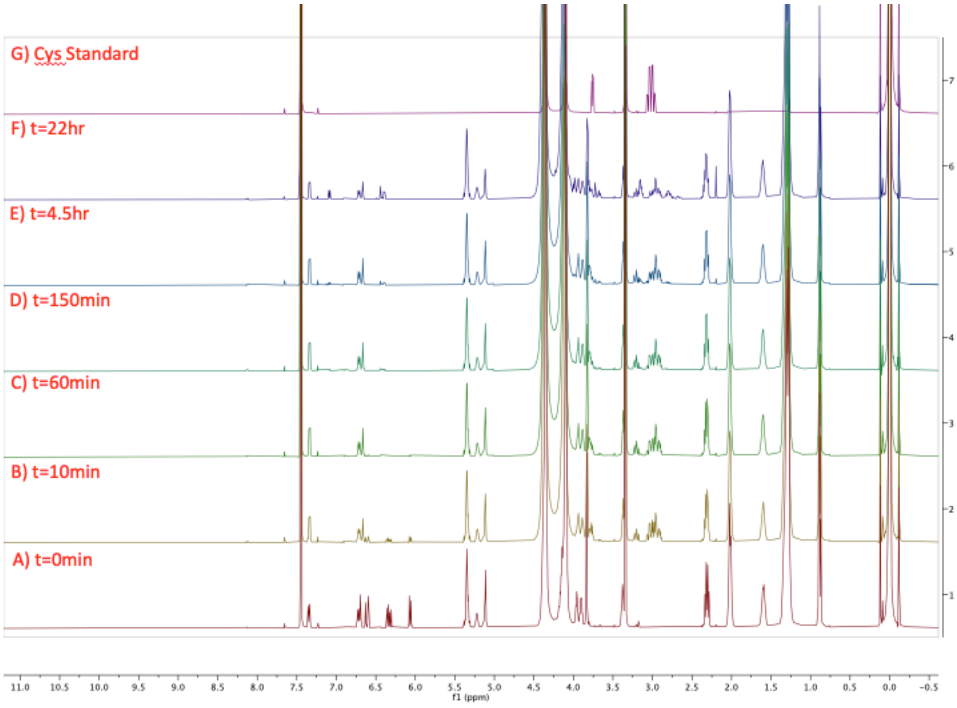


Figure 4.13 Time-dependent NMR analysis for lipid 4.2b in $CDCl_3$:CD_3OD:D_2O = 65:25:4 (v/v) upon treatment with Cys. Trace A: lipid **4.2b** before Cys addition. Trace B to F: spectra for lipid **4.2b** after Cys treatment taken over time. Trace G: Cys standard.

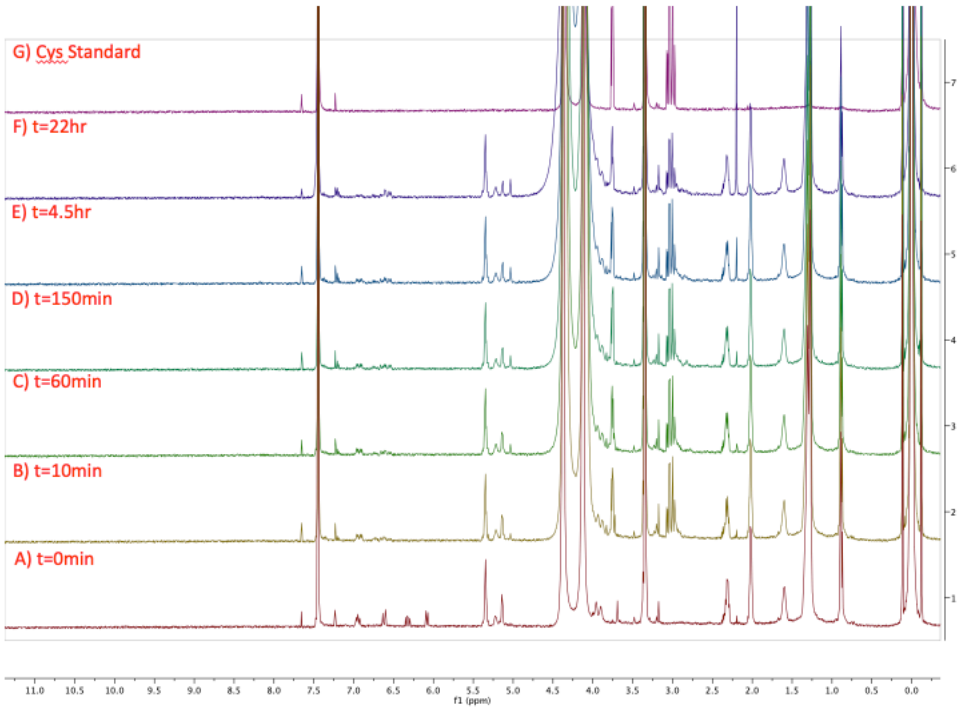


Figure 4.14 Time-dependent NMR analysis for lipid 4.2c in $CDCl_3$:CD_3OD:D_2O = 65:25:4 (v/v) upon treatment with Cys. Trace A: lipid **4.2c** before Cys addition. Trace B to F: spectra for lipid **4.2c** after Cys treatment taken over time. Trace G: Cys standard.

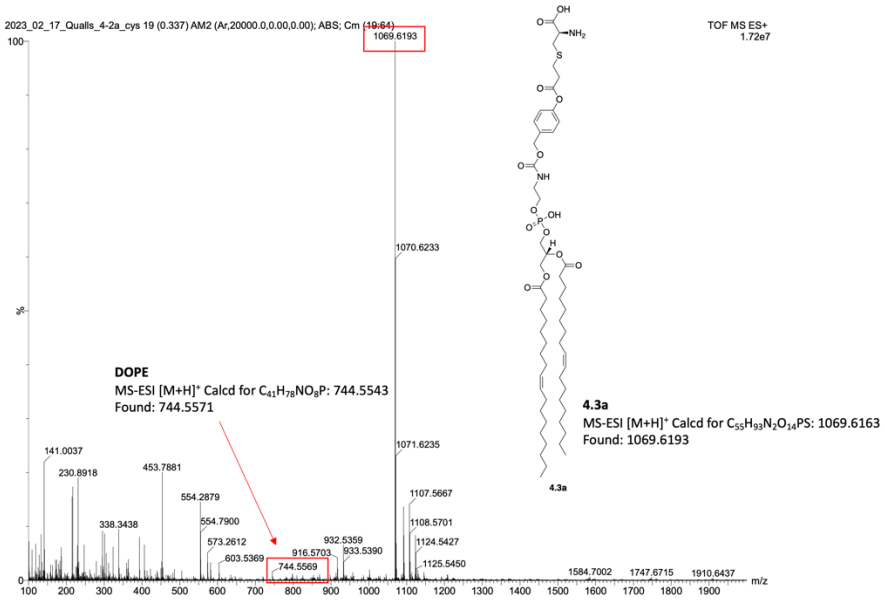


Figure 4.15 Mass spectrum including a peak matching lipid 4.3a and DOPE after treating free lipid 4.2a with Cys.

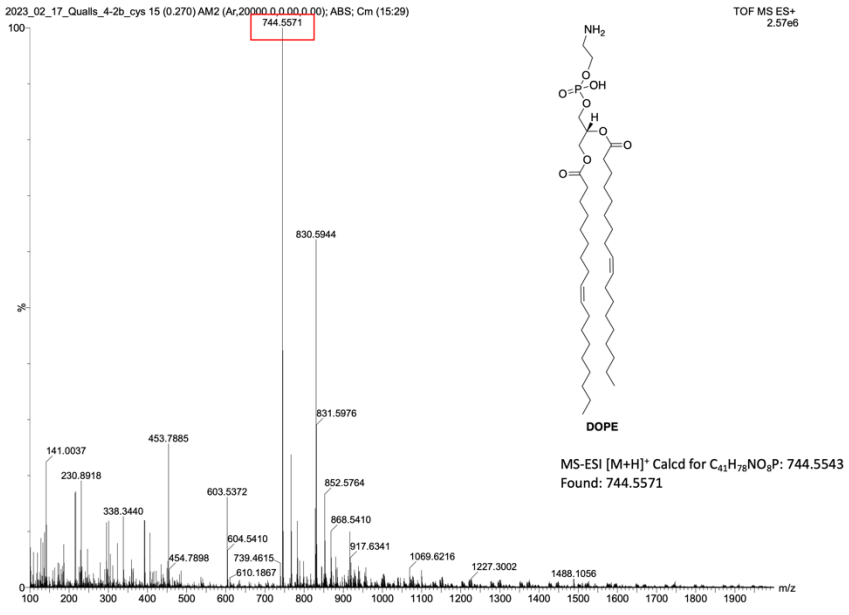


Figure 4.16 Mass spectrum including a peak matching DOPE after treating free lipid 4.2b with Cys.

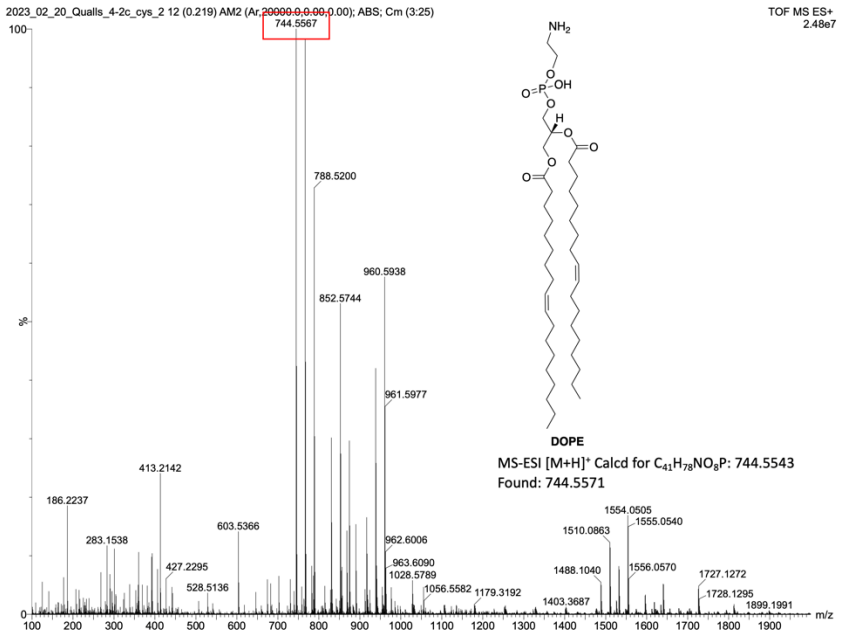


Figure 4.17 Mass spectrum including a peak matching DOPE after treating free lipid 4.2c with Cys.

or **4.2c** (Figure 4.17) treated with Cys, the DOPE peak could be clearly observed, indicating that these lipids underwent all steps to fully decompose and release free DOPE.

4.19. Conclusion

In conclusion, we have designed and synthesized two classes of stimuli-responsive liposomes, those that generally respond to thiols, and also lipid switches that are designed to be activated specifically by Cys, which is significantly upregulated during cancer onset. These lipids shared similar design strategies including a metabolite triggered headgroup, a SIL, and a non-bilayer forming lipid scaffold. Specifically, general thiol responsive lipid **4.1a** contained three major features including a thiol-responsive disulfide headgroup, a thioquinone methide-generating DSIL, and a non-bilayer forming DOPE lipid. Lipid **4.1b** was also synthesized in an attempt to increase reactivity which featured an electron withdrawing nitro group on the pyridyl group. Similarly, Cys responsive lipids **4.2a-c** also contained three features including a Cys-responsive acrylate headgroup, quinone methide-generating SIL, and non-bilayer forming DOPE. Analogs of this lipid type were created including the original **4.2a** in addition to **4.2b**, which featured an activating EWG around the aromatic SIL and **4.2c** with a deactivating EDG.

After synthesizing these innovative lipids, they were incorporated into liposomes and underwent excessive tuning of membrane stability by altering the liposome composition. Significant triggered release of hydrophobic dye NR dye was achieved for a general thiol-responsive lipid, and minimal release was seen from the Cys-responsive lipids when treated with Cys. The lipids' reactions with thiols were analyzed, and the results indicate that decomposition of lipids **4.1a** and **4.2a-c** is sufficient to result in the release of the hydrophobic dye NR, although no changes in liposomal particle sizes were observed by DLS. Although few platforms have been previously explored in liposome research, thiols and specifically amino acid Cys is an exciting target for triggered release considering it is significantly upregulated during cancer onset compared to healthy cells due to its vital role in cancer cellular homeostasis and survival. We demonstrated that lipids which respond both generally to thiol-containing biomolecules as well as selectively to Cys serve as exciting liposome systems for harnessing disease-associated thiols to trigger liposomal release. We envision that similar design strategies can be used to target additional

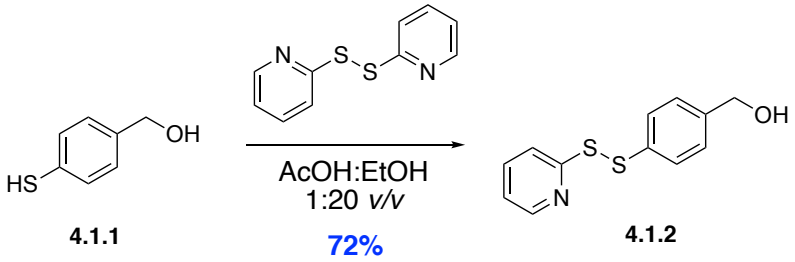
aberrantly expressed metabolites in order to develop future liposomal release platforms for controlled, triggered content release for therapeutic applications.

4.20. Synthesis and experimental procedure

General experimental

Reagents and solvents were generally purchased from Sigma-Aldrich or Fisher Scientific and used as received. Egg-PC (L-α-phosphatidylcholine, mixed isomers from chicken eggs), DPPC 1,2-dipalmitoyl-*sn*-glycero-3-phosphocholine, DOPE 1,2-dioleoyl-*sn*-glycero-3-phosphoethanolamine, PA 1,2-dioleoyl-*sn*-glycero-3-phosphate (sodium salt), DOTAP (1,2-dioleoyl-3-trimethylammonium-propane, chloride salt) and Rd-PE (L-α-phosphatidylethanolamine-*N*-(lissamine rhodamine B sulfonyl) (ammonium salt)) were purchased from Avanti Polar Lipids, Inc. (Alabaster, AL). Dry solvents were obtained from a Pure Solv MD-7 solvent delivery system purchased from Innovative Technologies, Inc. Column chromatography was performed using 230 – 400 mesh silica gel purchased from Sorbent Technologies (Norcross, GA). NMR spectra were obtained using a Bruker 500 MHz spectrometer. Mass spectra were obtained with JEOL DART-AccuTOF and Waters Synapt G2-Si mass spectrometers (Milford, MA). Liposome extruder and polycarbonate membranes were obtained from Avestin (Ottawa, Canada). Water for liposome preparation and assays was purified via a Millipore water system (≥18 MW·cm triple water purification system). Small quantities (<5 mg) were weighed on a Mettler Toledo XS105 dual range analytical balance. DLS measurements were performed using a Malvern Zetasizer Nano ZS instrument equipped with a He-Ne 633 nm laser and a temperature controller at a scattering angle of 173°. Plots were generated using Origin Pro 2022. All error bars in plots show the standard errors of at least three experimental replicates.

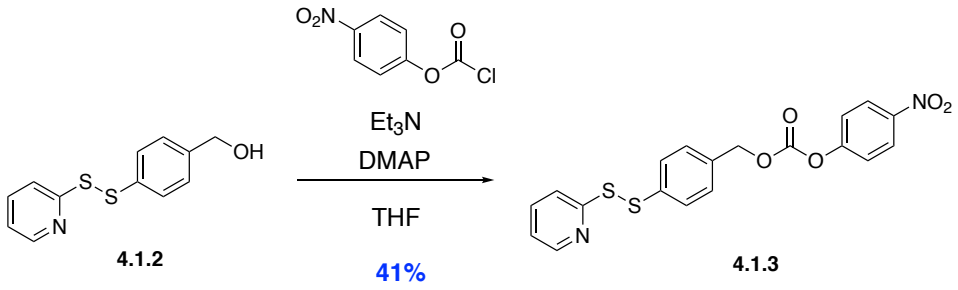
Synthesis



4-(Pyridin-2-yldisulfaneyl)phenyl)methanol (4.1.2)

To a solution of 2,2'-dipyridyl disulfide (0.3614g, 1.641 mmol, 2.3 eq) in acetic acid (AcOH) / ethanol (EtOH) (1/20 *v/*v, 3 mL, degassed for 5 min by N_2) under Ar, a solution of 4-mercaptobenzyl alcohol (**4.1.1**) (0.100 g, 0.7133 mmol, 1 eq) was added dropwise over 20 min. The reaction was allowed to stir at rt for 12 hr. After being concentrated under reduced pressure, the crude was subjected to silica gel column chromatography using gradient elution from hexanes to 50% EtOAc in hexanes to obtain **4.1.2** as a yellow oil (127.2 mg, 0.5101 mmol, 72% yield). R_f = 0.45 (50:50 EtOAc/Hex).

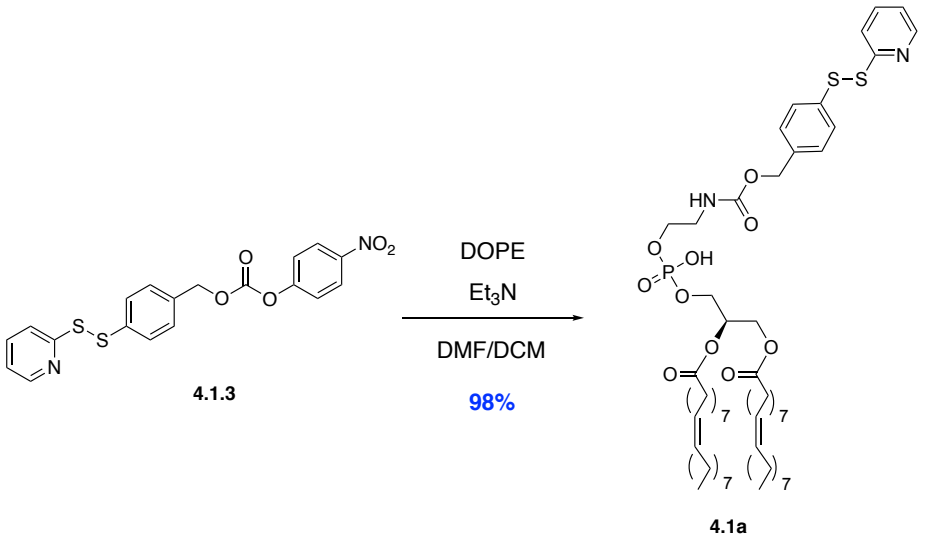
^{1}H NMR (500 MHz, $CDCl_3$) δ 8.40 (s, 1H), 7.66 – 7.55 (m, 2H), 7.47 (d, *J* = 7.8 Hz, 2H), 7.27 (d, *J* = 6.7 Hz, 2H), 7.10 – 7.04 (m, 1H), 4.62 (s, 2H). ^{13}C NMR (126 MHz, $CDCl_3$) δ 159.60, 149.44, 140.52, 137.38, 135.05, 127.74, 127.69, 120.95, 119.68, 64.41.



4-Nitrophenyl (4-(pyridin-2-yldisulfaneyl)benzyl) carbonate (4.1.3)

To a solution of 4-nitrophenyl chloroformate (0.1439 g, 0.7141 mmol, 1.4 eq) in dry THF (5 mL) under Ar at 0 ° C, a solution of (4-(pyridin-2-yldisulfaneyl)phenyl)methanol (**4.1.2**) (0.1272 g, 0.5202 mmol, 1 eq), DMAP (0.02493 g, 0.2040 mmol, 0.4 eq), and TEA (0.4052 mL, 2.9076 mmol, 5.7 eq) in dry tetrahydrofuran (THF, 5 mL) was added dropwise over 10 min. The mixture was warmed to rt over 1 hr and stirred for 15 hr. THF was evaporated *in vacuo*, and the resulting residue was dissolved in EtOAc (20 mL) and washed with 5 x 50 mL sat. sodium bicarbonate ($NaHCO_3$) and 1 x 50 mL brine, dried over Na_2SO_4, filtered, and concentrated under reduced pressure. The crude was subjected to silica gel column chromatography using gradient elution from hexanes to 20% EtOAc in hexanes to obtain **4.1.3** as a white solid (87.3 mg, 0.2106mmol, 41% yield). R_f = 0.53 (30% EtOAc/Hex).

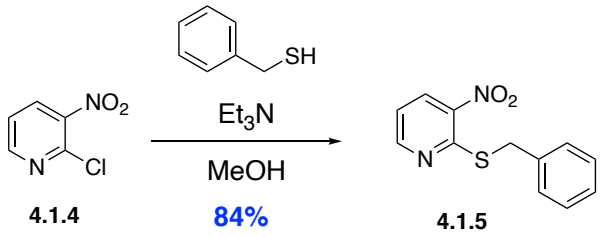
^{1}H NMR (500 MHz, $CDCl_3$) δ 8.48 (d, *J* = 6.2 Hz, 1H), 8.26 (d, *J* = 9.2 Hz, 2H), 7.62 (d, *J* = 3.4 Hz, 2H), 7.56 (d, *J* = 8.4 Hz, 2H), 7.37 (t, *J* = 8.8 Hz, 4H), 7.12 (d, *J* = 5.1 Hz, 1H), 5.25 (s, 2H). ^{13}C NMR (126 MHz, $CDCl_3$) δ 159.18, 155.44, 152.38, 149.70, 145.43, 137.34, 133.23, 129.48, 127.41, 125.30, 121.74, 121.10, 119.68, 70.28.



(2*R*)-3-((Hydroxy(2-((((4-(pyridin-2-yldisulfaneyl)benzyl)oxy)carbonyl)amino)ethoxy) phosphoryl)oxy)propane-1,2-diyl (9*E*,9'*E*)-bis(octadec-9-enoate) (4.1a)

4-Nitrophenyl (4-(pyridin-2-yldisulfaneyl)benzyl) carbonate (**4.1.3**) (29.1 mg, 0.0702 mmol, 1.3 eq) and DOPE (40 mg, 0.0538 mmol, 1 eq) were combined in a 50 mL round bottom flask (RBF) under Ar. A mix of 50/50 dry DMF/$CHCl_3$ (6 mL) was used to dissolve the starting materials at 0 °C. Next, TEA was added into the reaction (0.0225 mL, 0.1613 mmol, 3 eq). The reaction was allowed to warm up to rt and further stirred overnight before being quenched by pouring into 100 mL 0.5 M hydrochloric acid (HCl). The aqueous layer was then extracted with 3 × 25 mL $CHCl_3$. The combined organic layer was next washed with 50 mL water five times and once with 50 mL brine. After being dried over Na_2SO_4, filtered, and concentrated under reduced pressure, the crude was subjected to silica gel column chromatography using gradient elution from chloroform to 15% MeOH in $CHCl_3$ to obtain **4.1a** as a white solid (53.7 mg, 0.05268 mmol, 98% yield). R_f = 0.46 (20% MeOH/$CHCl_3$).

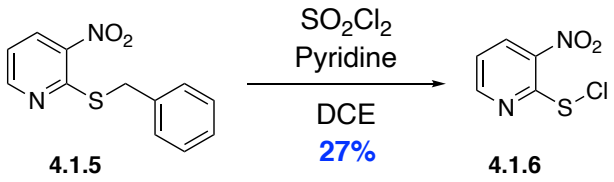
^{1}H NMR (500 MHz, 20% CD_3OD-$CDCl_3$) δ 8.18 (d, *J* = 5.0 Hz, 1H), 7.45 (d, *J* = 4.6 Hz, 2H), 7.24 (s, 1H), 7.06 (d, *J* = 8.0 Hz, 2H), 6.93 (q, *J* = 4.6 Hz, 1H), 5.10 (q, *J* = 5.2 Hz, 4H), 4.97 (dt, *J* = 8.9, 4.3 Hz, 1H), 4.80 (s, 2H), 4.13 (dd, *J* = 12.0, 3.3 Hz, 2H), 3.90 (dd, *J* = 12.0, 6.9 Hz, 1H), 3.74 – 3.62 (m, 4H), 2.06 (ddd, *J* = 9.5, 5.6, 2.3 Hz, 4H), 1.77 (q, *J* = 6.3 Hz, 8H), 1.35 (ddt, *J* = 13.9, 9.5, 5.5 Hz, 4H), 1.06 (t, *J* = 15.1 Hz, 45H), 0.64 (t, *J* = 6.8 Hz, 7H). ^{13}C NMR (126 MHz, MeOD) δ 173.64, 173.28, 159.16, 156.95, 148.98, 137.64, 135.90, 135.51, 129.73, 129.71, 129.37, 129.34, 128.40, 127.24, 121.07, 119.76, 70.18, 65.68, 64.23, 63.36, 62.33, 33.89, 33.74, 31.61, 29.45, 29.43, 29.34, 29.21, 29.01, 28.96, 28.93, 28.86, 28.84, 28.82, 28.79, 26.90, 26.87, 24.60, 24.55, 22.35, 13.59. ^{31}P NMR (202 MHz, CD_3OD-$CDCl_3$) δ 2.81.MS-ESI $[M+H]^+$ Calcd for $C_{54}H_{87}N_2O_{10}PS_2$: 1019.5618; Found: 1019.5645



2-(Benzylthio)-3-nitropyridine (4.1.5)

2-Chloro-3-nitropyridine (**4.1.4**) (0.50 g, 3.154 mmol, 1eq) was added to a pressure vessel in dry MeOH (10 mL). To the solution was added benzyl mercaptan (0.5876 g, 4.731mmol, 1.5 eq) and TEA (0.660 mL, 4.731 mmol, 1.5 eq). The mixture was heated to reflux and stirred for 5 hr, then cooled to rt, after which the mixture was diluted in $CHCl_3$ (20 mL) and concentrated under reduced pressure. The crude was subjected to silica gel column chromatography using gradient elution from hexanes to 10% EtOAc in hexanes to obtain **4.1.5** as a yellow solid (0.6546 g, 2.658 mmol, 84% yield). R_f = 0.52 (25% EtOAc/Hex).

^{1}H NMR (500 MHz, $CDCl_3$) δ 8.64 (dd, *J* = 4.6, 1.6 Hz, 1H), 8.39 (dt, *J* = 8.2, 1.4 Hz, 1H), 7.39 – 7.33 (m, 2H), 7.28 – 7.21 (m, 2H), 7.21 – 7.16 (m, 1H), 7.16 – 7.09 (m, 1H), 4.42 (s, 2H). ^{13}C NMR (126 MHz, $CDCl_3$) δ 157.75, 153.08, 141.72, 136.86, 133.71, 129.45, 128.59, 127.37, 118.93, 35.38.

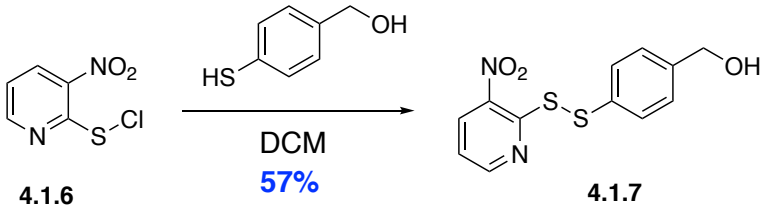


4.1.5 4.1.6

3-Nitropyridin-2-yl hypochlorothioite (4.1.6)

2-(Benzylthio)-3-nitropyridine (**4.1.5**) (0.5546 g, 2.252 mmol, 1eq) was dissolved in 1,2-dichloroethane (DCE, 10 mL) and cooled to 0° C. SO_2Cl_2 (2.9275 mL, 2.9276 mmol, 1.3 eq) and pyridine (4 drops) were then added to the mixture, which was stirred for 3 hr at 0 ° C. The mixture was concentrated under reduced pressure and the crude was subjected to silica gel column chromatography using gradient elution from hexanes to 50% EtOAc in hexanes to obtain **4.1.6** as a yellow solid (0.4292 g, 0.6138 mmol, 27% yield). R_f = 0.60 (75% EtOAc/Hex).

^{1}H NMR (500 MHz, $CDCl_3$) δ 8.95 (dd, *J* = 4.6, 1.6 Hz, 1H), 8.62 – 8.51 (m, 1H), 7.44 (dd, *J* = 8.3, 4.6 Hz, 1H), 2.17 (s, 1H). ^{13}C NMR (126 MHz, $CDCl_3$) δ 155.19, 153.51, 133.66, 120.79.

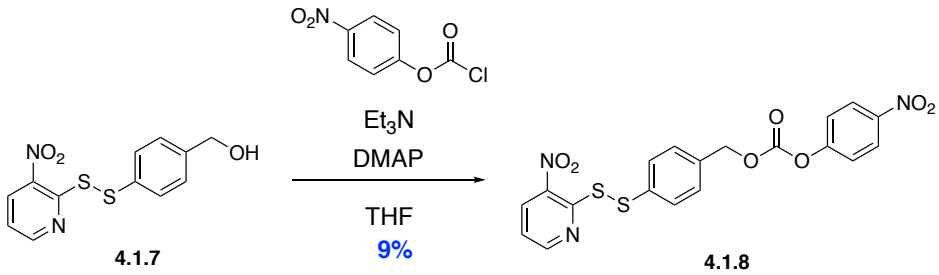


4.1.6 4.1.7

(4-((3-Nitropyridin-2-yl)disulfaneyl)phenyl)methanol (4.1.7)

3-Nitro-2-pyridinesulfenyl chloride (**4.1.6**) (0.16314 g, 0.8559 mmol, 1.5 eq) was dissolved in dry DCM (5 mL) and cooled to 0 ° C. A solution of 4-mercaptobenzyl alcohol (0.080 g, 0.5706 mmol, 1 eq) in dry DCM (5 mL) was added to the **4.1.6** solution dropwise over 5 min. The reaction was allowed to warm up to rt and further stirred for 12 hr, after which it was diluted in DCM and washed with 5 x 50 mL sat. $NaHCO_3$ and 1 x 50 mL brine, dried over Na_2SO_4, filtered, and concentrated under reduced pressure. The crude was subjected to silica gel column chromatography using gradient elution from DCM to 0.5% MeOH in DCM to obtain **4.1.7** as a yellow oil (9. 63 mg, 0.3272 mmol, 57 % yield). R_f = 0.55 (5% DCM/MeOH).

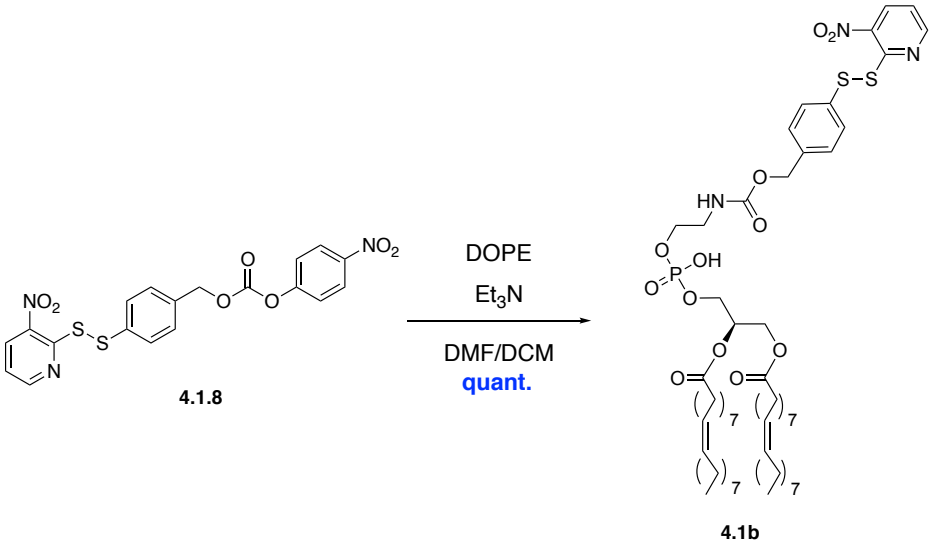
^{1}H NMR (500 MHz, $CDCl_3$) δ 8.83 (dd, *J* = 4.6, 1.6 Hz, 1H), 8.52 (dd, *J* = 8.1, 1.6 Hz, 1H), 7.56 (d, *J* = 8.2 Hz, 2H), 7.35 (dd, *J* = 8.2, 4.5 Hz, 1H), 7.28 (d, *J* = 8.0 Hz, 2H), 4.66 (s, 2H). ^{13}C NMR (126 MHz, $CDCl_3$) δ 156.51, 153.93, 142.76, 140.86, 135.48, 133.96, 130.06, 127.68, 121.23, 64.90.



4-Nitrophenyl (4-((3-nitropyridin-2-yl)disulfaneyl)benzyl) carbonate (4.1.8)

To a solution of 4-nitrophenyl chloroformate (0.06998 g, 0.3472 mmol, 1.4 eq) in dry THF (5 mL) under Ar at 0 ° C, a solution of (4-((3-nitropyridin-2-yl)disulfaneyl)phenyl)methanol (**4.1.7**) (0.0730 g, 0.248 mmol, 1 eq), DMAP (0.01212 g, 0.0992 mmol, 0.4 eq), and TEA (0.197 mL, 1.4136 mmol, 5.7 eq) in dry THF (5 mL) was added dropwise over 10 min. The mixture was warmed to rt over 1 hr and stirred for 15 hr. THF was evaporated *in vacuo*, and the resulting residue was dissolved in DCM (30 mL) and washed with 5 x 50 mL sat. $NaHCO_3$ and once with 50 mL brine, dried over Na_2SO_4, filtered, and concentrated under reduced pressure. The crude was subjected to silica gel column chromatography using gradient elution from hexanes to 20% EtOAc in hexanes to obtain **4.1.8** as a yellow oil (10.2 mg, 0.0222 mmol, 9 % yield). R_f = 0.60 (50% EtOAc/Hex).

^{1}H NMR (500 MHz, $CDCl_3$) δ 8.82 (dd, *J* = 4.6, 1.6 Hz, 1H), 8.54 (dd, *J* = 8.2, 1.6 Hz, 1H), 8.29 – 8.23 (m, 2H), 7.58 (d, *J* = 8.4 Hz, 2H), 7.36 (td, *J* = 8.4, 3.7 Hz, 5H), 5.24 (s, 2H). ^{13}C NMR (126 MHz, $CDCl_3$) δ 156.00, 155.45, 153.84, 152.39, 145.47, 142.70, 137.41, 133.87, 133.62, 129.33, 129.23, 125.31, 121.73, 121.26, 70.28.

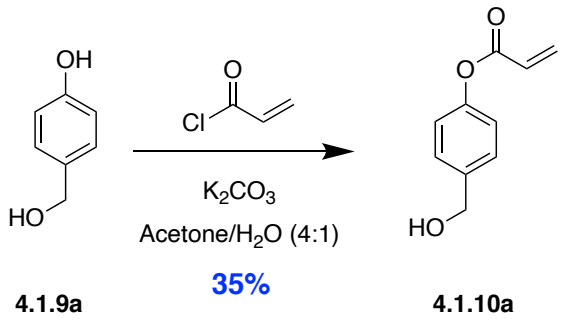


(2*R*)-3-((Hydroxy(2-((((4-((3-nitropyridin-2-yl)disulfaneyl)benzyl)oxy)carbonyl)amino)ethoxy) phosphoryl)oxy)propane-1,2-diyl (9*E*,9'*E*)-bis(octadec-9-enoate) (4.1b)

4-Nitrophenyl (4-((3-nitropyridin-2-yl)disulfaneyl)benzyl) carbonate (**4.1.8**) (10.2 mg, 0.0222 mmol, 1.2 eq) and DOPE (14 mg, 0.0185 mmol, 1 eq) were combined in a 50 mL RBF under Ar. A mix of 50/50 dry DMF/ $CHCl_3$ (6 mL) was used to dissolve the starting materials at 0 ° C. Next, TEA (0.0093 mL, 0.0666 mmol, 3 eq) was added into the reaction. The reaction was allowed to warm up to rt and further stirred overnight before being quenched by pouring into 100 mL 0.5 M HCl. The aqueous layer was then extracted with 3 × 25 mL $CHCl_3$. The combined organic layer was next washed with 5 x 50 mL water and 1 x 50 mL brine. After being dried over Na_2SO_4, filtered, and concentrated under reduced pressure, the crude was subjected to silica gel column chromatography using gradient elution from chloroform to 20% MeOH in $CHCl_3$ to obtain **4.1b** as a yellow oil (19.70 mg, 0.0185 mmol, 100% yield). R_f = 0.60 (20% MeOH/$CHCl_3$).

^{1}H NMR (500 MHz, 20% CD_3OD-$CDCl_3$) δ 8.73 (d, *J* = 4.4 Hz, 1H), 8.44 (d, *J* = 8.1 Hz, 1H), 7.42 (d, *J* = 7.5 Hz, 2H), 7.28 (dd, *J* = 8.2, 4.7 Hz, 1H), 7.14 (d, *J* = 8.0 Hz, 2H), 5.26 (q, *J* = 5.4 Hz, 4H), 5.13 (s, 1H), 4.96 (d, *J* = 23.5 Hz, 2H), 4.27 (d, *J* = 12.4 Hz, 1H), 4.04 (dd, *J* = 12.2, 7.0 Hz, 1H), 3.83 (d, *J* = 28.5 Hz, 4H), 2.18 (q, *J* = 5.6 Hz, 4H), 1.93 (q, *J* = 6.6 Hz, 8H), 1.50 – 1.46 (m, 4H), 1.26 – 1.15 (m, 49H), 0.80 (d, *J* = 7.1 Hz, 7H). ^{13}C NMR (126 MHz, $CDCl_3$) δ 173.78, 173.42, 155.69, 153.74, 142.51, 135.73, 133.84, 129.83, 129.47, 129.45, 129.19, 128.23, 121.29, 70.25, 65.81, 64.32, 63.46, 62.43, 33.99, 33.84, 31.69, 29.54, 29.52, 29.44, 29.30, 29.09, 29.05, 29.02, 28.96, 28.94, 28.91, 28.88,

26.99, 26.96, 24.68, 24.63, 22.44, 13.73.MS-ESI $[M+H]^+$ Calcd for $C_{54}H_{86}N_3O_{12}PS_2$: 1064.5469; Found: 1064.5483

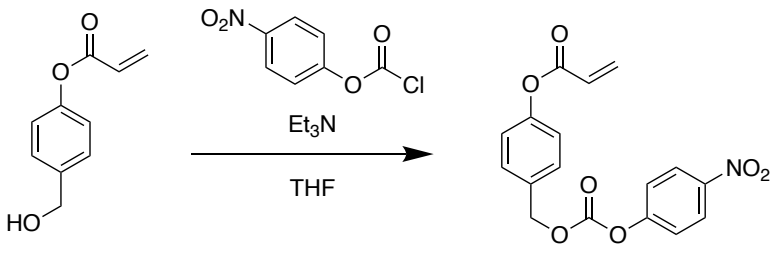


4.1.9a **4.1.10a**

4-(Hydroxymethyl)phenyl acrylate (4.1.10a)

A solution of potassium carbonate (0.835 g, 6.042 mmol, 1.5 eq) in acetone/H_2O (4/1 *v/v*, 25 mL) under Ar was cooled to 0° C, after which acryloyl chloride (0.36456 g, 4.028 mmol, 1 eq) was added. Then, a solution of 4-hydroxybenzyl alcohol (**4.1.9a**) (0.5 g, 4.028 mmol, 1 eq) dissolved in 5 mL acetone was added dropwise to the reaction mixture over 20 min. The reaction was allowed to stir at rt for 3 hr. After addition of 25 mL brine, the aqueous layer was then extracted with 3 × 25 mL DCM. The combined organic layer was next dried over Na_2SO_4, filtered, and concentrated under reduced pressure. The crude was subjected to silica gel column chromatography using gradient elution from hexanes to 30% EtOAc in hexanes to obtain **4.1.10a** as a clear oil (251.8 mg, 1.413 mmol, 35% yield). R_f = 0.53 (50:50 EtOAc/Hex).

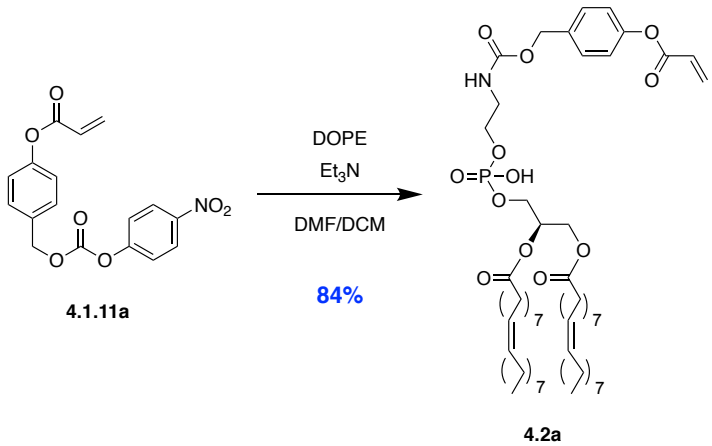
^{1}H NMR (500 MHz, $CDCl_3$) δ 7.39 (d, *J* = 8.1 Hz, 2H), 7.13 – 7.08 (m, 2H), 6.60 (dd, *J* = 17.3, 1.4 Hz, 1H), 6.34 (dd, *J* = 17.3, 10.4 Hz, 1H), 6.05 (dd, *J* = 10.4, 1.3 Hz, 1H), 4.63 (s, 2H). ^{13}C NMR (126 MHz, $CDCl_3$) δ 164.80, 149.37, 138.80, 132.31, 127.60, 127.42, 120.99, 63.32.



4-((((4-Nitrophenoxy)carbonyl)oxy)methyl)phenyl acrylate (4.1.11a)

4-(Hydroxymethyl)phenyl acrylate (**4.1.10a**) (0.2518 g, 1.413 mmol, 1 eq) was dissolved in 5 mL THF under Ar, and TEA (0.3940 mL, 2.826 mmol, 2 eq) was added. The reaction was cooled to 0 ° C, after which 4-nitrophenyl chloroformate (0.3418 g, 1.696 mmol, 1.2 eq) was added slowly. The reaction was allowed to warm up to rt and further stirred overnight. Next, the THF was evaporated, and the residue was dissolved in DCM (20 mL), after which the organic layer was washed with saturated $NaHCO_3$ (5 x 50 mL) and once with 50 mL brine. After being dried over Na_2SO_4, filtered, and concentrated under reduced pressure, the crude was subjected to silica gel column chromatography using gradient elution from hexanes to 20% EtOAc in hexanes to obtain **4.1.11a** as a clear oil (187 mg, 0.5447 mmol, 39% yield). R_f = 0.40 (30:70 EtOAc/Hex).

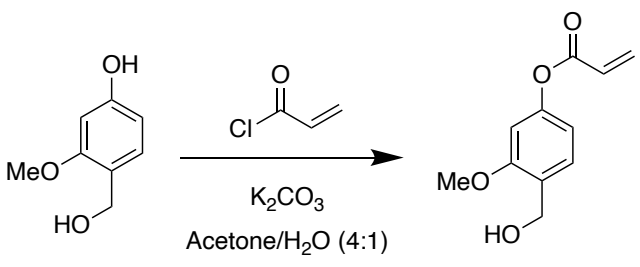
^{1}H NMR (500 MHz, $CDCl_3$) δ 8.28 (d, *J* = 9.2 Hz, 2H), 7.48 (d, *J* = 8.7 Hz, 2H), 7.39 (d, *J* = 9.2 Hz, 2H), 7.19 (d, *J* = 8.5 Hz, 2H), 6.62 (dd, *J* = 17.4, 1.5 Hz, 1H), 6.33 (ddd, *J* = 17.3, 10.5, 1.3 Hz, 1H), 6.04 (dd, *J* = 10.5, 1.4 Hz, 1H), 5.30 (s, 2H). ^{13}C NMR (126 MHz, $CDCl_3$) 164.36, 155.50, 152.44, 151.13, 145.47, 132.94, 131.86, 130.06, 127.73, 125.32, 122.01, 121.79, 70.28.



(2*R*)-3-(((2-((((4-(Acryloyloxy)benzyl)oxy)carbonyl)amino)ethoxy)(hydroxy)phosphoryl)oxy) propane-1,2-diyl dioleate (4.2a)

4-((((4-Nitrophenoxy)carbonyl)oxy)methyl)phenyl acrylate (**4.1.11a**) (0.02768 g, 0.08064 mmol, 1.5 eq) and DOPE (40 mg, 0.05376 mmol, 1 eq) were combined in a 50 mL RBF under Ar. A mix of 50/50 dry DMF/$CHCl_3$ (6 mL) was used to dissolve the starting materials at 0 ° C. Next, TEA was added into the reaction (0.02248 mL, 0.1613 mmol, 3 eq). The reaction was allowed to warm up to rt and further stirred overnight before being quenched by pouring into 100 mL 0.5 M HCl. The aqueous layer was then extracted with 3 × 25 mL $CHCl_3$. The combined organic layer was next washed with 5 x 50 mL water and 1 x 50 mL brine. After being dried over Na_2SO_4, filtered, and concentrated under reduced pressure, the crude was subjected to silica gel column chromatography using gradient elution from $CHCl_3$ to 20% MeOH in $CHCl_3$ to obtain **4.2a** as a white solid (42.8 mg, 0.04514 mmol, 84% yield). R_f = 0.55 (20% MeOH/$CHCl_3$).

^{1}H NMR (500 MHz, 20% CD_3OD-$CDCl_3$) δ 7.10 (d, *J* = 8.2 Hz, 2H), 6.82 (d, *J* = 8.1 Hz, 2H), 6.31 (d, *J* = 17.2 Hz, 1H), 6.04 (dd, *J* = 17.3, 10.5 Hz, 1H), 5.77 (d, *J* = 10.4 Hz, 1H), 5.09 – 5.00 (m, 4H), 4.94 (dq, *J* = 8.6, 5.0 Hz, 1H), 4.80 (s, 2H), 4.10 (dd, *J* = 12.0, 3.1 Hz, 1H), 3.86 (dd, *J* = 12.0, 6.9 Hz, 1H), 3.72 – 3.58 (m, 4H), 3.12 – 3.07 (m, 2H), 2.02 (dt, *J* = 7.2, 3.8 Hz, 4H), 1.75 – 1.69 (m, 8H), 1.31 (dq, *J* = 14.8, 5.5 Hz, 4H), 1.02 (dd, *J* = 19.0, 10.6 Hz, 41H), 0.59 (t, *J* = 6.7 Hz, 6H). ^{13}C NMR (126 MHz, MeOD) δ 173.57, 173.22, 164.49, 157.01, 150.02, 134.03, 132.44, 129.59, 129.25, 128.71, 127.33, 121.22, 70.16, 70.09, 65.66, 64.12, 63.29, 62.31, 41.06, 33.79, 33.64, 31.52, 29.35, 29.24, 29.11, 28.92, 28.89, 28.84, 28.77, 28.74, 28.70, 26.79, 26.76, 24.52, 24.46, 22.25, 13.44. ^{31}P NMR (202 MHz, CD_3OD-$CDCl_3$) δ -3.27. MS-ESI $[M+Na]^+$ Calcd for $C_{52}H_{86}NO_{12}P$: 970.5785; Found: 970.5826

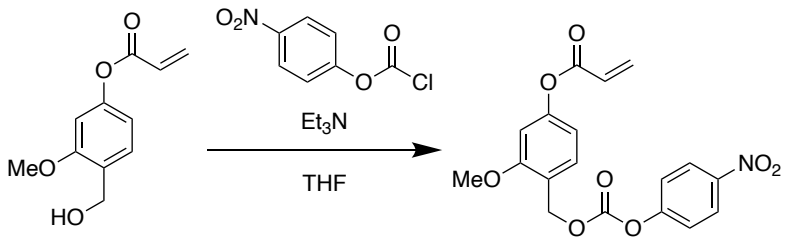


4.1.9b **4.1.10b**

4-(Hydroxymethyl)-3-methoxyphenyl acrylate (4.1.10b)

A solution of potassium carbonate (0.6723 g, 4.8645 mmol, 1.5 eq) in acetone/H_2O (4/1 *v/v*, 25 mL) under Ar was cooled to 0 ° C, after which acryloyl chloride (0.2620 mL, 3.243 mmol, 1 eq) was added. Then, a solution of 4-(hydroxymethyl)-3-methoxyphenol (**4.1.9b**) (0.5 g, 3.243 mmol, 1 eq) dissolved in 5 mL acetone was added dropwise to the reaction mixture over 20 min. The reaction was allowed to stir at rt for 3 hr. After addition of 25 mL brine, the aqueous layer was then extracted with 3 × 25 mL DCM. The combined organic layer was next dried over Na_2SO_4, filtered, and concentrated under reduced pressure. The crude was subjected to silica gel column chromatography using gradient elution from hexanes to 30% EtOAc in hexanes to obtain **4.1.10b** as a clear oil (7.50 mg, 0.3602 mmol, 11% yield). R_f = 0.52 (50:50 EtOAc/Hex).

^{1}H NMR (500 MHz, $CDCl_3$) δ 7.36 (d, *J* = 8.2 Hz, 1H), 6.72 (dd, *J* = 8.2, 2.2 Hz, 1H), 6.67 (d, *J* = 2.2 Hz, 1H), 6.61 (dd, *J* = 17.3, 1.2 Hz, 1H), 6.33 (dd, *J* = 17.3, 10.4 Hz, 1H), 6.05 (dd, *J* = 10.4, 1.2 Hz, 1H), 4.65 (s, 2H), 3.84 (s, 3H). ^{13}C NMR (126 MHz, $CDCl_3$) δ 164.88, 157.74, 150.82, 132.81, 128.74, 127.72, 126.97, 113.07, 104.35, 60.17, 60.15, 55.41.



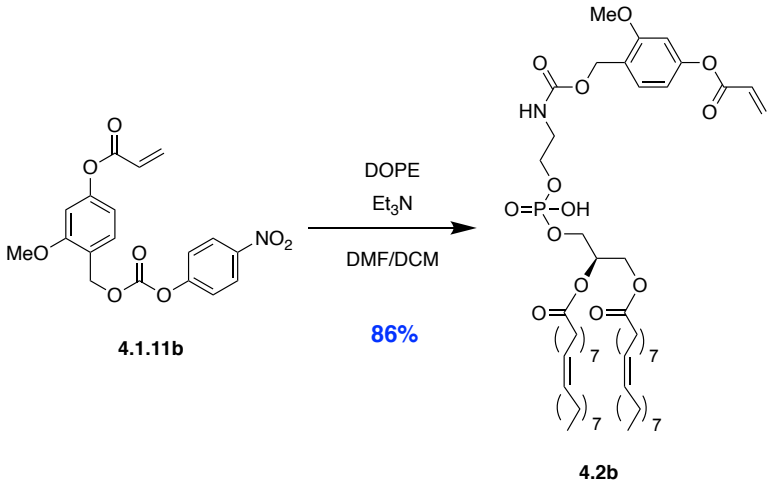
4.1.10b **4.1.11b**

3-Methoxy-4-((((4-nitrophenoxy)carbonyl)oxy)methyl)phenyl acrylate (4.1.11b)

4-(Hydroxymethyl)-3-methoxyphenyl acrylate (**4.1.10b**) (0.0744 g, 0.3573 mmol, 1 eq) was dissolved in 5 mL THF under Ar, and TEA (0.0996 mL, 0.7146 mmol, 2 eq) was added. The reaction was cooled to 0 ° C, after which 4-nitrophenyl chloroformate (0.08642 g, 0.4288 mmol, 1.2 eq) was added slowly. The reaction was allowed to warm up to rt and further stirred overnight. Next, the THF was evaporated, and the residue was dissolved in DCM (20 mL), after which the organic layer was washed with saturated $NaHCO_3$ (5 x 50 mL) and once with 50 mL brine. After being

dried over Na_2SO_4, filtered, and concentrated under reduced pressure, the crude was subjected to silica gel column chromatography using gradient elution from hexanes to 20% EtOAc in hexanes to obtain **4.1.11b** as a clear oil (66.7 mg, 0.1787 mmol, 50% yield). R_f = 0.49 (30:70 EtOAc/Hex).

^{1}H NMR (500 MHz, $CDCl_3$) δ 8.26 (d, *J* = 9.2 Hz, 2H), 7.42 (d, *J* = 8.2 Hz, 1H), 7.39 (d, *J* = 9.2 Hz, 2H), 6.77 (dd, *J* = 8.2, 2.2 Hz, 1H), 6.74 (d, *J* = 2.3 Hz, 1H), 6.62 (d, *J* = 17.4 Hz, 1H), 6.33 (dd, *J* = 17.3, 10.5 Hz, 1H), 6.04 (d, *J* = 11.7 Hz, 1H), 5.34 (s, 2H), 3.87 (s, 3H). ^{13}C NMR (126 MHz, $CDCl_3$) ^{13}C NMR (126 MHz, $CDCl_3$) δ 164.50, 158.79, 155.75, 152.59, 152.55, 145.46, 133.12, 131.31, 127.82, 125.38, 121.89, 120.34, 113.49, 105.07, 66.24, 55.89.

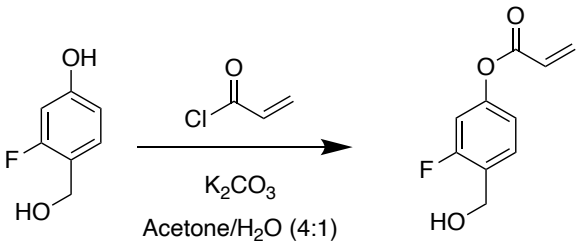


4.1.11b **4.2b**

(2*R*)-3-(((2-((((4-(Acryloyloxy)-2-methoxybenzyl)oxy)carbonyl)amino)ethoxy)(hydroxy) phosphoryl)oxy)propane-1,2-diyl dioleate (4.2b)

3-Methoxy-4-((((4-nitrophenoxy)carbonyl)oxy)methyl)phenyl acrylate (**4.1.11b**) (0.0667 g, 0.1787 mmol, 1.5 eq) and DOPE (88.61 mg, 0.1191 mmol, 1 eq) were combined in a 50 mL RBF under Ar. A mix of 50/50 dry DMF/$CHCl_3$ (6 mL) was used to dissolve the starting materials at 0 ° C. Next, TEA was added into the reaction (0.0498 mL, 0.3573 mmol, 3 eq). The reaction was allowed to warm up to rt and further stirred overnight before being quenched by pouring into 100 mL 0.5 M HCl. The aqueous layer was then extracted with 3 × 25 mL $CHCl_3$. The combined organic layer was next washed with 5 x 50 mL water and 1 x 50 mL brine. After being dried over Na_2SO_4, filtered, and concentrated under reduced pressure, the crude was subjected to silica gel

column chromatography using gradient elution from chloroform to 20% MeOH in $CHCl_3$ to obtain **4.2b** as a white solid (99.7 mg, 0.1019 mmol, 86% yield). R_f = 0.54 (20% MeOH/$CHCl_3$). ^{1}H NMR (500 MHz, 20% CD_3OD-$CDCl_3$) δ 7.34 (d, *J* = 7.9 Hz, 1H), 6.72 (d, *J* = 8.1 Hz, 2H), 6.61 (dd, *J* = 17.3, 1.2 Hz, 1H), 6.34 (dd, *J* = 17.3, 10.4 Hz, 1H), 6.07 (dd, *J* = 10.4, 1.2 Hz, 1H), 5.40 – 5.29 (m, 4H), 5.23 (dq, *J* = 5.5, 2.4 Hz, 1H), 5.13 (s, 2H), 4.39 (dd, *J* = 12.1, 3.1 Hz, 1H), 4.20 – 4.15 (m, 1H), 4.01 – 3.88 (m, 4H), 3.83 (s, 3H), 3.39 (q, *J* = 5.1 Hz, 2H), 2.35 – 2.28 (m, 4H), 2.02 (q, *J* = 6.1 Hz, 8H), 1.60 (h, *J* = 6.4 Hz, 4H), 1.32 (td, *J* = 15.1, 4.8 Hz, 40H), 0.89 (t, *J* = 6.8 Hz, 6H). ^{13}C NMR (126 MHz, MeOD) δ 173.64, 173.29, 164.52, 157.73, 151.19, 132.53, 129.63, 129.30, 129.29, 127.37, 122.19, 112.80, 104.28, 70.17, 70.11, 64.18, 63.32, 62.32, 61.40, 55.12, 41.11, 33.82, 33.67, 31.54, 29.38, 29.36, 29.14, 28.94, 28.92, 28.90, 28.86, 28.80, 28.77, 28.75, 28.73, 26.82, 26.79, 24.54, 24.49, 22.28, 13.48. ^{31}P NMR (202 MHz, CD_3OD-$CDCl_3$) δ -3.34. MS-ESI $[M+Na]^+$ Calcd for $C_{53}H_{88}NO_{13}P$: 1000.5891; Found: 1000.5898



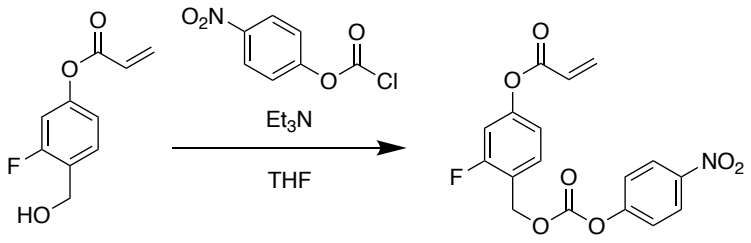
4.1.9c **4.1.10c**

3-Fluoro-4-(hydroxymethyl)phenyl acrylate (4.1.10c)

A solution of potassium carbonate (0.7293 g, 5.277 mmol, 1.5 eq) in acetone/H_2O (4/1 *v/v*, 25 mL) under Ar was cooled to 0 ° C, after which acryloyl chloride (0.2843 mL, 3.518 mmol, 1 eq) was added. Then, a solution of 3-fluoro-4-(hydroxymethyl)phenol (**4.1.9c**) (0.5 g, 3.518 mmol, 1 eq) dissolved in 5 mL acetone was added dropwise to the reaction mixture over 20 min. The reaction was allowed to stir at rt for 3 hr. After addition of 25 mL brine, the aqueous layer was then extracted with 3 × 25 mL DCM. The combined organic layer was next dried over Na_2SO_4, filtered, and concentrated under reduced pressure. The crude was subjected to silica gel column

chromatography using gradient elution from hexanes to 30% EtOAc in hexanes to obtain **4.1.10c** as a clear oil (0.4625 g, 2.3576 mmol, 67% yield). R_f = 0.54 (50:50 EtOAc/Hex).

^{1}H NMR (500 MHz, $CDCl_3$) δ 7.44 (t, *J* = 8.3 Hz, 1H), 6.93 (dd, *J* = 8.4, 2.4 Hz, 1H), 6.88 (dd, *J* = 10.4, 2.4 Hz, 1H), 6.59 (d, *J* = 17.2 Hz, 1H), 6.29 (dd, *J* = 17.4, 10.5 Hz, 1H), 6.03 (d, *J* = 11.7 Hz, 1H), 4.66 (s, 2H). ^{13}C NMR (126 MHz, $CDCl_3$) δ 164.34, 160.95, 158.98, 150.26, 133.03, 129.35, 125.75, 117.06, 117.03, 109.11, 57.51, 48.92, 48.75, 48.58, 48.41, 48.24.

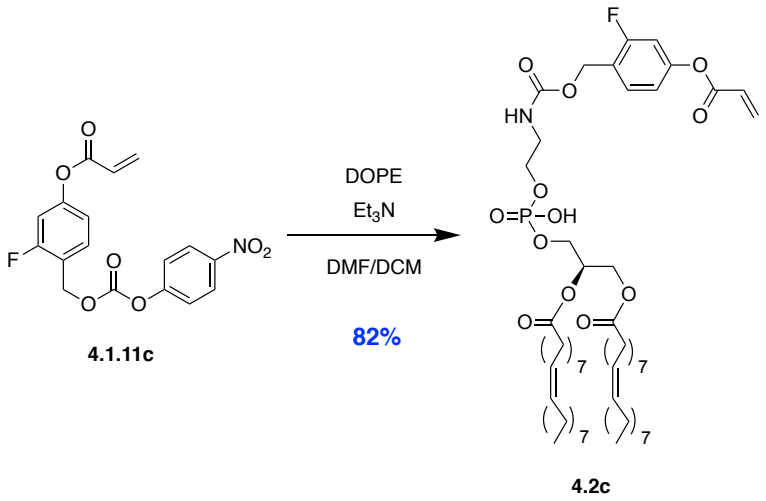


4.1.10c **4.1.11c**

3-Fluoro-4-((((4-nitrophenoxy)carbonyl)oxy)methyl)phenyl acrylate (4.1.11c)

3-Fluoro-4-(hydroxymethyl)phenyl acrylate (**4.1.10c**) (0.4625 g, 2.3576 mmol, 1 eq) was dissolved in 5 mL THF under Ar, and TEA (0.6572 mL, 4.7152 mmol, 2 eq) was added. The reaction was cooled to 0 ° C, after which 4-nitrophenyl chloroformate (0.5702 g, 2.8291 mmol, 1.2 eq) was added slowly. The reaction was allowed to warm up to rt and further stirred overnight. Next, the THF was evaporated, and the residue was dissolved in DCM (20 mL), after which the organic layer was washed with saturated $NaHCO_3$ (5 x 50 mL) and 1 x 50 mL brine. After being dried over Na_2SO_4, filtered, and concentrated under reduced pressure, the crude was subjected to silica gel column chromatography using gradient elution from hexanes to 20% EtOAc in hexanes to obtain **4.1.11c** as a clear oil (0.4201 g, 1.1628 mmol, 49% yield). R_f = 0.45 (30:70 EtOAc/Hex).

^{1}H NMR (500 MHz, $CDCl_3$) δ 8.30 – 8.23 (m, 2H), 7.50 (t, *J* = 8.1 Hz, 1H), 7.42 – 7.35 (m, 2H), 7.04 – 6.98 (m, 2H), 6.62 (d, *J* = 18.6 Hz, 1H), 6.31 (dd, *J* = 17.3, 10.4 Hz, 1H), 6.06 (d, *J* = 10.4 Hz, 1H), 5.35 (s, 2H). ^{13}C NMR (126 MHz, $CDCl_3$) δ 163.85, 162.17, 160.18, 155.47, 152.34, 145.48, 133.49, 131.65, 127.37, 125.31, 121.78, 119.23, 117.77, 109.93, 64.32.



(2*R*)-3-(((2-((((4-(Acryloyloxy)-2-fluorobenzyl)oxy)carbonyl)amino)ethoxy)(hydroxy) phosphoryl)oxy)propane-1,2-diyl dioleate (4.2c)

3-fluoro-4-((((4-Nitrophenoxy)carbonyl)oxy)methyl)phenyl acrylate (**4.1.11c**) (0.04734 g, 0.1310 mmol, 1.5 eq) and DOPE (65 mg, 0.08736 mmol, 1 eq) were combined in a 50 mL RBF under Ar. A mix of 50/50 dry DMF/ $CHCl_3$ (6 mL) was used to dissolve the starting materials at 0 ° C. Next, TEA was added into the reaction (0.03653 mL, 0.2621 mmol, 3 eq). The reaction was allowed to warm up to rt and further stirred overnight before being concentrated under reduced pressure. The crude residue was subjected to silica gel column chromatography using gradient elution from $CHCl_3$ to 20% MeOH in $CHCl_3$ to obtain **4.2c** as a white solid (68.94 mg, 0.07135 mmol, 82% yield). R_f = 0.56 (20% MeOH/$CHCl_3$).

^{1}H NMR (500 MHz, 20% CD_3OD-$CDCl_3$) δ 7.44 (t, *J* = 8.3 Hz, 1H), 6.94 (t, *J* = 8.9 Hz, 1H), 6.70 – 6.49 (m, 2H), 6.31 (dd, *J* = 17.3, 10.5 Hz, 1H), 6.06 (d, *J* = 10.5 Hz, 1H), 5.35 (p, *J* = 5.3 Hz, 4H), 5.21 (s, 1H), 5.13 (d, *J* = 7.9 Hz, 2H), 4.41 – 4.32 (m, 1H), 4.14 (dd, *J* = 12.1, 6.8 Hz, 1H), 4.00 – 3.85 (m, 4H), 3.40 – 3.37 (m, 2H), 2.33 – 2.26 (m, 4H), 2.01 (q, *J* = 6.4 Hz, 8H), 1.59 (t, *J* = 7.7 Hz, 4H), 1.36 – 1.25 (m, 45H), 0.88 (t, *J* = 6.8 Hz, 6H). ^{13}C NMR (126 MHz, MeOD) δ 173.93, 173.59, 164.30, 157.03, 151.49, 133.45, 131.08, 130.14, 129.79, 127.52, 121.60, 117.52, 111.33, 109.77, 103.00, 70.48, 64.66, 63.79, 62.70, 60.28, 41.64, 34.30, 34.15, 32.01, 30.89, 29.86, 29.79, 29.63, 29.41, 29.27, 27.31, 24.97, 22.77, 14.12. ^{31}P NMR (202 MHz, CD_3OD-$CDCl_3$) δ -2.59. ^{19}F NMR (471 MHz, MeOD) δ -115.65. MS-ESI $[M+Na]^+$ Calcd for $C_{52}H_{85}FNO_{12}P$: 988.5691; Found: 988.5688.

Experiment protocols

Preparation of liposomes for nile red release assays

Stock solutions of 5 mM **4.1a**, **4.1b**, **4.2a**, **4.2b**, and **4.2c**, 5 mM Nile Red, 32.46 mM Egg PC, 34.1 mM DPPC, 5 mM PA, and 30 mM DOTAP were prepared in 50:50 $CHCl_3$:MeOH and were stored at −20 °C after preparation. To prepare liposomes, a thin film was created by pipetting the appropriate volumes of the stock solution of each lipid component and NR into a clean vial according to calculations to obtain a mixture of 2 mM of total lipid content with the desired molar percentage of each component. As an example, for 300 µL of 2 mM liposomes composed of 20% **4.1a**, 20% Egg-PC, 50% DOPE, 10% PA, and 5% NR, 24 µL **4.1a** stock (120 nmol), 3.7 µL Egg-PC (120 nmols), 8.9 µL DOPE (300 nmols), and 12 µL PA (60 nmols) and 6 µL NR stock (30 nmol) were combined. A nitrogen stream was then used to evaporate the solvent and the resulting lipid film was subsequently dried for at least 1 hr under vacuum. Then, the lipids were hydrated with 1 × PBS (pH = 7.4) at 60 °C in a water bath for 3 sets of 20 min with vortexing after each set. Liposomes then underwent 10 freeze-thaw cycles between a -80 °C dry ice-acetone bath and a 60 °C water bath, and vortexing was performed at a low speed between each cycle. Last, the liposome solutions were extruded through a 200 nm membrane filter for 15 passes using a LiposoFast extruder (Avestin, Inc.) and were stored at 4 °C for use within 1 day.

Nile red release studies

For fluorescence-based release studies, 100 µL samples of liposome vesicles were added into a sub-micro cuvette cell (Starna Cells, Inc). First, an initial fluorescence scan was obtained (excitation wavelength of 552 nm, emission wavelength scanned from 580 nm to 700 nm, excitation slit = 5 nm, emission slit = 10 nm). For NR release studies with 10 mM Cys or GSH treatments, stock solutions were first created. A 400 mM Cys stock was created by dissolving 242.32 mg Cys in 5 mL 1 x PBS pH 7.4 buffer, and a 400 mM GSH stock was made by dissolving 614.66 mg GSH in 5 mL 1 x PBS pH 7.4 buffer. These solutions then underwent pH adjustment back to pH = 7.4 by addition of saturated sodium hydroxide (NaOH), were aliquoted into Eppendorf tubes, flash frozen in a -80 °C dry ice-acetone bath, stored at −20 °C after preparation,

and used within 5 days. To prepare the liposome treatment solutions containing 10 mM treatment, 2.56 µL of the 400 mM stock solution was then added into 100 µL liposome solution in a cuvette and fluorescence scans were taken on set timescale until a plateau was reached. For samples treated with buffer only, 2.56 µL of 1x PBS pH 7.4 was added to 100 µL liposome samples fluorescence measurements taken as described. Data presented in plots indicate emission intensity values at 635 nm, which were converted into a percentage of initial fluorescence intensity based on the initial scan before adding stimuli. Experiments were run at least 3 times with different batches of liposomes. Averaged data were reported with error bars denoting standard error.

Dynamic light scattering (DLS) analysis of liposome size.

DLS measurements were carried out with a Malvern Zetasizer Nano ZS instrument equipped with a 4.0 mW laser operating at l = 633 nm. Liposome samples were both before and after treatment (10 mM Cys or 10 mM GSH, incubation for 12 hr (**4.1a**) or 5 hr (**4.2a**, **4.2b**) and diluted 10 times with 1 x PBS pH 7.4. All samples were determined at a scattering angle of 173° at 20 °C. The data reported were the average of three tests with error bars indicating standard error.

Thin layer chromatography analysis of thiol-mediated cleavage of free lipids 4.1a, 4.1b, and 4.2a

Free lipid (**4.1a**, **4.1b**, or **4.2a**) was dissolved in 65:25 $CHCl_3$:MeOH at 2 mM. Stock solutions of 40 mM TCEP, GSH, and Cys were prepared in MQ H_2O. For example, to create the 40 mM Cys solution, 10 mg Cys was dissolved in 2.07 mL MQ H_2O. To prepare the lipid treatment samples, 200 µL of 2 mM lipid was prepared in a vial in 65:25 $CHCl_3$ $CHCl_3$:MeOH, and 8 µL of the treatment solution was added to obtain a treatment concentration of 1.5 mM and final solution of 65:25:4 $CHCl_3$:MeOH:H_2O to maintain solubility of both lipid and Cys. Small aliquots were used to prepare TLC plates at 0 min, 5 min, 10 min, 15 min, 20 min, 25 min, 30 min, and 3 hr. These TLC plates were first photographed under a UV lamp and again after staining with $KMnO_4$ and mind heating.

Time-dependent NMR analysis of lipids 4.2a-c after cysteine treatment

First, 2 mM of lipids **4.2a-c** were dissolved in $CDCl_3/CD_3OD/D_2O$=65/25/4 (v/v) in an NMR tube, and an initial scan was taken. Then, a stock solution of 400 mM Cys in D_2O was prepared by dissolving 24.232 mg of Cys in 0.5 mL D_2O, then that solution was diluted to 47 mM Cys in D_2O by combining 11.75 µL of 400 mM stock with 88.25 µL D_2O. Cys solutions were prepared immediately before use. Next, separate samples of 2.09 mM of either **4.2a**, **4.2b**, or **4.2c** were prepared in $CDCl_3/CD_3OD$=65/25 (v/v). For example, 2 mg of **4.2a** was dissolved in 0.938.7 µL $CDCl_3/CD_3OD$=65/25 (v/v) for a concentration of 2.09 mM. To prepare a sample for analysis, 590 µL of 2.09 mM **4.2a-c** in $CDCl_3/CD_3OD$=65/25 (v/v) was added to a clean NMR tube. Then, immediately before acquiring spectra, 24 µL of 47 mM Cys stock solution in D_2O was added to achieve a final concentration of 2 mM of either **4.2a**, **4.2b**, or **4.2c**, 2 mM Cys, and a final solution composition of $CDCl_3/CD_3OD/D_2O$=65/25/4 (v/v). The tube was then inverted to mix, and spectra were then taken over time.

Mass spectrometry analysis of lipids 4.1a-b and 4.2a-c after cysteine treatment

First, 94 µL of a 5 mM stock solution (470 nmols) of **4.1a-b** or **4.2a-c** was dried down in a vial. Then, a stock solution of 23.5 mM Cys in H_2O was prepared by dissolving 14.24 mg of Cys in 5 mL H_2O. Cys solutions were prepared immediately before use. The lipids films were next dissolved in 900 µL of $CHCl_3/CH_3OH$=65/25 (v/v), and 40 µL of the Cys in H_2O was added to achieve a final solution composed of 500 µM lipid **4.1a**, **4.1b**, **4.2a**, **4.2b**, or **4.2c** and 1 mM Cys dissolved in 940 µL of $CHCl_3/CH_3OH/H_2O$=65/25/4 (v/v). The vials were mixed, incubated for 12 hr, and MS spectra were then taken.

Chapter 5. Advances Toward ROS Triggered Artificial Transmembrane Signaling with Synthetic Integral Membrane Proteins

Experiments in Chapter 5 include contributions from Megan L. Qualls and Dr. Michael D. Best. MLQ designed the synthetic routes, synthesized, and characterized all compounds. MLQ and MDB contributed to the design of the transmembrane signaling compounds. MLQ and MDB contributed to the writing of Chapter 5. MDB directed the project.

5.1. Abstract

Communication between cells, responses to external stimuli, and internal cell signaling depend on the complex systems of signal transduction pathways. These pathways are pivotal mechanisms which control cell development and survival. A majority of these pathways require a directed transmission across lipid membranes, typically initiated by an external receptor recognizing a primary messenger, followed by a transduction of the signal inside the cell via release of a secondary messenger. Artificial chemical models can be created to mimic these biological pathways in order to study the basic principles of signal transduction across a membrane. ROS regulate signal transduction pathways that control diverse physiological parameters such as growth factor stimulation response and inflammatory responses. Dysregulated ROS signaling contributes to the development of a multitude of diseases, such as type 2 diabetes mellitus (T2DM), aging, and cancer, and the associated upregulation of ROS results in cellular damage from oxidative stress. Herein, we set out to develop a simple ROS-responsive synthetic system for use in artificial ROS signal transduction. The system was designed to contain (1) an ROS-responsive headgroup, (2) multiple bilayer-spanning self-immolating linkers (SIL), and (3) a cleavage responsive fluorophore. The hydrophobic SIL regions facilitate the insertion of the molecules into liposome bilayers, and the ROS-responsive boronic acid headgroup initiates a self-immolating cascade reaction which was designed to result in the release of a fluorophore inside the vesicle, as evidenced by fluorescence turn-on. In order to vary their bilayer spanning capabilities, multiple signaling compounds (**5.1a-b**) with variable lengths were designed. Synthesis of these compounds proved to be difficult due to an unproductive final step. Advances towards this system will be discussed as well as the synthetic strategies attempted.

5.2. Introduction

Living cells must communicate both internally and with surrounding cells. Communication between cells, internal cell signaling, and internal responses to external stimuli depend on the complex systems of signal transduction pathways. These pathways are pivotal mechanisms which control cell development and survival. In biological systems, lipid bilayer membranes allow cells to form compartments, or spatial separation of different areas of the cell, to allow for physical decoupling of physiological processes on either side of the membrane. These compartmentalization systems are important for maintaining cell homeostasis, such as ion balance, but it is crucial that chemical information be communicated between the two sides of a bilayers via signal transduction pathways.[459]

A majority of these pathways require a directed transmission across lipid membranes, mediated by membrane-spanning proteins. These transmembrane signals are typically initiated by an external receptor recognizing a primary messenger, followed by a transduction of the signal inside the cell via release of a secondary messenger. Two major categories of membrane proteins are G-protein coupled receptors (GPCRs) and receptor tyrosine kinases. GPCRs undergo pivoting conformational changes in the membrane, followed by G-protein association, which initiates a cascade of events resulting in highly efficient energy mobilization.[460, 461] Conversely, receptor tyrosine kinases are typically composed of two receptor units which come together to bind multivalent ligands and form activated dimers, triggering tyrosine phosphorylation on intracellular substrate proteins.[462, 463]

Artificial chemical models can be created to mimic these biological pathways in order to study the basic principles of signal transduction across a membrane and have shown promise for applications in drug delivery,[464] sensing,[465, 466] and disease treatment,[467] Additionally, lipid vesicles are being used to create artificial cells via bottom-up synthetic biology in order to further study the structure and function of living membranes.[166, 468, 469] Molecular systems have been developed that utilize synthetic systems which mimic biological signaling pathways, but with simplified mechanisms that don't exist in biological systems.[470, 471] For example, Clayden and co-

workers reported a system that mimics GPCR signal transduction.[472] Biological GPCRs are comprised of seven transmembrane helices and undergo conformational changes in the membrane in response to a selective ligand binding at an extracellular site, producing changes through the bilayer to the cytosolic terminus which initiate signaling cascades.[473-475] The GPCR synthetic mimic consisted of a bilayer spanning helical foldamer core ligated to a metal-centered binding site on one end, and on the opposite end was a conformationally responsive pyrene fluorophore. Upon external ligand (Boc-L-Pro or Boc-D-Pro) binding, the foldamer's conformation was perturbed, resulting in changes in fluorescence, thereby mimicking the conformational change of GPCRs in response to ligand binding. Similarly, Schrader and co-workers reported a synthetic system which also facilitated messenger-induced transmembrane signaling.[476] Upon addition of the external primary messenger diethylenetriamine (DET), the transmembrane units bearing tryptophan–dansyl (Trp–Dan) donor–acceptor fluorescence resonance energy transfer (FRET) pairs came together to form a heterodimeric complex, engaging FRET signal on the inside of the vesicle membrane.

Apart from conformational change and dimerization, another signaling method is controlled membrane translocation, which has been developed to transport molecular transducers from one side of a lipid bilayer membrane to the other.[477, 478] These synthetic transducers are typically non-membrane spanning and are composed of a sensing head and a reactive tail. A chemical reaction involving the sensor head group with the target stimulus such as pH,[477, 479] light,[480] or small molecules ethylenediaminetetraacetic acid (EDTA),[478] or GSH,[481] results in a change in physiochemical properties (i.e. hydrophobicity), and the transducer can then undergo translocation from the exterior side of the bilayer to the interior side. Then, the reactive tail, which is typically a pro-catalyst, undergoes activation by metal ion complexation and is then able to hydrolyze an encapsulated intra-vesicular non-fluorescent substrate to form a fluorescent product. The fluorescence signal produced from this reaction is the signaling event and represents the intra-vesicular response of the signal transduction pathway. Although these three methods of artificial signaling are promising, additional work is needed to expand the target

stimulus as well as development of additional signaling method types beyond conformational change, dimerization, and translocation.

Another promising stimulus target for an artificial signaling platform is ROS. ROS regulate signal transduction pathways that control diverse physiological parameters such as growth factor stimulation response and inflammatory responses.[482, 483] Dysregulated ROS signaling may contribute to the development of a multitude of diseases such as T2DM, heart disease, aging, and cancer, and the associated upregulation of ROS in disease states results in cellular damage from oxidative stress.[483-488] Specifically, cancer cells have been shown to contain elevated ROS concentrations ~2 orders of magnitude greater than those in normal cells (~100 μM compared to ~20 nM).[489] Indeed, it is a promising endeavor to develop a synthetic signaling system in which the target stimulus is ROS. The system could potentially be used to study both ROS signaling and sensing via the second messenger in order to help understand and alleviate dysregulated ROS signaling in biological systems.

Herein, we set out to develop a simple ROS-responsive synthetic system for use in artificial ROS signal transduction. The system was designed to contain (1) an ROS-responsive headgroup, (2) multiple bilayer-spanning self-immolating linkers (SIL), and (3) a cleavage responsive fluorophore. The hydrophobic SIL regions facilitate the insertion of the molecules into liposome bilayers, and the ROS-responsive boronic acid headgroup is designed to initiate a self-immolating cascade reaction which results in the release of a fluorophore inside the vesicle, as evidenced by fluorescence turn-on. In order to vary their bilayer spanning capabilities, multiple signaling compounds (**5.1a-b**) with variable lengths were designed. Synthesis of these compounds proved to be difficult due to an unproductive final step. Advances towards this system will be discussed as well as the synthetic strategy attempted.

5.3. Design and synthesis of ROS triggered synthetic integral membrane proteins

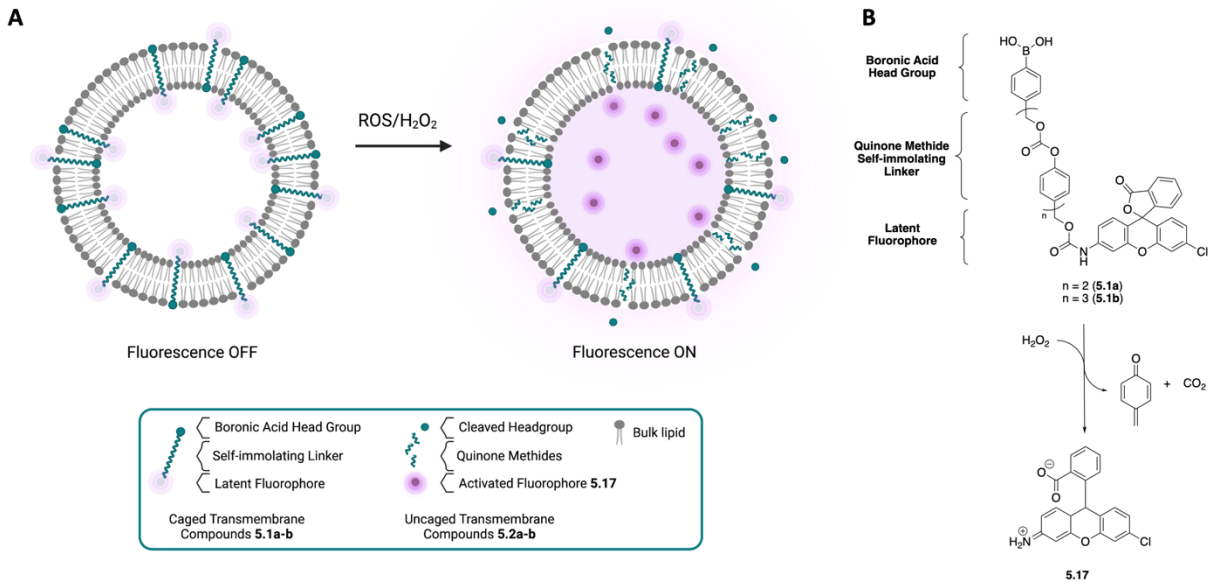
As shown in Scheme 5.1A, the system was designed to include an ROS-responsive hydrophilic headgroup, multiple hydrophobic quinone methide-generating SILs, and a cleavage-responsive

latent chloro-rhodamine (ClR) fluorophore (**5.1a-b**). The hydrophobic SIL regions facilitate the insertion of the molecules into liposome bilayer, and the ROS-responsive boronic acid headgroup is available on the vesicle surface. Upon ROS addition, a self-immolating cascade reaction is initiated, which is designed to result in the release of the fluorophore **5.17** inside the vesicle, as evidenced by internal fluorescence turn-on (Scheme 5.1B). This ClR fluorophore was chosen because it had previously been shown to need only one reactive site caged to control fluorescence, was colorless and non-fluorescence when caged (latent), was insensitive to pH changes, and hydrolysis of the amide bond between fluorophore and scaffold results in a highly fluorescent compound (**5.17**) due to a change in its spiral structure.[490] The design of the full signaling cascade is shown in Scheme 5.2. Upon ROS (H_2O_2) treatment, the boronic acid group of **5.1a-b** is expected to be cleaved, which produces a phenoxide anion (**5.2a-b**) that initiates the self-immolation cascade reaction including quinone methide formation and final release of linker, CO_2, and fluorophore **5.16**. After undergoing spiral-ring opening, highly fluorescent **5.17** is formed.

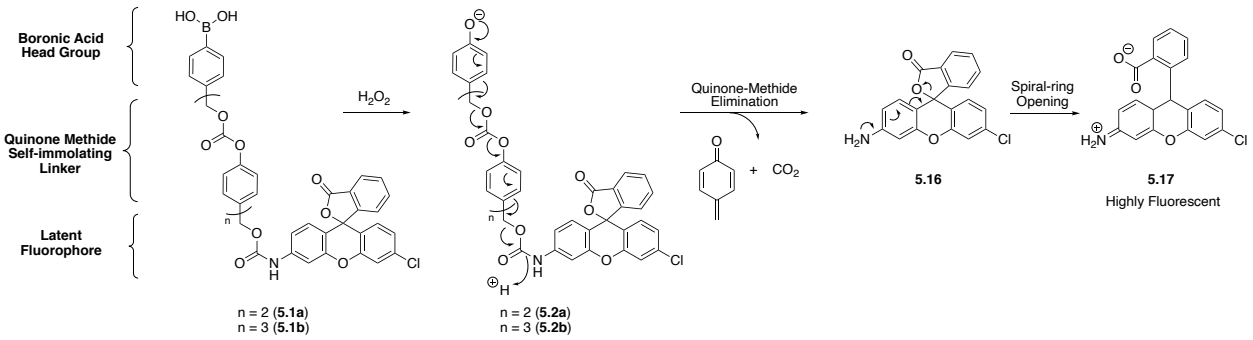
In order to vary their bilayer spanning capabilities, multiple signaling compounds with variable lengths were designed including n = 2 SIL units (**5.1a**) and n = 3 SIL units (**5.1b**) (Figure 5.1). These lengths were chosen in order to increase the likelihood of the transduction compound being capable of spanning the bilayer membrane. The liposomal membrane is composed largely of commercially available phospholipids, which contain a hydrophilic headgroup and FA tail that is typically 10 - 20 carbons long with varying degrees of unsaturation. The average overall tail length is n_c x l_{cc} where n_c is the number of carbon atoms in the chain and l_{cc} is the average carbon-carbon bond length projected on a hydrocarbon chain (l_{cc}=0.126 nm).[491] The length and saturation of the tail greatly influences the bilayer thickness, and bilayers composed of common single-type mono-unsaturated tail phospholipids have been found to have the following membrane hydrophobic thicknesses: ~2.2 nm for 1,2-dimyristoleoyl-*sn*-glycero-3-phosphocholine (DMCP, C=14), ~3.6 nm for 1,2-dioleoyl-*sn*-glycero-3-phosphocholine (DOPC, C=18), ~4.5 nm for 1,2-dierucoyl-*sn*-glycero-3-phosphocholine (C=22), and ~5 nm for 1,2-dihexacosenoyl-*sn*-glycero-3-phosphocholine (C=26).[492] It was found that the designed compounds showed approximate

molecular lengths of ~3.9 nm (**5.1a**) and ~4.9 nm (**5.1b**) (Figure 5.1A), and the compounds were similar to the hydrophobic thickness of a lipid bilayer membrane composed of DMPC (~2.2 nm) or DOPC (~3.6 nm). However, the lipid bilayer could be tuned with longer or shorter acyl chain length PC lipids in order to improve incorporation of compounds **5.1a-b**. The optimized structures according to the Corey–Pauling–Koltun (CPK) model are shown in Figure 5.1B.

The preliminary synthesis strategy for accessing transmembrane signaling molecules **5.1a-b** is shown in Scheme 5.3. To begin, 4-(hydroxymethyl)phenol (**5.2**) was protected with *tert*-butyldimethylsilyl chloride (TBDMS-Cl) to form **5.3**. The phenol of **5.3** was reacted with 4-nitrophenyl chloroformate to form the activated carbonate SIL **5.4**. In the original synthetic route, **5.4** was to be reacted with 4-(hydroxymethyl)phenylboronic acid pinacol ester to append the boronate head group and form **5.5**, however the polarity of **5.4** and **5.5** were nearly identical, making purification impossible. To resolve this issue, compound **5.3** instead underwent triphosgene coupling with 4-(hydroxymethyl)phenylboronic acid pinacol ester to form **5.5**. Next, the TBDMS ether of **5.5** was deprotected with *p*-toluenesulfonic acid (*p*-TsOH) to form **5.6**. Then, the primary alcohol of **5.6** was reacted with **5.4** in order to attach a second SIL and form **5.7**, which then again underwent silyl ether deprotection with *p*-TsOH to form **5.8**. To achieve a compounds with 3 SILs, **5.8** was reacted again with **5.4** to form **5.9**, and then was subsequently silyl deprotected with *p*-TsOH to make **5.10**, which contained a boronate head, three SILs, and a free hydroxyl. Design of the steps to access **5.1a-b** is shown in Scheme 5.4A. Compounds **5.8** and **5.10** were designed to undergo triphosgene coupling with fluorophore **5.16** to form **5.11,** or **5.12**, respectively. Synthesis of compounds proved to be unproductive. If synthesis of **5.11,** or **5.12** had been successful, citric acid was to be used to deprotect the boronate and form the final products, which would have possessed a boronic acid headgroup, two (**5.1a**) or three (**5.1b**) SILs, and latent fluorophore. Formation of fluorophore **5.16** is shown in Scheme 5.4B and involved the reaction of 3-aminophenol (**5.13**), 3-chlorophenol (**5.15**), phthalic anhydride (**5.13**) in methanesulfonic acid (MsOH) as previously described.[490]



Scheme 5.1 Design of ROS-responsive artificial signal transduction system. (A) The system (**5.1a-b**) includes ROS-responsive, hydrophilic boronic acid headgroup, multiple hydrophobic quinone methide-generating self-immolating linkers (SILs), and a cleavage-responsive latent ClR fluorophore. The hydrophobic SIL regions facilitate the insertion of the molecules into liposome bilayer, and the ROS-responsive boronic acid headgroup is available on the vesicle surface. Upon ROS addition, oxidation is designed to initiate a self-immolating cascade reaction, which results in the release of the fluorophore inside the vesicle, as evidenced by internal fluorescence turn-on. (B) Chemical structures of **5.1a-b** before and after ROS (H_2O_2) treatment and formation of highly fluorescent **5.17**.



Scheme 5.2 Design of the full signaling cascade of compounds 5.1a-b. Upon ROS (H_2O_2) addition, the boronic acid group of **5.1a-b** is cleaved, which is designed to produce a phenoxide anion (**5.2a-b**), initiating the self-immolation cascade reaction. Following the SIL cascade reaction is the release of quinone methide linker, CO_2, and fluorophore **5.16**. After undergoing spiral-ring opening, highly fluorescent **5.17** is formed.

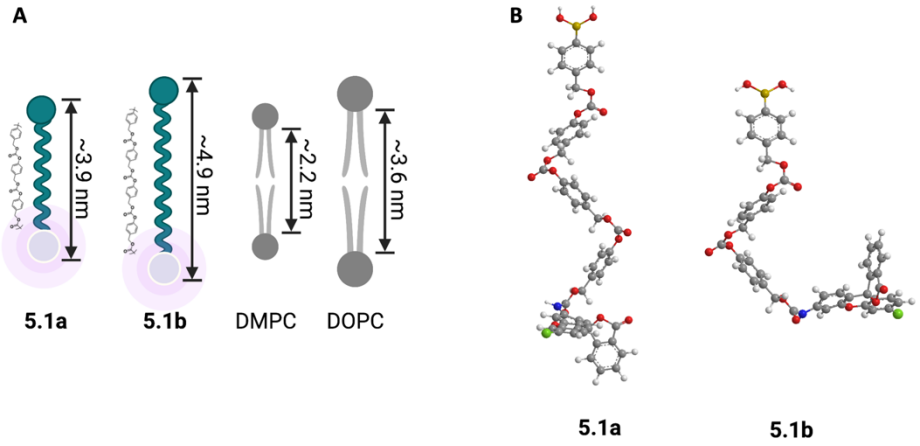
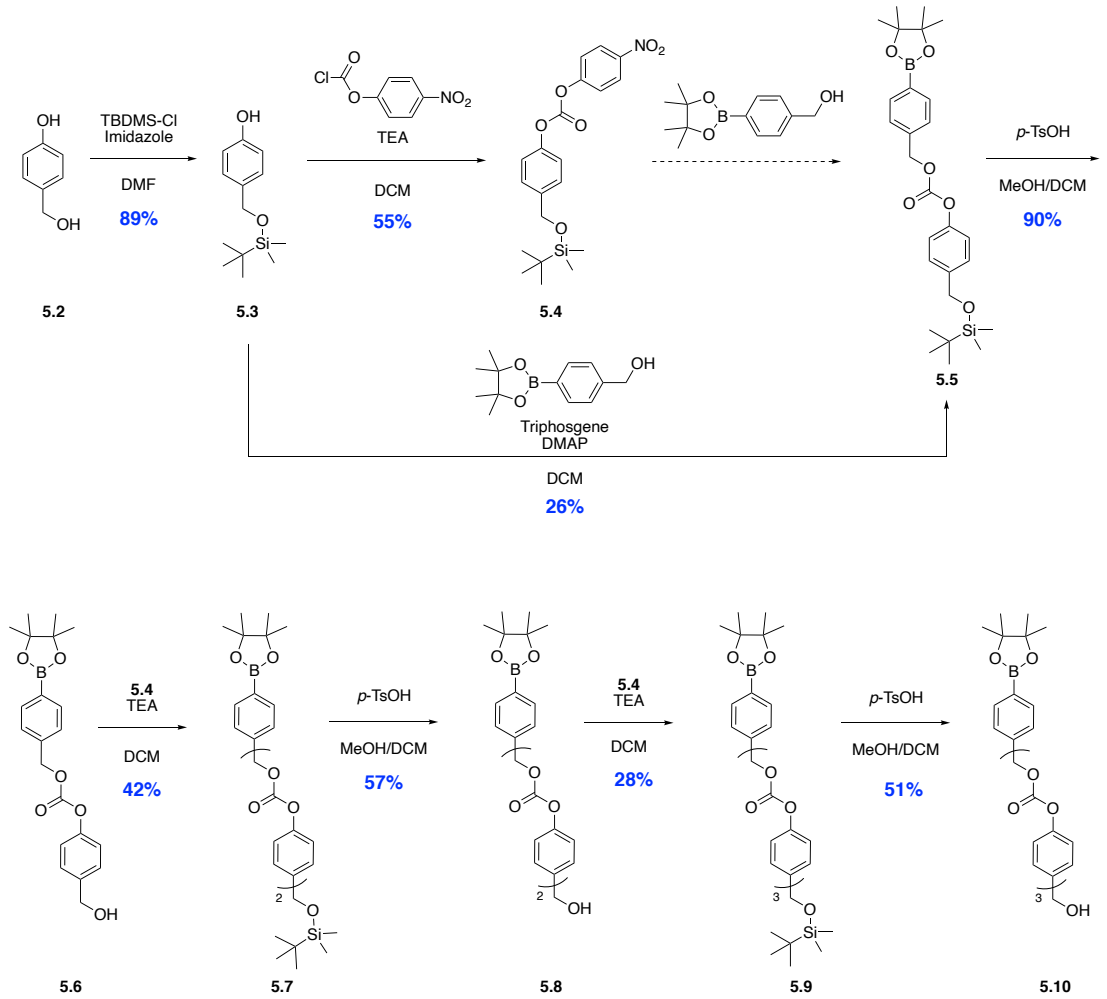
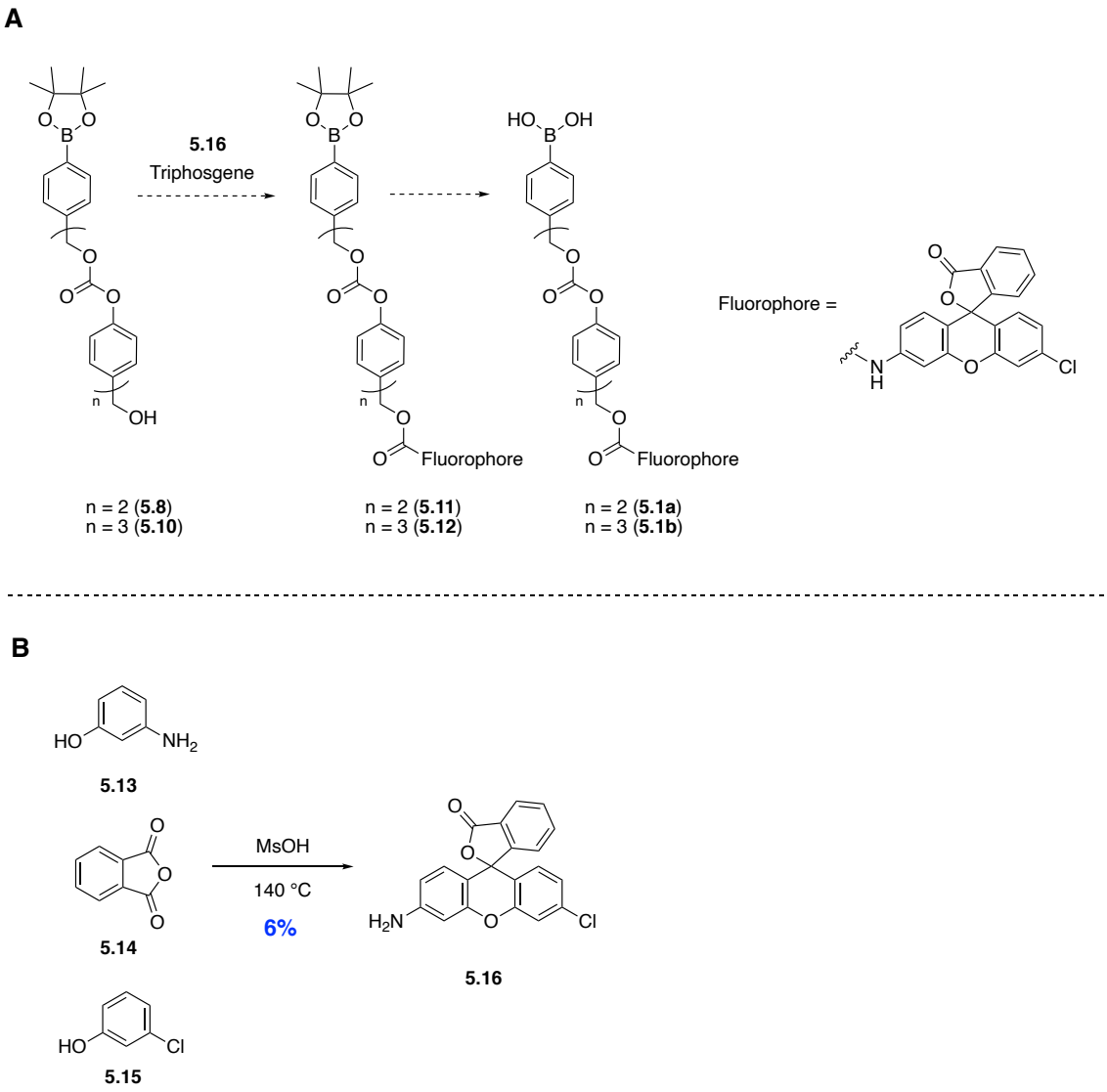


Figure 5.1 Design of lipid bilayer spanning compounds 5.1a-b. (A) Cartoon illustration of transducers which show molecular lengths of ~3.9 nm (**5.1a**) and ~4.9 nm (**5.1b**) compared to the hydrophobic thickness of DMPC (~2.2 nm) and DOPC (~3.6 nm). (B) The optimized structures of transducers. Here the white, gray, blue, yellow, green, and red balls represent H, C, N, B, Cl and O atoms, respectively. The molecules are shown in the CPK model.



Scheme 5.3 Synthetic scheme for accessing transmembrane signaling molecules 5.8 and 5.10. First, 4-(hydroxymethyl)phenol (**5.2**) was protected with TBDMS-Cl to form **5.3**, which was then activated with 4-nitrophenyl chloroformate to form **5.4**. Originally, **5.4** was to be reacted with 4-(hydroxymethyl)phenylboronic acid pinacol ester to form **5.5**, but difficult purification led to an alternative route in which **5.3** underwent triphosgene coupling with 4-(hydroxymethyl)phenylboronic acid pinacol ester to form **5.5**. Next, the TBDMS ether of **5.5** was deprotected with *p*-TsOH to form **5.6**, followed by reaction with **5.4** to attach a second SIL and form **5.7**, which then again underwent silyl ether deprotection with *p*-TsOH to form **5.8**. To achieve a compound with 3 SILs, **5.8** was reacted again with **5.4** to form **5.9**, and then was subsequently silyl deprotected with *p*-TsOH to make **5.10**, which bared a boronate head, three SILs, and a free hydroxyl.



Scheme 5.4 Synthetic design of signaling molecules 5.1a and 5.1b. (A) Compounds **5.8** and **5.10** were designed to undergo triphosgene coupling with fluorophore **5.16** to form **5.11** and **5.12**, respectively, which proved unproductive. Further plans involved citric acid for deprotection of the boronate to form the final products, which would have possessed a boronic acid headgroup, two (**5.1a**) or three (**5.1b**) SILs, and latent fluorophore. (B) Formation of fluorophore **5.16** involved the reaction of 3-aminophenol (**5.13**), 3-chlorophenol (**5.15**), phthalic anhydride (**5.13**) in MsOH as previously described.[490]

5.4. Conclusions

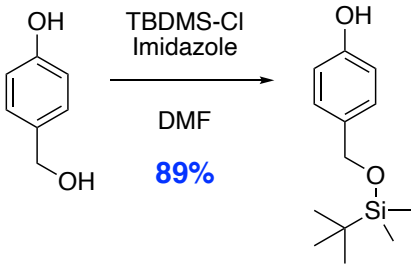
In conclusion, we designed an ROS-responsive synthetic system for use in artificial ROS signal transduction. Synthetic signal transduction compounds **5.1a-b** were designed and initial progress towards their formation was completed. Signaling molecules **5.1a-b** were designed to contain three major units including an ROS-responsive headgroup, either two (**5.1a**) or three (**5.1b**) bilayer-spanning self-immolating linkers, and a cleavage-responsive fluorophore. Although synthesis of these compounds proved to be difficult due to an unproductive second-to-last step, advances towards this system include platform design and synthesis of precursors. Additional work is being undertaken to complete the synthesis of **5.1a-b**, after which fluorescence microscopy will be used to assess ROS-responsive signaling and fluorescence turn-on within the liposome, as well as liposome morphology studies via DLS and TEM. While it has not been widely studied in transmembrane signaling research, it is a worthwhile endeavor to develop a synthetic signaling system in which the target stimulus is ROS considering how dysregulated ROS signaling can contribute to the development of a multitude of diseases. We envision that the system could potentially be used to study both ROS signaling and sensing via the second messenger in order to help understand and alleviate dysregulated ROS signaling in biological systems, and that the system could be adapted to other biological targets to further advance artificial signaling research.

5.5. Synthesis and experimental procedure

General experimental

Reagents and solvents were generally purchased from Sigma-Aldrich or Fisher Scientific and used as received. Dry solvents were obtained from a Pure Solv MD-7 solvent delivery system purchased from Innovative Technologies, Inc. Column chromatography was performed using 230 – 400 mesh silica gel purchased from Sorbent Technologies (Norcross, GA). NMR spectra were obtained using a Varian 500 MHz spectrometer. Mass spectra were obtained with JEOL DART-AccuTOF and Waters Synapt G2-Si mass spectrometers (Milford, MA). Small quantities (<5 mg) were weighed on a Mettler Toledo XS105 dual range analytical balance.

Synthesis

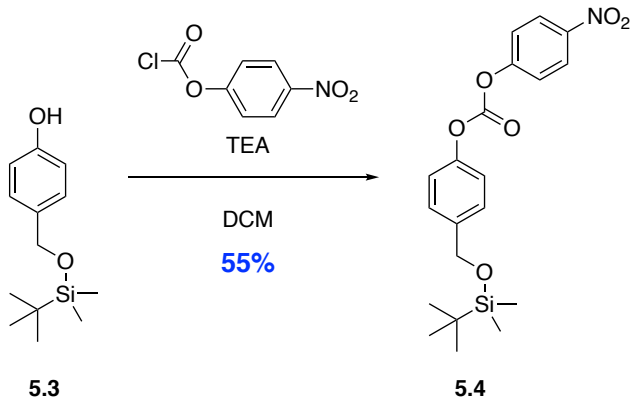


5.2 **5.3**

4-(((*tert*-Butyldimethylsilyl)oxy)methyl)phenol (5.3)

4-(Hydroxymethyl)phenol (0.5 g, 4.028 mmol, 1 eq) in DMF (40 mL) under Ar was cooled to 0 °C, after which Imidazole (0.329 g, 4.833 mmol, 1.2 eq) and *tert*-butylchlorodimethylsilane (0.7285 g, x 4.833 mmol, x 1.2 eq) were added. The reaction was allowed to stir at rt for 1.5 hr. After addition of 25 mL anhydrous ether, the organic layer was then washed saturated with ammonium chloride (25mL) and brine (25 mL). The combined organic layer was next dried over Na_2SO_4, filtered, and concentrated under reduced pressure. The crude was subjected to silica gel column chromatography using gradient elution from hexanes to 25% EtOAc in hexanes to obtain **5.3** as a yellow oil (0.8559 g, 3.59 mmol, 89 % yield). R_f = 0.55 (25:75 EtOAc/Hex).

^{1}H NMR (500 MHz, $CDCl_3$) (δ 7.19 (d, *J* = 8.7 Hz, 2H), 6.78 (d, *J* = 8.6 Hz, 2H), 5.23 (s, 1H), 4.67 (s, 2H), 0.94 (s, 9H), 0.10 (s, 6H). ^{13}C NMR (126 MHz, $CDCl_3$) δ 154.80, 133.62, 127.98, 115.24, 64.95, 26.12, 18.59, -5.02.

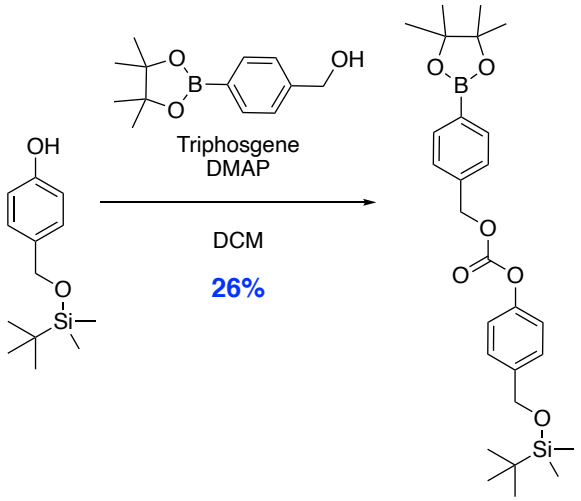


5.3 **5.4**

4-(((*tert*-Butyldimethylsilyl)oxy)methyl)phenyl (4-nitrophenyl) carbonate (5.4)

4-(((*tert*-Butyldimethylsilyl)oxy)methyl)phenol (**5.3**) (0.5 g, 2.0973 mmol, 1 eq) was dissolved in DCM under Ar. After TEA (1.46 mL, 10.4865 mmol, 5 eq) addition, 4-nitrophenyl chloroformate (1.2982 g, 6.2919 mmol, 3 eq) was added slowly and the reaction was stirred overnight at rt The reaction was diluted in DCM (30 mL), after which the organic layer was washed with 1 M HCl (1 x 25 mL) and once with 25 mL brine. After being dried over Na_2SO_4, filtered, and concentrated under reduced pressure, the crude was subjected to silica gel column chromatography using gradient elution from 30% DCM in hexanes to 70% DCM in hexanes to obtain **5.4** as a white powder (0.4656 g, 1.154 mmol, 55% yield). R_f = 0.75 (10:90 Hex/DCM).

^{1}H NMR (500 MHz, $CDCl_3$) δ 8.35 – 8.28 (m, 2H), 7.49 (d, *J* = 9.3 Hz, 2H), 7.39 (d, *J* = 8.9 Hz, 2H), 7.24 (d, *J* = 8.7 Hz, 2H), 4.76 (s, 2H), 0.95 (s, 10H), 0.11 (s, 6H). ^{13}C NMR (126 MHz, $cdcl_3$) δ 155.46, 151.26, 149.65, 145.74, 140.25, 127.35, 125.54, 121.88, 120.58, 64.38, 26.07, 18.53, -5.14.



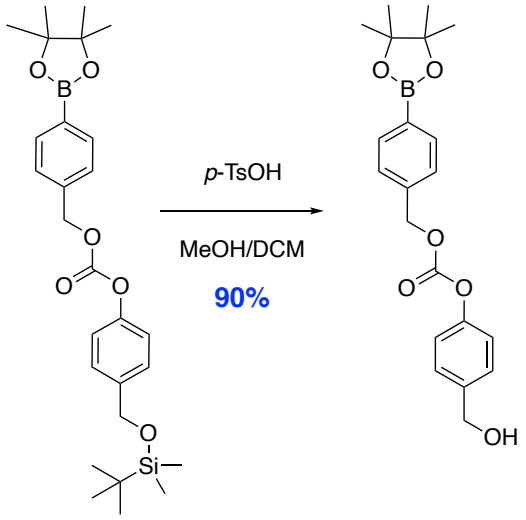
5.3 **5.5**

4-(((*tert*-Butyldimethylsilyl)oxy)methyl)phenyl (4-(4,4,5,5-tetramethyl-1,3,2-dioxaborolan-2-yl)benzyl) carbonate (5.5)

4-(((*tert*-Butyldimethylsilyl)oxy)methyl)phenol (**5.3**) (2 g, 8.39 mmol, 1 eq) was dissolved in DCM (40 mL) under Ar, then 4-dimethylaminopyridine (DMAP) (4.1 g, 33.56mmol, 4 eq) was added to the solution. The reaction was cooled to 0 ° C, after which triphosgene (0.9959 g, 3.356 mmol, 0.4 eq) was added. The reaction stirred at rt for 20 min. In a separate flask under Ar, 4-

(hydroxymethyl)phenylboronic acid pinacol ester (5.892 g, 25.17 mmol, 3 eq) was dissolved in DCM (40 mL), then this solution was added dropwise to the original reaction vessel over 20 min. The reaction was run overnight, after which it was diluted in DCM (30 mL), and the organic layer was washed with water (3 x 25 mL) and brine (1 x 25 mL). Next, the crude was dried over Na_2SO_4, filtered, and concentrated under reduced pressure, and was then subjected to silica gel column chromatography using gradient elution from hexanes to 10% EtOAc in hexanes to obtain **5.5** as a white solid (1.0749 g, 2.1563 mmol, 26% yield). R_f = 0.40 (10:90 Hex/DCM).

^{1}H NMR (500 MHz, $CDCl_3$) δ 7.84 (d, *J* = 8.2 Hz, 2H), 7.43 (d, *J* = 8.3 Hz, 2H), 7.32 (d, *J* = 8.8 Hz, 2H), 7.13 (d, *J* = 8.7 Hz, 2H), 5.28 (s, 2H), 4.72 (s, 2H), 1.35 (s, 12H), 0.94 (s, 9H), 0.09 (s, 6H). ^{13}C NMR (126 MHz, $CDCl_3$) δ 153.86, 150.12, 139.46, 137.89, 135.25, 127.62, 127.16, 120.88, 84.07, 70.25, 64.49, 26.08, 25.02, 18.54, -5.13. ^{11}B NMR (160 MHz, $cdcl_3$) δ 30.82.



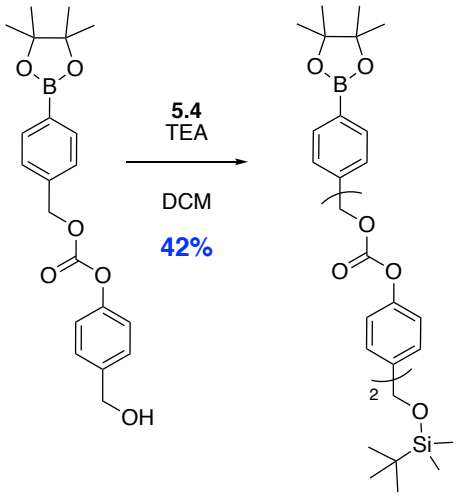
5.5 **5.6**

4-(Hydroxymethyl)phenyl (4-(4,4,5,5-tetramethyl-1,3,2-dioxaborolan-2-yl)benzyl) carbonate (5.6)

4-(((*tert*-Butyldimethylsilyl)oxy)methyl)phenyl (4-(4,4,5,5-tetramethyl-1,3,2-dioxaborolan-2-yl)benzyl) carbonate (**5.5**) (1.0749 g, 2.1563 mmol, 1 eq) was dissolved in DCM/MeOH (1/1 *v/v*, 20 mL) under Ar. Next, *p*-TsOH (0.03713 g, 0.21563 mmol, 0.1 eq) was added and the reaction was stirred for 1 hr and monitored by TLC. The reaction was then diluted in EtOAc (50 mL), and

the organic layer was washed with saturated $NaHCO_3$ (1 x 20 mL), dried over Na_2SO_4, filtered, and concentrated under reduced pressure. Finally, the crude was subjected to silica gel column chromatography using gradient elution from hexanes to 35% EtOAc in hexanes to obtain **5.6** as a white solid (0.7452 g, 0.7452 mmol, 90% yield). R_f = 0.40 (50:50 EtOAc/Hex).

^{1}H NMR (500 MHz, $CDCl_3$) δ 7.84 (d, *J* = 7.7 Hz, 2H), 7.43 (d, *J* = 7.6 Hz, 2H), 7.37 (d, *J* = 8.2 Hz, 2H), 7.16 (d, *J* = 8.6 Hz, 2H), 5.28 (s, 2H), 4.68 (s, 2H), 1.35 (s, 12H). ^{13}C NMR (126 MHz, $CDCl_3$) δ 153.76, 150.64, 138.89, 137.80, 135.25, 128.21, 127.63, 121.28, 84.08, 70.33, 64.81, 25.00. ^{11}B NMR (160 MHz, cdcl$_3$) δ 30.72.

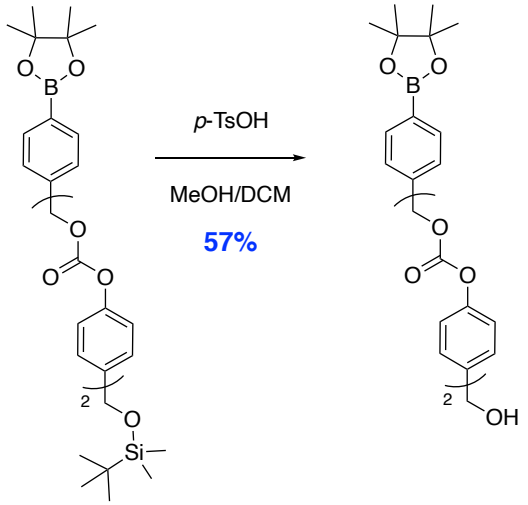


5.6 **5.7**

4-((((4-(((*tert*-Butyldimethylsilyl)oxy)methyl)phenoxy)carbonyl)oxy)methyl)phenyl (4-(4,4,5,5-tetramethyl-1,3,2-dioxaborolan-2-yl)benzyl) carbonate (5.7)

First, 4-(hydroxymethyl)phenyl (4-(4,4,5,5-tetramethyl-1,3,2-dioxaborolan-2-yl)benzyl) carbonate (**5.6**) (0.6808 g, 2.395 mmol, 1.12 eq) was dissolved in DCM (20 mL) under Ar, followed by addition of TEA (1.335 mL, 9.58 mmol, 4 eq) and 4-(((*tert*-butyldimethylsilyl)oxy)methyl)phenyl (4-nitrophenyl) carbonate (**5.4**) (0.863 g, 2.1388 mmol, 1 eq). The reaction was allowed to stir at rt overnight. Next, the reaction was then diluted in DCM (20 mL) and the organic layer was washed with water (3 x 25 mL), brine (1 x 25 mL), dried over Na_2SO_4, filtered, and concentrated under reduced pressure. The crude was then subjected to

silica gel column chromatography using gradient elution from hexanes to 10% EtOAc in hexanes to obtain **5.7** as a white solid (0.5827 g, 0.8984 mmol, 42% yield). R_f = 0.70 (25:75 EtOAc/Hex). ^{1}H NMR (500 MHz, cdcl$_3$) δ 7.86 (d, *J* = 8.2 Hz, 2H), 7.46 (t, *J* = 8.4 Hz, 4H), 7.34 (d, *J* = 8.8 Hz, 2H), 7.22 (d, *J* = 8.6 Hz, 2H), 7.15 (d, *J* = 8.7 Hz, 2H), 5.30 (s, 2H), 5.25 (s, 2H), 4.74 (s, 2H), 1.36 (s, 12H), 0.95 (s, 9H), 0.11 (s, 6H). ^{13}C NMR (126 MHz, cdcl$_3$) δ 153.79, 153.54, 151.45, 150.04, 139.46, 137.70, 135.24, 132.81, 129.99, 127.63, 127.14, 121.44, 120.84, 115.17, 84.04, 70.37, 69.58, 64.45, 26.05, 24.98, 18.50, -5.15.



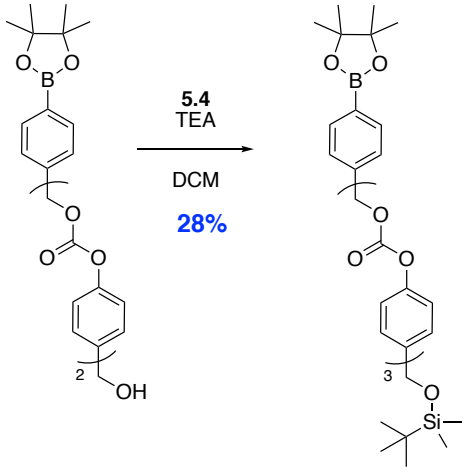
4-((((4-(Hydroxymethyl)phenoxy)carbonyl)oxy)methyl)phenyl (4-(4,4,5,5-tetramethyl-1,3,2-dioxaborolan-2-yl)benzyl) carbonate (5.8)

4-((((4-(((*tert*-Butyldimethylsilyl)oxy)methyl)phenoxy)carbonyl)oxy)methyl)phenyl (4-(4,4,5,5-tetramethyl-1,3,2-dioxaborolan-2-yl)benzyl) carbonate (**5.7**) (0.5827 g, 0.8984 mmol, 1 eq) was dissolved in DCM/MeOH (1/1 *v/v*, 20 mL) under Ar. Next, *p*-TsOH (0.01547 g, 0.08984 mmol, 0.1 eq) was added and the reaction was stirred for 1 hr and monitored by TLC. The reaction was then diluted in EtOAc (20 mL), and the organic layer was washed with saturated $NaHCO_3$ (1 x 20 mL), dried over Na_2SO_4, filtered, and concentrated under reduced pressure. Finally, the crude was subjected to silica gel column chromatography using gradient elution from hexanes to 30% EtOAc

in hexanes to obtain **5.8** as a white solid (0.2715 g, 0.5081 mmol, 57% yield). R_f = 0.45 (50:50 EtOAc/Hex).

^{1}H NMR (500 MHz, cdcl$_3$) δ 7.87 – 7.81 (m, 2H), 7.45 (dd, *J* = 11.4, 8.5 Hz, 4H), 7.38 (d, *J* = 7.6 Hz, 2H), 7.19 (dd, *J* = 21.4, 8.7 Hz, 6H), 5.29 (s, 2H), 5.25 (s, 2H), 4.70 (s, 2H), 1.35 (s, 12H).

^{13}C NMR (126 MHz, cdcl$_3$) δ 153.74, 153.57, 151.51, 150.62, 138.92, 137.71, 135.27, 132.75, 130.05, 128.24, 127.67, 121.50, 121.28, 84.09, 70.44, 69.71, 64.84, 25.01. ^{11}B NMR (160 MHz, cdcl$_3$) δ 30.73.

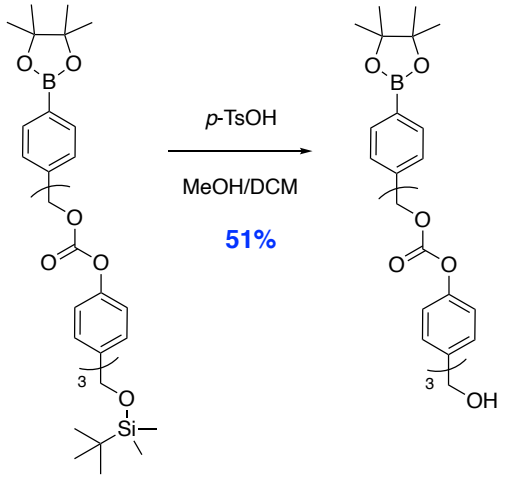


5.8 **5.9**

4-((((4-((((4-(((*tert*-Butyldimethylsilyl)oxy)methyl)phenoxy)carbonyl)oxy)methyl)phenoxy)carbonyl)oxy)methyl)phenyl (4-(4,4,5,5-tetramethyl-1,3,2-dioxaborolan-2-yl)benzyl) carbonate (5.9)

First, 4-((((4-(hydroxymethyl)phenoxy)carbonyl)oxy)methyl)phenyl (4-(4,4,5,5-tetramethyl-1,3,2-dioxaborolan-2-yl)benzyl) carbonate (**5.8**) (0.220 g, 0.4117 mmol, 1.2 eq) was dissolved in DCM (10 mL) under Ar, followed by addition of TEA (0.1913 mL, 1.3724 mmol, 4 eq) and 4-(((*tert*-butyldimethylsilyl)oxy)methyl)phenyl (4-nitrophenyl) carbonate (**5.4**) (0.13844 g, 0.3431 mmol, 1 eq). The reaction was allowed to stir at rt overnight. Next, the reaction was then diluted in DCM (20 mL) and the organic layer was washed with water (3 x 25 mL), brine (1 x 25 mL), dried over Na_2SO_4, filtered, and concentrated under reduced pressure. The crude was then subjected to

silica gel column chromatography using gradient elution from hexanes to 10% EtOAc in hexanes to obtain **5.9** as a white solid (0.5827 g, 0.8984 mmol, 42% yield). R_f = 0.40 (25:75 EtOAc/Hex). ^{1}H NMR (500 MHz, $CDCl_3$) δ 7.84 (d, *J* = 8.1 Hz, 2H), 7.45 (dd, *J* = 12.6, 8.3 Hz, 6H), 7.33 (d, *J* = 8.5 Hz, 2H), 7.21 (dd, *J* = 8.6, 2.8 Hz, 4H), 7.13 (d, *J* = 8.5 Hz, 2H), 5.29 (s, 2H), 5.25 (d, *J* = 5.2 Hz, 4H), 4.72 (s, 2H), 1.35 (s, 12H), 0.94 (s, 9H), 0.10 (d, *J* = 1.4 Hz, 6H). ^{13}C NMR (126 MHz, $CDCl_3$) δ 153.83, 153.57, 153.54, 151.53, 151.43, 150.07, 139.48, 137.71, 135.26, 132.88, 132.68, 130.04, 130.00, 127.64, 127.18, 121.49, 121.44, 120.84, 115.69, 84.09, 70.43, 69.77, 69.60, 64.48, 29.82, 26.06, 24.99, 18.52, -5.15. ^{11}B NMR (160 MHz, $CDCl_3$) δ 30.62.



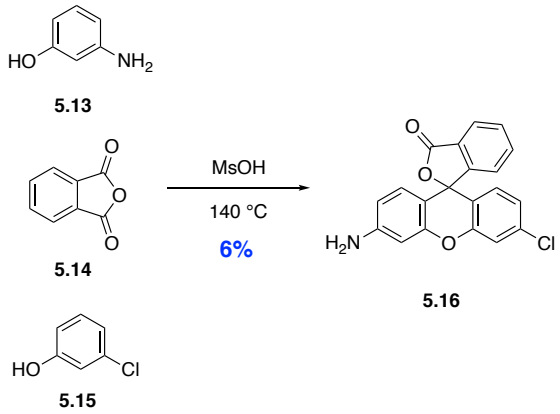
5.9 **5.10**

4-((((4-((((4-(Hydroxymethyl)phenoxy)carbonyl)oxy)methyl)phenoxy)carbonyl)oxy)methyl)phenyl (4-(4,4,5,5-tetramethyl-1,3,2-dioxaborolan-2-yl)benzyl) carbonate (5.10)

4-((((4-((((4-(((*tert*-Butyldimethylsilyl)oxy)methyl)phenoxy)carbonyl)oxy)methyl)phenoxy)carbonyl)oxy)methyl)phenyl (4-(4,4,5,5-tetramethyl-1,3,2-dioxaborolan-2-yl)benzyl) carbonate (**5.9**) (0.0910 g, 0.11393 mmol, 1 eq) was dissolved in DCM/MeOH (1/1 *v/v*, 20 mL) under Ar. Next, *p*-TsOH (0.001962 g, 0.011393 mmol, 0.1 eq) was added and the reaction was stirred for 1 hr and monitored by TLC. The reaction was then diluted in EtOAc (20 mL), and the organic layer was washed with saturated $NaHCO_3$ (3 x 20 mL), brine (1 x 25 mL), dried over Na_2SO_4, filtered, and concentrated under

reduced pressure. Finally, the crude was subjected to silica gel column chromatography using gradient elution from hexanes to 30% EtOAc in hexanes to obtain **5.10** as a white solid (0.2715 g, 0.5081 mmol, 57% yield). R_f = 0.43 (50:50 EtOAc/Hex).

^{1}H NMR (500 MHz, $CDCl_3$) δ 7.85 (d, *J* = 7.5 Hz, 2H), 7.45 (dd, *J* = 11.8, 7.9 Hz, 6H), 7.37 (d, *J* = 8.1 Hz, 2H), 7.21 (d, *J* = 8.1 Hz, 4H), 7.16 (d, *J* = 8.1 Hz, 2H), 5.29 (s, 2H), 5.25 (d, *J* = 3.6 Hz, 4H), 4.68 (s, 2H), 1.35 (s, 12H). ^{13}C NMR (126 MHz, $CDCl_3$) δ 153.73, 153.56, 153.53, 151.54, 151.46, 150.60, 138.95, 137.70, 135.26, 132.81, 132.67, 130.05, 130.03, 128.97, 128.21, 127.65, 121.50, 121.46, 121.24, 84.09, 70.43, 69.79, 69.68, 64.77, 25.00. ^{11}B NMR (160 MHz, $CDCl_3$) δ 31.33.



3'-Amino-6'-chloro-3*H*-spiro[isobenzofuran-1,9'-xanthen]-3-one (5.16)

3-Aminophenol (0.5457 g, 5 mmol, 1 eq), 3-chlorophenol (0.6428 g, 5 mmol, 1 eq), and phthalic anhydride (0.7405 g, 5 mmol, 1 eq) were dissolved in MsOH (10 mL) at rt The reaction was refluxed at 140 ° C for 40 hr. After cooling to rt, the reaction was poured over 300 g of ice cubes. The mixture was neutralized with 10% NaOH, and the aqueous layer was then extracted with DCM 3 × 50 mL. The combined organic layers were washed with 10% NaOH (3 x 50 mL), dried over Na_2SO_4, filtered, and concentrated under reduced pressure. Finally, the crude was subjected to silica gel column chromatography using gradient elution from hexanes to 30% EtOAc in hexanes to obtain **5.16** as an orange solid (0.0995 g, 0.2845 mmol, 6% yield). R_f = 0.43 (50:50 EtOAc/Hex).

^{1}H NMR (500 MHz, $CDCl_3$) δ 8.00 (d, *J* = 7.6 Hz, 1H), 7.68 – 7.63 (m, 1H), 7.60 (t, *J* = 7.4 Hz, 1H), 7.26 (s, 1H), 7.14 (d, *J* = 7.6 Hz, 1H), 6.96 (dd, *J* = 8.4, 2.1 Hz, 1H), 6.70 (d, *J* = 8.5 Hz, 1H), 6.56 –

6.47 (m, 2H), 6.34 (dd, *J* = 8.6, 2.3 Hz, 1H). ^{13}C NMR (126 MHz, $CDCl_3$) δ 171.27, 169.49, 153.01, 152.28, 152.00, 149.21, 135.99, 135.20, 129.92, 129.30, 129.20, 126.78, 125.21, 124.03, 118.15, 117.37, 112.18, 108.25, 101.49, 83.24.

References

1. Olzmann, J. A.; Carvalho, P., Dynamics and functions of lipid droplets. *Nat. Rev. Mol. Cell Biol.* **2019,** *20* (3), 137-155.
2. Marsh, D., Thermodynamics of phospholipid self-assembly. *Biophys. J.* **2012,** *102* (5), 1079-1087.
3. Glass Christopher, K.; Jerrold, O.; Inflammation, M., Lipid Signaling in the Etiology of Insulin Resistance. *Cell Metab.* **2012,** *15*, 635-645.
4. Wang, J.; Yu, C.; Zhuang, J.; Qi, W.; Jiang, J.; Liu, X.; Zhao, W.; Cao, Y.; Wu, H.; Qi, J., The role of phosphatidylserine on the membrane in immunity and blood coagulation. *Biomark. Res.* **2022,** *10* (1), 1-23.
5. Storck, E. M.; Özbalci, C.; Eggert, U. S., Lipid cell biology: a focus on lipids in cell division. *Annu. Rev. Biochem* **2018,** *87*, 839-869.
6. Huijbregts, R. P.; Topalof, L.; Bankaitis, V. A., Lipid metabolism and regulation of membrane trafficking. *Traffic* **2000,** *1* (3), 195-202.
7. Hiller-Sturmhöfel, S.; Bartke, A., The endocrine system: an overview. *Alcohol Res.* **1998,** *22* (3), 153.
8. Zampelas, A.; Magriplis, E., New insights into cholesterol functions: a friend or an enemy? MDPI: 2019; Vol. 11, p 1645.
9. Wang, J.; Chen, Y.-L.; Li, Y.-K.; Chen, D.-K.; He, J.-F.; Yao, N., Functions of Sphingolipids in Pathogenesis During Host–Pathogen Interactions. *Front. Microbiol.* **2021,** *12*, 701041.
10. Harayama, T.; Riezman, H., Understanding the diversity of membrane lipid composition. *Nat. Rev. Mol. Cell Biol.* **2018,** *19* (5), 281-296.
11. Gunstone, F. D., *Fatty Acid and Lipid Chemistry*. Springer: 1996.
12. Yamashita, A.; Hayashi, Y.; Nemoto-Sasaki, Y.; Ito, M.; Oka, S.; Tanikawa, T.; Waku, K.; Sugiura, T., Acyltransferases and transacylases that determine the fatty acid composition of glycerolipids and the metabolism of bioactive lipid mediators in mammalian cells and model organisms. *Prog. Lipid Res.* **2014,** *53*, 18-81.
13. Tanguy, E.; Wang, Q.; Moine, H.; Vitale, N., Phosphatidic acid: from pleiotropic functions to neuronal pathology. *Front. Cell. Neurosci.* **2019,** *13*, 2.
14. Small, D. M., *The Physical Chemistry of Lipids: From Alkanes to Phospholipids*. Springer: 1986; Vol. 4, p 1-672.
15. Calzada, E.; Onguka, O.; Claypool, S. M., Phosphatidylethanolamine metabolism in health and disease. *Int. Rev. Cell Mol. Biol.* **2016,** *321*, 29-88.
16. Svennerholm, L., Distribution and fatty acid composition of phosphoglycerides in normal human brain. *J. Lipid Res.* **1968,** *9* (5), 570-579.
17. Kim, H.-Y.; Huang, B. X.; Spector, A. A., Phosphatidylserine in the brain: metabolism and function. *Prog. Lipid Res.* **2014,** *56*, 1-18.
18. Leventis, P. A.; Grinstein, S., The distribution and function of phosphatidylserine in cellular membranes. *Annu. Rev. Biophys.* **2010,** *39*, 407-427.
19. Nie, J.; Hao, X.; Chen, D.; Han, X.; Chang, Z.; Shi, Y., A novel function of the human CLS1 in phosphatidylglycerol synthesis and remodeling. *Biochim. Biophys. Acta. Mol. Cell. Biol. Lipids* **2010,** *1801* (4), 438-445.

20. Batrouni, A. G.; Baskin, J. M., The chemistry and biology of phosphatidylinositol 4-phosphate at the plasma membrane. *Biorg. Med. Chem.* **2021,** *40*, 116190.
21. Šegota, S., Spontaneous formation of vesicles. *Adv. Colloid Interface Sci.* **2006,** *121* (1-3), 51-75.
22. Israelachvili, J. N.; Mitchell, D. J.; Ninham, B. W., Theory of self-assembly of hydrocarbon amphiphiles into micelles and bilayers. *Journal of the Chemical Society, Faraday Transactions 2: Molecular and Chemical Physics* **1976,** *72*, 1525-1568.
23. Bangham, A. D.; Horne, R., Negative staining of phospholipids and their structural modification by surface-active agents as observed in the electron microscope. *J. Mol. Biol.* **1964,** *8* (5), 660-IN10.
24. Horne, R.; Bangham, A.; Whittaker, V., Negatively stained lipoprotein membranes. *Nature* **1963,** *200* (4913), 1340-1340.
25. Marsh, D., *Handbook of lipid bilayers*. CRC press: 2013.
26. De Gier, J.; Mandersloot, J.; Van Deenen, L., Lipid composition and permeability of liposomes. *Biochim. Biophys. Acta, Biomembr.* **1968,** *150* (4), 666-675.
27. Blok, M.; Van der Neut-Kok, E.; Van Deenen, L.; De Gier, J., The effect of chain length and lipid phase transitions on the selective permeability properties of liposomes. *Biochim. Biophys. Acta, Biomembr.* **1975,** *406* (2), 187-196.
28. Kranenburg, M.; Smit, B., Phase behavior of model lipid bilayers. *J. Phys. Chem. B* **2005,** *109* (14), 6553-6563.
29. Israelachvili, J. N., Van der Waals forces in biological systems. *Q. Rev. Biophys.* **1973,** *6* (4), 341-387.
30. van Swaay, D.; DeMello, A., Microfluidic methods for forming liposomes. *Lab on a Chip* **2013,** *13* (5), 752-767.
31. Bangham, A.; De Gier, J.; Greville, G., Osmotic properties and water permeability of phospholipid liquid crystals. *Chem. Phys. Lipids* **1967,** *1* (3), 225-246.
32. Dua, J.; Rana, A.; Bhandari, A., Liposome: methods of preparation and applications. *Int. J. Pharm. Stud. Res.* **2012,** *3* (2), 14-20.
33. Saunders, L.; Perrin, J.; Gammack, D., Ultrasonic irradiation of some phospholipid sols. *J. Pharm. Pharmacol.* **1962,** *14* (1), 567-572.
34. Torchilin, V. P.; Torchilin, V.; Weissig, V., *Liposomes: a practical approach*. Oxford University Press: 2003.
35. Mendez, R.; Banerjee, S., Sonication-based basic protocol for liposome synthesis. *Methods Mol. Biol.* **2017**, 255-260.
36. Olson, F.; Hunt, C.; Szoka, F.; Vail, W.; Papahadjopoulos, D., Preparation of liposomes of defined size distribution by extrusion through polycarbonate membranes. *Biochim. Biophys. Acta, Biomembr.* **1979,** *557* (1), 9-23.
37. Schneider, T.; Sachse, A.; Röβling, G.; Brandl, M., Generation of contrast-carrying liposomes of defined size with a new continuous high pressure extrusion method. *Int. J. Pharm.* **1995,** *117* (1), 1-12.
38. Ong, S. G. M.; Chitneni, M.; Lee, K. S.; Ming, L. C.; Yuen, K. H., Evaluation of extrusion technique for nanosizing liposomes. *Pharmaceutics* **2016,** *8* (4), 36.

39. Lombardo, D.; Kiselev, M. A., Methods of liposomes preparation: formation and control factors of versatile nanocarriers for biomedical and nanomedicine application. *Pharmaceutics* **2022,** *14* (3), 543.
40. Batzri, S.; Korn, E. D., Single bilayer liposomes prepared without sonication. *Biochim. Biophys. Acta, Biomembr.* **1973,** *298* (4), 1015-1019.
41. Charcosset, C.; Juban, A.; Valour, J.-P.; Urbaniak, S.; Fessi, H., Preparation of liposomes at large scale using the ethanol injection method: Effect of scale-up and injection devices. *Chem. Eng. Res. Des.* **2015,** *94*, 508-515.
42. Justo, O. R.; Moraes, Â. M., Analysis of process parameters on the characteristics of liposomes prepared by ethanol injection with a view to process scale-up: Effect of temperature and batch volume. *Chem. Eng. Res. Des.* **2011,** *89* (6), 785-792.
43. Gouda, A.; Sakr, O. S.; Nasr, M.; Sammour, O., Ethanol injection technique for liposomes formulation: An insight into development, influencing factors, challenges and applications. *J. Drug. Deliv. Sci. Techno.* **2021,** *61*, 102174.
44. Shaker, S.; Gardouh, A. R.; Ghorab, M. M., Factors affecting liposomes particle size prepared by ethanol injection method. *Res. Pharm. Sci.* **2017,** *12* (5), 346.
45. Woodle, M. C.; Papahadjopoulos, D., Liposome preparation and size characterization. *Meth. Enzymol.* **1989,** *171*, 193-217.
46. Kanásová, M.; Nesměrák, K., Systematic review of liposomes' characterization methods. *Monatsh. Chem.* **2017,** *148*, 1581-1593.
47. Edwards, K. A.; Baeumner, A. J., Analysis of liposomes. *Talanta* **2006,** *68* (5), 1432-1441.
48. Helvig, S.; Azmi, I. D.; Moghimi, S. M.; Yaghmur, A., Recent advances in cryo-TEM imaging of soft lipid nanoparticles. *AIMS Biophys.* **2015,** *2* (2), 116-130.
49. Almgren, M.; Edwards, K.; Karlsson, G., Cryo transmission electron microscopy of liposomes and related structures. *Colloids Surf., A* **2000,** *174* (1-2), 3-21.
50. Di Cola, E.; Grillo, I.; Ristori, S., Small angle X-ray and neutron scattering: powerful tools for studying the structure of drug-loaded liposomes. *Pharmaceutics* **2016,** *8* (2), 10.
51. Lombardo, D.; Calandra, P.; Kiselev, M. A., Structural characterization of biomaterials by means of small angle X-rays and neutron scattering (SAXS and SANS), and light scattering experiments. *Molecules* **2020,** *25* (23), 5624.
52. Kinnun, J. J.; Scott, H. L.; Ashkar, R.; Katsaras, J., Biomembrane structure and material properties studied with neutron scattering. *Front. Chem.* **2021,** *9*, 642851.
53. Zorec, B.; Préat, V.; Miklavčič, D.; Pavšelj, N., Active enhancement methods for intra-and transdermal drug delivery: a review. *Slov. Med. J.* **2013,** *82* (5).
54. Sultana, A.; Zare, M.; Thomas, V.; Kumar, T. S.; Ramakrishna, S., Nano-based drug delivery systems: Conventional drug delivery routes, recent developments and future prospects. *Med. Drug Discv.* **2022**, 100134.
55. Mitchell, M. J.; Billingsley, M. M.; Haley, R. M.; Wechsler, M. E.; Peppas, N. A.; Langer, R., Engineering precision nanoparticles for drug delivery. *Nat. Rev. Drug Discov.* **2021,** *20* (2), 101-124.
56. Zhang, X.-y.; Zhang, P.-y., Polymersomes in nanomedicine-A review. *Curr. Nanosci.* **2017,** *13* (2), 124-129.
57. Wang, J.; Li, B.; Qiu, L.; Qiao, X.; Yang, H., Dendrimer-based drug delivery systems: history, challenges, and latest developments. *J. Biol. Eng.* **2022,** *16* (1), 1-12.

58. Perumal, S.; Atchudan, R.; Lee, W., A review of polymeric micelles and their applications. *Polymers* **2022,** *14* (12), 2510.
59. Guterres, S. S.; Alves, M. P.; Pohlmann, A. R., Polymeric nanoparticles, nanospheres and nanocapsules, for cutaneous applications. *Drug Target Insights* **2007,** *2*, 117739280700200002.
60. Valcourt, D. M.; Dang, M. N.; Scully, M. A.; Day, E. S., Nanoparticle-mediated co-delivery of Notch-1 antibodies and ABT-737 as a potent treatment strategy for triple-negative breast cancer. *ACS Nano* **2020,** *14* (3), 3378-3388.
61. Anselmo, A. C.; Mitragotri, S., Nanoparticles in the clinic: An update. *Bioeng. Transl. Med.* **2019,** *4* (3), e10143.
62. Li, X.; Zhang, Y.; Liu, G.; Zhou, L.; Xue, Y.; Liu, M., Recent progress in the applications of gold-based nanoparticles towards tumor-targeted imaging and therapy. *RSC Adv.* **2022,** *12* (13), 7635-7651.
63. Attia, N. F.; Abd El-Monaem, E. M.; El-Aqapa, H. G.; Elashery, S. E.; Eltaweil, A. S.; El Kady, M.; Khalifa, S. A.; Hawash, H. B.; El-Seedi, H. R., Iron oxide nanoparticles and their pharmaceutical applications. *Appl. Surf. Sci.* **2022,** *11*, 100284.
64. Devi, S.; Kumar, M.; Tiwari, A.; Tiwari, V.; Kaushik, D.; Verma, R.; Bhatt, S.; Sahoo, B. M.; Bhattacharya, T.; Alshehri, S., Quantum dots: An emerging approach for cancer therapy. *Front. Mater.* **2022,** *8*, 585.
65. Ahmadi, F.; Sodagar-Taleghani, A.; Ebrahimnejad, P.; Moghaddam, S. P. H.; Ebrahimnejad, F.; Asare-Addo, K.; Nokhodchi, A., A review on the latest developments of mesoporous silica nanoparticles as a promising platform for diagnosis and treatment of cancer. *Int. J. Pharm.* **2022**, 122099.
66. Debnath, S. K.; Srivastava, R., Drug delivery with carbon-based nanomaterials as versatile nanocarriers: progress and prospects. *Front. Nanosci.* **2021,** *3*, 644564.
67. Huang, K.-W.; Hsu, F.-F.; Qiu, J. T.; Chern, G.-J.; Lee, Y.-A.; Chang, C.-C.; Huang, Y.-T.; Sung, Y.-C.; Chiang, C.-C.; Huang, R.-L., Highly efficient and tumor-selective nanoparticles for dual-targeted immunogene therapy against cancer. *Sci. Adv.* **2020,** *6* (3), eaax5032.
68. Xu, C.; Nam, J.; Hong, H.; Xu, Y.; Moon, J. J., Positron emission tomography-guided photodynamic therapy with biodegradable mesoporous silica nanoparticles for personalized cancer immunotherapy. *ACS Nano* **2019,** *13* (10), 12148-12161.
69. Shi, Z.; Zhou, Y.; Fan, T.; Lin, Y.; Zhang, H.; Mei, L., Inorganic nano-carriers based smart drug delivery systems for tumor therapy. *Smart Mater. Med.* **2020,** *1*, 32-47.
70. Wang, J.; Potocny, A. M.; Rosenthal, J.; Day, E. S., Gold nanoshell-linear tetrapyrrole conjugates for near infrared-activated dual photodynamic and photothermal therapies. *ACS Omega* **2019,** *5* (1), 926-940.
71. Yang, W.; Liang, H.; Ma, S.; Wang, D.; Huang, J., Gold nanoparticle based photothermal therapy: Development and application for effective cancer treatment. *Sustain. Mater. Technol.* **2019,** *22*, e00109.
72. Sibuyi, N. R. S.; Moabelo, K. L.; Fadaka, A. O.; Meyer, S.; Onani, M. O.; Madiehe, A. M.; Meyer, M., Multifunctional gold nanoparticles for improved diagnostic and therapeutic applications: a review. *Nanoscale Res. Lett.* **2021,** *16*, 1-27.

73. Arias, L. S.; Pessan, J. P.; Vieira, A. P. M.; Lima, T. M. T. d.; Delbem, A. C. B.; Monteiro, D. R., Iron oxide nanoparticles for biomedical applications: A perspective on synthesis, drugs, antimicrobial activity, and toxicity. *Antibiotics* **2018,** *7* (2), 46.
74. Manshian, B. B.; Jiménez, J.; Himmelreich, U.; Soenen, S. J., Personalized medicine and follow-up of therapeutic delivery through exploitation of quantum dot toxicity. *Biomaterials* **2017,** *127*, 1-12.
75. Sercombe, L.; Veerati, T.; Moheimani, F.; Wu, S. Y.; Sood, A. K.; Hua, S., Advances and challenges of liposome assisted drug delivery. *Front. Pharmacol.* **2015,** *6*, 286.
76. Dhaval, M.; Vaghela, P.; Patel, K.; Sojitra, K.; Patel, M.; Patel, S.; Dudhat, K.; Shah, S.; Manek, R.; Parmar, R., Lipid-based emulsion drug delivery systems—a comprehensive review. *Drug Deliv. Transl. Res.* **2022**, 1-24.
77. Xu, L.; Wang, X.; Liu, Y.; Yang, G.; Falconer, R. J.; Zhao, C.-X., Lipid nanoparticles for drug delivery. *Adv. Biomed. Res.* **2022,** *2* (2), 2100109.
78. Fenton, O. S.; Olafson, K. N.; Pillai, P. S.; Mitchell, M. J.; Langer, R., Advances in biomaterials for drug delivery. *Adv. Mater.* **2018,** *30* (29), 1705328.
79. Leung, A. K.; Tam, Y. Y. C.; Chen, S.; Hafez, I. M.; Cullis, P. R., Microfluidic mixing: a general method for encapsulating macromolecules in lipid nanoparticle systems. *J. Phys. Chem. B.* **2015,** *119* (28), 8698-8706.
80. Cheng, X.; Lee, R. J., The role of helper lipids in lipid nanoparticles (LNPs) designed for oligonucleotide delivery. *Adv. Drug Deliv. Rev.* **2016,** *99*, 129-137.
81. Kulkarni, J. A.; Witzigmann, D.; Leung, J.; Tam, Y. Y. C.; Cullis, P. R., On the role of helper lipids in lipid nanoparticle formulations of siRNA. *Nanoscale* **2019,** *11* (45), 21733-21739.
82. Li, Y.; Tenchov, R.; Smoot, J.; Liu, C.; Watkins, S.; Zhou, Q., A comprehensive review of the global efforts on COVID-19 vaccine development. *ACS Cent. Sci.* **2021,** *7* (4), 512-533.
83. Cross, R., Without these lipid shells, there would be no mRNA vaccines for COVID-19. *Chem. Eng. News.* **2021,** *99* (8), 144.
84. Emergency Use Authorization (Eua) of the Pfizer-Biontech Covid-19 Vaccine to Prevent Coronavirus Disease 2019 (COVID-19) in Individuals 16 Years of Age and Older. https://www.fda.gov/media/144414/download (accessed 2-26-2023).
85. Emergency Use Authorization (Eua) of the Moderna Covid-19 Vaccine to Prevent Coronavirus Disease 2019 (Covid-19) in Individuals 18 Years of Age and Older. https://www.fda.gov/media/144638/download (accessed 2-26-2023).
86. Pfizer-Biontech Covid-19 Vaccine- BNT162b2 Injection, Suspension. https://dailymed.nlm.nih.gov/dailymed/drugInfo.cfm?setid=908ecbe7-2f1b-42dd-94bf-f917ec3c5af8 (accessed 2-26-2023).
87. DeFrancesco, L., Whither COVID-19 vaccines? *Nat. Biotechnol.* **2020,** *38* (10), 1132-1145.
88. Sabnis, S.; Kumarasinghe, E. S.; Salerno, T.; Mihai, C.; Ketova, T.; Senn, J. J.; Lynn, A.; Bulychev, A.; McFadyen, I.; Chan, J., A novel amino lipid series for mRNA delivery: improved endosomal escape and sustained pharmacology and safety in non-human primates. *Mol. Ther.* **2018,** *26* (6), 1509-1519.
89. Yanez Arteta, M.; Kjellman, T.; Bartesaghi, S.; Wallin, S.; Wu, X.; Kvist, A. J.; Dabkowska, A.; Székely, N.; Radulescu, A.; Bergenholtz, J., Successful reprogramming of cellular protein production through mRNA delivered by functionalized lipid nanoparticles. *Proc. Natl. Acad. Sci.* **2018,** *115* (15), E3351-E3360.

90. Vaccines and Related Biological Products Advisory Committee Meeting. Moderna COVID-19 Vaccine, FDA Briefing Document.
91. Schoenmaker, L.; Witzigmann, D.; Kulkarni, J. A.; Verbeke, R.; Kersten, G.; Jiskoot, W.; Crommelin, D. J., mRNA-lipid nanoparticle COVID-19 vaccines: Structure and stability. *Int. J. Pharm.* **2021,** *601*, 120586.
92. Zhang, C.; Ma, Y.; Zhang, J.; Kuo, J. C.-T.; Zhang, Z.; Xie, H.; Zhu, J.; Liu, T., Modification of lipid-based nanoparticles: an efficient delivery system for nucleic acid-based immunotherapy. *Molecules* **2022,** *27* (6), 1943.
93. Yamashiro, D. J.; Maxfield, F. R., Kinetics of endosome acidification in mutant and wild-type Chinese hamster ovary cells. *J. Cell. Biol.* **1987,** *105* (6), 2713-2721.
94. Kulkarni, J. A.; Cullis, P. R.; Van Der Meel, R., Lipid nanoparticles enabling gene therapies: from concepts to clinical utility. *Nucleic Acid Ther.* **2018,** *28* (3), 146-157.
95. Setten, R. L.; Rossi, J. J.; Han, S.-p., The current state and future directions of RNAi-based therapeutics. *Nat. Rev. Drug Discov.* **2019,** *18* (6), 421-446.
96. Tenchov, R.; Bird, R.; Curtze, A. E.; Zhou, Q., Lipid nanoparticles– from liposomes to mRNA vaccine delivery, a landscape of research diversity and advancement. *ACS Nano* **2021,** *15* (11), 16982-17015.
97. Gregoriadis, G.; Ryman, B., Liposomes as carriers of enzymes or drugs: a new approach to the treatment of storage diseases. *Biochem. J.* **1971,** *124* (5), 58P.
98. Gregoriadis, G., Drug entrapment in liposomes. *FEBS Lett.* **1973,** *36* (3), 292-296.
99. Mirzavi, F.; Barati, M.; Soleimani, A.; Vakili-Ghartavol, R.; Jaafari, M. R.; Soukhtanloo, M., A review on liposome-based therapeutic approaches against malignant melanoma. *Int. J. Pharm.* **2021,** *599*, 120413.
100. Wang, G.; Li, R.; Parseh, B.; Du, G., Prospects and challenges of anticancer agents' delivery via chitosan-based drug carriers to combat breast cancer: A review. *Carbohydr. Polym.* **2021,** *268*, 118192.
101. Watson, D. S.; Endsley, A. N.; Huang, L., Design considerations for liposomal vaccines: influence of formulation parameters on antibody and cell-mediated immune responses to liposome associated antigens. *Vaccine* **2012,** *30* (13), 2256-72.
102. Man, F.; Gawne, P. J.; R, T. M. d. R., Nuclear imaging of liposomal drug delivery systems: A critical review of radiolabelling methods and applications in nanomedicine. *Adv. Drug Deliv. Rev.* **2019,** *143*, 134-160.
103. Dos Santos Rodrigues, B.; Banerjee, A.; Kanekiyo, T.; Singh, J., Functionalized liposomal nanoparticles for efficient gene delivery system to neuronal cell transfection. *Int. J. Pharm.* **2019,** *566*, 717-730.
104. Allen, T. M.; Cullis, P. R., Liposomal drug delivery systems: from concept to clinical applications. *Adv. Drug Deliv. Rev.* **2013,** *65* (1), 36-48.
105. Liu, P.; Chen, G.; Zhang, J., A Review of Liposomes as a Drug Delivery System: Current Status of Approved Products, Regulatory Environments, and Future Perspectives. *Molecules* **2022,** *27* (4).
106. Dymek, M.; Sikora, E., Liposomes as biocompatible and smart delivery systems–The current state. *Adv. Colloid Interface Sci.* **2022**, 102757.

107. Chang, C. C.; Liu, D. Z.; Lin, S. Y.; Liang, H. J.; Hou, W. C.; Huang, W. J.; Chang, C. H.; Ho, F. M.; Liang, Y. C., Liposome encapsulation reduces cantharidin toxicity. *Food Chem. Toxicol.* **2008,** *46* (9), 3116-21.
108. Chang, H. I.; Yeh, M. K., Clinical development of liposome-based drugs: formulation, characterization, and therapeutic efficacy. *Int. J. Nanomedicine* **2012,** *7*, 49-60.
109. Allen, T. M.; Hansen, C. B.; de Menezes, D. E. L., Pharmacokinetics of long-circulating liposomes. *Adv. Drug Deliv. Rev.* **1995,** *16* (2-3), 267-284.
110. Gabizon, A. A., Selective tumor localization and improved therapeutic index of anthracyclines encapsulated in long-circulating liposomes. *Cancer Res.* **1992,** *52* (4), 891-896.
111. Bhalani, D. V.; Nutan, B.; Kumar, A.; Singh Chandel, A. K., Bioavailability Enhancement Techniques for Poorly Aqueous Soluble Drugs and Therapeutics. *Biomedicines* **2022,** *10* (9), 2055.
112. Wu, J., The enhanced permeability and retention (EPR) effect: The significance of the concept and methods to enhance its application. *J. Pers. Med.* **2021,** *11* (8), 771.
113. Sharifi, M.; Cho, W. C.; Ansariesfahani, A.; Tarharoudi, R.; Malekisarvar, H.; Sari, S.; Bloukh, S. H.; Edis, Z.; Amin, M.; Gleghorn, J. P., An updated review on EPR-based solid tumor targeting nanocarriers for cancer treatment. *Cancers* **2022,** *14* (12), 2868.
114. Lentz, B. R.; Carpenter, T. J.; Alford, D. R., Spontaneous fusion of phosphatidylcholine small unilamellar vesicles in the fluid phase. *Biochemistry* **1987,** *26* (17), 5389-5397.
115. Gaber, B. P.; Sheridan, J. P., Kinetic and thermodynamic studies of the fusion of small unilamellar phospholipid vesicles. *Biochim. Biophys. Acta, Biomembr.* **1982,** *685* (1), 87-93.
116. Juliano, R. á.; Stamp, D., The effect of particle size and charge on the clearance rates of liposomes and liposome encapsulated drugs. *Biochem. Biophys. Res. Commun.* **1975,** *63* (3), 651-658.
117. Miller, C. R.; Bondurant, B.; McLean, S. D.; McGovern, K. A.; O'Brien, D. F., Liposome–cell interactions in vitro: effect of liposome surface charge on the binding and endocytosis of conventional and sterically stabilized liposomes. *Biochemistry* **1998,** *37* (37), 12875-12883.
118. Campbell, R. B.; Fukumura, D.; Brown, E. B.; Mazzola, L. M.; Izumi, Y.; Jain, R. K.; Torchilin, V. P.; Munn, L. L., Cationic charge determines the distribution of liposomes between the vascular and extravascular compartments of tumors. *Cancer Res.* **2002,** *62* (23), 6831-6836.
119. Fenske, D. B.; Cullis, P. R., Encapsulation of drugs within liposomes by pH-gradient techniques. *J. Liposome Res.* **2007,** *2*, 27-50.
120. Liu, J.-J.; Hong, R.-L.; Cheng, W.-F.; Hong, K.; Chang, F.-H.; Tseng, Y.-L., Simple and efficient liposomal encapsulation of topotecan by ammonium sulfate gradient: stability, pharmacokinetic and therapeutic evaluation. *Anti-cancer drugs* **2002,** *13* (7), 709-717.
121. Mayer, L. D.; Bally, M. B.; Hope, M. J.; Cullis, P. R., Techniques for encapsulating bioactive agents into liposomes. *Chem. Phys. Lipids* **1986,** *40* (2-4), 333-345.
122. Castile, J. D.; Taylor, K. M., Factors affecting the size distribution of liposomes produced by freeze–thaw extrusion. *Int. J. Pharm.* **1999,** *188* (1), 87-95.

123. Anzai, K.; Yoshida, M.; Kirino, Y., Change in intravesicular volume of liposomes by freeze-thaw treatment as studied by the ESR stopped-flow technique. *Biochim. Biophys. Acta, Biomembr.* **1990,** *1021* (1), 21-26.
124. Agashe, H.; Lagisetty, P.; Awasthi, S.; Awasthi, V., Improved formulation of liposome-encapsulated hemoglobin with an anionic non-phospholipid. *Colloids Surf., B* **2010,** *75* (2), 573-583.
125. Immordino, M. L.; Dosio, F.; Cattel, L., Stealth liposomes: review of the basic science, rationale, and clinical applications, existing and potential. *Int. J. Nanomed.* **2006,** *1* (3), 297.
126. Nie, S., Understanding and overcoming major barriers in cancer nanomedicine. *Nanomedicine* **2010,** *5* (4), 523-528.
127. Cˇeh, B.; Winterhalter, M.; Frederik, P. M.; Vallner, J. J.; Lasic, D. D., Stealth® liposomes: from theory to product. *Adv. Drug Deliv. Rev.* **1997,** *24* (2-3), 165-177.
128. Zalipsky, S.; Hansen, C. B.; de Menezes, D. E. L.; Allen, T. M., Long-circulating, polyethylene glycol-grafted immunoliposomes. *J. Control. Release* **1996,** *39* (2-3), 153-161.
129. Eloy, J. O.; Petrilli, R.; Trevizan, L. N. F.; Chorilli, M., Immunoliposomes: A review on functionalization strategies and targets for drug delivery. *Colloids Surf., B* **2017,** *159*, 454-467.
130. Kelemen, L. E., The role of folate receptor α in cancer development, progression and treatment: cause, consequence or innocent bystander? *Int. J. Cancer* **2006,** *119* (2), 243-250.
131. Zwicke, G. L.; Ali Mansoori, G.; Jeffery, C. J., Utilizing the folate receptor for active targeting of cancer nanotherapeutics. *Nano Rev.* **2012,** *3* (1), 18496.
132. Lee, W.; Im, H.-J., Theranostics based on liposome: looking back and forward. *Nucl. Med. Mol. Imaging.* **2019,** *53*, 242-246.
133. Nakamura, Y.; Mochida, A.; Choyke, P. L.; Kobayashi, H., Nanodrug delivery: is the enhanced permeability and retention effect sufficient for curing cancer? *Bioconjug. Chem.* **2016,** *27* (10), 2225-2238.
134. Alam, S.; Mattern-Schain, S.; Best, M., *Targeting and triggered release using lipid-based supramolecular assemblies as medicinal nanocarriers*. Elsevier: 2017; p 329-362.
135. Allen, T. M.; Cullis, P. R., Liposomal drug delivery systems: From concept to clinical applications. *Adv. Drug Del. Rev.* **2013,** *65* (1), 36-48.
136. Pak, C. C.; Ali, S.; Janoff, A. S.; Meers, P., Triggerable liposomal fusion by enzyme cleavage of a novel peptide–lipid conjugate. *Biochim. Biophys. Acta, Biomembr.* **1998,** *1372* (1), 13-27.
137. Sun, Y.; Yan, Y.; Wang, M.; Chen, C.; Xu, H.; Lu, J. R., Controlled release of hydrophilic guest molecules from photoresponsive nucleolipid vesicles. *ACS Appl. Mater. Interfaces* **2013,** *5* (13), 6232-6236.
138. Koyanagi, T.; Cifelli, J. L.; Leriche, G.; Onofrei, D.; Holland, G. P.; Yang, J., Thiol-triggered release of intraliposomal content from liposomes made of extremophile-inspired tetraether lipids. *Bioconjug. Chem.* **2017,** *28* (8), 2041-2045.

139. Dey, S.; Patel, A.; Raina, K.; Pradhan, N.; Biswas, O.; Thummer, R. P.; Manna, D., A stimuli-responsive anticancer drug delivery system with inherent antibacterial activities. *Chem. Commun.* **2020,** *56* (11), 1661-1664.
140. Lou, J.; Qualls, M. L.; Hudson, M. M.; McBee, D. P.; Baccile, J. A.; Best, M. D., Reactive Oxygen Species (ROS) Activated Liposomal Cell Delivery using a Boronate-Caged Guanidine Lipid. *Chem. Eur. J.* **2022,** *28* (46), e202201057.
141. Ghavami, M.; Shiraishi, T.; Nielsen, P. E., Enzyme-triggered release of the antisense octaarginine-pna conjugate from phospholipase A2 sensitive liposomes. *ACS Appl. Bio Mater.* **2020,** *3* (2), 1018-1025.
142. Thamphiwatana, S.; Gao, W.; Pornpattananangkul, D.; Zhang, Q.; Fu, V.; Li, J.; Li, J.; Obonyo, M.; Zhang, L., Phospholipase A2-responsive antibiotic delivery via nanoparticle-stabilized liposomes for the treatment of bacterial infection. *J. Mater. Chem. B* **2014,** *2* (46), 8201-8207.
143. Zhu, G.; Mock, J. N.; Aljuffali, I.; Cummings, B. S.; Arnold, R. D., Secretory phospholipase A2 responsive liposomes. *J. Pharm. Sci.* **2011,** *100* (8), 3146-3159.
144. Samoshin, A. V.; Veselov, I. S.; Chertkov, V. A.; Yaroslavov, A. A.; Grishina, G. V.; Samoshina, N. M.; Samoshin, V. V., Fliposomes: new amphiphiles based on trans-3, 4-bis (acyloxy)-piperidine able to perform a pH-triggered conformational flip and cause an instant cargo release from liposomes. *Tetrahedron Lett.* **2013,** *54* (41), 5600-5604.
145. Viricel, W.; Mbarek, A.; Leblond, J., Switchable lipids: conformational change for fast pH-triggered cytoplasmic delivery. *Angew. Chem. Int. Ed.* **2015,** *54* (43), 12743-12747.
146. Sagar, R.; Lou, J.; Watson, A. J.; Best, M. D., Zinc Triggered Release of Encapsulated Cargo from Liposomes via a Synthetic Lipid Switch. *Bioconjug. Chem.* **2021,** *32* (12), 2485-2496.
147. Lou, J.; Carr, A. J.; Watson, A. J.; Mattern-Schain, S. I.; Best, M. D., Calcium-Responsive Liposomes via a Synthetic Lipid Switch. *Chem. Eur. J.* **2018,** *24* (14), 3599-3607.
148. Lou, J.; Schuster, J. A.; Barrera, F. N.; Best, M. D., ATP-Responsive Liposomes via Screening of Lipid Switches Designed to Undergo Conformational Changes upon Binding Phosphorylated Metabolites. *J. Am. Chem. Soc.* **2022,** *144* (8), 3746-3756.
149. Paliwal, S. R.; Paliwal, R.; Vyas, S. P., A review of mechanistic insight and application of pH-sensitive liposomes in drug delivery. *Drug Deliv.* **2015,** *22* (3), 231-242.
150. McCarley, R. L., Redox-responsive delivery systems. *Annu. Rev. Anal. Chem.* **2012,** *5*, 391-411.
151. Fouladi, F.; Steffen, K. J.; Mallik, S., Enzyme-responsive liposomes for the delivery of anticancer drugs. *Bioconjug. Chem.* **2017,** *28* (4), 857-868.
152. Lou, J.; Carr, A. J.; Watson, A. J.; Mattern-Schain, S. I.; Best, M. D., Calcium-Responsive Liposomes via a Synthetic Lipid Switch. *Chem. Eur. J.* **2018,** *24* (14), 3599-3607.
153. Zhang, X.; Alves, D. S.; Lou, J.; Hill, S. D.; Barrera, F. N.; Best, M. D., Boronic acid liposomes for cellular delivery and content release driven by carbohydrate binding. *Chem. Commun.* **2018,** *54* (48), 6169-6172.
154. Lou, J.; Zhang, X.; Best, M. D., Lipid Switches: Stimuli-Responsive Liposomes through Conformational Isomerism Driven by Molecular Recognition. *Chem. Eur. J.* **2019,** *25* (1), 20-25.
155. Sagar, R.; Lou, J.; Watson, A. J.; Best, M. D., Zinc triggered release of encapsulated cargo from liposomes via a synthetic lipid switch. *Bioconjug. Chem.* **2021,** *32* (12), 2485-2496.

156. Shum, P.; Kim, J.-M.; Thompson, D. H., Phototriggering of liposomal drug delivery systems. *Adv. Drug Deliv. Rev.* **2001,** *53* (3), 273-284.
157. Leung, S. J.; Romanowski, M., Light-activated content release from liposomes. *Theranostics* **2012,** *2* (10), 1020.
158. Puri, A., Phototriggerable liposomes: current research and future perspectives. *Pharmaceutics* **2013,** *6* (1), 1-25.
159. Kneidl, B.; Peller, M.; Winter, G.; Lindner, L. H.; Hossann, M., Thermosensitive liposomal drug delivery systems: state of the art review. *Int. J. Nanomed.* **2014,** *9*, 4387.
160. Dicheva, B. M.; Koning, G. A., Targeted thermosensitive liposomes: an attractive novel approach for increased drug delivery to solid tumors. *Expert Opin. Drug Deliv.* **2014,** *11* (1), 83-100.
161. Sirsi, S. R.; Borden, M. A., State-of-the-art materials for ultrasound-triggered drug delivery. *Adv. Drug Deliv. Rev.* **2014,** *72*, 3-14.
162. Boissenot, T.; Bordat, A.; Fattal, E.; Tsapis, N., Ultrasound-triggered drug delivery for cancer treatment using drug delivery systems: From theoretical considerations to practical applications. *J. Control. Release* **2016,** *241*, 144-163.
163. Bayer, A. M.; Alam, S.; Mattern-Schain, S. I.; Best, M. D., Triggered liposomal release through a synthetic phosphatidylcholine analogue bearing a photocleavable moiety embedded within the sn-2 acyl chain. *Chem. Eur. J.* **2014,** *20* (12), 3350-7.
164. Lou, J.; Carr, A. J.; Watson, A. J.; Mattern-Schain, S. I.; Best, M. D., Calcium-responsive liposomes via a synthetic lipid switch. *Chem. Eur. J.* **2018,** *24* (14), 3599-3607.
165. Lou, J.; Best, M. D., Calcium-responsive liposomes: Toward ion-mediated targeted drug delivery. *Methods Enzymol.* **2020,** *640*, 105-129.
166. Qualls, M. L.; Sagar, R.; Lou, J.; Best, M. D., Demolish and Rebuild: Controlling Lipid Self-Assembly toward Triggered Release and Artificial Cells. *J. Phys. Chem. B* **2021,** *125* (47), 12918-12933.
167. Lou, J.; Best, M. D., A general approach to enzyme-responsive liposomes. *Chem. Eur. J.* **2020,** *26* (39), 8597-8607.
168. Lou, J.; Best, M. D., Reactive oxygen species-responsive liposomes via boronate-caged phosphatidylethanolamine. *Bioconjugate Chem.* **2020,** *31* (9), 2220-2230.
169. Lou, J.; Schuster, J. A.; Barrera, F. N.; Best, M. D., ATP-responsive liposomes via screening of lipid switches designed to undergo conformational changes upon binding phosphorylated metabolites. *J. Am. Chem. Soc.* **2022,** *144* (8), 3746-3756.
170. Bottcher, S. E.; Lou, J.; Best, M. D., Liposome triggered content release through molecular recognition of inositol trisphosphate. *Chem. Commun.* **2022,** *58* (28), 4520-4523.
171. Lou, J.; Sagar, R.; Best, M. D., Metabolite-Responsive Liposomes Employing Synthetic Lipid Switches Driven by Molecular Recognition Principles. *Acc. Chem. Res.* **2022,** *55* (20), 2882-2891.
172. Lou, J.; Best, M. D., Strategies for altering lipid self-assembly to trigger liposome cargo release. *Chem. Phys. Lipids.* **2020,** *232*, 104966.
173. Sevier, C. S.; Kaiser, C. A., Formation and transfer of disulphide bonds in living cells. *Nat. Rev. Mol. Cell Biol.* **2002,** *3* (11), 836-847.
174. Bechtel, T. J.; Weerapana, E., From structure to redox: The diverse functional roles of disulfides and implications in disease. *Proteomics* **2017,** *17* (6), 1600391.

175. Wouters, M. A.; Fan, S. W.; Haworth, N. L., Disulfides as redox switches: from molecular mechanisms to functional significance. *Antioxid. Redox Signal.* **2010,** *12* (1), 53-91.
176. Hatahet, F.; Ruddock, L. W., Protein disulfide isomerase: a critical evaluation of its function in disulfide bond formation. *Antioxid. Redox Signal.* **2009,** *11* (11), 2807-2850.
177. Beaupre, D. M.; Weiss, R. G., Thiol-and disulfide-based stimulus-responsive soft materials and self-assembling systems. *Molecules* **2021,** *26* (11), 3332.
178. Singh, R.; Whitesides, G. M., *The Chemistry of Sulfur-Containing Functional Groups*. J. Wiley and Sons, Ltd: London, 1993; p 633-658.
179. Bulleid, N. J.; Ellgaard, L., Multiple ways to make disulfides. *Trends Biochem. Sci.* **2011,** *36* (9), 485-492.
180. Herrmann, J. M.; Riemer, J., Mitochondrial disulfide relay: redox-regulated protein import into the intermembrane space. *J. Biol. Chem.* **2012,** *287* (7), 4426-4433.
181. Hock, N.; Racaniello, G. F.; Aspinall, S.; Denora, N.; Khutoryanskiy, V. V.; Bernkop-Schnürch, A., Thiolated nanoparticles for biomedical applications: mimicking the workhorses of our body. *Adv. Sci.* **2022,** *9* (1), 2102451.
182. Anderson, M. E., Glutathione: an overview of biosynthesis and modulation. *Chem. Biol. Interact.* **1998,** *111*, 1-14.
183. Wu, G.; Fang, Y.-Z.; Yang, S.; Lupton, J. R.; Turner, N. D., Glutathione metabolism and its implications for health. *J. Nutr.* **2004,** *134* (3), 489-492.
184. Lu, S. C., Regulation of glutathione synthesis. *Mol. Aspects Med.* **2009,** *30* (1-2), 42-59.
185. Niu, B.; Liao, K.; Zhou, Y.; Wen, T.; Quan, G.; Pan, X.; Wu, C., Application of glutathione depletion in cancer therapy: Enhanced ROS-based therapy, ferroptosis, and chemotherapy. *Biomaterials* **2021,** *277*, 121110.
186. Combs, J. A.; DeNicola, G. M., The non-essential amino acid cysteine becomes essential for tumor proliferation and survival. *Cancers* **2019,** *11* (5), 678.
187. Jensen, K. S.; Hansen, R. E.; Winther, J. R., Kinetic and thermodynamic aspects of cellular thiol–disulfide redox regulation. *Antioxid. Redox Signal.* **2009,** *11* (5), 1047-1058.
188. Mahmood, D. F. D.; Abderrazak, A.; El Hadri, K.; Simmet, T.; Rouis, M., The thioredoxin system as a therapeutic target in human health and disease. *Antioxid. Redox Signal.* **2013,** *19* (11), 1266-1303.
189. Gilbert, H. F.; McLean, V., Molecular and cellular aspects of thiol-disulfide exchange. *Adv. Enzymol. Relat. Areas Mol. Biol.* **1993,** *63*, 69-69.
190. Witt, A. C.; Lakshminarasimhan, M.; Remington, B. C.; Hasim, S.; Pozharski, E.; Wilson, M. A., Cysteine p K a depression by a protonated glutamic acid in human DJ-1. *Biochemistry* **2008,** *47* (28), 7430-7440.
191. Shaked, Z. e.; Szajewski, R. P.; Whitesides, G. M., Rates of thiol-disulfide interchange reactions involving proteins and kinetic measurements of thiol pKa values. *Biochemistry* **1980,** *19* (18), 4156-4166.
192. Wilson, J. M.; Bayer, R. J.; Hupe, D., Structure-reactivity correlations for the thiol-disulfide interchange reaction. *J. Am. Chem. Soc.* **1977,** *99* (24), 7922-7926.
193. Pace, C. N.; Grimsley, G. R.; Thomson, J. A.; Barnett, B. J., Conformational stability and activity of ribonuclease T1 with zero, one, and two intact disulfide bonds. *J. Biol. Chem.* **1988,** *263* (24), 11820-11825.

194. Katz, B.; Kossiakoff, A., The crystallographically determined structures of atypical strained disulfides engineered into subtilisin. *J. Biol. Chem.* **1986,** *261* (33), 15480-15485.
195. Fass, D.; Thorpe, C., Chemistry and enzymology of disulfide cross-linking in proteins. *Chem. Rev.* **2018,** *118* (3), 1169-1198.
196. Schafer, F. Q.; Buettner, G. R., Redox environment of the cell as viewed through the redox state of the glutathione disulfide/glutathione couple. *Free Radical Biol. Med.* **2001,** *30* (11), 1191-1212.
197. Aoki, D.; Aibara, G.; Uchida, S.; Takata, T., A rational entry to cyclic polymers via selective cyclization by self-assembly and topology transformation of linear polymers. *J. Am. Chem. Soc.* **2017,** *139* (20), 6791-6794.
198. Andrén, O. C.; Fernandes, A. P.; Malkoch, M., Heterogeneous rupturing dendrimers. *J. Am. Chem. Soc.* **2017,** *139* (48), 17660-17666.
199. Son, S.; Namgung, R.; Kim, J.; Singha, K.; Kim, W. J., Bioreducible polymers for gene silencing and delivery. *Acc. Chem. Res.* **2012,** *45* (7), 1100-1112.
200. Yu, B.; Zheng, Y.; Yuan, Z.; Li, S.; Zhu, H.; De La Cruz, L. K.; Zhang, J.; Ji, K.; Wang, S.; Wang, B., Toward direct protein S-persulfidation: a prodrug approach that directly delivers hydrogen persulfide. *J. Am. Chem. Soc.* **2018,** *140* (1), 30-33.
201. Samuel, N.; Singh, M.; Yamaguchi, K.; Regen, S. L., Polymerized-depolymerized vesicles. Reversible thiol-disulfide-based phosphatidylcholine membranes. *J. Am. Chem. Soc.* **1985,** *107* (1), 42-47.
202. Carnall, J. M.; Waudby, C. A.; Belenguer, A. M.; Stuart, M. C.; Peyralans, J. J.-P.; Otto, S., Mechanosensitive self-replication driven by self-organization. *Science* **2010,** *327* (5972), 1502-1506.
203. Zhang, Q.; Deng, Y.-X.; Luo, H.-X.; Shi, C.-Y.; Geise, G. M.; Feringa, B. L.; Tian, H.; Qu, D.-H., Assembling a natural small molecule into a supramolecular network with high structural order and dynamic functions. *J. Am. Chem. Soc.* **2019,** *141* (32), 12804-12814.
204. Canadell, J.; Goossens, H.; Klumperman, B., Self-healing materials based on disulfide links. *Macromolecules* **2011,** *44* (8), 2536-2541.
205. Yoon, J. A.; Kamada, J.; Koynov, K.; Mohin, J.; Nicolaÿ, R.; Zhang, Y.; Balazs, A. C.; Kowalewski, T.; Matyjaszewski, K., Self-healing polymer films based on thiol–disulfide exchange reactions and self-healing kinetics measured using atomic force microscopy. *Macromolecules* **2012,** *45* (1), 142-149.
206. Kleine, T. S.; Nguyen, N. A.; Anderson, L. E.; Namnabat, S.; LaVilla, E. A.; Showghi, S. A.; Dirlam, P. T.; Arrington, C. B.; Manchester, M. S.; Schwiegerling, J., High refractive index copolymers with improved thermomechanical properties via the inverse vulcanization of sulfur and 1, 3, 5-triisopropenylbenzene. *ACS Macro Lett.* **2016,** *5* (10), 1152-1156.
207. Zhang, Y.; Glass, R. S.; Char, K.; Pyun, J., Recent advances in the polymerization of elemental sulphur, inverse vulcanization and methods to obtain functional Chalcogenide Hybrid Inorganic/Organic Polymers (CHIPs). *Polym. Chem.* **2019,** *10* (30), 4078-4105.
208. Ling, L.; Ismail, M.; Du, Y.; Yao, C.; Li, X., Lipoic acid-derived cross-linked liposomes for reduction-responsive delivery of anticancer drug. *Int. J. Pharm.* **2019,** *560*, 246-260.
209. Kılıç, A.; Jadidi, M. F.; Özer, H. Ö.; Kök, F. N., The effect of thiolated phospholipids on formation of supported lipid bilayers on gold substrates investigated by surface-sensitive methods. *Colloids Surf. B. Biointerfaces* **2017,** *160*, 117-125.

210. Viricel, W.; Mbarek, A.; Leblond, J., Switchable Lipids: Conformational Change for Fast pH-Triggered Cytoplasmic Delivery. *Angew. Chem. Int. Ed. Engl.* **2015,** *54* (43), 12743-7.
211. Karanth, H.; Murthy, R. S., pH-sensitive liposomes--principle and application in cancer therapy. *J. Pharm. Pharmacol.* **2007,** *59* (4), 469-83.
212. Paliwal, S. R.; Paliwal, R.; Vyas, S. P., A review of mechanistic insight and application of pH-sensitive liposomes in drug delivery. *Drug Deliv.* **2015,** *22* (3), 231-42.
213. Ferreira Ddos, S.; Lopes, S. C.; Franco, M. S.; Oliveira, M. C., pH-sensitive liposomes for drug delivery in cancer treatment. *Ther. Deliv.* **2013,** *4* (9), 1099-123.
214. Andresen, T. L.; Thompson, D. H.; Kaasgaard, T., Enzyme-triggered nanomedicine: drug release strategies in cancer therapy. *Mol. Membr. Biol.* **2010,** *27* (7), 353-63.
215. Hu, Q.; Katti, P. S.; Gu, Z., Enzyme-responsive nanomaterials for controlled drug delivery. *Nanoscale* **2014,** *6* (21), 12273-86.
216. Zhang, X.; Alves, D. S.; Lou, J.; Hill, S. D.; Barrera, F. N.; Best, M. D., Boronic acid liposomes for cellular delivery and content release driven by carbohydrate binding. *Chem. Commun.* **2018,** *54* (48), 6169-6172.
217. Ong, W.; Yang, Y.; Cruciano, A. C.; McCarley, R. L., Redox-triggered contents release from liposomes. *J. Am. Chem. Soc.* **2008,** *130* (44), 14739-44.
218. Lou, J.; Best, M. D., Reactive Oxygen Species-Responsive Liposomes via Boronate-Caged Phosphatidylethanolamine. *Bioconjug. Chem.* **2020,** *31* (9), 2220-2230.
219. Maeda, H., The tumor blood vessel as an ideal target for macromolecular anticancer agents. *J. Control. Release* **1992,** *19* (1-3), 315-324.
220. Maeda, H.; Nakamura, H.; Fang, J., The EPR effect for macromolecular drug delivery to solid tumors: Improvement of tumor uptake, lowering of systemic toxicity, and distinct tumor imaging in vivo. *Adv. Drug Deliv. Rev.* **2013,** *65* (1), 71-79.
221. Bibi, S.; Lattmann, E.; Mohammed, A. R.; Perrie, Y., Trigger release liposome systems: local and remote controlled delivery? *J. Microencapsul.* **2012,** *29* (3), 262-76.
222. Lee, Y.; Thompson, D. H., Stimuli-responsive liposomes for drug delivery. *WIREs Nanomed. Nanobi.* **2017,** *9* (5).
223. Pattni, B. S.; Chupin, V. V.; Torchilin, V. P., New Developments in Liposomal Drug Delivery. *Chem. Rev.* **2015,** *115* (19), 10938-66.
224. Derakhshankhah, H.; Jafari, S., Cell penetrating peptides: A concise review with emphasis on biomedical applications. *Biomed. Pharmacother.* **2018,** *108*, 1090-1096.
225. Popilski, H.; Feinshtein, V.; Kleiman, S.; Mattarei, A.; Garofalo, M.; Salmaso, S.; Stepensky, D., Doxorubicin liposomes cell penetration enhancement and its potential drawbacks for the tumor targeting efficiency. *Int. J. Pharm.* **2021,** *592*, 120012.
226. Bendas, G., Immunoliposomes. *BioDrugs* **2001,** *15* (4), 215-224.
227. Puri, A.; Loomis, K.; Smith, B.; Lee, J.-H.; Yavlovich, A.; Heldman, E.; Blumenthal, R., Lipid-based nanoparticles as pharmaceutical drug carriers: from concepts to clinic. *Crit. Rev. Ther. Drug Carrier Syst.* **2009,** *26* (6).
228. Torres, A. G.; Gait, M. J., Exploiting cell surface thiols to enhance cellular uptake. *Trends Biotechnol.* **2012,** *30* (4), 185-190.
229. Chuard, N.; Gasparini, G.; Moreau, D.; Lorcher, S.; Palivan, C.; Meier, W.; Sakai, N.; Matile, S., Strain-Promoted Thiol-Mediated Cellular Uptake of Giant Substrates: Liposomes and Polymersomes. *Angew. Chem. Int. Ed. Engl.* **2017,** *56* (11), 2947-2950.

230. Abegg, D.; Gasparini, G.; Hoch, D. G.; Shuster, A.; Bartolami, E.; Matile, S.; Adibekian, A., Strained Cyclic Disulfides Enable Cellular Uptake by Reacting with the Transferrin Receptor. *J. Am. Chem. Soc.* **2017,** *139* (1), 231-238.
231. Gasparini, G.; Matile, S., Protein delivery with cell-penetrating poly(disulfide)s. *Chem. Commun.* **2015,** *51* (96), 17160-2.
232. Azimi, I.; Matthias, L. J.; Center, R. J.; Wong, J. W.; Hogg, P. J., Disulfide bond that constrains the HIV-1 gp120 V3 domain is cleaved by thioredoxin. *J. Biol. Chem.* **2010,** *285* (51), 40072-80.
233. Ryser, H. J.-P.; Flückiger, R., Keynote review: progress in targeting HIV-1 entry. *Drug Discov. Today* **2005,** *10* (16), 1085-1094.
234. Gasparini, G.; Bang, E. K.; Molinard, G.; Tulumello, D. V.; Ward, S.; Kelley, S. O.; Roux, A.; Sakai, N.; Matile, S., Cellular uptake of substrate-initiated cell-penetrating poly(disulfide)s. *J. Am. Chem. Soc.* **2014,** *136* (16), 6069-74.
235. Gasparini, G.; Sargsyan, G.; Bang, E. K.; Sakai, N.; Matile, S., Ring Tension Applied to Thiol-Mediated Cellular Uptake. *Angew. Chem. Int. Ed. Engl.* **2015,** *54* (25), 7328-31.
236. Kung, V. T.; Redemann, C. T., Synthesis of carboxyacyl derivatives of phosphatidylethanolamine and use as an efficient method for conjugation of protein to liposomes. *Biochim. Biophys. Acta, Biomembr.* **1986,** *862* (2), 435-439.
237. Schelté, P.; Boeckler, C.; Frisch, B.; Schuber, F., Differential reactivity of maleimide and bromoacetyl functions with thiols: application to the preparation of liposomal diepitope constructs. *Bioconjug. Chem.* **2000,** *11* (1), 118-123.
238. Nakano, Y.; Mori, M.; Nishinohara, S.; Takita, Y.; Naito, S.; Kato, H.; Taneichi, M.; Komuro, K.; Uchida, T., Surface-linked liposomal antigen induces IgE-selective unresponsiveness regardless of the lipid components of liposomes. *Bioconjug. Chem.* **2001,** *12* (3), 391-395.
239. Bourel-Bonnet, L.; Pécheur, E.-I.; Grandjean, C.; Blanpain, A.; Baust, T.; Melnyk, O.; Hoflack, B.; Gras-Masse, H., Anchorage of synthetic peptides onto liposomes via hydrazone and α-oxo hydrazone bonds. Preliminary functional investigations. *Bioconjug. Chem.* **2005,** *16* (2), 450-457.
240. Said Hassane, F.; Frisch, B.; Schuber, F., Targeted liposomes: convenient coupling of ligands to preformed vesicles using "click chemistry". *Bioconjug. Chem.* **2006,** *17* (3), 849-854.
241. Zhang, H.; Ma, Y.; Sun, X.-L., Chemically-selective surface glyco-functionalization of liposomes through Staudinger ligation. *Chem. Commun.* **2009,** (21), 3032-3034.
242. Losey, E. A.; Smith, M. D.; Meng, M.; Best, M. D., Microplate-based analysis of protein-membrane binding interactions via immobilization of whole liposomes containing a biotinylated anchor. *Bioconjug. Chem.* **2009,** *20* (2), 376-83.
243. Sechi, S.; Chait, B. T., Modification of cysteine residues by alkylation. A tool in peptide mapping and protein identification. *Anal. Chem.* **1998,** *70* (24), 5150-5158.
244. Zhang, L.; Tong, H.; Garewal, M.; Ren, G., Optimized negative-staining electron microscopy for lipoprotein studies. *Biochim. Biophys. Acta* **2013,** *1830* (1), 2150-9.
245. Patel, N. R.; Piroyan, A.; Nack, A. H.; Galati, C. A.; McHugh, M.; Orosz, S.; Keeler, A. W.; O'Neal, S.; Zamboni, W. C.; Davis, B., Design, synthesis, and characterization of folate-

targeted platinum-loaded theranostic nanoemulsions for therapy and imaging of ovarian cancer. *Mol. Pharm.* **2016,** *13* (6), 1996-2009.
246. Siwowska, K.; Haller, S.; Bortoli, F.; Benesova, M.; Groehn, V.; Bernhardt, P.; Schibli, R.; Müller, C., Preclinical comparison of albumin-binding radiofolates: Impact of linker entities on the in vitro and in vivo properties. *Mol. Pharm.* **2017,** *14* (2), 523-532.
247. Sun, L.; Wu, Q.; Peng, F.; Liu, L.; Gong, C., Strategies of polymeric nanoparticles for enhanced internalization in cancer therapy. *Colloids and Surfaces B: Biointerfaces* **2015,** *135*, 56-72.
248. Vlahov, I. R.; Leamon, C. P., Engineering folate–drug conjugates to target cancer: from chemistry to clinic. *Bioconjugate Chem.* **2012,** *23* (7), 1357-1369.
249. Fernández, M.; Javaid, F.; Chudasama, V., Advances in targeting the folate receptor in the treatment/imaging of cancers. *Chem. Sci.* **2018,** *9* (4), 790-810.
250. Fernandes, G. F. S.; Denny, W. A.; Dos Santos, J. L., Boron in drug design: Recent advances in the development of new therapeutic agents. *Eur. J. Med. Chem.* **2019,** *179*, 791-804.
251. Hall, D. G., *Boronic acids: preparation, applications in organic synthesis and medicine*. John Wiley & Sons: 2006.
252. Lorand, J. P.; EDWARDS, J. O., Polyol complexes and structure of the benzeneboronate ion. *J. Org. Chem.* **1959,** *24* (6), 769-774.
253. Wulff, G., Selective binding to polymers via covalent bonds. The construction of chiral cavities as specific receptor sites. *Pure Appl. Chem.* **1982,** *54* (11), 2093-2102.
254. Wiskur, S. L.; Lavigne, J. J.; Ait-Haddou, H.; Lynch, V.; Chiu, Y. H.; Canary, J. W.; Anslyn, E. V., pKa Values and Geometries of Secondary and Tertiary Amines Complexed to Boronic Acids Implications for Sensor Design. *Org. Lett.* **2001,** *3* (9), 1311-1314.
255. Ni, W.; Kaur, G.; Springsteen, G.; Wang, B.; Franzen, S., Regulating the fluorescence intensity of an anthracene boronic acid system: a B–N bond or a hydrolysis mechanism? *Bioorg. Chem.* **2004,** *32* (6), 571-581.
256. Zhu, L.; Shabbir, S. H.; Gray, M.; Lynch, V. M.; Sorey, S.; Anslyn, E. V., A Structural Investigation of the N− B Interaction in an o-(N, N-Dialkylaminomethyl) arylboronate System. *J. Am. Chem. Soc.* **2006,** *128* (4), 1222-1232.
257. Collins, B. E.; Sorey, S.; Hargrove, A. E.; Shabbir, S. H.; Lynch, V. M.; Anslyn, E. V., Probing Intramolecular B− N Interactions in Ortho-Aminomethyl Arylboronic Acids. *J. Org. Chem.* **2009,** *74* (11), 4055-4060.
258. Cambre, J. N.; Sumerlin, B. S., Biomedical applications of boronic acid polymers. *Polymer* **2011,** *52* (21), 4631-4643.
259. Sun, X.; James, T. D., Glucose sensing in supramolecular chemistry. *Chem. Rev.* **2015,** *115* (15), 8001-8037.
260. Jin, S.; Wang, J.; Li, M.; Wang, B., Synthesis, evaluation, and computational studies of naphthalimide-based long-wavelength fluorescent boronic acid reporters. *Chem. Eur. J.* **2008,** *14* (9), 2795-2804.
261. Zhai, W.; Sun, X.; James, T. D.; Fossey, J. S., Boronic acid-based carbohydrate sensing. *Chem. Asian J.* **2015,** *10* (9), 1836-1848.
262. Franzen, S.; Ni, W.; Wang, B., Study of the mechanism of electron-transfer quenching by boron− nitrogen adducts in fluorescent sensors. *J. Phys. Chem. B.* **2003,** *107* (47), 12942-12948.

263. Chapin, B. M.; Metola, P.; Vankayala, S. L.; Woodcock, H. L.; Mooibroek, T. J.; Lynch, V. M.; Larkin, J. D.; Anslyn, E. V., Disaggregation is a mechanism for emission turn-on of ortho-aminomethylphenylboronic acid-based saccharide sensors. *J. Am. Chem. Soc.* **2017,** *139* (15), 5568-5578.
264. Sun, X.; James, T. D.; Anslyn, E. V., Arresting "loose bolt" internal conversion from− B (OH) 2 groups is the mechanism for emission turn-on in ortho-aminomethylphenylboronic acid-based saccharide sensors. *J. Am. Chem. Soc.* **2018,** *140* (6), 2348-2354.
265. Sun, X.; Chapin, B. M.; Metola, P.; Collins, B.; Wang, B.; James, T. D.; Anslyn, E. V., The mechanisms of boronate ester formation and fluorescent turn-on in ortho-aminomethylphenylboronic acids. *Nat. Chem.* **2019,** *11* (9), 768-778.
266. O'Neill, M. A.; Eberhard, S.; Albersheim, P.; Darvill, A. G., Requirement of borate cross-linking of cell wall rhamnogalacturonan II for Arabidopsis growth. *Science* **2001,** *294* (5543), 846-849.
267. Chen, X.; Schauder, S.; Potier, N.; Van Dorsselaer, A.; Pelczer, I.; Bassler, B. L.; Hughson, F. M., Structural identification of a bacterial quorum-sensing signal containing boron. *Nature* **2002,** *415* (6871), 545-549.
268. Aung, Y.-Y.; Kristanti, A. N.; Lee, H. V.; Fahmi, M. Z., Boronic-acid-modified nanomaterials for biomedical applications. *ACS Omega* **2021,** *6* (28), 17750-17765.
269. Li, D.; Chen, Y.; Liu, Z., Boronate affinity materials for separation and molecular recognition: structure, properties and applications. *Chem. Soc. Rev.* **2015,** *44* (22), 8097-8123.
270. Duggan, P. J.; Tyndall, E. M., Boron acids as protective agents and catalysts in synthesis. *J. Chem. Soc., Perkin Trans. 1* **2002,** (11), 1325-1339.
271. Mancini, R. S.; Lee, J. B.; Taylor, M. S., Boronic esters as protective groups in carbohydrate chemistry: processes for acylation, silylation and alkylation of glycoside-derived boronates. *Org. Biomol. Chem.* **2017,** *15* (1), 132-143.
272. Yan, J.; Springsteen, G.; Deeter, S.; Wang, B., The relationship among pKa, pH, and binding constants in the interactions between boronic acids and diols—it is not as simple as it appears. *Tetrahedron* **2004,** *60* (49), 11205-11209.
273. Brooks, W. L.; Deng, C. C.; Sumerlin, B. S., Structure–reactivity relationships in boronic acid–diol complexation. *ACS Omega* **2018,** *3* (12), 17863-17870.
274. Springsteen, G.; Wang, B., A detailed examination of boronic acid–diol complexation. *Tetrahedron* **2002,** *58* (26), 5291-5300.
275. Pizer, R.; Tihal, C., Equilibria and reaction mechanism of the complexation of methylboronic acid with polyols. *Inorg. Chem.* **1992,** *31* (15), 3243-3247.
276. Aguirre-Chagala, Y. E.; Santos, J. L.; Huang, Y.; Herrera-Alonso, M., Phenylboronic acid-installed polycarbonates for the pH-dependent release of diol-containing molecules. *ACS Macro Lett.* **2014,** *3* (12), 1249-1253.
277. Zhu, J.-Y.; Lei, Q.; Yang, B.; Jia, H.-Z.; Qiu, W.-X.; Wang, X.; Zeng, X.; Zhuo, R.-X.; Feng, J.; Zhang, X.-Z., Efficient nuclear drug translocation and improved drug efficacy mediated by acidity-responsive boronate-linked dextran/cholesterol nanoassembly. *Biomaterials* **2015,** *52*, 281-290.
278. Li, Y.; Xiao, W.; Xiao, K.; Berti, L.; Luo, J.; Tseng, H. P.; Fung, G.; Lam, K. S., Inside Back Cover: Well-Defined, Reversible Boronate Crosslinked Nanocarriers for Targeted Drug

Delivery in Response to Acidic pH Values and cis-Diols (Angew. Chem. Int. Ed. 12/2012). *Angew. Chem. Int. Ed.* **2012,** *51* (12), 3027-3027.
279. Zhao, Z.; Yao, X.; Zhang, Z.; Chen, L.; He, C.; Chen, X., Boronic acid shell-crosslinked dextran-b-PLA micelles for acid-responsive drug delivery. *Macromol. Biosci.* **2014,** *14* (11), 1609-1618.
280. He, L.; Fullenkamp, D. E.; Rivera, J. G.; Messersmith, P. B., pH responsive self-healing hydrogels formed by boronate–catechol complexation. *Chem. Commun.* **2011,** *47* (26), 7497-7499.
281. Nakahata, M.; Mori, S.; Takashima, Y.; Hashidzume, A.; Yamaguchi, H.; Harada, A., pH- and sugar-responsive gel assemblies based on boronate–catechol interactions. *ACS Macro Lett.* **2014,** *3* (4), 337-340.
282. Pettignano, A.; Grijalvo, S.; Haering, M.; Eritja, R.; Tanchoux, N.; Quignard, F.; Díaz, D. D., Boronic acid-modified alginate enables direct formation of injectable, self-healing and multistimuli-responsive hydrogels. *Chem. Commun.* **2017,** *53* (23), 3350-3353.
283. Heleg-Shabtai, V.; Aizen, R.; Orbach, R.; Aleman-Garcia, M. A.; Willner, I., Gossypol-cross-linked boronic acid-modified hydrogels: a functional matrix for the controlled release of an anticancer drug. *Langmuir* **2015,** *31* (7), 2237-2242.
284. Negri, G. E.; Deming, T. J., Protein Complexation and pH Dependent Release Using Boronic Acid Containing PEG-Polypeptide Copolymers. *Macromol. Biosci.* **2017,** *17* (1), 1600136.
285. Su, J.; Chen, F.; Cryns, V. L.; Messersmith, P. B., Catechol polymers for pH-responsive, targeted drug delivery to cancer cells. *J. Am. Chem. Soc.* **2011,** *133* (31), 11850-11853.
286. Yilmaz, M. D.; Xue, M.; Ambrogio, M. W.; Buyukcakir, O.; Wu, Y.; Frasconi, M.; Chen, X.; Nassar, M. S.; Stoddart, J. F.; Zink, J. I., Sugar and pH dual-responsive mesoporous silica nanocontainers based on competitive binding mechanisms. *Nanoscale* **2015,** *7* (3), 1067-1072.
287. Tan, L.; Yang, M.-Y.; Wu, H.-X.; Tang, Z.-W.; Xiao, J.-Y.; Liu, C.-J.; Zhuo, R.-X., Glucose- and pH-responsive nanogated ensemble based on polymeric network capped mesoporous silica. *ACS Appl. Mater. Interfaces* **2015,** *7* (11), 6310-6316.
288. Liu, J.; Luo, Z.; Zhang, J.; Luo, T.; Zhou, J.; Zhao, X.; Cai, K., Hollow mesoporous silica nanoparticles facilitated drug delivery via cascade pH stimuli in tumor microenvironment for tumor therapy. *Biomaterials* **2016,** *83*, 51-65.
289. Broaders, K. E.; Grandhe, S.; Fréchet, J. M., A biocompatible oxidation-triggered carrier polymer with potential in therapeutics. *J. Am. Chem. Soc.* **2011,** *133* (4), 756-758.
290. Zhang, Q.; Zhang, F.; Chen, Y.; Dou, Y.; Tao, H.; Zhang, D.; Wang, R.; Li, X.; Zhang, J., Structure–property correlations of reactive oxygen species-responsive and hydrogen peroxide-eliminating materials with anti-oxidant and anti-inflammatory activities. *Chem. Mater.* **2017,** *29* (19), 8221-8238.
291. de Gracia Lux, C.; Joshi-Barr, S.; Nguyen, T.; Mahmoud, E.; Schopf, E.; Fomina, N.; Almutairi, A., Biocompatible polymeric nanoparticles degrade and release cargo in response to biologically relevant levels of hydrogen peroxide. *J. Am. Chem. Soc.* **2012,** *134* (38), 15758-15764.
292. Lee, S.; Stubelius, A.; Olejniczak, J.; Jang, H.; Huu, V. A. N.; Almutairi, A., Chemical amplification accelerates reactive oxygen species triggered polymeric degradation. *Biomater. Sci.* **2018,** *6* (1), 107-114.

293. Hoang, T. T.; Smith, T. P.; Raines, R. T., A Boronic Acid Conjugate of Angiogenin that Shows ROS-Responsive Neuroprotective Activity. *Angew. Chem.* **2017,** *129* (10), 2663-2666.
294. Qiu, F. Y.; Zhang, M.; Ji, R.; Du, F. S.; Li, Z. C., Oxidation-Responsive Polymer–Drug Conjugates with a Phenylboronic Ester Linker. *Macromol. Rapid Commun.* **2015,** *36* (22), 2012-2018.
295. Lee, S.; Stubelius, A.; Hamelmann, N.; Tran, V.; Almutairi, A., Inflammation-responsive drug-conjugated dextran nanoparticles enhance anti-inflammatory drug efficacy. *ACS Appl. Mater. Interfaces* **2018,** *10* (47), 40378-40387.
296. Chou, D. H.-C.; Webber, M. J.; Tang, B. C.; Lin, A. B.; Thapa, L. S.; Deng, D.; Truong, J. V.; Cortinas, A. B.; Langer, R.; Anderson, D. G., Glucose-responsive insulin activity by covalent modification with aliphatic phenylboronic acid conjugates. *Proc. Natl. Acad. Sci.* **2015,** *112* (8), 2401-2406.
297. Gaballa, H.; Theato, P., Glucose-responsive polymeric micelles via boronic acid–diol complexation for insulin delivery at neutral pH. *Biomacromolecules* **2019,** *20* (2), 871-881.
298. Gaballa, H.; Shang, J.; Meier, S.; Theato, P., The glucose-responsive behavior of a block copolymer featuring boronic acid and glycine. *J. Polym. Sci., Part A: Polym. Chem.* **2019,** *57* (3), 422-431.
299. Dong, Y.; Wang, W.; Veiseh, O.; Appel, E. A.; Xue, K.; Webber, M. J.; Tang, B. C.; Yang, X.-W.; Weir, G. C.; Langer, R., Injectable and glucose-responsive hydrogels based on boronic acid–glucose complexation. *Langmuir* **2016,** *32* (34), 8743-8747.
300. Qian, C.; Chen, Y.; Zhu, S.; Yu, J.; Zhang, L.; Feng, P.; Tang, X.; Hu, Q.; Sun, W.; Lu, Y., ATP-responsive and near-infrared-emissive nanocarriers for anticancer drug delivery and real-time imaging. *Theranostics* **2016,** *6* (7), 1053.
301. James, T. D.; Sandanayake, K. S.; Shinkai, S., A glucose-selective molecular fluorescence sensor. *Angew. Chem., Int. Ed. Engl.* **1994,** *33* (21), 2207-2209.
302. James, T. D.; Sandanayake, K. S.; Iguchi, R.; Shinkai, S., Novel saccharide-photoinduced electron transfer sensors based on the interaction of boronic acid and amine. *J. Am. Chem. Soc.* **1995,** *117* (35), 8982-8987.
303. Arimori, S.; Bell, M. L.; Oh, C. S.; Frimat, K. A.; James, T. D., Modular fluorescence sensors for saccharides. *J. Chem. Soc., Perkin Trans. 1* **2002,** (6), 803-808.
304. Arimori, S.; Bell, M. L.; Oh, C. S.; Frimat, K. A.; James, T. D., Modular fluorescence sensors for saccharides. *Chem. Commun.* **2001,** (18), 1836-1837.
305. Whyte, G. F.; Vilar, R.; Woscholski, R., Molecular recognition with boronic acids—applications in chemical biology. *J. Chem. Biol.* **2013,** *6*, 161-174.
306. Liu, Z.; He, H., Synthesis and applications of boronate affinity materials: from class selectivity to biomimetic specificity. *Acc. Chem. Res.* **2017,** *50* (9), 2185-2193.
307. Saito, S.; Maeda, T.; Nakazumi, H.; Colyer, C. L., An application of polymer-enhanced capillary transient isotachophoresis with an emissive boronic acid functionalized squarylium dye as an on-capillary labeling agent for gram-positive bacteria. *Anal. Sci.* **2013,** *29* (1), 157-159.
308. Golabi, M.; Kuralay, F.; Jager, E. W.; Beni, V.; Turner, A. P., Electrochemical bacterial detection using poly (3-aminophenylboronic acid)-based imprinted polymer. *Biosens. Bioelectron.* **2017,** *93*, 87-93.

309. Yang, P.; Bam, M.; Pageni, P.; Zhu, T.; Chen, Y. P.; Nagarkatti, M.; Decho, A. W.; Tang, C., Trio act of boronolectin with antibiotic-metal complexed macromolecules toward broad-spectrum antimicrobial efficacy. *ACS Infect. Dis.* **2017,** *3* (11), 845-853.
310. Pearce, O. M.; Läubli, H., Sialic acids in cancer biology and immunity. *Glycobiology* **2016,** *26* (2), 111-128.
311. Otsuka, H.; Uchimura, E.; Koshino, H.; Okano, T.; Kataoka, K., Anomalous binding profile of phenylboronic acid with N-acetylneuraminic acid (Neu5Ac) in aqueous solution with varying pH. *J. Am. Chem. Soc.* **2003,** *125* (12), 3493-3502.
312. Sanjoh, M.; Miyahara, Y.; Kataoka, K.; Matsumoto, A., Phenylboronic acids-based diagnostic and therapeutic applications. *Anal. Sci.* **2014,** *30* (1), 111-117.
313. Bondioli, L.; Ruozi, B.; Belletti, D.; Forni, F.; Vandelli, M. A.; Tosi, G., Sialic acid as a potential approach for the protection and targeting of nanocarriers. *Expert Opin. Drug Deliv.* **2011,** *8* (7), 921-937.
314. Qing, G.; Lu, Q.; Xiong, Y.; Zhang, L.; Wang, H.; Li, X.; Liang, X.; Sun, T., New opportunities and challenges of smart polymers in post-translational modification proteomics. *Adv. Mater.* **2017,** *29* (20), 1604670.
315. Wang, S.; Yin, D.; Wang, W.; Shen, X.; Zhu, J.-J.; Chen, H.-Y.; Liu, Z., Targeting and imaging of cancer cells via monosaccharide-imprinted fluorescent nanoparticles. *Sci. Rep.* **2016,** *6* (1), 22757.
316. Yin, D.; Wang, S.; He, Y.; Liu, J.; Zhou, M.; Ouyang, J.; Liu, B.; Chen, H.-Y.; Liu, Z., Surface-enhanced Raman scattering imaging of cancer cells and tissues via sialic acid-imprinted nanotags. *Chem. Commun.* **2015,** *51* (100), 17696-17699.
317. Yin, D.; Li, X.; Ma, Y.; Liu, Z., Targeted cancer imaging and photothermal therapy via monosaccharide-imprinted gold nanorods. *Chem. Commun.* **2017,** *53* (50), 6716-6719.
318. Forssen, E.; Willis, M., Ligand-targeted liposomes. *Adv. Drug Deliv. Rev.* **1998,** *29* (3), 249-271.
319. Van Elssen, C. H.; Frings, P. W.; Bot, F. J.; Van de Vijver, K. K.; Huls, M. B.; Meek, B.; Hupperets, P.; Germeraad, W. T.; Bos, G. M., Expression of aberrantly glycosylated Mucin-1 in ovarian cancer. *Histopathology* **2010,** *57* (4), 597-606.
320. Bhatia, R.; Gautam, S. K.; Cannon, A.; Thompson, C.; Hall, B. R.; Aithal, A.; Banerjee, K.; Jain, M.; Solheim, J. C.; Kumar, S.; Batra, S. K., Cancer-associated mucins: role in immune modulation and metastasis. *Cancer Metastasis Rev.* **2019,** *38* (1-2), 223-236.
321. Munkley, J., The role of sialyl-Tn in cancer. *Int. J. Mol. Sci.* **2016,** *17* (3), 275.
322. Büll, C.; Stoel, M. A.; den Brok, M. H.; Adema, G. J., Sialic acids sweeten a tumor's life. *Cancer Res.* **2014,** *74* (12), 3199-3204.
323. Munkley, J., The glycosylation landscape of pancreatic cancer. *Oncology letters* **2019,** *17* (3), 2569-2575.
324. Jourdian, G. W.; Dean, L.; Roseman, S., The sialic acids. XI. A periodate-resorcinol method for the quantitative estimation of free sialic acids and their glycosides. *J. Biol. Chem.* **1971,** *246* (2), 430-5.
325. Mahal, L. K.; Yarema, K. J.; Bertozzi, C. R., Engineering chemical reactivity on cell surfaces through oligosaccharide biosynthesis. *Science* **1997,** *276* (5315), 1125-8.
326. Bull, S. D.; Davidson, M. G.; van den Elsen, J. M.; Fossey, J. S.; Jenkins, A. T.; Jiang, Y. B.; Kubo, Y.; Marken, F.; Sakurai, K.; Zhao, J.; James, T. D., Exploiting the reversible covalent

bonding of boronic acids: recognition, sensing, and assembly. *Acc. Chem. Res.* **2013,** *46* (2), 312-26.
327. Fang, H.; Kaur, G.; Wang, B., Progress in boronic acid-based fluorescent glucose sensors. *J. Fluoresc.* **2004,** *14* (5), 481-9.
328. James, T. D.; Sandanayake, K. S.; Shinkai, S., Chiral discrimination of monosaccharides using a fluorescent molecular sensor. *Nature* **1995,** *374* (6520), 345.
329. James, T. D.; Sandanayake, K. S.; Shinkai, S., Saccharide sensing with molecular receptors based on boronic acid. *Angew. Chem., Int. Ed. Engl.* **1996,** *35* (17), 1910-1922.
330. Jin, S.; Cheng, Y.; Reid, S.; Li, M.; Wang, B., Carbohydrate recognition by boronolectins, small molecules, and lectins. *Med. Res. Rev.* **2010,** *30* (2), 171-257.
331. Kuivila, H. G.; Keough, A. H.; Soboczenski, E. J., Areneboronates from diols and polyols. *J. Org. Chem.* **1954,** *19* (5), 780-783.
332. Sun, X.; Zhai, W.; Fossey, J. S.; James, T. D., Boronic acids for fluorescence imaging of carbohydrates. *Chem. Commun.* **2016,** *52* (17), 3456-69.
333. Wang, W.; Gao, X.; Wang, B., Boronic acid-based sensors. *Curr. Org. Chem.* **2002,** *6* (14), 1285-1317.
334. Wiskur, S. L.; Ait-Haddou, H.; Lavigne, J. J.; Anslyn, E. V., Teaching old indicators new tricks. *Acc. Chem. Res.* **2001,** *34* (12), 963-72.
335. Zhai, W.; Sun, X.; James, T. D.; Fossey, J. S., Boronic Acid-Based Carbohydrate Sensing. *Chem. Asian J.* **2015,** *10* (9), 1836-48.
336. Cairo, C. W.; Gestwicki, J. E.; Kanai, M.; Kiessling, L. L., Control of multivalent interactions by binding epitope density. *J. Am. Chem. Soc.* **2002,** *124* (8), 1615-9.
337. Gestwicki, J. E.; Cairo, C. W.; Strong, L. E.; Oetjen, K. A.; Kiessling, L. L., Influencing receptor-ligand binding mechanisms with multivalent ligand architecture. *J. Am. Chem. Soc.* **2002,** *124* (50), 14922-33.
338. Kiessling, L. L.; Gestwicki, J. E.; Strong, L. E., Synthetic multivalent ligands as probes of signal transduction. *Angew. Chem. Int. Ed.* **2006,** *45* (15), 2348-68.
339. Liang, P. H.; Wang, S. K.; Wong, C. H., Quantitative analysis of carbohydrate-protein interactions using glycan microarrays: determination of surface and solution dissociation constants. *J. Am. Chem. Soc.* **2007,** *129* (36), 11177-84.
340. Mammen, M.; Choi, S. K.; Whitesides, G. M., Polyvalent Interactions in Biological Systems: Implications for Design and Use of Multivalent Ligands and Inhibitors. *Angew. Chem. Int. Ed.* **1998,** *37* (20), 2754-2794.
341. Zhang, X.; Zhang, S.; Baek, S. J.; Best, M. D., A Boronic Acid Assay for the Detection of Mucin-1 Glycoprotein from Cancer Cells. *ChemBioChem* **2017,** *18* (16), 1578-1582.
342. Yang, W.; He, H.; Drueckhammer, D. G., Computer-guided design in molecular recognition: design and synthesis of a glucopyranose receptor. *Angew. Chem. Int. Ed.* **2001,** *40* (9), 1714-1718.
343. James, T. D.; Samankumara Sandanayake, K. R. A.; Shinkai, S., Chiral discrimination of monosaccharides using a fluorescent molecular sensor. *Nature* **1995,** *374* (6520), 345-347.
344. Eggert, H.; Frederiksen, J.; Morin, C.; Norrild, J. C., A new glucose-selective fluorescent bisboronic acid. first report of strong α-Furanose complexation in aqueous solution at physiological pH1. *J. Org. Chem.* **1999,** *64* (11), 3846-3852.

345. Karnati, V. V.; Gao, X.; Gao, S.; Yang, W.; Ni, W.; Sankar, S.; Wang, B., A glucose-selective fluorescence sensor based on boronicacid-diol recognition. *Bioorg. Med. Chem. Lett.* **2002,** *12* (23), 3373-3377.
346. Yang, W.; Fan, H.; Gao, X.; Gao, S.; Karnati, V. V.; Ni, W.; Hooks, W. B.; Carson, J.; Weston, B.; Wang, B., The first fluorescent diboronic acid sensor specific for hepatocellular carcinoma cells expressing sialyl Lewis X. *Chem. Biol.* **2004,** *11* (4), 439-48.
347. Losey, E. A.; Smith, M. D.; Meng, M.; Best, M. D., Microplate-based analysis of protein-membrane binding interactions via immobilization of whole liposomes containing a biotinylated anchor. *Bioconjugate Chem.* **2009,** *20* (2), 376-83.
348. Lammerts van Bueren, A.; Finn, R.; Ausio, J.; Boraston, A. B., Alpha-glucan recognition by a new family of carbohydrate-binding modules found primarily in bacterial pathogens. *Biochemistry* **2004,** *43* (49), 15633-42.
349. Meddens, M. J.; Thompson, J.; Leijh, P. C.; van Furth, R., Role of granulocytes in the induction of an experimental endocarditis with a dextran-producing Streptococcus sanguis and its dextran-negative mutant. *Br. J. Exp. Pathol.* **1984,** *65* (2), 257-65.
350. Banas, J. A.; Vickerman, M. M., Glucan-binding proteins of the oral streptococci. *Crit. Rev. Oral. Biol. Med.* **2003,** *14* (2), 89-99.
351. Shabbir, S. H.; Joyce, L. A.; da Cruz, G. M.; Lynch, V. M.; Sorey, S.; Anslyn, E. V., Pattern-based recognition for the rapid determination of identity, concentration, and enantiomeric excess of subtly different threo diols. *J. Am. Chem. Soc.* **2009,** *131* (36), 13125-13131.
352. Springsteen, G.; Wang, B., Alizarin Red S. as a general optical reporter for studying the binding of boronic acids with carbohydrates. *Chem. Commun.* **2001,** (17), 1608-1609.
353. Ruozi, B.; Belletti, D.; Tombesi, A.; Tosi, G.; Bondioli, L.; Forni, F.; Vandelli, M. A., AFM, ESEM, TEM, and CLSM in liposomal characterization: a comparative study. *Int. J. Nanomed.* **2011,** *6*, 557.
354. Fisher, R. K.; Mattern-Schain, S. I.; Best, M. D.; Kirkpatrick, S. S.; Freeman, M. B.; Grandas, O. H.; Mountain, D. J. H., Improving the efficacy of liposome-mediated vascular gene therapy via lipid surface modifications. *J. Surg. Res.* **2017,** *219*, 136-144.
355. Šturm, L.; Poklar Ulrih, N., Basic methods for preparation of liposomes and studying their interactions with different compounds, with the emphasis on polyphenols. *Int. J. Mol. Sci* **2021,** *22* (12), 6547.
356. Low, C.-Y.; Rotstein, C., Emerging fungal infections in immunocompromised patients. *F1000 Med. Rep.* **2011,** *3*.
357. Sobel, J. D.; Chaim, W., Treatment of Torulopsis glabrata vaginitis: retrospective review of boric acid therapy. *Clin Infect Dis* **1997,** *24* (4), 649-52.
358. Iavazzo, C.; Gkegkes, I. D.; Zarkada, I. M.; Falagas, M. E., Boric acid for recurrent vulvovaginal candidiasis: the clinical evidence. *J. Womens Health (Larchmt)* **2011,** *20* (8), 1245-55.
359. De Seta, F.; Schmidt, M.; Vu, B.; Essmann, M.; Larsen, B., Antifungal mechanisms supporting boric acid therapy of Candida vaginitis. *J. Antimicrob. Chemother.* **2009,** *63* (2), 325-36.

360. De Seta, F.; Hunter, M.; Larsen, B., In vitro evaluation of small molecule inhibitors and probiotic byproducts on growth and viability of vaginal microorganisms. *Br. J. Med. Med. Res.* **2014,** *4* (36), 5779.
361. Cabib, E.; Blanco, N.; Arroyo, J., Presence of a large beta(1-3)glucan linked to chitin at the Saccharomyces cerevisiae mother-bud neck suggests involvement in localized growth control. *Eukaryot. Cell* **2012,** *11* (4), 388-400.
362. Abbott, D. W.; Martens, E. C.; Gilbert, H. J.; Cuskin, F.; Lowe, E. C., Coevolution of yeast mannan digestion: Convergence of the civilized human diet, distal gut microbiome, and host immunity. *Gut Microbes* **2015,** *6* (5), 334-9.
363. Orlean, P.; Menon, A. K., Thematic review series: lipid posttranslational modifications. GPI anchoring of protein in yeast and mammalian cells, or: how we learned to stop worrying and love glycophospholipids. *J. Lipid Res.* **2007,** *48* (5), 993-1011.
364. Komath, S. S.; Singh, S. L.; Pratyusha, V. A.; Sah, S. K., Generating anchors only to lose them: The unusual story of glycosylphosphatidylinositol anchor biosynthesis and remodeling in yeast and fungi. *IUBMB Life* **2018,** *70* (5), 355-383.
365. Yeul, V. S.; Rayalu, S. S., Unprecedented chitin and chitosan: A chemical overview. *J. Polym. Environ.* **2013,** *21* (2), 606-614.
366. Nworu, C. S.; Ihim, S. A.; Okoye, F. B.; Esimone, C. O.; Adikwu, M. U.; Akah, P. A., Immunomodulatory and immunorestorative activities of β-d-glucan-rich extract and polysaccharide fraction of mushroom, Pleurutus tuberregium. *Pharm. Biol.* **2015,** *53* (11), 1555-1566.
367. Hu, X.; Shi, Y.; Zhang, P.; Miao, M.; Zhang, T.; Jiang, B., D-Mannose: Properties, production, and applications: An overview. *Compr. Rev. Food Sci. Food Saf.* **2016,** *15* (4), 773-785.
368. Mayer, F. L.; Wilson, D.; Hube, B., Candida albicans pathogenicity mechanisms. *Virulence* **2013,** *4* (2), 119-128.
369. Kim, J.; Sudbery, P., Candida albicans, a major human fungal pathogen. *J. Microbiol.* **2011,** *49* (2), 171-177.
370. Kim, K.-J.; Sung, W. S.; Suh, B. K.; Moon, S.-K.; Choi, J.-S.; Kim, J. G.; Lee, D. G., Antifungal activity and mode of action of silver nano-particles on Candida albicans. *Biometals* **2009,** *22* (2), 235-242.
371. Kim, J.; Sudbery, P., Candida albicans, a major human fungal pathogen. *J. Microbiol.* **2011,** *49* (2), 171-177.
372. Chen, Y. L.; Montedonico, A. E.; Kauffman, S.; Dunlap, J. R.; Menn, F. M.; Reynolds, T. B., Phosphatidylserine synthase and phosphatidylserine decarboxylase are essential for cell wall integrity and virulence in Candida albicans. *Mol. Microbiol.* **2010,** *75* (5), 1112-1132.
373. Greenspan, P.; Mayer, E. P.; Fowler, S. D., Nile red: a selective fluorescent stain for intracellular lipid droplets. *J. Cell. Biol.* **1985,** *100* (3), 965-973.
374. Liang, X.; Yue, X.; Dai, Z.; Kikuchi, J., Photoresponsive liposomal nanohybrid cerasomes. *Chem. Commun.* **2011,** *47* (16), 4751-3.
375. Wright, A. T.; Zhong, Z.; Anslyn, E. V., A functional assay for heparin in serum using a designed synthetic receptor. *Angew. Chem.* **2005,** *117* (35), 5825-5828.

376. Zhong, Z.; Anslyn, E. V., A colorimetric sensing ensemble for heparin. *J. Am. Chem. Soc.* **2002,** *124* (31), 9014-9015.
377. Springsteen, G.; Wang, B., Alizarin Red S. as a general optical reporter for studying the binding of boronic acids with carbohydrates. *Chemical Communications* **2001,** (17), 1608-1609.
378. Winson, M.; áPereira Morais, M. P.; ávan den Elsen, J. M.; Jonathan, P., Dye displacement assay for saccharide detection with boronate hydrogels. *Chem. Commun.* **2009,** (5), 532-534.
379. Tomsho, J. W.; Benkovic, S. J., Elucidation of the mechanism of the reaction between phenylboronic acid and a model diol, Alizarin Red S. *J. Org. Chem.* **2012,** *77* (5), 2098-2106.
380. Lampard, E. V.; Sedgwick, A. C.; Sombuttan, T.; Williams, G. T.; Wannalerse, B.; Jenkins, A. T. A.; Bull, S. D.; James, T. D., Dye displacement assay for saccharides using benzoxaborole hydrogels. *ChemistryOpen* **2018,** *7* (3), 266-268.
381. Kopatz, I.; Remy, J. S.; Behr, J. P., A model for non-viral gene delivery: through syndecan adhesion molecules and powered by actin. *J. Gene Med.* **2004,** *6* (7), 769-776.
382. Yang, B. Y.; Gray, J. S.; Montgomery, R., The glycans of horseradish peroxidase. *Carbohydr. Res.* **1996,** *287* (2), 203-212.
383. Dulaney, S. B.; Huang, X., Strategies in synthesis of heparin/heparan sulfate oligosaccharides: 2000–present. *Adv. Carbohydr. Chem. Biochem.* **2021,** *80*, 121-164.
384. Ahirwar, R.; Bariar, S.; Balakrishnan, A.; Nahar, P., BSA blocking in enzyme-linked immunosorbent assays is a non-mandatory step: a perspective study on mechanism of BSA blocking in common ELISA protocols. *RSC Adv.* **2015,** *5* (121), 100077-100083.
385. Killian, J. A.; de Kruijff, B., Nonbilayer lipids affect peripheral and integral membrane proteins via changes in the lateral pressure profile. *Biochim. Biophys. Acta, Biomembr.* **2004,** *1666* (1-2), 275-288.
386. Lou, J.; Carr, A. J.; Watson, A. J.; Mattern-Schain, S. I.; Best, M. D., Calcium-Responsive Liposomes via a Synthetic Lipid Switch. *Chemistry* **2018,** *24* (14), 3599-3607.
387. Bulbake, U.; Doppalapudi, S.; Kommineni, N.; Khan, W., Liposomal formulations in clinical use: an updated review. *Pharmaceutics* **2017,** *9* (2), 12.
388. Bhatia, R.; Gautam, S. K.; Cannon, A.; Thompson, C.; Hall, B. R.; Aithal, A.; Banerjee, K.; Jain, M.; Solheim, J. C.; Kumar, S.; Batra, S. K., Cancer-associated mucins: role in immune modulation and metastasis. *Cancer Metastasis Rev* **2019,** *38* (1-2), 223-236.
389. Munkley, J., The role of sialyl-Tn in cancer. *International journal of molecular sciences* **2016,** *17* (3), 275.
390. Buskas, T.; Thompson, P.; Boons, G.-J., Immunotherapy for cancer: synthetic carbohydrate-based vaccines. *Chem. Commun.* **2009,** (36), 5335-5349.
391. Wilson, R. M.; Danishefsky, S. J., A vision for vaccines built from fully synthetic tumor-associated antigens: from the laboratory to the clinic. *J. Am. Chem. Soc.* **2013,** *135* (39), 14462-14472.
392. Angata, T.; Varki, A., Chemical diversity in the sialic acids and related α-keto acids: an evolutionary perspective. *Chem. Rev.* **2002,** *102* (2), 439-470.
393. Chen, X.; Varki, A., Advances in the biology and chemistry of sialic acids. *ACS Chem. Biol.* **2010,** *5* (2), 163-176.

394. Kikkeri, R.; Padler-Karavani, V.; Diaz, S.; Verhagen, A.; Yu, H.; Cao, H.; Langereis, M. A.; De Groot, R. J.; Chen, X.; Varki, A., Quantum dot nanometal surface energy transfer based biosensing of sialic acid compositions and linkages in biological samples. *Anal. Chem.* **2013,** *85* (8), 3864-3870.
395. Varki, A.; Cummings, R. D.; Esko, J. D.; Freeze, H. H.; Stanley, P.; Bertozzi, C. R.; Hart, G. W.; Etzler, M. E., *Essentials of Glycobiology*. 2nd ed.; Cold Spring Harbor Press: Cold Spring Harbor, NY, 2009.
396. Kim, Y. J.; Varki, A., Perspectives on the significance of altered glycosylation of glycoproteins in cancer. *Glycoconjugate J.* **1997,** *14* (5), 569-576.
397. Cazet, A.; Julien, S.; Bobowski, M.; Krzewinski-Recchi, M.-A.; Harduin-Lepers, A.; Groux-Degroote, S.; Delannoy, P., Consequences of the expression of sialylated antigens in breast cancer. *Carbohydr. Res.* **2010,** *345* (10), 1377-1383.
398. Levonis, S. M.; Kiefel, M. J.; Houston, T. A., Boronolectin with divergent fluorescent response specific for free sialic acid. *Chem. Commun.* **2009,** (17), 2278-2280.
399. Rabuka, D.; Parthasarathy, R.; Lee, G. S.; Chen, X.; Groves, J. T.; Bertozzi, C. R., Hierarchical assembly of model cell surfaces: synthesis of mucin mimetic polymers and their display on supported bilayers. *J. Am. Chem. Soc.* **2007,** *129* (17), 5462-71.
400. Liang, X.; Yue, X.; Dai, Z.; Kikuchi, J., Photoresponsive liposomal nanohybrid cerasomes. *Chem Commun (Camb)* **2011,** *47* (16), 4751-3.
401. MacDonald, R. I., Characteristics of self-quenching of the fluorescence of lipid-conjugated rhodamine in membranes. *J. Biol. Chem.* **1990,** *265* (23), 13533-13539.
402. Chen, Y. L.; Montedonico, A. E.; Kauffman, S.; Dunlap, J. R.; Menn, F. M.; Reynolds, T. B., Phosphatidylserine synthase and phosphatidylserine decarboxylase are essential for cell wall integrity and virulence in Candida albicans. *Mol. Microbiol.* **2010,** *75* (5), 1112-32.
403. Pattni, B. S.; Chupin, V. V.; Torchilin, V. P., New developments in liposomal drug delivery. *Chem. Rev.* **2015,** *115* (19), 10938-10966.
404. Lasic, D. D.; Needham, D., The ''Stealth'' liposome: A prototypical biomaterial. *Chem. Rev.* **1995,** *95* (8), 2601-2628.
405. Gao, H.; Zhang, Q.; Yu, Z.; He, Q., Cell-penetrating peptide-based intelligent liposomal systems for enhanced drug delivery. *Curr. Pharm. Biotechnol.* **2014,** *15* (3), 210-219.
406. Koren, E.; Torchilin, V. P., Cell-penetrating peptides: breaking through to the other side. *Trends Mol. Med.* **2012,** *18* (7), 385-393.
407. Manjappa, A. S.; Chaudhari, K. R.; Venkataraju, M. P.; Dantuluri, P.; Nanda, B.; Sidda, C.; Sawant, K. K.; Murthy, R. S. R., Antibody derivatization and conjugation strategies: Application in preparation of stealth immunoliposome to target chemotherapeutics to tumor. *J. Control. Release* **2011,** *150* (1), 2-22.
408. Zhang, X.; Alves, D. S.; Lou, J.; Hill, S. D.; Barrera, F. N.; Best, M. D., Boronic acid liposomes for cellular delivery and content release driven by carbohydrate binding. *Chem. Commun.* **2018,** *54* (48), 6169-6172.
409. Qualls, M. L.; Hagewood, H.; Lou, J.; Mattern-Schain, S. I.; Zhang, X.; Mountain, D. J.; Best, M. D., Bis-boronic acid liposomes for carbohydrate recognition and cellular delivery. *ChemBioChem* **2022,** *23* (21), e202200402.

410. Qualls, M. L.; Lou, J.; McBee, D. P.; Baccile, J. A.; Best, M. D., Cyclic Disulfide Liposomes for Membrane Functionalization and Cellular Delivery. *Chem. Eur. J.* **2022,** *28* (45), e202201164.
411. Kirpotin, D.; Hong, K.; Mullah, N.; Papahadjopoulos, D.; Zalipsky, S., Liposomes with detachable polymer coating: destabilization and fusion of dioleoylphosphatidylethanolamine vesicles triggered by cleavage of surface-grafted poly (ethylene glycol). *FEBS Lett.* **1996,** *388* (2-3), 115-118.
412. Senter, P. D.; Pearce, W. E.; Greenfield, R. S., Development of a drug-release strategy based on the reductive fragmentation of benzyl carbamate disulfides. *The Journal of Organic Chemistry* **1990,** *55* (9), 2975-2978.
413. Zheng, Y.; Shen, Y.; Meng, X.; Wu, Y.; Zhao, Y.; Wu, C., Stabilizing p-Dithiobenzyl Urethane Linkers without Rate-Limiting Self-Immolation for Traceless Drug Release. *ChemMedChem* **2019,** *14* (12), 1196-1203.
414. Zalipsky, S.; Mullah, N.; Engbers, C.; Hutchins, M. U.; Kiwan, R., Thiolytically cleavable dithiobenzyl urethane-linked polymer–protein conjugates as macromolecular prodrugs: reversible PEGylation of proteins. *Bioconjug. Chem.* **2007,** *18* (6), 1869-1878.
415. Qian, L.; Fu, J.; Yuan, P.; Du, S.; Huang, W.; Li, L.; Yao, S. Q., Intracellular Delivery of Native Proteins Facilitated by Cell-Penetrating Poly (disulfide) s. *Angew. Chem.* **2018,** *130* (6), 1548-1552.
416. Aoyama, E.; Fuchida, H.; Oshikawa, Y.; Uchinomiya, S.; Ojida, A., Intracellular delivery of chemical probes using a glutathione-responsive traceless tag. *Chem. Commun.* **2016,** *52* (49), 7715-7718.
417. Jones, L. R.; Goun, E. A.; Shinde, R.; Rothbard, J. B.; Contag, C. H.; Wender, P. A., Releasable luciferin− transporter conjugates: Tools for the real-time analysis of cellular uptake and release. *J. Am. Chem. Soc.* **2006,** *128* (20), 6526-6527.
418. Zalipsky, S.; Qazen, M.; Walker, J. A.; Mullah, N.; Quinn, Y. P.; Huang, S. K., New detachable poly (ethylene glycol) conjugates: cysteine-cleavable lipopolymers regenerating natural phospholipid, diacyl phosphatidylethanolamine. *Bioconjug. Chem.* **1999,** *10* (5), 703-707.
419. Ong, W.; Yang, Y.; Cruciano, A. C.; McCarley, R. L., Redox-triggered contents release from liposomes. *J. Am. Chem. Soc.* **2008,** *130* (44), 14739-14744.
420. Zhang, Z.-Y.; Smith, B. D., Synthesis and characterization of NVOC-DOPE, a caged photoactivatable derivative of dioleoylphosphatidylethanolamine. *Bioconjug. Chem.* **1999,** *10* (6), 1150-1152.
421. Lou, J.; Best, M. D., A General Approach to Enzyme-Responsive Liposomes. *Chem. Eur. J.* **2020,** *26* (39), 8597-8607.
422. Israelachvili, J. N.; Mitchell, D. J.; Ninham, B. W., Theory of self-assembly of lipid bilayers and vesicles. *Biochim. Biophys. Acta, Biomembr.* **1977,** *470* (2), 185-201.
423. Litzinger, D. C.; Huang, L., Phosphatodylethanolamine liposomes: drug delivery, gene transfer and immunodiagnostic applications. *Biochim. Biophys. Acta, Biomembr.* **1992,** *1113* (2), 201-227.
424. Siegel, D.; Epand, R., The mechanism of lamellar-to-inverted hexagonal phase transitions in phosphatidylethanolamine: implications for membrane fusion mechanisms. *Biophys. J.* **1997,** *73* (6), 3089-3111.

425. Veremeeva, P. N.; Lapteva, V. L.; Palyulin, V. A.; Sybachin, A. V.; Yaroslavov, A. A.; Zefirov, N. S., Bispidinone-based molecular switches for construction of stimulus-sensitive liposomal containers. *Tetrahedron* **2014,** *70* (7), 1408-1411.
426. Jimah, J. R.; Schlesinger, P. H.; Tolia, N. H., Liposome disruption assay to examine lytic properties of biomolecules. *Bio-protoc.* **2017,** *7* (15), e2433-e2433.
427. Ha, Y.; Koo, Y.; Park, S.-K.; Kim, G.-E.; Oh, H. B.; Kim, H. R.; Kwon, J.-H., Liposome leakage and increased cellular permeability induced by guanidine-based oligomers: effects of liposome composition on liposome leakage and human lung epithelial barrier permeability. *RSC Adv.* **2021,** *11* (51), 32000-32011.
428. Shen, R.; Yang, J.; Luo, H.; Wang, B.; Jiang, Y., A sensitive fluorescent probe for cysteine and Cu2+ based on 1, 8-naphthalimide derivatives and its application in living cells imaging. *Tetrahedron* **2017,** *73* (4), 373-377.
429. Yu, Y.; Yang, J.; Xu, X.; Jiang, Y.; Wang, B., A novel fluorescent probe for highly sensitive and selective detection of cysteine and its application in cell imaging. *Sens. Actuators, B* **2017,** *251*, 902-908.
430. Zhang, H.; Feng, W.; Feng, G., A simple and readily available fluorescent turn-on probe for cysteine detection and bioimaging in living cells. *Dyes Pigm.* **2017,** *139*, 73-78.
431. Zhou, X.; Guo, D.; Jiang, Y.; Gong, D.-m.; Zhao, X.-j.; Zhou, L.-y., A novel AIEE and EISPT fluorescent probe for selective detection of cysteine. *Tetrahedron Letters* **2017,** *58* (33), 3214-3218.
432. Wei, L.-F.; Thirumalaivasan, N.; Liao, Y.-C.; Wu, S.-P., Fluorescent coumarin-based probe for cysteine and homocysteine with live cell application. *Spectrochim. Acta, Part A* **2017,** *183*, 204-208.
433. Kang, Y.-F.; Qiao, H.-X.; Meng, Y.-L.; Xin, Z.-H.; Ge, L.-P.; Zheng, J.-N.; Wang, Y.-N., A simple and sensitive fluorescent probe for specific detection of cysteine. *J. Chem. Sci.* **2017,** *129*, 1219-1223.
434. Chen, C.; Zhou, L.; Huang, X.; Liu, W., Rapid detection of intracellular Cys over Hcy and GSH using a novel two-photon coumarinocoumarin-based colorimetric and fluorescent probe. *J. Mater. Chem. B* **2017,** *5* (29), 5892-5897.
435. Dai, X.; Zhang, T.; Liu, Y.-Z.; Yan, T.; Li, Y.; Miao, J.-Y.; Zhao, B.-X., A ratiometric fluorescent probe for cysteine and its application in living cells. *Sens. Actuators, B* **2015,** *207*, 872-877.
436. Feng, S.; Fang, Y.; Feng, W.; Xia, Q.; Feng, G., A colorimetric and ratiometric fluorescent probe with enhanced near-infrared fluorescence for selective detection of cysteine and its application in living cells. *Dyes Pigm.* **2017,** *146*, 103-111.
437. Tong, H.; Zhao, J.; Li, X.; Zhang, Y.; Ma, S.; Lou, K.; Wang, W., Orchestration of dual cyclization processes and dual quenching mechanisms for enhanced selectivity and drastic fluorescence turn-on detection of cysteine. *Chem. Commun.* **2017,** *53* (25), 3583-3586.
438. Liu, X.; Yang, D.; Chen, W.; Yang, L.; Qi, F.; Song, X., A red-emitting fluorescent probe for specific detection of cysteine over homocysteine and glutathione with a large Stokes shift. *Sens. Actuators, B* **2016,** *234*, 27-33.

439. Nawimanage, R. R.; Prasai, B.; Hettiarachchi, S. U.; McCarley, R. L., Cascade reaction-based, near-infrared multiphoton fluorescent probe for the selective detection of cysteine. *Anal. Chem.* **2017,** *89* (12), 6886-6892.
440. Fu, Y.-J.; Li, Z.; Li, C.-Y.; Li, Y.-F.; Wu, P.; Wen, Z.-H., Borondipyrrolemethene-based fluorescent probe for distinguishing cysteine from biological thiols and its application in cell image. *Dyes Pigm.* **2017,** *139*, 381-387.
441. Fan, W.; Huang, X.; Shi, X.; Wang, Z.; Lu, Z.; Fan, C.; Bo, Q., A simple fluorescent probe for sensing cysteine over homocysteine and glutathione based on PET. *Spectrochim. Acta, Part A* **2017,** *173*, 918-923.
442. Song, X.; Dong, B.; Kong, X.; Wang, C.; Zhang, N.; Lin, W., A sensitive and selective red fluorescent probe for imaging of cysteine in living cells and animals. *Anal. Methods* **2017,** *9* (12), 1891-1896.
443. Liu, Y.; Xiang, K.; Tian, B.; Zhang, J., Rhodol-based far-red fluorescent probe for the detection of cysteine and homocysteine over glutathione. *Luminescence* **2017,** *32* (1), 78-85.
444. Fu, Z.-H.; Han, X.; Shao, Y.; Fang, J.; Zhang, Z.-H.; Wang, Y.-W.; Peng, Y., Fluorescein-based chromogenic and ratiometric fluorescence probe for highly selective detection of cysteine and its application in bioimaging. *Anal. Chem.* **2017,** *89* (3), 1937-1944.
445. Xue, S.; Ding, S.; Zhai, Q.; Zhang, H.; Feng, G., A readily available colorimetric and near-infrared fluorescent turn-on probe for rapid and selective detection of cysteine in living cells. *Biosens. Bioelectron.* **2015,** *68*, 316-321.
446. Lv, H.-M.; Yuan, D.-H.; Liu, W.; Chen, Y.; Au, C.-T.; Yin, S.-F., A highly selective ESIPT-based fluorescent probe for cysteine sensing and its bioimaging application in living cells. *Sens. Actuators, B* **2016,** *233*, 173-179.
447. Yu, Y.; Xu, H.; Zhang, W.; Han, Q.; Wang, B.; Jiang, Y., A novel near-infrared fluorescent probe for cysteine in living cells based on a push-pull dicyanoisophorone system. *J. Photochem. Photobiol. A.* **2017,** *346*, 215-220.
448. Liu, G.; Liu, D.; Han, X.; Sheng, X.; Xu, Z.; Liu, S. H.; Zeng, L.; Yin, J., A hemicyanine-based colorimetric and ratiometric fluorescent probe for selective detection of cysteine and bioimaging in living cell. *Talanta* **2017,** *170*, 406-412.
449. Xiao, Y.; Guo, Y.; Dang, R.; Yan, X.; Xu, P.; Jiang, P., A dansyl-based fluorescent probe for the highly selective detection of cysteine based on a d-PeT switching mechanism. *RSC Adv.* **2017,** *7* (34), 21050-21053.
450. Wang, P.; Wang, Q.; Huang, J.; Li, N.; Gu, Y., A dual-site fluorescent probe for direct and highly selective detection of cysteine and its application in living cells. *Biosens. Bioelectron.* **2017,** *92*, 583-588.
451. Yan, F.; Sun, X.; Zu, F.; Bai, Z.; Jiang, Y.; Fan, K.; Wang, J., Fluorescent probes for detecting cysteine. *Methods Appl. Fluoresc.* **2018,** *6* (4), 042001.
452. Mosey, R. A.; Floreancig, P. E., Versatile approach to α-alkoxy carbamate synthesis and stimulus-responsive alcohol release. *Org. Biomol. Chem.* **2012,** *10* (39), 7980-7985.
453. Alouane, A.; Labruère, R.; Le Saux, T.; Schmidt, F.; Jullien, L., Self-immolative spacers: kinetic aspects, structure–property relationships, and applications. *Angew. Chem. Int. Ed.* **2015,** *54* (26), 7492-7509.

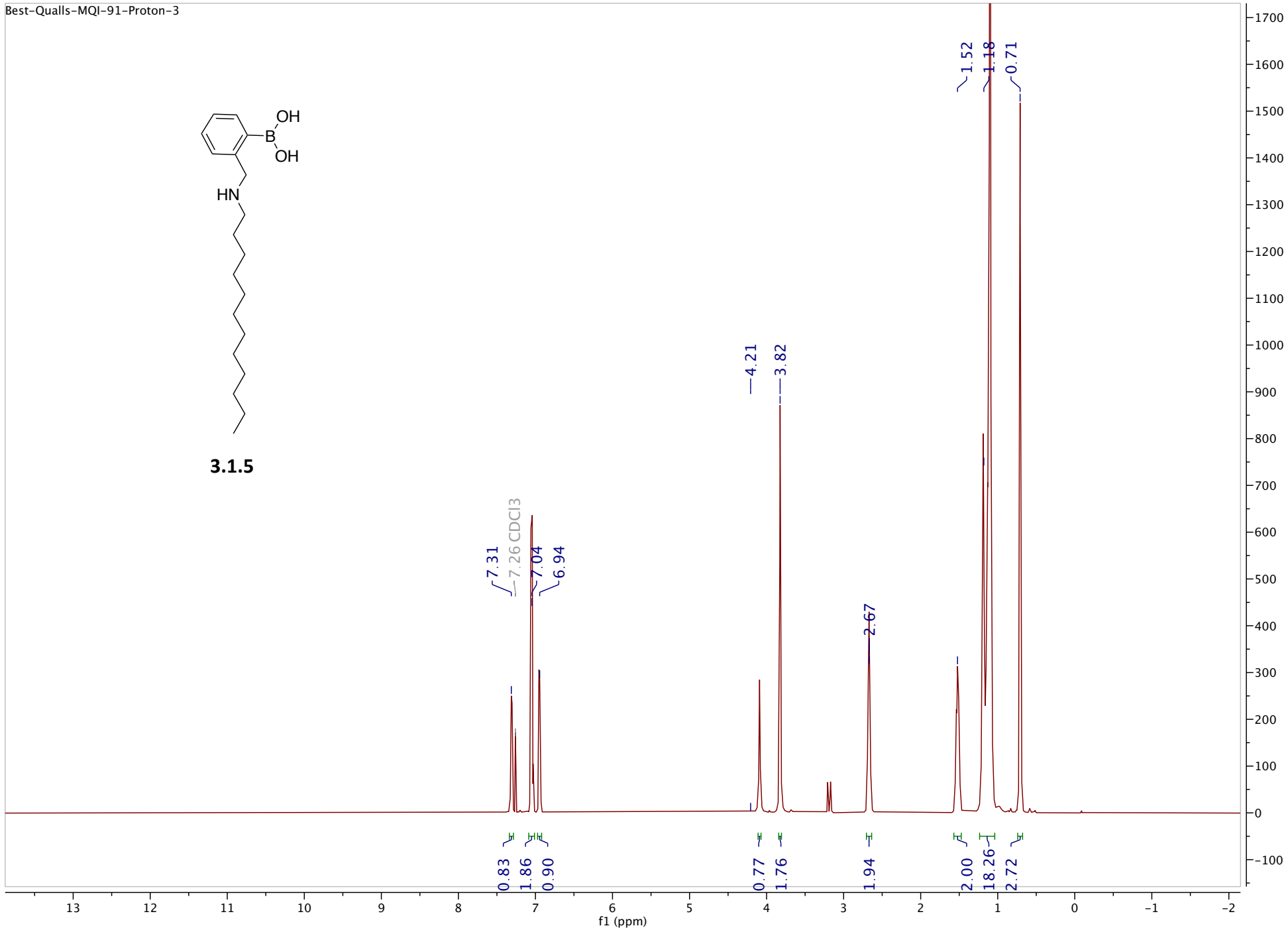
454. Alouane, A.; Labruère, R.; Le Saux, T.; Aujard, I.; Dubruille, S.; Schmidt, F.; Jullien, L., Light Activation for the Versatile and Accurate Kinetic Analysis of Disassembly of Self-Immolative Spacers. *Chem. Eur. J.* **2013,** *19* (35), 11717-11724.
455. Schmid, K. M.; Jensen, L.; Phillips, S. T., A self-immolative spacer that enables tunable controlled release of phenols under neutral conditions. *J. Org. Chem.* **2012,** *77* (9), 4363-4374.
456. Hay, M.; Sykes, B.; Denny, W.; O'Connor, C., Substituent effects on the kinetics of reductively-initiated fragmentation of nitrobenzyl carbamates designed as triggers for bioreductive prodrugs. *J. Chem. Soc., Perkin Trans. 1* **1999,** (19), 2759-2770.
457. Robbins, J. S.; Schmid, K. M.; Phillips, S. T., Effects of electronics, aromaticity, and solvent polarity on the rate of azaquinone–methide-mediated depolymerization of aromatic carbamate oligomers. *J. Org. Chem.* **2013,** *78* (7), 3159-3169.
458. Weinert, E. E.; Dondi, R.; Colloredo-Melz, S.; Frankenfield, K. N.; Mitchell, C. H.; Freccero, M.; Rokita, S. E., Substituents on quinone methides strongly modulate formation and stability of their nucleophilic adducts. *J. Am. Chem. Soc.* **2006,** *128* (36), 11940-11947.
459. Krauss, G., *Biochemistry of signal transduction and regulation*. John Wiley & Sons: 2006.
460. Baldwin, J. M., Structure and function of receptors coupled to G proteins. *Curr. Opin. Cell Biol.* **1994,** *6* (2), 180-190.
461. Strader, C. D.; Fong, T. M.; Tota, M. R.; Underwood, D.; Dixon, R. A., Structure and function of G protein-coupled receptors. *Annu. Rev. Biochem* **1994,** *63* (1), 101-132.
462. Yarden, Y.; Ullrich, A., Molecular analysis of signal transduction by growth factors. *Biochemistry* **1988,** *27* (9), 3113-3119.
463. Schlessinger, J., Cell signaling by receptor tyrosine kinases. *Cell* **2000,** *103* (2), 211-225.
464. Quinn, Z.; Mao, W.; Xia, Y.; John, R.; Wan, Y., Conferring receptors on recipient cells with extracellular vesicles for targeted drug delivery. *Bioact. Mater.* **2021,** *6* (3), 749-756.
465. Clapham, D. E., TRP channels as cellular sensors. *Nature* **2003,** *426* (6966), 517-524.
466. Lister, F. G.; Eccles, N.; Pike, S. J.; Brown, R. A.; Whitehead, G. F.; Raftery, J.; Webb, S. J.; Clayden, J., Bis-pyrene probes of foldamer conformation in solution and in phospholipid bilayers. *Chem. Sci.* **2018,** *9* (33), 6860-6870.
467. Jonathan, M.-C.; Adrián, S.-H.; Gonzalo, A., Type II nuclear receptors with potential role in Alzheimer disease. *Mol. Aspects Med.* **2021,** *78*, 100940.
468. Vance, J. A.; Devaraj, N. K., Membrane mimetic chemistry in artificial cells. *J. Am. Chem. Soc.* **2021,** *143* (22), 8223-8231.
469. Herianto, S.; Chien, P.-J.; Ho, J.-a. A.; Tu, H.-L., Liposome-based artificial cells: From gene expression to reconstitution of cellular functions and phenotypes. *Biomater. Adv.* **2022**, 213156.
470. Morstein, J.; Dacheux, M. A.; Norman, D. D.; Shemet, A.; Donthamsetti, P. C.; Citir, M.; Frank, J. A.; Schultz, C.; Isacoff, E. Y.; Parrill, A. L., Optical control of lysophosphatidic acid signaling. *J. Am. Chem. Soc.* **2020,** *142* (24), 10612-10616.
471. Peng, S.; Barba-Bon, A.; Pan, Y. C.; Nau, W. M.; Guo, D. S.; Hennig, A., Phosphorylation-Responsive Membrane Transport of Peptides. *Angew. Chem. Int. Ed.* **2017,** *56* (49), 15742-15745.

472. Lister, F. G.; Le Bailly, B. A.; Webb, S. J.; Clayden, J., Ligand-modulated conformational switching in a fully synthetic membrane-bound receptor. *Nat. Chem.* **2017,** *9* (5), 420-425.
473. Nussinov, R.; Tsai, C.-J.; Liu, J., Principles of allosteric interactions in cell signaling. *J. Am. Chem. Soc.* **2014,** *136* (51), 17692-17701.
474. Groves, J. T.; Kuriyan, J., Molecular mechanisms in signal transduction at the membrane. *Nat. Struct. Mol. Biol.* **2010,** *17* (6), 659-665.
475. Gurevich, V. V.; Gurevich, E. V., GPCR monomers and oligomers: it takes all kinds. *Trends Neurosci.* **2008,** *31* (2), 74-81.
476. Bernitzki, K.; Schrader, T., Entirely artificial signal transduction with a primary messenger. *Angew. Chem.* **2009,** *121* (43), 8145-8149.
477. Langton, M. J.; Keymeulen, F.; Ciaccia, M.; Williams, N. H.; Hunter, C. A., Controlled membrane translocation provides a mechanism for signal transduction and amplification. *Nat. Chem.* **2017,** *9* (5), 426-430.
478. Langton, M. J.; Williams, N. H.; Hunter, C. A., Recognition-controlled membrane translocation for signal transduction across lipid bilayers. *J. Am. Chem. Soc.* **2017,** *139* (18), 6461-6466.
479. Langton, M. J.; Scriven, L. M.; Williams, N. H.; Hunter, C. A., Triggered release from lipid bilayer vesicles by an artificial transmembrane signal transduction system. *J. Am. Chem. Soc.* **2017,** *139* (44), 15768-15773.
480. Yang, H.; Du, S.; Ye, Z.; Wang, X.; Yan, Z.; Lian, C.; Bao, C.; Zhu, L., A system for artificial light signal transduction via molecular translocation in a lipid membrane. *Chem. Sci.* **2022,** *13* (8), 2487-2494.
481. Liu, S.; Xing, Y.; Yan, T.; Li, Y.; Tian, R.; Hou, J.; Xu, J.; Wang, T.; Liu, J., Regulation of artificial supramolecular transmembrane signal transduction by selenium-containing artificial enzyme receptors. *Nano Res.* **2022**, 1-6.
482. Sinenko, S. A.; Starkova, T. Y.; Kuzmin, A. A.; Tomilin, A. N., Physiological signaling functions of reactive oxygen species in stem cells: from flies to man. *Front. Cell Dev. Biol.* **2021,** *9*, 714370.
483. Finkel, T., Signal transduction by reactive oxygen species. *J. Cell Biol.* **2011,** *194* (1), 7-15.
484. Forrester, S. J.; Kikuchi, D. S.; Hernandes, M. S.; Xu, Q.; Griendling, K. K., Reactive oxygen species in metabolic and inflammatory signaling. *Circ. Res.* **2018,** *122* (6), 877-902.
485. Brown, D. I.; Griendling, K. K., Regulation of signal transduction by reactive oxygen species in the cardiovascular system. *Circ. Res.* **2015,** *116* (3), 531-549.
486. Fubini, B.; Hubbard, A., Reactive oxygen species (ROS) and reactive nitrogen species (RNS) generation by silica in inflammation and fibrosis. *Free Radical Biol. Med.* **2003,** *34* (12), 1507-1516.
487. Davalli, P.; Mitic, T.; Caporali, A.; Lauriola, A.; D'Arca, D., ROS, cell senescence, and novel molecular mechanisms in aging and age-related diseases. *Oxid. Med. Cell. Longev.* **2016,** *2016*.
488. Sosa, V.; Moliné, T.; Somoza, R.; Paciucci, R.; Kondoh, H.; LLeonart, M. E., Oxidative stress and cancer: an overview. *Ageing Res. Rev.* **2013,** *12* (1), 376-390.
489. Szatrowski, T. P.; Nathan, C. F., Production of large amounts of hydrogen peroxide by human tumor cells. *Cancer Res.* **1991,** *51* (3), 794-798.

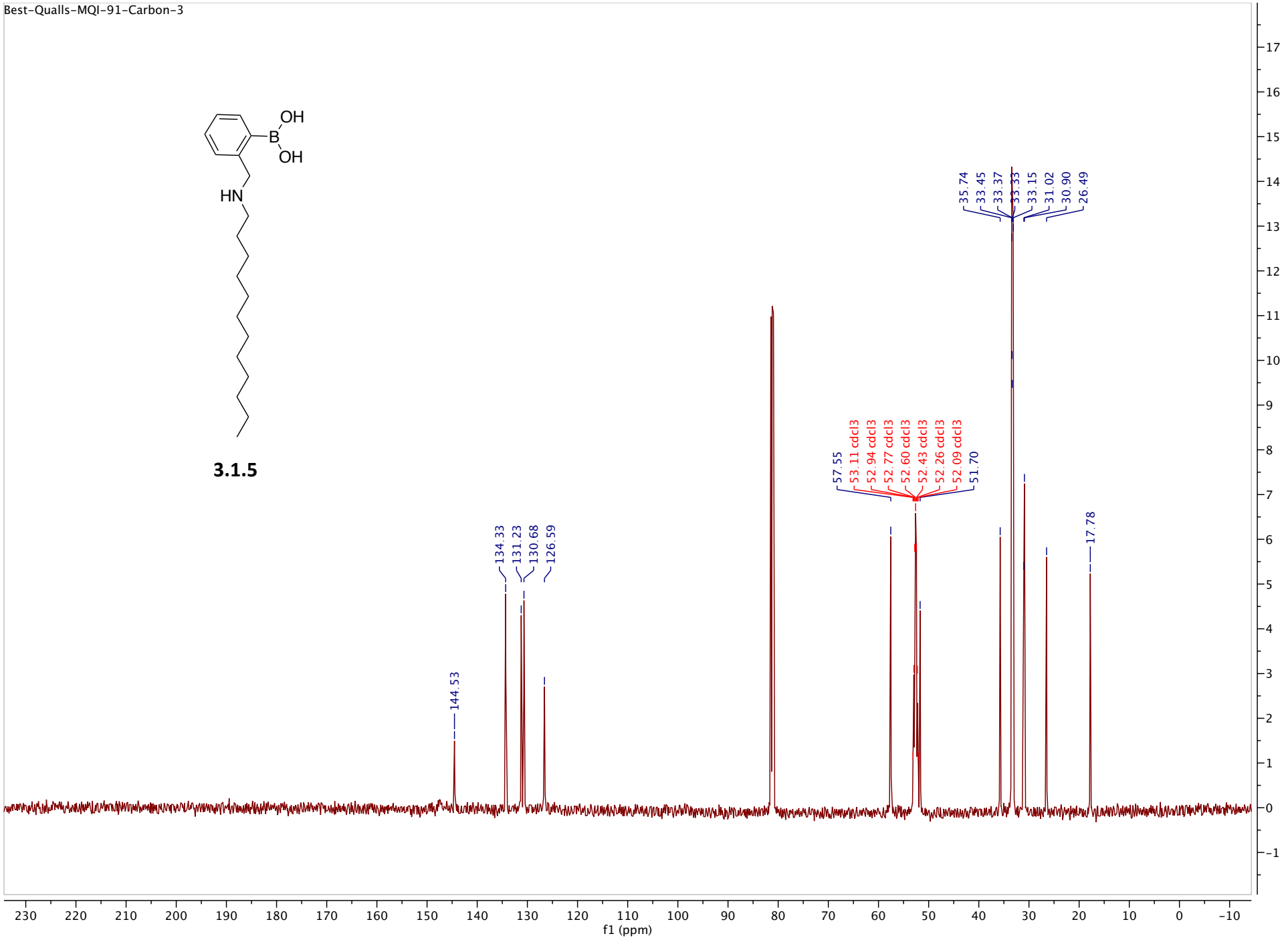
490. Li, Z.; Li, Y.; Liu, Y.; Zheng, Y.; Shen, J.; He, X.; Peng, B., One-step activated fluorescence bioimaging of γ-glutamyltransferase activity in living cancer cells based on chloro-rhodamine probe. *Dyes Pigm.* **2022,** *199*, 109962.
491. Boal, D. H., *Mechanics of the Cell*. 2nd ed.; Cambridge University Press: 2012.
492. Frallicciardi, J.; Melcr, J.; Siginou, P.; Marrink, S. J.; Poolman, B., Membrane thickness, lipid phase and sterol type are determining factors in the permeability of membranes to small solutes. *Nat. Commun.* **2022,** *13* (1), 1605.

Appendix

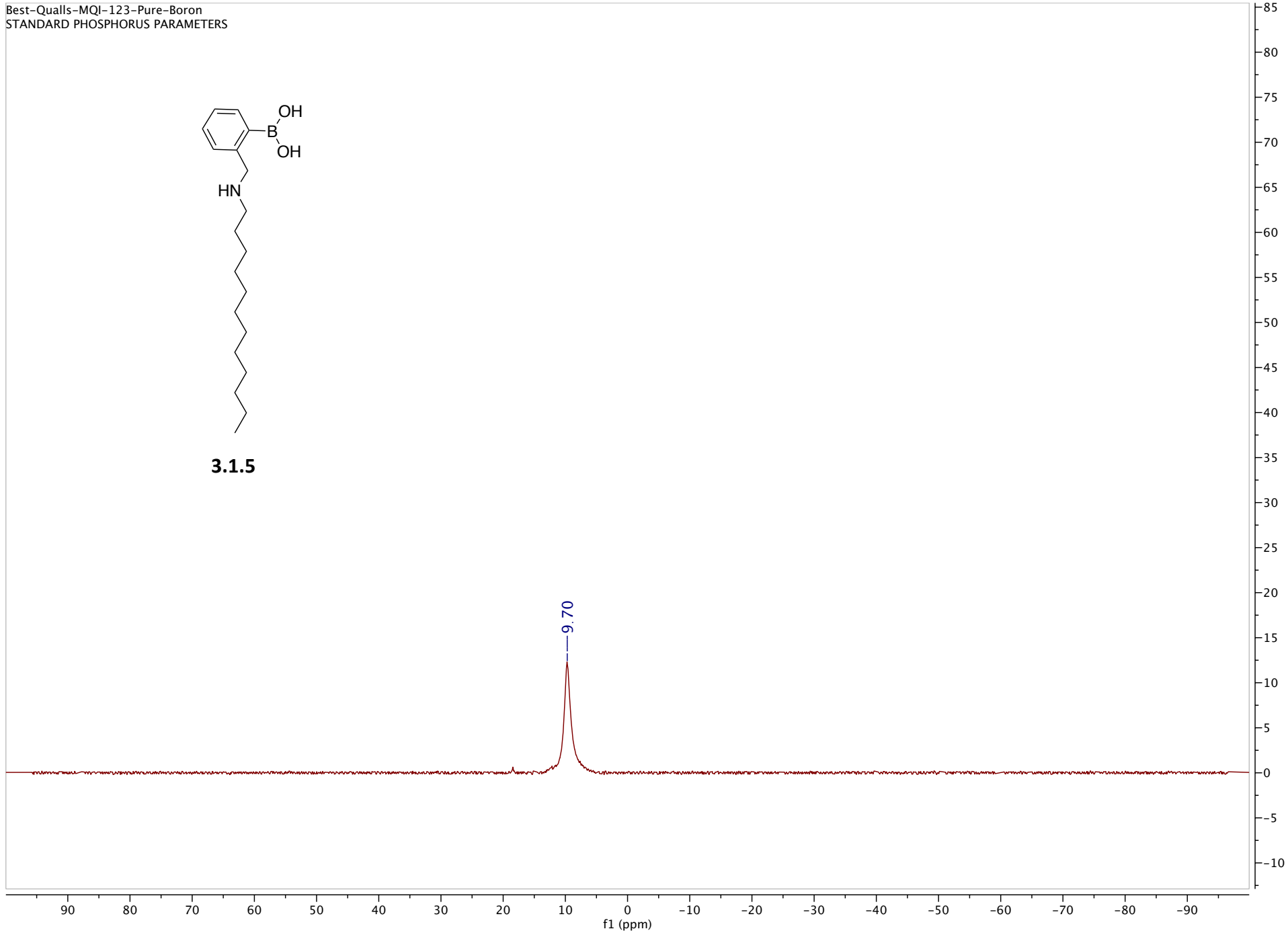
^{1}H NMR


Best-Qualls-MQI-91-Proton-3
OH
B
OH
HN
3.1.5
7.31
7.26 CDCl3
7.04
6.94
4.21
3.82
2.67
1.52
1.18
0.71
0.83
1.86
0.90
0.77
1.76
1.94
2.00
18.26
2.72
f1 (ppm)

^{13}C NMR

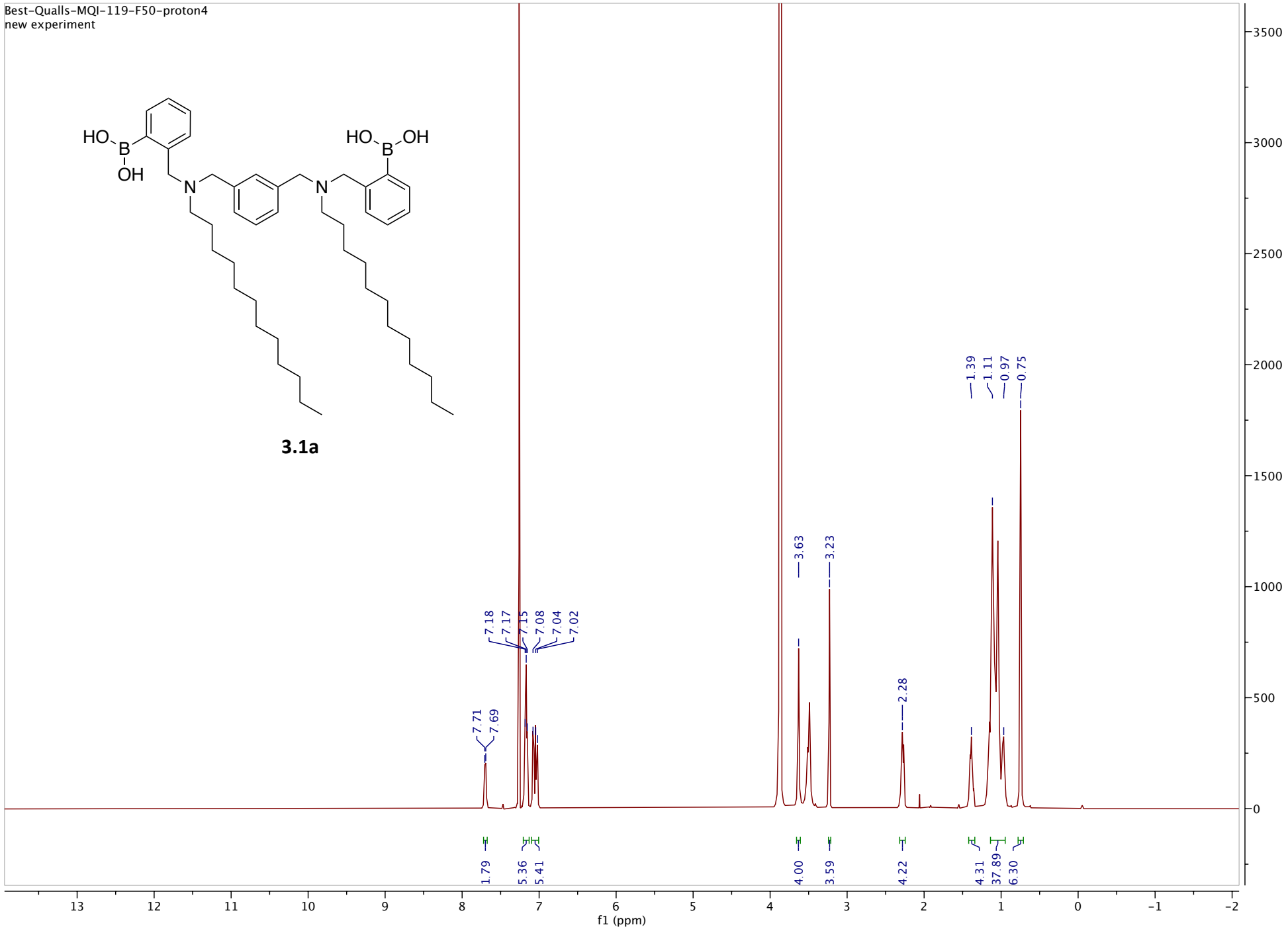

Best-Qualls-MQI-91-Carbon-3
OH
B
OH
HN
3.1.5
144.53
134.33
131.23
130.68
126.59
57.55
53.11 cdcl3
52.94 cdcl3
52.77 cdcl3
52.60 cdcl3
52.43 cdcl3
52.26 cdcl3
52.09 cdcl3
51.70
35.74
33.45
33.37
33.33
33.15
31.02
30.90
26.49
17.78
f1 (ppm)

^{11}B NMR

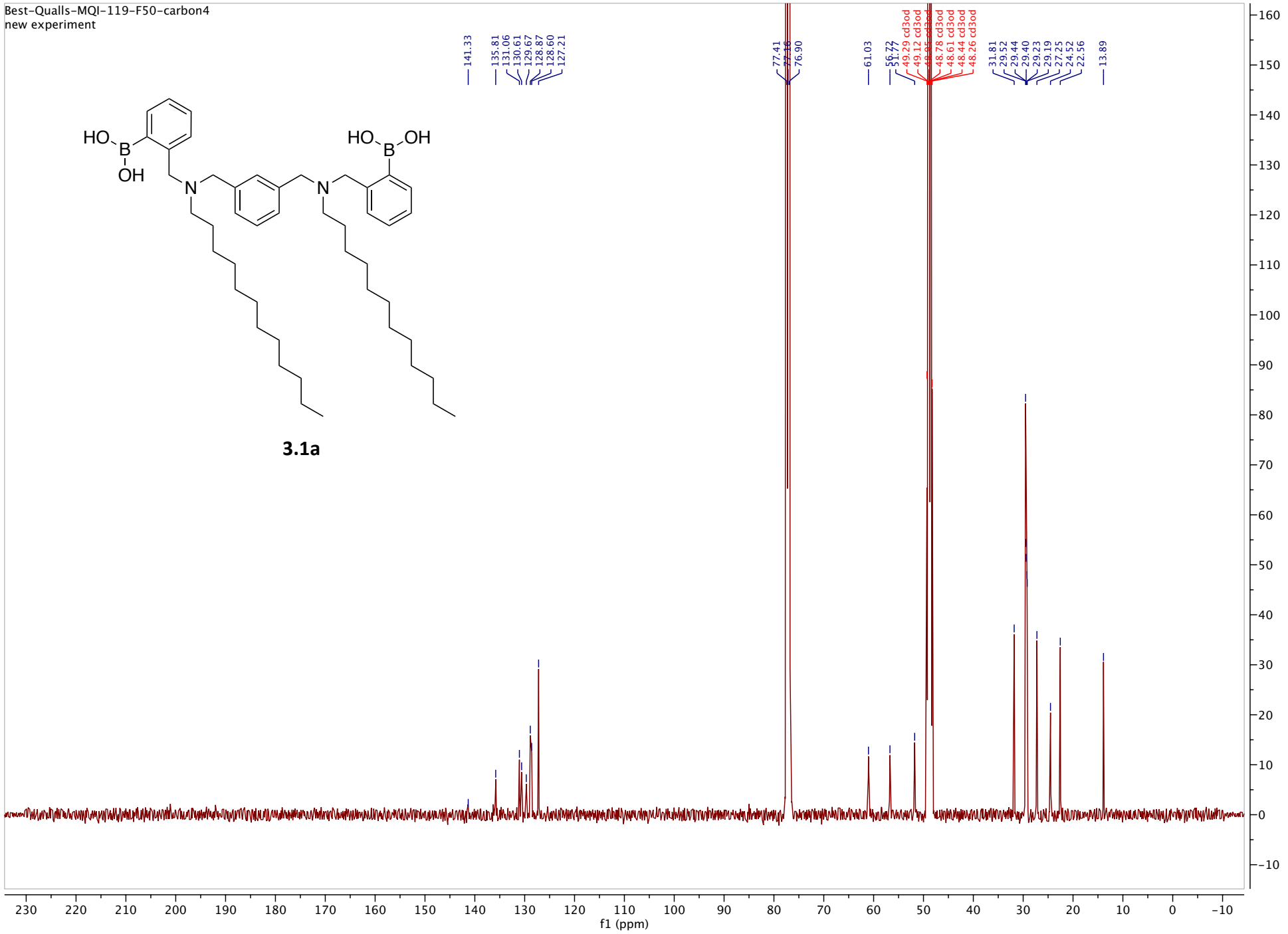

Best-Qualls-MQI-123-Pure-Boron
STANDARD PHOSPHORUS PARAMETERS
OH
B
OH
HN
9.70
f1 (ppm)

3.1.5

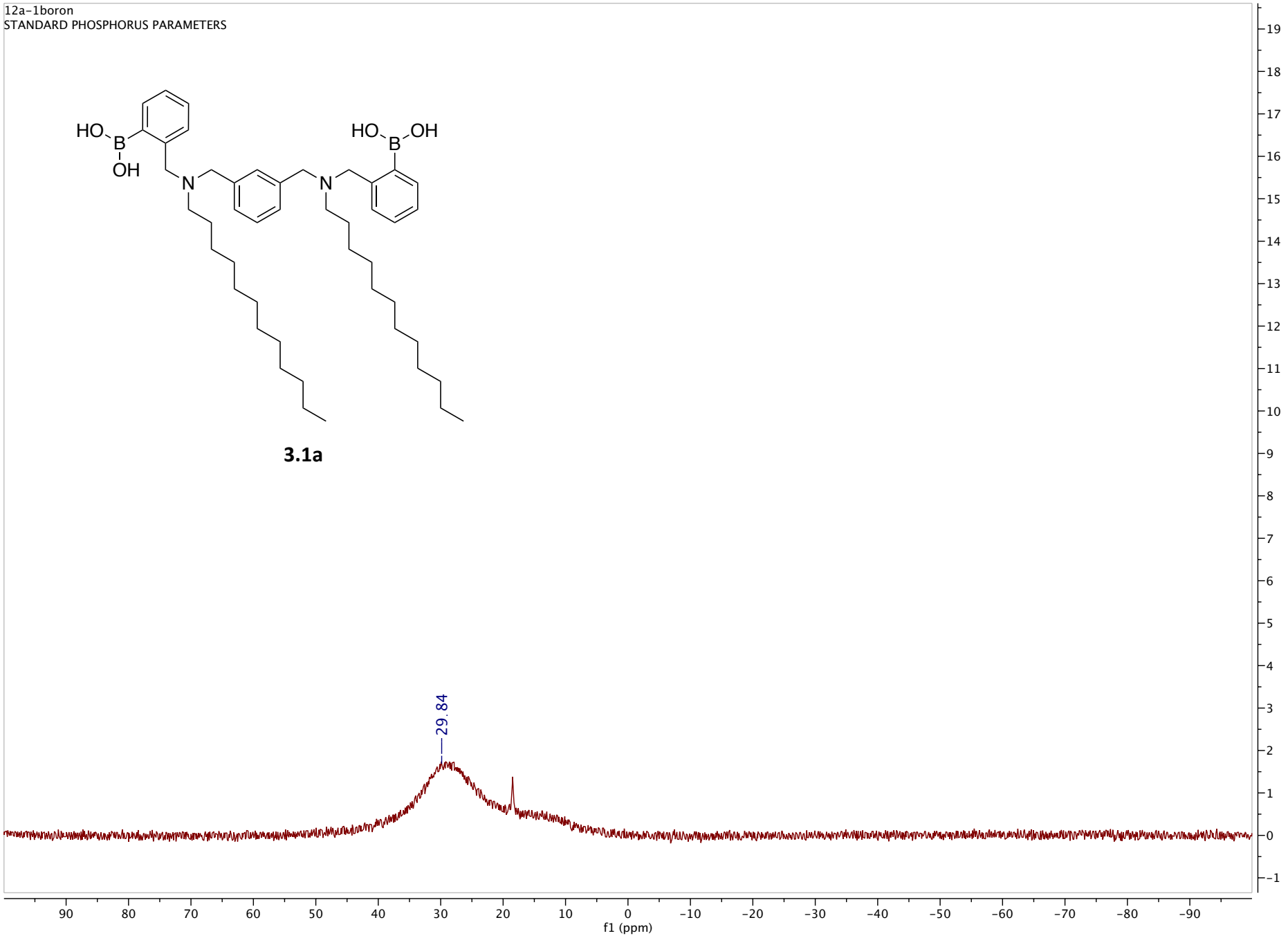
^{1}H NMR


Best-Qualls-MQI-119-F50-proton4
new experiment
HO
B
OH
N
HO
B
OH
N
3.1a
7.71
7.69
7.18
7.17
7.15
7.08
7.04
7.02
3.63
3.23
2.28
1.39
1.11
0.97
0.75
1.79
5.36
5.41
4.00
3.59
4.22
4.31
37.89
6.30
f1 (ppm)

^{13}C NMR

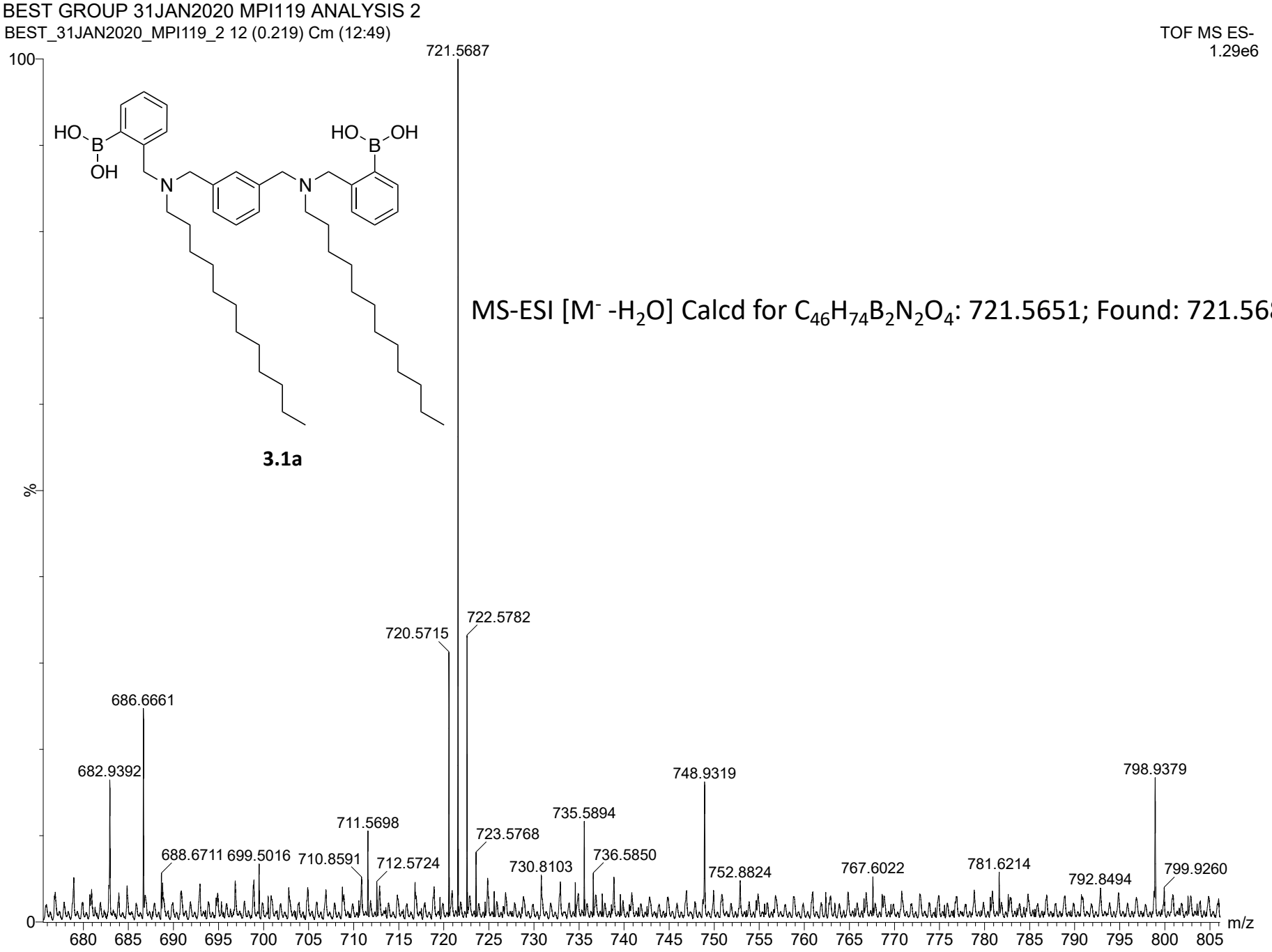

Best-Qualls-MQI-119-F50-carbon4
new experiment
141.33
135.81
131.06
130.61
129.67
128.87
128.60
127.21
77.41
77.16
76.90
61.03
56.72
51.77
49.29 cd3od
49.12 cd3od
48.78 cd3od
48.61 cd3od
48.44 cd3od
48.26 cd3od
31.81
29.52
29.44
29.40
29.23
29.19
27.25
24.52
22.56
13.89
HO
B
OH
N
HO
B
OH
N
3.1a
f1 (ppm)

^{11}B NMR


12a-1boron
STANDARD PHOSPHORUS PARAMETERS
HO
B
OH
N
N
HO
B
OH
29.84
f1 (ppm)

3.1a

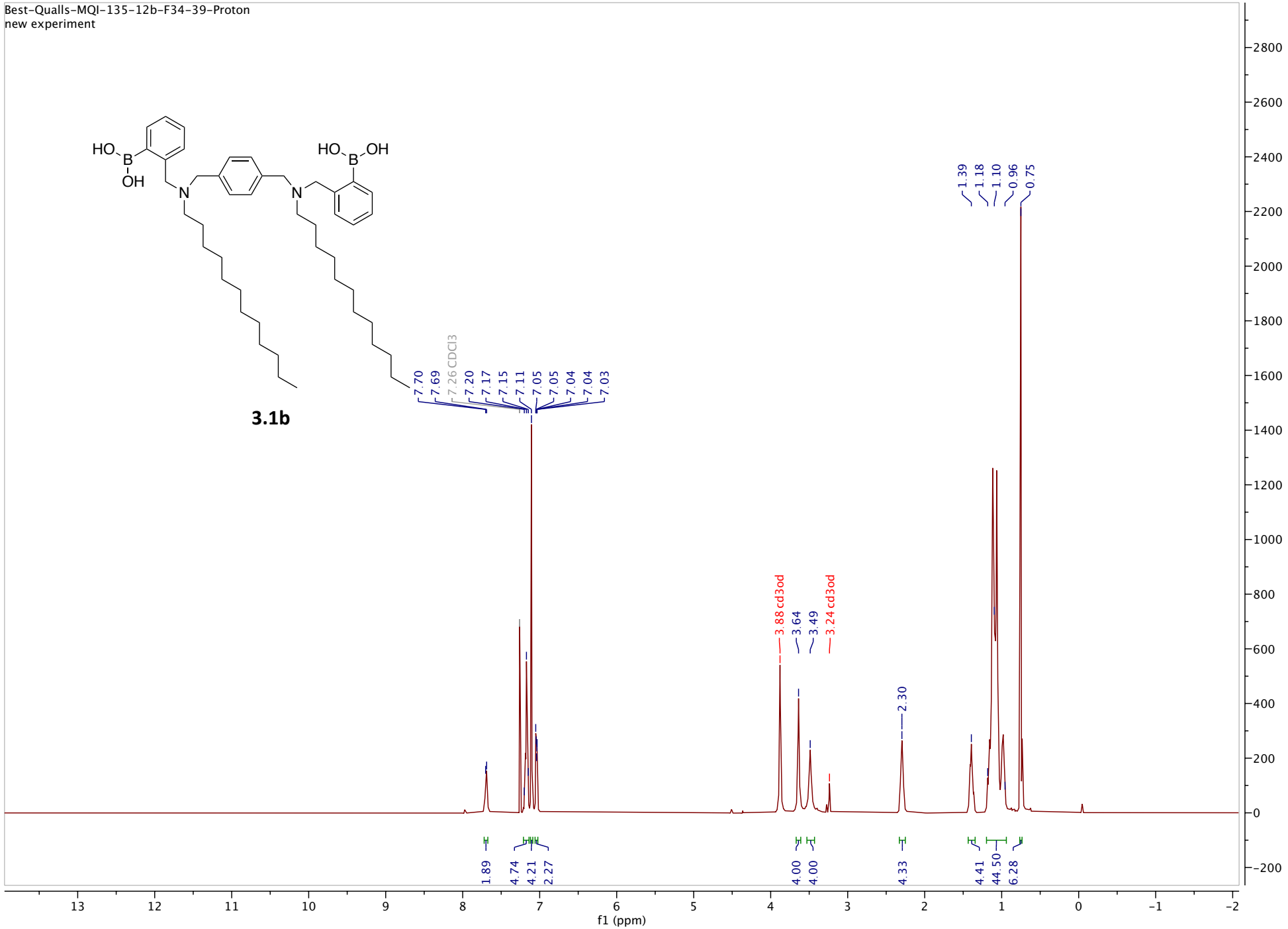
ESI-MS



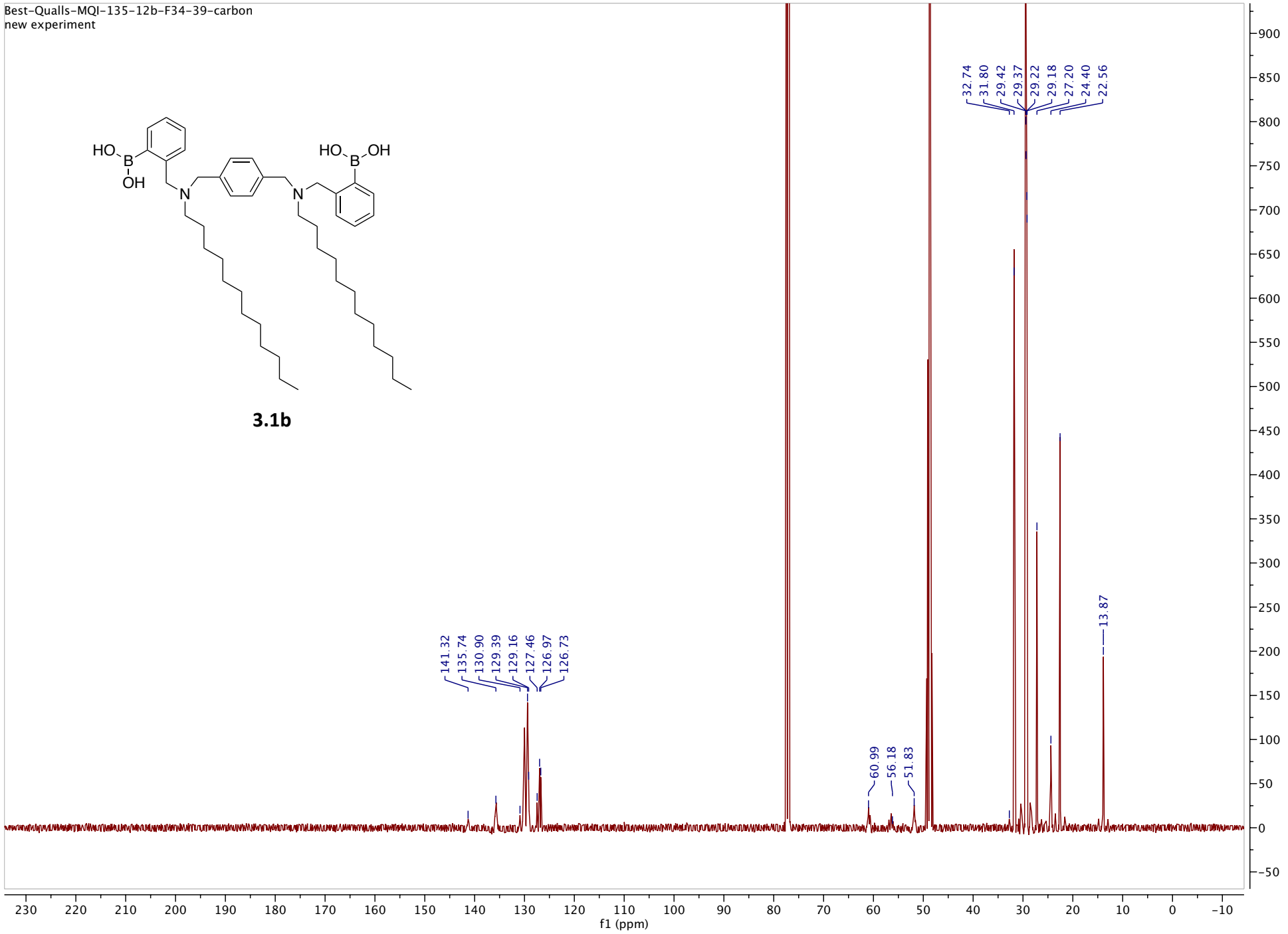
3.1a

MS-ESI [M^- -H_2O] Calcd for $C_{46}H_{74}B_2N_2O_4$: 721.5651; Found: 721.5687

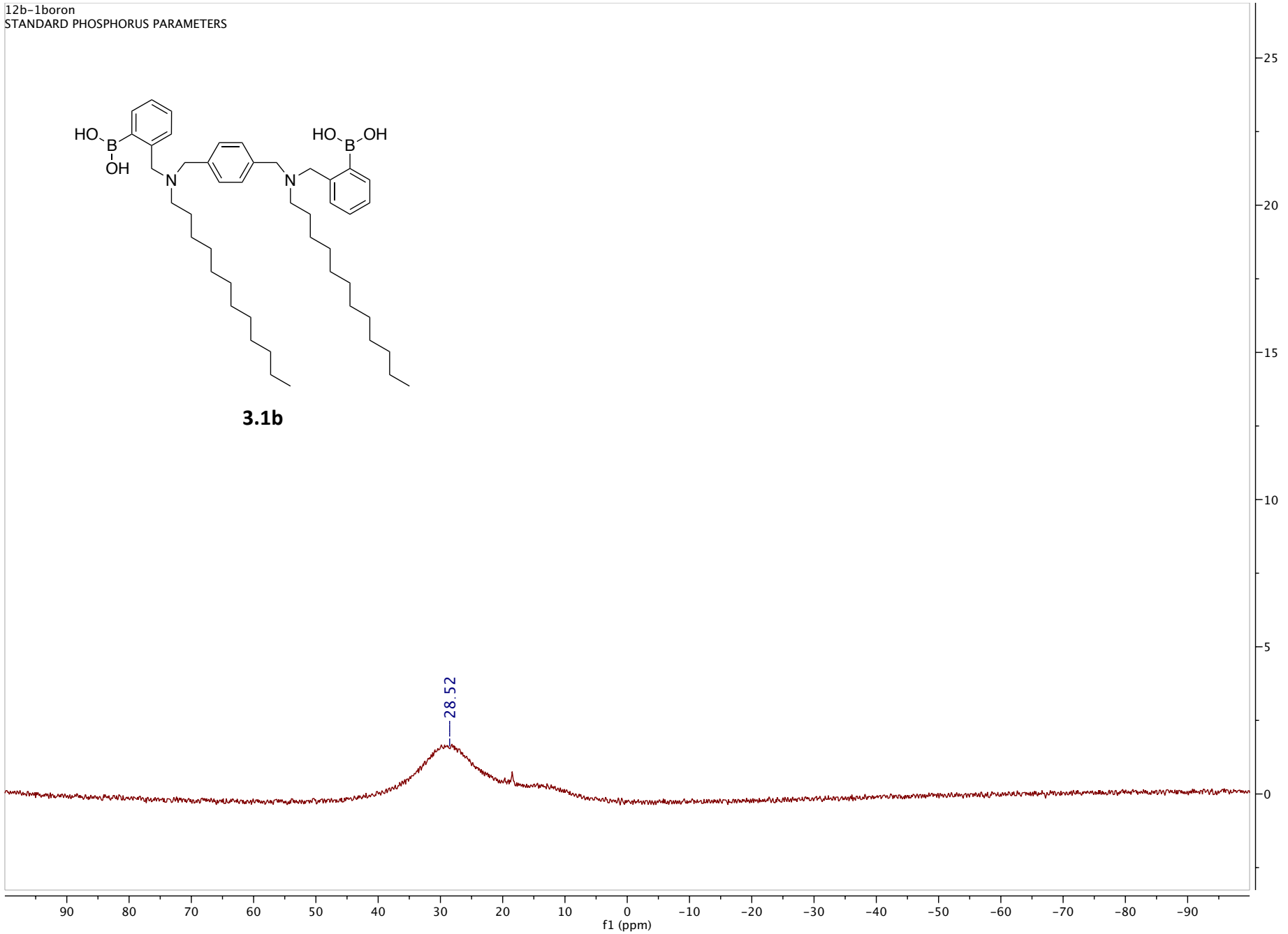
^{1}H NMR


Best-Qualls-MQI-135-12b-F34-39-Proton
new experiment
HO
B
OH
N
HO
B
OH
3.1b
7.70
7.69
7.26 CDCl3
7.20
7.17
7.15
7.11
7.05
7.05
7.04
7.04
7.03
1.39
1.18
1.10
0.96
0.75
3.88 cd3od
3.64
3.49
3.24 cd3od
2.30
1.89
4.74
4.21
2.27
4.00
4.00
4.33
4.41
44.50
6.28
f1 (ppm)

^{13}C NMR

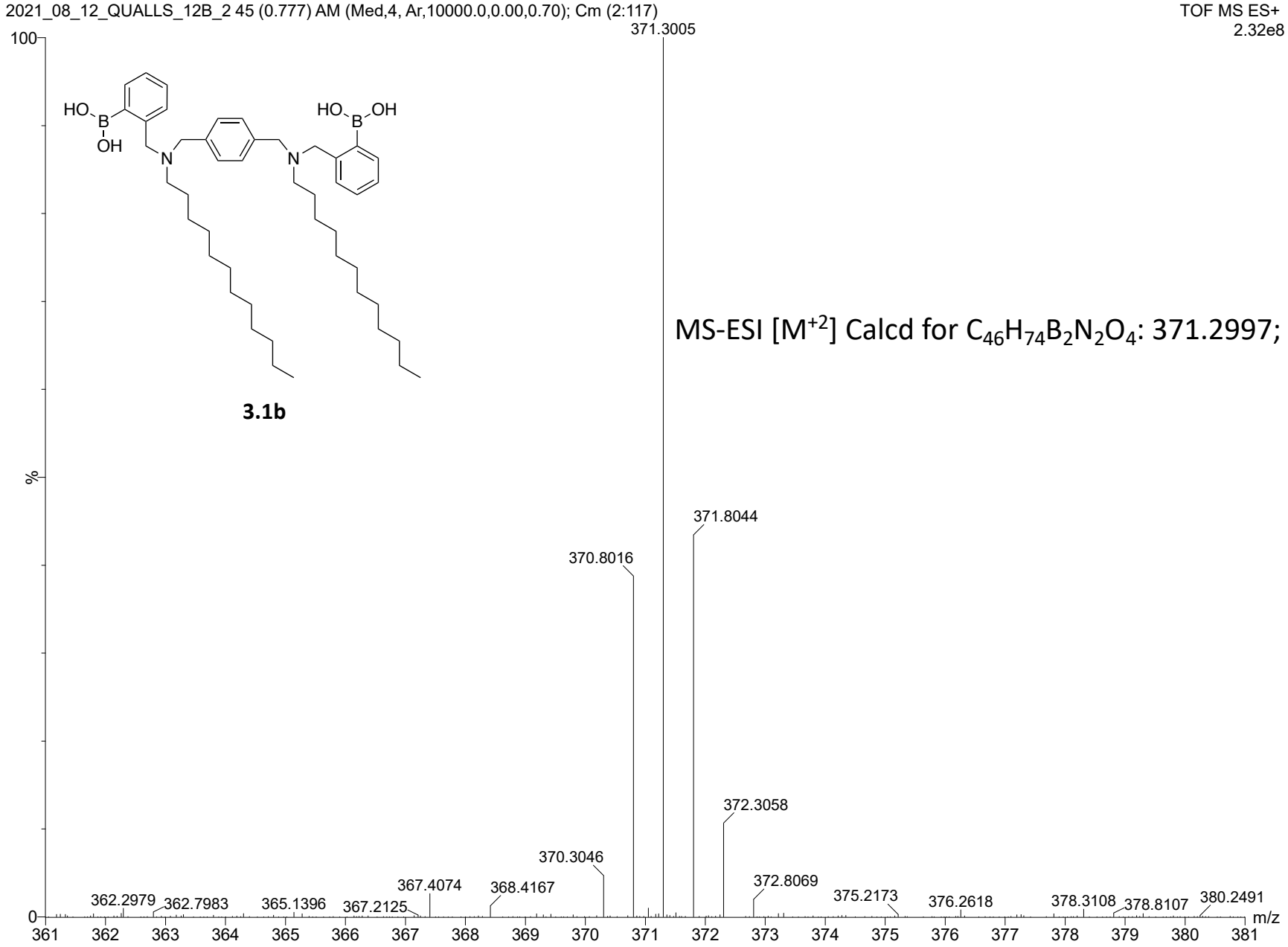

Best-Qualls-MQI-135-12b-F34-39-carbon
new experiment
HO
B
OH
N
HO
B
OH
N
3.1b
32.74
31.80
29.42
29.37
29.22
29.18
27.20
24.40
22.56
141.32
135.74
130.90
129.39
129.16
127.46
126.97
126.73
60.99
56.18
51.83
13.87
f1 (ppm)

^{11}B NMR


12b-1boron
STANDARD PHOSPHORUS PARAMETERS
HO
B
OH
N
N
HO
B
OH
28.52
25
20
15
10
5
0
90
80
70
60
50
40
30
20
10
0
-10
-20
-30
-40
-50
-60
-70
-80
-90
f1 (ppm)

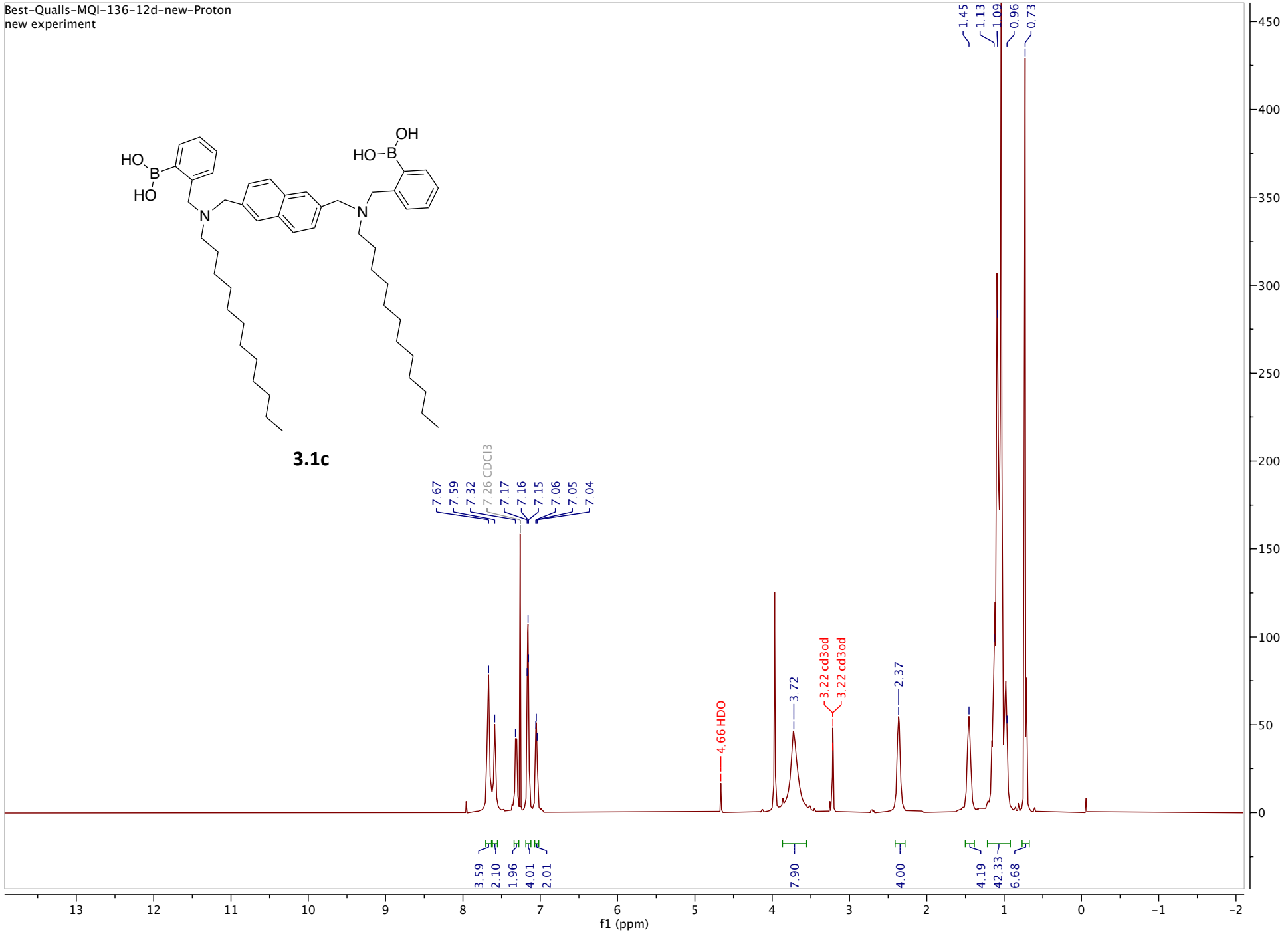
3.1b

ESI-MS

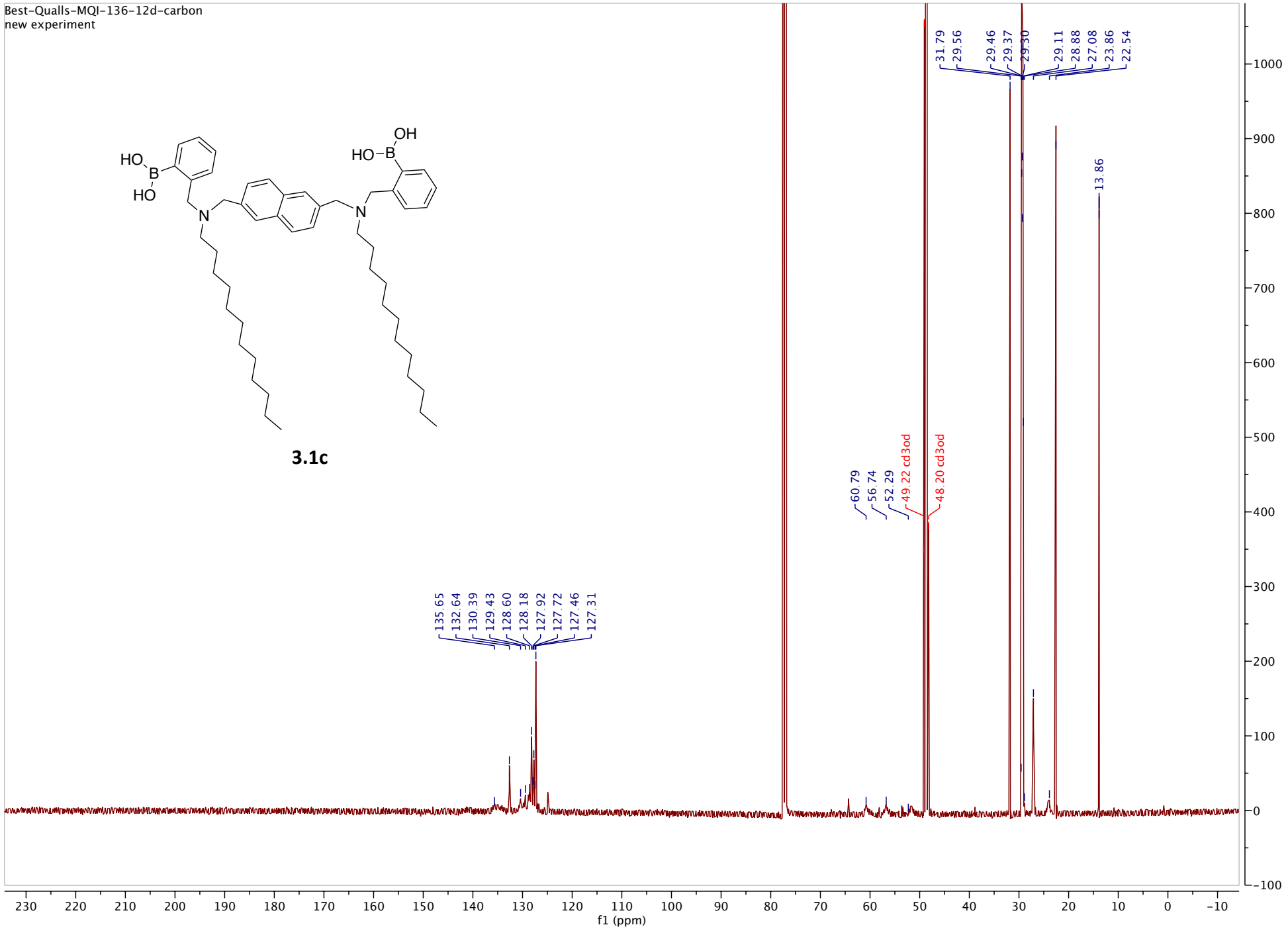


MS-ESI [M^{+2}] Calcd for $C_{46}H_{74}B_2N_2O_4$: 371.2997; Found: 371.3005

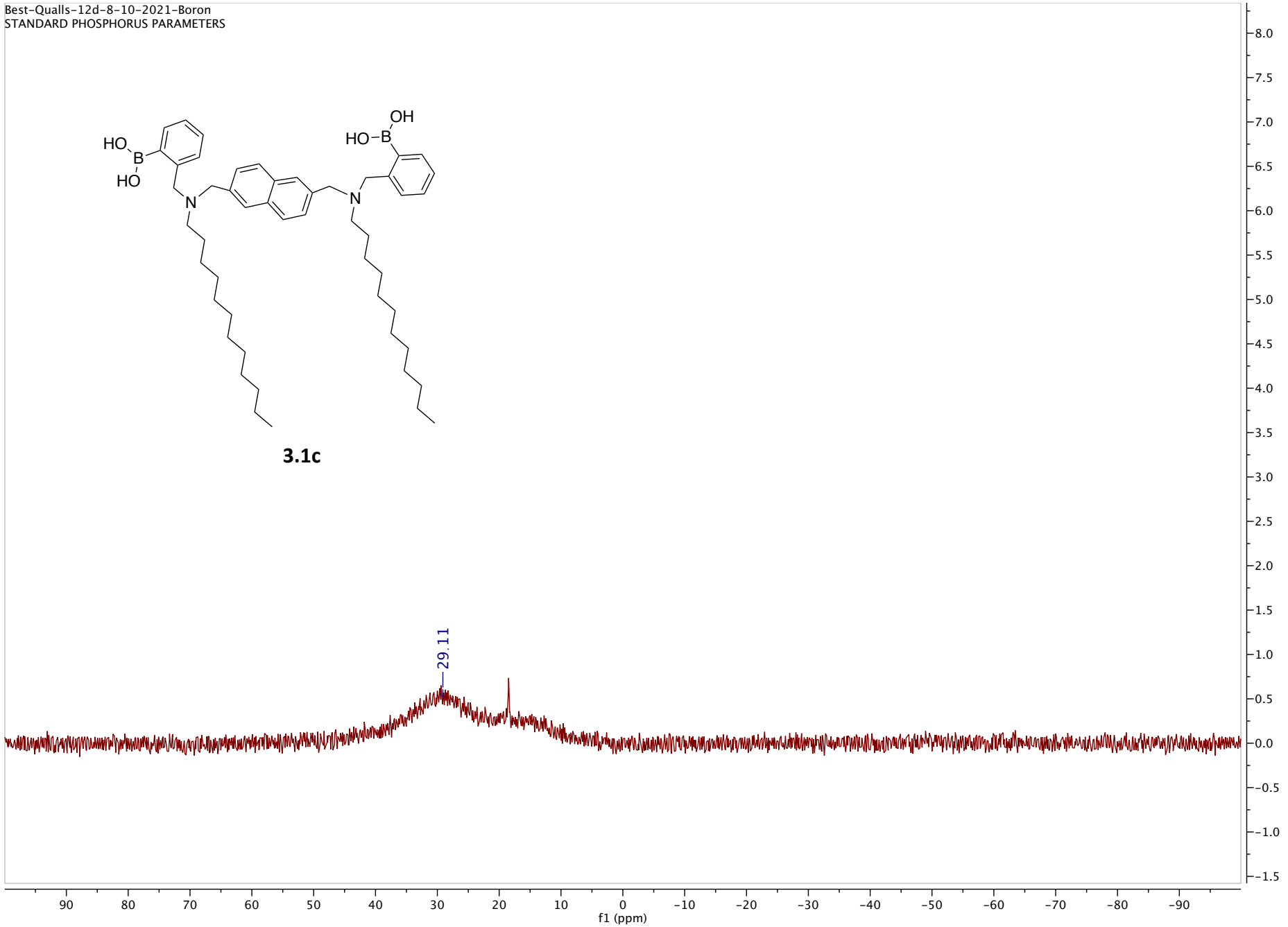
^{1}H NMR


Best-Qualls-MQI-136-12d-new-Proton
new experiment
HO
B
HO
OH
HO–B
N
N
3.1c
7.67
7.59
7.32
7.26 CDCl3
7.17
7.16
7.15
7.06
7.05
7.04
4.66 HDO
3.72
3.22 cd3od
3.22 cd3od
2.37
1.45
1.13
1.09
0.96
0.73
3.59
2.10
1.96
4.01
2.01
7.90
4.00
4.19
42.33
6.68
f1 (ppm)

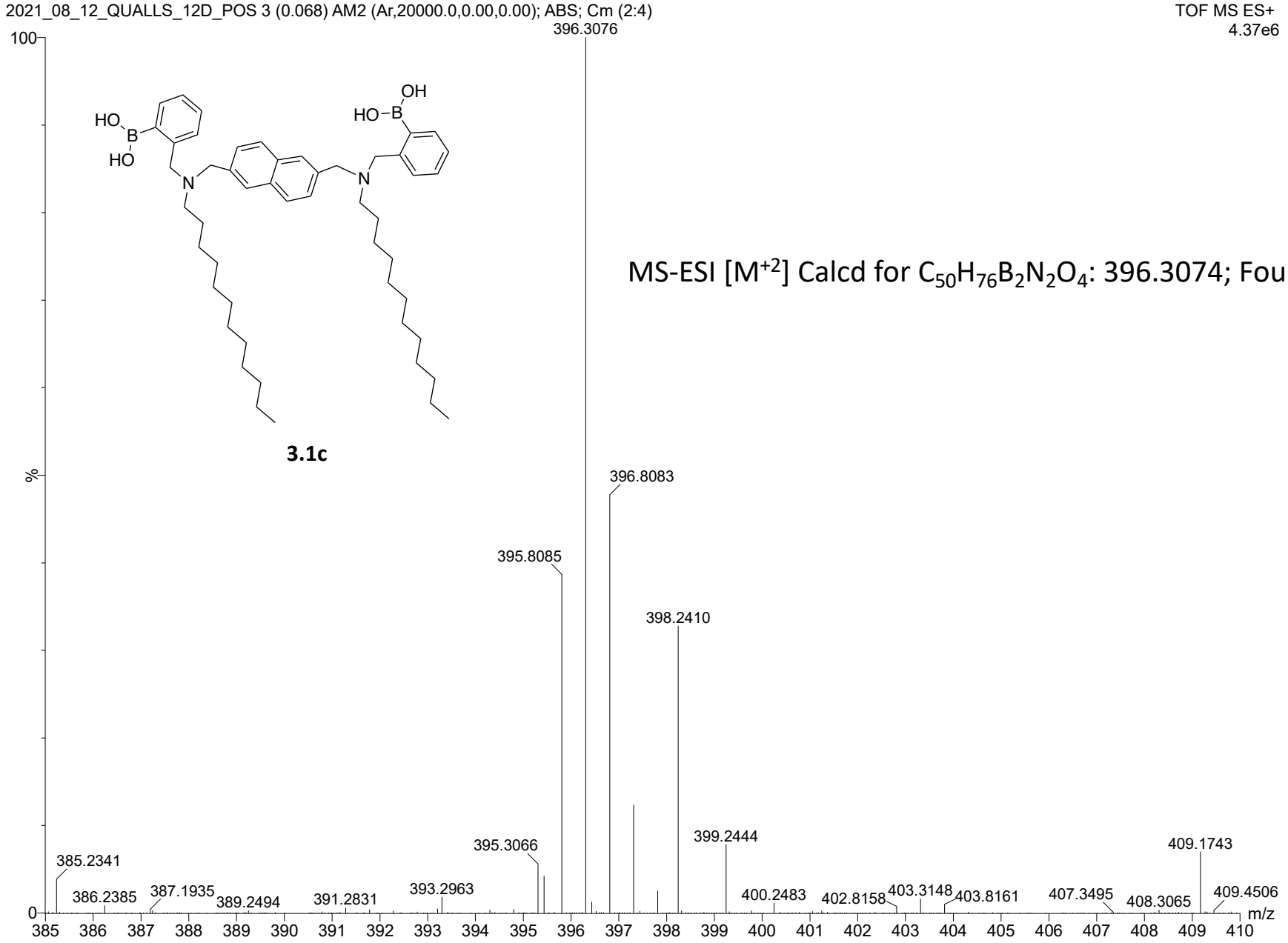
^{13}C NMR


Best-Qualls-MQI-136-12d-carbon
new experiment
HO
B
HO
OH
HO–B
N
N
3.1c
31.79
29.56
29.46
29.37
29.30
29.11
28.88
27.08
23.86
22.54
13.86
60.79
56.74
52.29
49.22 cd3od
48.20 cd3od
135.65
132.64
130.39
129.43
128.60
128.18
127.92
127.72
127.46
127.31
f1 (ppm)

^{11}B NMR


Best-Qualls-12d-8-10-2021-Boron
STANDARD PHOSPHORUS PARAMETERS
HO
B
HO
N
OH
HO–B
N
3.1c
29.11
8.0
7.5
7.0
6.5
6.0
5.5
5.0
4.5
4.0
3.5
3.0
2.5
2.0
1.5
1.0
0.5
0.0
-0.5
-1.0
-1.5
90
80
70
60
50
40
30
20
10
0
-10
-20
-30
-40
-50
-60
-70
-80
-90
f1 (ppm)

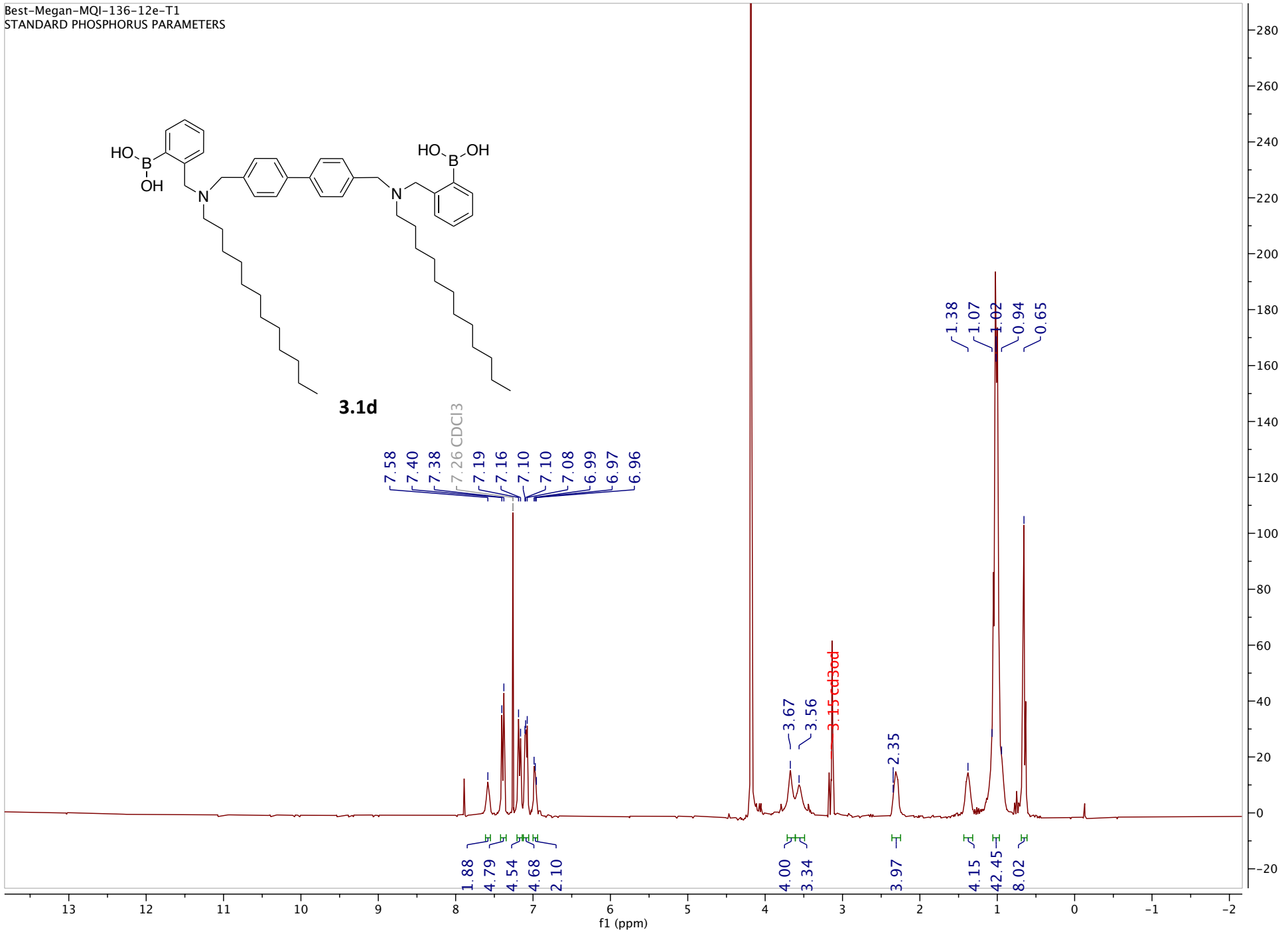
ESI-MS



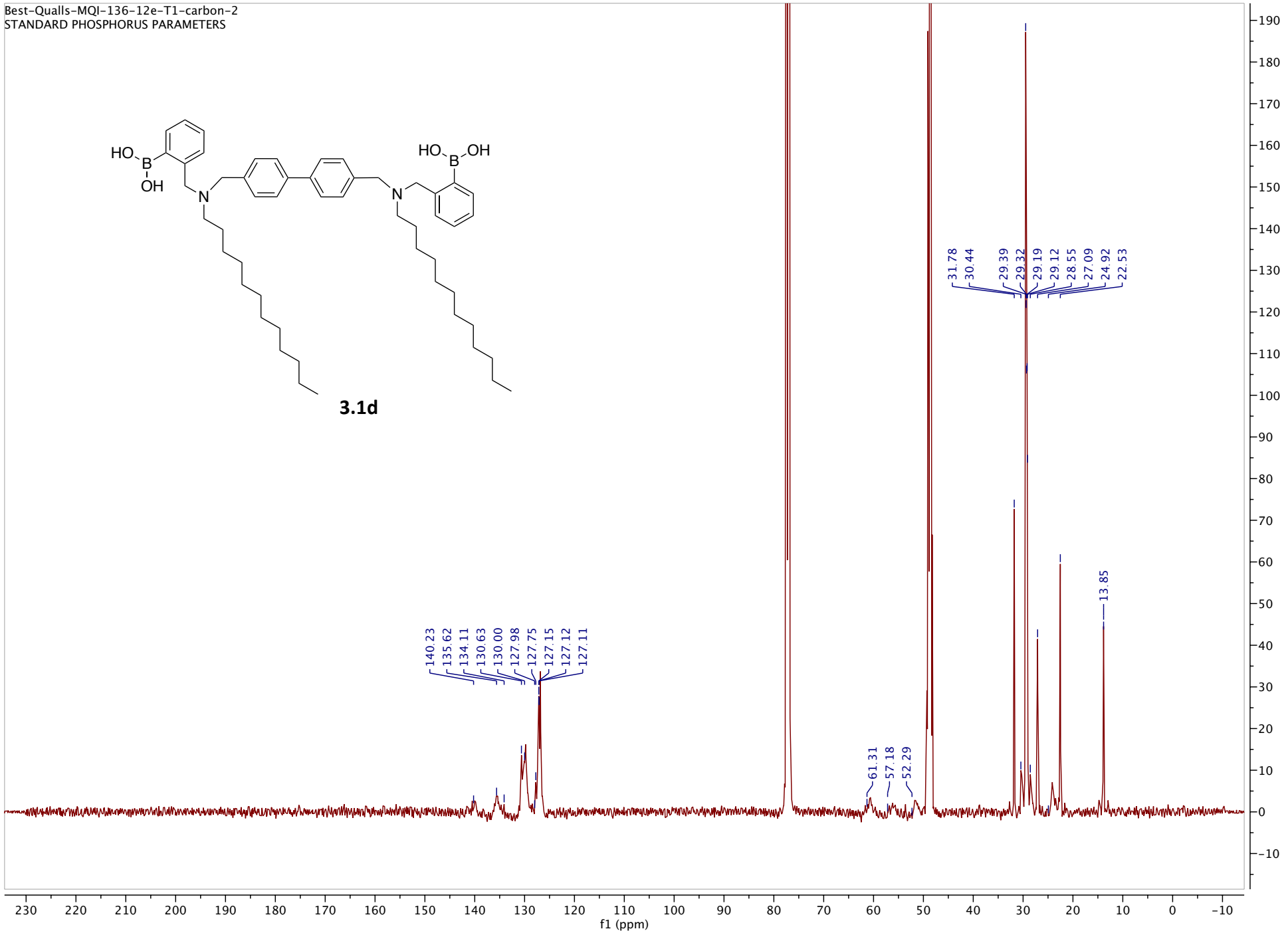
3.1c

MS-ESI [M^{+2}] Calcd for $C_{50}H_{76}B_2N_2O_4$: 396.3074; Found: 396.3076

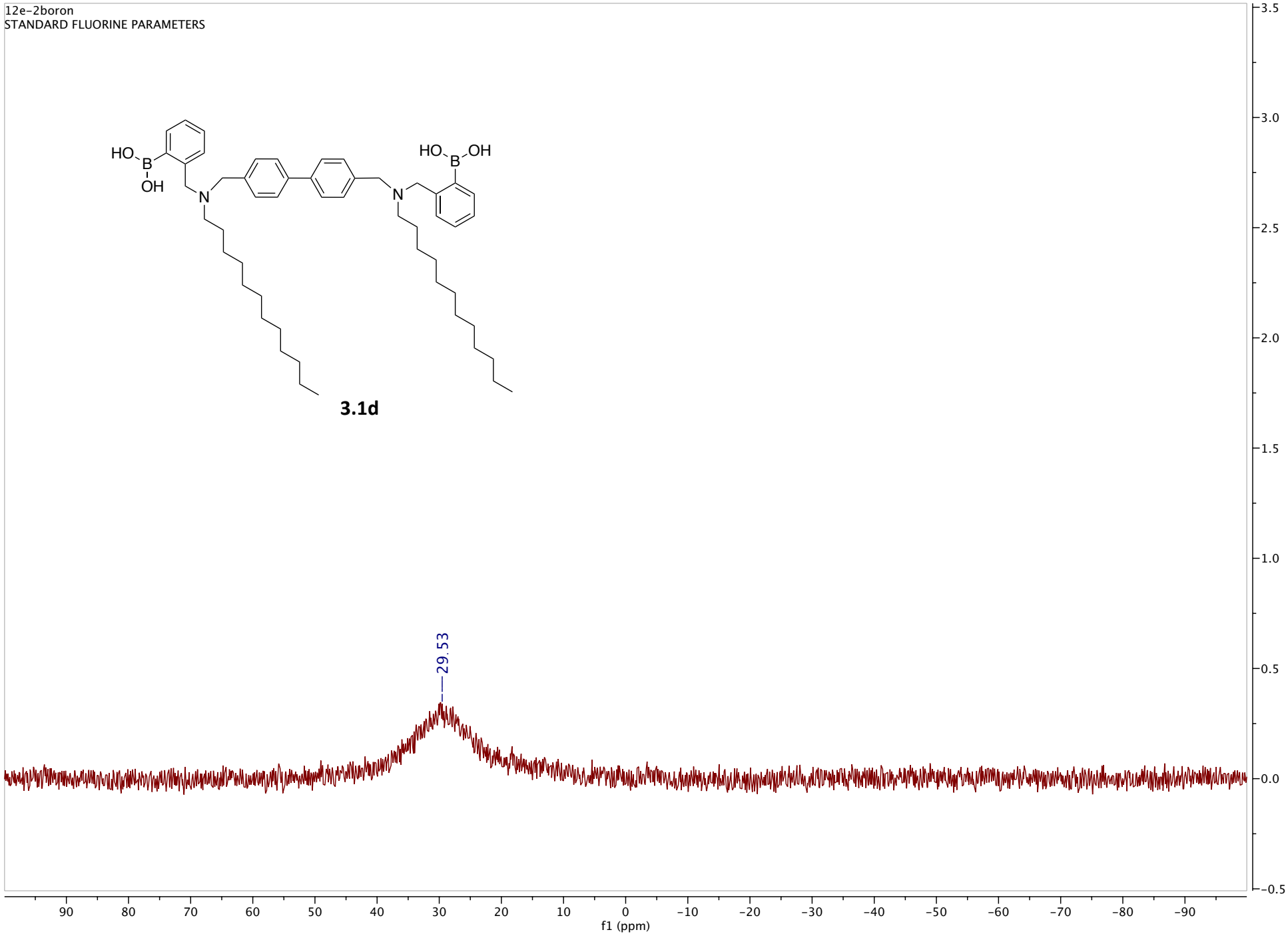
^{1}H NMR


Best-Megan-MQI-136-12e-T1
STANDARD PHOSPHORUS PARAMETERS
HO
B
OH
N
HO
B
OH
N
3.1d
7.58
7.40
7.38
7.26 CDCl3
7.19
7.16
7.10
7.10
7.08
6.99
6.97
6.96
1.38
1.07
1.02
0.94
0.65
3.67
3.56
3.15 cd3od
2.35
1.88
4.79
4.54
4.68
2.10
4.00
3.34
3.97
4.15
42.45
8.02
f1 (ppm)

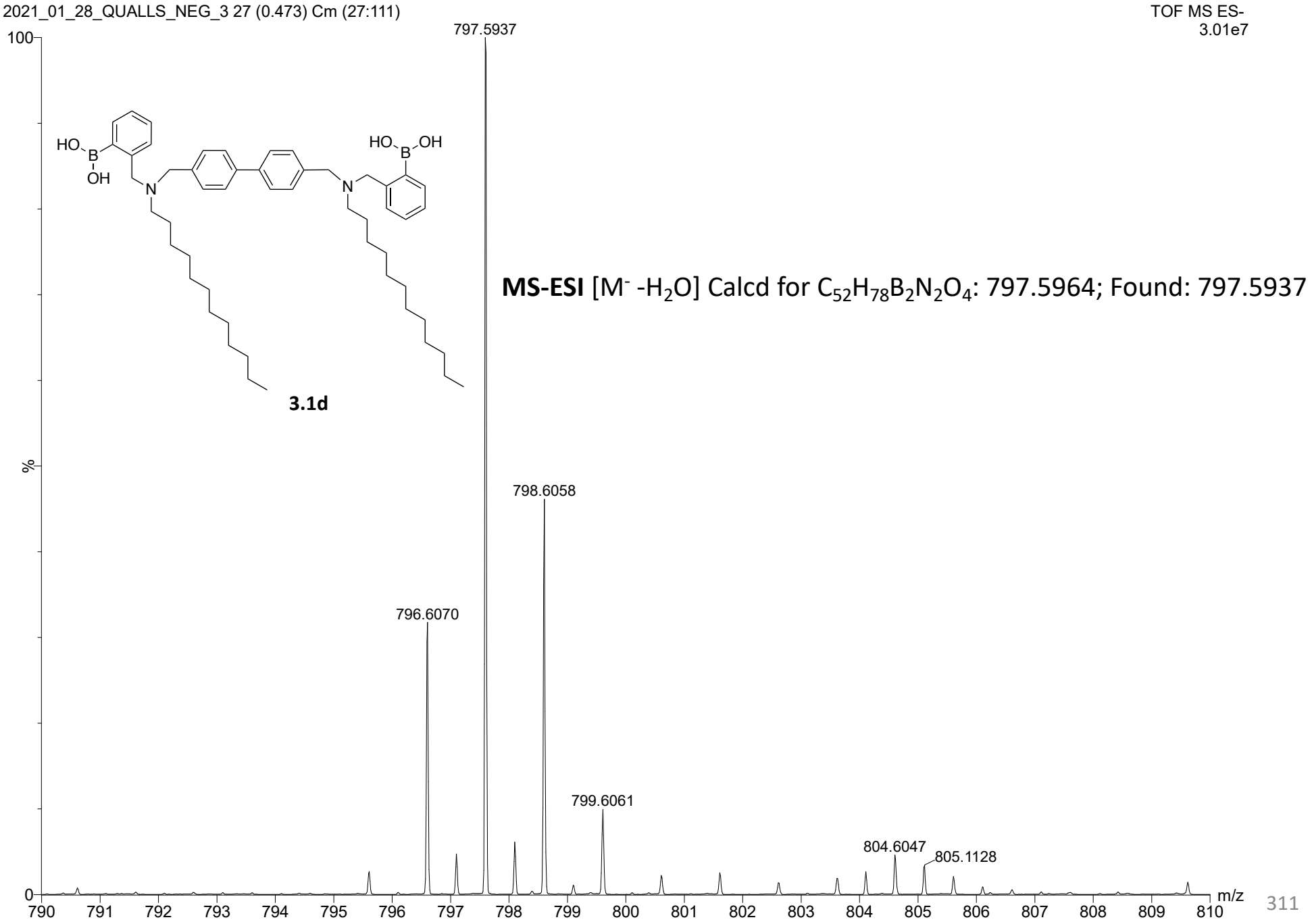
^{13}C NMR


Best-Qualls-MQI-136-12e-T1-carbon-2
STANDARD PHOSPHORUS PARAMETERS
HO
B
OH
N
HO
B
OH
N
3.1d
140.23
135.62
134.11
130.63
130.00
127.98
127.75
127.15
127.12
127.11
61.31
57.18
52.29
31.78
30.44
29.39
29.32
29.19
29.12
28.55
27.09
24.92
22.53
13.85
f1 (ppm)

^{11}B NMR

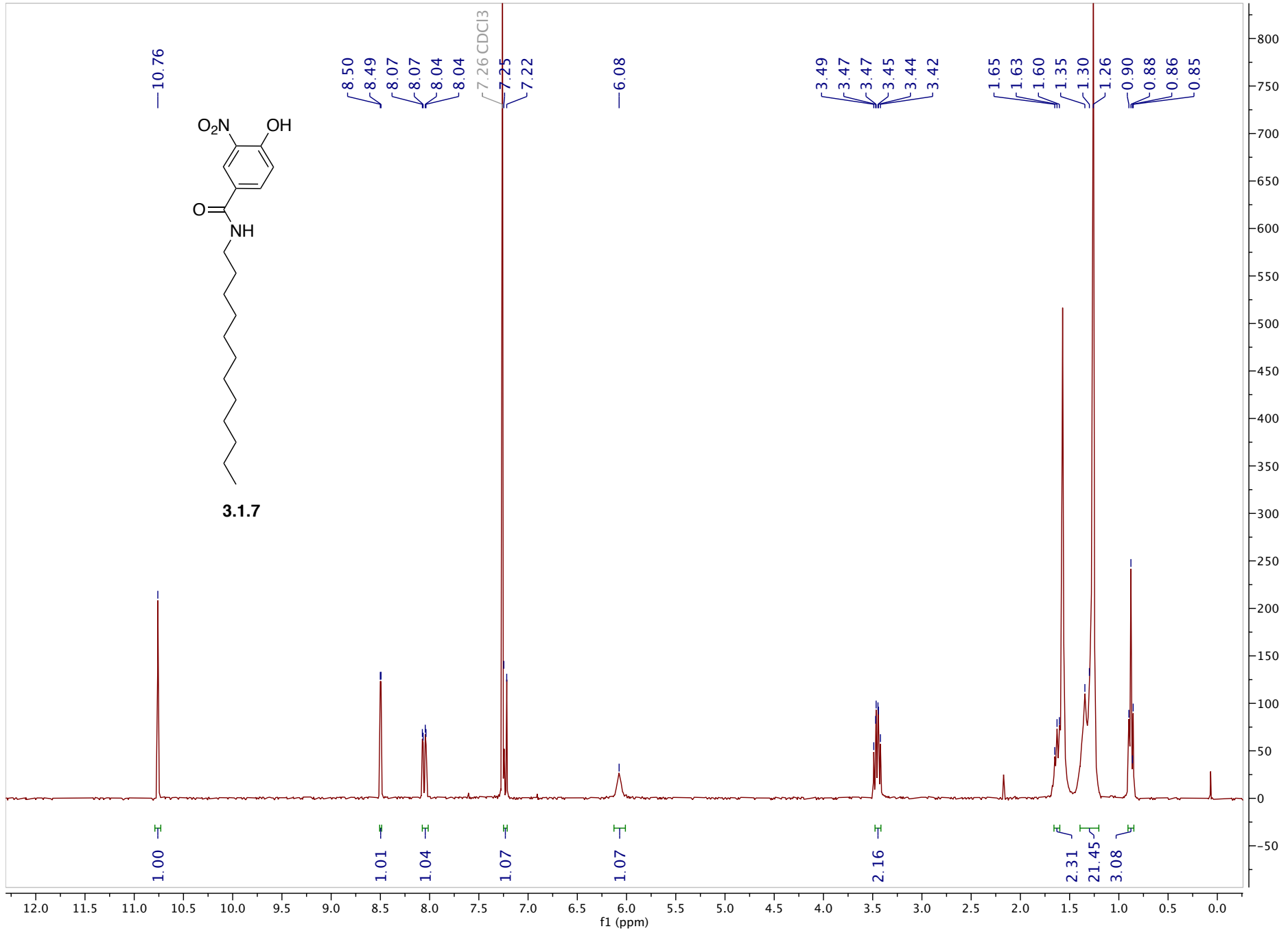

12e-2boron
STANDARD FLUORINE PARAMETERS
HO
B
OH
N
N
HO
B
OH
3.1d
29.53
3.5
3.0
2.5
2.0
1.5
1.0
0.5
0.0
-0.5
90
80
70
60
50
40
30
20
10
0
-10
-20
-30
-40
-50
-60
-70
-80
-90
f1 (ppm)

ESI-MS

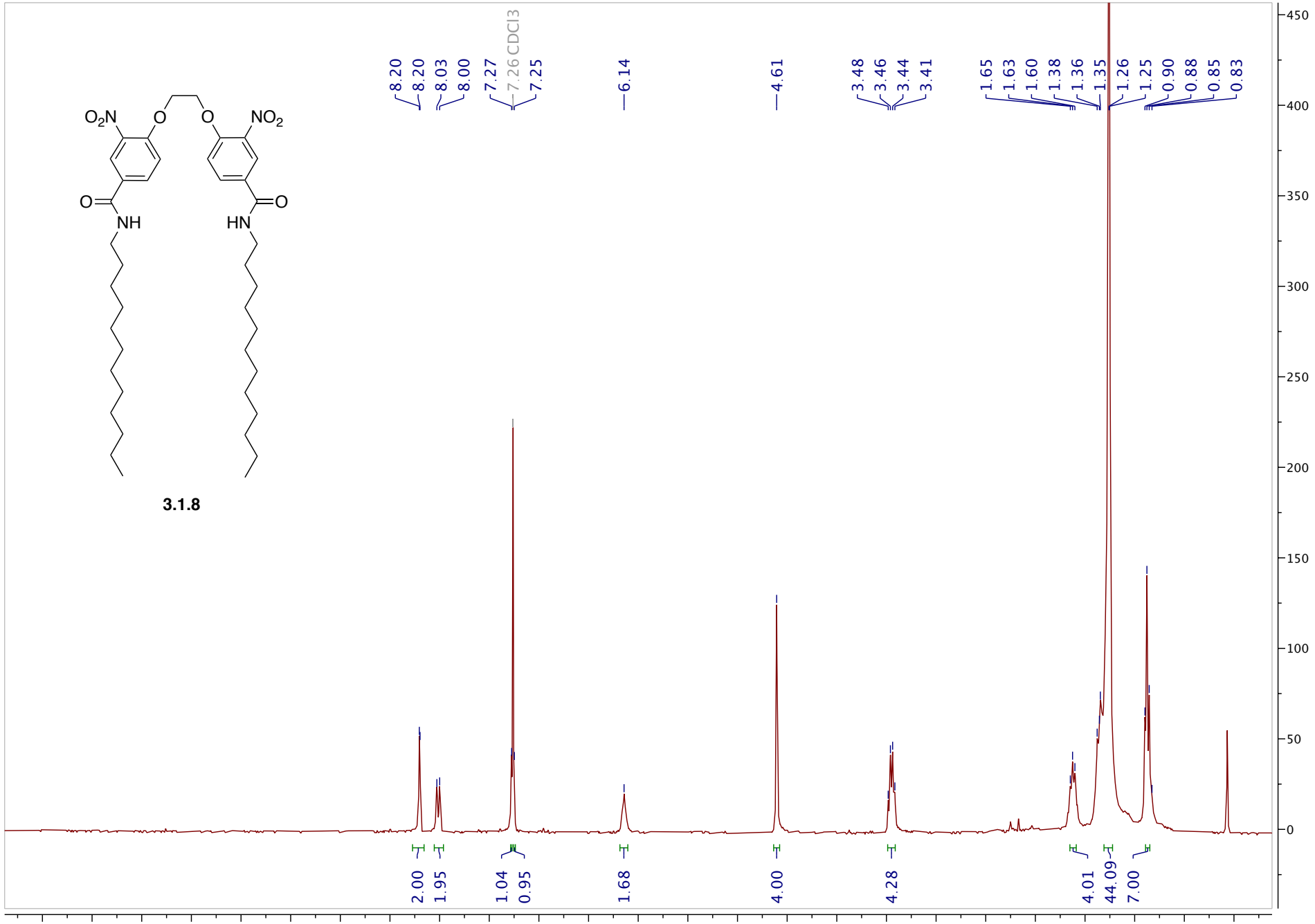


MS-ESI [M^- -H_2O] Calcd for $C_{52}H_{78}B_2N_2O_4$: 797.5964; Found: 797.5937

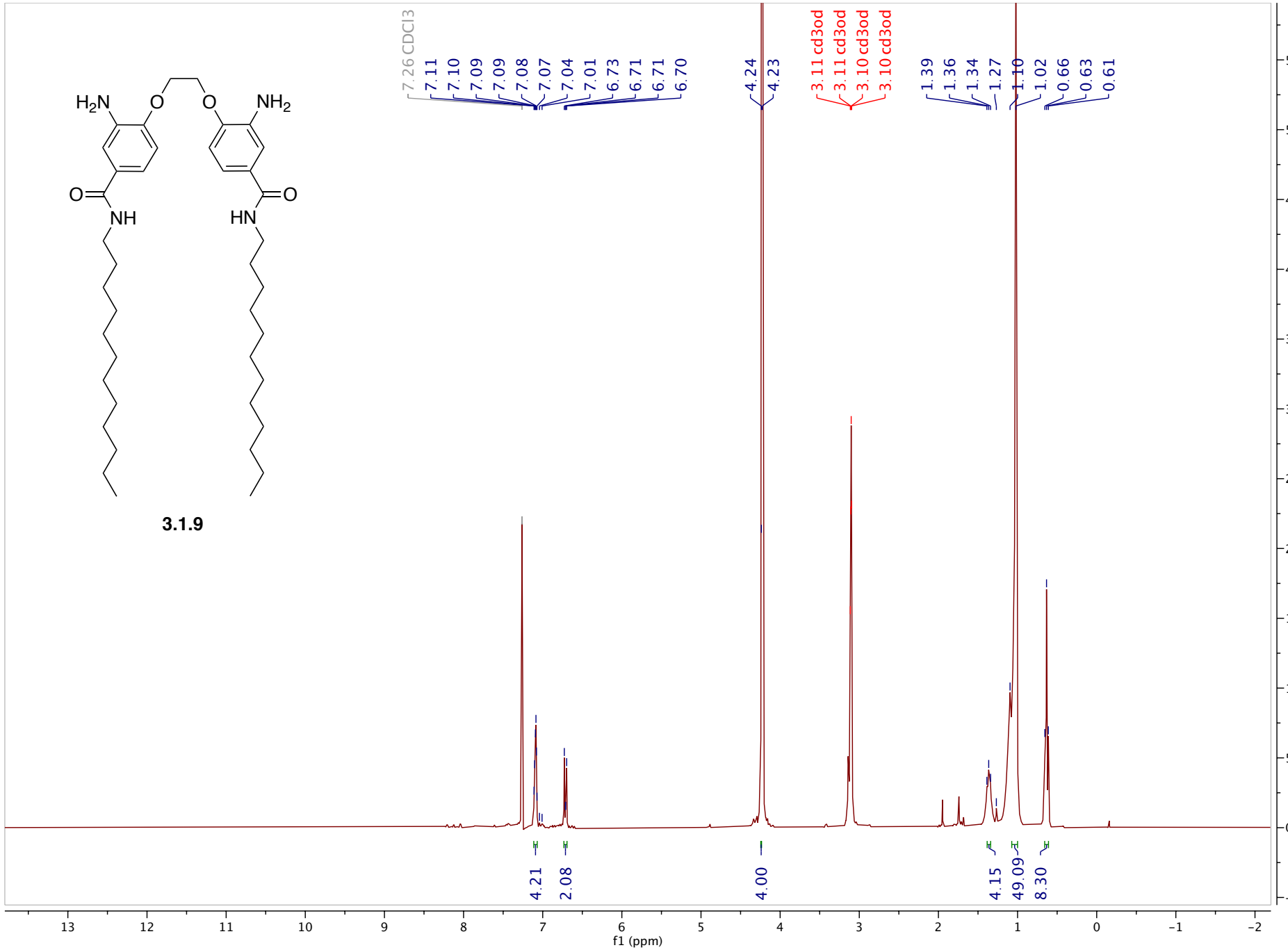
^{1}H NMR


10.76
8.50
8.49
8.07
8.07
8.04
8.04
7.26 CDCl3
7.25
7.22
6.08
3.49
3.47
3.47
3.45
3.44
3.42
1.65
1.63
1.60
1.35
1.30
1.26
0.90
0.88
0.86
0.85
O2N
OH
O
NH
3.1.7
1.00
1.01
1.04
1.07
1.07
2.16
2.31
21.45
3.08
f1 (ppm)

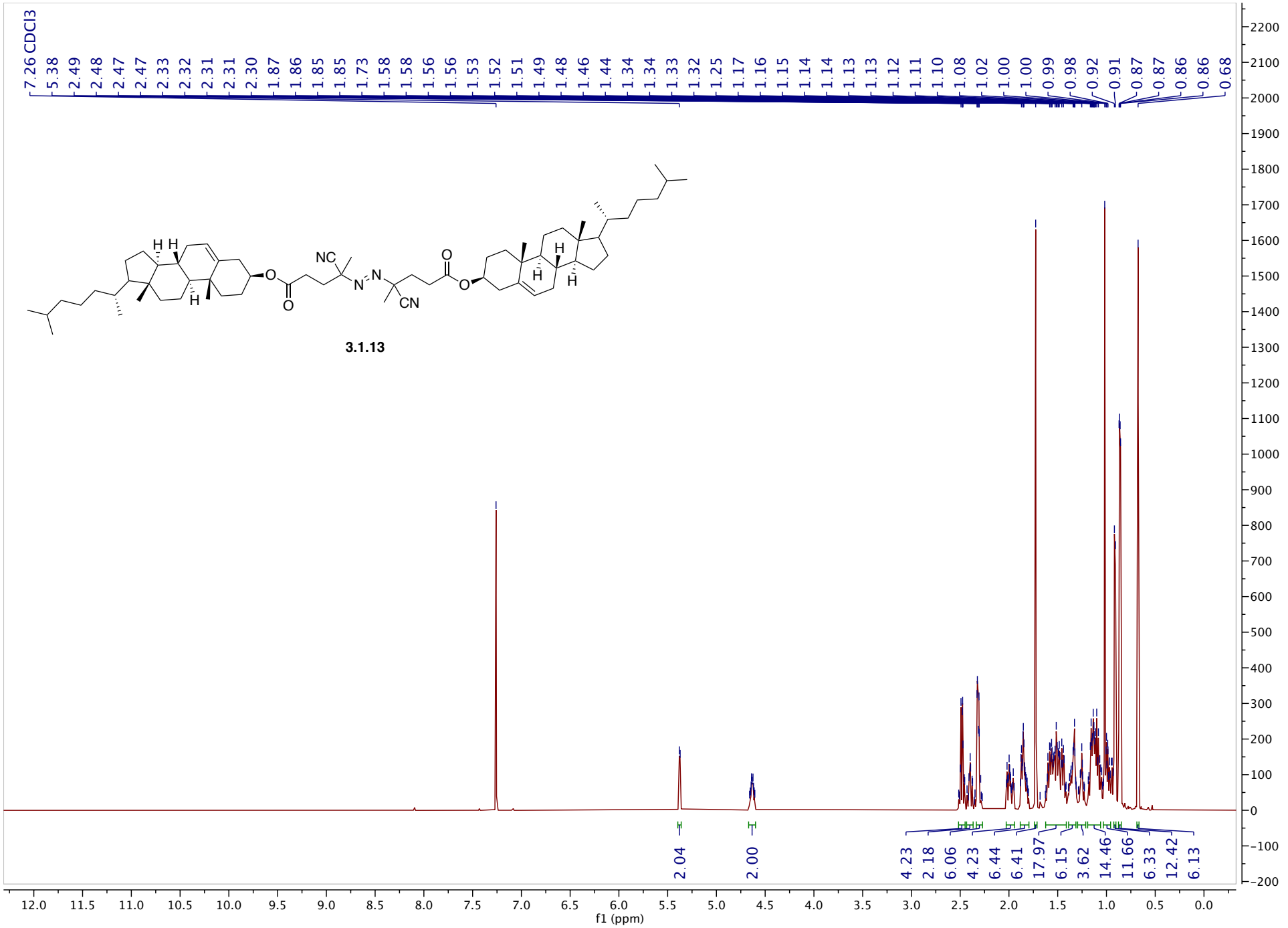
^{1}H NMR


O2N
O
O
NO2
O
NH
HN
O
3.1.8
8.20
8.20
8.03
8.00
7.27
7.26 CDCl3
7.25
6.14
4.61
3.48
3.46
3.44
3.41
1.65
1.63
1.60
1.38
1.36
1.35
1.26
1.25
0.90
0.88
0.85
0.83
2.00
1.95
1.04
0.95
1.68
4.00
4.28
4.01
44.09
7.00
f1 (ppm)

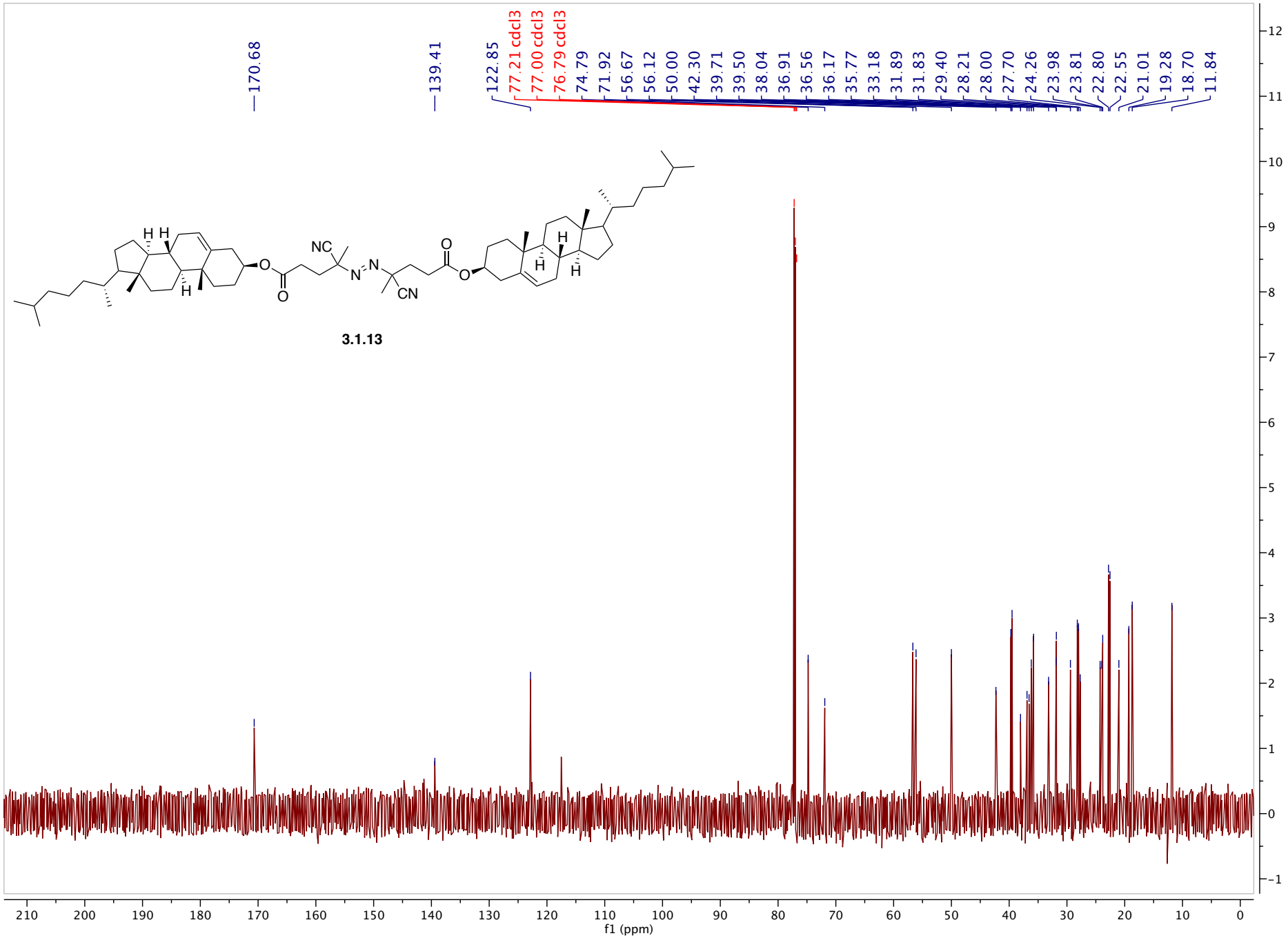
^{1}H NMR


H2N
O
O
NH2
O
NH
HN
O
3.1.9
7.26 CDCl3
7.11
7.10
7.09
7.09
7.08
7.07
7.04
7.01
6.73
6.71
6.71
6.70
4.24
4.23
3.11 cd3od
3.11 cd3od
3.10 cd3od
3.10 cd3od
1.39
1.36
1.34
1.27
1.10
1.02
0.66
0.63
0.61
4.21
2.08
4.00
4.15
49.09
8.30
f1 (ppm)

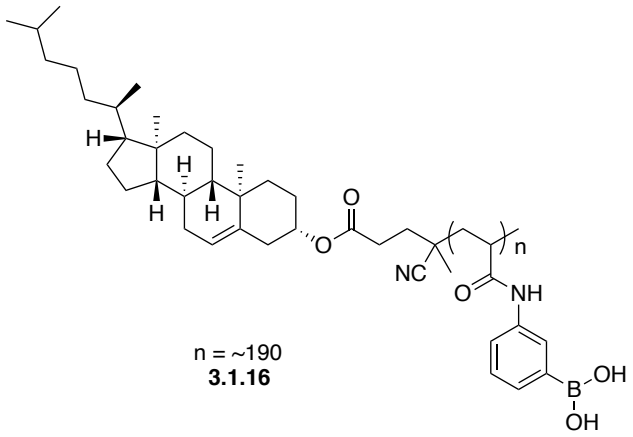
^{1}H NMR


7.26 CDCl3
5.38 2.49 2.48 2.47 2.47 2.33 2.32 2.31 2.31 2.30 1.87 1.86 1.85 1.85 1.73 1.58 1.58 1.56 1.56 1.53 1.52 1.51 1.49 1.48 1.46 1.44 1.34 1.34 1.33 1.32 1.25 1.17 1.16 1.15 1.14 1.14 1.13 1.13 1.12 1.11 1.10 1.08 1.02 1.00 1.00 0.99 0.98 0.92 0.91 0.87 0.87 0.86 0.86 0.68
NC
CN
O
N
H
3.1.13
2.04
2.00
4.23 2.18 6.06 4.23 6.44 6.41 17.97 6.15 3.62 14.46 11.66 6.33 12.42 6.13
f1 (ppm)

^{13}C NMR

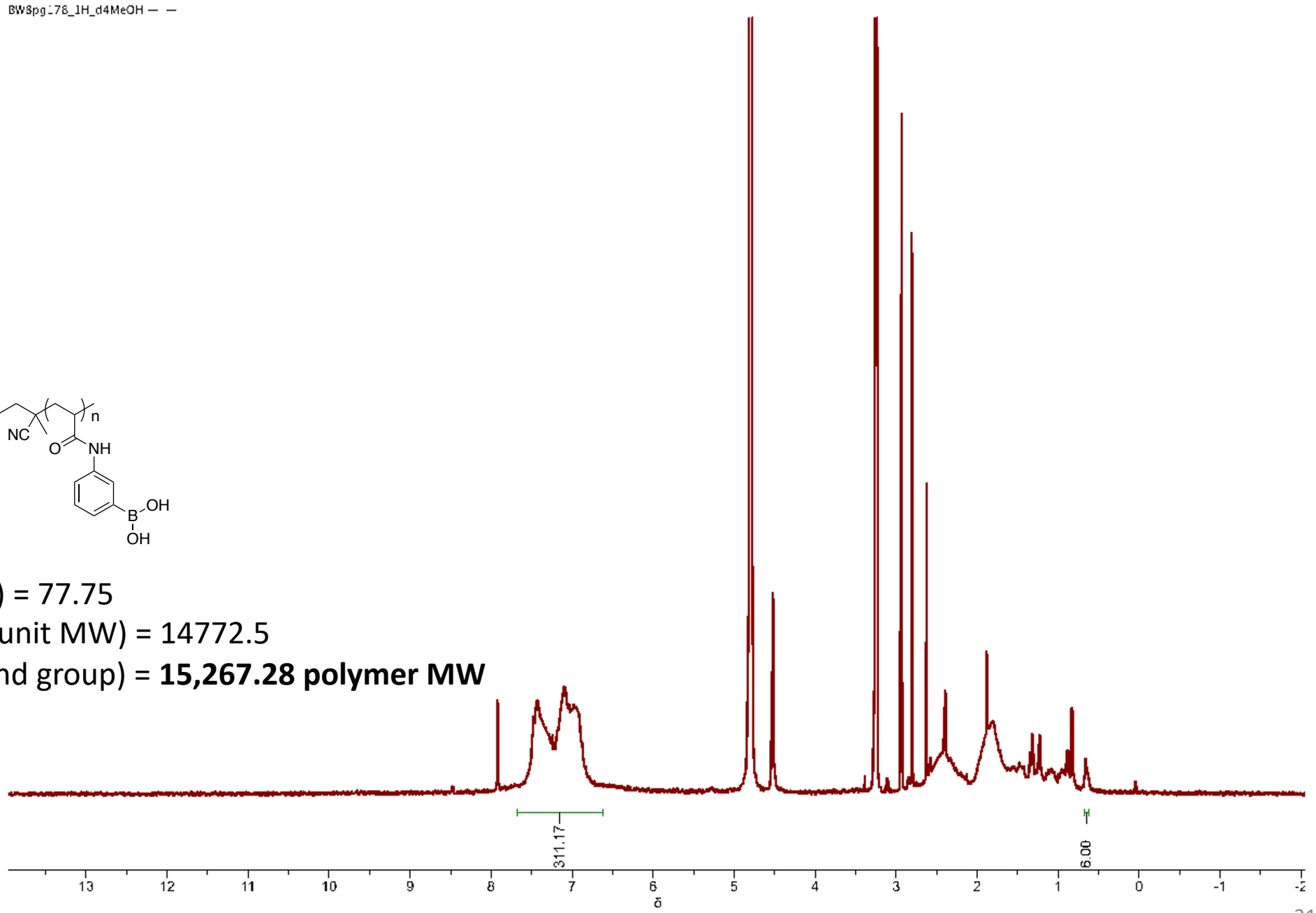

170.68
139.41
122.85
77.21 cdcl3
77.00 cdcl3
76.79 cdcl3
74.79
71.92
56.67
56.12
50.00
42.30
39.71
39.50
38.04
36.91
36.56
36.17
35.77
33.18
31.89
31.83
29.40
28.21
28.00
27.70
24.26
23.98
23.81
22.80
22.55
21.01
19.28
18.70
11.84
NC
CN
O
N
H
3.1.13
f1 (ppm)

^{1}H NMR

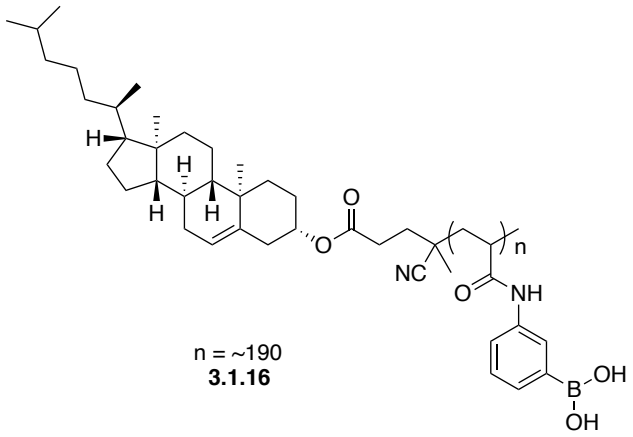


n = ~190
3.1.16

311/4 (# aromatic H) = 77.75
77.75 * 190 (repeat unit MW) = 14772.5
14772.5 + 494.78 (end group) = **15,267.28 polymer MW**

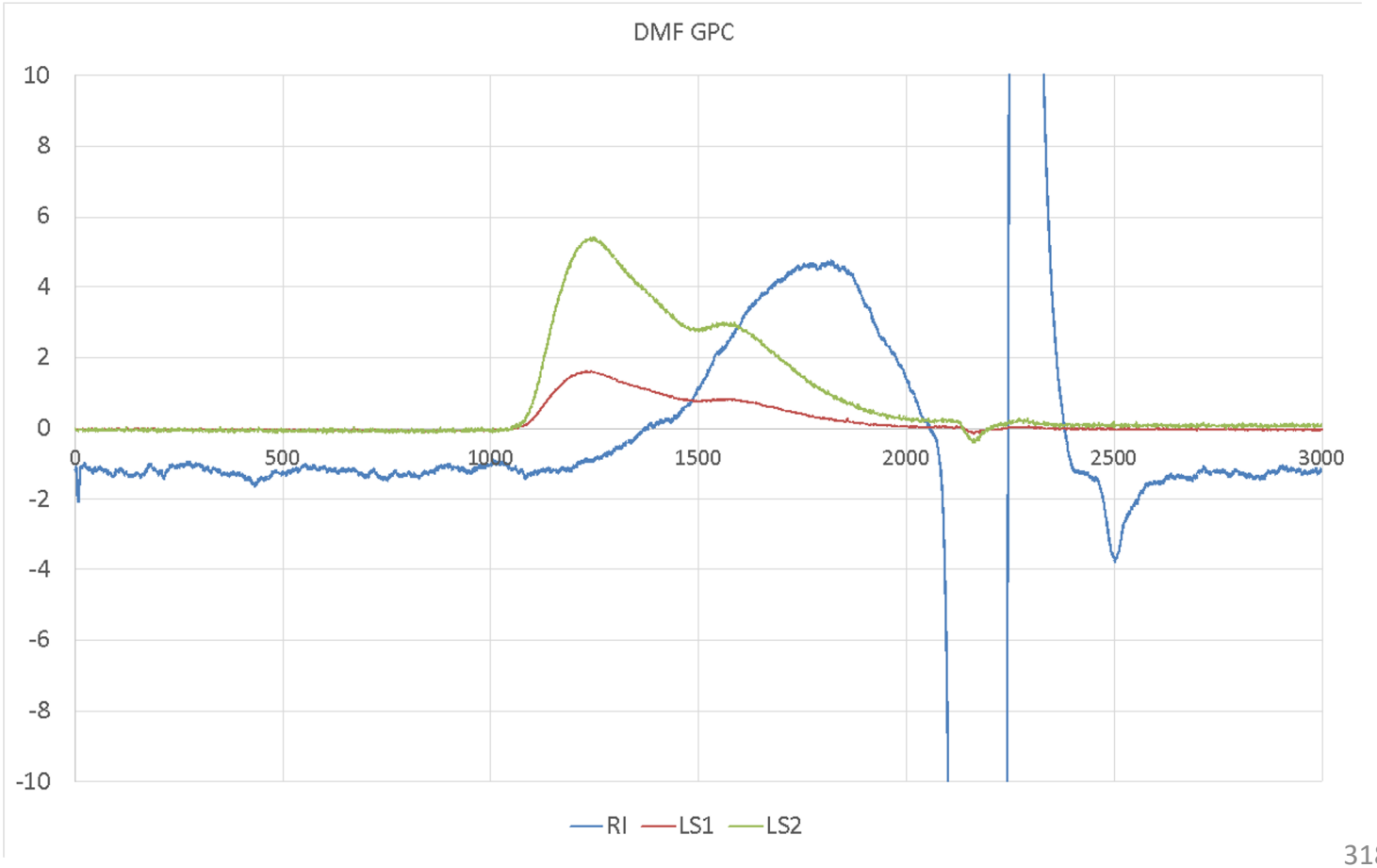


GPC-DMF

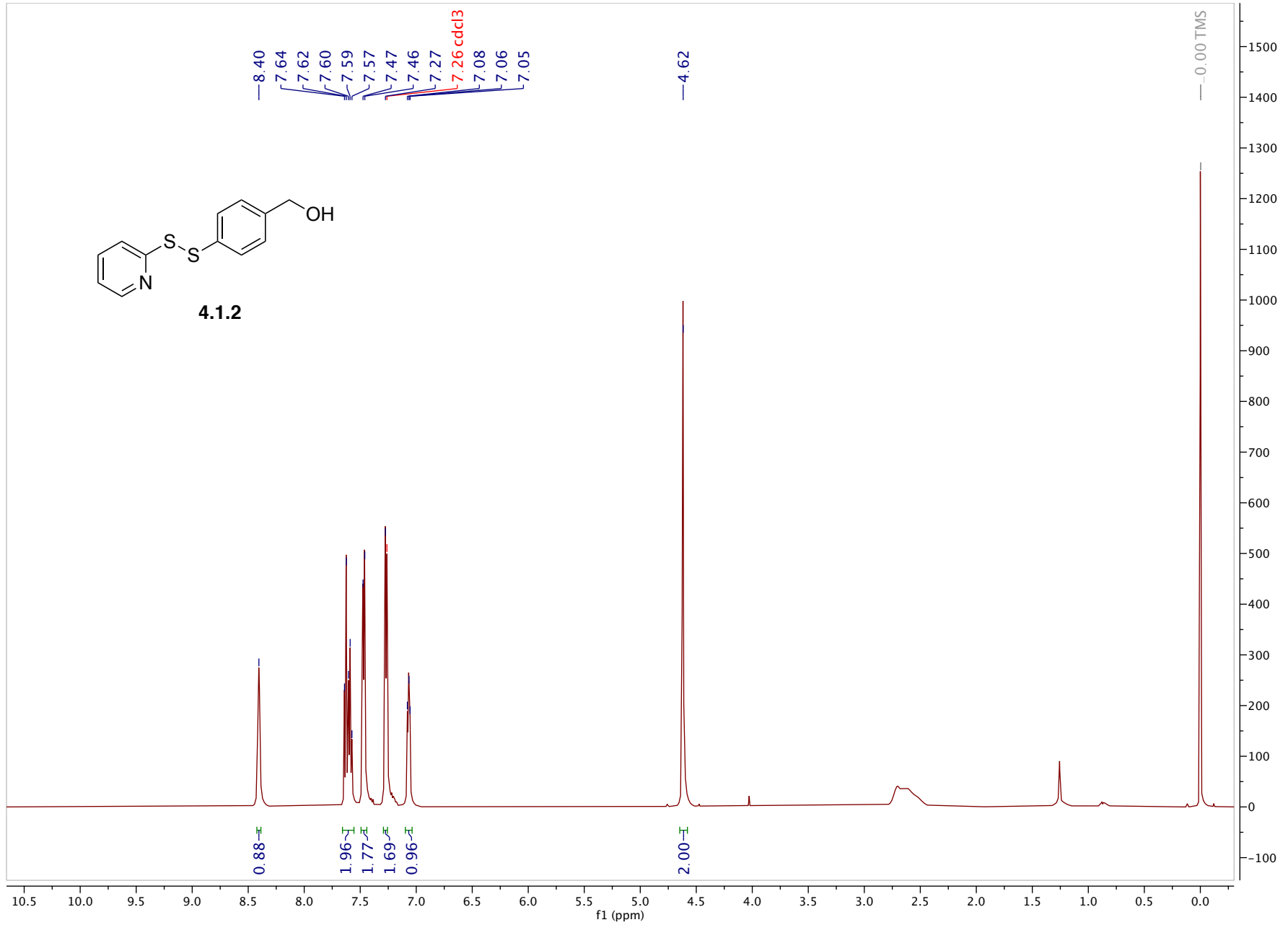


n = ~190
3.1.16

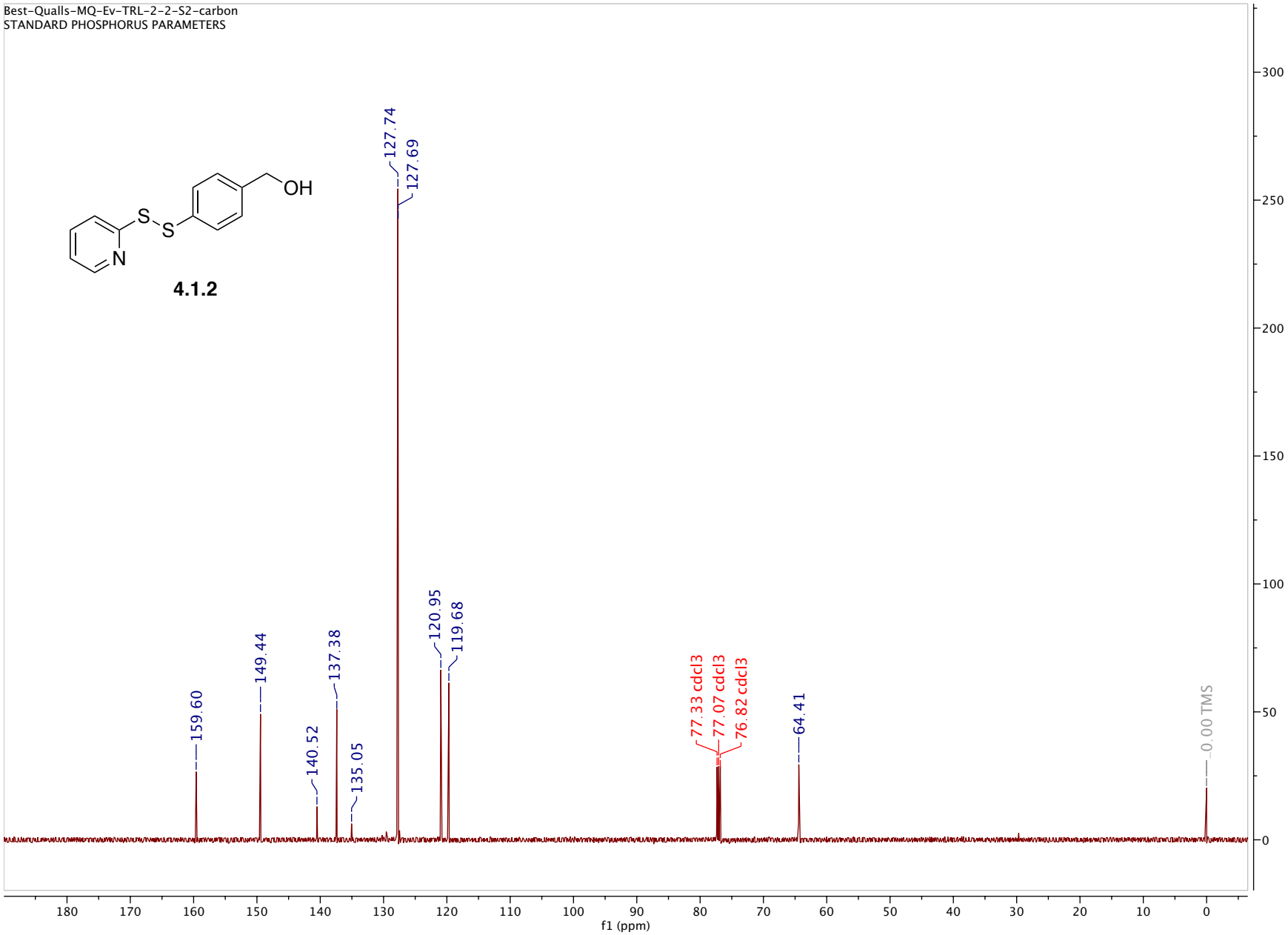
Peak No.	Mp	Mn	Mw	Mz	Mz+1	Mv	PD
1	15873.5	15337.9	88839.3	494388	1391560	-1	5.79216



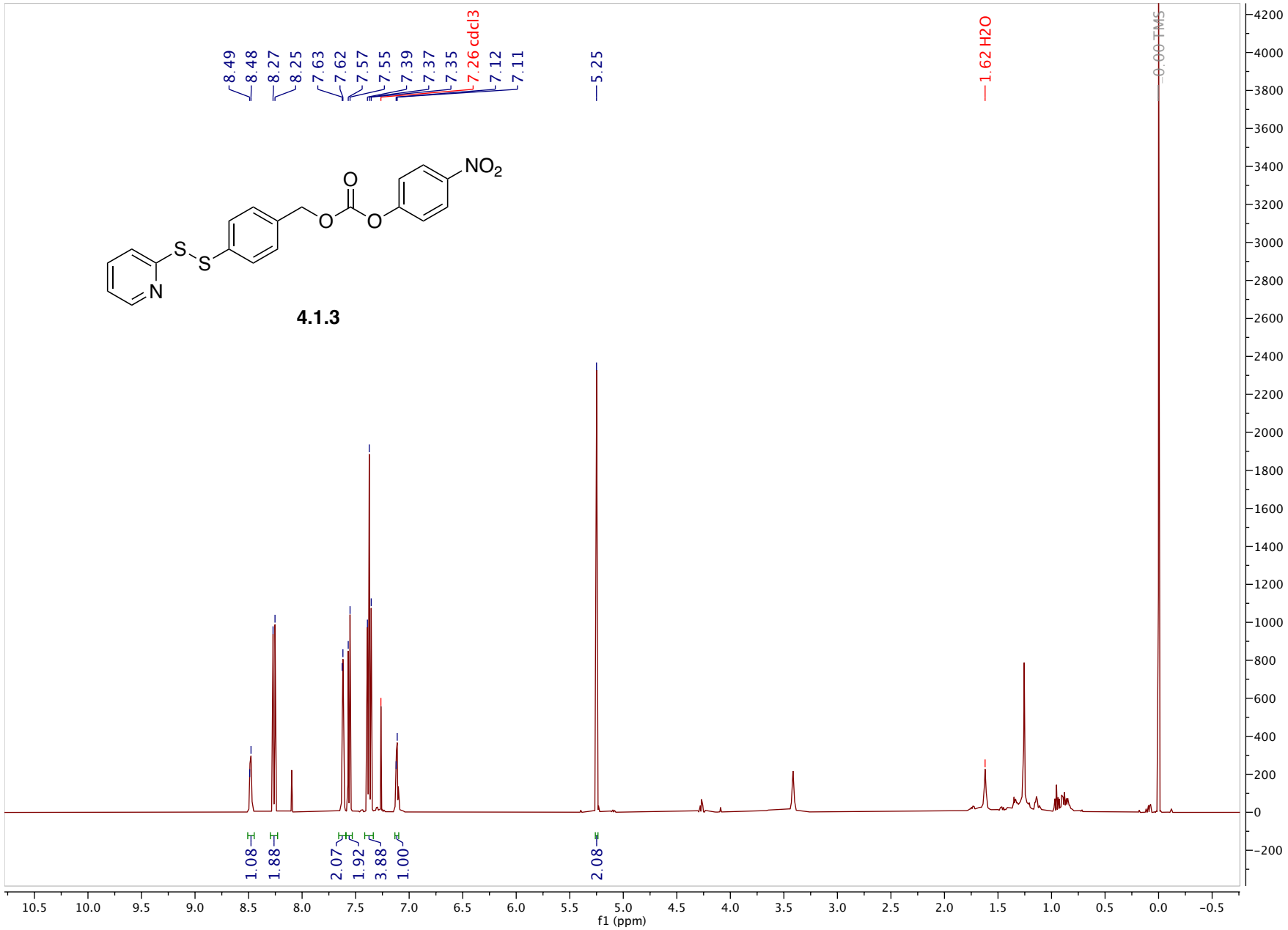
^{1}H NMR


8.40
7.64
7.62
7.60
7.59
7.57
7.47
7.46
7.27
7.26 cdcl3
7.08
7.06
7.05
4.62
0.00 TMS
OH
S
S
N
4.1.2
0.88
1.96
1.77
1.69
0.96
2.00
f1 (ppm)

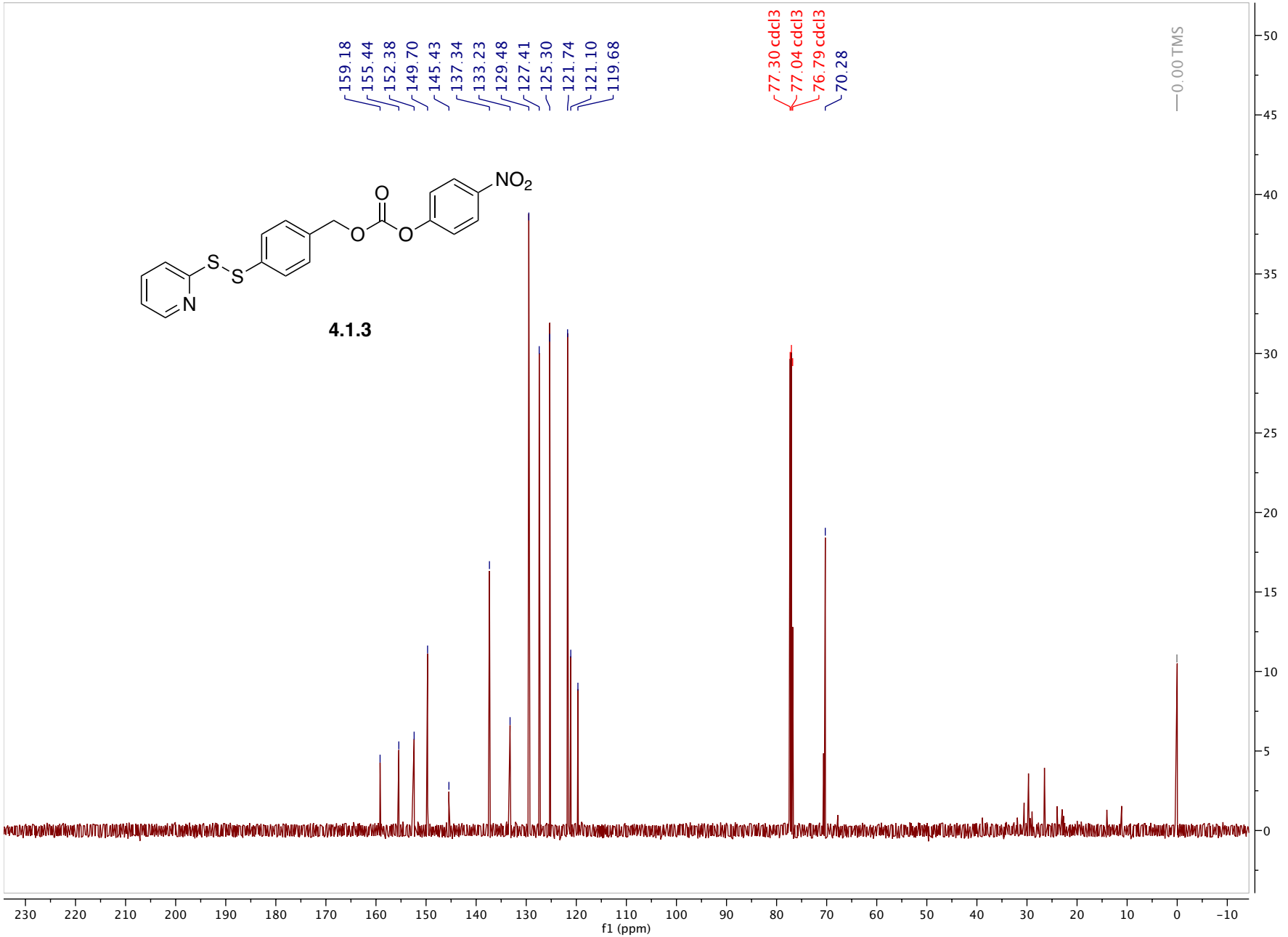
^{13}C NMR


Best-Qualls-MQ-Ev-TRL-2-2-S2-carbon
STANDARD PHOSPHORUS PARAMETERS
OH
S
S
N
4.1.2
159.60
149.44
140.52
137.38
135.05
127.74
127.69
120.95
119.68
77.33 cdcl3
77.07 cdcl3
76.82 cdcl3
64.41
0.00 TMS
f1 (ppm)

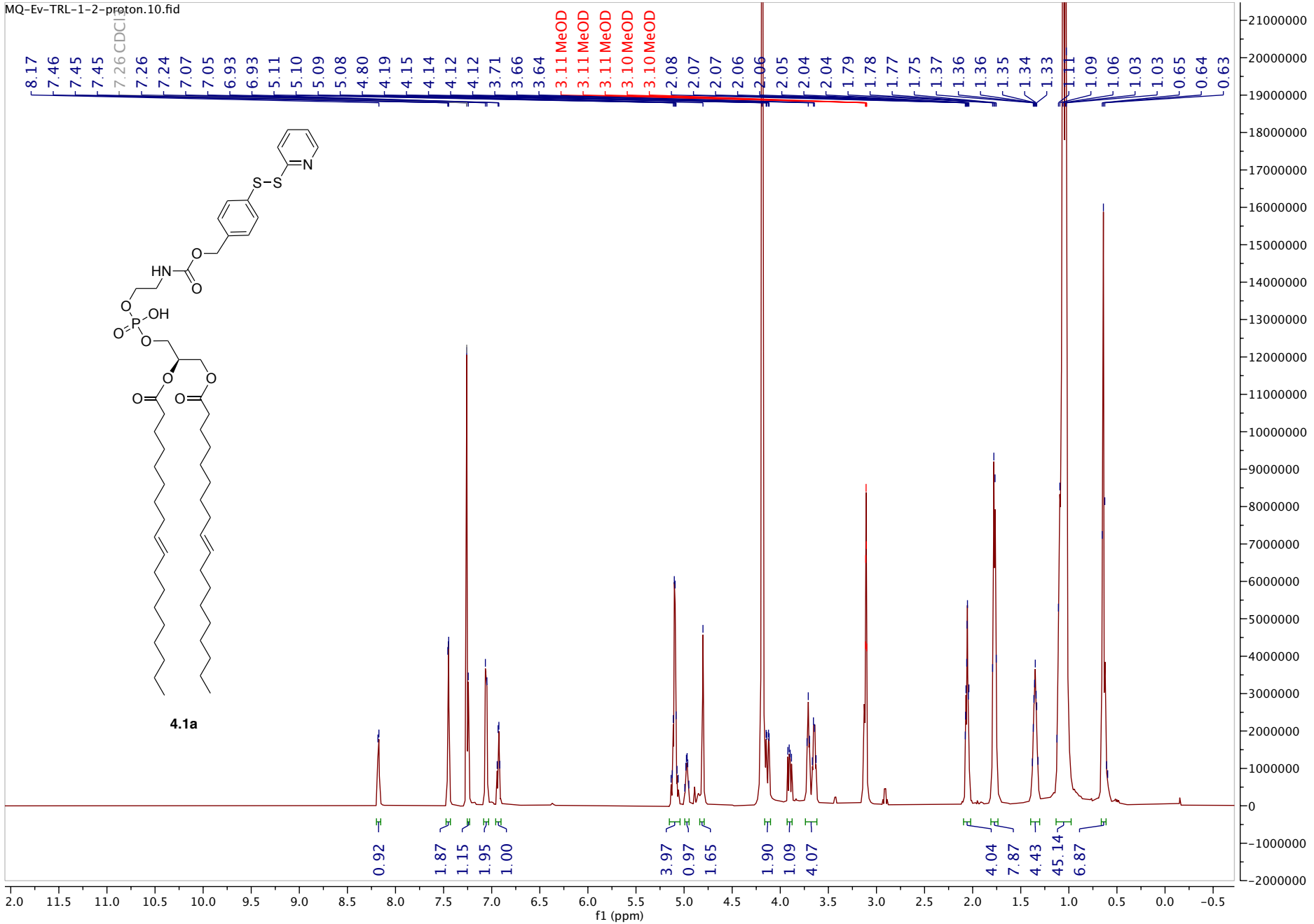
^{1}H NMR


8.49
8.48
8.27
8.25
7.63
7.62
7.57
7.55
7.39
7.37
7.35
7.26 cdcl3
7.12
7.11
5.25
1.62 H2O
0.00 TMS
NO2
O
O
O
S
S
N
4.1.3
1.08
1.88
2.07
1.92
3.88
1.00
2.08
f1 (ppm)

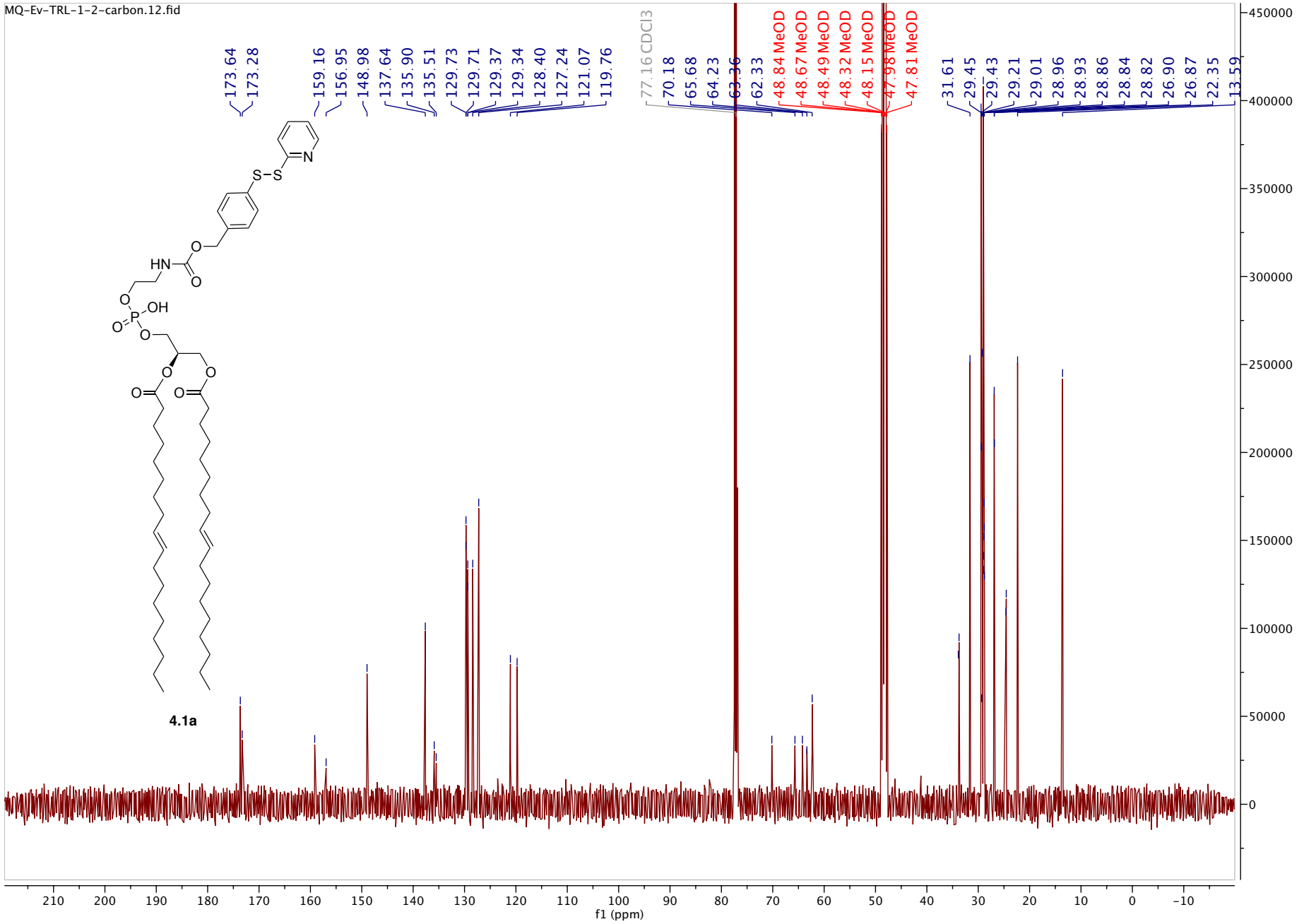
^{13}C NMR


159.18
155.44
152.38
149.70
145.43
137.34
133.23
129.48
127.41
125.30
121.74
121.10
119.68
77.30 cdcl3
77.04 cdcl3
76.79 cdcl3
70.28
0.00 TMS
NO2
O
O
O
S
S
N
4.1.3
f1 (ppm)

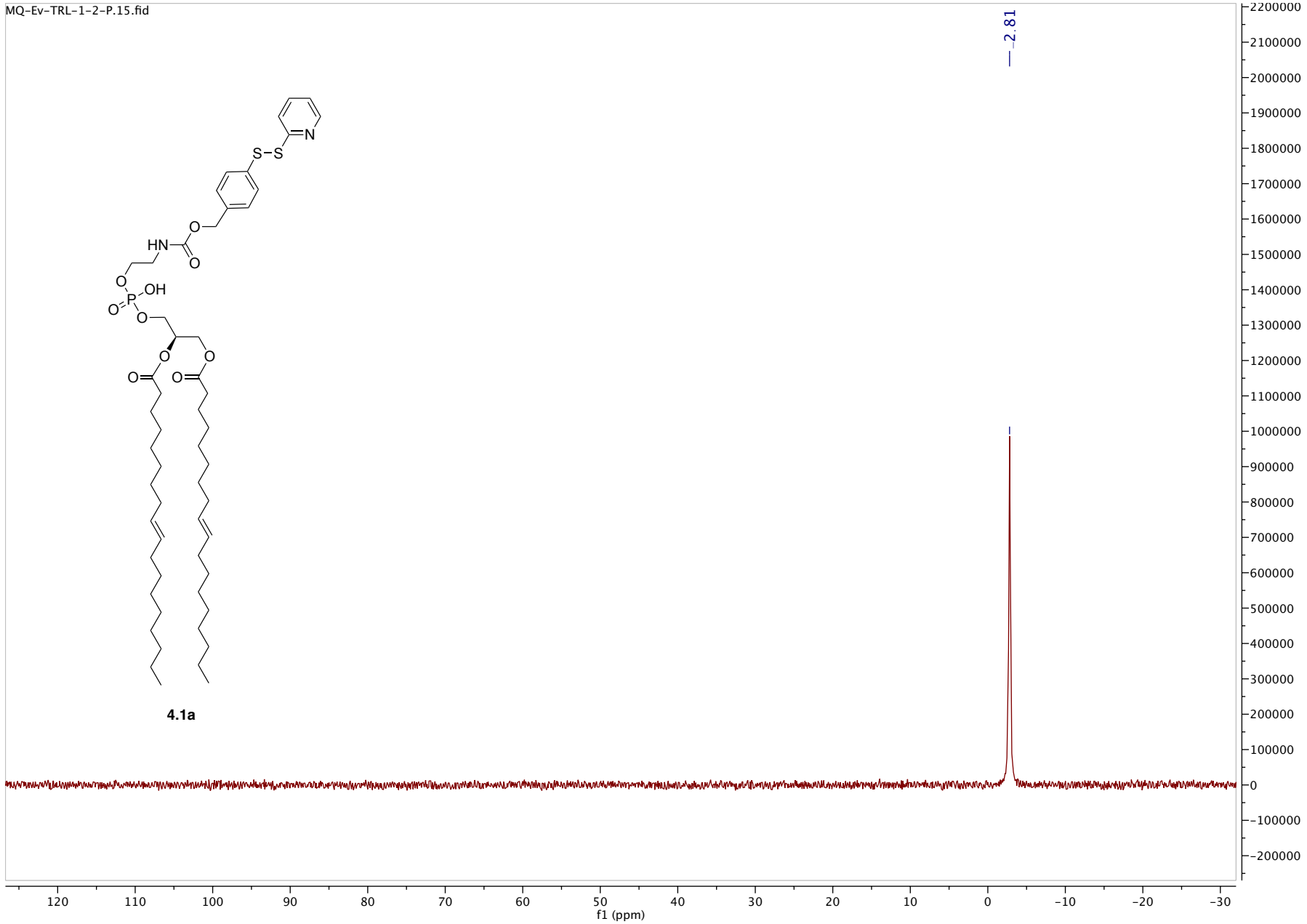
^{1}H NMR


MQ-Ev-TRL-1-2-proton.10.fid
7.26 CDCl3
3.11 MeOD
3.10 MeOD
4.1a
0.92
1.87
1.15
1.95
1.00
3.97
0.97
1.65
1.90
1.09
4.07
4.04
7.87
4.43
45.14
6.87
f1 (ppm)

^{13}C NMR

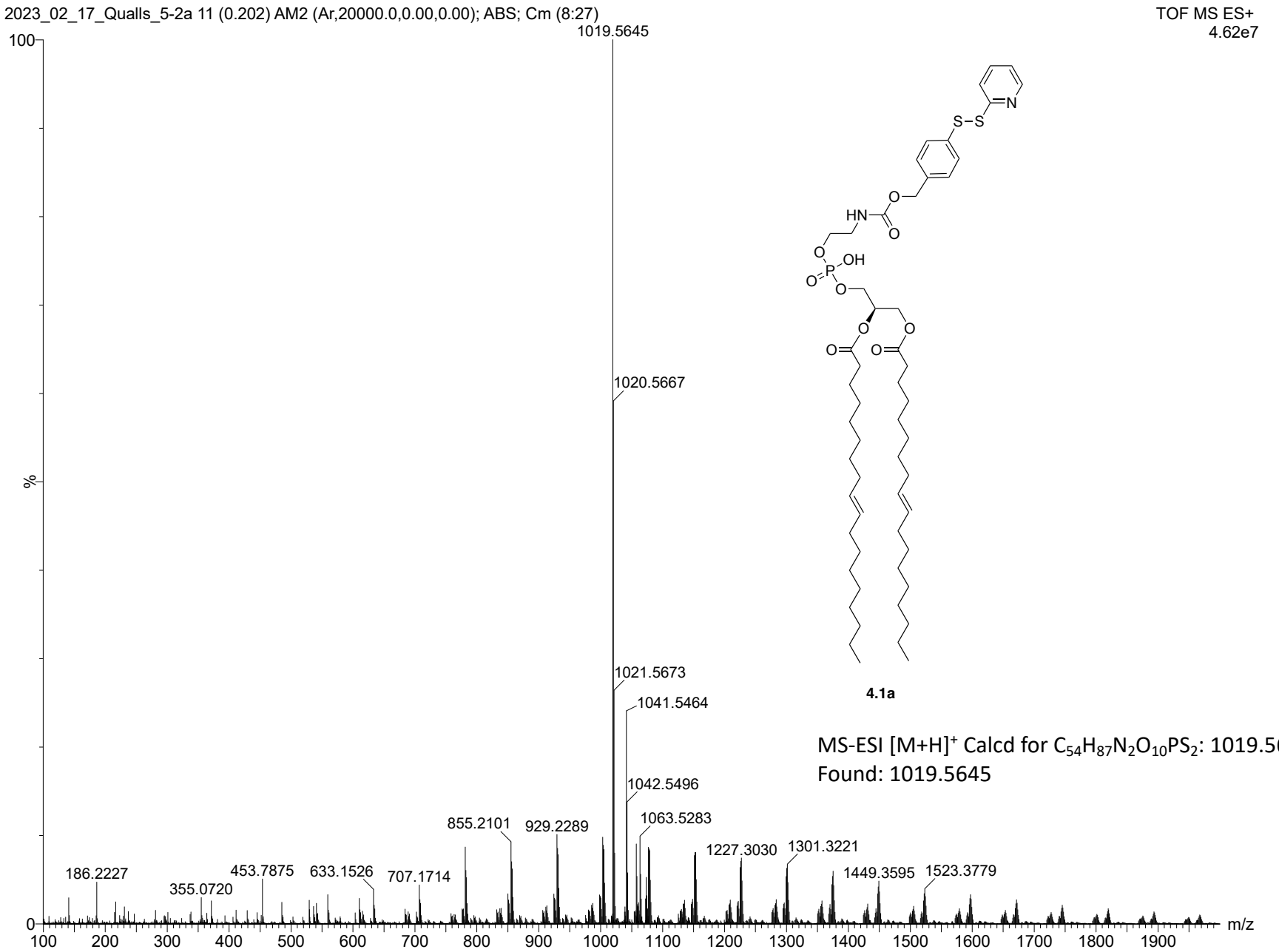

MQ-Ev-TRL-1-2-carbon.12.fid
173.64
173.28
159.16
156.95
148.98
137.64
135.90
135.51
129.73
129.71
129.37
129.34
128.40
127.24
121.07
119.76
77.16 CDCl3
70.18
65.68
64.23
63.36
62.33
48.84 MeOD
48.67 MeOD
48.49 MeOD
48.32 MeOD
48.15 MeOD
47.98 MeOD
47.81 MeOD
31.61
29.45
29.43
29.21
29.01
28.96
28.93
28.86
28.84
28.82
26.90
26.87
22.35
13.59
HN
OH
4.1a
f1 (ppm)

^{31}P NMR



ESI-MS

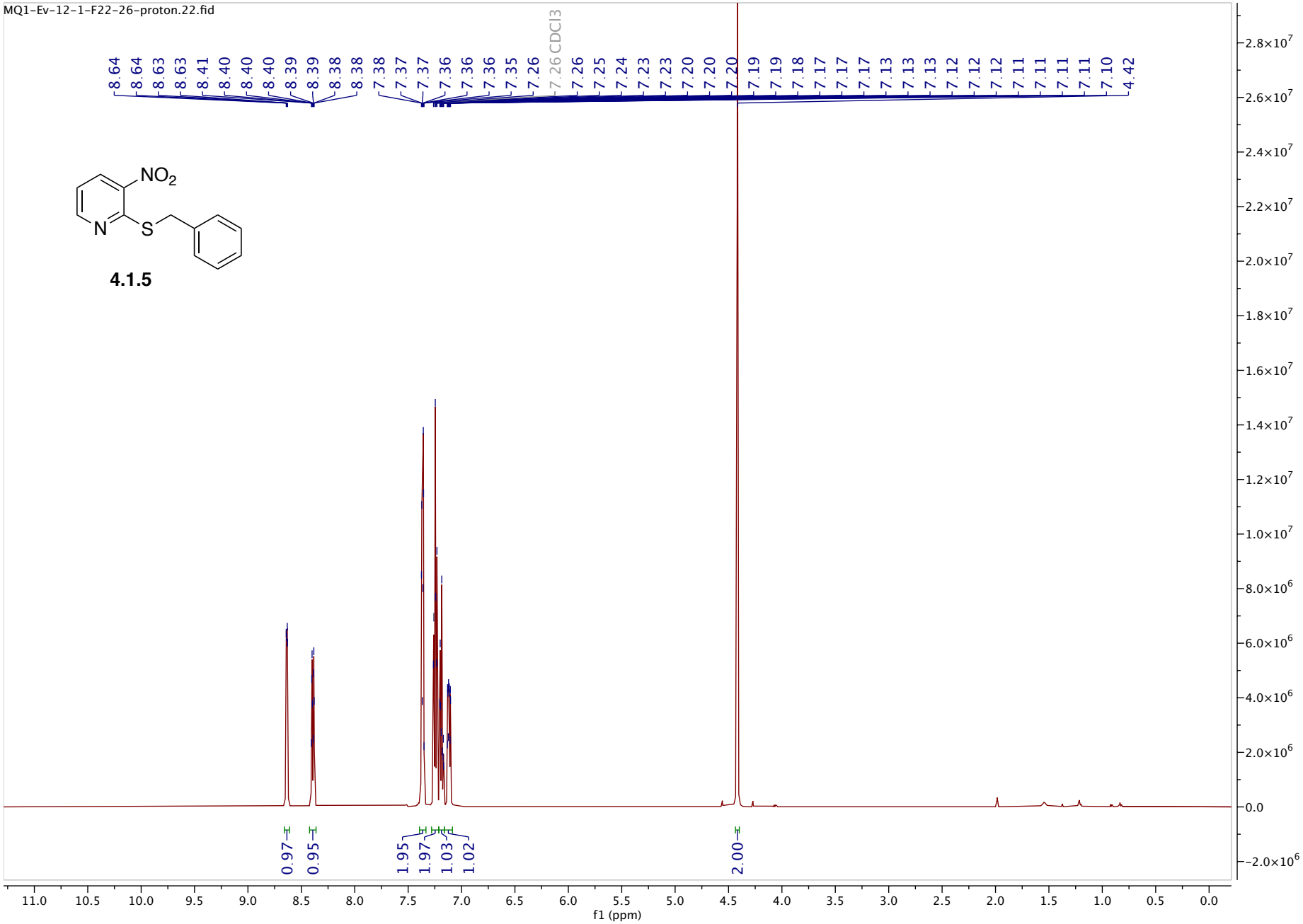
Sample: Pure **4.1a**



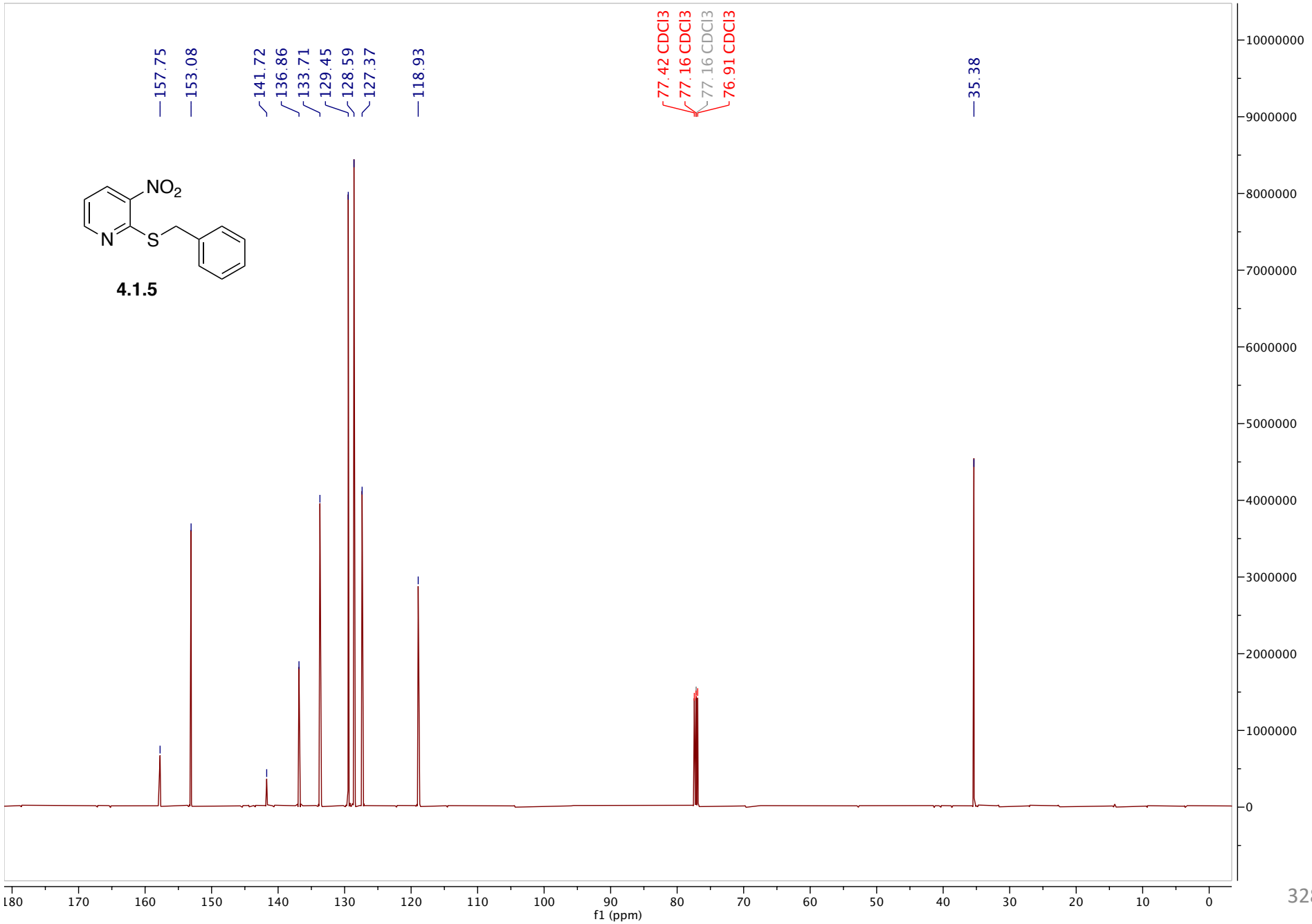
4.1a

MS-ESI $[M+H]^+$ Calcd for $C_{54}H_{87}N_2O_{10}PS_2$: 1019.5618
Found: 1019.5645

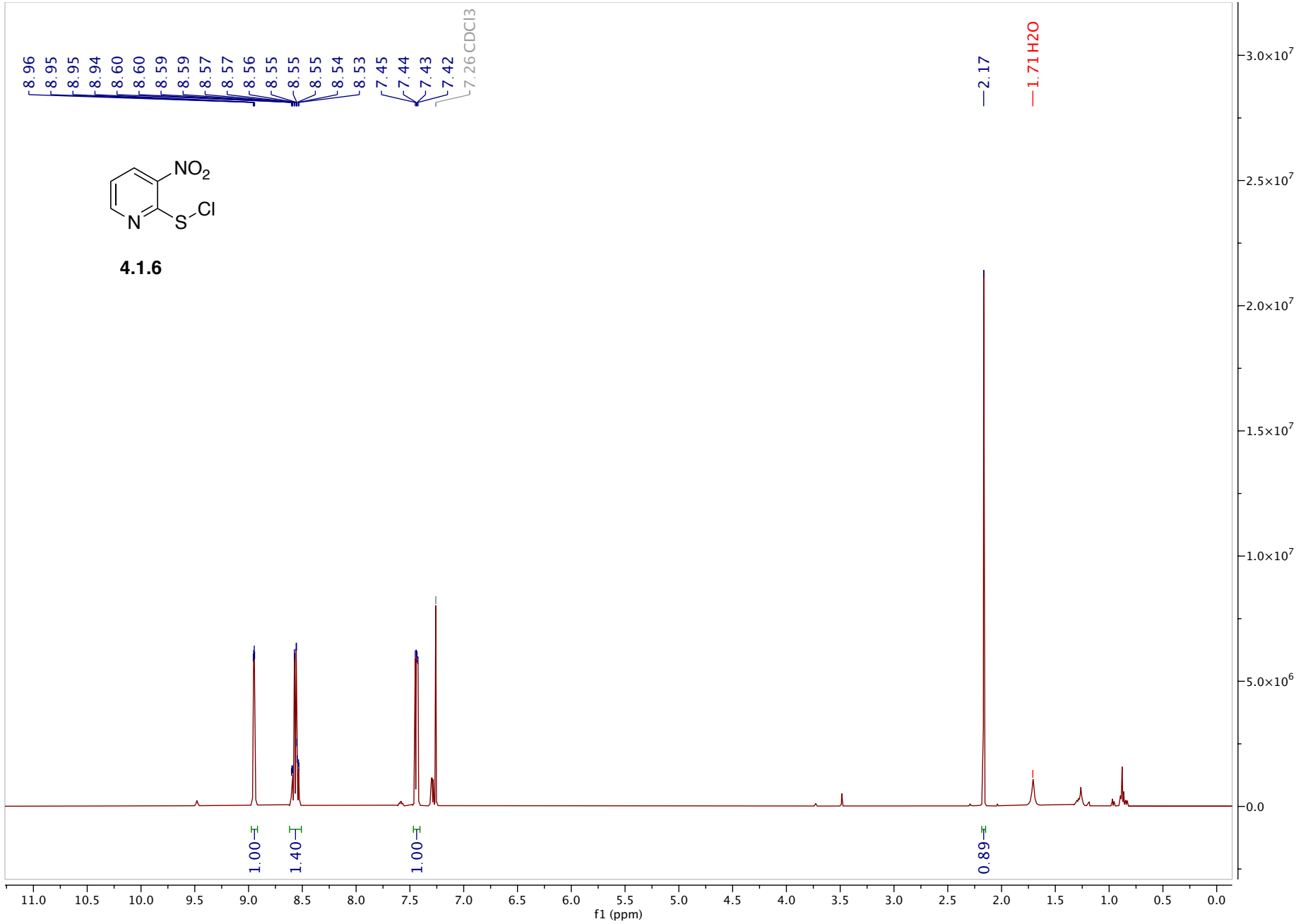
^{1}H NMR


MQ1-Ev-12-1-F22-26-proton.22.fid
8.64 8.64 8.63 8.63 8.41 8.40 8.40 8.40 8.39 8.39 8.38 8.38 7.38 7.37 7.37 7.36 7.36 7.36 7.35 7.26 7.26 CDCl3 7.26 7.25 7.24 7.23 7.23 7.20 7.20 7.20 7.19 7.19 7.18 7.17 7.17 7.17 7.13 7.13 7.13 7.12 7.12 7.12 7.11 7.11 7.11 7.11 7.10 4.42
NO2
N
S
4.1.5
0.97 0.95 1.95 1.97 1.03 1.02 2.00
f1 (ppm)

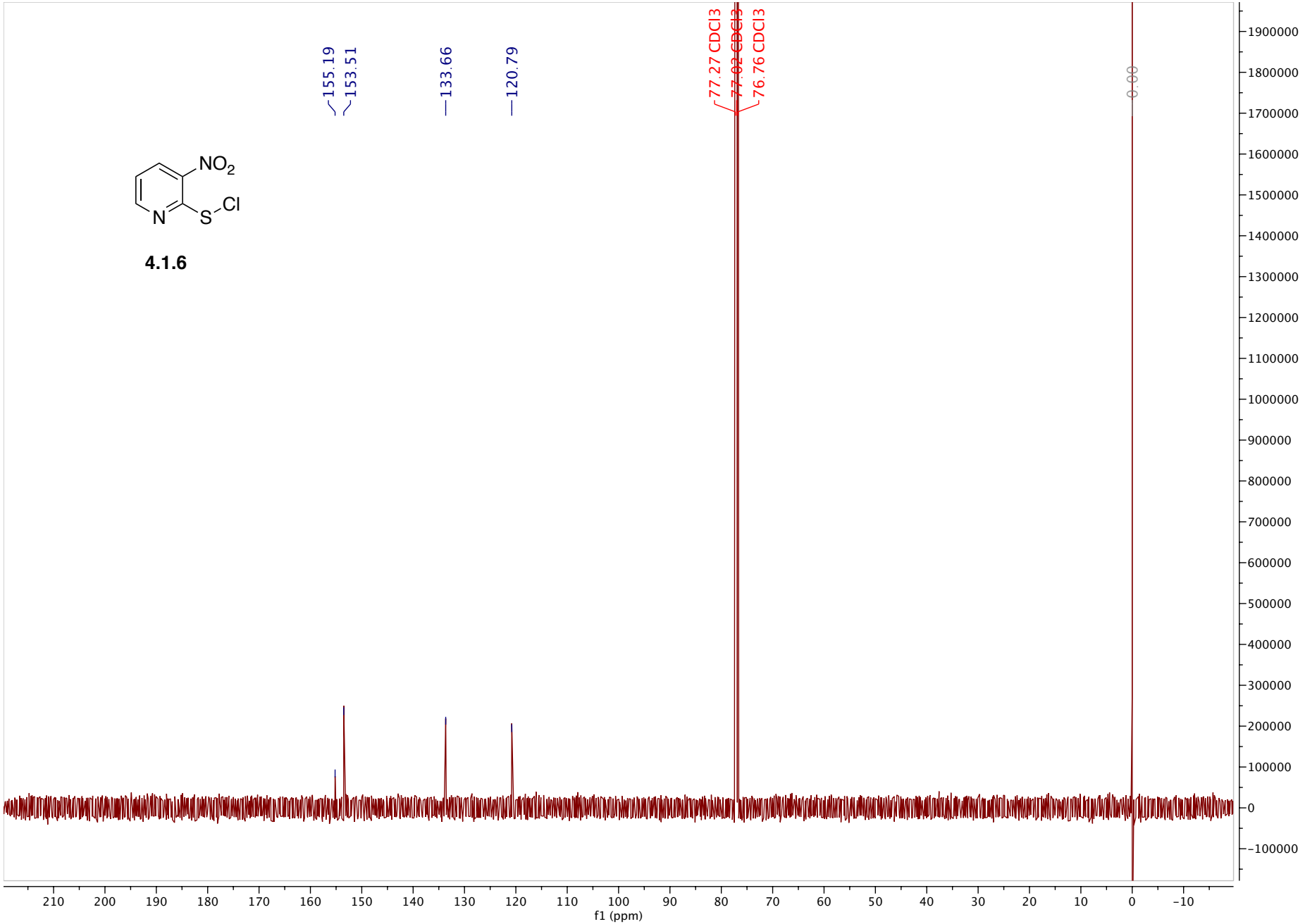
^{13}C NMR


157.75
153.08
141.72
136.86
133.71
129.45
128.59
127.37
118.93
77.42 CDCl3
77.16 CDCl3
77.16 CDCl3
76.91 CDCl3
35.38
NO2
N
S
4.1.5
10000000
9000000
8000000
7000000
6000000
5000000
4000000
3000000
2000000
1000000
0
180
170
160
150
140
130
120
110
100
90
80
70
60
50
40
30
20
10
0
f1 (ppm)

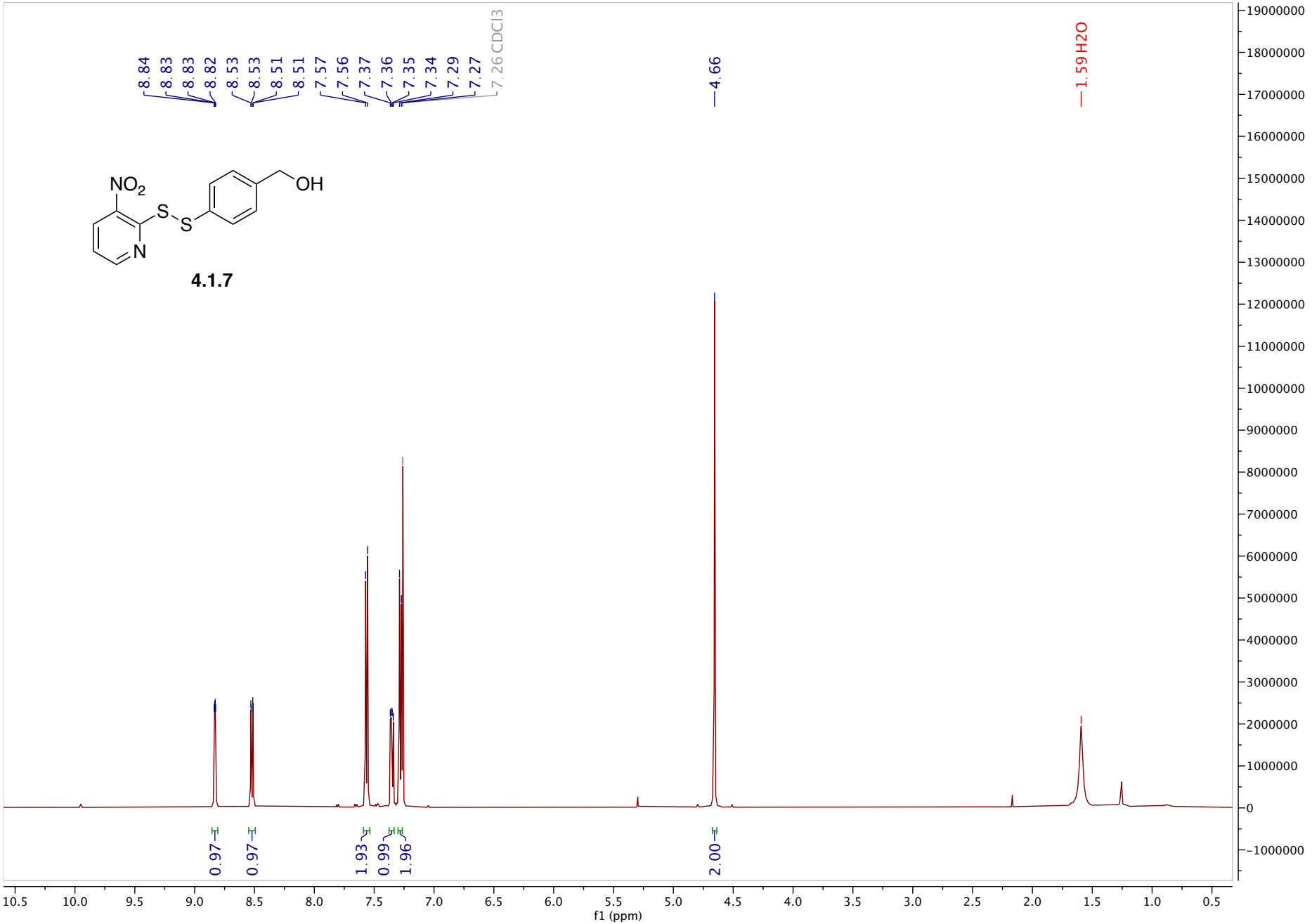
^{1}H NMR


8.96
8.95
8.95
8.94
8.60
8.60
8.59
8.59
8.57
8.57
8.56
8.55
8.55
8.55
8.54
8.53
7.45
7.44
7.43
7.42
7.26 CDCl3
2.17
1.71 H2O
NO2
Cl
N
S
4.1.6
3.0×10^7
2.5×10^7
2.0×10^7
1.5×10^7
1.0×10^7
5.0×10^6
0.0
1.00
1.40
1.00
0.89
11.0
10.5
10.0
9.5
9.0
8.5
8.0
7.5
7.0
6.5
6.0
5.5
5.0
4.5
4.0
3.5
3.0
2.5
2.0
1.5
1.0
0.5
0.0
f1 (ppm)

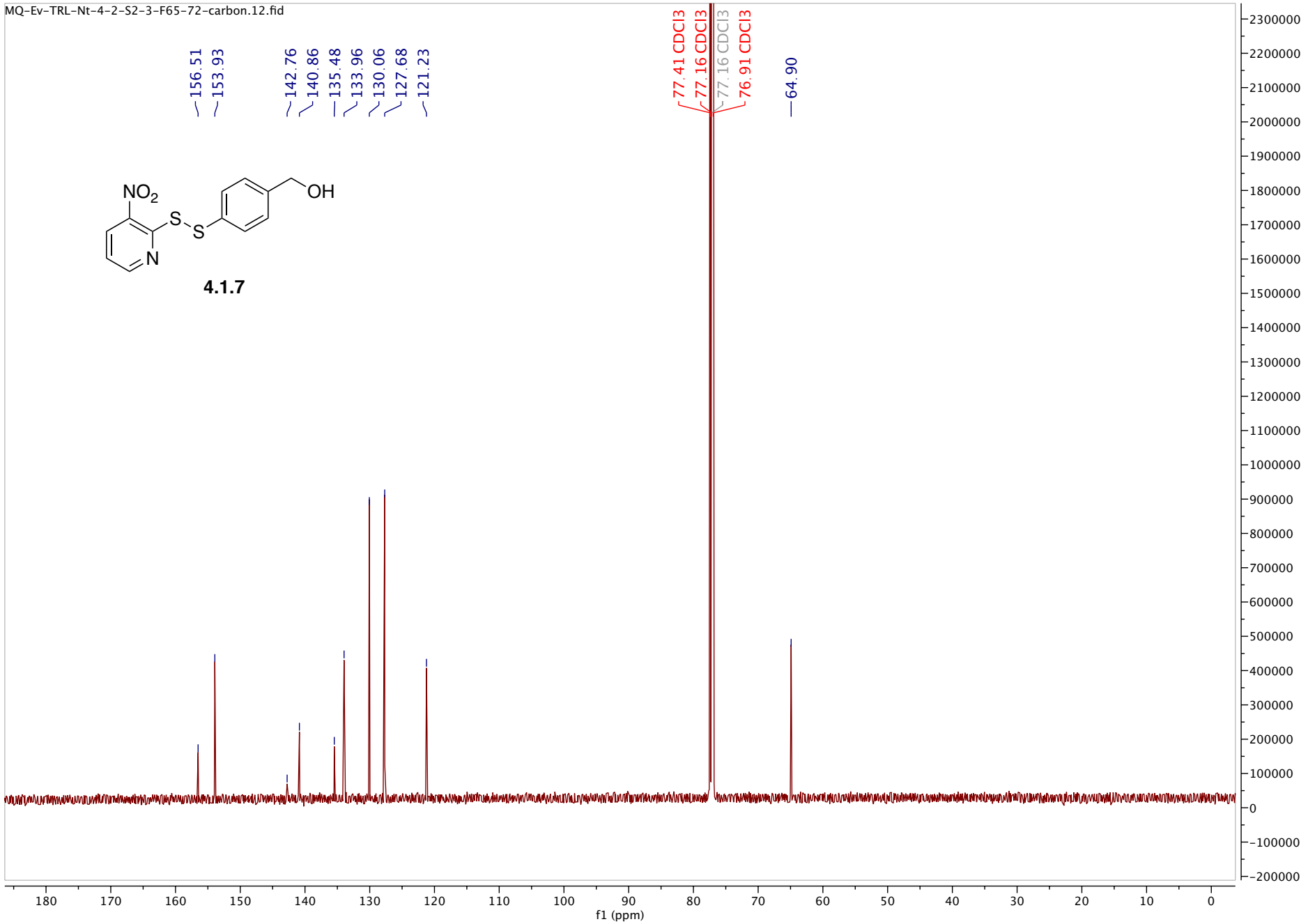
^{13}C NMR


155.19
153.51
133.66
120.79
77.27 CDCl3
77.02 CDCl3
76.76 CDCl3
0.00
NO2
Cl
S
N
4.1.6
f1 (ppm)

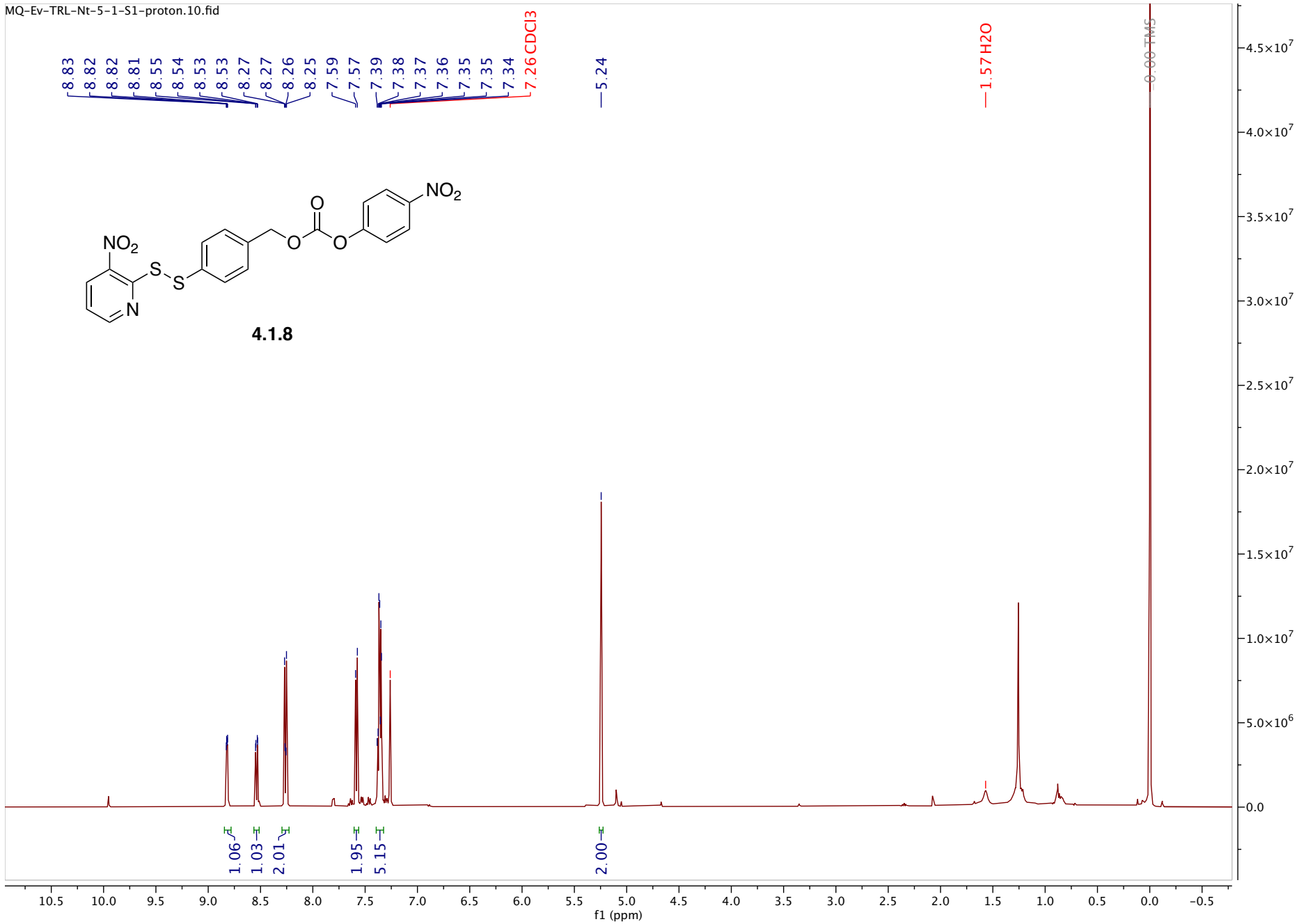
^{1}H NMR


8.84
8.83
8.83
8.82
8.53
8.53
8.51
8.51
7.57
7.56
7.37
7.36
7.35
7.34
7.29
7.27
7.26 CDCl3
4.66
1.59 H2O
NO2
S
S
OH
N
4.1.7
0.97
0.97
1.93
0.99
1.96
2.00
f1 (ppm)

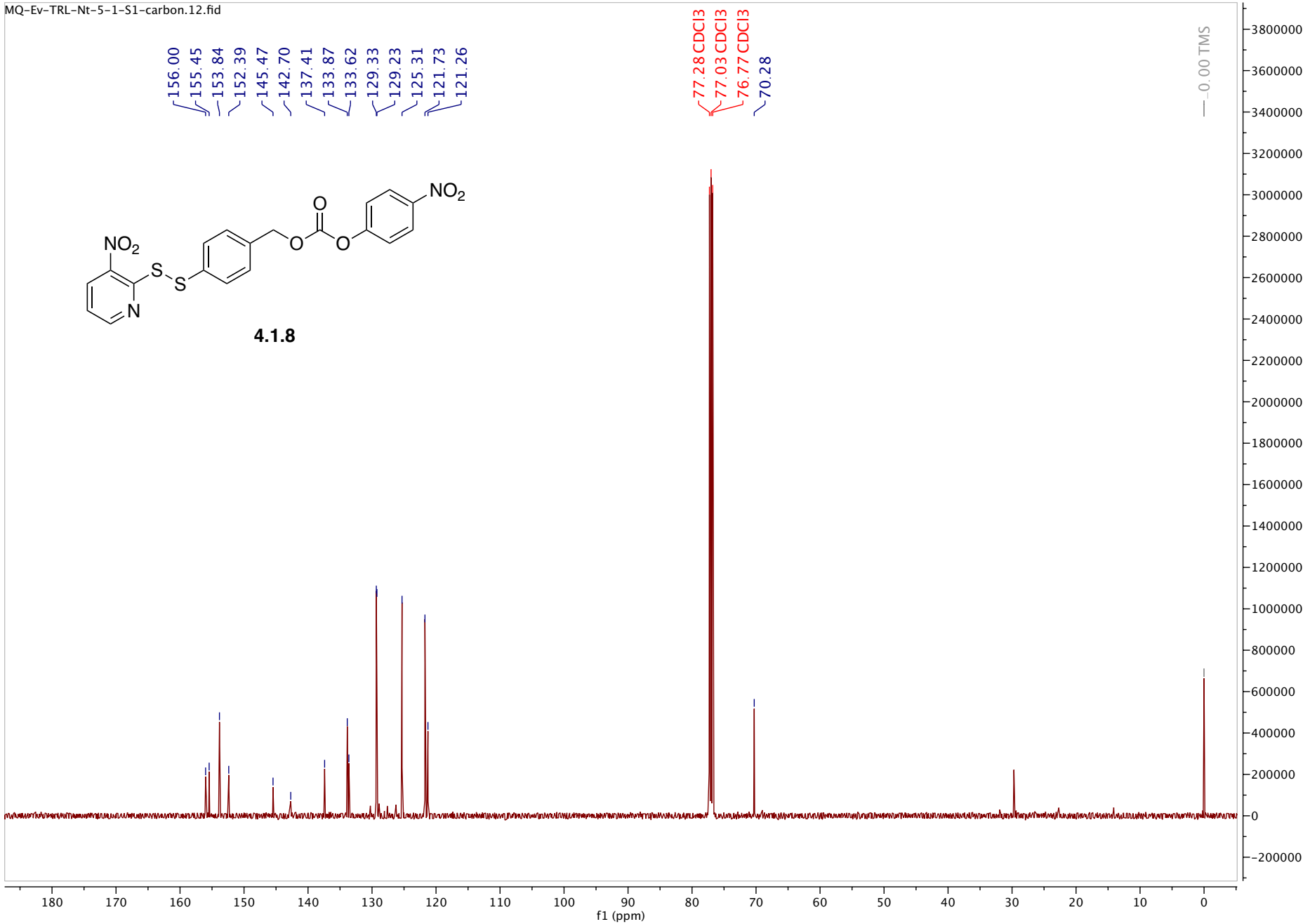
^{13}C NMR


MQ-Ev-TRL-Nt-4-2-S2-3-F65-72-carbon.12.fid
156.51
153.93
142.76
140.86
135.48
133.96
130.06
127.68
121.23
77.41 CDCl3
77.16 CDCl3
77.16 CDCl3
76.91 CDCl3
64.90
NO2
S
S
OH
N
4.1.7
f1 (ppm)

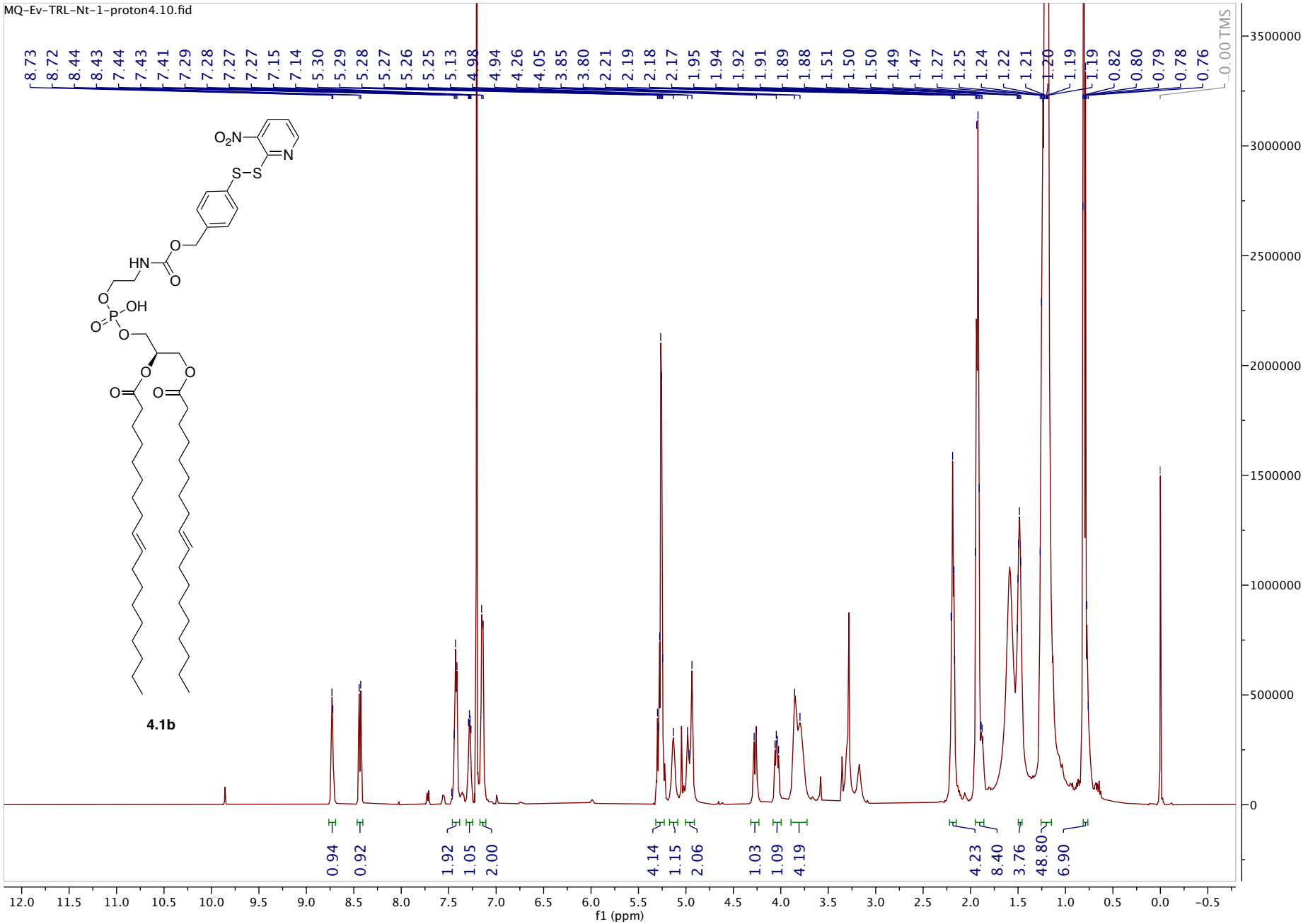
^{1}H NMR


MQ-Ev-TRL-Nt-5-1-S1-proton.10.fid
8.83
8.82
8.82
8.81
8.55
8.54
8.53
8.53
8.27
8.27
8.26
8.25
7.59
7.57
7.39
7.38
7.37
7.36
7.35
7.35
7.34
7.26 CDCl3
5.24
1.57 H2O
0.00 TMS
NO2
O
O
O
NO2
S
S
N
4.1.8
4.5×10^7
4.0×10^7
3.5×10^7
3.0×10^7
2.5×10^7
2.0×10^7
1.5×10^7
1.0×10^7
5.0×10^6
0.0
1.06
1.03
2.01
1.95
5.15
2.00
10.5
10.0
9.5
9.0
8.5
8.0
7.5
7.0
6.5
6.0
5.5
5.0
4.5
4.0
3.5
3.0
2.5
2.0
1.5
1.0
0.5
0.0
-0.5
f1 (ppm)

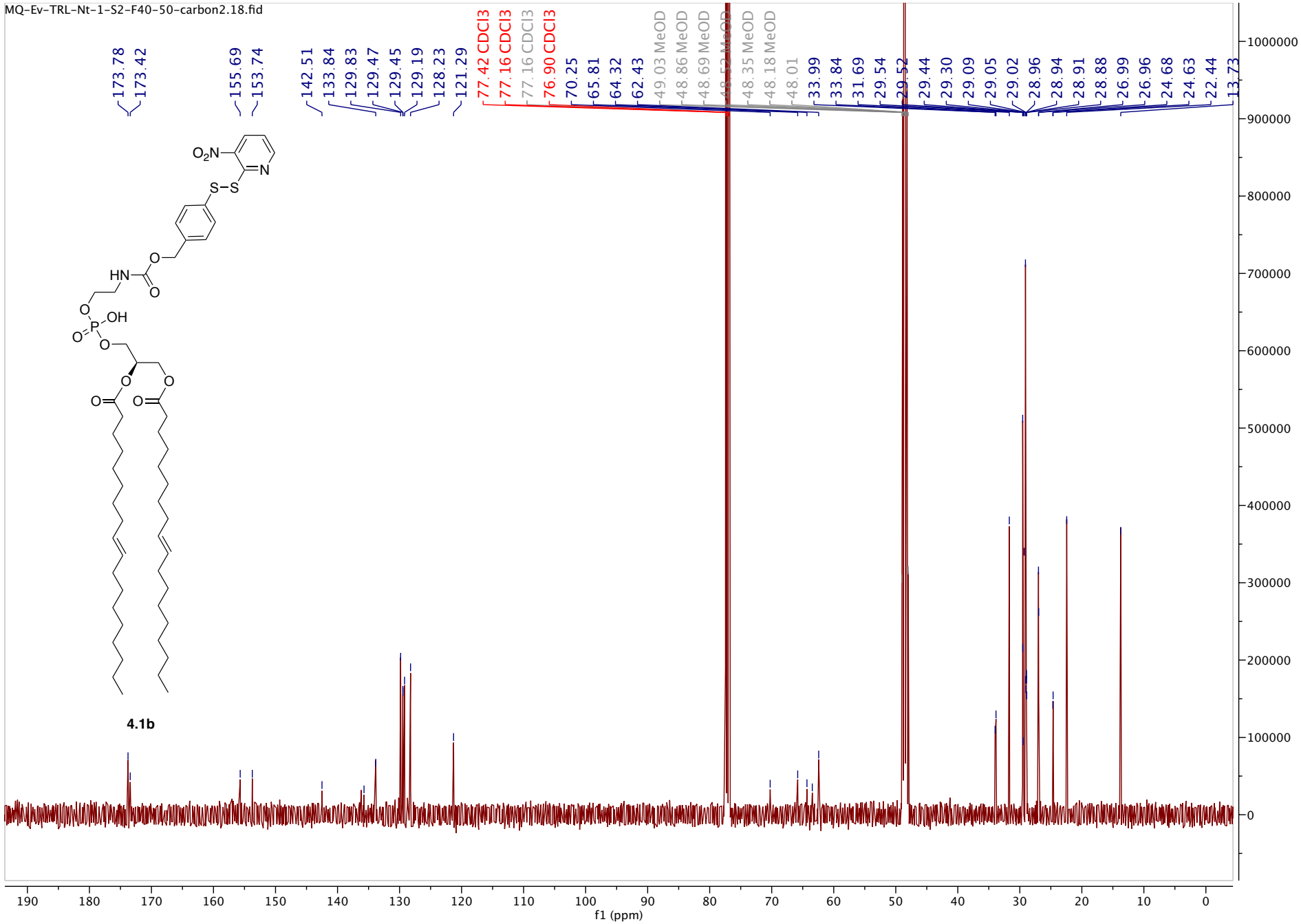
^{13}C NMR


MQ-Ev-TRL-Nt-5-1-S1-carbon.12.fid
156.00
155.45
153.84
152.39
145.47
142.70
137.41
133.87
133.62
129.33
129.23
125.31
121.73
121.26
77.28 CDCl3
77.03 CDCl3
76.77 CDCl3
70.28
0.00 TMS
NO2
S
S
O
O
O
NO2
N
4.1.8
f1 (ppm)

^{1}H NMR

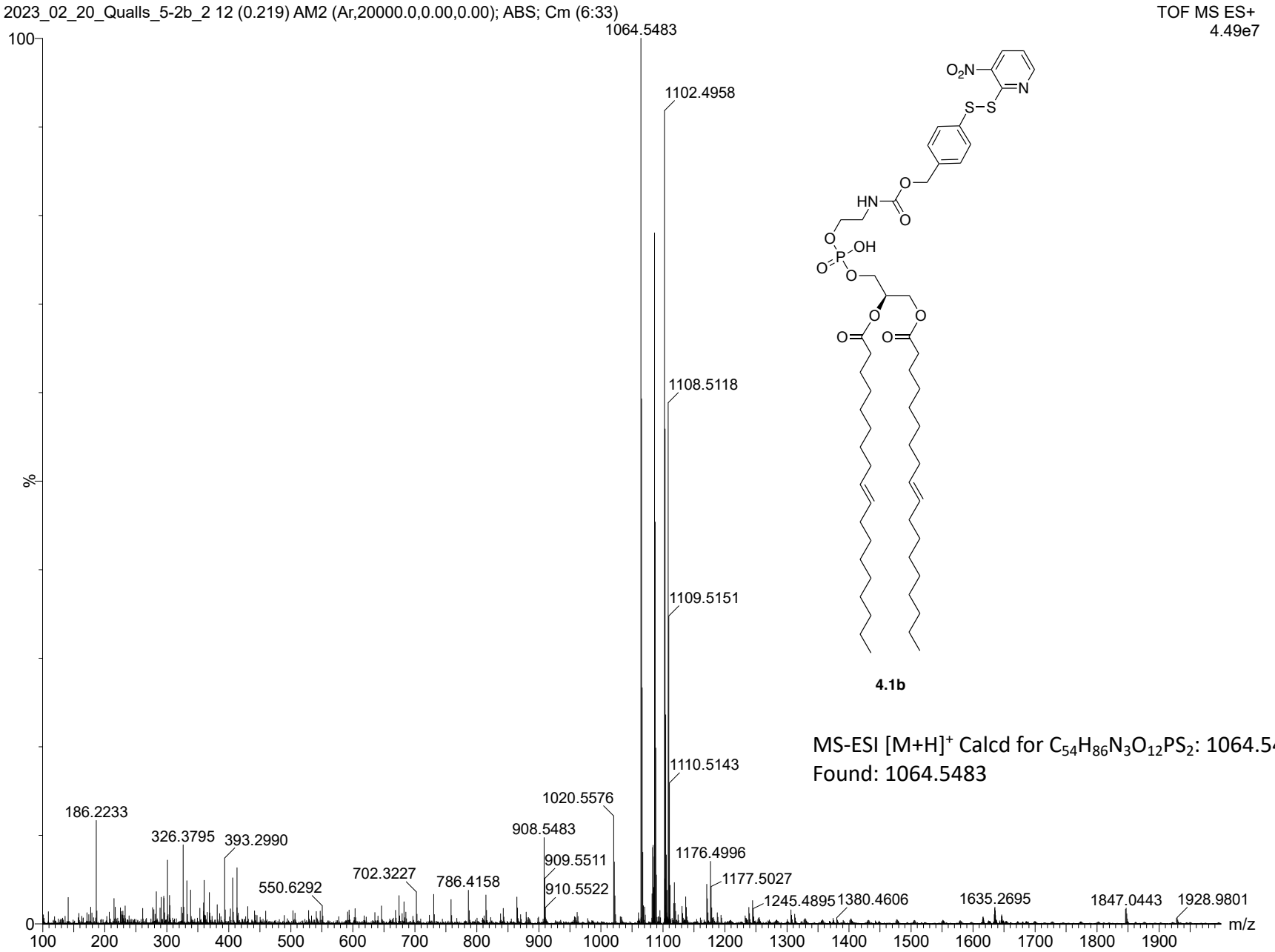

MQ-Ev-TRL-Nt-1-proton4.10.fid
8.73 8.72 8.44 8.43 7.44 7.43 7.41 7.29 7.28 7.27 7.27 7.15 7.14 5.30 5.29 5.28 5.27 5.26 5.25 5.13 4.98 4.94 4.26 4.05 3.85 3.80 2.21 2.19 2.18 2.17 1.95 1.94 1.92 1.91 1.89 1.88 1.51 1.50 1.50 1.49 1.47 1.27 1.25 1.24 1.22 1.21 1.20 1.19 0.82 0.80 0.79 0.78 0.76 0.00 TMS
4.1b
0.94 0.92 1.92 1.05 2.00 4.14 1.15 2.06 1.03 1.09 4.19 4.23 8.40 3.76 48.80 6.90
f1 (ppm)

^{13}C NMR


MQ-Ev-TRL-Nt-1-S2-F40-50-carbon2.18.fid
173.78
173.42
155.69
153.74
142.51
133.84
129.83
129.47
129.45
129.19
128.23
121.29
77.42 CDCl3
77.16 CDCl3
77.16 CDCl3
76.90 CDCl3
70.25
65.81
64.32
62.43
49.03 MeOD
48.86 MeOD
48.69 MeOD
48.52 MeOD
48.35 MeOD
48.18 MeOD
48.01
33.99
33.84
31.69
29.54
29.52
29.44
29.30
29.09
29.05
29.02
28.96
28.94
28.91
28.88
26.99
26.96
24.68
24.63
22.44
13.73
1000000
900000
800000
700000
600000
500000
400000
300000
200000
100000
0
190
180
170
160
150
140
130
120
110
100
90
80
70
60
50
40
30
20
10
0
f1 (ppm)
4.1b

ESI-MS

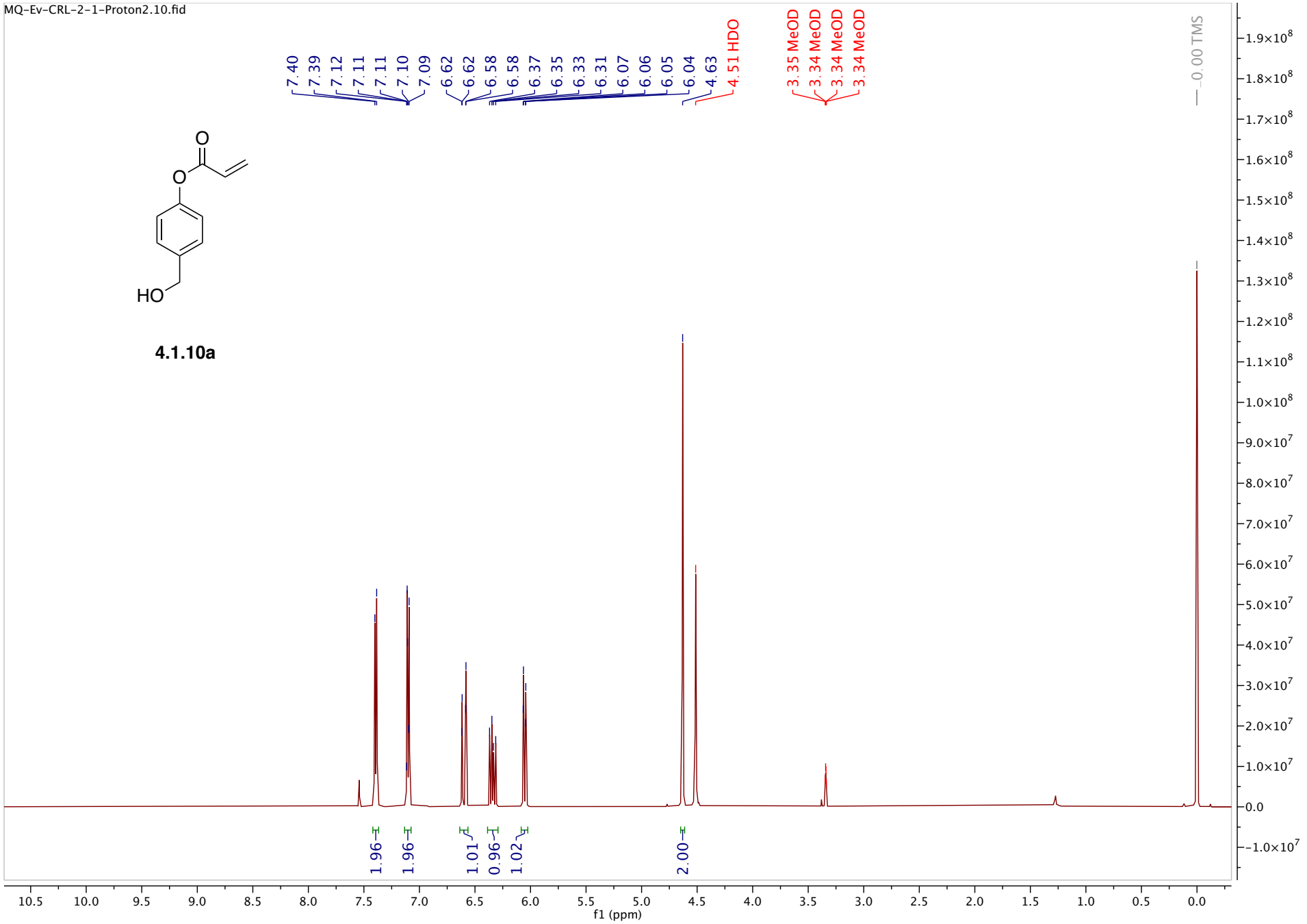
Sample: Pure **4.1b**



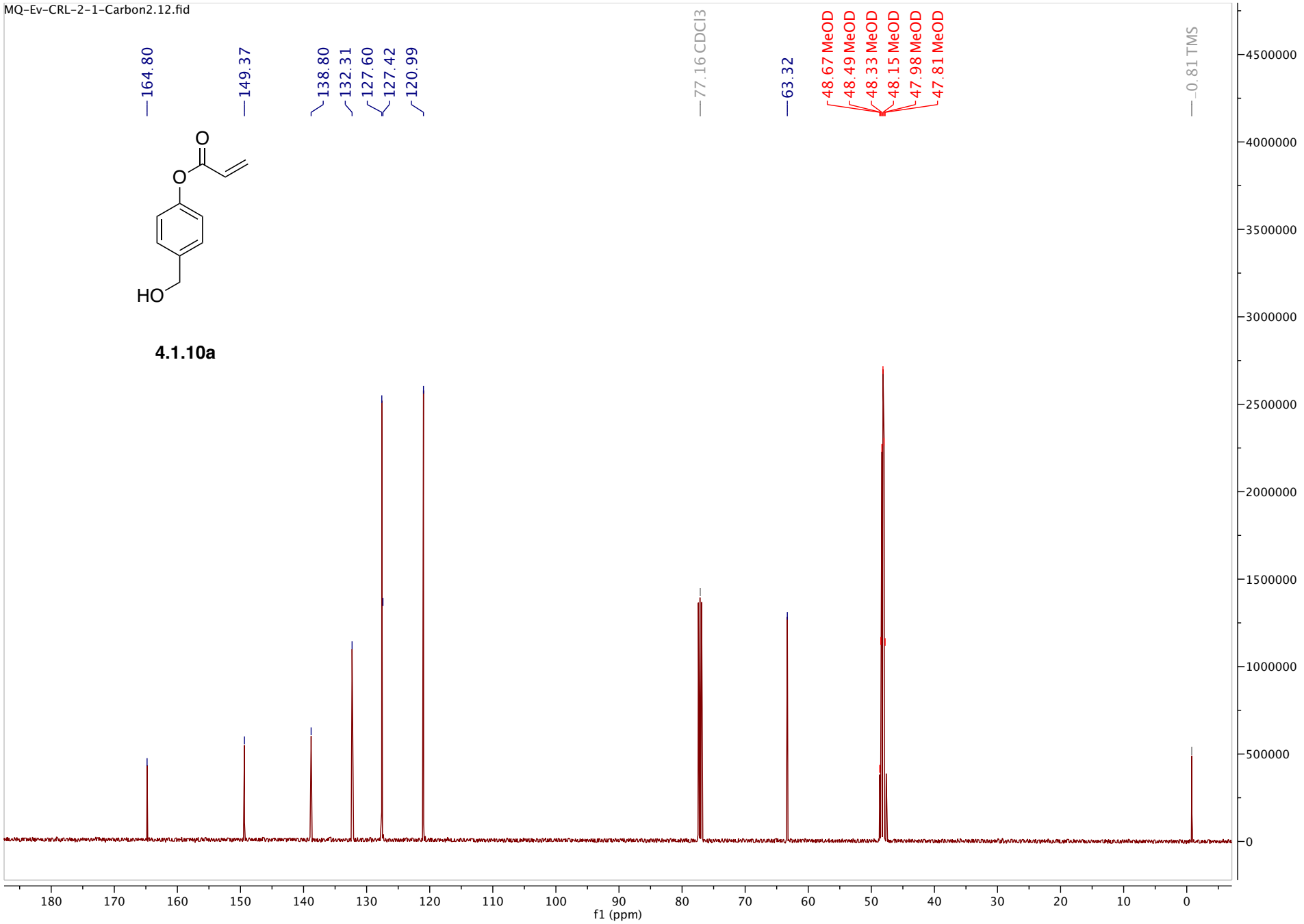
4.1b

MS-ESI $[M+H]^+$ Calcd for $C_{54}H_{86}N_3O_{12}PS_2$: 1064.5469
Found: 1064.5483

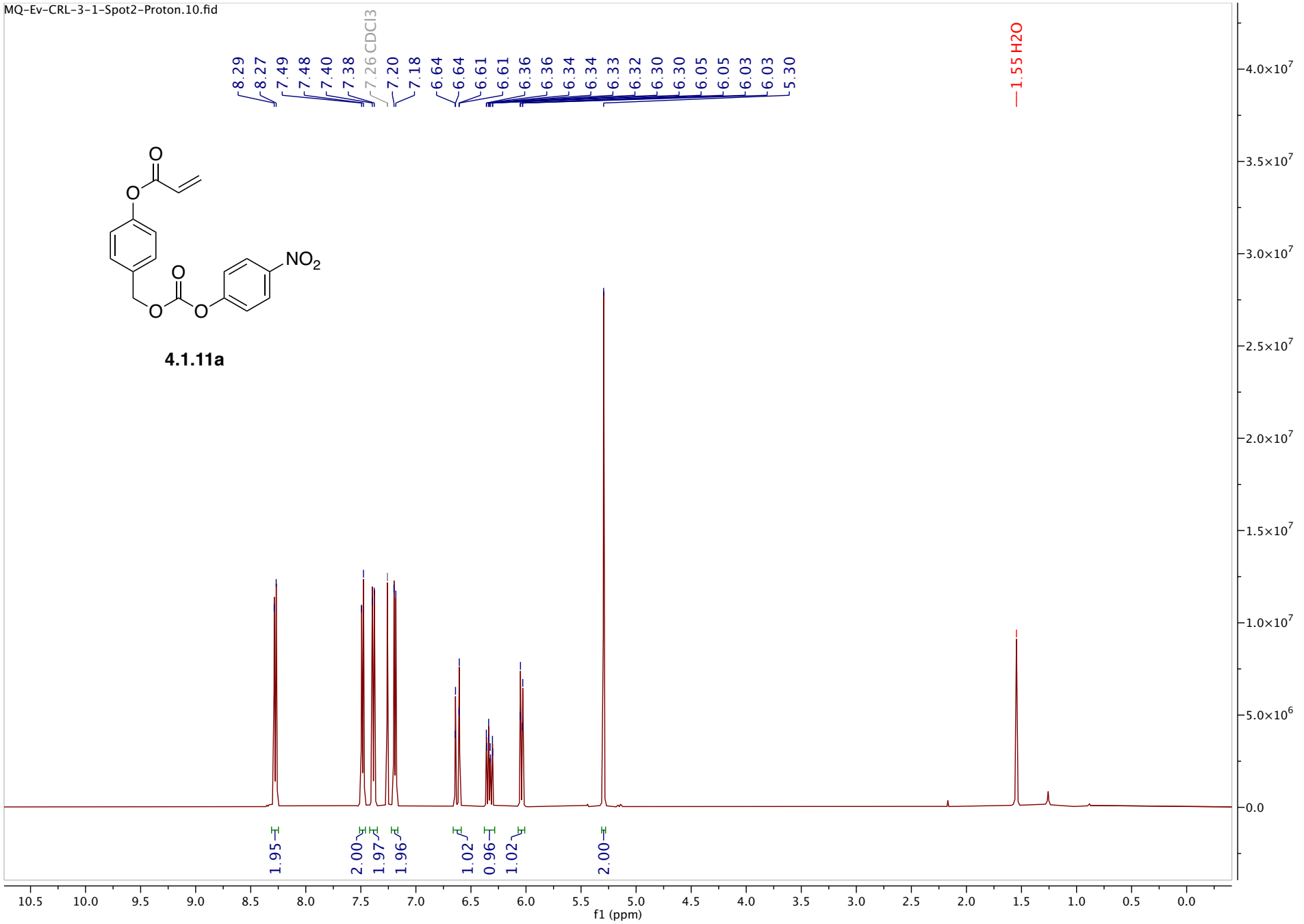
^{1}H NMR


MQ-Ev-CRL-2-1-Proton2.10.fid
7.40
7.39
7.12
7.11
7.11
7.10
7.09
6.62
6.62
6.58
6.58
6.37
6.35
6.33
6.31
6.07
6.06
6.05
6.04
4.63
4.51 HDO
3.35 MeOD
3.34 MeOD
3.34 MeOD
3.34 MeOD
0.00 TMS
O
O
HO
4.1.10a
1.96
1.96
1.01
0.96
1.02
2.00
f1 (ppm)

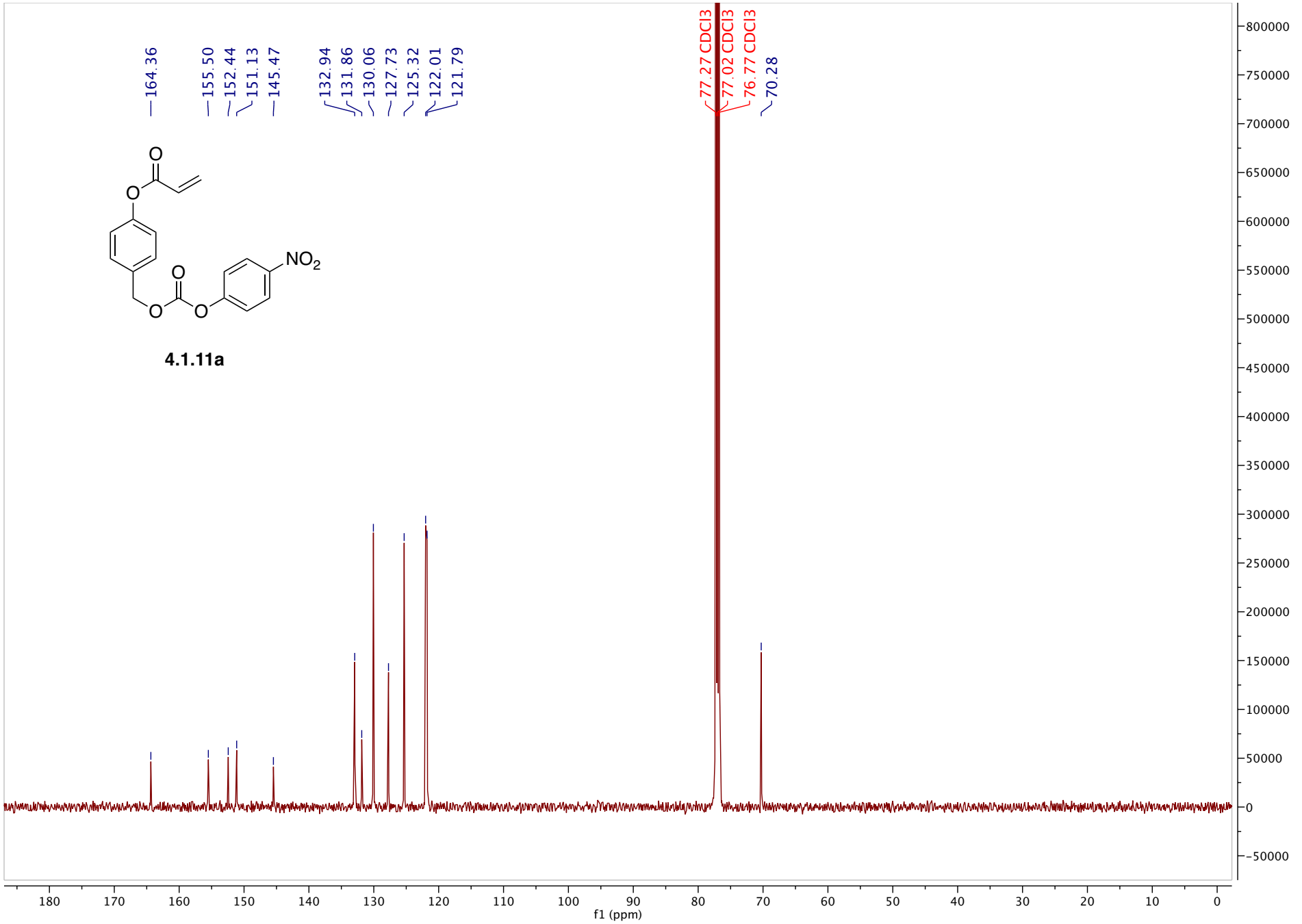
^{13}C NMR


MQ-Ev-CRL-2-1-Carbon2.12.fid
164.80
149.37
138.80
132.31
127.60
127.42
120.99
77.16 CDCl3
63.32
48.67 MeOD
48.49 MeOD
48.33 MeOD
48.15 MeOD
47.98 MeOD
47.81 MeOD
0.81 TMS
O
O
HO
4.1.10a
4500000
4000000
3500000
3000000
2500000
2000000
1500000
1000000
500000
0
180
170
160
150
140
130
120
110
100
90
80
70
60
50
40
30
20
10
0
f1 (ppm)

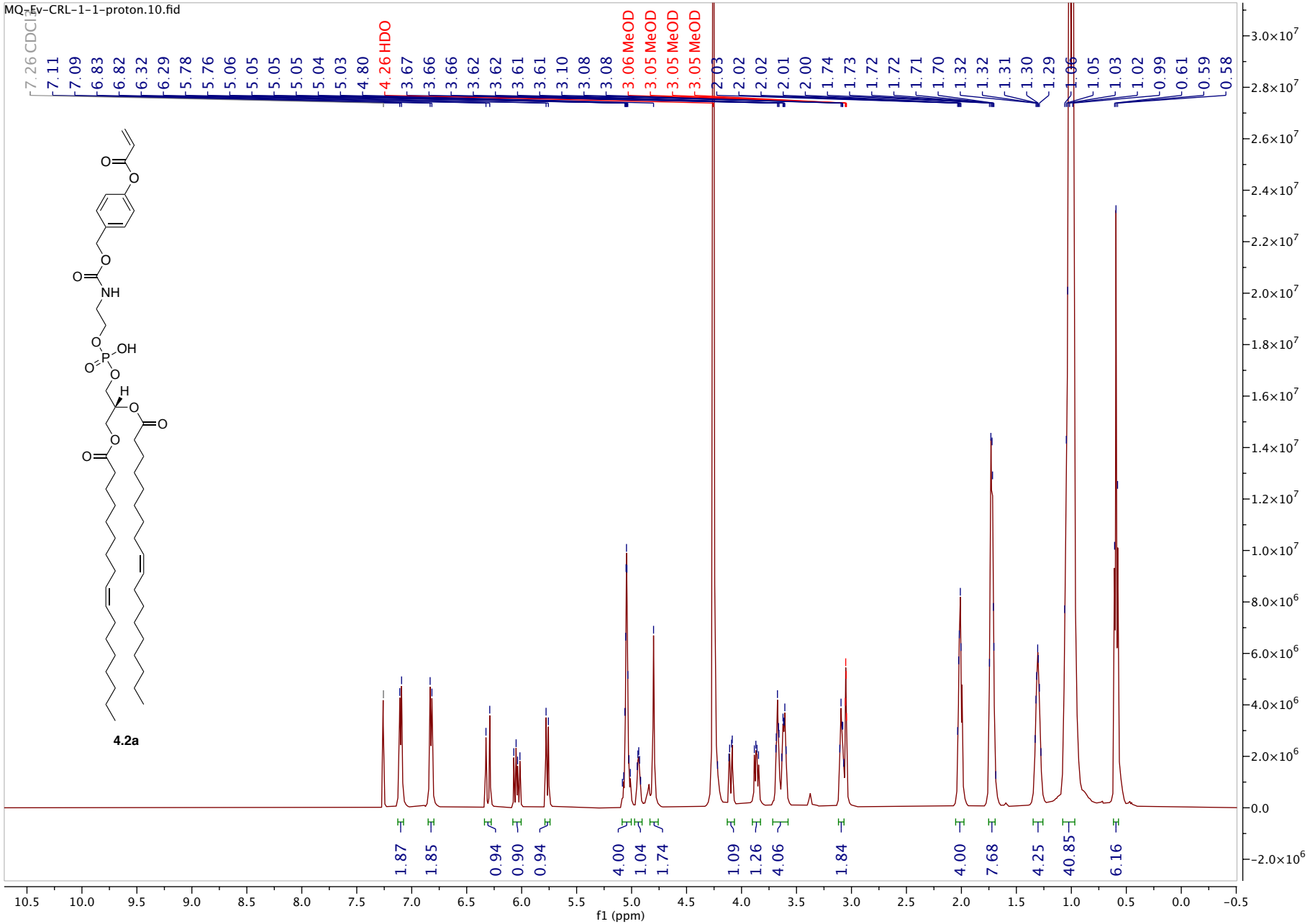
^{1}H NMR


MQ-Ev-CRL-3-1-Spot2-Proton.10.fid
8.29
8.27
7.49
7.48
7.40
7.38
7.26 CDCl3
7.20
7.18
6.64
6.64
6.61
6.61
6.36
6.36
6.34
6.34
6.33
6.32
6.30
6.30
6.05
6.05
6.03
6.03
5.30
1.55 H2O
NO2
4.1.11a
1.95
2.00
1.97
1.96
1.02
0.96
1.02
2.00
f1 (ppm)

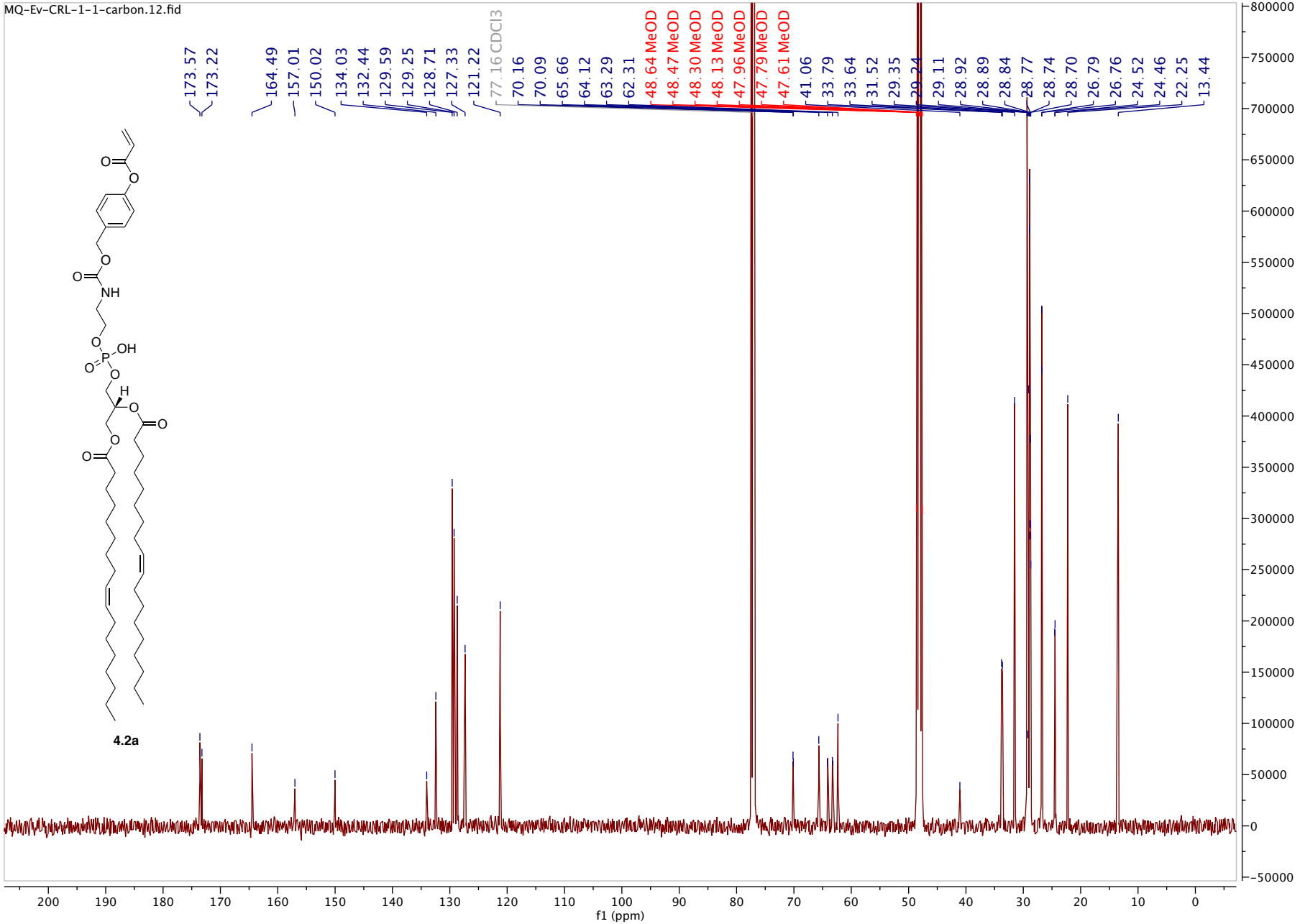
^{13}C NMR


164.36
155.50
152.44
151.13
145.47
132.94
131.86
130.06
127.73
125.32
122.01
121.79
77.27 CDCl3
77.02 CDCl3
76.77 CDCl3
70.28
O
O
O
O
O
NO2
4.1.11a
f1 (ppm)

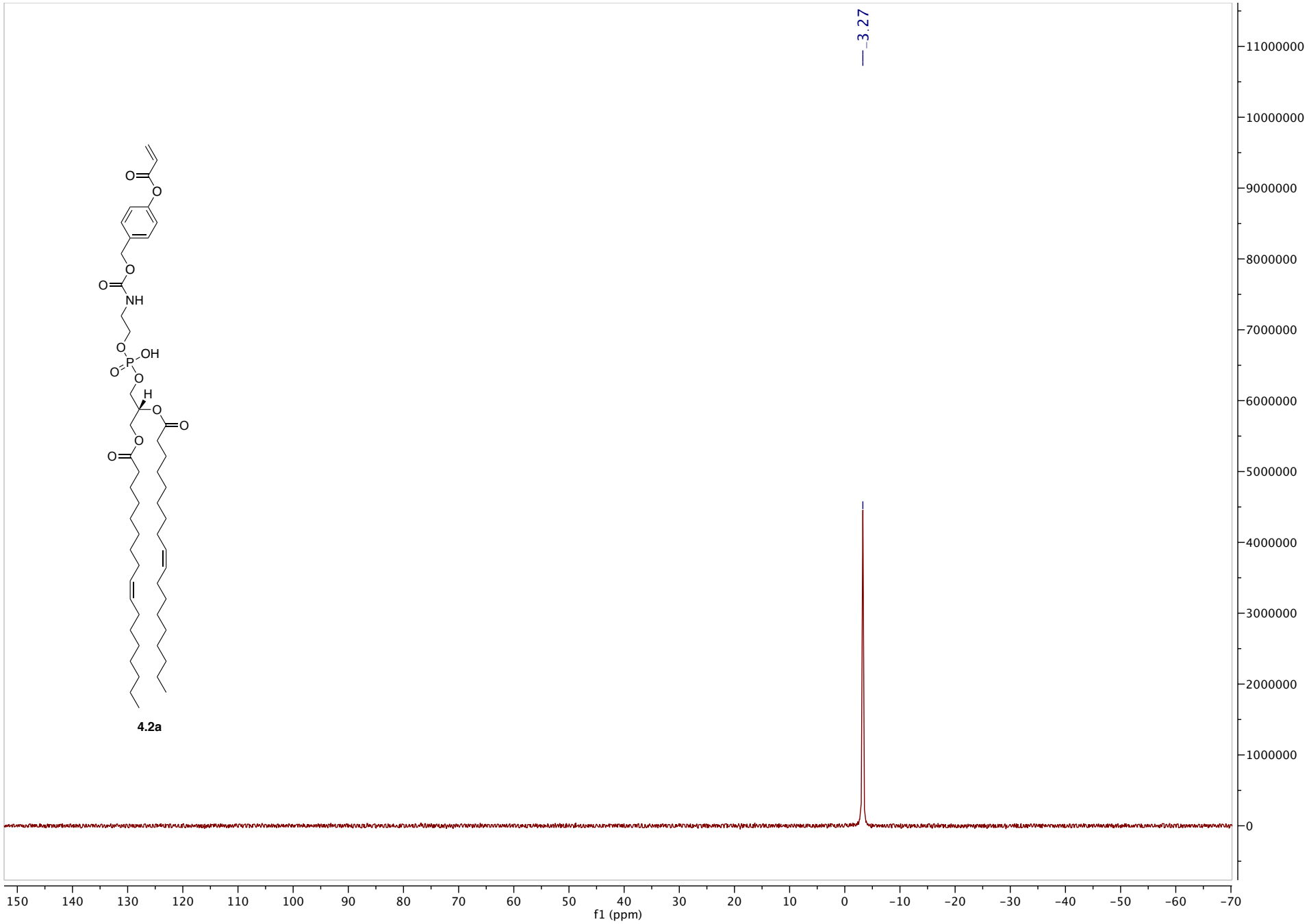
^{1}H NMR


MQ-Ev-CRL-1-1-proton.10.fid
7.26 CDCl3
7.11 7.09 6.83 6.82 6.32 6.29 5.78 5.76 5.06 5.05 5.05 5.05 5.04 5.03 4.80 4.26 HDO 3.67 3.66 3.66 3.62 3.62 3.61 3.61 3.10 3.08 3.08 3.06 MeOD 3.05 MeOD 3.05 MeOD 3.05 MeOD 2.03 2.02 2.02 2.01 2.00 1.74 1.73 1.72 1.72 1.71 1.70 1.32 1.32 1.31 1.30 1.29 1.06 1.05 1.03 1.02 0.99 0.61 0.59 0.58
NH
OH
H
4.2a
1.87 1.85 0.94 0.90 0.94 4.00 1.04 1.74 1.09 1.26 4.06 1.84 4.00 7.68 4.25 40.85 6.16
f1 (ppm)

^{13}C NMR


MQ-Ev-CRL-1-1-carbon.12.fid
173.57
173.22
164.49
157.01
150.02
134.03
132.44
129.59
129.25
128.71
127.33
121.22
77.16 CDCl3
70.16
70.09
65.66
64.12
63.29
62.31
48.64 MeOD
48.47 MeOD
48.30 MeOD
48.13 MeOD
47.96 MeOD
47.79 MeOD
47.61 MeOD
41.06
33.79
33.64
31.52
29.35
29.24
29.11
28.92
28.89
28.84
28.77
28.74
28.70
26.79
26.76
24.52
24.46
22.25
13.44
4.2a
f1 (ppm)

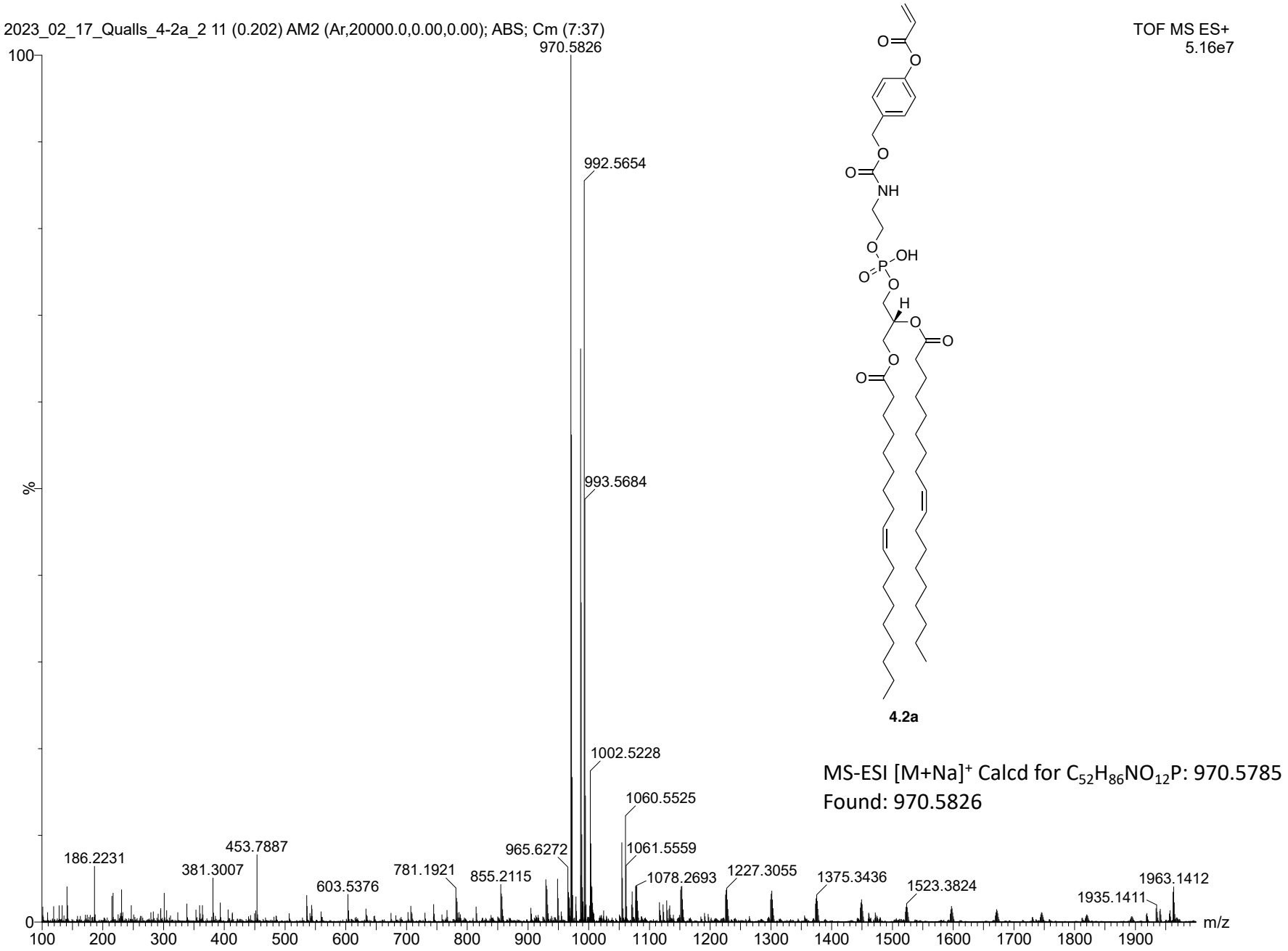
^{31}P NMR


3.27
11000000
10000000
9000000
8000000
7000000
6000000
5000000
4000000
3000000
2000000
1000000
0
150 140 130 120 110 100 90 80 70 60 50 40 30 20 10 0 −10 −20 −30 −40 −50 −60 −70
f1 (ppm)
O
O
O
NH
O
O
P
OH
O
O
H
O
O
O
O
O

4.2a

ESI-MS

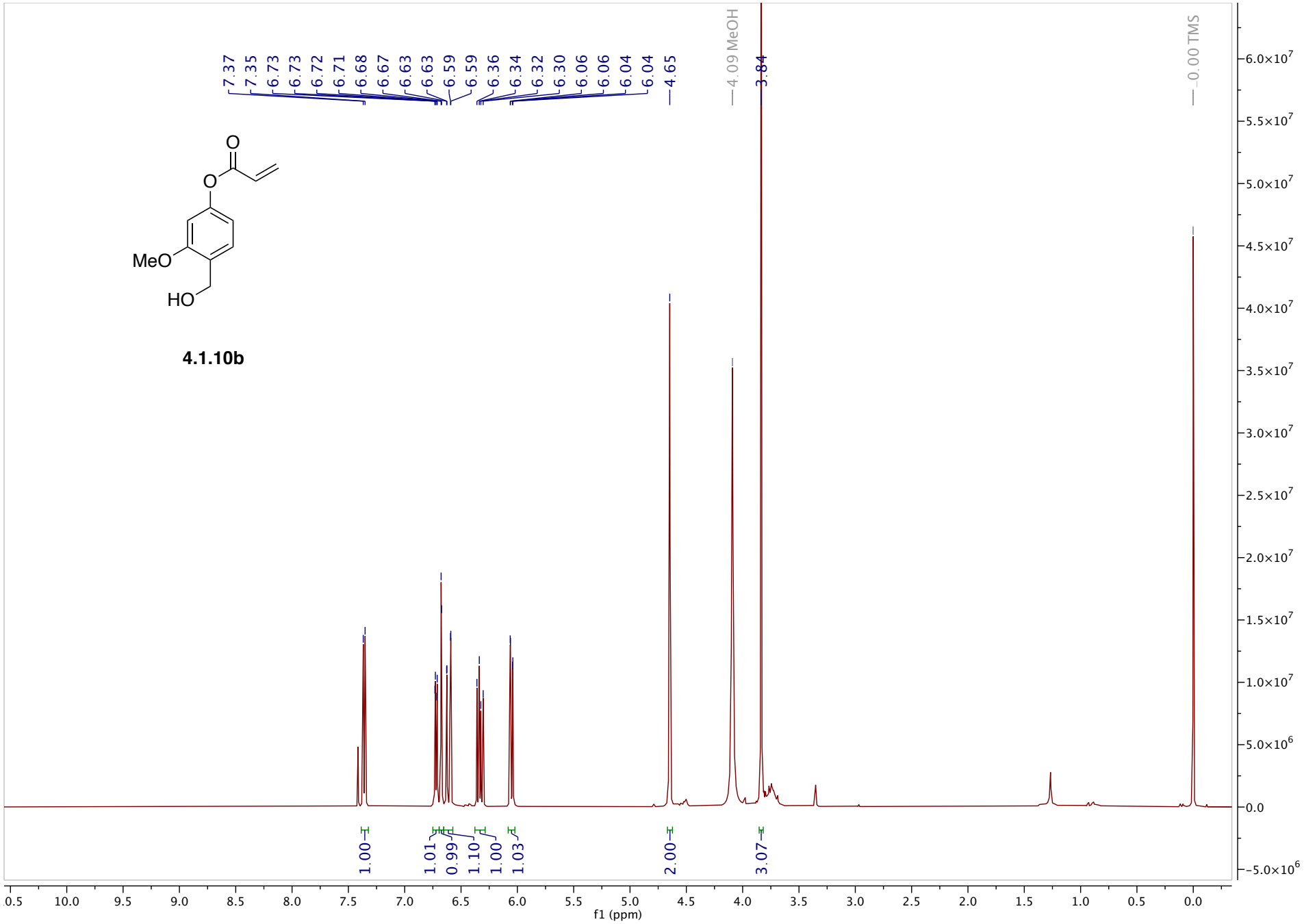
Sample: Pure **4.2a**



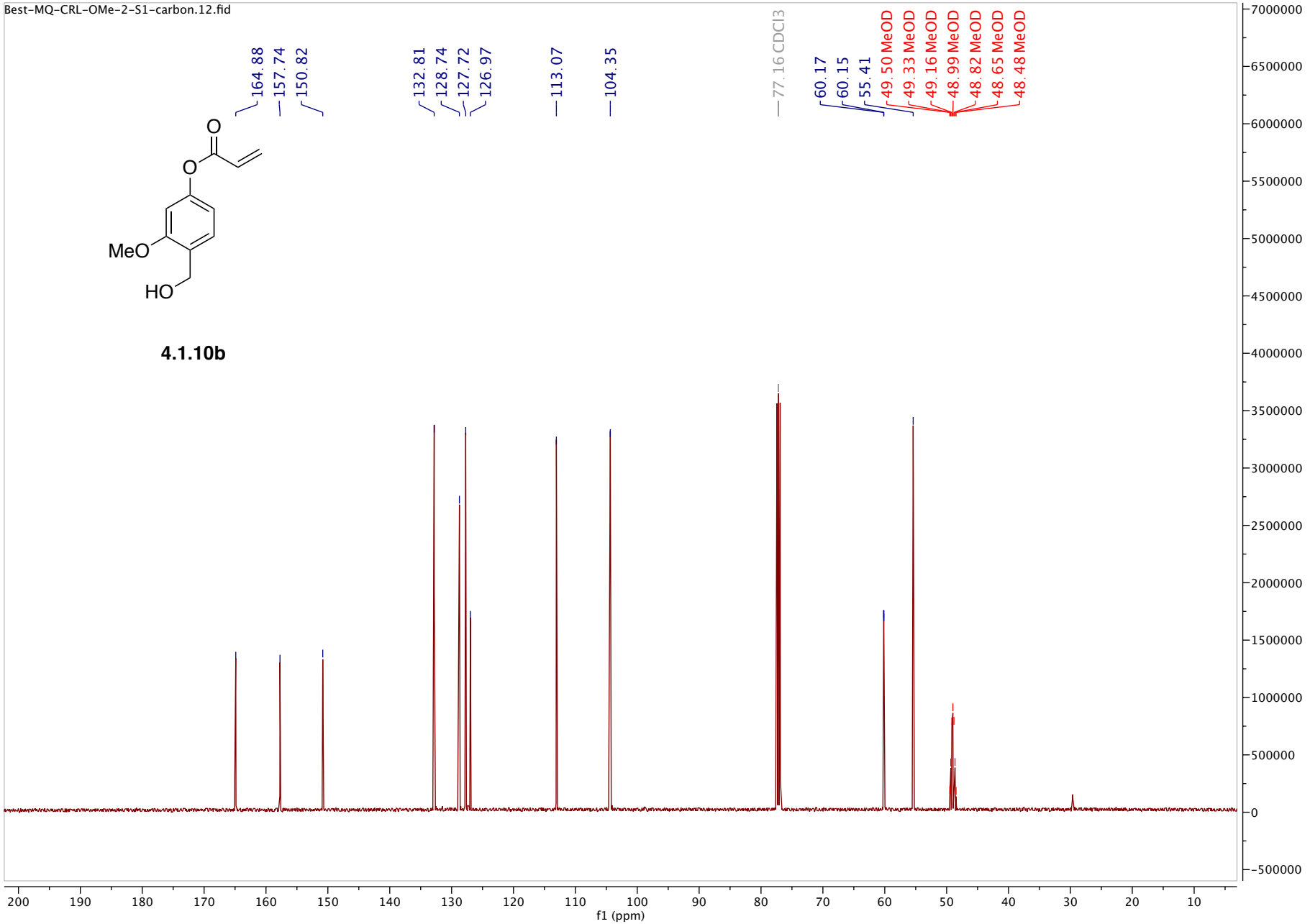
4.2a

MS-ESI $[M+Na]^+$ Calcd for $C_{52}H_{86}NO_{12}P$: 970.5785
Found: 970.5826

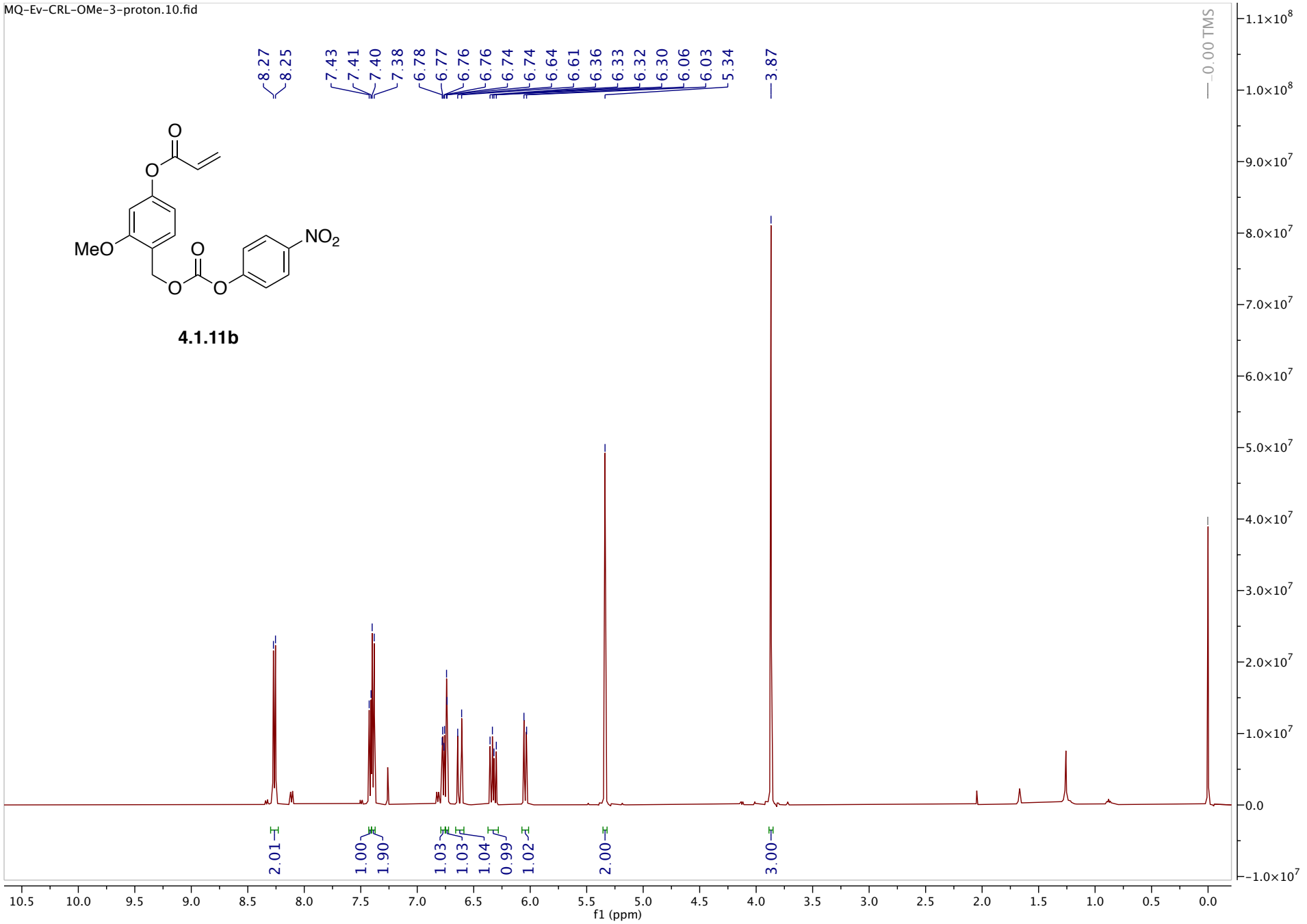
^{1}H NMR


7.37
7.35
6.73
6.73
6.72
6.71
6.68
6.67
6.63
6.63
6.59
6.59
6.36
6.34
6.32
6.30
6.06
6.06
6.04
6.04
4.65
4.09 MeOH
3.84
0.00 TMS
O
O
MeO
HO
4.1.10b
1.00
1.01
0.99
1.10
1.00
1.03
2.00
3.07
f1 (ppm)

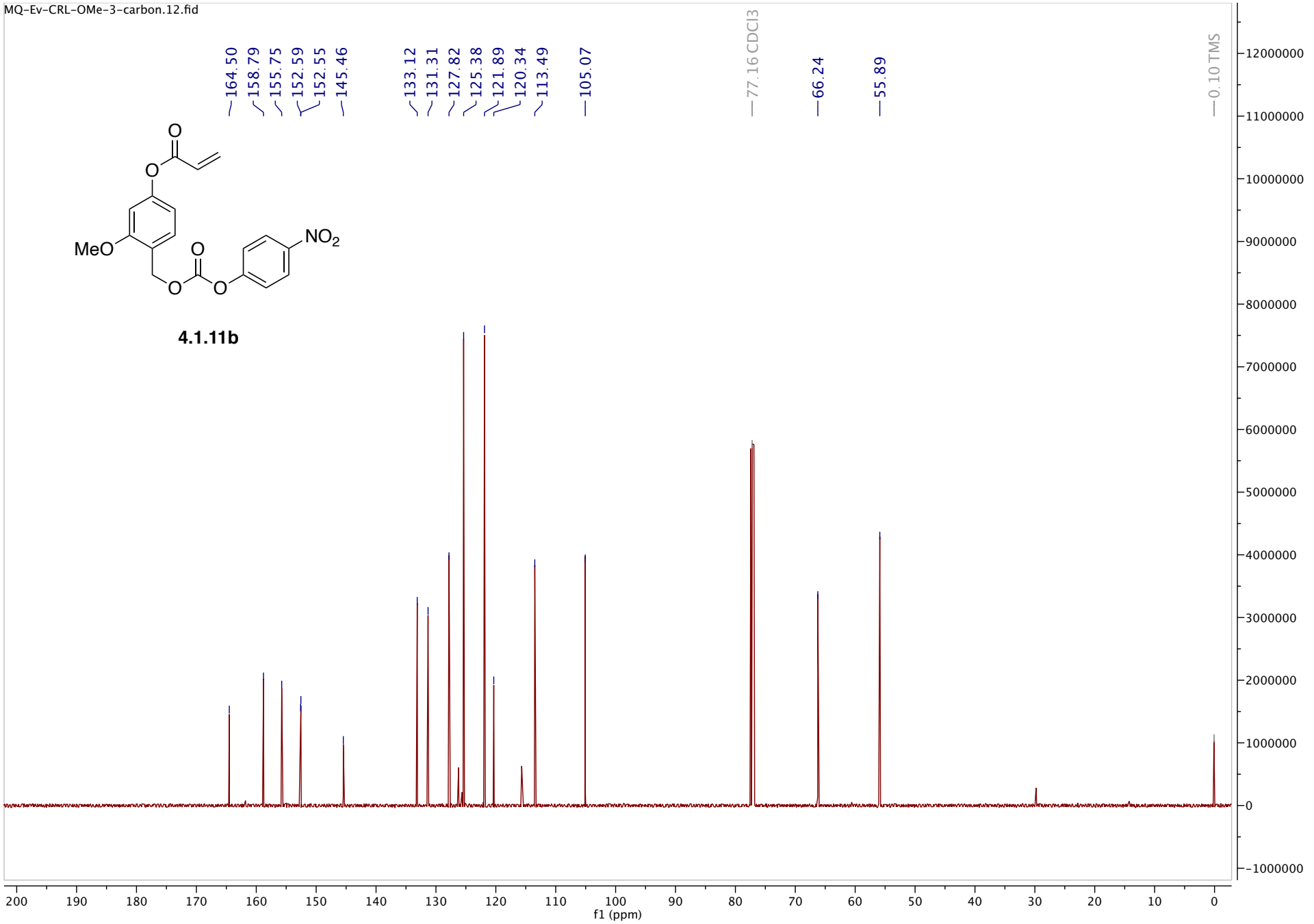
^{13}C NMR


Best-MQ-CRL-OMe-2-S1-carbon.12.fid
164.88
157.74
150.82
132.81
128.74
127.72
126.97
113.07
104.35
77.16 CDCl3
60.17
60.15
55.41
49.50 MeOD
49.33 MeOD
49.16 MeOD
48.99 MeOD
48.82 MeOD
48.65 MeOD
48.48 MeOD
O
O
MeO
HO
4.1.10b
f1 (ppm)

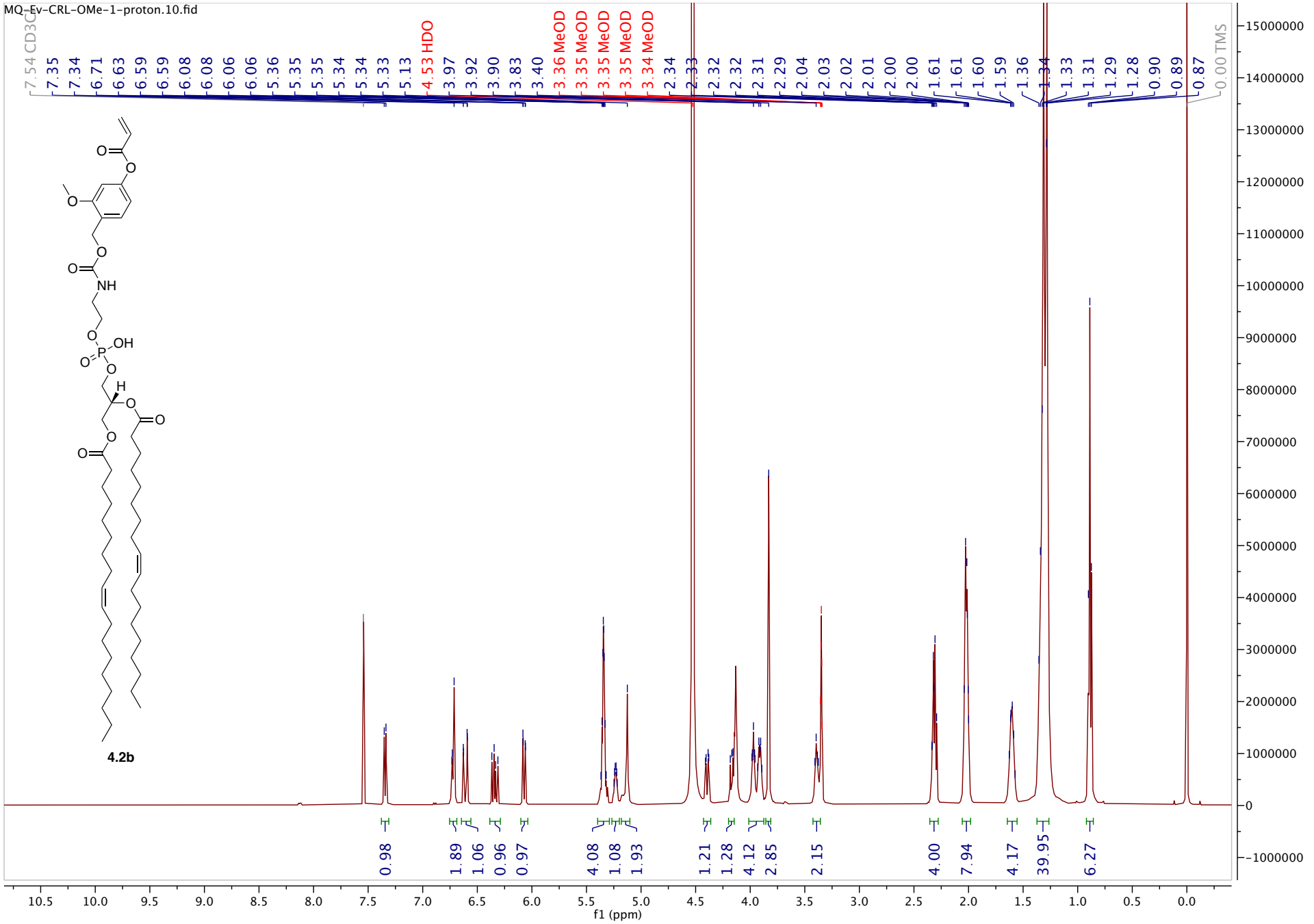
^{1}H NMR


MQ-Ev-CRL-OMe-3-proton.10.fid
8.27
8.25
7.43
7.41
7.40
7.38
6.78
6.77
6.76
6.76
6.74
6.74
6.64
6.61
6.36
6.33
6.32
6.30
6.06
6.03
5.34
3.87
0.00 TMS
MeO
NO2
4.1.11b
2.01
1.00
1.90
1.03
1.03
1.04
0.99
1.02
2.00
3.00
f1 (ppm)

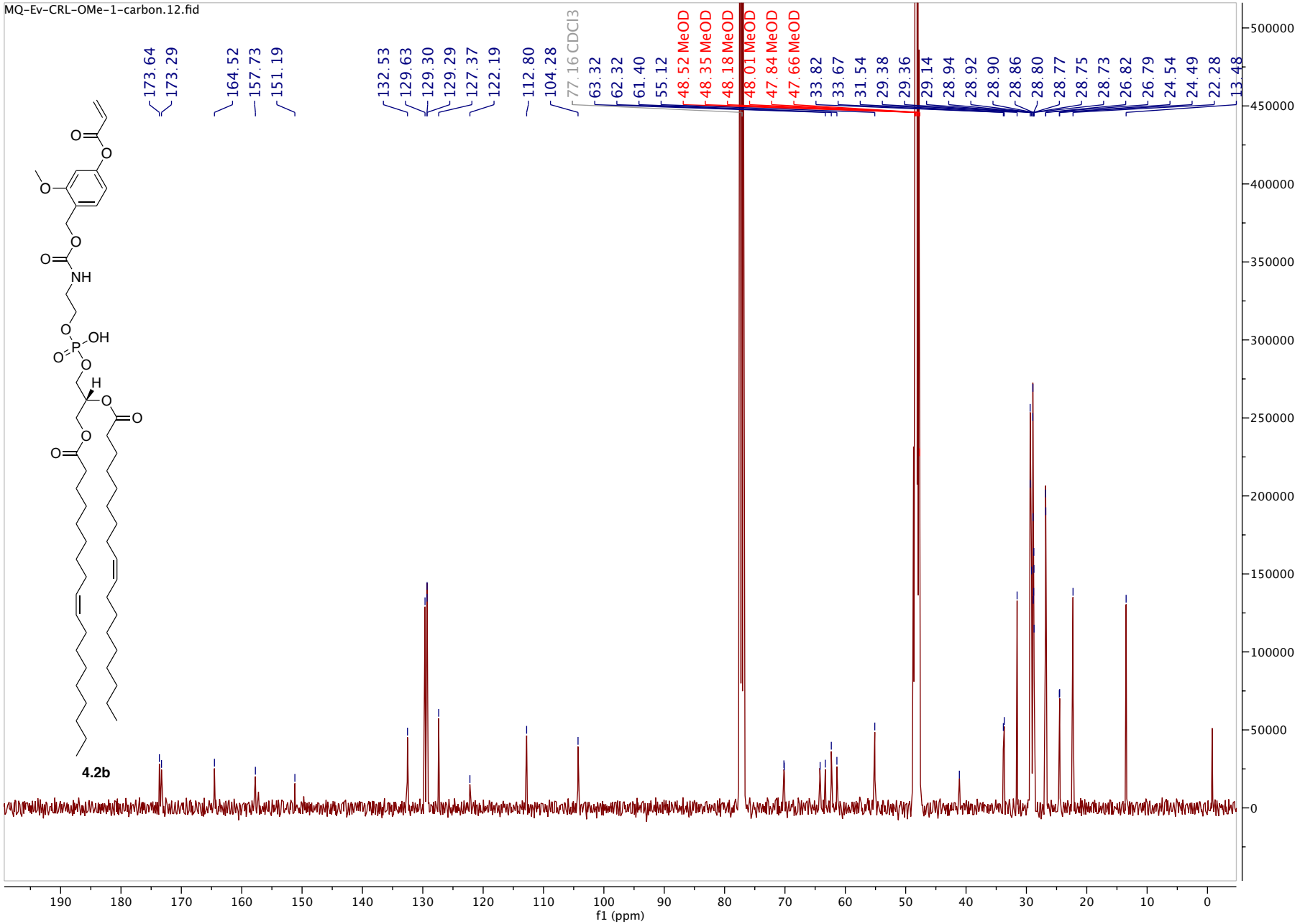
^{13}C NMR


MQ-Ev-CRL-OMe-3-carbon.12.fid
164.50
158.79
155.75
152.59
152.55
145.46
133.12
131.31
127.82
125.38
121.89
120.34
113.49
105.07
77.16 CDCl3
66.24
55.89
0.10 TMS
MeO
O
O
O
O
O
NO2
4.1.11b
f1 (ppm)

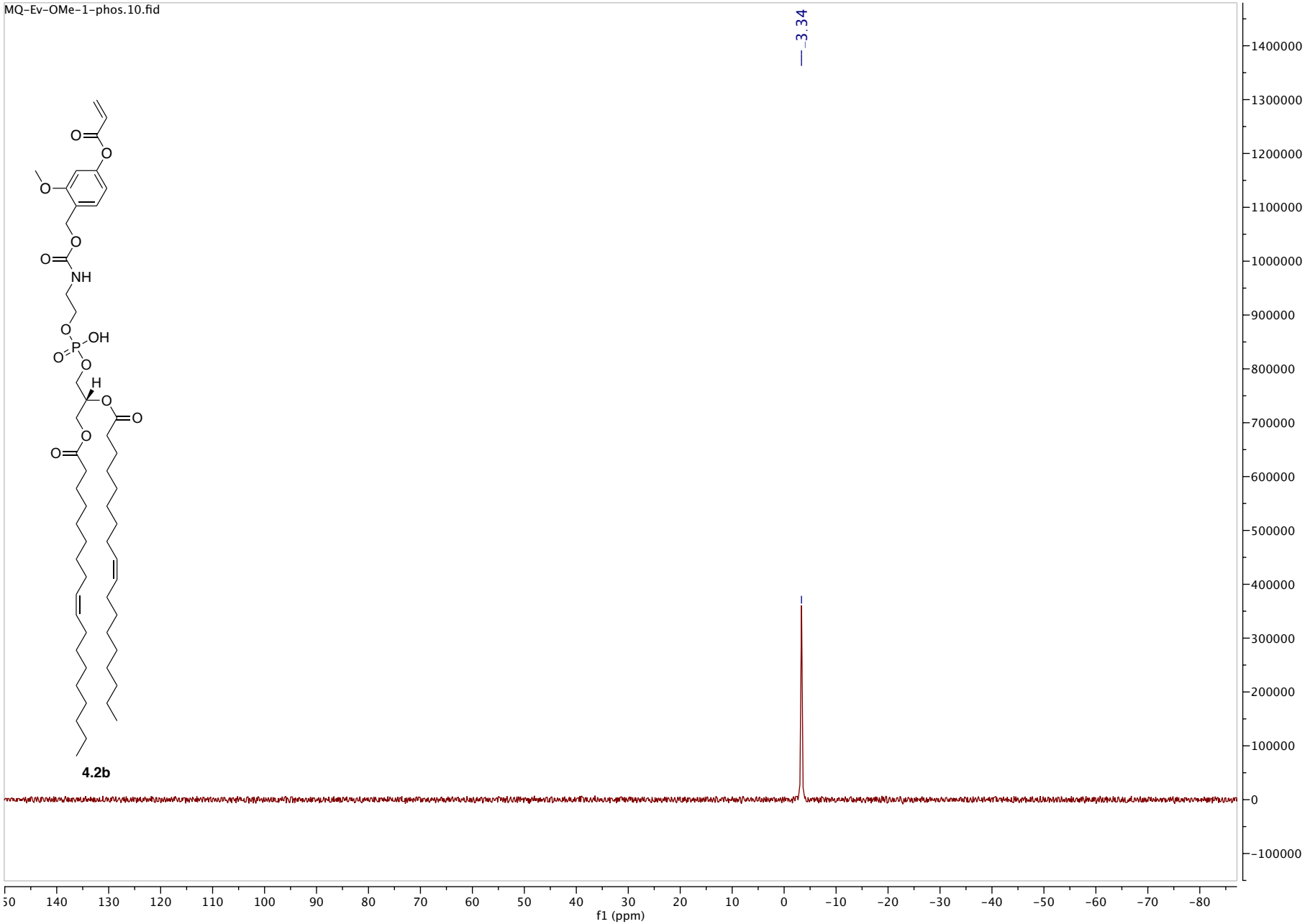
^{1}H NMR


MQ-Ev-CRL-OMe-1-proton.10.fid
7.54 CD3OD
7.35
7.34
6.71
6.63
6.59
6.59
6.08
6.08
6.06
6.06
5.36
5.35
5.35
5.34
5.34
5.33
5.13
4.53 HDO
3.97
3.92
3.90
3.83
3.40
3.36 MeOD
3.35 MeOD
3.35 MeOD
3.35 MeOD
3.34 MeOD
2.34
2.33
2.32
2.32
2.31
2.29
2.04
2.03
2.02
2.01
2.00
2.00
1.61
1.61
1.60
1.59
1.36
1.34
1.33
1.31
1.29
1.28
0.90
0.89
0.87
0.00 TMS
0.98
1.89
1.06
0.96
0.97
4.08
1.08
1.93
1.21
1.28
4.12
2.85
2.15
4.00
7.94
4.17
39.95
6.27
f1 (ppm)
4.2b

^{13}C NMR

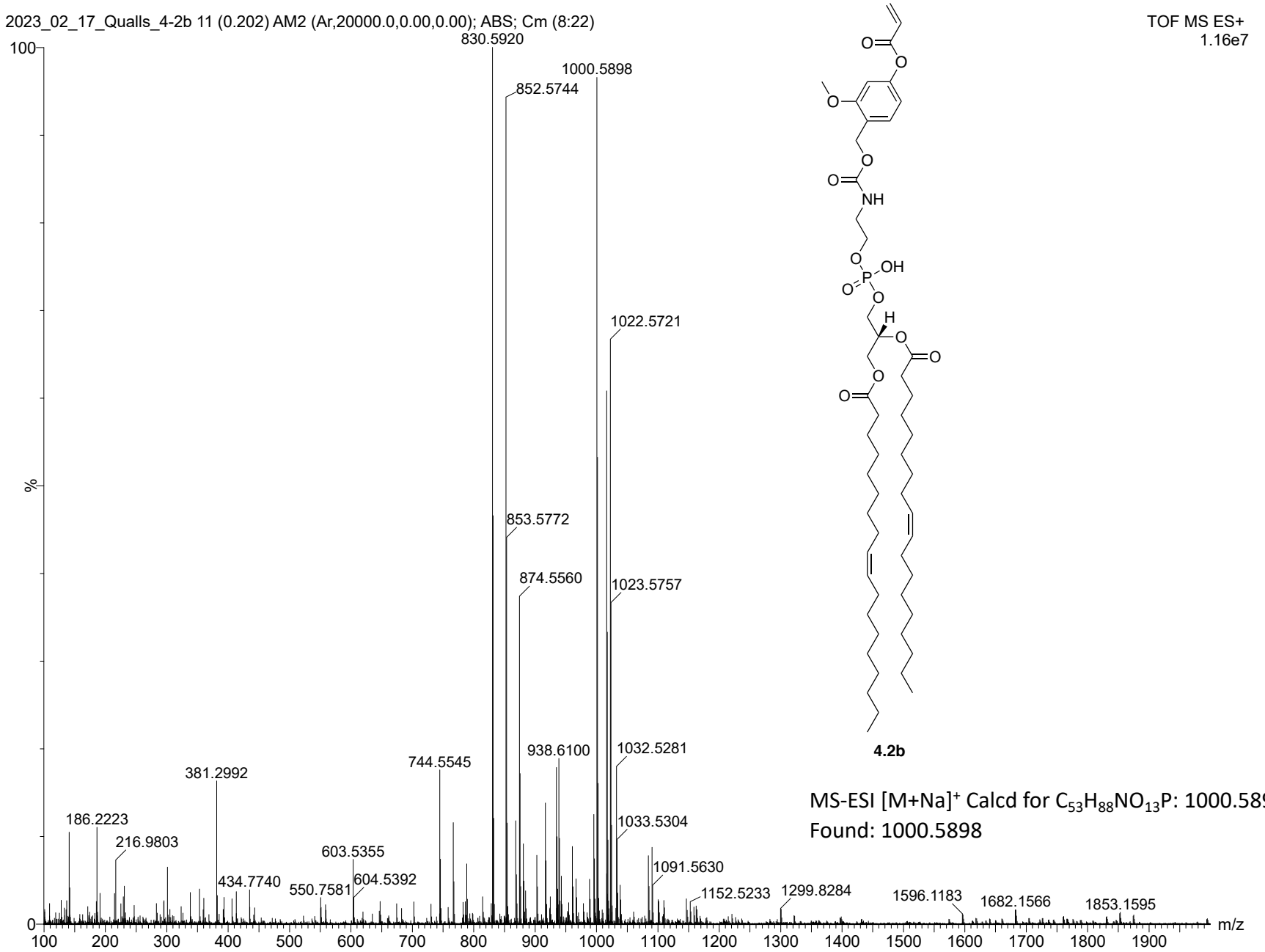

MQ-Ev-CRL-OMe-1-carbon.12.fid
173.64
173.29
164.52
157.73
151.19
132.53
129.63
129.30
129.29
127.37
122.19
112.80
104.28
77.16 CDCl3
63.32
62.32
61.40
55.12
48.52 MeOD
48.35 MeOD
48.18 MeOD
48.01 MeOD
47.84 MeOD
47.66 MeOD
33.82
33.67
31.54
29.38
29.36
29.14
28.94
28.92
28.90
28.86
28.80
28.77
28.75
28.73
26.82
26.79
24.54
24.49
22.28
13.48
4.2b
f1 (ppm)

^{31}P NMR



ESI-MS

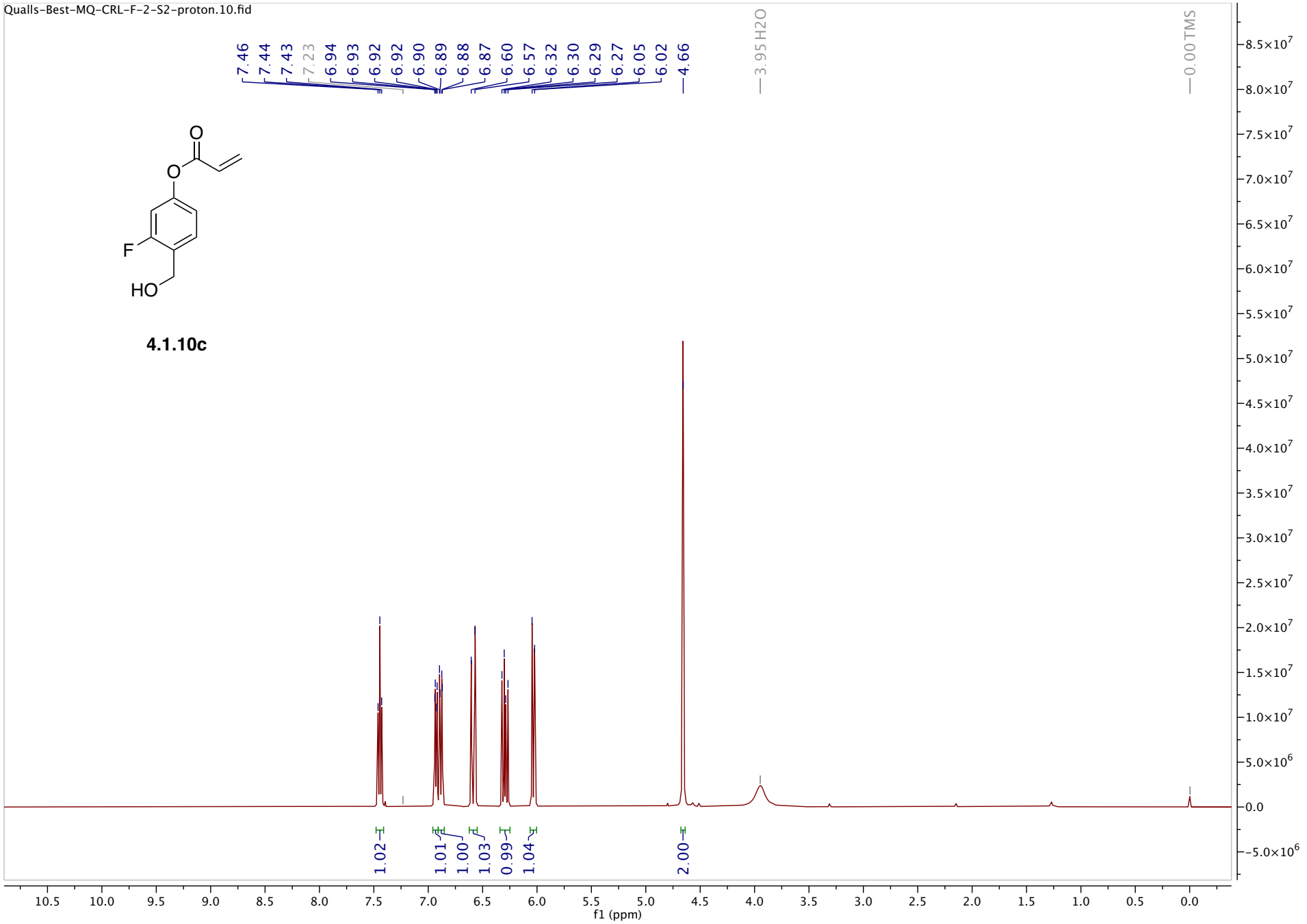
Sample: Pure **4.2b**



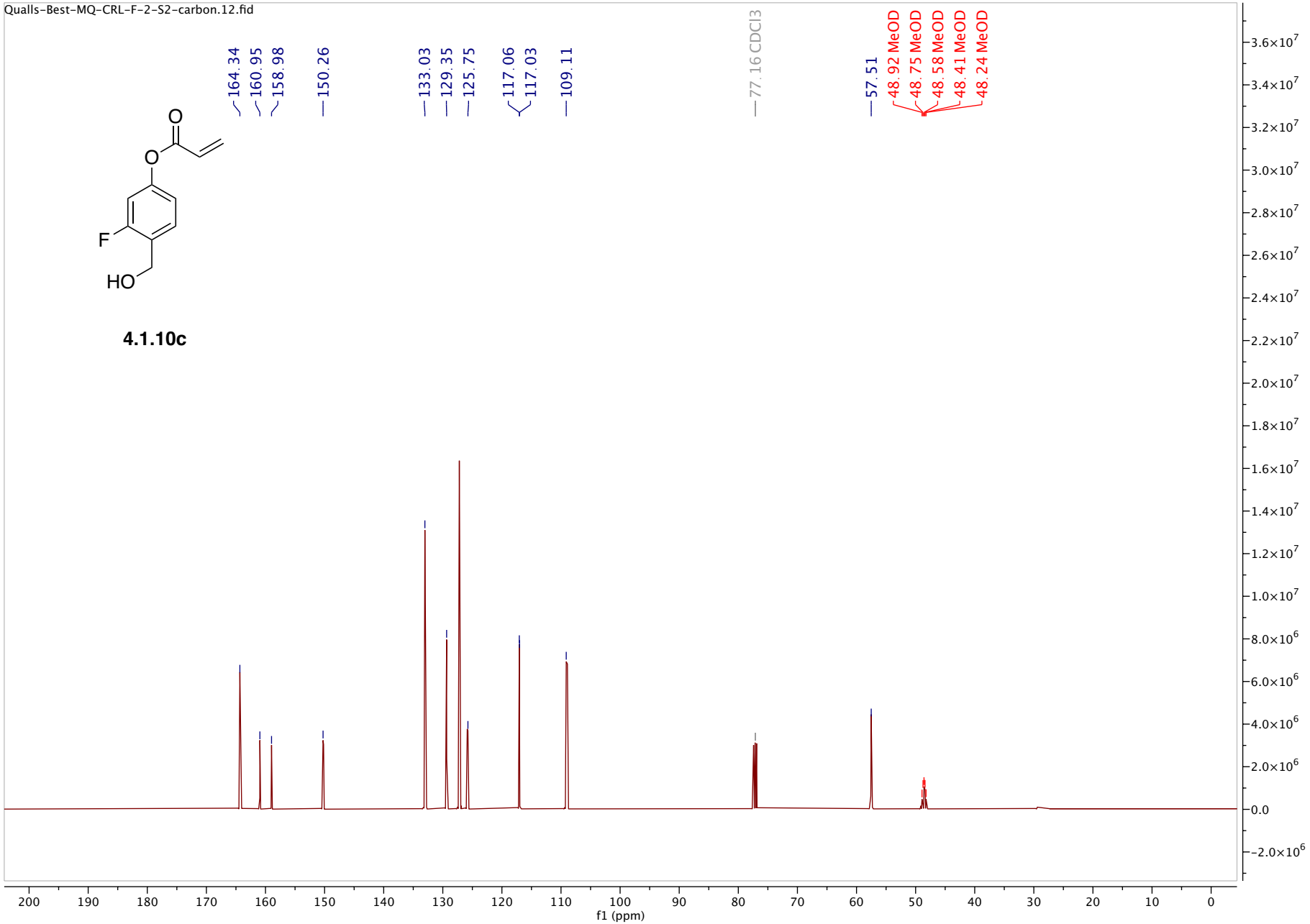
4.2b

MS-ESI $[M+Na]^+$ Calcd for $C_{53}H_{88}NO_{13}P$: 1000.5891
Found: 1000.5898

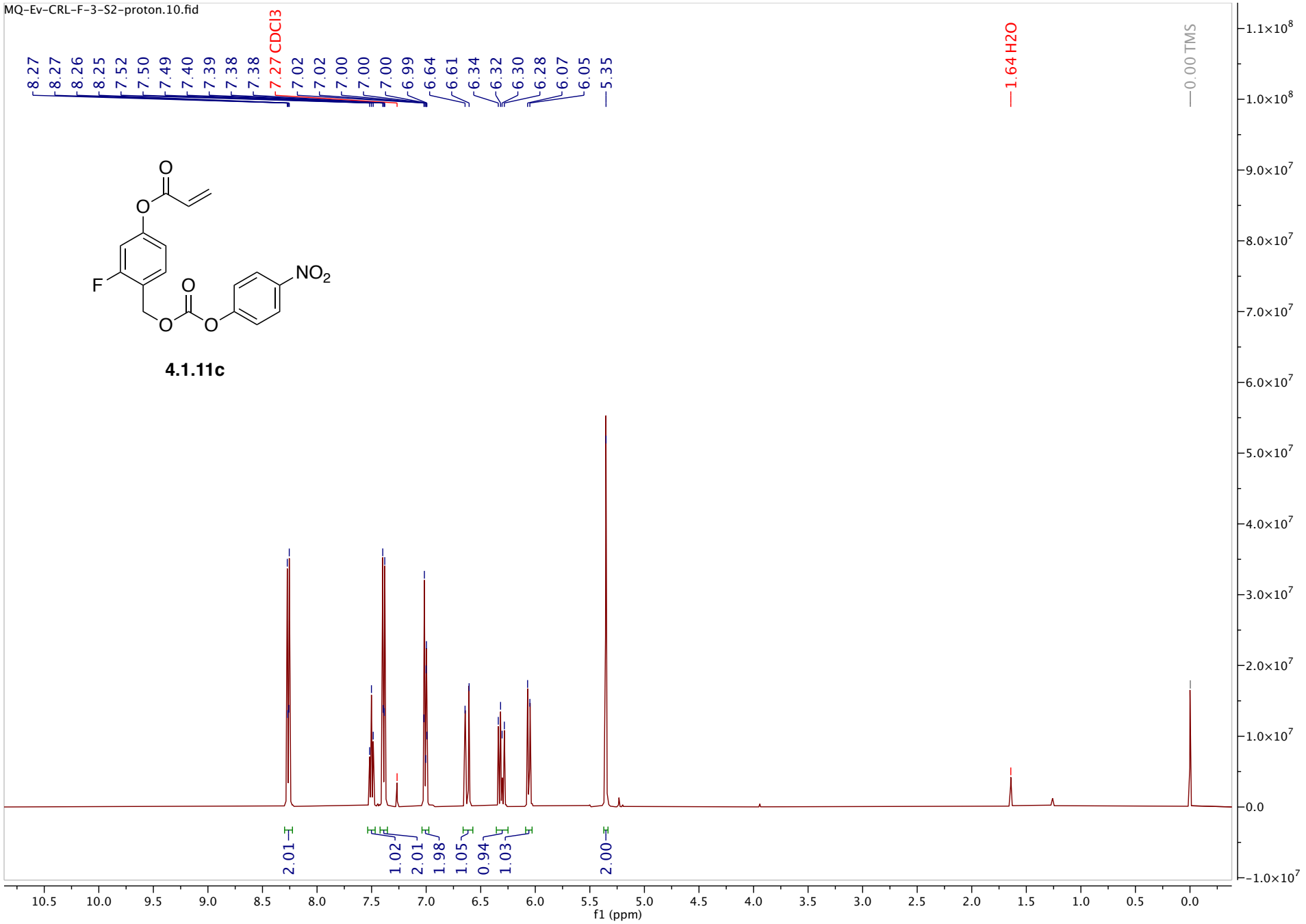
^{1}H NMR


Qualls-Best-MQ-CRL-F-2-S2-proton.10.fid
7.46
7.44
7.43
7.23
6.94
6.93
6.92
6.92
6.90
6.89
6.88
6.87
6.60
6.57
6.32
6.30
6.29
6.27
6.05
6.02
4.66
3.95 H2O
0.00 TMS
O
O
F
HO
4.1.10c
1.02
1.01
1.00
1.03
0.99
1.04
2.00
f1 (ppm)

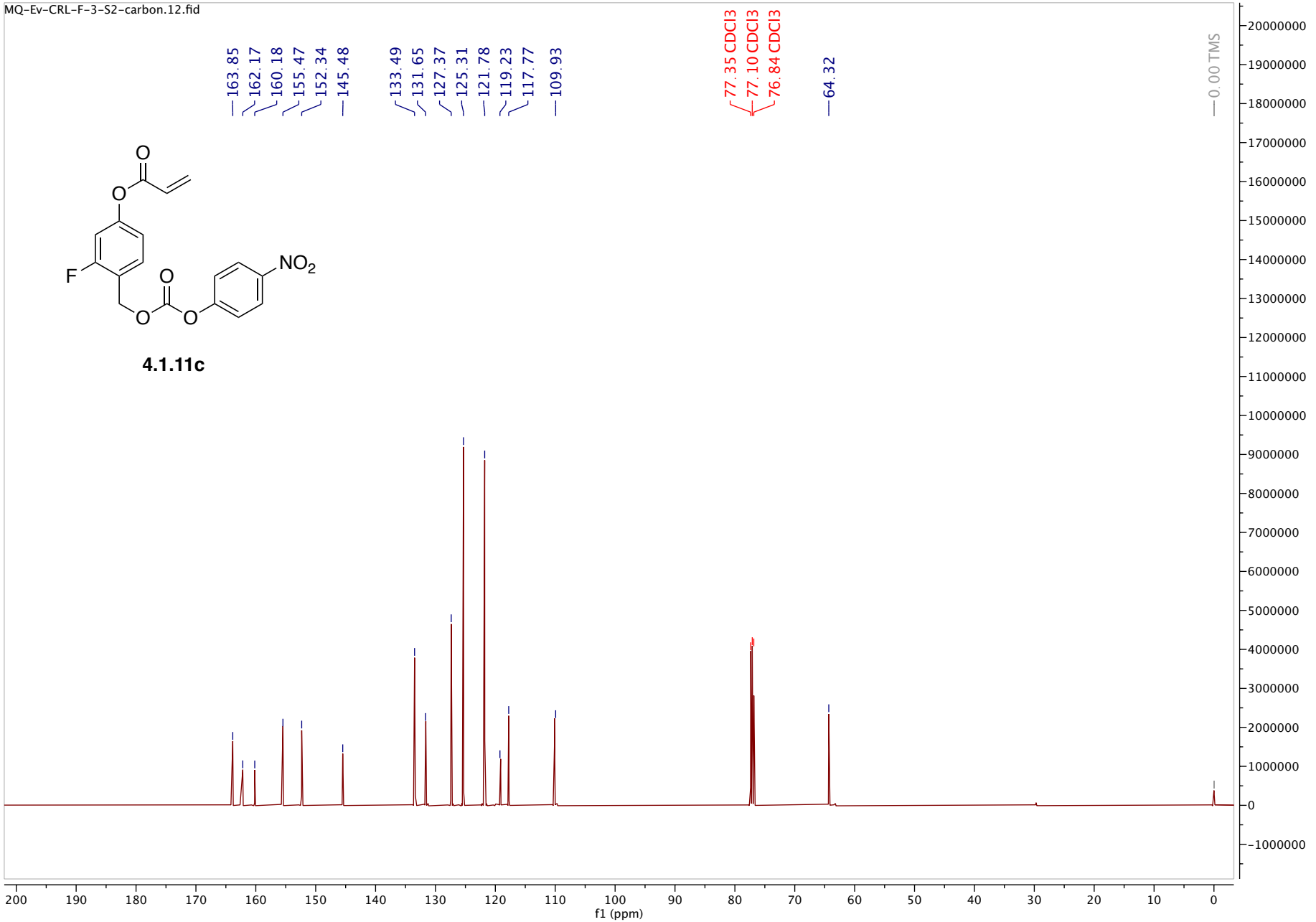
^{13}C NMR


Qualls-Best-MQ-CRL-F-2-S2-carbon.12.fid
164.34
160.95
158.98
150.26
133.03
129.35
125.75
117.06
117.03
109.11
77.16 CDCl3
57.51
48.92 MeOD
48.75 MeOD
48.58 MeOD
48.41 MeOD
48.24 MeOD
O
O
F
HO
4.1.10c
f1 (ppm)

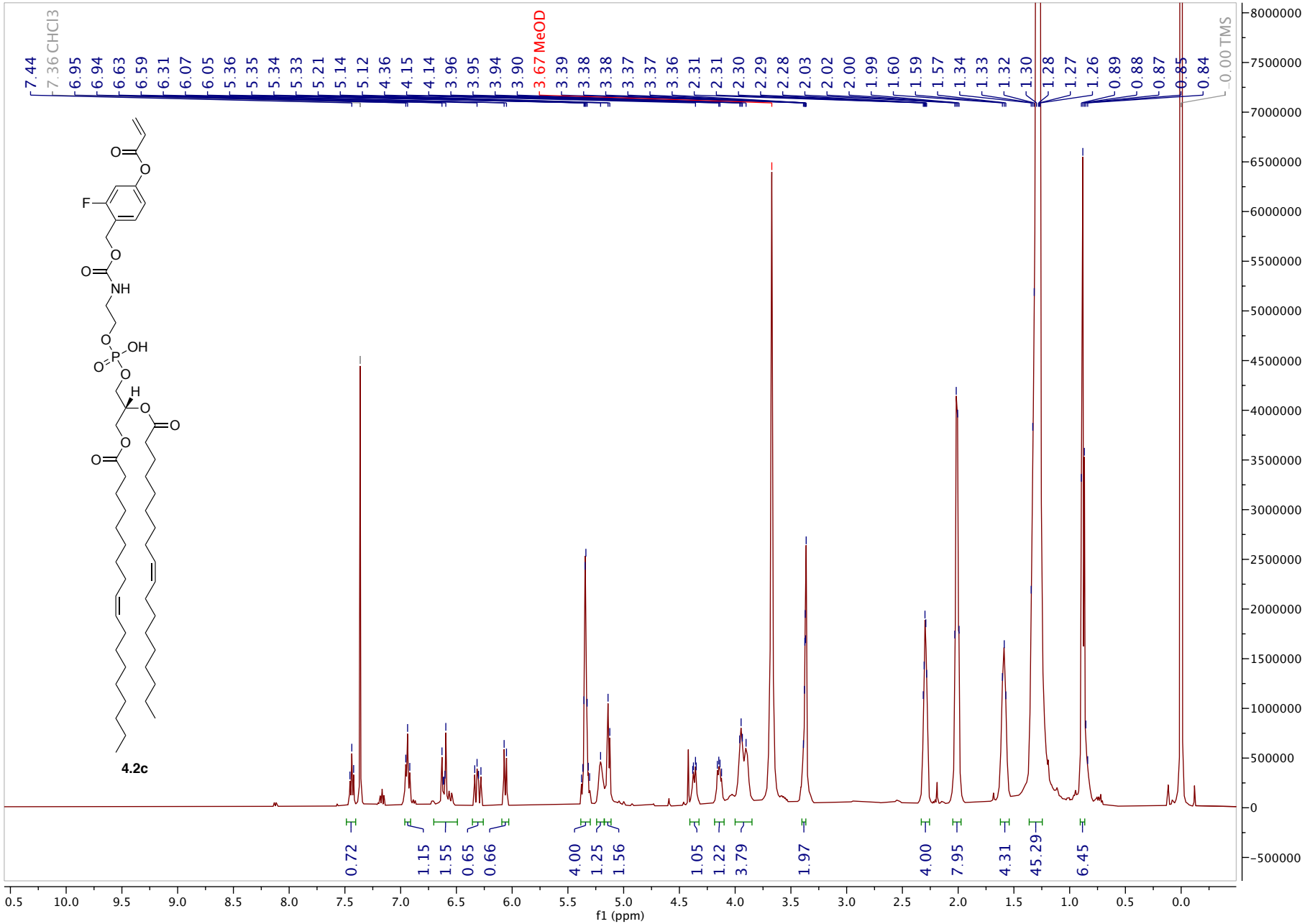
^{1}H NMR


MQ-Ev-CRL-F-3-S2-proton.10.fid
8.27
8.27
8.26
8.25
7.52
7.50
7.49
7.40
7.39
7.38
7.38
7.27 CDCl3
7.02
7.02
7.00
7.00
7.00
6.99
6.64
6.61
6.34
6.32
6.30
6.28
6.07
6.05
5.35
1.64 H2O
0.00 TMS
O
O
F
O
O
O
NO2
4.1.11c
2.01
1.02
2.01
1.98
1.05
0.94
1.03
2.00
f1 (ppm)

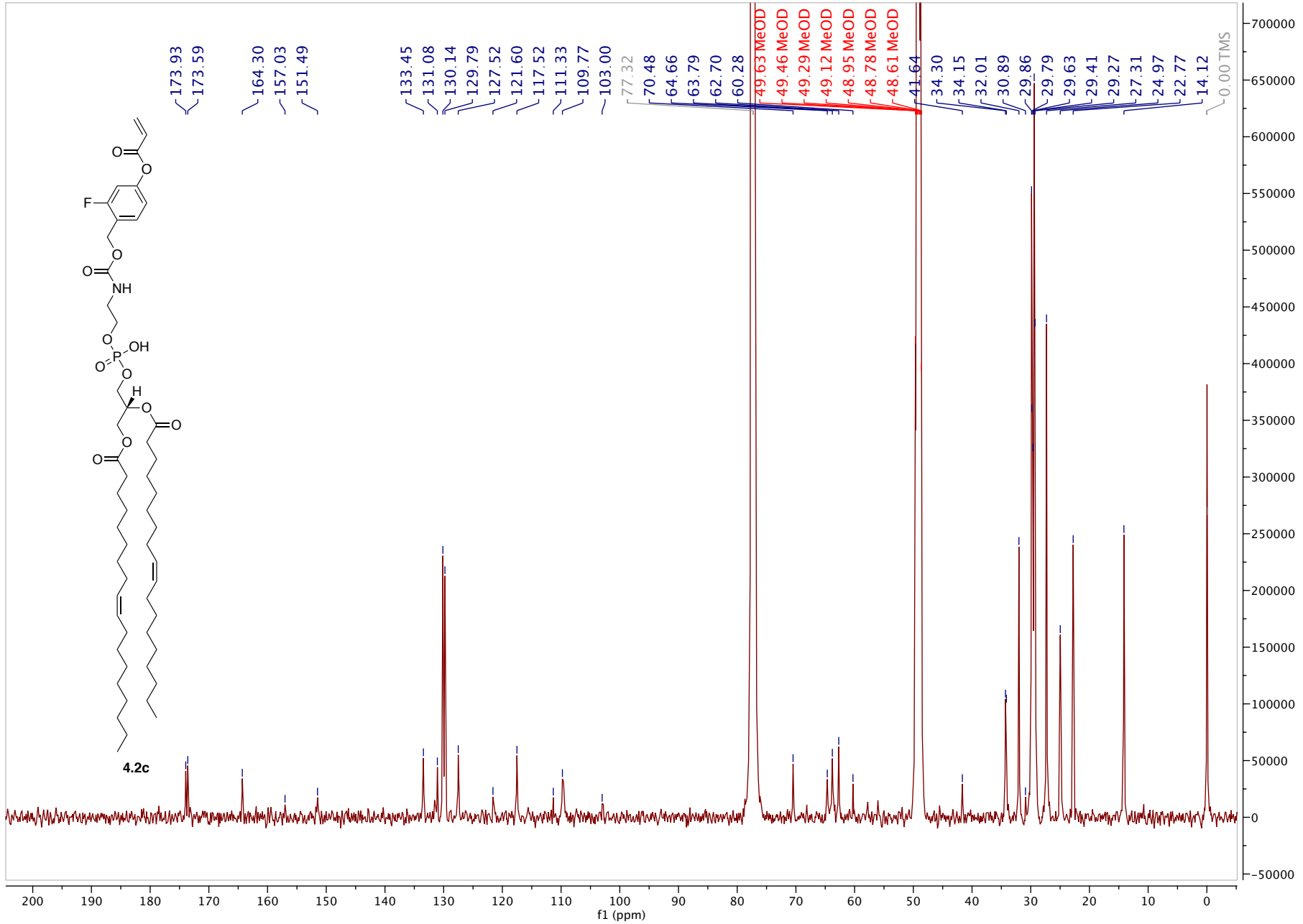
^{13}C NMR


MQ-Ev-CRL-F-3-S2-carbon.12.fid
163.85
162.17
160.18
155.47
152.34
145.48
133.49
131.65
127.37
125.31
121.78
119.23
117.77
109.93
77.35 CDCl3
77.10 CDCl3
76.84 CDCl3
64.32
0.00 TMS
F
O
NO2
4.1.11c
f1 (ppm)

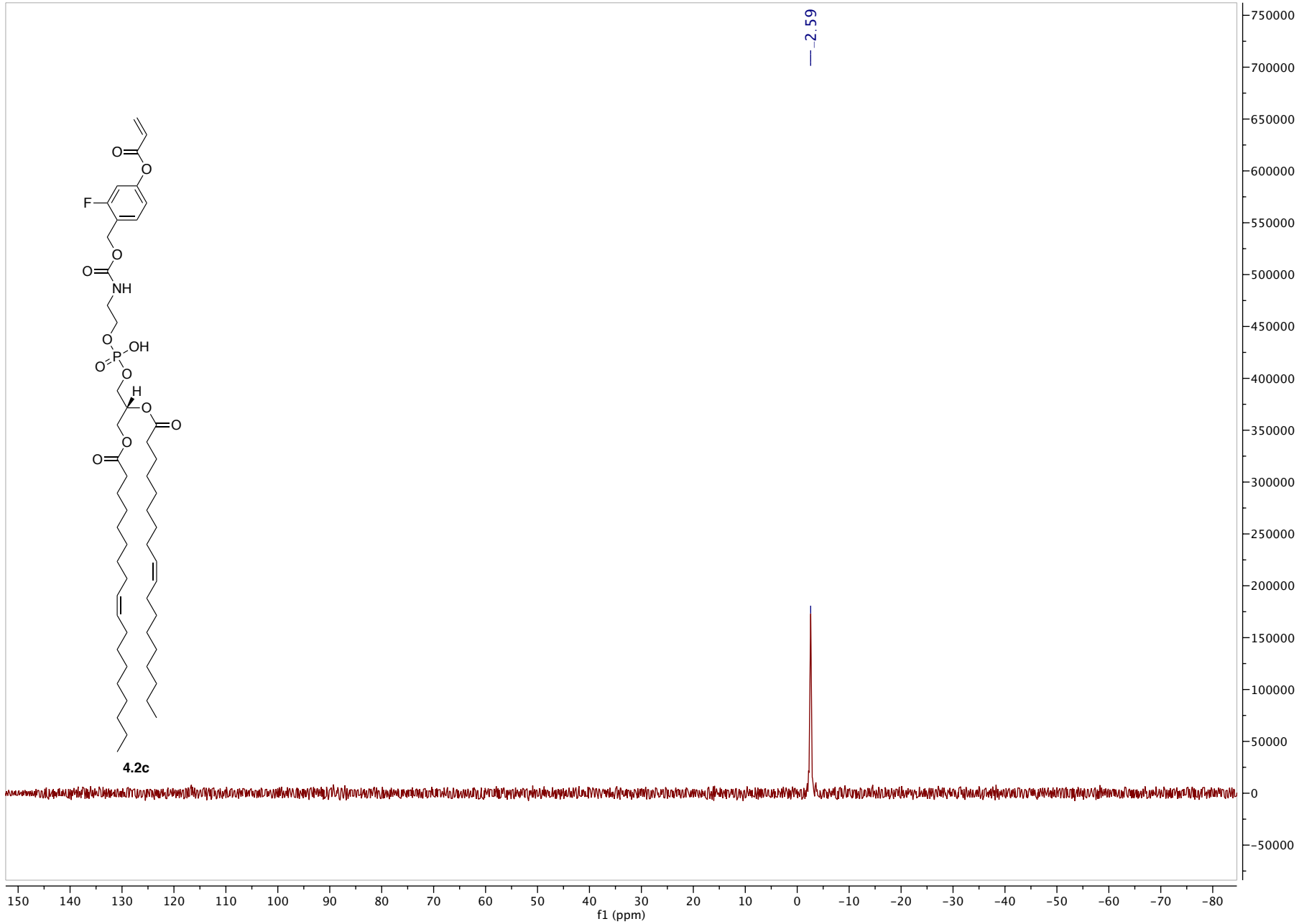
^{1}H NMR


7.44
7.36 CHCl3
6.95
6.94
6.63
6.59
6.31
6.07
6.05
5.36
5.35
5.34
5.33
5.21
5.14
5.12
4.36
4.15
4.14
3.96
3.95
3.94
3.90
3.67 MeOD
3.39
3.38
3.38
3.37
3.37
3.36
2.31
2.31
2.30
2.29
2.28
2.03
2.02
2.00
1.99
1.60
1.59
1.57
1.34
1.33
1.32
1.30
1.28
1.27
1.26
0.89
0.88
0.87
0.85
0.84
0.00 TMS
4.2c
0.72
1.15
1.55
0.65
0.66
4.00
1.25
1.56
1.05
1.22
3.79
1.97
4.00
7.95
4.31
45.29
6.45
f1 (ppm)

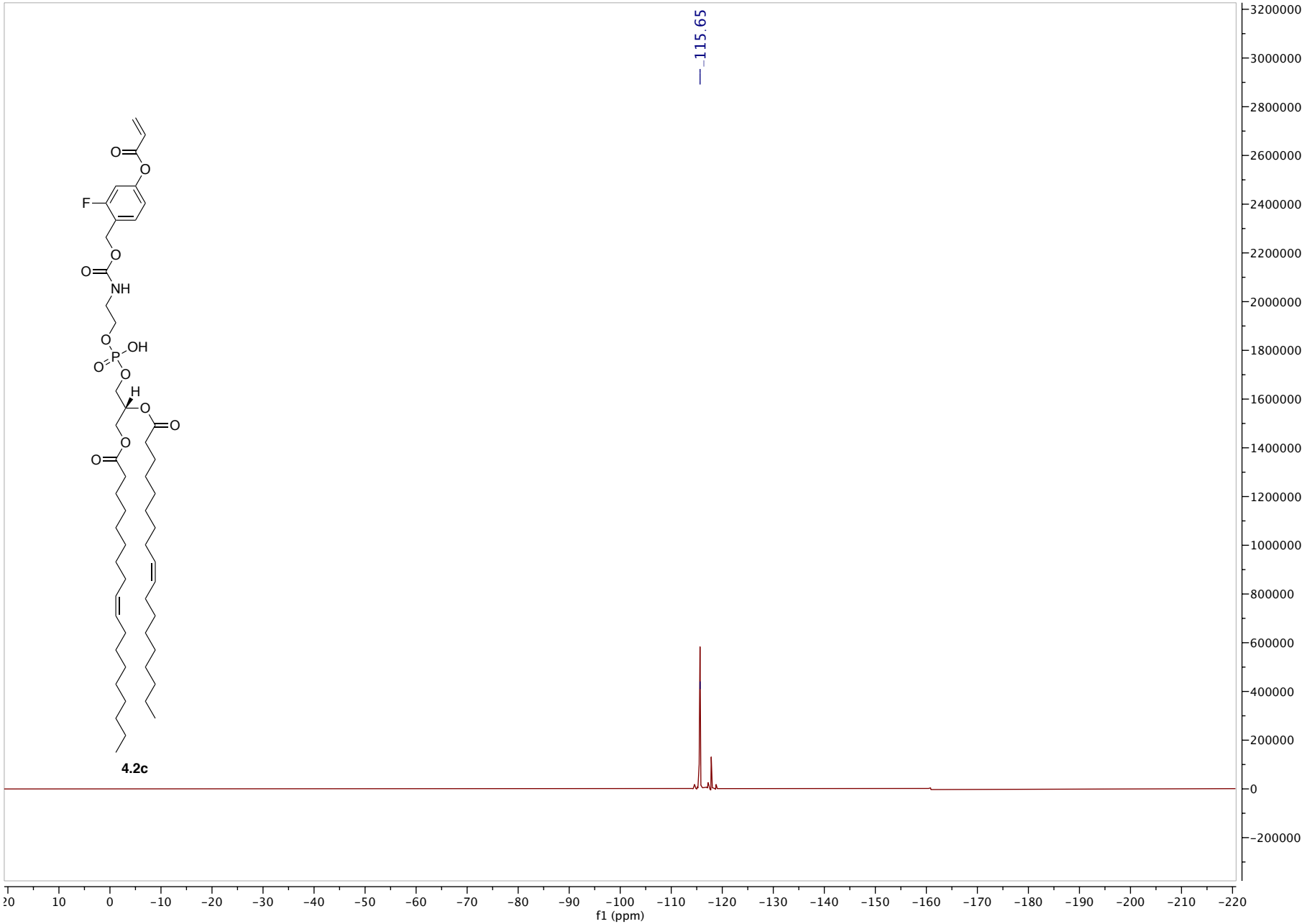
^{13}C NMR


173.93
173.59
164.30
157.03
151.49
133.45
131.08
130.14
129.79
127.52
121.60
117.52
111.33
109.77
103.00
77.32
70.48
64.66
63.79
62.70
60.28
49.63 MeOD
49.46 MeOD
49.29 MeOD
49.12 MeOD
48.95 MeOD
48.78 MeOD
48.61 MeOD
41.64
34.30
34.15
32.01
30.89
29.86
29.79
29.63
29.41
29.27
27.31
24.97
22.77
14.12
0.00 TMS
4.2c
f1 (ppm)

^{31}P NMR

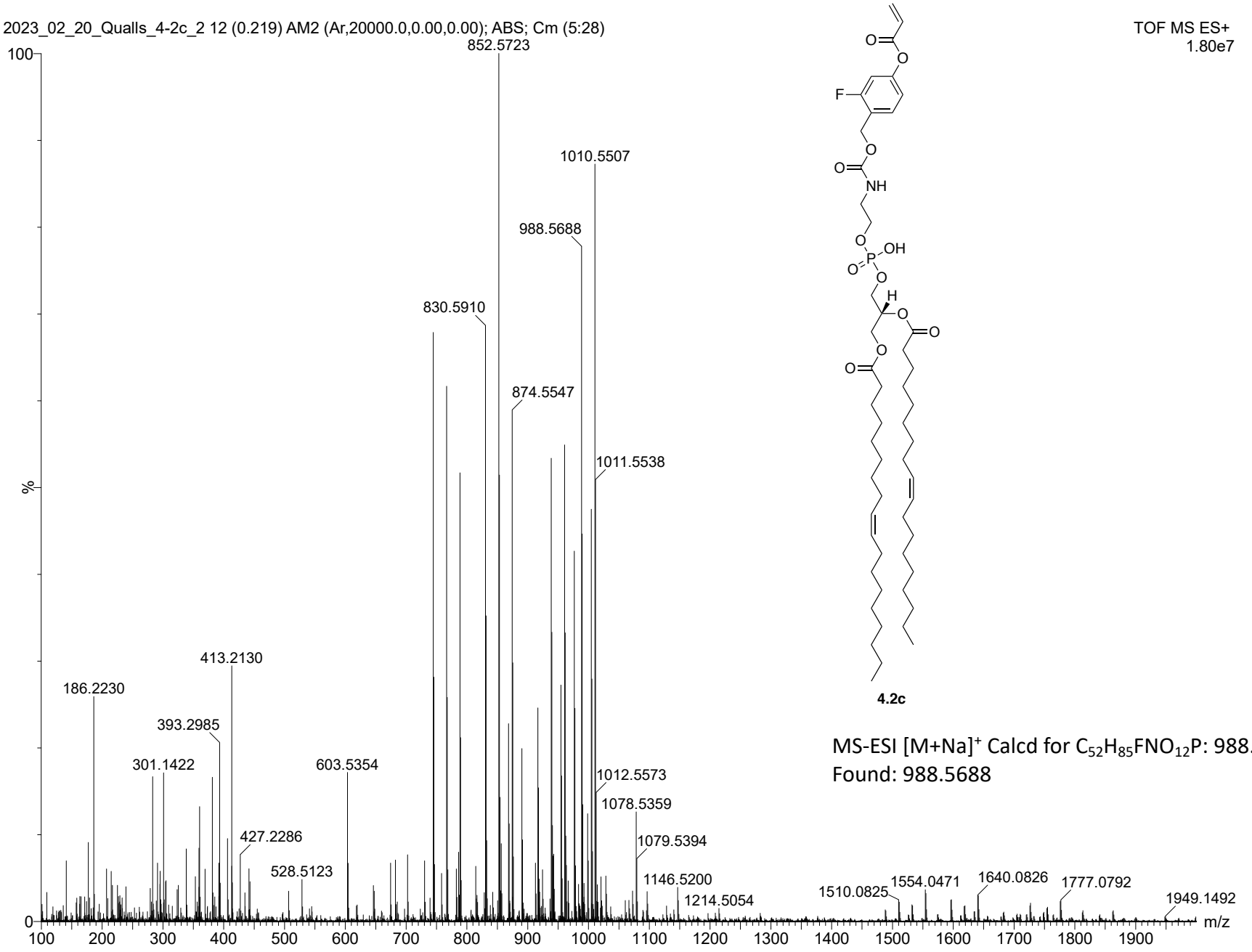

-2.59
4.2c
750000
700000
650000
600000
550000
500000
450000
400000
350000
300000
250000
200000
150000
100000
50000
0
-50000
150 140 130 120 110 100 90 80 70 60 50 40 30 20 10 0 -10 -20 -30 -40 -50 -60 -70 -80
f1 (ppm)

^{19}F NMR



ESI-MS

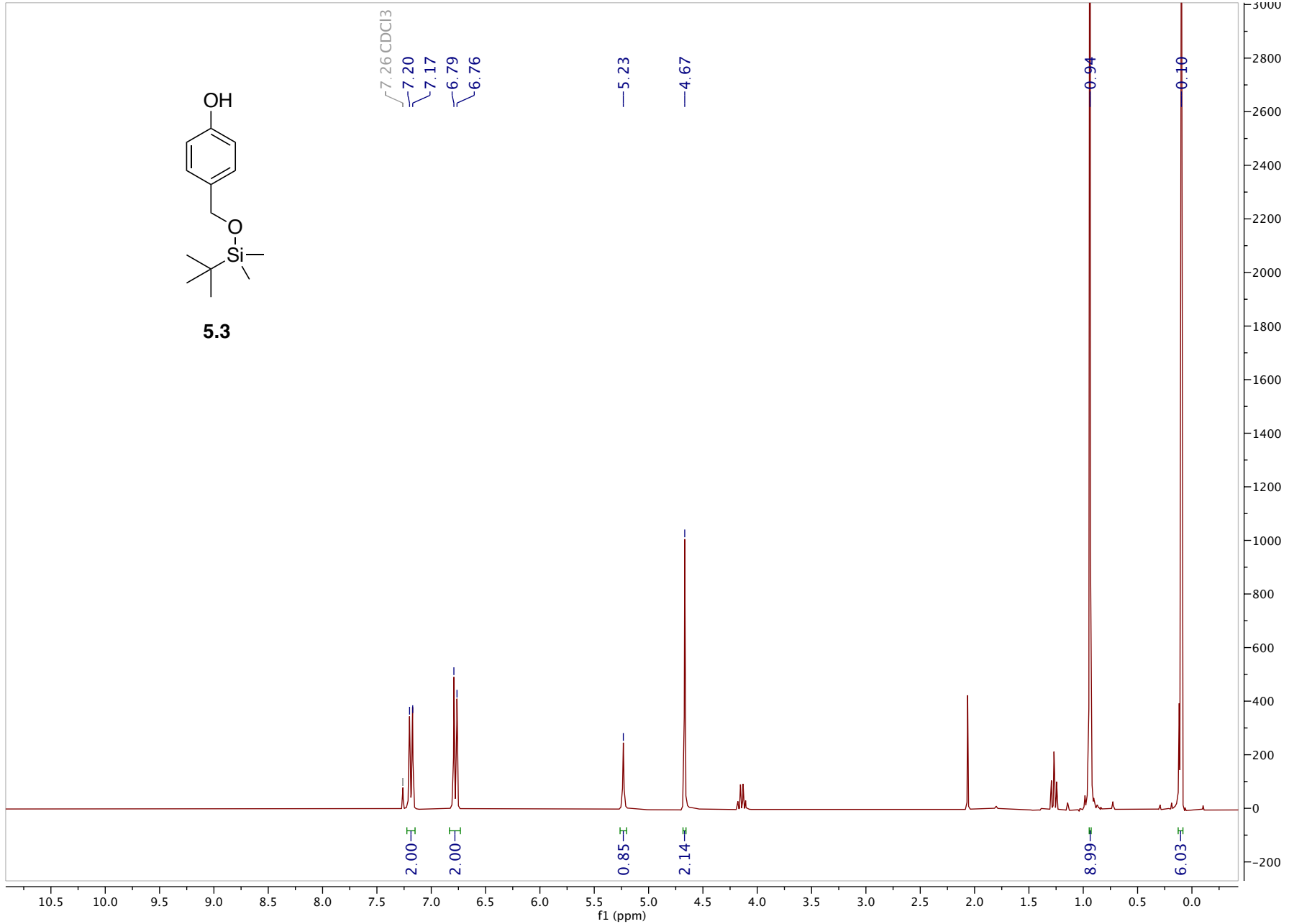
Sample: Pure **4.2c**



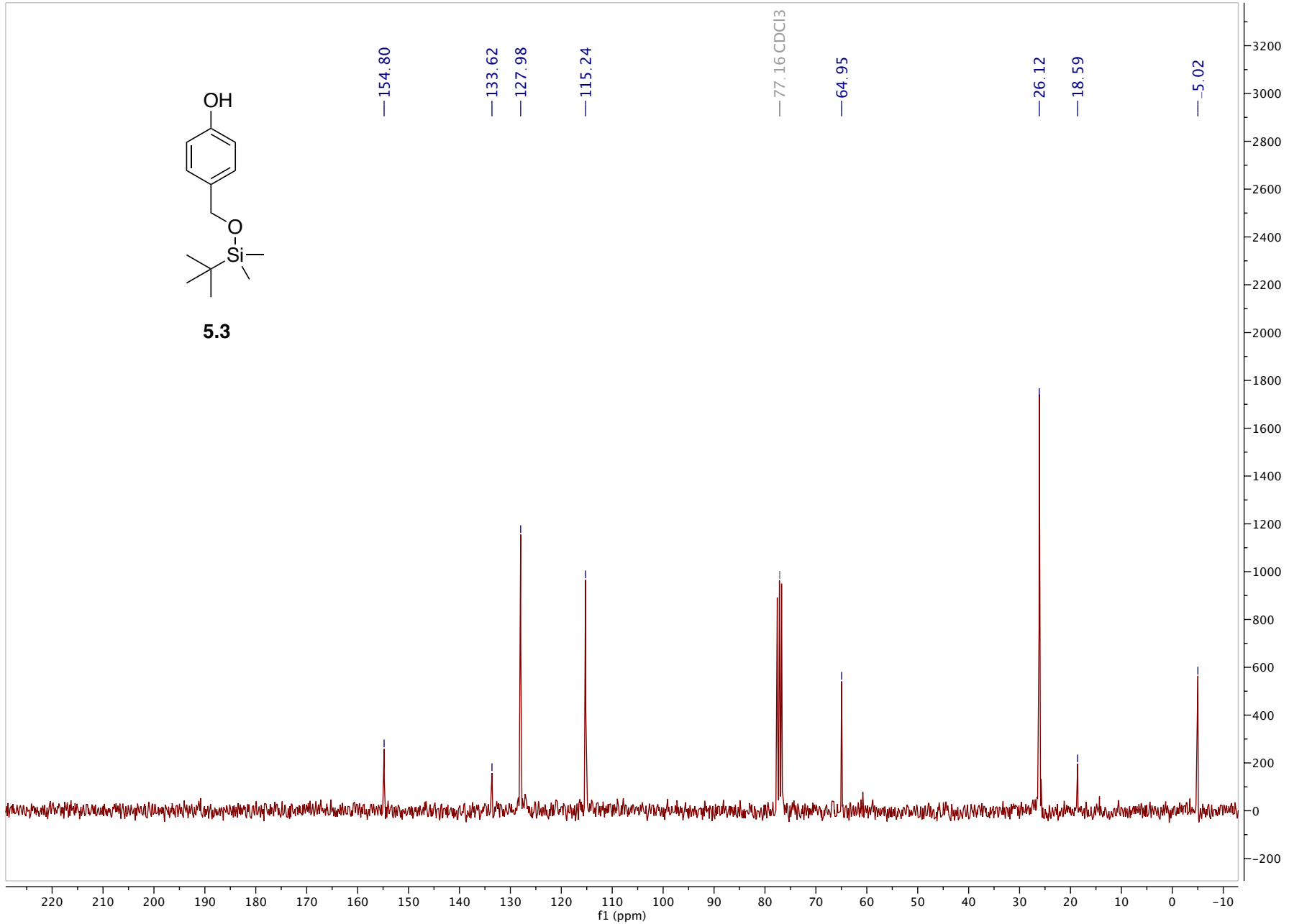
4.2c

MS-ESI $[M+Na]^+$ Calcd for $C_{52}H_{85}FNO_{12}P$: 988.5691
Found: 988.5688

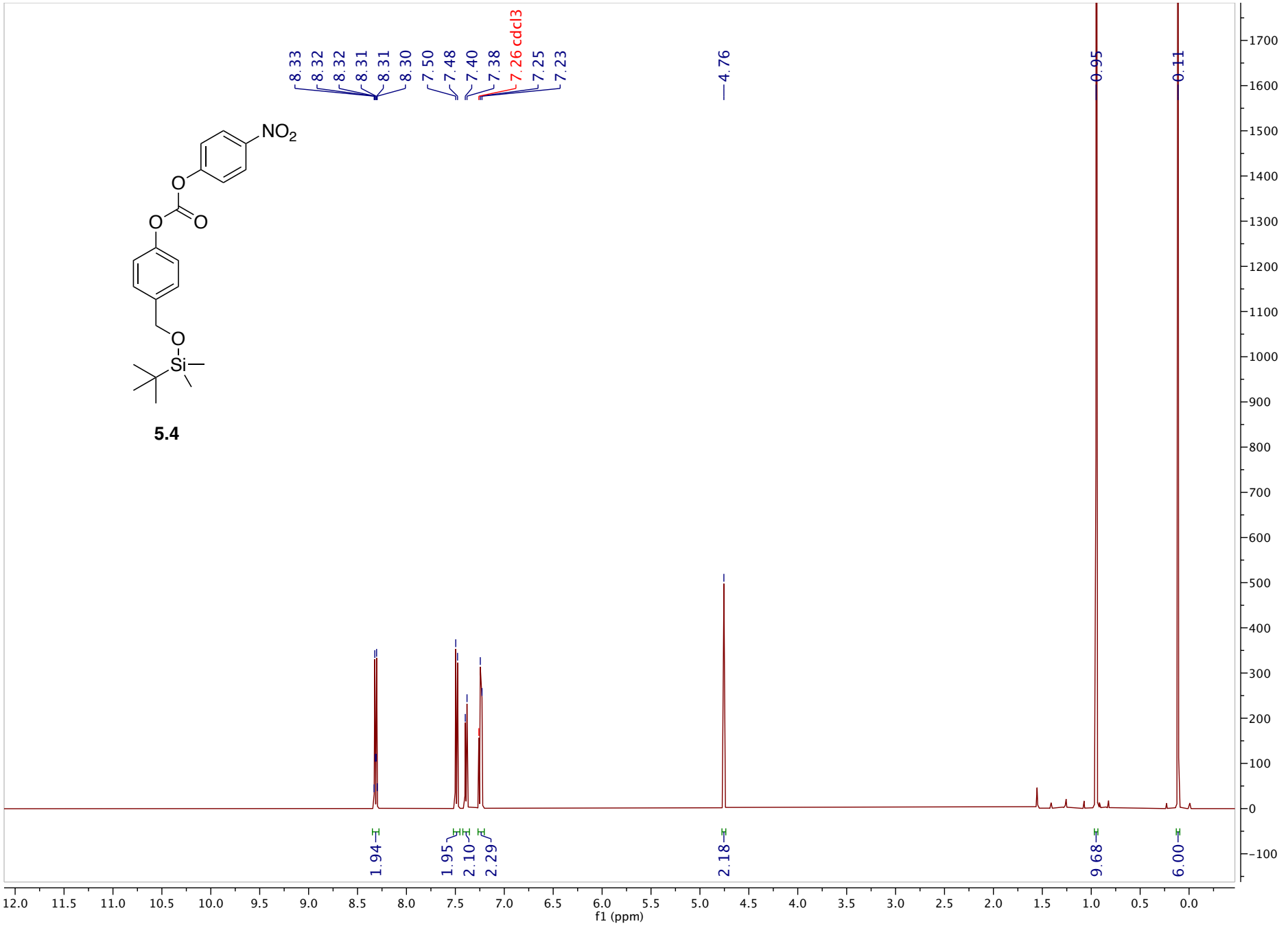
^{1}H NMR


OH
O
Si
5.3
7.26 CDCl3
7.20
7.17
6.79
6.76
5.23
4.67
0.94
0.10
2.00
2.00
0.85
2.14
8.99
6.03
f1 (ppm)

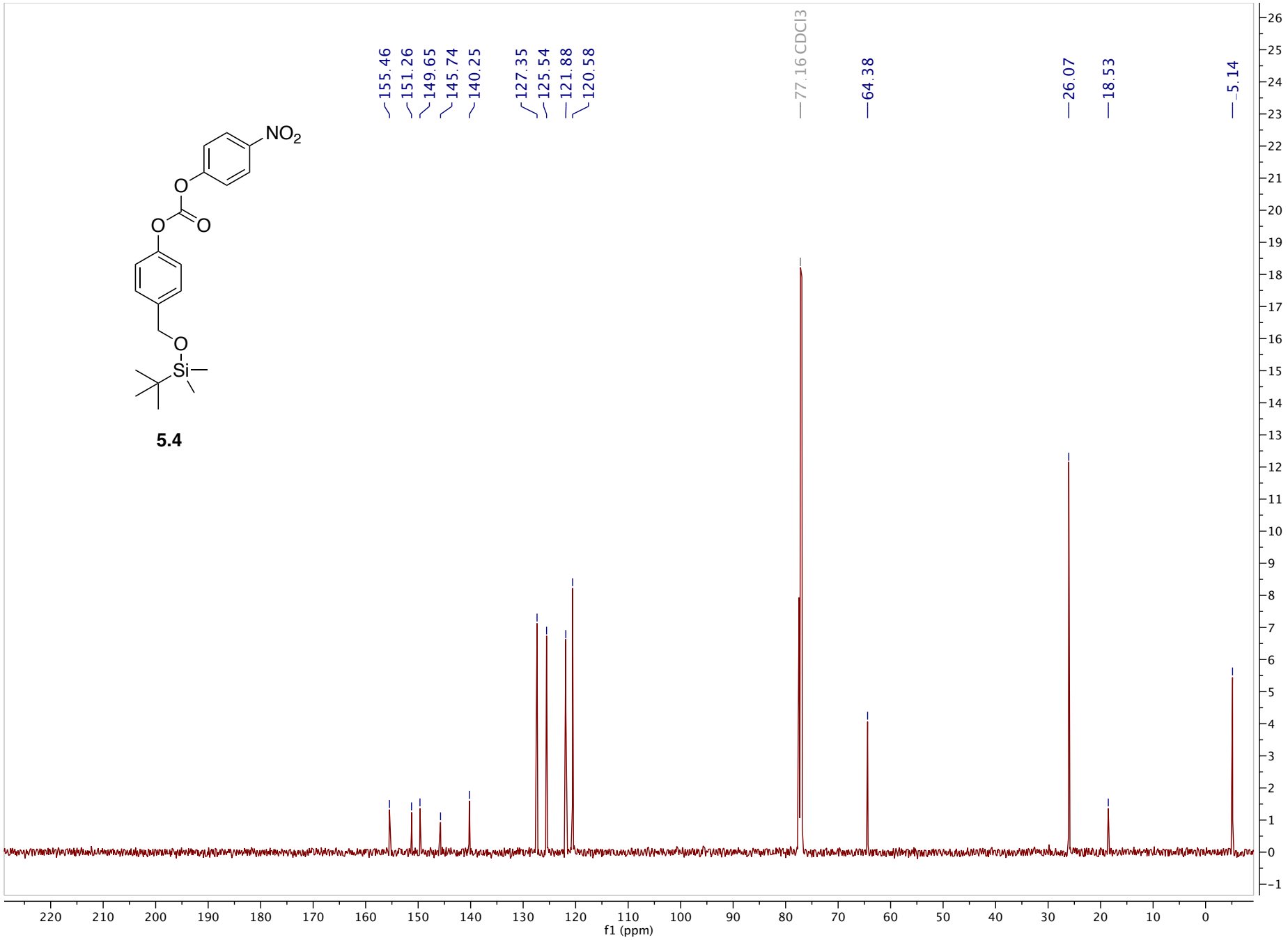
^{13}C NMR


OH
O
Si
5.3
154.80
133.62
127.98
115.24
77.16 CDCl3
64.95
26.12
18.59
5.02
f1 (ppm)

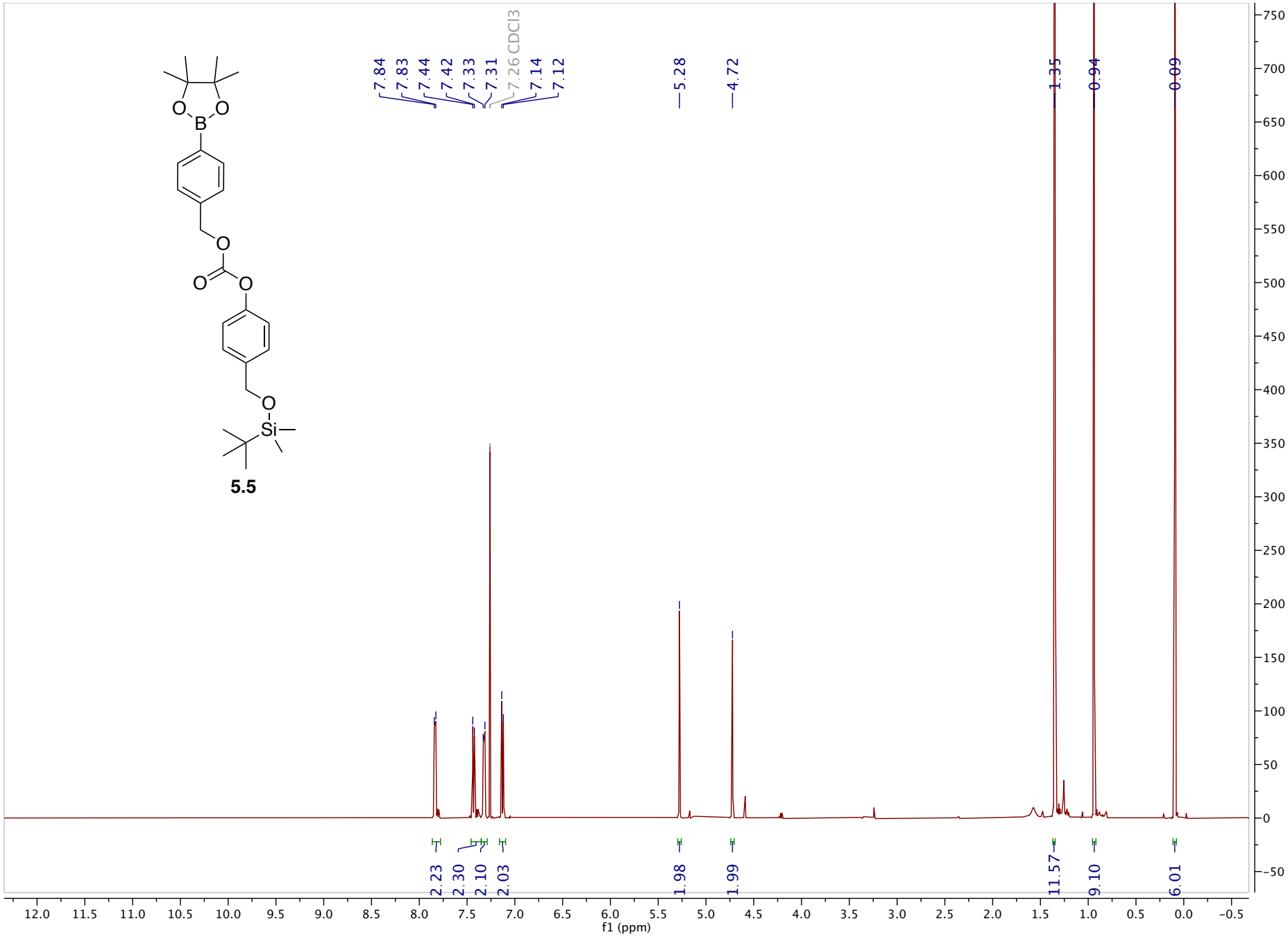
^{1}H NMR


8.33
8.32
8.32
8.31
8.31
8.30
7.50
7.48
7.40
7.38
7.26 cdcl3
7.25
7.23
4.76
0.95
0.11
NO2
O
O
O
O
Si
5.4
1.94
1.95
2.10
2.29
2.18
9.68
6.00
f1 (ppm)

^{13}C NMR

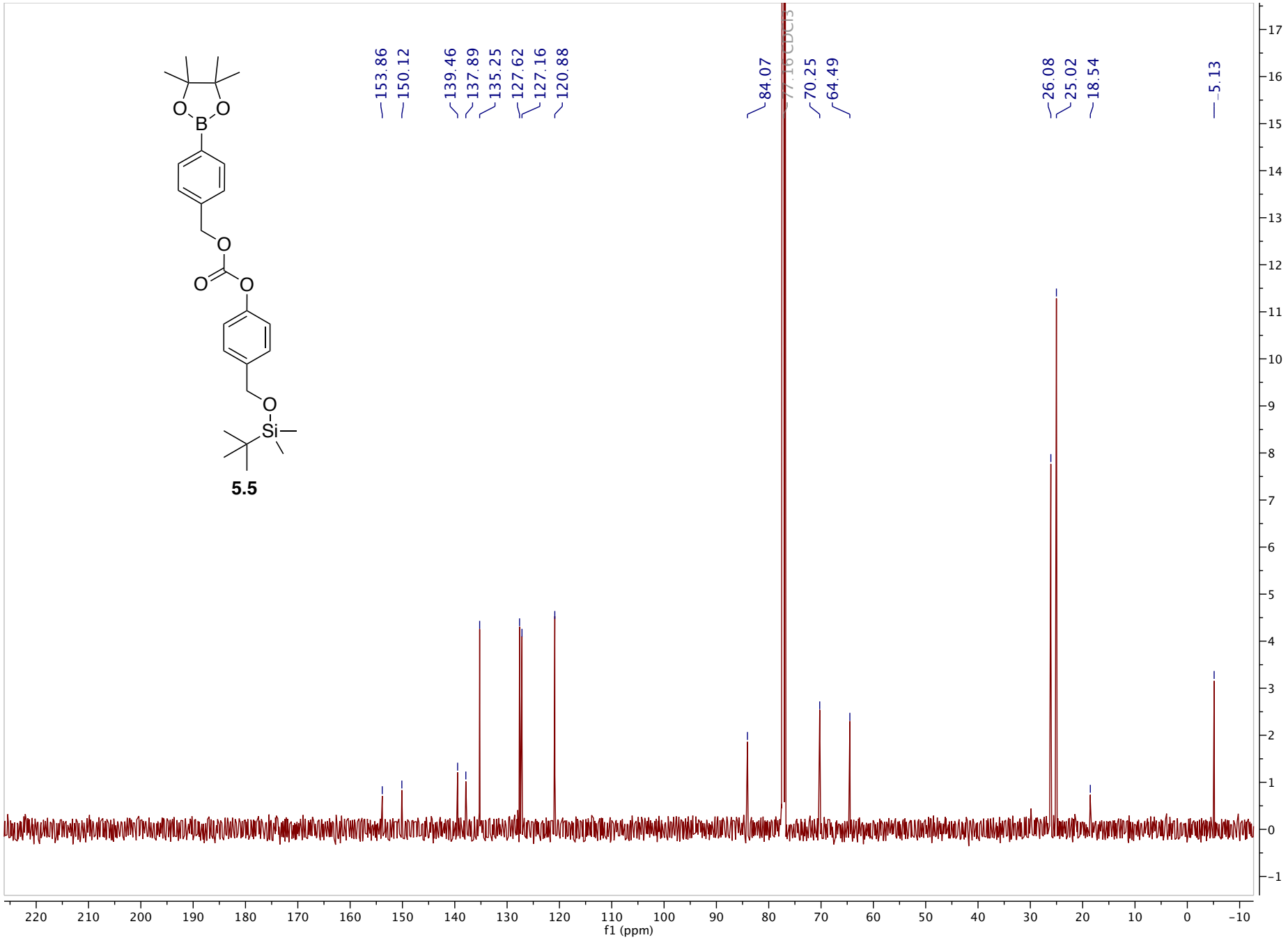

155.46
151.26
149.65
145.74
140.25
127.35
125.54
121.88
120.58
77.16 CDCl3
64.38
26.07
18.53
5.14
NO2
O
O
O
O
Si
5.4
f1 (ppm)

^{1}H NMR


7.84
7.83
7.44
7.42
7.33
7.31
7.26 CDCl3
7.14
7.12
5.28
4.72
1.35
0.94
0.09
2.23
2.30
2.10
2.03
1.98
1.99
11.57
9.10
6.01
f1 (ppm)

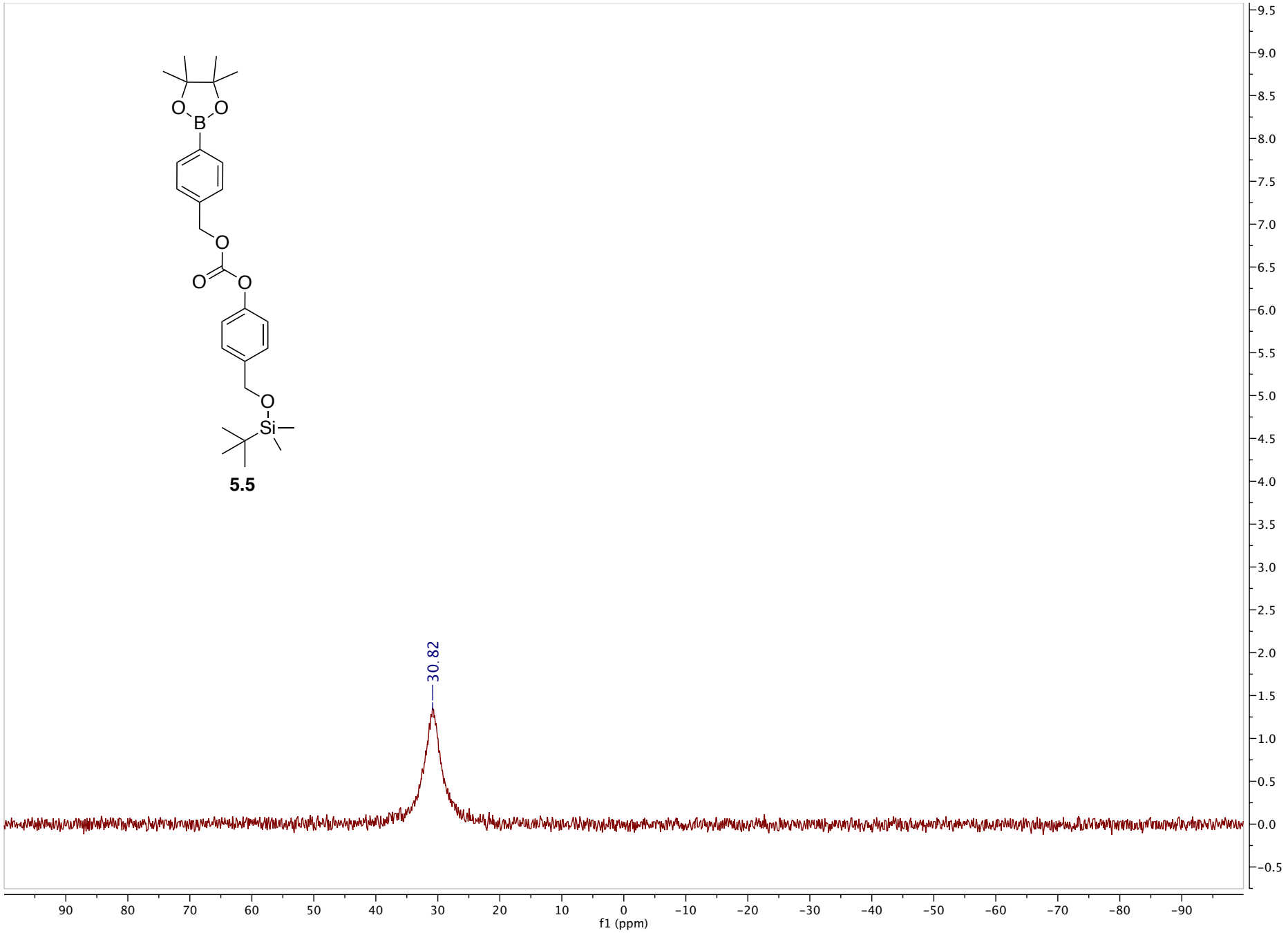
5.5

^{13}C NMR

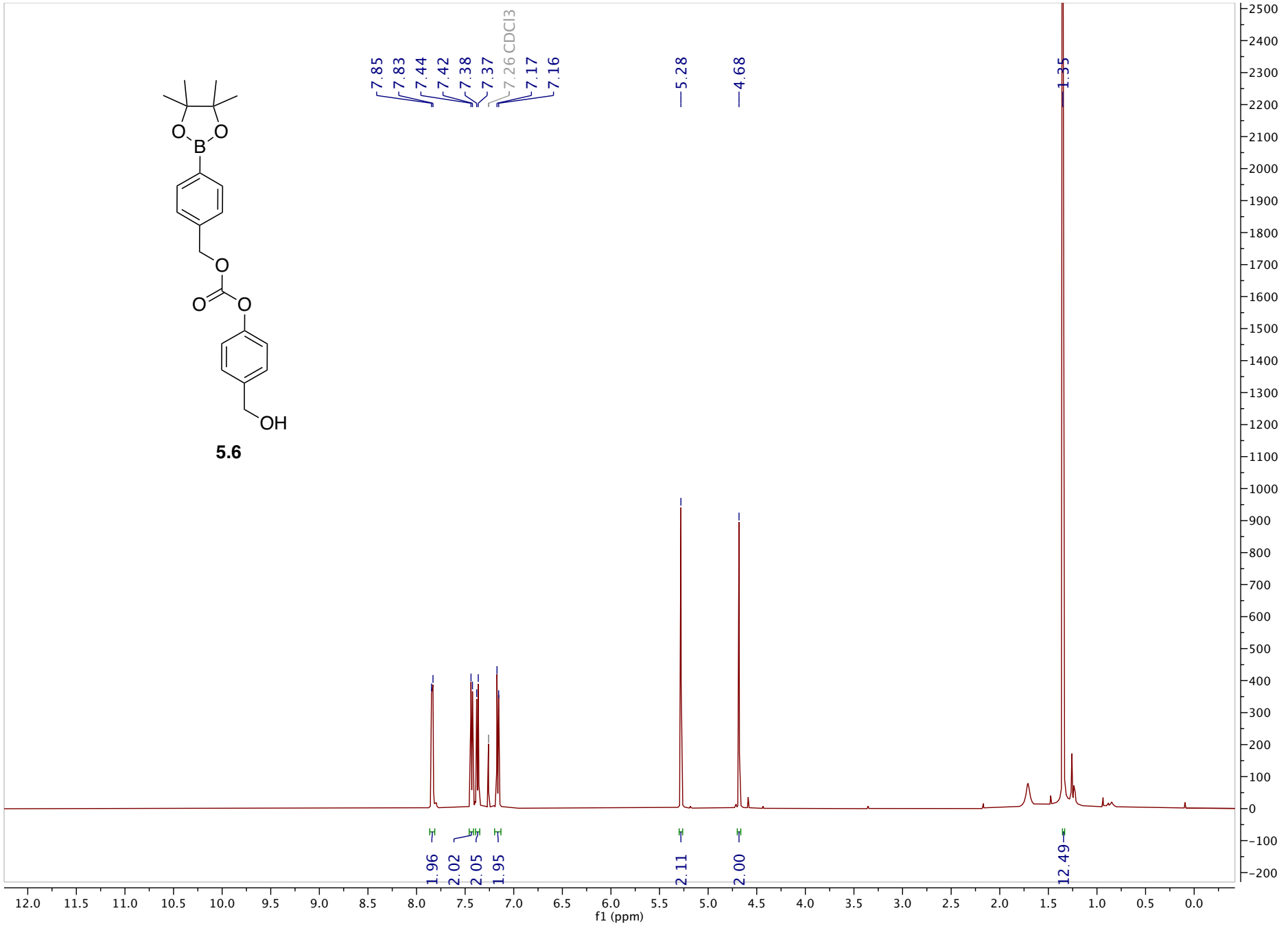

153.86
150.12
139.46
137.89
135.25
127.62
127.16
120.88
84.07
77.16 CDCl3
70.25
64.49
26.08
25.02
18.54
5.13
f1 (ppm)

5.5

^{11}B NMR

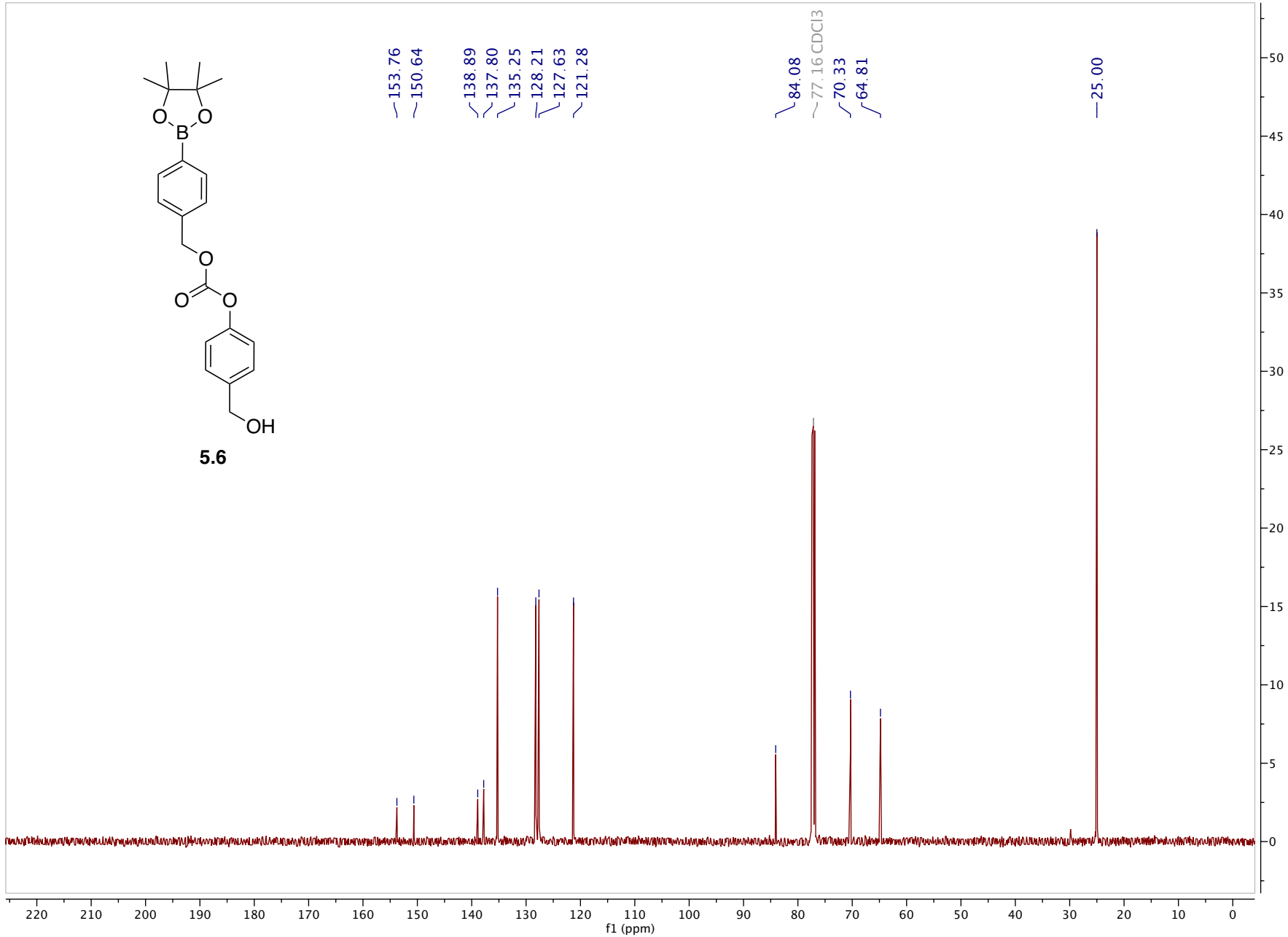

O
B
O
O
O
O
O
Si
5.5
30.82
9.5
9.0
8.5
8.0
7.5
7.0
6.5
6.0
5.5
5.0
4.5
4.0
3.5
3.0
2.5
2.0
1.5
1.0
0.5
0.0
-0.5
90
80
70
60
50
40
30
20
10
0
-10
-20
-30
-40
-50
-60
-70
-80
-90
f1 (ppm)

^{1}H NMR

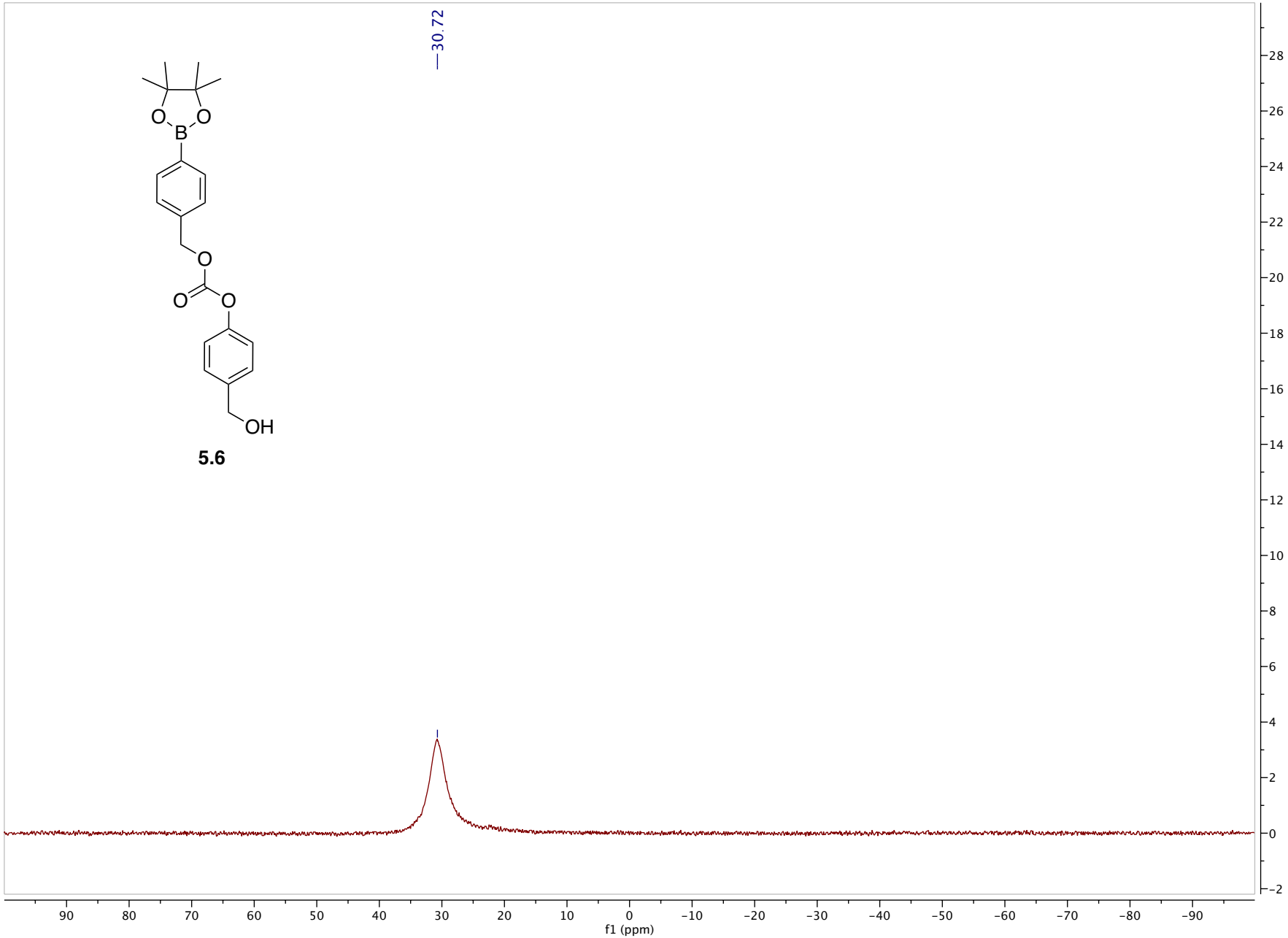

7.85
7.83
7.44
7.42
7.38
7.37
7.26 CDCl3
7.17
7.16
5.28
4.68
1.35
1.96
2.02
2.05
1.95
2.11
2.00
12.49
f1 (ppm)

5.6

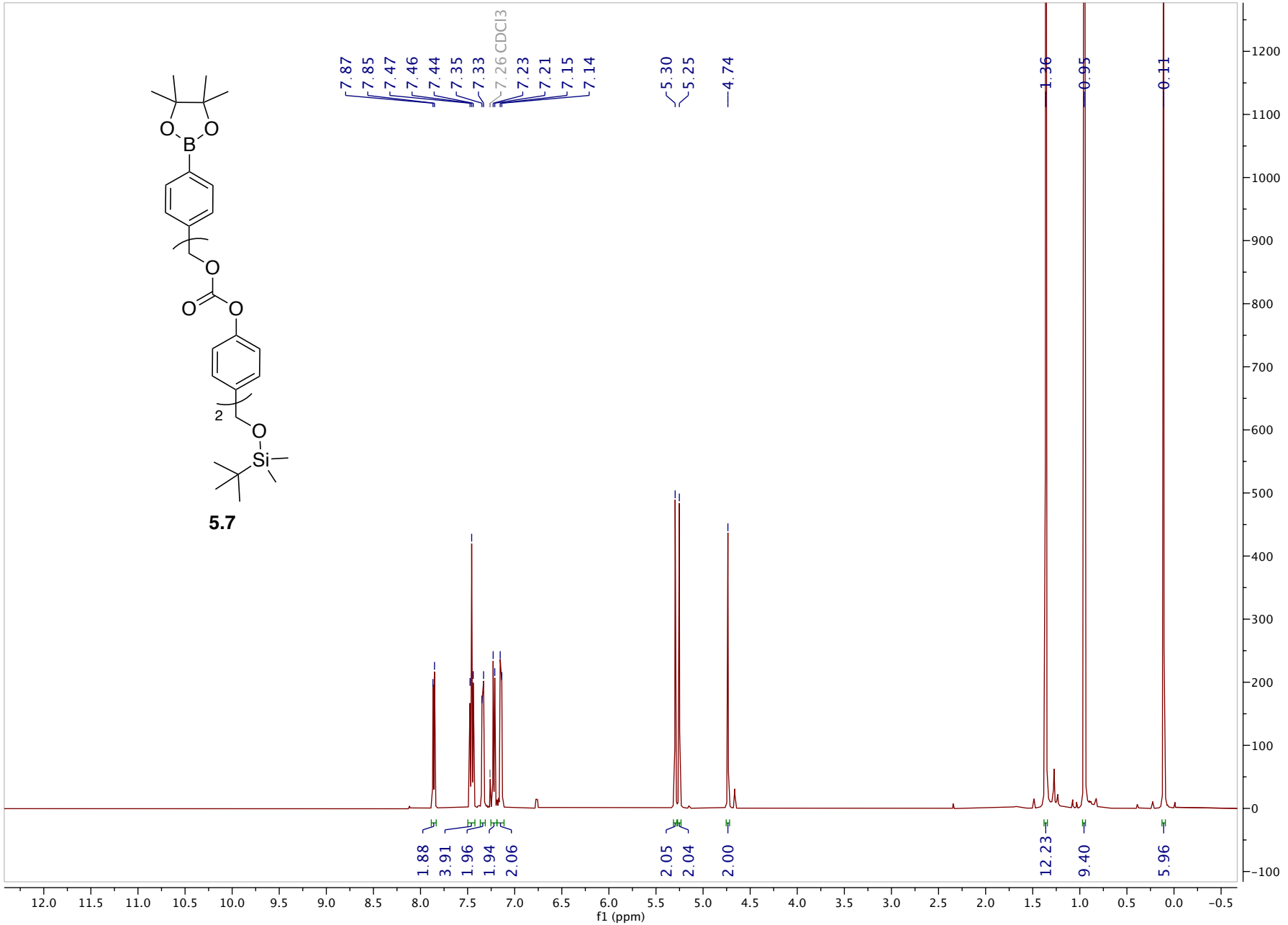
^{13}C NMR


153.76
150.64
138.89
137.80
135.25
128.21
127.63
121.28
84.08
77.16 CDCl3
70.33
64.81
25.00
O
B
O
O
O
O
OH
5.6
f1 (ppm)

^{11}B NMR

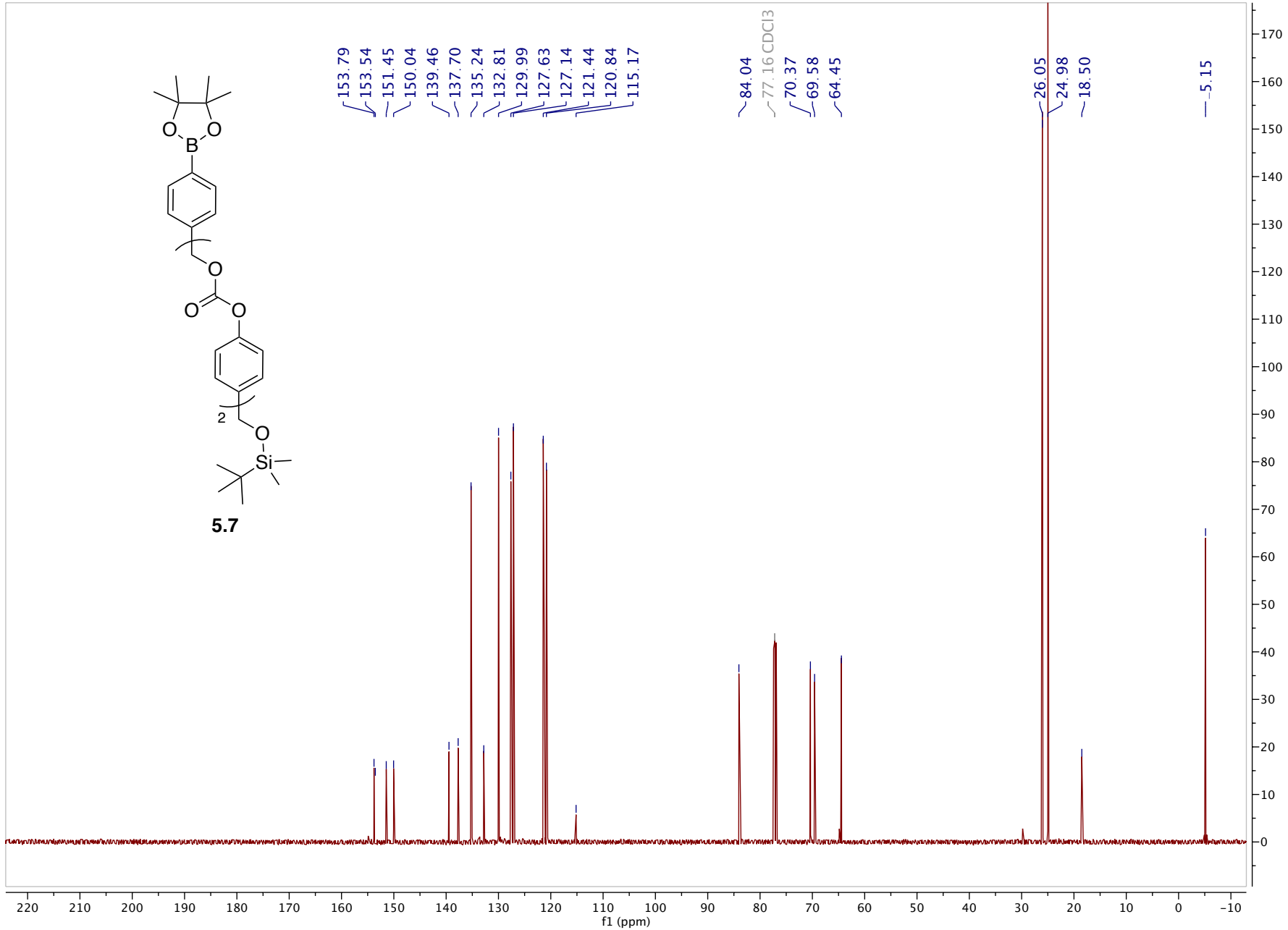

30.72
O
B
O
O
O
O
OH
5.6
28
26
24
22
20
18
16
14
12
10
8
6
4
2
0
−2
90
80
70
60
50
40
30
20
10
0
−10
−20
−30
−40
−50
−60
−70
−80
−90
f1 (ppm)

^{1}H NMR

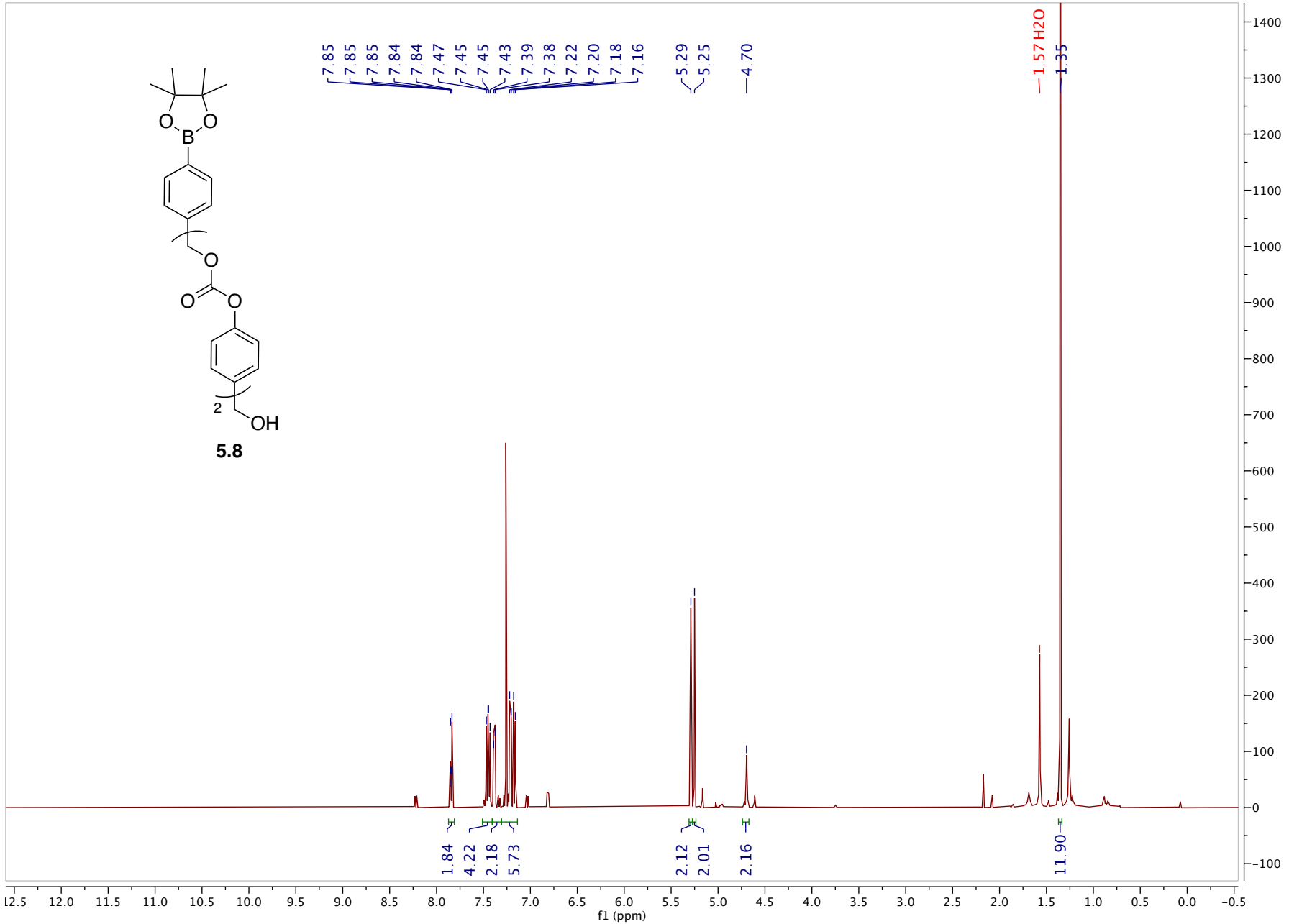

7.87
7.85
7.47
7.46
7.44
7.35
7.33
7.26 CDCl3
7.23
7.21
7.15
7.14
5.30
5.25
4.74
1.36
0.95
0.11
1.88
3.91
1.96
1.94
2.06
2.05
2.04
2.00
12.23
9.40
5.96
f1 (ppm)

5.7

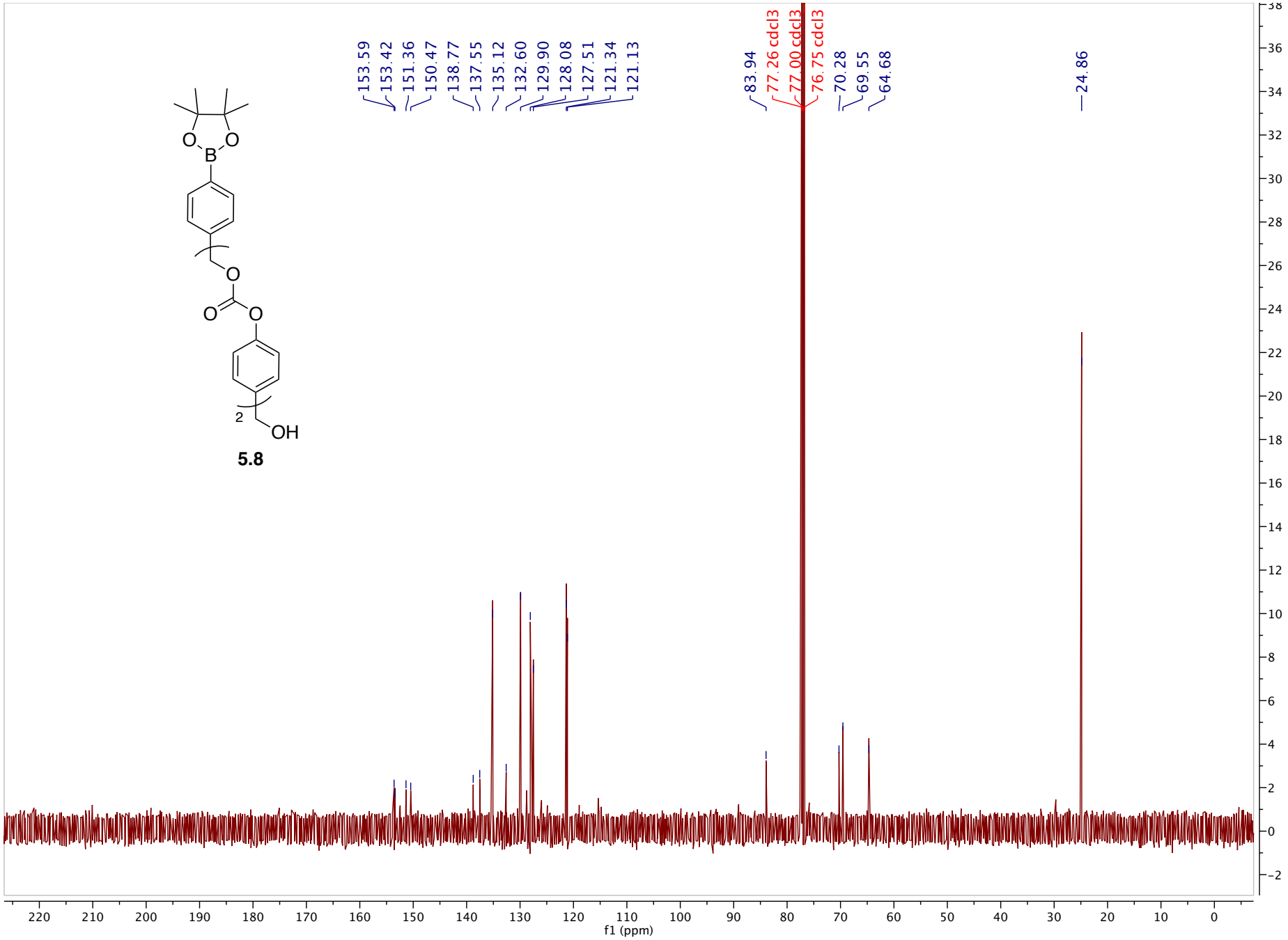
^{13}C NMR


153.79
153.54
151.45
150.04
139.46
137.70
135.24
132.81
129.99
127.63
127.14
121.44
120.84
115.17
84.04
77.16 CDCl3
70.37
69.58
64.45
26.05
24.98
18.50
5.15
5.7
f1 (ppm)

^{1}H NMR

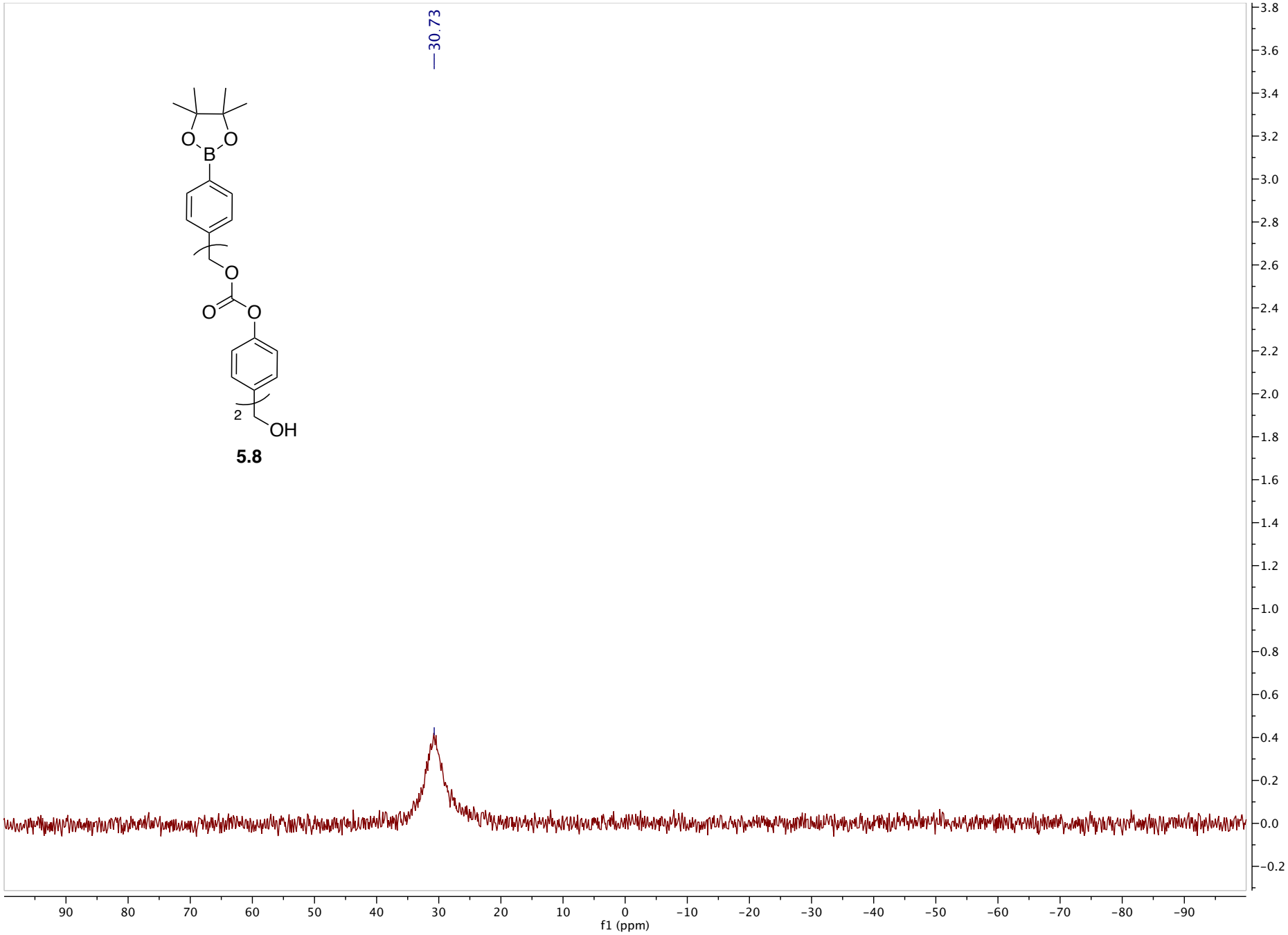

7.85
7.85
7.85
7.84
7.84
7.47
7.45
7.45
7.43
7.39
7.38
7.22
7.20
7.18
7.16
5.29
5.25
4.70
1.57 H2O
1.35
O
B
O
O
O
O
2
OH
5.8
1.84
4.22
2.18
5.73
2.12
2.01
2.16
11.90
f1 (ppm)

^{13}C NMR

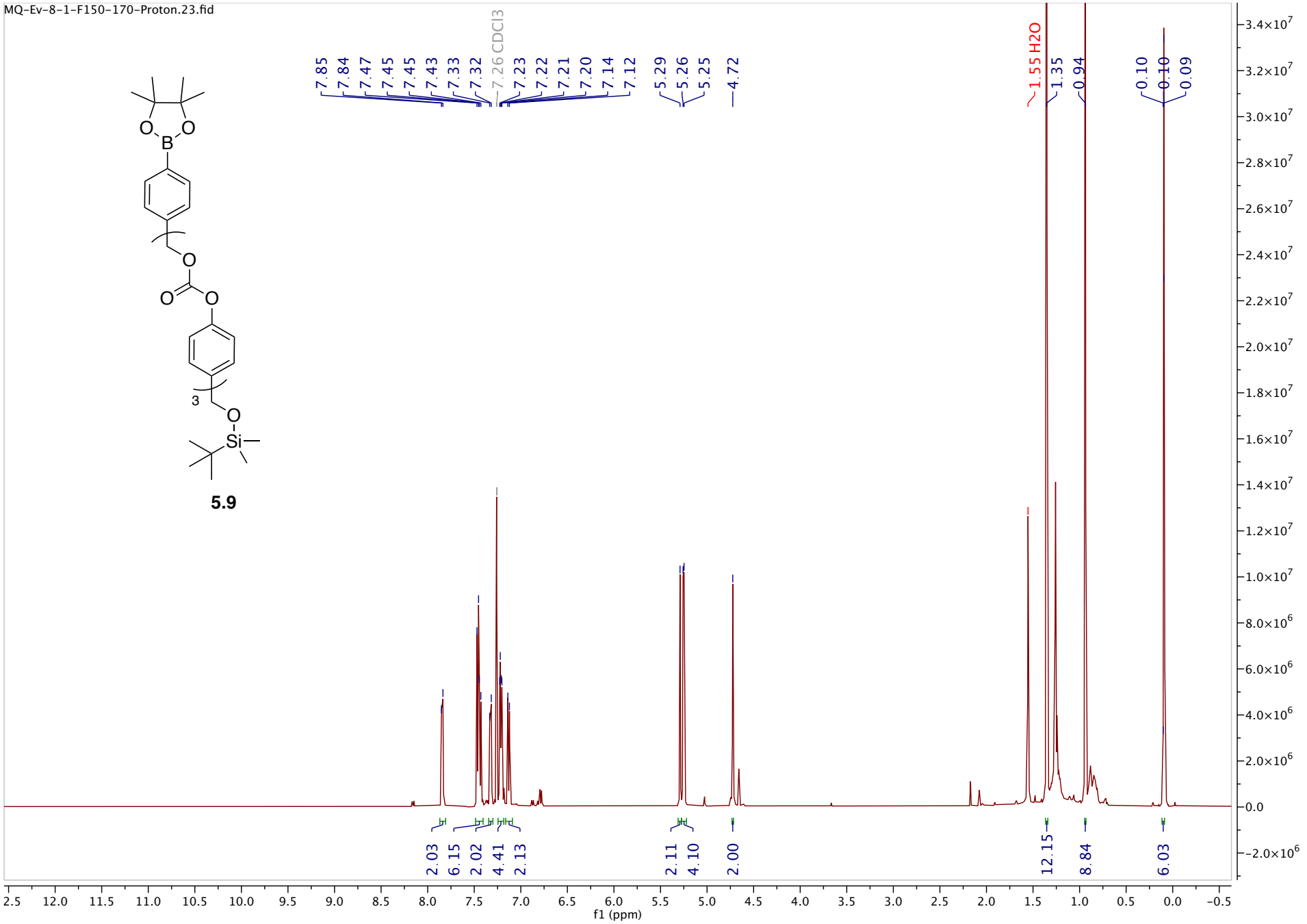

153.59
153.42
151.36
150.47
138.77
137.55
135.12
132.60
129.90
128.08
127.51
121.34
121.13
83.94
77.26 cdcl3
77.00 cdcl3
76.75 cdcl3
70.28
69.55
64.68
24.86
O
B
O
O
O
O
2
OH
f1 (ppm)

5.8

^{11}B NMR

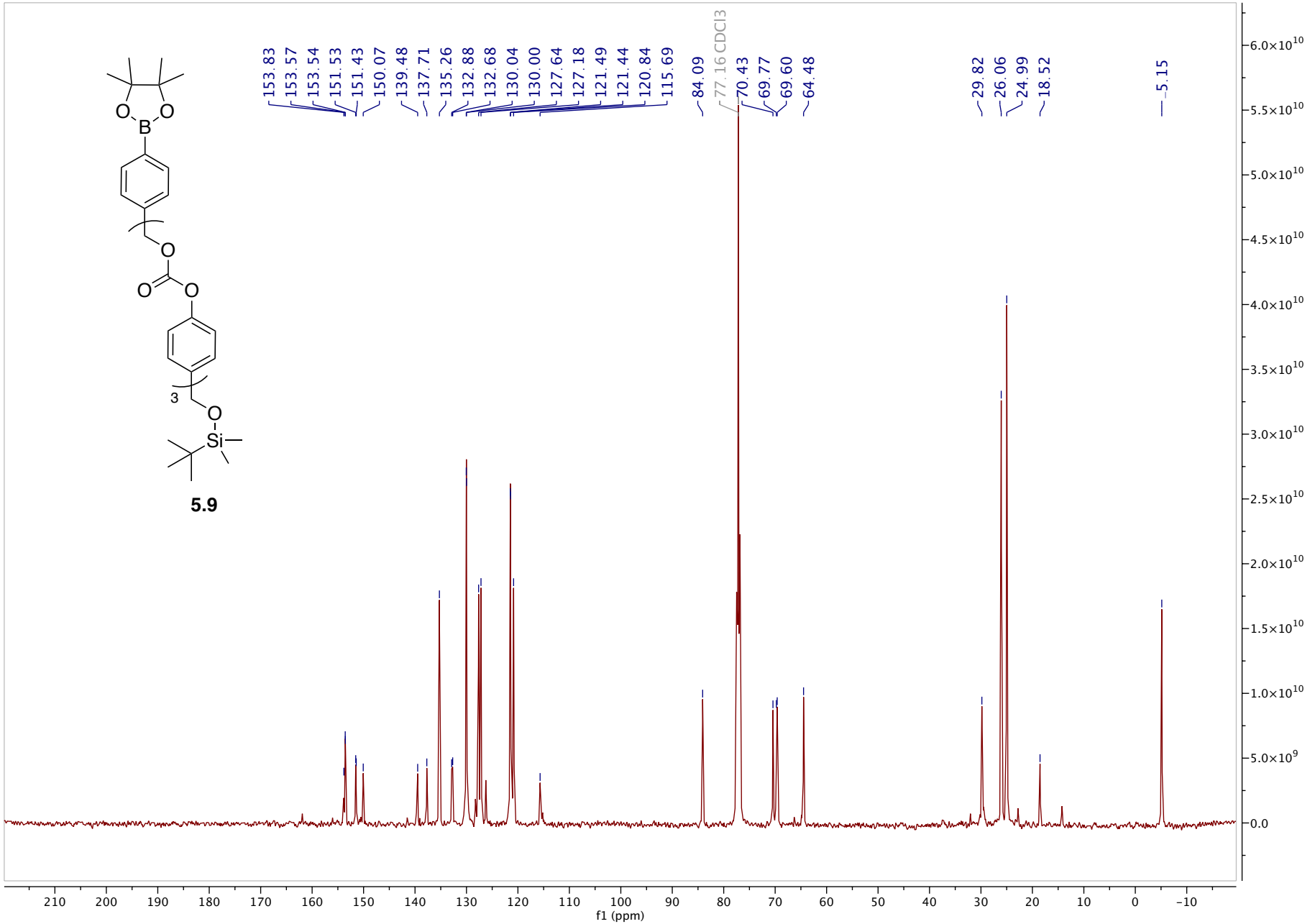

30.73
O
B
O
O
O
O
2
OH
5.8
3.8
3.6
3.4
3.2
3.0
2.8
2.6
2.4
2.2
2.0
1.8
1.6
1.4
1.2
1.0
0.8
0.6
0.4
0.2
0.0
-0.2
90
80
70
60
50
40
30
20
10
0
-10
-20
-30
-40
-50
-60
-70
-80
-90
f1 (ppm)

^{1}H NMR


MQ-Ev-8-1-F150-170-Proton.23.fid
7.85
7.84
7.47
7.45
7.45
7.43
7.33
7.32
7.26 CDCl3
7.23
7.22
7.21
7.20
7.14
7.12
5.29
5.26
5.25
4.72
1.55 H2O
1.35
0.94
0.10
0.10
0.09
2.03
6.15
2.02
4.41
2.13
2.11
4.10
2.00
12.15
8.84
6.03
f1 (ppm)

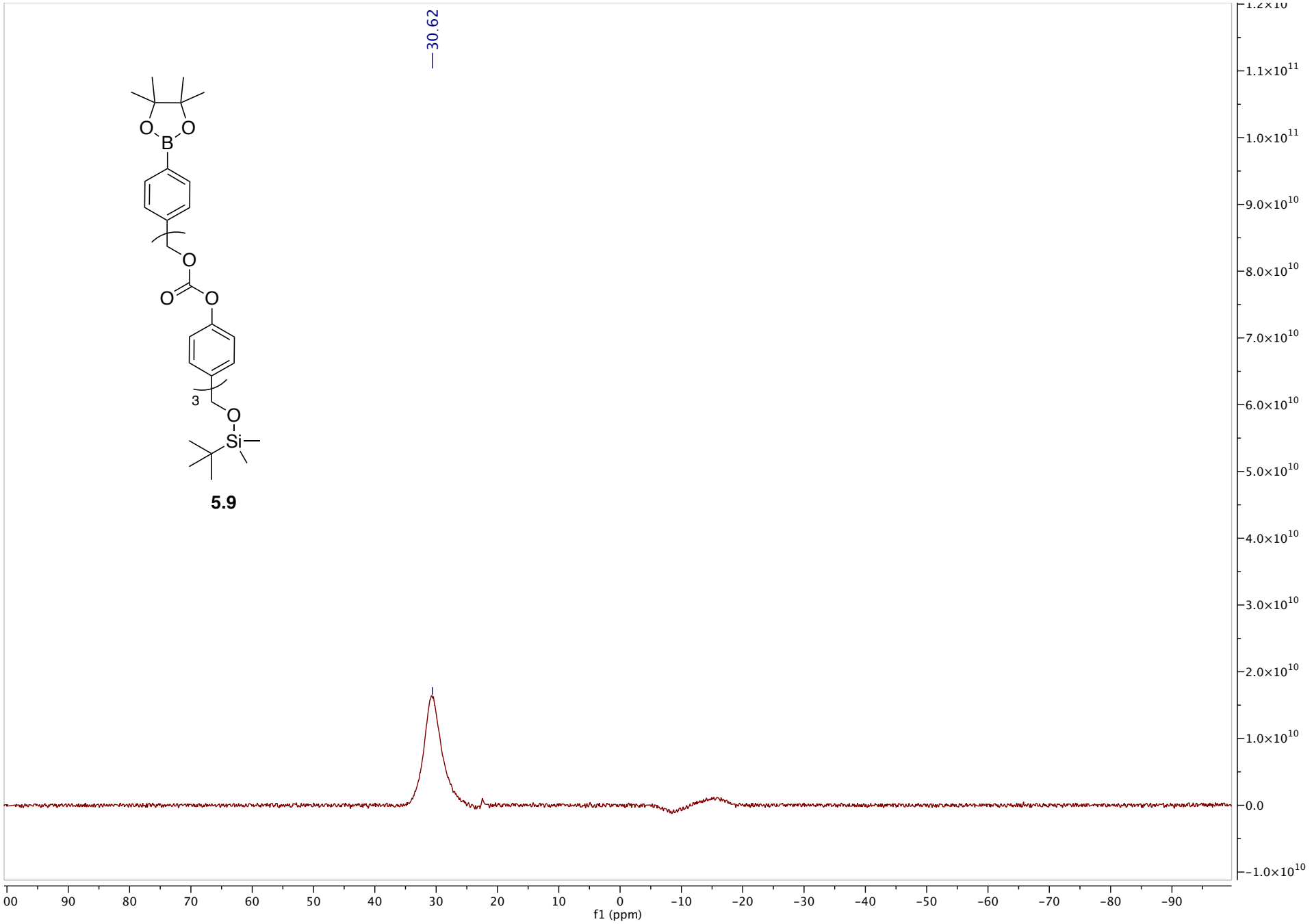
5.9

^{13}C NMR

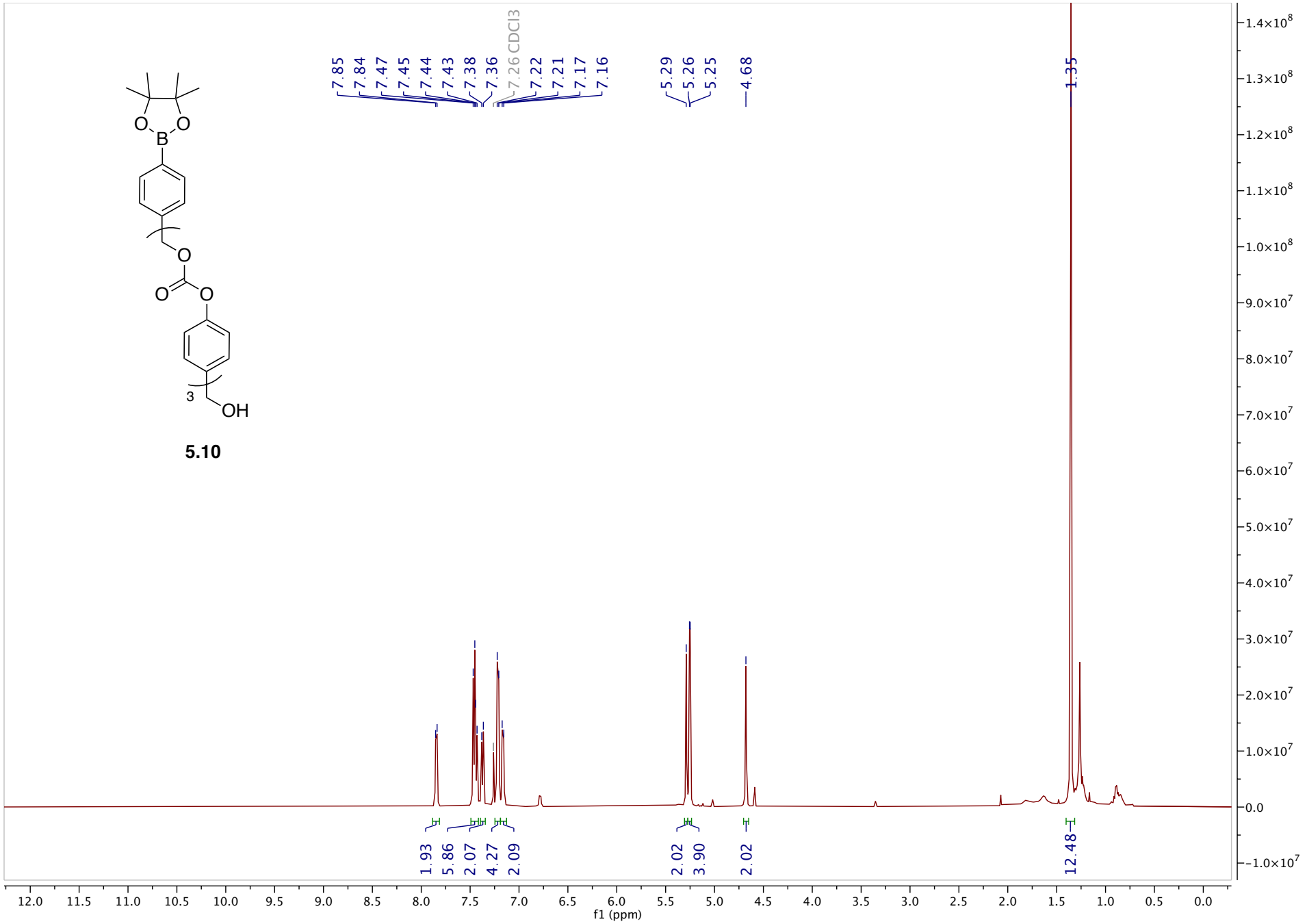

153.83
153.57
153.54
151.53
151.43
150.07
139.48
137.71
135.26
132.88
132.68
130.04
130.00
127.64
127.18
121.49
121.44
120.84
115.69
84.09
77.16 CDCl3
70.43
69.77
69.60
64.48
29.82
26.06
24.99
18.52
5.15
6.0×10^10
5.5×10^10
5.0×10^10
4.5×10^10
4.0×10^10
3.5×10^10
3.0×10^10
2.5×10^10
2.0×10^10
1.5×10^10
1.0×10^10
5.0×10^9
0.0
210 200 190 180 170 160 150 140 130 120 110 100 90 80 70 60 50 40 30 20 10 0 −10
f1 (ppm)

5.9

^{11}B NMR


30.62
O
B
O
O
O
O
3
O
Si
5.9
1.2×10
1.1×10^11
1.0×10^11
9.0×10^10
8.0×10^10
7.0×10^10
6.0×10^10
5.0×10^10
4.0×10^10
3.0×10^10
2.0×10^10
1.0×10^10
0.0
-1.0×10^10
00 90 80 70 60 50 40 30 20 10 0 -10 -20 -30 -40 -50 -60 -70 -80 -90
f1 (ppm)

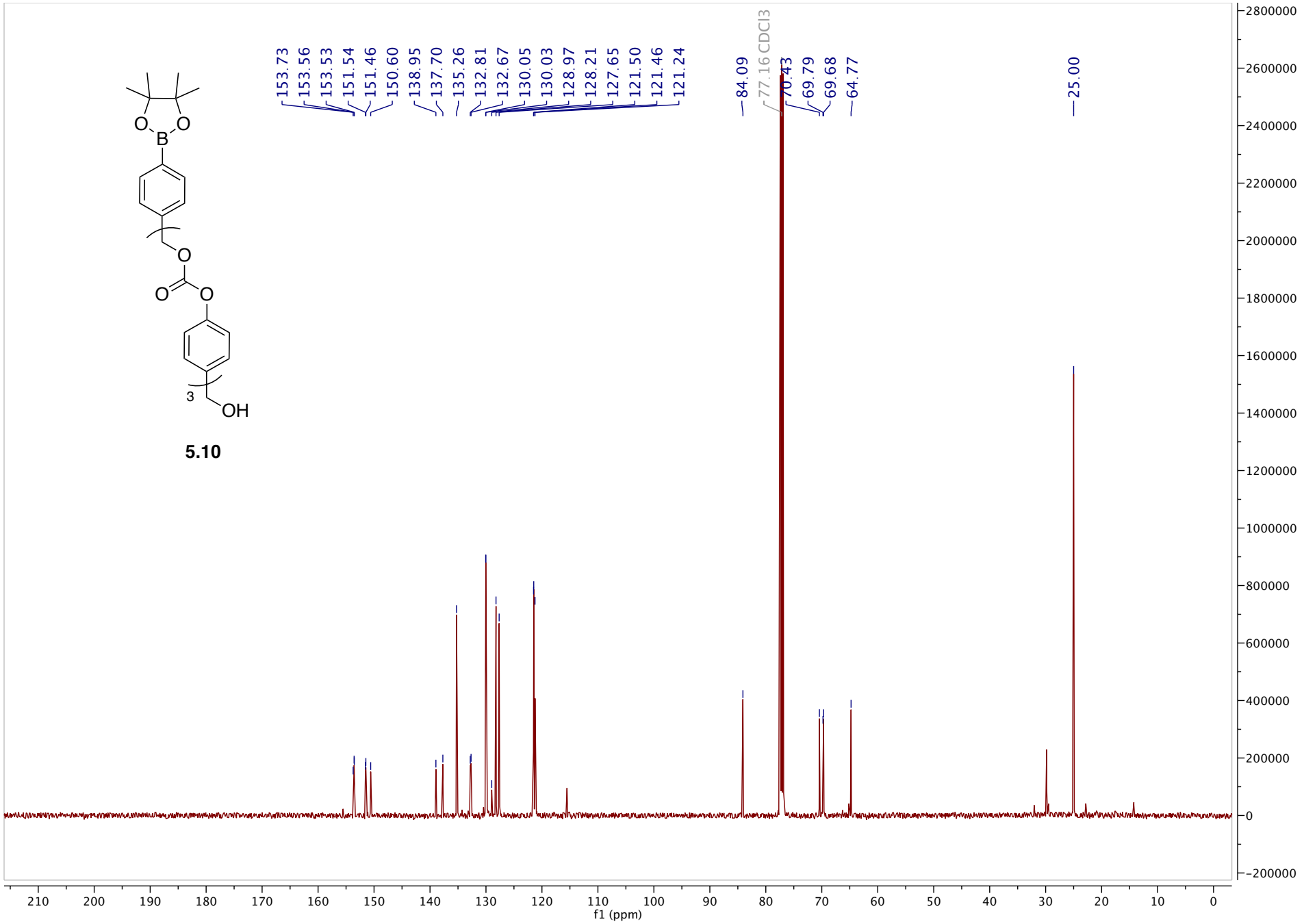
^{1}H NMR


7.85
7.84
7.47
7.45
7.44
7.43
7.38
7.36
7.26 CDCl3
7.22
7.21
7.17
7.16
5.29
5.26
5.25
4.68
1.35
1.93
5.86
2.07
4.27
2.09
2.02
3.90
2.02
12.48
f1 (ppm)

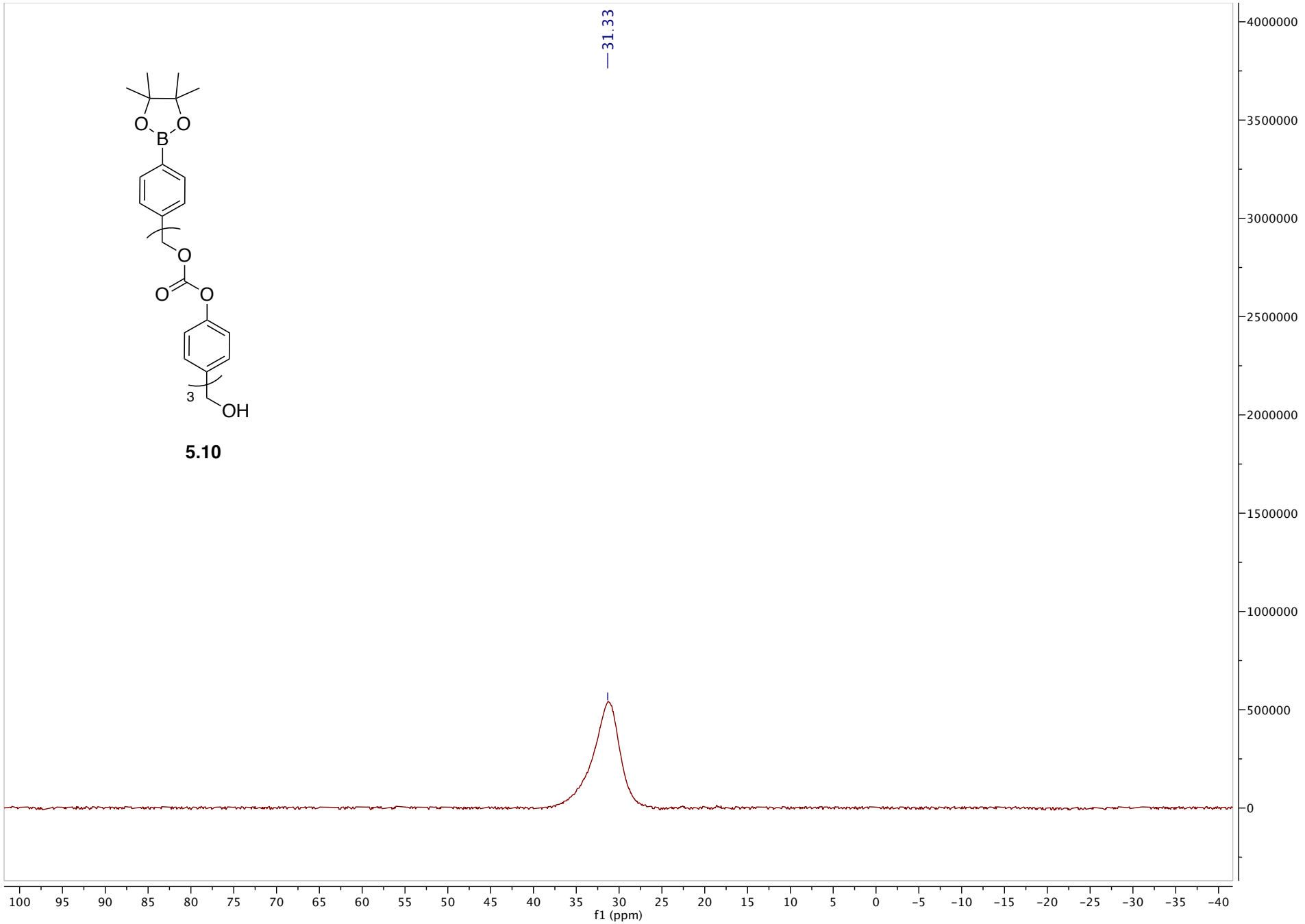
O
B
O
O
O
O
3
OH

5.10

^{13}C NMR


153.73
153.56
153.53
151.54
151.46
150.60
138.95
137.70
135.26
132.81
132.67
130.05
130.03
128.97
128.21
127.65
121.50
121.46
121.24
84.09
77.16 CDCl3
70.43
69.79
69.68
64.77
25.00
O
B
O
O
O
O
3
OH
5.10
f1 (ppm)

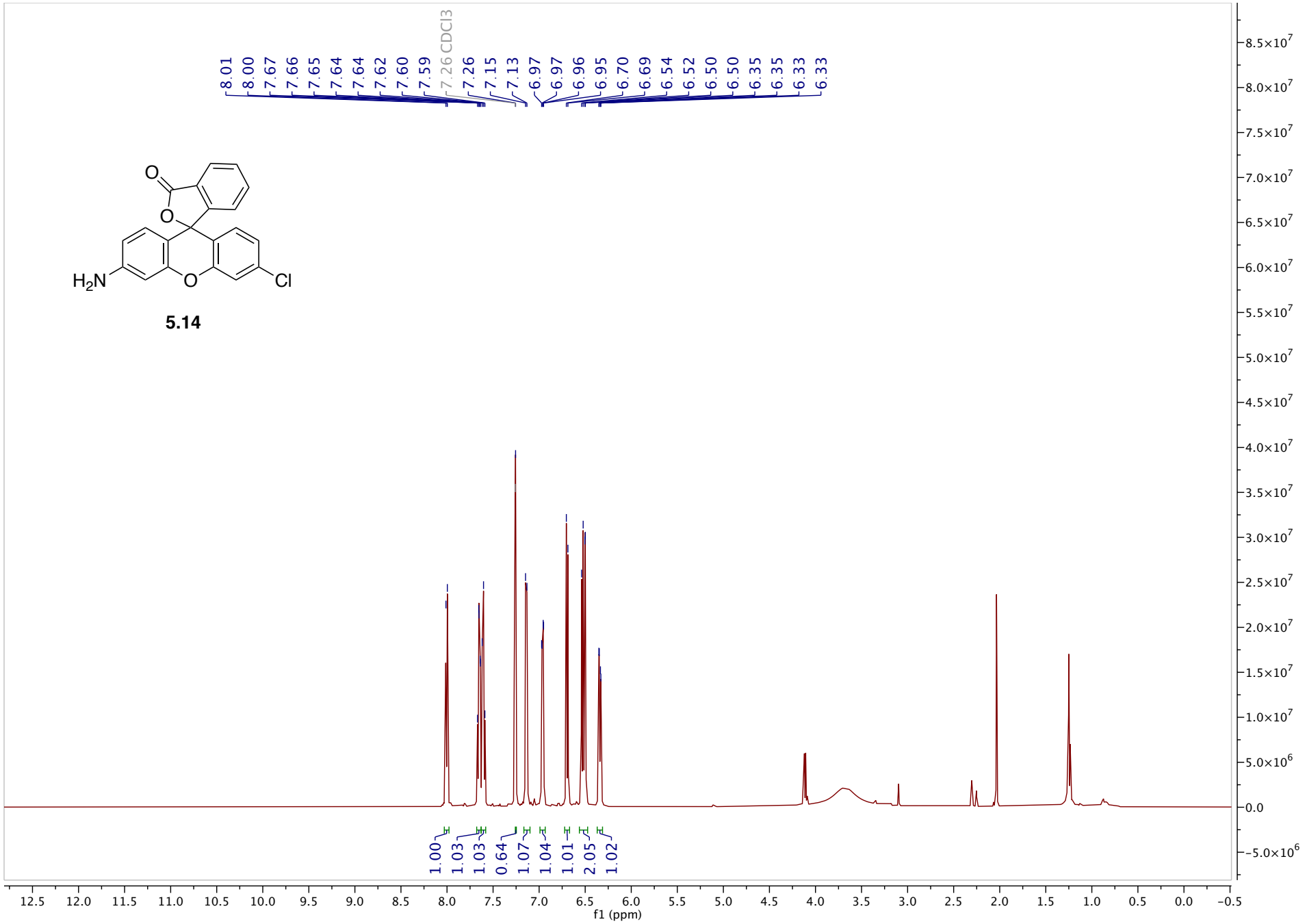
^{11}B NMR


31.33
4000000
3500000
3000000
2500000
2000000
1500000
1000000
500000
0
100 95 90 85 80 75 70 65 60 55 50 45 40 35 30 25 20 15 10 5 0 -5 -10 -15 -20 -25 -30 -35 -40
f1 (ppm)

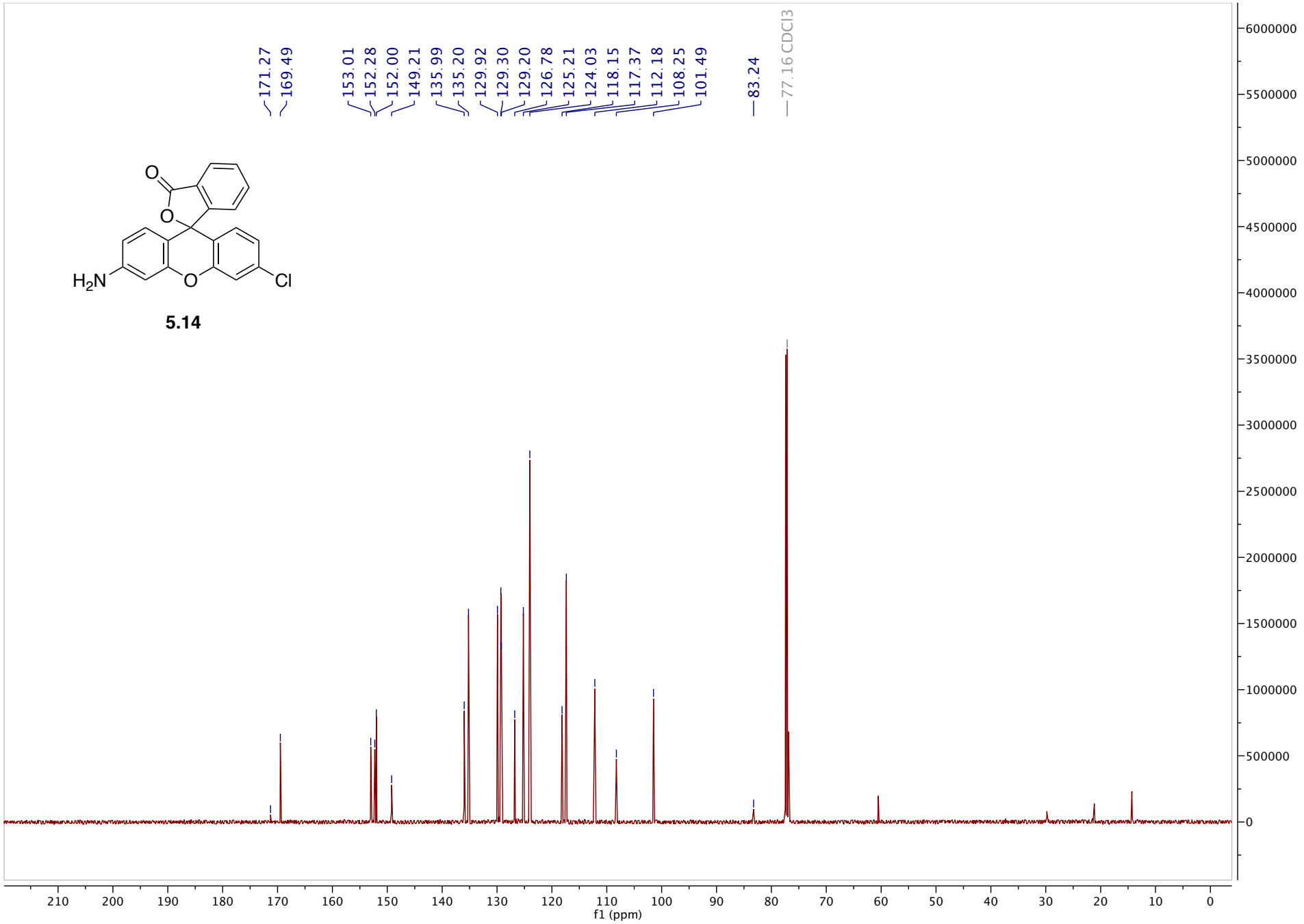
O
B
O
O
O
O
3
OH

5.10

^{1}H NMR


8.01
8.00
7.67
7.66
7.65
7.64
7.64
7.62
7.60
7.59
7.26 CDCl3
7.26
7.15
7.13
6.97
6.97
6.96
6.95
6.70
6.69
6.54
6.52
6.50
6.50
6.35
6.35
6.33
6.33
O
O
H2N
O
Cl
5.14
1.00
1.03
1.03
0.64
1.07
1.04
1.01
2.05
1.02
f1 (ppm)

^{13}C NMR


171.27
169.49
153.01
152.28
152.00
149.21
135.99
135.20
129.92
129.30
129.20
126.78
125.21
124.03
118.15
117.37
112.18
108.25
101.49
83.24
77.16 CDCl3
O
O
H2N
O
Cl
5.14
6000000
5500000
5000000
4500000
4000000
3500000
3000000
2500000
2000000
1500000
1000000
500000
0
210
200
190
180
170
160
150
140
130
120
110
100
90
80
70
60
50
40
30
20
10
0
f1 (ppm)

Vita

Megan L. Qualls was born in 1996 in Stockbridge, Georgia, and raised in Bartlett, Tennessee. Despite receiving little formal education, she found solace in the few classes she attended and was particularly inspired by biology and chemistry. She viewed higher education as a way to rise up from her circumstances, and after gaining acceptance to The University of Tennessee, Knoxville, she pursued knowledge for nearly a decade. She first obtained her bachelor's degree in Nutrition with a concentration in Cellular and Molecular Nutrition Science and minor in Chemistry and graduated summa cum laude within the Chancellor's Honors Program in 2018. During her undergraduate studies, she participated in research in a Biomedical Nutrition Science lab under the supervision of Dr. Dallas Donohoe where she studied the metabolic function of the microbial-derived metabolite butyrate toward dietary colorectal cancer prevention. She also conducted research in the polymer chemistry lab of Dr. Brian K. Long where she obtained experience in organic synthesis through the synthesis of organometallic olefin polymerization catalysts. Throughout her studies, science drove her curiosity and she realized that chemistry is the foundation to understand all biological issues, so she decided to pursue further education in organic chemistry. She then enrolled in the chemistry Ph.D. program at the University of Tennessee, Knoxville in August 2018. After joining Dr. Michael D. Best's research lab, she spent five years studying organic chemistry and chemical biology. Her graduate research, which is discussed in this dissertation, focused primarily on the development of various surface-modified liposomes for enhanced cellular delivery and triggered release purposes.